Lessons from the ICU
Under the Auspices of the European Society of Intensive Care Medicine
Series Editors: Maurizio Cecconi · Daniel De Backer

Chiara Robba
Antonio Messina
Adrian Wong
Antoine Vieillard-Baron *Editors*

Basic Ultrasound Skills "Head to Toe" for General Intensivists

Springer

Lessons from the ICU
Under the Auspices of the European Society of Intensive Care Medicine

Series Editors

Maurizio Cecconi
Head Dept Anesthesia and ICU, Humanitas Research Hospital
Head Dept Anesthesia and ICU
Rozzano, Milano, Milano, Italy

Daniel De Backer
Dept Intensive Care, Université Libre de Bruxelles Dept Intensive Care Erasme University
Bruxelles, Brussels Hoofdst.ge., Belgium

Lessons from the ICU is a Book Series published by Springer under the auspices of the *European Society of Intensive Care Medicine* (ESICM). The aim of the Series is to provide focused and state-of-the-art reviews of central topics in Intensive Care. Ultimately, its mission is to transfer the latest knowledge to the bedside in order to improve patient outcomes. Accordingly, the ESICM has also developed *Lessons from the ICU* with the vision or providing the best resources for everyone working in Intensive Care.

Each volume presents a comprehensive review of topical issues in Intensive Care. The volumes are intended to cover the majority of aspects that intensive care professionals are likely to encounter in the course of their career. Books offer an excellent guide for residents who are new to the ICU, and for allied professionals, senior consultants as well as nurses and allied healthcare professionals.

The chapters are organized in a way that allows the reader to quickly familiarize or reacquaint themselves with the pathophysiological background before moving on to diagnosis and treatment. Each chapter includes a list of Take Home Messages, as well as practical examples that apply theoretical knowledge in real clinical scenarios. Each volume in the Series is edited by international Key Opinion Leaders in Intensive Care, and each chapter is written by experts in the field.

In summary, this Series represents a valuable contribution to fill the gap in the current Intensive Care literature by providing top-quality literature reviews that can be easily digested and used at the bedside to improve patient outcomes.

Indexed in Scopus

Corresponding Series Editors and responsible for new book proposals :
Maurizio Cecconi @ maurizio.cecconi@hunimed.eu
Daniel De Backer @ ddebacke@ulb.ac.be

Chiara Robba • Antonio Messina • Adrian Wong
Antoine Vieillard-Baron
Editors

Basic Ultrasound Skills "Head to Toe" for General Intensivists

Springer

Editors
Chiara Robba
Anesthesia and Intensive Care
Ospedale Policlinico San Martino
Genova, Italy

Antonio Messina
Department of Biomedical Sciences
IRCCS Humanitas Research Hospital
Rozzano, Milano, Italy

Adrian Wong
Department of Critical Care
King's College Hospital
London, UK

Antoine Vieillard-Baron
Intensive Care Medicine Unit
Hôpital Ambroise-Paré
Boulogne-Billancourt, France

ISSN 2522-5928 ISSN 2522-5936 (electronic)
Lessons from the ICU
ISBN 978-3-031-32461-1 ISBN 978-3-031-32462-8 (eBook)
https://doi.org/10.1007/978-3-031-32462-8

© European Society of Intensive Care Medicine 2023
This work is subject to copyright. All rights are solely and exclusively licensed by the Publisher, whether the whole or part of the material is concerned, specifically the rights of translation, reprinting, reuse of illustrations, recitation, broadcasting, reproduction on microfilms or in any other physical way, and transmission or information storage and retrieval, electronic adaptation, computer software, or by similar or dissimilar methodology now known or hereafter developed.
The use of general descriptive names, registered names, trademarks, service marks, etc. in this publication does not imply, even in the absence of a specific statement, that such names are exempt from the relevant protective laws and regulations and therefore free for general use.
The publisher, the authors, and the editors are safe to assume that the advice and information in this book are believed to be true and accurate at the date of publication. Neither the publisher nor the authors or the editors give a warranty, expressed or implied, with respect to the material contained herein or for any errors or omissions that may have been made. The publisher remains neutral with regard to jurisdictional claims in published maps and institutional affiliations.

This Springer imprint is published by the registered company Springer Nature Switzerland AG
The registered company address is: Gewerbestrasse 11, 6330 Cham, Switzerland

Contents

1 **Introduction** 1
Adrian Wong, Chiara Robba, Antonio Messina, and Antoine Vieillard-Baron

2 **General Principles of Ultrasound** 5
Olusegun Olusanya

I Heart

3 **Detection and Interpretation of Left Ventricular Systolic Dysfunction by Basic Critical Care Echocardiography** 21
Edouard Jullien and Antoine Vieillard-Baron

4 **Evaluation for Right Ventricular Failure** 29
Bruno Evrard, Marine Goudelin, and Philippe Vignon

5 **Evaluation of Haemodynamically Important Pericardial Effusion** 47
Michelle S. Chew, Jonathan Aron, and Meriam Åström Aneq

6 **Evaluation for Severe Hypovolemia** 59
Max Rosenthal and Paul Mayo

7 **Evaluation for Acute, Severe Left-Sided Valvulopathy** 75
Alexander Astell, Erica Clarke Whalen, and Robert T. Arntfield

II Lung

8 **Pneumothorax** 93
Silvia Mongodi, Giulia Salve, and Francesco Mojoli

9 **Pleural Effusion in Critically Ill Patients** 107
Luigi Vetrugno, Fabrizio Tritapepe, Valentina Angelini, Salvatore Maurizio Maggiore, and Giovanni Volpicelli

10 **Airway Ultrasound for the Intensivist** 121
Ashraf Al-Tayar, Serene SP Ho, and Adrian Wong

11 **Ultrasound Assessment of the Respiratory Muscles** 137
Annemijn H. Jonkman, Nuttapol Rittayamai, Annia Schreiber, Laurent Brochard, and Alberto Goffi

III Abdomen

12 **Triage or Clinical Suspicion for Aortic Syndromes** 171
Federico Dazzi, Francesco Corradi, Erika Taddei, Giada Cucciolini, and Francesco Forfori

13 **Assessment of Kidneys and Urinary Tract** 189
Adrian Wong and Serene SP Ho

14 **Assessment of Traumatic Acute Abdomen** 199
Kelvin Wong, Dae Hyeon Kim, and Mangala Narasimhan

15 **Ecographic Assessment of Nontraumatic Acute Abdomen** 211
Martina Fregonese, Beatrice Vigna, Edoardo De Robertis, and Gianmaria Cammarota

IV Vessels

16 **Ultrasound-Guided Cannulation** 233
Michel Slama, Yoann Zerbib, Clément Brault, and Julien Maizel

17 **Deep Venous Thrombosis** 251
Massimo Lamperti, Boris Tufegdzic, and Amit Jain

V Brain

18 **Cranial Ultrasound for Intracerebral Pathology** 275
Aarti Sarwal

19 **Role of Brain Ultrasound for the Assessment of Intracranial Hypertension** 291
Corina Puppo

20 **Transcranial Doppler (TCD): Clinical Applications in Acute Brain Injury** 309
Carla Bittencourt Rynkowski, Juliana Caldas, and Fabio Silvio Taccone

21 **Regional Anaesthesia for the Intensivist** 325
Edmund Chan, Cosmin Balan, and Amit Pawa

VI Ultrasound Training

22 **Training in Ultrasound for Intensivists** 357
Laura Galarza

VII Integration of Different US Skills in Clinical Scenarios at the Bedside

23 **Combined Echocardiography and Lung Ultrasound in Shocked Patient** 371
Luigi Vetrugno, Fabrizio Tritapepe, Marco Ventin, Gian Marco Anzellotti, and Salvatore Maurizio Maggiore

24 **Role of Lung Ultrasound and Echocardiography in Acute Respiratory Failure, Acute Respiratory Distress Syndrome, and Weaning in Mechanically Ventilated Patients** 387
Luigi Pisani, Marry R. Smit, and Pieter R. Tuinman

25 **Use of Ultrasound for the Assessment of Fluid Responsiveness in Critically Ill Patients** 409
Filippo Sanfilippo, Stephen Huang, and Alberto Noto

26 **Extended-FAST Protocol in Polytrauma Patients** 433
Francesco Corradi, Federico Dazzi, Erika Taddei, Giada Cucciolini, and Samuele Ferrari

Contributors

Ashraf Al-Tayar Critical Care, Security Forces Hospital, Dammam, Saudi Arabia

Meriam Åström Aneq Department of Clinical Physiology, Linköping University Hospital, Linköping, Sweden

Valentina Angelini Department of Innovative Technologies in Medicine and Dentistry, Gabriele d'Annunzio University of Chieti-Pescara, Chieti, Italy

Gian Marco Anzellotti Clinical Department of Anesthesiology, Critical Care Medicine and Emergency, SS Annunziata Hospital, Chieti, Italy

Robert T. Arntfield Division of Emergency Medicine and Division of Critical Care Medicine, Schulich School of Medicine and Dentistry, Western University, London, ON, Canada

Jonathan Aron Intensive Care Unit, St. George University Hospital, London, UK

Alexander Astell Section of Critical Care Medicine, Department of Medicine, University of Manitoba, Winnipeg, MB, Canada

Cosmin Balan Cardiovascular Anesthesia and Intensive Care Medicine, Prof. Dr. C.C. Iliescu Institute for Emergency Cardiovascular Diseases, Bucharest, Romania

Antoine Vieillard Baron Intensive Care Medicine Unit, Assistance Publique-Hôpitaux de Paris, University Hospital Ambroise Paré, Boulogne-Billancourt, France

INSERM UMR-1018, CESP, Team Kidney and Heart, University of Versailles Saint-Quentin-en-Yvelines, Villejuif, France

Clément Brault Médecine Intensive Réanimation, CHU Sud, Amiens, France

Laurent Brochard Interdepartmental Division of Critical Care Medicine, University of Toronto, Toronto, ON, Canada

St. Michael's Hospital and Li Ka Shing Knowledge Institute, Keenan Research Centre, Toronto, ON, Canada

Juliana Caldas Escola Bahiana de Medicina e Saúde Pública, Salvador, Brazil

Instituto D'Or de Pesquisa e Ensino (IDOR), Salvador, Brazil

Gianmaria Cammarota University of Perugia, Perugia, Italy

Edmund Chan Department of Theatres, Anaesthesia & Perioperative Medicine, Guy's & St Thomas' NHS Foundation Trust, London, UK

Michelle S. Chew Department of Anaesthesia and Intensive Care, Biomedical and Clinical Sciences, Linköping University, Linköping, Sweden

Francesco Corradi Department of Surgical, Medical, Molecular Pathology and Critical Care Medicine, University of Pisa, Pisa, Italy

Giada Cucciolini Department of Surgical, Medical, Molecular Pathology and Critical Care Medicine, University of Pisa, Pisa, Italy

Federico Dazzi Department of Surgical, Medical, Molecular Pathology and Critical Care Medicine, University of Pisa, Pisa, Italy

Edoardo De Robertis University of Perugia, Perugia, Italy

Bruno Evrard Medical-Surgical ICU and Inserm CIC 1435, Dupuytren Teaching Hospital, Limoges, France

Samuele Ferrari Department of Surgical, Medical, Molecular Pathology and Critical Care Medicine, University of Pisa, Pisa, Italy

Francesco Forfori Department of Surgical, Medical, Molecular Pathology and Critical Care Medicine, University of Pisa, Pisa, Italy

Martina Fregonese University of Perugia, Perugia, Italy

Laura Galarza Department of Intensive Care, Hospital General Universitario de Castellón, Castellón de la Plana, Spain

Alberto Goffi Interdepartmental Division of Critical Care Medicine, University of Toronto, Toronto, ON, Canada

St. Michael's Hospital and Li Ka Shing Knowledge Institute, Keenan Research Centre, Toronto, ON, Canada

Marine Goudelin Medical-Surgical ICU and Inserm CIC 1435, Dupuytren Teaching Hospital, Limoges, France

Serene SP Ho Cavendish Clinic, London, UK

Stephen Huang Intensive Care Medicine, Nepean Hospital, The University of Sydney, Sydney, NSW, Australia

Amit Jain Anesthesiology Institute, Cleveland Clinic Abu Dhabi, Abu Dhabi, UAE

Annemijn H. Jonkman Department of Intensive Care Medicine, Erasmus Medical Center, Rotterdam, The Netherlands

Edouard Jullien Intensive Care Unit, University Hospital Ambroise Paré, APHP, Boulogne-Billancourt, France

Dae Hyeon Kim Pulmonary and Critical Care Medicine, Northwell Health, New Hyde Park, NY, USA

Massimo Lamperti Anesthesiology Institute, Cleveland Clinic Abu Dhabi, Abu Dhabi, UAE

Salvatore Maurizio Maggiore Department of Innovative Technologies in Medicine and Dentistry, Gabriele d'Annunzio University of Chieti-Pescara, Chieti, Italy

Clinical Department of Anesthesiology, Critical Care Medicine and Emergency, SS Annunziata Hospital, Chieti, Italy

Department of Innovative Technologies in Medicine and Dentistry, University of Chieti-Pescara, Chieti, Italy

Julien Maizel Médecine Intensive Réanimation, CHU Sud, Amiens, France

Paul Mayo Division of Pulmonary, Critical Care, and Sleep Medicine, Department of Medicine, Northwell Health LIJ/NSUH Medical Center, Donald and Barbara Zucker School of Medicine at Hofstra/Northwell, Hempstead, NY, USA

Antonio Messina Department of Biomedical Sciences, Humanitas Clinical and Research Center—IRCCS, Rozzano, Italy

Francesco Mojoli Dipartimento di Scienze Clinico-Chirurgiche, Diagnostiche e Pediatriche, Università di Pavia, Pavia, Italy

Silvia Mongodi Anestesia e Rianimazione 1, Fondazione IRCCS Policlinico San Matteo, Pavia, Italy

Mangala Narasimhan Critical Care, Northwell Health, New Hyde Park, NY, USA

Alberto Noto Division of Anesthesia and Intensive Care, Department of Human Pathology of the Adult and Evolutive Age "Gaetano Barresi", University of Messina, Policlinico "G. Martino", Messina, Italy

Olusegun Olusanya Barts Heart Centre, London, UK

Amit Pawa Department of Theatres, Anaesthesia & Perioperative Medicine, Guy's & St Thomas' NHS Foundation Trust, London, UK

Luigi Pisani Mahidol Oxford Research Unit (MORU), Bangkok, Thailand

Corina Puppo Critical Care Unit, Clinics Hospital, Universidad de la Republica, Uruguay, Montevideo, Uruguay

Nuttapol Rittayamai Division of Respiratory Diseases and Tuberculosis, Department of Medicine, Faculty of Medicine Siriraj Hospital, Mahidol University, Bangkok, Thailand

Chiara Robba Anesthesia and Intensive Care, Ospedale Policlinico San Martino, IRCCS per l'Oncologia e le Neuroscienze, Genoa, Italy

Department of Surgical Sciences and Integrated Diagnostics (DISC), University of Genoa, Genoa, Italy

Max Rosenthal Department of Internal Medicine, Prisma Health, University of South Carolina School of Medicine Greenville, Greenville, SC, USA

Carla Bittencourt Rynkowski Intensive Care Unit of Cristo Redentor Hospital, Porto Alegre, Brazil

Intensive Care Unit, Ernesto Dornelles Hospital, Porto Alegre, Brazil

Giulia Salve Dipartimento di Scienze Clinico-Chirurgiche, Diagnostiche e Pediatriche, Università di Pavia, Pavia, Italy

Filippo Sanfilippo Department of Anaesthesia and Intensive Care, "Policlinico-San Marco" University Hospital, Catania, Italy

Division of Anaesthesia and Intensive Care, Department of General Surgery and Medical-Surgical Specialty, University of Catania, Catania, Italy

Aarti Sarwal Neurocritical Care, Department of Neurology, Atrium Wake Forest School of Medicine, Winston Salem, NC, USA

Annia Schreiber Interdepartmental Division of Critical Care Medicine, University of Toronto, Toronto, ON, Canada

St. Michael's Hospital and Li Ka Shing Knowledge Institute, Keenan Research Centre, Toronto, ON, Canada

Michel Slama Médecine Intensive Réanimation, CHU Sud, Amiens, France

Marry R. Smit Department of Intensive Care, Amsterdam UMC, Amsterdam, The Netherlands

Fabio Silvio Taccone Department of Intensive Care, Hôpital Erasme, Université Libre de Bruxelles, Bruxelles, Belgium

Erika Taddei Department of Surgical, Medical, Molecular Pathology and Critical Care Medicine, University of Pisa, Pisa, Italy

Fabrizio Tritapepe Department of Innovative Technologies in Medicine and Dentistry, Gabriele d'Annunzio University of Chieti-Pescara, Chieti, Italy

Clinical Department of Anesthesiology, Critical Care Medicine and Emergency, SS Annunziata Hospital, Chieti, Italy

Boris Tufegdzic Anesthesiology Institute, Cleveland Clinic Abu Dhabi, Abu Dhabi, UAE

Pieter R. Tuinman Department of Intensive Care, Amsterdam UMC, Amsterdam, The Netherlands

Marco Ventin Department of Surgery, Massachusetts General Hospital, Harvard Medical School, Boston, MA, USA

Luigi Vetrugno Department of Medical, Oral and Biotechnological Sciences, University of Chieti-Pescara, Chieti, Italy

Clinical Department of Anesthesiology, Critical Care Medicine and Emergency, SS Annunziata Hospital, Chieti, Italy

Antoine Vieillard-Baron Intensive Care Unit, University Hospital Ambroise Paré, APHP, Boulogne-Billancourt, France

CESP, UMR 1018, Université Paris Saclay, Paris, France

Beatrice Vigna Presidio Ospedaliero "Santa Maria della Stella" di Orvieto, Orvieto, Italy

Philippe Vignon Medical-Surgical ICU and Inserm CIC 1435, Dupuytren Teaching Hospital, Limoges, France

Giovanni Volpicelli Department of Emergency Medicine, San Luigi Gonzaga University Hospital, Torino, Italy

Erica Clarke Whalen Section of Critical Care Medicine, Department of Medicine, University of Manitoba, Winnipeg, MB, Canada

Adrian V. K. Wong Department of Critical Care, King's College Hospital, London, UK

Kelvin Wong Pulmonary and Critical Care Medicine, Northwell Health, New Hyde Park, NY, USA

Yoann Zerbib Médecine Intensive Réanimation, CHU Sud, Amiens, France

Introduction

Adrian Wong, Chiara Robba, Antonio Messina, and Antoine Vieillard-Baron

Contents

References – 3

© The Author(s), under exclusive license to Springer Nature Switzerland AG 2023
C. Robba et al. (eds.), *Basic Ultrasound Skills "Head to Toe" for General Intensivists*, Lessons from the ICU,
https://doi.org/10.1007/978-3-031-32462-8_1

1

The use of ultrasound has evolved well beyond the confines of radiology (and cardiology) over the last decades. It has become integral to the delivery of modern critical care medicine as a diagnostic and monitoring tool, and as an aid to procedural and management planning. There is no single organ in the body that cannot be imaged using ultrasound.

Given that a core business of intensive care medicine (ICM) is the manipulation of the circulation and haemodynamics, the use of echocardiography to diagnose and guide interventions is to be expected. The collaboration between cardiologists and intensivists was totally informal, without defined training pathways—enthusiastic colleagues were simply encouraged to pick up the probe and scan. These arrangements were created in silos and there was a clear need to ensure that colleagues everywhere had the opportunity to train in the modality and gain the necessary skill set.

There was a natural progression to extend ultrasound examinations beyond the heart, in line with the holistic, whole-body approach that is ICM [1]. Examinations of the lung, abdomen and brain became part and parcel of the armamentarium of the Intensivists (albeit at different pace) and were broadly termed Critical Care Ultrasonography (CCUS).

However, it is not surprising that the journey to develop ultrasound as a key tool in ICM has not been without challenges and resistance both within and outside the Specialty [2]. Key points of deliberation include defining the competencies, training pathways and governance of the scans. These issues are key to ensuring quality and standards are maintained.

Recognizing this, collaborative projects involving like-minded individuals and professional societies culminated in large national level courses both in the USA [3, 4] and Europe. Several landmark papers were published in subsequent years that attempted to define the various required competencies in both critical care echocardiography and general CCUS [5–8]. These also attempted to provide some guidance in the number of scans that would be required for the trainee to gain the necessary competencies.

National societies started to operationalize recommendations into their own curriculum and training programmes, but the differences between the various guidelines was a source of uncertainty. Clarity and transparency (alongside supporting resources—of which this book forms a part) and an adaptation to knowledge and studies are necessary for setting standards to which both trainers and trainees adhere/aspire. It took more than a decade from the seminal papers before, in 2021, the European Society of Intensive Care Medicine (ESICM) produced the most recent consensus statement with expert recommendations on basic CCUS for intensivists working in general ICU and neuro ICU [9]. The document included 74 statements: 7 for brain; 20 for lung; 20 for heart; 20 for abdomen; 7 for vascular ultrasound. These represent the most up-to-date and robust consensus on the required competencies available for CCUS, and they are expected to form the foundation for development of more advanced skill sets.

The aim of this book is to provide a comprehensive, clear and practical approach to bedside CCUS, including chapters on the heart, lung, abdomen, vessels and brain systems. Moreover, two specific sections on general principles of the ultrasound and on the training programmes for intensivists are included. Considering the volume of information provided, we specifically asked the experts involved to maintain a consistent methodology throughout the chapters, mainly focused on reporting and

explaining the basic skills considered "standard level" to evaluate organ function using an accessible and practical approach.

The Editors hope to design a pathway of knowledge and clinical application of basic CCUS skills, based on the first ESICM consensus on this topic [9] and presented at the General Intensive Care Ultrasound (GenIUS) course, firstly presented at the ESICM congress in 2022 in Paris. The GenIUS course consists of a 2-day training programme with hands-on learning and theoretical insights which have been discussed in this book by CCUS experts.

Reflecting the structure of the GenIUS course and the ESICM guidelines, this book is an essential tool for all the intensivists and residents interested in "Head to Toe" US for ICM. It should provide the basics upon which an Intensivist can build the skills to accurately interpret US images and integrate them into clinical management of the critically ill patient.

In summary, CCUS has progressed over the last decades, and it is becoming a standard of care and part of routine practice for the management of critically ill patients. We hope that this book will help in a gradual pushing of boundaries as this skill continues to mature, together with the implementation of new devices and techniques to suit the evolving clinical needs. We thus hope to provide adequate resources that support such evolution.

References

1. Lichtenstein D, Axler O. Intensive use of general ultrasound in the intensive care unit. Prospective study of 150 consecutive patients. Intensive Care Med. 1993;19(6):353–5. https://doi.org/10.1007/BF01694712.
2. Galarza L, Wong A, Malbrain MLNG. The state of critical care ultrasound training in Europe: a survey of trainers and a comparison of available accreditation programmes. Anaesthesiol Intensive Ther. 2017;49(5):382–6. https://doi.org/10.5603/AIT.a2017.0075. Epub 2017 Dec 1.
3. Patrawalla P, Narasimhan M, Eisen L, Shiloh AL, Koenig S, Mayo P. A regional, cost-effective, collaborative model for critical care fellows' ultrasonography education. J Intensive Care Med. 2020;35(12):1447–52.
4. Greenstein YY, Littauer R, Narasimhan M, Mayo PH, Koenig SJ. Effectiveness of a critical care ultrasonography course. Chest. 2017;151(1):34–40.
5. Mayo PH, Beaulieu Y, Doelken P, Feller-Kopman D, Harrod C, Kaplan A, Oropello J, Vieillard-Baron A, Axler O, Lichtenstein D, Maury E. American College of Chest Physicians/La Société de Réanimation de Langue Française statement on competence in critical care ultrasonography. Chest. 2009;135(4):1050–60. https://doi.org/10.1378/chest.08-2305.
6. Expert Round Table on Ultrasound in ICU. International expert statement on training standards for critical care ultrasonography. Intensive Care Med. 2011;37:1077–83.
7. Expert Round Table on Echocardiography in ICU. International consensus statement on training standards for advanced critical care echocardiography. Intensive Care Med. 2014;40:654–66.
8. Wong A, Galarza L, Forni L, De Backer D, Slama M, Cholley B, Mayo P, McLean A, Vieillard-Baron A, Lichtenstein D, Volpicelli G, Arntfield R, Martin-Loeches I, Istrate GM, Duška F, ESICM Critical Care Ultrasound Group. Recommendations for core critical care ultrasound competencies as a part of specialist training in multidisciplinary intensive care: a framework proposed by the European Society of Intensive Care Medicine (ESICM). Crit Care. 2020;24(1):393. https://doi.org/10.1186/s13054-020-03099-8.
9. Robba C, Wong A, Poole D, et al. Basic ultrasound head-to-toe skills for intensivists in the general and neuro intensive care unit population: consensus and expert recommendations of the European Society of Intensive Care Medicine. Intensive Care Med. 2021;47:1347–67. https://doi.org/10.1007/s00134-021-06486-z.

General Principles of Ultrasound

Olusegun Olusanya

Contents

2.1 Introduction – 6

2.2 What Happens to Sound Waves as They Travel? – 7
2.2.1 Attenuation – 7
2.2.2 Reflection – 8
2.2.3 Refraction – 9
2.2.4 Scattering – 9

2.3 How Is an Ultrasound Image Generated? – 9

2.4 Principles of Pulsed Echo – 12

2.5 Transducers and Image Formation – 13

2.6 Principles of Doppler Ultrasound – 14

2.7 Limitations of Diagnostic Ultrasound – 16

2.8 Ultrasound Artefacts – 16

2.9 Artefacts Related to 2D Imaging – 17

2.10 Artefacts Related to Doppler Imaging – 17

Further Reading – 18

© The Author(s), under exclusive license to Springer Nature Switzerland AG 2023
C. Robba et al. (eds.), *Basic Ultrasound Skills "Head to Toe" for General Intensivists*, Lessons from the ICU,
https://doi.org/10.1007/978-3-031-32462-8_2

2

Learning Objectives

- To describe the physical properties of a sound wave
- To understand the relationship between frequency, wavelength, and propagation velocity of sound in a medium
- To understand the physics of reflection and the generation of an ultrasound image
- To understand the principles of Doppler ultrasound
- To understand some of the common artefacts in ultrasound imaging

2.1 Introduction

From a beautiful aria to the crunch of dry leaves underfoot, sounds form a significant part of our human experience. The recognition of sound waves as a form of energy, which can be analysed and manipulated, has allowed us to make great strides—particularly in the field of medical imaging.

Sound waves are waves of mechanical energy which travel parallel to the direction of propagation—hence they are called "longitudinal" waves. The energy source that generates the sound waves transmits the energy into the medium around it, causing compression of the molecules as the energy travels. The molecules next to this area of compression remain evenly spaced out—this is referred to as an area of "rarefaction." A repeated cycle of areas of compression and rarefaction are the components of a sound wave.

If this wave of compression and rarefaction is represented as a graph—with energy (termed amplitude) on the y axis and time on the x axis, a two-dimensional representation of the wave can be obtained. The resulting visual is a sine wave, with compression and rarefaction represented by positive and negative deflections.

The distance between peaks is called the wavelength, and the number of completed cycles that occur every second is termed frequency. Seeing that velocity is a product of distance and time, this gives us our first key equation—propagation velocity is a product of the frequency and the wavelength (Fig. 2.1).

$$C = f \times \lambda \tag{2.1}$$

where C = propagation velocity, f = frequency, and λ = wavelength.

A key property of sound waves is that their propagation velocity is constant within a specific medium. As a result, it means that within a single medium, an increase in frequency results in a reduction in wavelength, and vice versa.

The frequency of ultrasound ties closely in with its characteristics. Audible ultrasound has a frequency of between 20 and 20,000 cycles per second, or Hertz (Hz). Higher frequency sound is heard as a higher "pitch," with the reverse being the case for lower frequency sound. Low frequency sound below the range of human hearing (i.e. less than 20 Hz) is termed "infrasound," while high frequency sound above the range of human hearing is termed "ultrasound."

Medical ultrasound uses frequencies of millions of cycles per second (megaHertz, or mHz). At the most basic level, diagnostic medical ultrasound involves transmitting ultrasound beams into soft tissue, detecting beams that are reflected back from these tissues, and converting those reflected signals into an image. We will discuss the specifics of this later in the chapter.

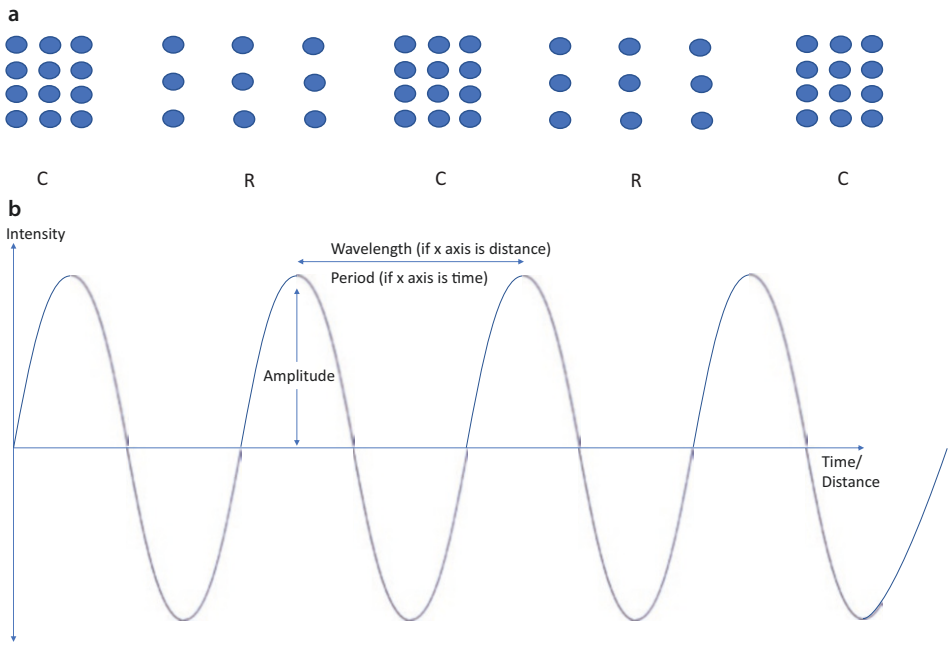

Fig. 2.1 **a** Compression and rarefaction. *C* compression; *R* rarefaction; **b** A sound wave represented as a sine wave, and broken down into its components

2.2 What Happens to Sound Waves as They Travel?

Sound waves have four important interactions of note:

- Attenuation
- Reflection
- Refraction
- Scattering

2.2.1 Attenuation

If a sound wave travels within a single medium, over time it loses energy and will eventually fade (think about how an object producing sound at a constant volume gets quieter the further away you travel, until you can no longer hear it). This is called attenuation, and can be expressed mathematically as a ratio of initial and final ultrasound energy (in this case, the unit of energy used is intensity—the amount of energy per second per square centimetre).

Attenuation is expressed using the same units that are conventionally used for ultrasound "loudness"—Decibels. (These are the same units that are used to express gain and dynamic range, which will be discussed later in the chapter)

$$\text{Attenuation} = 10 \log (I_1 / I_2) \text{dB} \tag{2.2}$$

where *I*1 and *I*2 refer to the initial and final intensities

Attenuation is affected by the initial frequency, the distance travelled, and the nature of the medium; as a result, an "attenuation coefficient" can be calculated for an individual medium which expresses the amount of attenuation in dB/cm/MHz. This coefficient is labelled alpha. For soft tissue, alpha works out as 0.5 cm/Db/MHz.

Due to the way ultrasound transducers work—that is, they require an ultrasound beam to be transmitted to an object and reflected back—calculating the true amount of attenuation an ultrasound beam undergoes before it is converted to an image requires doubling the depth that the object is from the transducer. This is termed round path attenuation and is calculated as

$$\text{Round path attenuation} = 2 \times \alpha \times \text{depth} \times \text{frequency} \tag{2.3}$$

At a certain depth, the returning signals are too small to generate an image. This depth is termed the penetration (P), and fits in to the formula above as:

$$\text{Maximum attenuation} = 2 \times \alpha \times \text{penetration} \times \text{frequency} \tag{2.3a}$$

Due to the fact that is constant, and penetration is fixed for each machine, this means that the primary determinant of attenuation of diagnostic ultrasound is *transmission frequency*—and thus the primary determinant for the depth of structures that can be imaged is also transmission frequency. There is, however, a trade-off between penetration and resolution—which will be discussed later on.

2.2.2 Reflection

When sound moves from one medium to another, and those two media have different densities, some interesting interactions can occur. In particular, echoes can be generated—just like the ones you hear when you speak in an enclosed area. Echoes are as a result of sound travelling between two media with a significant difference in a property known as acoustic impedance. Acoustic impedance (z) is related to the density of a medium and the sound propagation velocity within it, and is measured in Rayls.

$$Z = \rho \text{ x } C$$

When sound travels between two media with different acoustic impedances, a proportion of the sound is reflected. The relative intensity of the transmitted and reflected sound can be mathematically related in this equation:

$$\text{Reflected intensity} / \text{Incident intensity} = (z1 + z2)^2 / (z1 - z2)^2 \tag{2.4}$$

This ratio is termed the reflection coefficient, and is given the label R. As can be seen from the equation, if there is a large difference in Z1 and Z2, the coefficient will approach 1, meaning near complete reflection. If there is a small difference, the coefficient will approach zero, meaning continued propagation of the wave. Thus, clear image generation is dependent on tissue interfaces with different acoustic impedances. The other important aspect of this is the angle of incidence of the ultrasound beam—the above equation assumes perpendicular incidence of the beam. Not all

ultrasound beams travel, or are reflected, perpendicularly—this is one of the causes of ultrasound artefacts, which we will discuss later.

2.2.3 Refraction

The principle of refraction of light beams is classically demonstrated by light passing through a prism—where the light beam is shown to "bend." This is due to the light beam passing from air to glass, where there are two different propagation velocities. Ultrasound has the same property—when passing between two different media with different propagation velocities, the path of the ultrasound beam will change.

The law that defines this relationship is Snell's Law:

$$\sin\theta 1 / C1 = \sin\theta 2 / C2 \tag{2.5}$$

Where $\theta 1$ is the incident angle and $\theta 2$ is the reflected angle.

If the incident angle is 0°, the reflected angle is also 0°—hence no refraction occurs.

If C2 is significantly greater than C1, there will exist a particular incident angle that results in a reflected angle of 90°. Any further increase of the incident angle will result in a reflected angle of greater than 90°—i.e. total reflection of the beam. This is called the *critical angle*.

Refraction is another of the phenomena that results in the generation of ultrasound artefacts.

2.2.4 Scattering

When ultrasound beams hit small structures, rather than being reflected, the energy gets scattered in multiple directions. This results in multiple low-level echoes that interact with one another, and when detected by the transducer are displayed as "speckles" with a grey appearance.

If the structures are smaller than the wavelength of the beam, a special type of scattering called Rayleigh scattering occurs. This phenomenon is exploited as part of Doppler ultrasound, which we will discuss later in the chapter.

2.3 How Is an Ultrasound Image Generated?

In order to generate an image, a series of steps need to occur:

- Ultrasound needs to be transmitted into the body from the machine.
- Some of those ultrasound beams need to be reflected back to the machine.
- The machine needs to be able to detect these reflected beams and convert them into electrical signals.
- These electrical signals need to be converted into a visual display.

2

The majority of ultrasound machines utilize special crystals which utilize the Piezoelectric effect—when exposed to electricity, they vibrate at a certain frequency. This effect can also occur in reverse, as in a sound wave hitting the crystal is converted to an electrical signal. Hence these crystals act as both emitter and detector of ultrasound. Each Piezoelectric transducer can only vibrate at a single frequency, however; thus, traditional machines have different probes with different transducer frequencies to allow a wide range of diagnostic imaging (Fig. 2.2).

Some newer devices use mechanical transducers that can vibrate at, and detect, a range of frequencies. This allows for different types of images to be performed with a single probe.

Figure 2.3a demonstrates different probes, and Fig. 2.3b exposes the inner workings of a probe.

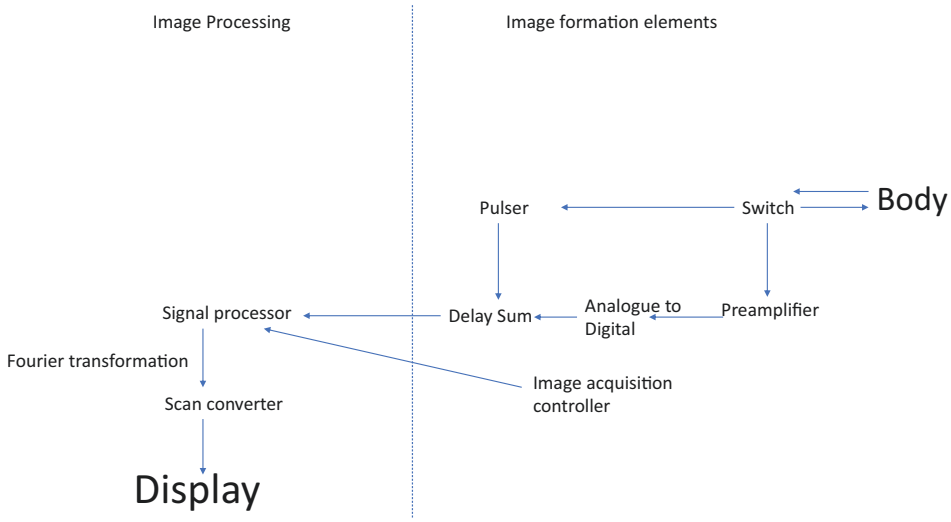

Fig. 2.2 Elements of an ultrasound machine

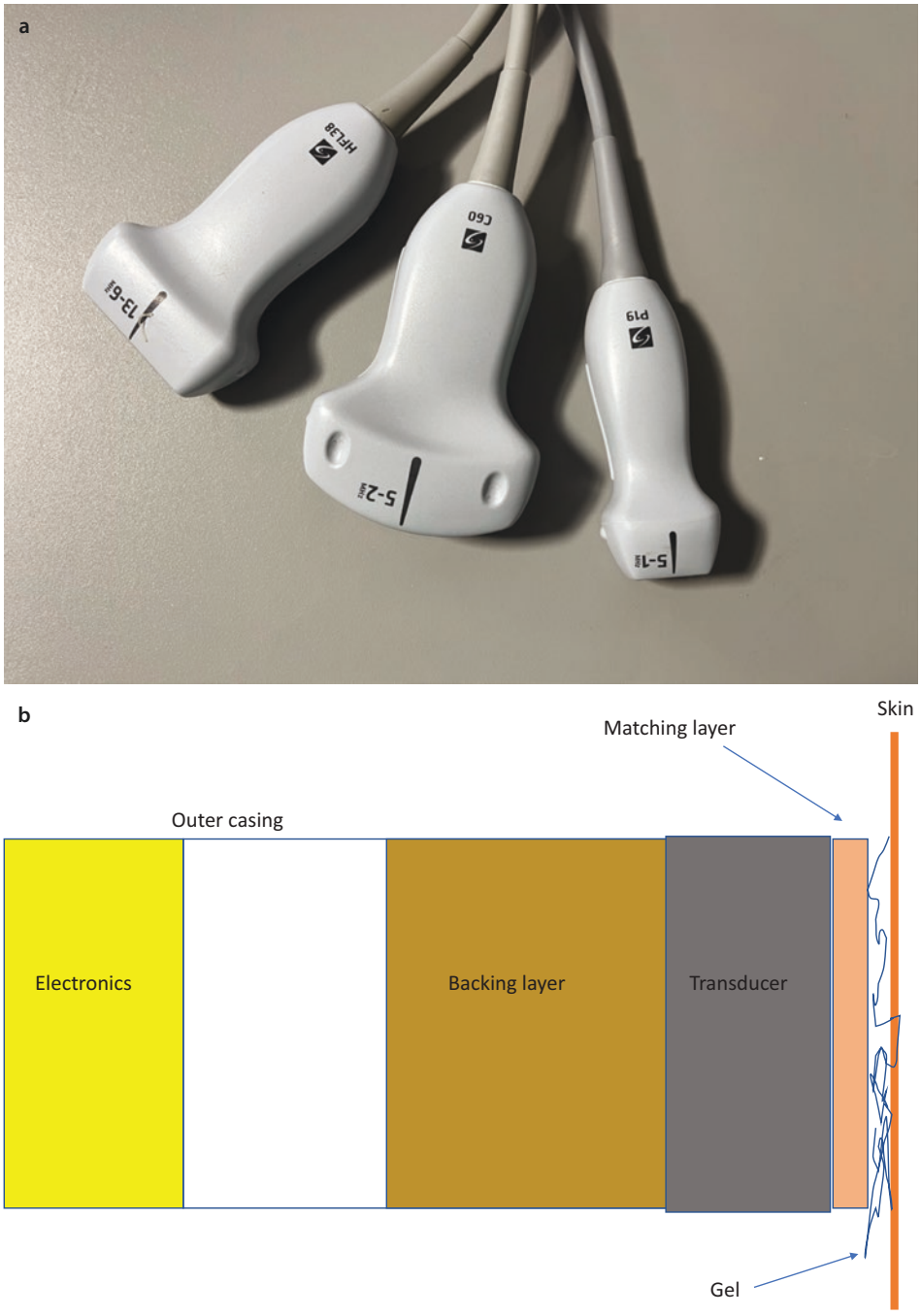

Fig. 2.3 **a** Left to right: Linear, Curvilinear, and phased array probes; **b** Elements of an ultrasound probe

2.4 Principles of Pulsed Echo

2

To generate an appropriate image, the transducer functions by emitting ultrasound in "pulses"—this allows it to transmit ultrasound beams for a certain period, and then listen for echoes. The standard pulse length is approximately three cycles, the proportion of time that the ultrasound transducer spends transmitting as a percentage of total time is called the duty factor.

The time taken for an echo to return to the transducer is a key variable for imaging. By dividing this time by 2, the depth of the reflector can be calculated:

$$D = (C \times t) / 2$$

The principle for this is demonstrated in Fig. 2.4.

Seeing that specific transducers have a maximum depth of penetration, it logically means that there is a maximum number of pulses that the machine can be set to deliver over time in order to facilitate imaging at that depth. The number of pulses per unit time is called the pulse repetition frequency, and the maximum PRF can be calculated as

$$\text{PRF} = c / 2 \times \text{Penetration depth}$$

Pulse repetition frequency is also important for determining the maximum number of images the machine can display every second—otherwise known as the frame rate.

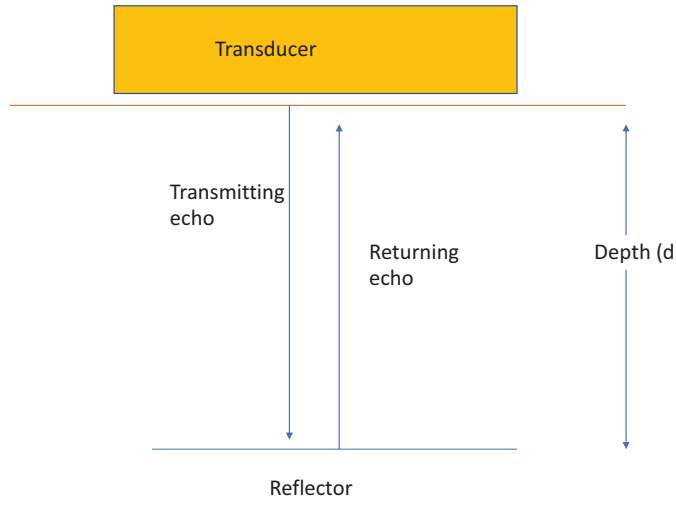

Fig. 2.4 Ultrasound "round trip" illustration

2.5 Transducers and Image Formation

The simplest form of ultrasound imaging involves a single transducer, emitting a series of pulses, receiving echoes, and displaying the echoes on a single graph showing their amplitude against the calculated depth. This is termed A mode (amplitude mode); it is rarely used now outside of ophthalmology.

If we convert those amplitudes into grayscale pixels, where a higher amplitude is displayed as bright and vice versa, we end up with a display showing light or dark colours against depth. This is termed "brightness" mode, or B mode.

Now, if we were able to take this transducer and have it pulse continuously over time, we can build an image of structures moving over this single thin beam of ultrasound. This is termed "motion" mode, or M mode.

All modern ultrasound machines use transducer elements arranged in "arrays." These fire sequentially, creating multiple M mode lines that are linked together by computer post processing to create the moving image that we see. This view is now termed B mode and is the standard diagnostic imaging technique that we use.

Some transducers allow for 3-dimensional (sometimes termed 4-dimensional) imaging by using a more complex transducer array known as a matrix array.

The ability for the ultrasound machine to discriminate between structures—the resolution—is an important quality, allowing for detailed accurate imaging. Resolution can be axial, lateral, or elevational. The two biggest factors affecting resolution are the transducer transmission frequency and the penetration depth; this must be borne in mind when performing diagnostic imaging (Fig. 2.5).

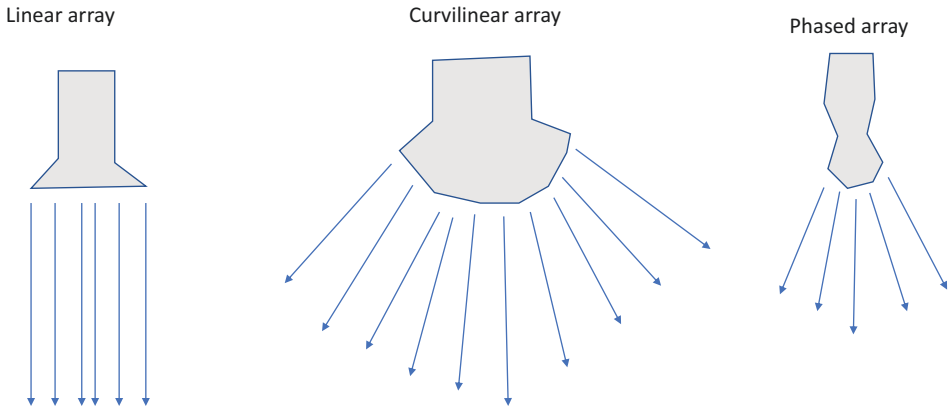

Fig. 2.5 Different probe arrays. Note that the different arrays result in the generation of slightly different images

2.6 Principles of Doppler Ultrasound

2

Sound transmitted from a moving object emits a different frequency depending on whether the object is moving towards or away from the receiver. (Think about how a car horn changes frequency as the car speeds past you). This is called the Doppler effect; and the change in frequency is called the Doppler shift (fD) (Figs. 2.6 and 2.7).

Fig. 2.6 Doppler principles

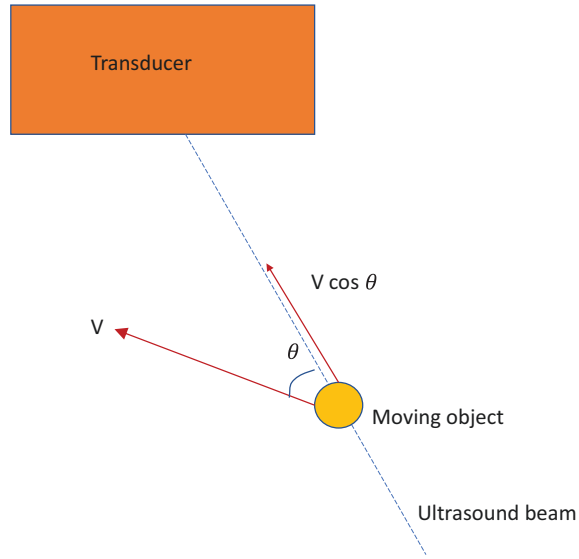

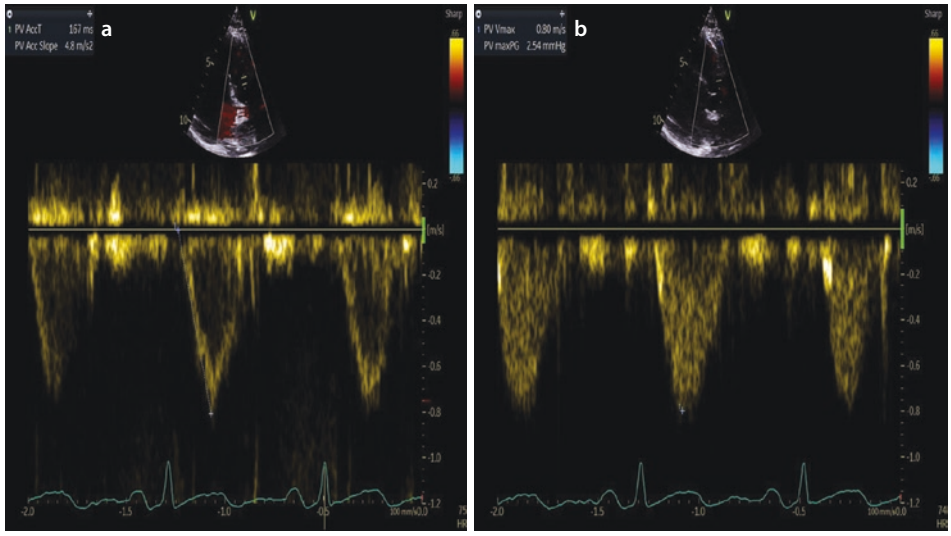

Fig. 2.7 **a** Pulse Wave Doppler—note the incompletely filled in envelope; **b** Continuous Wave Doppler

Doppler shift can be calculated using the equation

$$fD = \frac{2f^0 V \cos\theta}{C}$$

Where f^0 is the initial frequency, V is the velocity of the moving object, and θ is the Doppler angle (the angle between the direction of sound travel and the direction of movement of the object).

Doppler shift is useful in diagnostic ultrasound, as the movement of red blood cells or tissues result in a detectable Doppler shift. This can be detected and used to work out the direction and velocity of blood and/or tissue movement.

There are a number of types of Doppler ultrasound:

Continuous wave Doppler involves two separate transducers or elements—one dedicated to transmission, the other dedicated to receiving. This allows the detection of direction and a large range of velocities. However, it has the feature of range ambiguity—meaning it cannot resolve specific signals along its path.

Pulse wave Doppler involves the use of a single transducer or element which sends out pulses and receives them. This solves the above issue of range ambiguity and allows information to be obtained from a specific depth; however, the range of velocities it can detect is limited by aliasing—which will be discussed in the "artefacts" section.

Colour Doppler is a specialised form of pulse wave Doppler. It measures a range of pulsed Doppler signals in a sample box, and then converts the velocities and directions to colour signals. Direction is displayed on a scale of blue to red with classically blue used for flow away from the transducer and red being used for flow towards the transducer (Blue Away, Red Towards—BART). High velocity signals give more intense colour. A variant of this is power Doppler, which does not measure direction and looks purely at intensity. Another variant of this is tissue Doppler, which uses different filter techniques and focuses on movement of tissue rather than blood (Fig. 2.8).

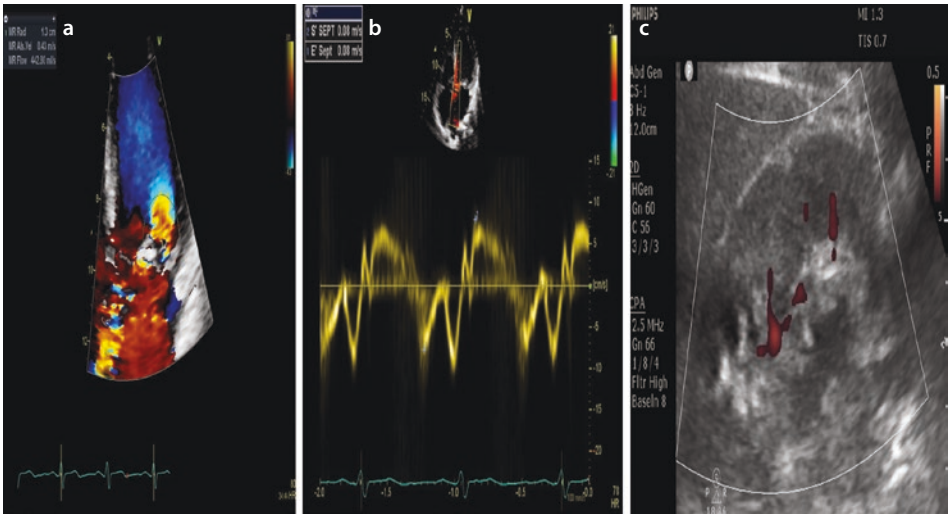

Fig. 2.8 Different types of Doppler. **a** Colour Doppler; **b** Tissue Doppler; **c** Power Doppler

2.7 Limitations of Diagnostic Ultrasound

The nature of ultrasound technology leads to some inherent limitations—and these are:

Resolution: axial and lateral resolution are affected by the frequency of the transmitted ultrasound beam, with a higher frequency resulting in better resolution. Harmonic imaging can be used to improve the lateral resolution and contrast.

Temporal resolution: This is the refresh speed of the ultrasound image; this is affected by the amount of "work" the machine has to do. So large imaging windows with multiple post processing effects (colour Doppler, for instance) will result in poor temporal resolution, while an M mode image results in high temporal resolution.

Imaging depth: Attenuation of ultrasound limits the depth of structures that can be imaged. Lower frequency ultrasound has a greater depth of penetration; this is traded off against worse resolution.

Bioeffects: Ultrasound is a form of energy. As it is transmitted through tissues, it is absorbed by the surrounding tissues—this manifests as thermal (heat) or mechanical effects (termed cavitation). The potential for heat generation is monitored by a parameter termed the Thermal Index (TI), while that for mechanical effects is monitored by the mechanical index (MI). As a result, ultrasound imaging should adhere to the principles of keeping the patient's exposure As Low As Reasonably Achievable (the ALARA principle).

The final limitation of ultrasound imaging is artefacts—which get their own section below.

2.8 Ultrasound Artefacts

Artefacts are display phenomena that do not represent the structures to be imaged properly. They occur because the ultrasound machine makes several idealised assumptions about the sound waves it transmits and receives:

- The ultrasound beam travels in a narrow straight line without deviation.
- Ultrasound is reflected back along the same narrow straight line on which it travelled.
- The speed of ultrasound is 1540 m/s regardless of medium.
- Attenuation is uniform regardless of medium.
- All echoes arise as a result of the most recent transmitted pulse.

In reality, ultrasound within tissues does not conform to these rules. There are three sets of these artefacts to deal with, generated during the use of 2D/B-mode imaging, colour, and 3D/4D imaging.

2.9 Artefacts Related to 2D Imaging

The main artefacts to consider here are:

- Reverberation artefacts (these include "comet tail" and "ring down" artefacts)
- Attenuation artefacts—Posterior acoustic enhancement, posterior acoustic shadowing, edge shadowing
- Side lobe artefacts
- Beam width/slice thickness artefacts
- Refraction artefacts—Ghosting and Mirror image artefacts

2.10 Artefacts Related to Doppler Imaging

There are two main artefacts to consider related to Doppler imaging:

- Aliasing
- Range ambiguity

Table 2.1 and Fig. 2.9 show examples of multiple artefacts.

Table 2.1 Examples of artefacts

Artifact	Explanation	Example
Posterior acoustic shadowing	A structure in the beam path causes significant attenuation	Gallstones (A)
Reverberation	A very strong reflector in the beam path causes multiple images to be generated	Pacing wire artefacts (B)
Posterior acoustic enhancement	The beam travels from an area of high attenuation to an area of low attenuation and back again, causing structures behind the low attenuation area to appear "bright"	A renal cyst (C)
Aliasing	Specific to pulse wave and colour Doppler, a structure moving faster than the set Nyquist limit of the transducer will appear to be moving "backwards"	Wrap around signal of high velocity pulmonic regurgitation (D)

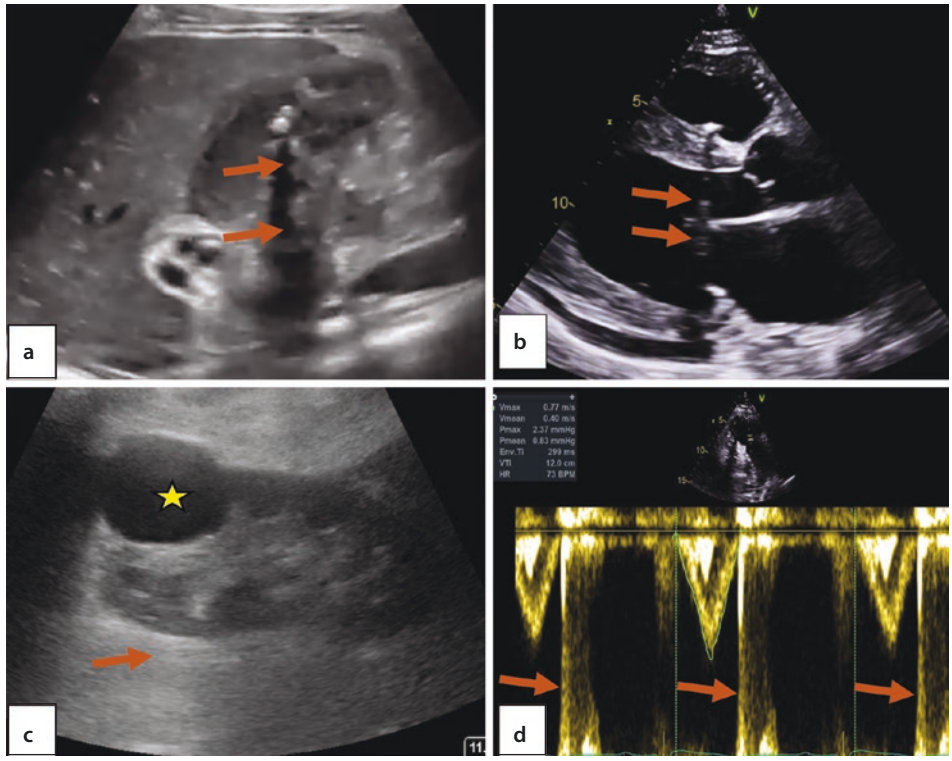

Fig. 2.9 Image artefacts. **a** Posterior acoustic shadowing (arrow); **b** Reverberation artefact from pacing wire (arrows); **c** Posterior acoustic enhancement (arrows) from renal cyst (star); **d** Aliasing from pulmonic regurgitation (arrows)

Take Home Messages

- Sound waves are longitudinal waves that can be defined by their propagation velocity, frequency, wavelength, and amplitude.
- Medical ultrasound involves the use of high frequency sound waves above the audible range of human hearing, in the range of 2–50 MHz.
- The main principles of diagnostic ultrasound involve transmitting ultrasound beams into tissues and detecting echoes; the intensity and depth of those echoes are then calculated and converted to a 2- or 3-dimensional image.
- Doppler imaging involves using the change in frequency of sound transmitted from an object in motion to detect both the direction and velocity of that object. It can be used to measure blood flow, and sometimes the movement of tissues.
- Medical ultrasound is limited by resolution, frame rate, depth of imaging, and its ability to generate artefacts.

Further Reading

Gill R. The physics and technology of diagnostic ultrasound: a practitioner's guide (second edition). High Frequency Publishing; 2020.

Heart

Contents

Chapter 3 **Detection and Interpretation of Left Ventricular Systolic Dysfunction by Basic Critical Care Echocardiography – 000**
Edouard Jullien and Antoine Vieillard-Baron

Chapter 4 **Evaluation for Right Ventricular Failure – 000**
Bruno Evrard, Marine Goudelin, and Philippe Vignon

Chapter 5 **Evaluation of Haemodynamically Important Pericardial Effusion – 000**
Michelle S. Chew, Jonathan Aron, and Meriam Åström Aneq

Chapter 6 **Evaluation for Severe Hypovolemia – 000**
Max Rosenthal and Paul Mayo

Chapter 7 **Evaluation for Acute, Severe Left-Sided Valvulopathy – 000**
Alexander Astell, Erica Clarke Whalen, and Robert T. Arntfield

Detection and Interpretation of Left Ventricular Systolic Dysfunction by Basic Critical Care Echocardiography

Edouard Jullien and Antoine Vieillard-Baron

Contents

3.1 Introduction – 22

3.2 Physiology and Anatomy of the Left Ventricle – 22

3.3 Main Parameters of LV Systolic Function – 23

3.4 Clinical Applications – 26

References – 27

© The Author(s), under exclusive license to Springer Nature Switzerland AG 2023
C. Robba et al. (eds.), *Basic Ultrasound Skills "Head to Toe" for General Intensivists*, Lessons from the ICU,
https://doi.org/10.1007/978-3-031-32462-8_3

Learning Objectives

- To understand how basically to evaluate LV systolic function, using simple parameters.
- To adequately interpret LV systolic dysfunction when present, according to LV size, LV filling pressure, and segmental wall motion.

3

3.1 Introduction

The use of critical care echocardiography (CCE) at the bedside is essential in managing critically ill patients. Recent guidelines have re-emphasized the basic skills that should be acquired by all intensivists [1]. The current chapter will focus on the detection and adequate interpretation of left ventricular (LV) systolic dysfunction by CCE according in part to the recent guidelines. Therefore, only transthoracic echocardiography (TTE) will be discussed, even though some studies suggest that a transesophageal approach could also be adequate for a quick and focused evaluation of LV systolic function [2]. The main clinical applications in critical care situations will be summarized. A quick reminder of LV anatomy and physiology, both of which are key to understanding how to use this technique accurately, will also be given.

3.2 Physiology and Anatomy of the Left Ventricle

The left ventricle is a semi-ellipse in shape, with relatively thick and rigid walls. Therefore, its diastolic elastance is high, in contrast to the right ventricle, which explains why the left ventricle is unable to dilate acutely [3, 4]. In fact, echocardiographic studies do not show any significant LV dilatation in the case of sepsis-related LV systolic dysfunction in patients with previously normal LV function [5]. Normal values of LV end-diastolic volume are widely distributed among the population, between 46 and 106 mL in females and 62 and 150 mL in males, depending on body surface area, which explains why LV size is better related to this area in square meters.

Within the myocardium, the striated muscle fibers are fan-shaped from the epicardium to the endocardium, leading to contraction of muscle fibers on different axes, a short and a long axis, associated with a twisting movement in the opposite direction from the tip to the base. Because the shortening is more pronounced in the short than in the long axis, eyeballing of LV systolic function, when performed, will be more efficient from a short-axis view. This also explains why techniques able to capture the LV twisting movement will be more sensitive in precisely evaluating LV systolic function, but this is beyond the scope of this chapter.

The left ventricle is vascularized by both the right and the left coronary artery. Seventeen walls are defined with their respective coronary perfusion [6]. Segmental wall motion abnormalities, when present, may thus indicate injury of one or more coronary arteries and may point toward a specific cause of LV systolic dysfunction, which is ischemia and acute coronary syndrome.

By definition, LV systolic function is dependent on LV afterload and so reflects the coupling between intrinsic LV contractility and vasomotor tone [7], as well as the ability of the left ventricle to maintain homeostasis (adapted or not to LV stroke volume/cardiac output). This means that LV systolic dysfunction can be related

either to an absolute alteration in LV performance or to an excessive LV afterload. Alternatively, a significant alteration in LV performance may be associated with preserved LV systolic function in the case of vasoplegia and unmasked after correction of blood pressure, as observed in septic shock [8]. LV systolic function should never be evaluated in isolation. Assessment of LV filling pressure by CCE allows intensivists to associate LV systolic dysfunction, if any, with a cardiogenic cause (LV filling pressure is then elevated) or with a "non-cardiogenic" cause, as septic cardiomyopathy (LV filling pressure is then normal or low).

To summarize these physiological considerations, accurate assessment of LV systolic function requires evaluation/measurement of LV size, LV filling pressure, and LV stroke volume, and detection of any wall motion abnormalities. Basic CCE should meet all these goals [1].

3.3 Main Parameters of LV Systolic Function

LV ejection fraction (EF), defined as the ratio between LV stroke volume and LV end-diastolic volume (EDV), is well accepted as a clinically useful measure of LV systolic function. For basic skills, only the single-plane Simpson method will be reported. It is based on an apical 4-chamber view, which allows physicians to measure EDV and end-systolic volume (ESV), with the machine calculating EF as EDV—ESV/EDV (Fig. 3.1). The normal value is considered to be between 52 and 72%. One frequent limitation in critically ill patients, especially when ventilated, is the non-optimal quality of the view, which limits adequate visualization of the endocardial borders, for which common risk factors are application of a PEEP $\geq$15 cmH_2O, weight gain >10%, and chest tube [9]. In the past, before technological improvement (machines, probes, software,..), TTE gave "adequate" images in only 36–70% of cases [10–12]. However, it has been reported that eyeballing may be accurate enough [13]. For such an approach, a parasternal short-axis view (Fig. 3.2) is more suitable because of the way the left ventricle shortens, as explained above.

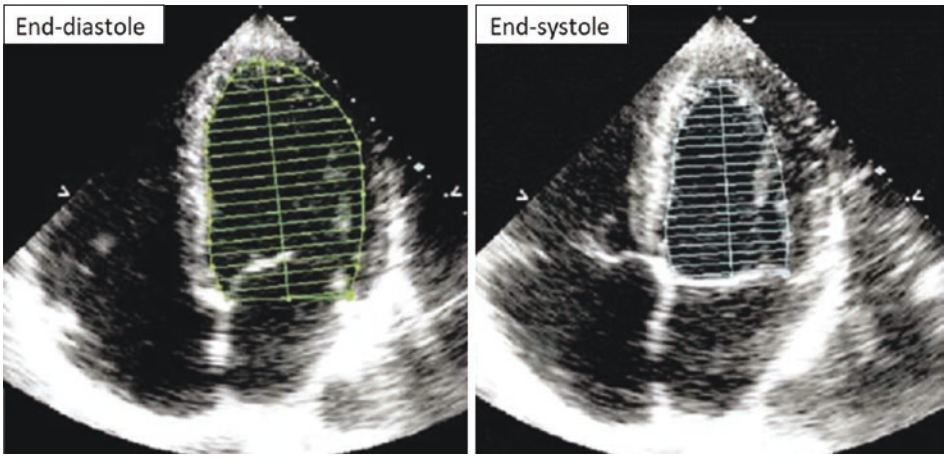

Fig. 3.1 LV ejection fraction on an apical 4-chamber view with the single-plane Simpson method

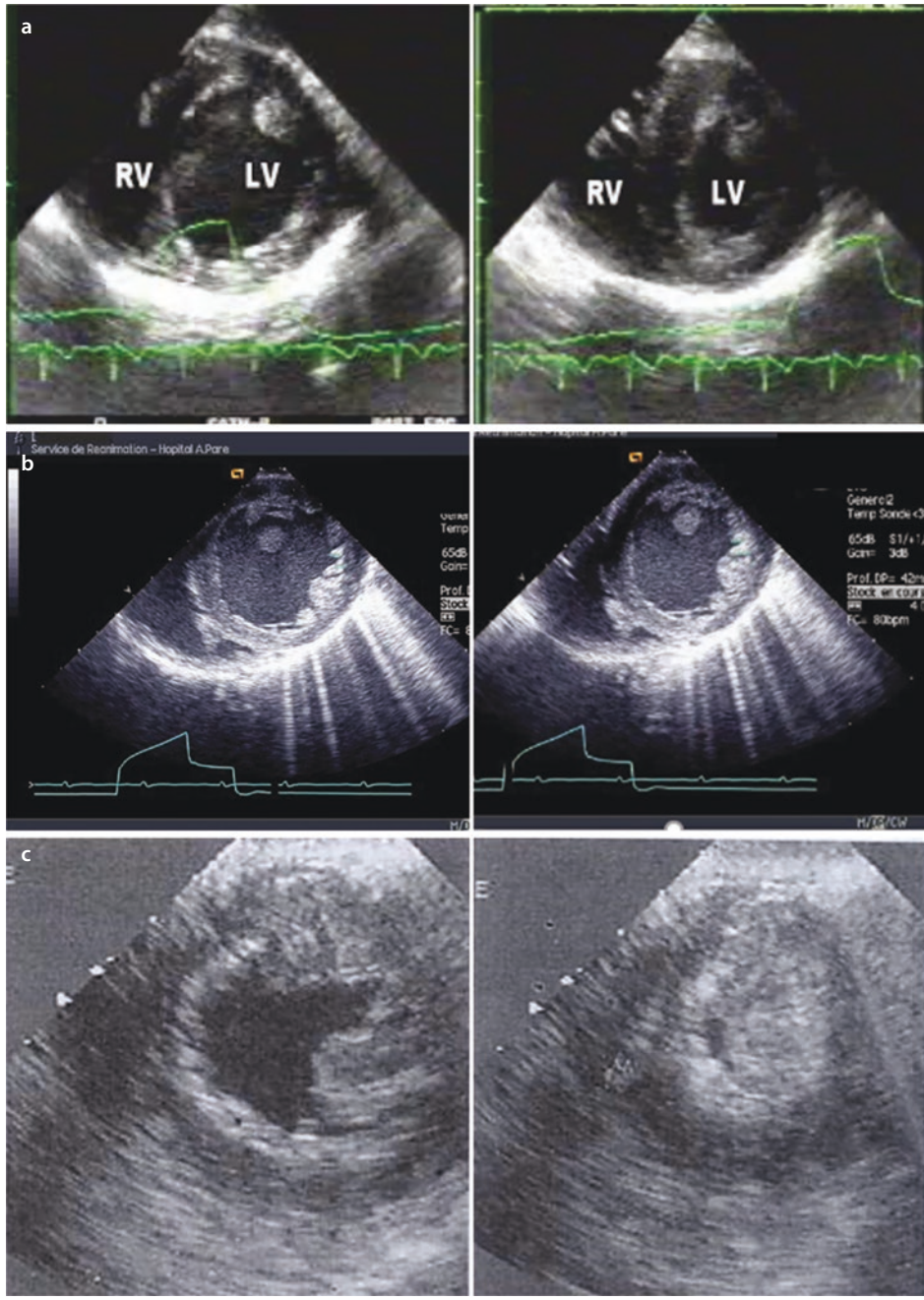

Fig. 3.2 Eyeballing of LV systolic function on a parasternal short-axis view. Left panel, end-diastole. Right panel, end-systole. Panel **a** Normal LV systolic function. Panel **b** Severely depressed LV systolic function. Panel **c** Supranormal LV systolic function (hyperkinetic left ventricle)

In critically ill patients, obtaining a precise value of LVEF is very rarely pertinent to patient management. More importantly, LV systolic function has to be classified in different categories, which could be severely impaired, moderately impaired, normal, or supranormal (i.e., hyperkinetic left ventricle) [8]. This approach may be much more efficient in discussing the appropriate strategy to improve hemodynamics (dobutamine, norepinephrine infusion, fluid expansion), even though no evidence base is currently available. In the case of a hyperkinetic left ventricle, a decreased EDV usually means hypovolemia, while a normal EDV means vasoplegia.

Evaluation of the mitral annulus during systole also allows physicians to evaluate LV systolic function, even though it was not strictly speaking considered as a basic skill in the recent guidelines [1]. An apical 4-chamber view is also required. Two approaches are available, either evaluation of the distance covered by the annulus during systole, which is called the mitral annulus plane systolic excursion (MAPSE), or the maximal velocity at which this movement occurs (S' wave velocity). While the former requires combination of 2D imaging with the time-motion study mode with an abnormal value <11 mm, the latter requires the combination of tissue Doppler imaging, with an abnormal value <8 cm/s (Fig. 3.3). It has been suggested that both parameters could be less load-dependent than the LVEF and so could be more reliable in assessing the intrinsic performance of the left ventricle.

As explained above, an adequate evaluation of LV systolic (dys)function requires evaluation of (1) whether the left ventricle is dilated (which means a decompensation of a chronic state) or not (which means that the injury is acute in a previously normal left ventricle), (2) whether LV filling pressure is elevated (meaning that in the case of shock this is a typical cardiogenic shock) or not (meaning that LV dysfunction is secondary to other mechanisms as in septic shock), and (3) whether there is any wall motion abnormality (meaning that LV dysfunction is probably due in part to cardiac ischemia). For LV filling pressure evaluation, basic skills only require the ability to detect a restrictive pattern of the mitral inflow, looking at the ratio between the early diastolic wave (E wave) and the end-diastolic wave (A wave) (Fig. 3.4).

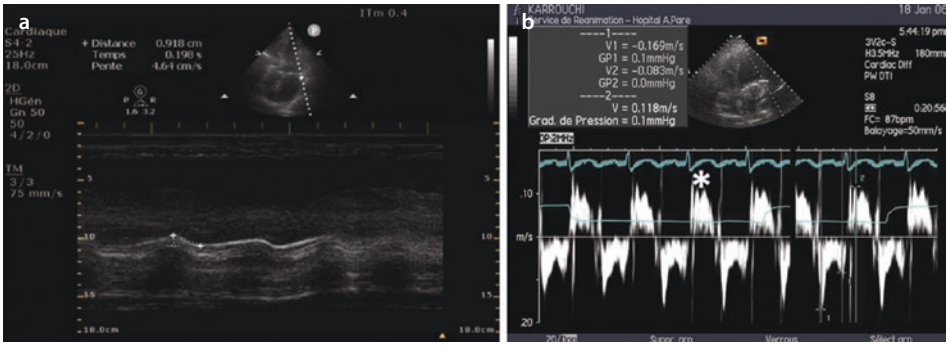

Fig. 3.3 Apical 4-chamber view in a patient with depressed LV systolic function. Panel **a** Mitral annular plane systolic excursion (MAPSE) using time-motion study. Panel **b** Maximal velocity (S' wave, *) using tissue Doppler imaging

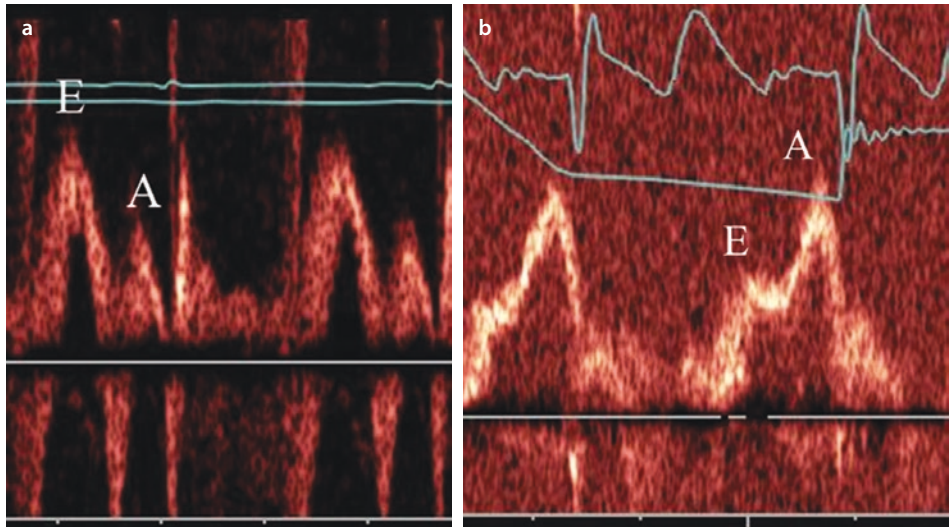

Fig. 3.4 Mitral inflow using pulsed wave Doppler on an apical 4-chamber view. Panel **a** Elevated LV filling pressure. Panel **b** Non-elevated LV filling pressure

3.4 Clinical Applications

Table 3.1 summarizes and simplifies the echo patterns of the different situations that may be encountered by physicians in the ICU. This has obviously to be interpreted in light of the clinical context. Basic skills in CCE should be adapted so as to clearly differentiate these different patterns, even though in the case of doubt, physicians should ask a more experienced practitioner for advice. In all of these potential situations, one more word has to be added regarding the evaluation of LV stroke volume. Basic skills for the heart require that physicians accurately evaluate the aortic velocity time integral (VTI) as an estimation of LV stroke volume [1]. For this, the pulsed wave sample volume should be placed in the LV outflow tract just before the aortic valve in an apical 5-chamber view. Like all static measurements, this must be done at end-expiration. In the case of LV systolic dysfunction, the aortic VTI could be used to select patients who could benefit from implantation of a VA ECMO in the case of severe cardiogenic shock [14], to identify in septic shock those patients with a potentially significant septic cardiomyopathy who could benefit from inotropic drugs [15], and to monitor the natural or assisted change in LV stroke volume.

Table 3.1 Main CCE patterns of different situations potentially involving LV systolic dysfunction. VTI is not reported as it could be widely distributed from a normal value to a very low value according to the severity of the injury and LV size. Notice, however, that septic cardiomyopathy has been reported to be optimally defined by an LVEF below 40% and a VTI below 14 cm [15]

	LV systolic dysfunction	LV size	LV filling pressure
Myocarditis	Global	Normal	Increased
Stress cardiomyopathy	Apical dyskinesia	Apical ballooning	Increased
Septic cardiomyopathy	Global	Normal	Normal or low
Decompensated chronic cardiomyopathy	Global	Increased	Increased
Acute myocardial ischemia	Segmental wall motion abnormality	Normal	Normal or increased

Summary

Basic skills for evaluating LV systolic dysfunction should be physiologically based and as simple as possible. While still open to discussion, the appropriate route is transthoracic. By evaluating LV systolic function, mainly by eyeballing LV size and LV filling pressure, and also by searching for wall-motion abnormalities, intensivists have all the clues needed to determine and understand the exact LV profile according to the clinical context. Addition of the aortic VTI would enable evaluation of the severity of LV systolic dysfunction and its adaptation to load conditions and monitoring of how it changes, under natural conditions or with mechanical or drug support.

Take-Home Messages

- Evaluation of LV systolic function requires measurement or eyeballing of LV ejection fraction.
- Aortic VTI should be also measured.
- Aortic 4- and 5-chamber views, as well as a parasternal short-axis view are mandatory.
- Adequate interpretation of LV systolic dysfunction requires evaluation of LV size, LV filling pressure, and segmental wall motion.

References

1. Robba C, Wong A, Poole D, Al Tayar A, Arntfield RT, Chew MS, Corradi F, Douflé G, Goffi A, Lamperti M, Mayo P, Messina A, Mongodi S, Narasimhan M, Puppo C, Sarwal A, Slama M, Taccone FS, Vignon P, Vieillard-Baron A. European Society of Intensive Care Medicine task force for critical care ultrasonography*. Basic ultrasound head-to-toe skills for intensivists in the gen-

eral and neuro intensive care unit population: consensus and expert recommendations of the European Society of Intensive Care Medicine. Intensive Care Med. 2021;47(12):1347–67. https://doi.org/10.1007/s00134-021-06486-z. Epub 2021 Oct 5.

2. Benjamin E, Griffin K, Leibowitz AB, Manasia A, Oropello JM, Geffroy V, DelGiudice R, Hufanda J, Rosen S, Goldman M. Goal-directed transesophageal echocardiography performed by intensivists to assess left ventricular function: comparison with pulmonary artery catheterization. J Cardiothorac Vasc Anesth. 1998;12(1):10–5. https://doi.org/10.1016/s1053-0770(98)90048-9.
3. Kumar A, Anel R, Bunnell E, Habet K, Zanotti S, Marshall S, Neumann A, Ali A, Cheang M, Kavinsky C, Parrillo JE. Pulmonary artery occlusion pressure and central venous pressure fail to predict ventricular filling volume, cardiac performance, or the response to volume infusion in normal subjects. Crit Care Med. 2004;32(3):691–9. https://doi.org/10.1097/01.ccm.0000114996.68110.c9.
4. Braunwald E, Heart disease. A textbook of cardiovascular medicine. 4th ed. W.B. Saunders Company; 1992.
5. Vieillard-Baron A. Septic cardiomyopathy. Ann Intensive Care. 2011;1(1):6. https://doi.org/10.1186/2110-5820-1-6.
6. Partridge JB, Anderson RH. Left ventricular anatomy: its nomenclature, segmentation, and planes of imaging. Clin Anat. 2009;22(1):77–84. https://doi.org/10.1002/ca.20646.
7. Robotham JL, Takata M, Berman M, Harasawa Y. Ejection fraction revisited. Anesthesiology. 1991;74(1):172–83. https://doi.org/10.1097/00000542-199101000-00026.
8. Repessé X, Charron C, Vieillard-Baron A. Evaluation of left ventricular systolic function revisited in septic shock. Crit Care. 2013;17(4):164. https://doi.org/10.1186/cc12755.
9. Cook CH, Praba AC, Beery PR, Martin LC. Transthoracic echocardiography is not cost-effective in critically ill surgical patients. J Trauma. 2002;52(2):280–4. https://doi.org/10.1097/00005373-200202000-00013.
10. Vignon P, Mentec H, Terré S, Gastinne H, Guéret P, Lemaire F. Diagnostic accuracy and therapeutic impact of transthoracic and transesophageal echocardiography in mechanically ventilated patients in the ICU. Chest. 1994;106(6):1829–34. https://doi.org/10.1378/chest.106.6.1829.
11. Heidenreich PA, Stainback RF, Redberg RF, Schiller NB, Cohen NH, Foster E. Transesophageal echocardiography predicts mortality in critically ill patients with unexplained hypotension. J Am Coll Cardiol. 1995;26(1):152–8. https://doi.org/10.1016/0735-1097(95)00129-n.
12. Slama MA, Novara A, Van de Putte P, Diebold B, Safavian A, Safar M, Ossart M, Fagon JY. Diagnostic and therapeutic implications of transesophageal echocardiography in medical ICU patients with unexplained shock, hypoxemia, or suspected endocarditis. Intensive Care Med. 1996;22(9):916–22. https://doi.org/10.1007/BF02044116.
13. Schiller NB, Foster E. Analysis of left ventricular systolic function. Heart. 1996;75(6 Suppl 2):17–26. https://doi.org/10.1136/hrt.75.6_suppl_2.17.
14. Donker D, Meuwese C, Braithwaite S, Broomé M, van der Heijden J, Hermens J, et al. Echocardiography in extracorporeal life support: a key player in procedural guidance, tailoring and monitoring. Perfusion. 2018;33:31–41. https://doi.org/10.1177/0267659118766438.
15. Geri G, Vignon P, Aubry A, Fedou AL, Charron C, Silva S, Repessé X, Vieillard-Baron A. Cardiovascular clusters in septic shock combining clinical and echocardiographic parameters: a post hoc analysis. Intensive Care Med. 2019;45(5):657–67. https://doi.org/10.1007/s00134-019-05596-z. Epub 2019 Mar 19.

Evaluation for Right Ventricular Failure

Bruno Evrard, Marine Goudelin and Philippe Vignon

Contents

4.1 Introduction – 30

4.2 From Physiology to Right Ventricular Failure – 31

4.3 Two-Dimensional Assessment of the Normal Right Ventricle – 32

4.4 Assessment of Right Ventricular Failure – 36

4.4.1 Right Ventricular Size – 36

4.4.2 Assessment of the Pattern of Contraction of the Interventricular Septum – 37

4.4.3 Assessment of the Inferior Vena Cava – 38

4.4.4 Assessment of Right Ventricular Free Wall Thickness – 39

4.5 Proposed Diagnostic Algorithm – 39

4.6 Conclusion – 42

References – 43

© The Author(s), under exclusive license to Springer Nature Switzerland AG 2023
C. Robba et al. (eds.), *Basic Ultrasound Skills "Head to Toe" for General Intensivists*, Lessons from the ICU,
https://doi.org/10.1007/978-3-031-32462-8_4

Learning Objectives

- Propose a definition of right ventricular failure.
- Describe the normal pattern of ejection of the thin-walled compliant right ventricle.
- Illustrate the paradoxical septal motion (in systole) and its significance in the presence of an enlarged right ventricle.
- List the main causes of right ventricular failure and describe their respective mechanisms.
- Describe how to identify a right ventricular dilatation using basic critical care echocardiography and discuss its pathophysiology.
- Illustrate the confounding factors which may lead to an erroneous assessment of right ventricular cavity size.
- Describe how to identify a congested inferior vena cava using basic critical care echocardiography and discuss its pathophysiology.
- Describe how to identify a hypertrophy of right ventricular free wall using basic critical care echocardiography and discuss its pathophysiology.
- Illustrate the two dimensional measurement of right ventricular cavity and of end-expiratory diameter of the inferior vena cava.
- Describe the typical findings associated with the main etiologies of right ventricular failure when assessing the patient using basic critical care echocardiography.

4.1 Introduction

Right ventricular failure (RVF) has currently no unanimously accepted definition. RVF can be defined as a *complex clinical syndrome characterized by insufficient delivery of blood from the RV in the setting of elevated systemic venous pressure* [1]. A recent statement defined acute RVF as a *rapidly progressive syndrome with systemic congestion resulting from impaired RV filling and/or reduced RV flow output* [2].

RVF develops in acute diseases which alter unfavorably RV loading conditions and/or decrease RV contractility. Accordingly, RVF is highly prevalent in critically ill patients. In addition, the frequent use of positive-pressure ventilation in the intensive care unit (ICU) may participate in the detrimental changes of RV loading conditions due to heart-lung interactions [3]. Accurate diagnosis is crucial, since RVF appears prognostic both in chronic and acute conditions [4–6].

Echocardiography is the first-line imaging modality used in ICU patients to assess RV morphology and function at the bedside, and to depict the potential consequences of RVF on left ventricular (LV) performance through ventricular interdependence. Qualitative assessment of (i) RV cavity dilatation and free wall thickness; (ii) pattern of contraction of the interventricular septum during the cardiac cycle; and (iii) size and respirophasic variations of the inferior vena cava (IVC) to detect systemic venous congestion is currently recommended to diagnose RVF using basic critical care echocardiography [7].

4.2 From Physiology to Right Ventricular Failure

The main physiological role of the RV is to facilitate venous return in maintaining low right atrial pressure (back pressure), thus participating in the normal regulation of cardiac output and systemic blood flow to meet organ needs. Unlike the LV, the RV is a volume pump with a thin free wall and high compliance. RV ejection mainly results from a bellows effect due to the traction of its free wall toward the interventricular septum by myocardial fibers shared with the LV, the shortening of longitudinal myocardial fibers pulling the tricuspid plane toward the apex and, to a lesser extent, from the thickening of RV free wall (◘ Fig. 4.1). Importantly, the two cardiac ventricles are functionally interdependent since they are located within the stiff pericardium, they share a common myocardial wall (interventricular septum), and they are intertwined by common myocardial fibers [2]. Physiologically, the RV ejects its stroke volume in a low-resistance pulmonary circulation. Accordingly, both the RV size and function are highly sensitive to its afterload. Any increase in pulmonary vascular resistance, especially when marked and abrupt, may rapidly have adverse consequences on RV function, and in turn on LV ejection due to ventricular interaction [8].

Increased RV afterload (pulmonary hypertension) constitutes the leading mechanism of RVF in ICU patients. To maintain its stroke volume, the RV exhibits a sequential functional and morphological adaption [9]. In the presence of an acute pulmonary hypertension, the initial homeometric adaptation (Anrep's effect) of the RV, which consists in increasing its contractility to maintain a normal ventriculo-arterial coupling, is frequently limited in critically ill patients [10]. This explains why ICU patients are often clinically assessed at the time of the subsequent heterometric adaptation (Frank–Starling's law) which uses the ability of the RV to acutely dilate to maintain its stroke volume despite elevated pulmonary vascular resistance [2]. This acute dilatation stretches the tricuspid ring and facilitates systolic regurgitation within the right atrium. The adaptive tricuspid regurgitation reduces RV pressure overload on the one hand, but induces a systemic venous and hepatic congestion, and reduces forward flow on the other. In addition, diastolic ventricular interaction will further reduce LV filling and cardiac output: RV acutely dilates at the expense of LV cavity since the sum of end-diastolic ventricular volumes remains constant within the stiff pericardium. Since RV functional adaptation and increased loading condition is not linear, a substantial RV dilatation may be encountered, whereas RV stroke volume is still preserved without systemic venous congestion [10]. This is presumably why there is no relationship between the RV systolic function (e.g., value of the Tricuspid Annulus Plane Systolic Excursion) and RV size and central venous pressure (marker of venous congestion) [11]. Accordingly, the assessment of RV systolic function is not part of the competence for basic critical care echocardiography [7]. Ultimately, when RV adaptation becomes insufficient as a result of a too abrupt increase in pulmonary artery pressure or long-standing pulmonary hypertension, RV-arterial coupling deteriorates. Clinically, a low cardiac output and systemic hypotension, elevated RV filling pressure and systemic venous congestion are then observed [2].

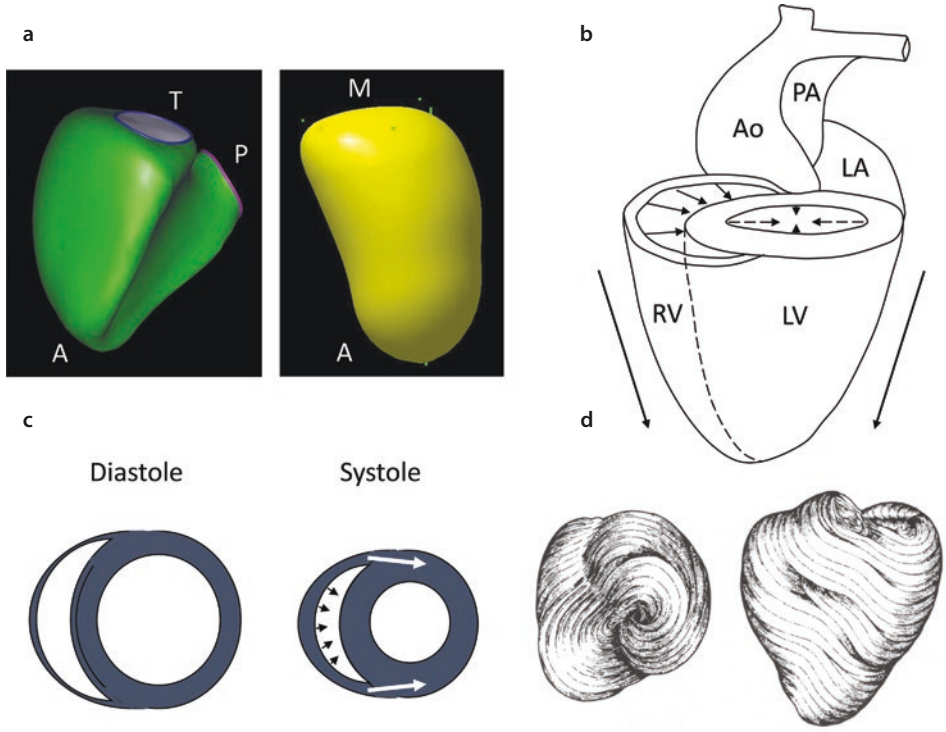

Fig. 4.1 Normal right ventricle. Panel **a** Anatomical shape of normal right (green model) and left (yellow model) ventricles depicted by three-dimensional echocardiography. Unlike the bullet-shaped left ventricle, the right ventricle has a complex anatomy which precludes the use of simple geometric assumptions to measure its volume with two-dimensional echocardiography. Panel **b** Schematic representation of the two ventricles with their respective pattern of contraction. Unlike the left ventricle, which mainly shortens along its short axis to generate a concentric contraction toward the centroid of its cavity (dashed arrows), the thin-walled right ventricle exhibits a bellows-like contraction pattern (short solid arrows) and a shortening along its long axis (contraction of longitudinal fibers, long solid arrows). Panel **c** Schematic representation of the short-axis view of the heart depicting the bellows-like inward motion of the right ventricular free wall during systole. The main component is the traction of the right ventricular free wall toward the interventricular septum secondary to the shortening of common myocardial fibers intertwining the two ventricles during left ventricular contraction (long white arrows). In contrast to the left ventricle, the thickening of the normally thin free wall has a small contribution to right ventricular stroke volume (short black arrows). Panel **d** Schematic representation of common myocardial fibers (spiral musculature) intertwining the two ventricles of a normal heart after resection of the pericardium. In addition to the ventricular septum, these common myocardial fibers contribute to the interaction between the two ventricles during the cardiac and respiratory cycle. (From Streeter, 1952). **Abbreviations**: *T* tricuspid ring; *P* pulmonary valve; *A* apex of the ventricles; *M* mitral ring; *LV* left ventricle; *RV* right ventricle; *Ao* ascending aorta; *PA* pulmonary artery; *LA* left atrium

4.3 Two-Dimensional Assessment of the Normal Right Ventricle

Although of similar volume, the RV cavity size appears smaller than that of the LV in the different two-dimensional echocardiography planes since it is wrapped around the LV ejection tract as a bellows (Fig. 4.1). Two-dimensional echocardiography assessment of RV size and function relies on the five transthoracic views which must be mastered at a basic level [12].

In the parasternal long-axis view, the RV outflow tract is located above the interventricular septum and aortic root, and appears much smaller than the LV cavity (Fig. 4.2). This view allows the measurement of RV and LV end-diastolic diameter to quantitatively confirm the RV dilatation, and the evaluation of RV free wall thickness. In the parasternal short-axis view, the RV cavity has a crescentic shape and is located anteriorly to the LV. At the LV mid-papillary level, the lateral, inferior, and anterior RV free wall are visualized (Fig. 4.2). Importantly, this view allows best analyzing the interventricular septal motion during the cardiac cycle. The apical four-chamber view is essential for the assessment of RV size and function [13]. In this view, the RV has a triangular shape and myocardial trabeculations are visible in the apical region. Both the RV lateral free wall and interventricular septum are visualized. RV end-diastolic area should visually appear no more than two-thirds of LV end-diastolic area [13]. The LV normally constitutes the entire cardiac apex. Importantly, the relative RV size compared to that of the LV may significantly vary from normal, larger, or smaller dimension according to the imaging plane [13]. Accordingly, particular attention should be directed toward obtaining a strict four-chamber view (i.e., LV outflow tract should not be visualized), with the transducer properly positioned over the cardiac apex (i.e., no foreshortening) and the LV being positioned in the center of the image. To avoid an overestimation of RV size, the operator should avoid any foreshortening and obtain the largest long-axis of the ventricles (Fig. 4.3). To avoid underestimating RV size, the operator should slightly rotate the transducer to obtain the imaging plane which yields

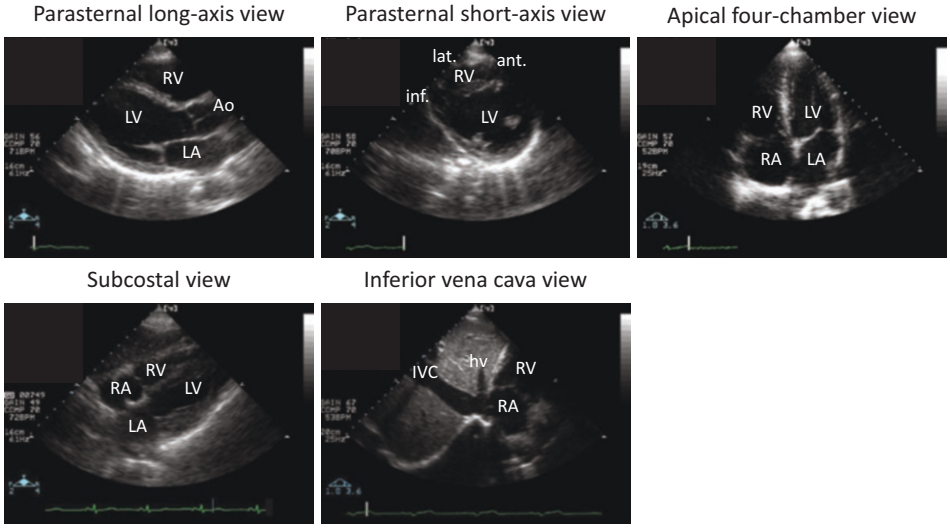

Fig. 4.2 Transthoracic two-dimensional views of a normal heart which must be mastered to perform basic critical care echocardiography. The right ventricle can be assessed in all views (see text for details). The parasternal long axis and the apical four-chamber views are best suited to evaluate right ventricular size. The parasternal short-axis view allows the assessment of the interventricular septal motion pattern. The subcostal long-axis view of the heart is used to evaluate the thickness of right ventricular free wall. The subcostal view centered on the inferior vena cava provides information on both its size and respiratory variations in spontaneously breathing patients. **Abbreviations**: *LV* left ventricle; *RV* right ventricle; *LA* left atrium; *RA* right atrium; *IVC* inferior vena cava; *inf.* Inferior free wall; *lat.* Lateral free wall; *ant.* Anterior free wall; *hv* hepatic veins

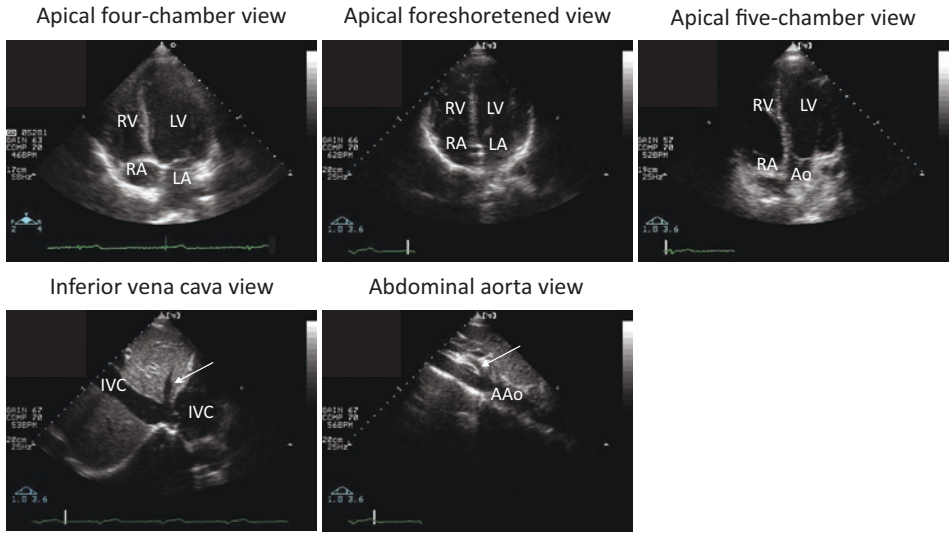

Fig. 4.3 Illustration of the main pitfalls to avoid in acquiring two-dimensional echocardiography views to assess the right ventricle in the apical four-chamber view (upper panels) and the inferior vena cava in the modified subcostal view (lower panels) (see text for details). Inaccurate estimation of the right ventricular cavity size when compared to that of the left ventricle may be the result of a foreshortened apical four-chamber view (upper mid panel) or a five-chamber view (upper right panel). The long-axis of the inferior vena cava and its junction with the hepatic vein (lower left panel, arrow) must be distinguished from the longitudinal view of the abdominal aorta with the take-off of collateral arteries (lower right panel, arrow). **Abbreviations**: *LV* left ventricle; *RV* right ventricle; *LA* left atrium; *RA* right atrium; *Ao* aorta; *IVC* inferior vena cava; *AAo* abdominal aorta

the largest RV cavity area [13]. The tricuspid valve plane (anterior and septal leaflets) appears slightly anterior to that of the mitral valve, and both the right atrium and interatrial septum can also be examined. The subcostal long-axis view allows best assessing RV free wall thickness (Fig. 4.2), which normally is <5 mm [14]. Epicardial fat should be distinguished from the myocardium to avoid erroneous interpretation of RV free wall thickness. This view also allows the examination of the interatrial septum. In contrast, the subcostal long-axis view of the heart does not allow to accurately assess the RV cavity size due to foreshortening and oblique angle imaging plane [13].

The assessment of IVC is part of RV evaluation since it connected to the right atrium and it indirectly reflects RV preload and systemic venous congestion in the presence of RVF. From the subcostal long-axis view of the heart, a 90° anticlockwise rotation of the probe allows imaging the IVC in its long-axis view (Fig. 4.2). Slight adjustment of the probe position (rotation and angulation) allows obtaining the adequate imaging plane which depicts the vessel in its true long axis (with IVC walls strictly parallel), the junction between the IVC and the right atrium, and the hepatic veins which lie approximately 0.5–3 cm proximal to the ostium of the right atrium [13]. In the absence of confounding factors (e.g., direct IVC compression by a liver disease), the size of the IVC results from the transmural pressure of the vessel (i.e., intravascular pressure minus abdominal pressure) and is influenced by cardiac preload. In spontaneously breathing patients, the IVC physiologically tends to collapse

during inspiration, with a reduction of its diameter exceeding 50%. Both the (end-expiration) IVC size and the amplitude of its reduction during inspiration correlate with right atrial pressure [13]. In further decreasing intrathoracic pressure, the sniff test increases IVC collapsibility. Importantly, increased inspiratory efforts in a patient who is dyspneic at rest tend to increase IVC collapse at inspiration, when compared to quiet respiration. The operator should ensure that respirophasic changes in IVC diameter are not the result of a cyclic translation of the IVC into another plane during respiration [13]. These respiratory variations are not observed in mechanically ventilated patients, since the IVC tends to dilate during insufflation due to a cyclic increase in its transmural pressure. Nevertheless, respiratory variations of the IVC size during positive-pressure ventilation are too small to be visually detected with two-dimensional echocardiography. A traditional pitfall is to erroneously image the abdominal aorta instead of the IVC, which anatomically runs parallel to it. The differential diagnosis is based on the pulsatility of the vessel, the frequent (calcified) atherosclerotic lesions, and the visualization of the take-off of abdominal arteries (Fig. 4.3). The measurement of the maximal IVC diameter is performed at end-expiration, just proximal to the junction with the hepatic veins, and strictly perpendicular to the vessel long axis/walls (Fig. 4.4). The measurement of IVC diameter has low inter-observer variation [4]. Although it is challenging to edict normal

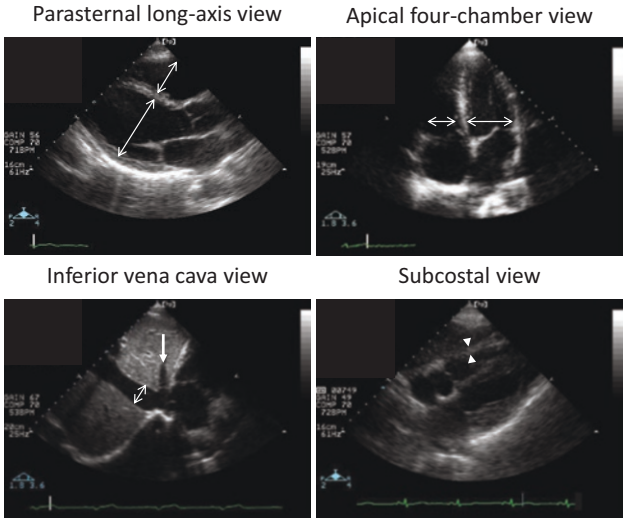

Fig. 4.4 Illustrative examples of two-dimensional measurements relevant for the assessment of patients with suspected right ventricular failure (see text for details). The end-diastolic (maximal) diameter of the right and left ventricular cavity is best measured in the parasternal long-axis view (upper left panel, double-headed arrows). Alternatively, this measurement can be performed in the apical four-chamber view at the base of the ventricles, above the atrio-ventricular valve planes (upper right panel, double-headed arrows). The end-expiration diameter of the inferior vena cava (maximal diameter in spontaneously breathing patients) is measured in the subcostal long-axis view of the vessel, just proximal to the junction of the hepatic veins (lower left panel, double-headed arrow) which lies approximately 0.5–3 cm proximal to the right atrium (lower left panel, thick arrow). The thickness of right ventricular free wall is best evaluated (rather than measured at a basic critical care echocardiography level) in the long-axis subcostal view of the heart (lower right panel, arrowheads)

values, the proximal IVC diameter typically ranges between 12 and 23 mm in normal adults [15]. Overall, the assessment of both the size and respiratory variations of the IVC provides information on the venous return and potential venous systemic congestion.

4.4 Assessment of Right Ventricular Failure

4.4.1 Right Ventricular Size

Unlike the LV, the thin-walled and compliant RV can acutely dilate in response to a pressure and/or volume overload, or to a decreased contractility [16]. RV cavity size is best assessed in the apical four-chamber view. When the RV dilatation is severe, its size visually exceeds that of LV cavity. The dilated RV has a round shaped apex. When the dilatation is severe, the RV apex constitutes the cardiac apical region instead of the LV. With increasing RV dilatation, its apical trabeculations become more prominent and the moderator band is fully visualized (Fig. 4.5). In our experience, recently trained residents for basic critical care echocardiography without previous experience in ultrasound satisfactorily identify RV dilatation in the apical four-chamber view when compared to the expert used as reference (Kappa: 0.71 [0.46–0.95] and 0.76 [0.64–3.89]) in ICU patients [17, 18]. When present, RV dilatation must be visually confirmed in the parasternal long- and short-axis views (Fig. 4.5).

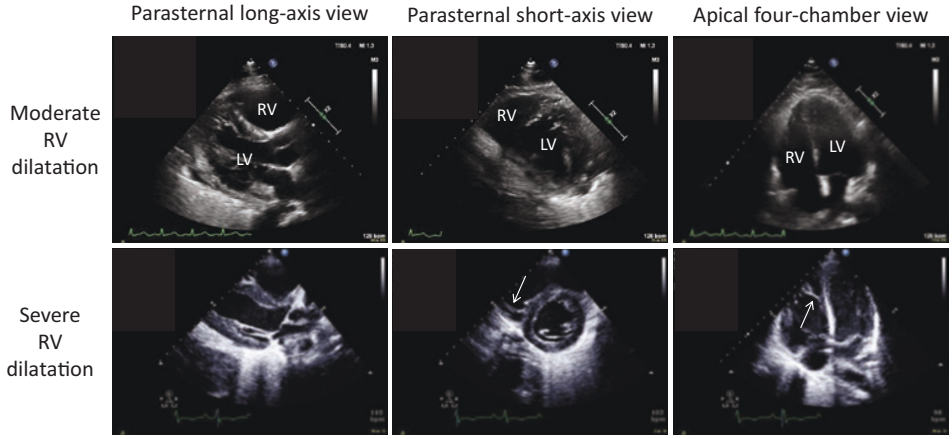

Fig. 4.5 Example of a moderate and severe dilatation of the right ventricle depicted by end-diastolic still-frames obtained in the parasternal long- and short-axis views and in the apical four-chamber view. Right ventricular dilatation must be visually confirmed in all these views when using the left ventricular cavity as a reference (see text for details). Note that the different image depth used in the two patients may lead to an erroneous semi-quantitative assessment of right ventricular enlargement if its cavity size is not compared to that of the left ventricle. In both the parasternal short-axis view and apical four-chamber view, the moderator band is fully depicted in the presence of a severely enlarged right ventricle (lower mid and right panel, arrows). **Abbreviations**: *RV* right ventricle; *LV* left ventricle

In addition, the visual diagnosis of RV dilatation should be confirmed by adequate measurements of its cavity, especially when moderate. Unlike the LV, the complex RV anatomy precludes the use of simple geometrical assumptions to accurately measure the volume of its cavity. Accordingly, internal end-diastolic RV diameter (basic level) or surface (advanced level) is measured to assess the size of its cavity, when using LV cavity size as a reference. The measurement of RV and LV end-diastolic diameter is preferably performed in the parasternal long-axis view [7]. RV cavity dilatation is confirmed when the RV/LV end-diastolic diameter ratio exceeds 0.6 [19]. RV dilatation is considered moderate when the ratio is less than one, and severe when it is greater or equal to one [20]. Alternatively, the same measurement may be performed in the apical four-chamber view (◘ Fig. 4.4), using the same diagnostic criteria for RV dilatation [17, 18]. The subcostal view is not ideally suited for the diagnosis of RV dilatation due to frequently inadequate imaging plane precluding accurate assessment of ventricular cavity size [13].

Since RV dilatation results in a functional tricuspid regurgitation and potentially increased filling pressure, the right atrium is also frequently dilated in the apical four-chamber view. In addition, when the normal interatrial pressure gradient is reversed due to markedly elevated right-sided pressure, the interatrial septum may bulge toward the left atrium throughout the cardiac and respiratory cycle [21].

4.4.2 Assessment of the Pattern of Contraction of the Interventricular Septum

Physiologically, the interventricular septal thickening mainly contributes to LV ejection [22]. The parasternal short-axis view is ideally suited to evaluate its pattern of contraction. The interventricular septum normally bulges toward the RV cavity throughout the cardiac cycle, according to the interventricular pressure gradient, and homogeneously thickens during systole to contribute to the LV concentric contraction toward the centroid of its cavity (◘ Fig. 4.6) [23]. The inversed sequence is observed during diastole [24].

In the presence of increased afterload, the RV contraction becomes stronger and longer than normal [25]. Accordingly, RV contraction extends while the LV starts relaxing, and the interventricular pressure gradient is reversed at end-systole. This results in a transient end-systolic flattening of the interventricular septum, or even an inversion of its normal curvature with a bulging toward the LV cavity in the most severe presentations (◘ Fig. 4.6). During diastole, the abnormal septal position frequently persists to a variable extent, according to the magnitude of RV diastolic pressure and/or worsened tricuspid regurgitation (volume overload) [8, 26]. At the onset of the subsequent systole, the abrupt increase of LV pressure resulting from its contraction restores the normal transseptal pressure and the interventricular septum moves toward the RV cavity. This abnormal interventricular septal motion is called "paradoxical septal motion" [20]. The identification of the paradoxical motion may be challenging, especially when subtle with only a mild and transient end-systolic flattening (◘ Fig. 4.6). In this case, a careful examination of the septal kinetic throughout the cardiac cycle on a low speed image loop is required. When pronounced, the paradoxical septal motion may also be depicted in the apical four-

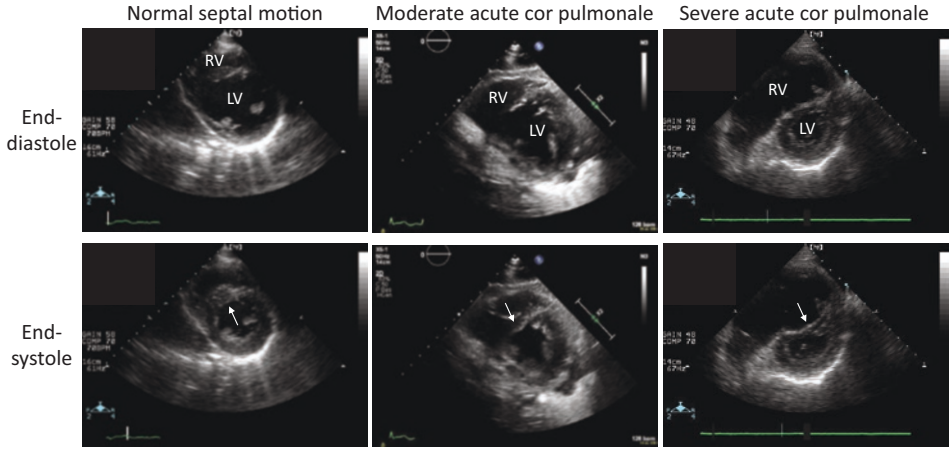

Fig. 4.6 Illustrative examples of qualitative (visual) assessment of the pattern of contraction of the interventricular septum in the parasternal short-axis view of the heart (see text for details). Normally, the left ventricle is round-shaped and bulges toward the right ventricle both at end-diastole (upper left panel) and at end-systole (lower left panel, arrow), since its intracavitary pressure exceeds that of the right ventricle throughout the cardiac cycle and its contraction is concentric toward the centroid of its cavity. In the presence of an abrupt pressure overload, the right ventricle enlarges and a paradoxical septal motion is depicted at end-systole. According to the severity of right ventricular afterloading, the cavity enlargement can be moderate (mid panels) or severe (right panels). At end-systole, the interventricular septum can be only flattened (lower mid panel, arrow) or its curvature can be reversed with the septum bulging toward the left ventricle (lower right panel, arrow). The left ventricle appears restricted in the stiff pericardium, proportionally to the severity of the right ventricular cavity dilatation. **Abbreviations**: *LV* left ventricle; *RV* right ventricle

chamber view. Nevertheless, in the long axis of the heart, an abnormal interventricular septal motion pattern may be secondary to a complete branch block leading to an asynergy of ventricular contraction (e.g., after open-heart surgery).

The association of RV dilatation and paradoxical septal motion echocardiographically defines the acute cor pulmonale (ACP) which suggests an abrupt increase of RV afterload, irrespective of its nature. According to the magnitude of RV dilatation, the ACP is coined "moderate" or "severe" [20].

4.4.3 Assessment of the Inferior Vena Cava

RVF is characterized by a systemic venous congestion which contributes to the development of organ failure (e.g., liver and renal failure) in reducing the perfusion pressure. In the subcostal view centered on IVC long axis, the vessel appears dilated with a reduced or absent normal inspiratory collapse in spontaneously breathing patients (Fig. 4.7). In the presence of a marked venous congestion, the sniff test fails to induce a transient reduction of IVC size. Although no specific threshold value is unanimously accepted, an end-expiratory (i.e., maximal) IVC diameter >23 mm can be proposed to characterize a dilated IVC, and is associated with a poor prognosis [4].

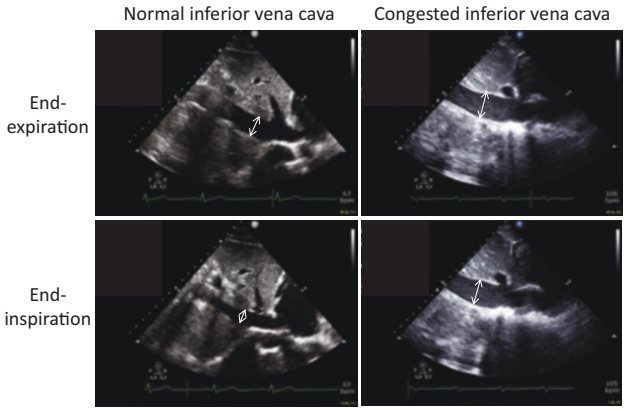

Fig. 4.7 Examination of the inferior vena cava in the modified subcostal view in a spontaneously breathing patient presenting with a right ventricular failure and in a normal volunteer for comparison. Physiologically, the inferior vena cava has a normal size and exhibits an inspiratory collapse which typically exceeds 50% of its end-expiratory diameter (left panels, double arrowheads). In contrast, patients with right ventricular failure develop systemic venous congestion which is reflected by both the enlargement of the inferior vena cava (increased end-expiratory diameter; upper right panel, double arrowhead: 29 mm) and the absence of its normal inspiratory collapse (lower right panel, double arrowhead: 27 mm)

In our experience, recently trained residents with a basic level in critical care echocardiography adequately identify a dilated IVC when compared with the expert (Kappa: 0.79 [0.63–0.94]) in ICU patients [18].

4.4.4 Assessment of Right Ventricular Free Wall Thickness

RV free wall hypertrophy is consistent with a RV remodeling in response to a chronically elevated afterload (pulmonary hypertension). It is best identified in the subcostal long-axis view or in the parasternal long-axis view of the heart [13]. In this case, the thickness of the RV free wall exceeds 6 mm and may reach up to 10 mm [14].

4.5 Proposed Diagnostic Algorithm

RVF is a heterogeneous syndrome. Basic critical care echocardiography may help in guiding diagnostic work-up (Table 4.1). In patients presenting with shock and systemic venous congestion, basic echocardiography allows to promptly rule out a tamponade which constitutes the main differential diagnosis of RVF.

In ICU patients, the most frequent cause of RVF is pulmonary hypertension (pressure overload). When a massive pulmonary embolism is suspected in a patient with circulatory failure, the presence of an ACP is highly evocative [27]. Transthoracic echocardiography is not sensitive but specific for the identification of intracavitary thrombus, which definitely links ACP to a massive pulmonary embolism (Fig. 4.8). In ventilated patients after a resuscitated cardiac arrest, transesophageal echocardiography has a higher diagnostic capacity for the diagnosis of entrapped thrombus

Table 4.1 Main causes of right ventricular failure in patients hospitalized in the intensive care unit and corresponding basic critical care echocardiography findings

Etiology	Basic critical care echocardiography findings
Right ventricular pressure overload (pulmonary hypertension)	
Acute pulmonary embolism	– RV dilatation – Paradoxical septal motion (systolic) – Regional wall motion abnormality (Mc Connell's sign) – Thrombus-in-transit or entrapped (proximal pulmonary artery, foramen ovale) – Congested IVC – Normal LV systolic function
Acute respiratory distress syndrome	– RV dilatation – Paradoxical septal motion (systolic) – Congested IVC – Normal LV systolic function – Normal left atrial size (absence of elevated left-sided pressure)
Exacerbation of chronic respiratory insufficiency	– RV hypertrophy (chronic pulmonary hypertension) – RV dilatation (marked in advanced stages) – Paradoxical septal motion (systolic/diastolic[a]) – Right atrial dilatation (chronically elevated right-sided pressure)
Cardiomyopathies	– Reduced LV systolic function – Left atrial dilatation reflecting chronically elevated LV filling pressure – Ventricular remodeling according to the cardiomyopathy: Dilated cardiomyopathy: RV and LV dilatation Infiltrative cardiomyopathy: RV and LV hypertrophy with small ventricular cavities and dilatation of both atria
Impaired right ventricular contractility	
RV myocardial infarction	– RV dilatation (marked) – Hypokinetic RV free wall with associated LV inferoseptal wall motion abnormality – Congested IVC
Sepsis	– RV dilatation (variable) – LV of normal size with global hypokinesia (septic cardiomyopathy) – Absence of atrial dilatation (low filling pressures)
Right ventricular volume overload	
Severe tricuspid regurgitation	– RV dilatation – Marked right atrial dilatation – Diastolic septal bulging toward LV cavity – Congested IVC – Preserved RV systolic function
Atrial septal defect	– RV dilatation – Marked right atrial dilatation – Anatomical defect of various size and position of the interatrial septum

Abbreviations: *RV* right ventricle; *LV* left ventricle; *IVC* inferior vena cava

[a] In the presence of associated right ventricular volume overload (severe tricuspid regurgitation)

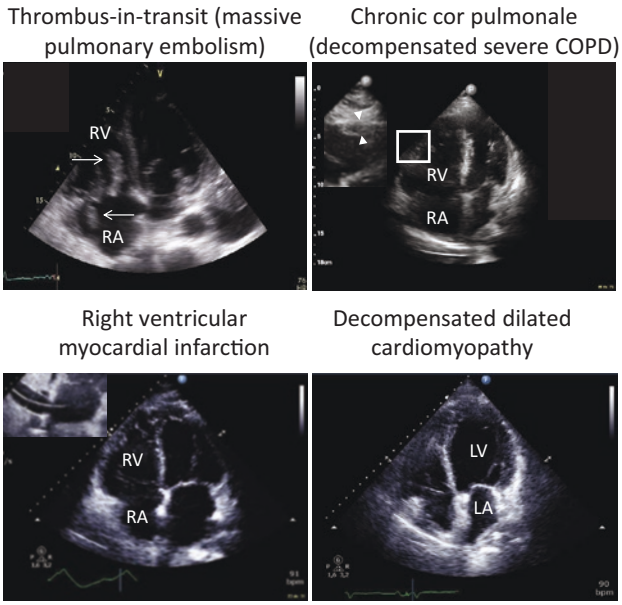

Fig. 4.8 Illustrative examples of different types of right ventricular failure when assessed from the apical four-chamber view (see text for details). In all cases, both the right ventricle and right atrium are moderately or severely dilated (i.e., larger than the respective left cavities). The presence of a thrombus-in-transit within right cardiac cavities is rare but specific of an acute massive pulmonary embolism (upper left panel, arrows) in a patient sustaining a circulatory failure. Severe hypertrophy of the right ventricular free wall (upper right panel, magnified image from a sub-costal long-axis view, arrowheads: 10 mm) is consistent with a long-standing pulmonary hypertension in a patient presenting with a decompensated chronic respiratory insufficiency and associated chronic cor pulmonale. Right ventricular cavity dilatation associated with a severely dilated inferior vena cava (lower left panel, zoomed image obtained from the modified sub-costal view, end-expiratory diameter: 28 mm, a temporary pacemaker probe is depicted) in the absence of significant pulmonary hypertension are the hallmarks of right ventricular myocardial infarction in shocked patients with systemic venous congestion. In the presence of a severe left ventricular systolic and diastolic dysfunction as in a patient with decompensated dilated cardiomyopathy, chronic post-capillary pulmonary hypertension results in right ventricular failure with a dilatation of the four cardiac cavities due to chronically elevated filling pressures (lower right panel). **Abbreviations**: *RV* right ventricle; *RA* right atrium; *LV* left ventricle; *LA* left atrium

[28]. In contrast, the absence of RV dilatation should prompt the frontline intensivist to consider alternative diagnoses [7]. In the ICU settings, the acute respiratory distress syndrome (ARDS) is the most frequent cause of RVF. The prevalence of ACP in ARDS patients who are under protective mechanical ventilation approximates 22%. Risk factors are pneumonia, $PaO_2/FiO_2 < 150$ mmHg, $PaCO_2 \geq 48$ mmHg, and driving pressure ≥18 cm H_2O [29]. In ARDS patients, the development of RVF is frequently associated with a deterioration of the respiratory condition [6]. The therapeutic strategy is mainly directed toward (i) keeping the systolic arterial pressure greater than pulmonary arterial pressure for best RV coronary flow, and (ii) unloading the RV with adequate ventilator settings, prone positioning, and inhaled Nitric Oxide [10]. In patients with exacerbated chronic respiratory failure, RV hypertrophy is frequently observed according to the level of underlying pulmonary hypertension and a chronic cor pulmonale may be depicted (Fig. 4.8). The subcostal view may

also depict ascites, which is indicative of pre-existing chronic RVF [10]. Patients with cardiomyopathies responsible for severe LV systolic and diastolic dysfunction may develop post-capillary pulmonary hypertension and subsequent RVF (Fig. 4.8). In contrast to pre-capillary pulmonary hypertension, which is typically characterized by a (systolic) paradoxical septal motion; these patients exhibit normal interventricular septal motion, but marked remodeling of the LV with an enlarged left atrium denoting chronically elevated LV filling pressure (Table 4.1).

When the RV dilatation is isolated (absence of paradoxical septal motion), intrinsically RV reduced contractility and/or volume overload should be raised. In the absence of advanced pulmonary hypertension, the main causes of decreased RV contractility in ICU patients are RV myocardial infarction and septic cardiomyopathy (Table 4.1). RV myocardial infarction is typically associated with an LV infarction in the myocardial territory supplied by the right coronary artery [30]. RV and LV dysfunction is common in septic patients [31]. Although isolated RV afterloading may be encountered in septic patients with ARDS since pneumonia remains the most frequent site of community-acquired septic shock, biventricular dysfunction may occur in patients who develop septic cardiomyopathy [32].

Patients with RVF are typically unresponsive to fluid challenge, which is usually deleterious in further increasing RV overload [33], and worsening both the systemic venous congestion and associated organ dysfunction (e.g., liver and renal failure). ICU patients with septic shock and a dilated IVC (end-respiratory diameter $\geq$25 mm) have been shown not to respond to fluid loading, with a specificity of at least 80% [34].

4.6 Conclusion

RVF is frequently encountered in ICU patients and results predominantly from an acute pulmonary hypertension, irrespective of its origins. In patients with circulatory failure and systemic venous congestion, basic critical echocardiography promptly rules out a tamponade and depicts RV enlargement with congested IVC. The presence of a paradoxical septal motion ascribes RV dilatation to a pressure overload, while hypertrophy of RV free wall reflects chronic and advanced pulmonary hypertension. RV dilatation associated with systolic dysfunction and systemic venous congestion suggest altered RV contractility. Basic critical care echocardiography provides clinically relevant information in critically ill patients with RVF, and helps the frontline physician in guiding both the diagnostic work-up and acute management.

Summary

Right ventricular failure refers to a rapidly progressive syndrome with systemic congestion resulting from impaired right ventricular filling and/or reduced right ventricular flow output. This condition develops in acute diseases which alter unfavorably right ventricular loading conditions and/or decrease right ventricular contractility. Accordingly, right ventricular failure is frequently encountered in critically ill patients and results predominantly from an acute pulmonary hypertension, irrespective of its origin. In patients with circulatory failure and systemic venous congestion, basic critical echocardiography promptly rules out a tamponade and depicts right ventricular enlargement with congested IVC. The

presence of a paradoxical septal motion ascribes right ventricular dilatation to a pressure overload, while hypertrophy of right ventricular free wall reflects chronic and advanced pulmonary hypertension. Right ventricular dilatation associated with systolic dysfunction and systemic venous congestion suggest altered myocardial contractility, such as right ventricular infarction or septic cardiomyopathy. Basic critical care echocardiography provides clinically relevant information in critically ill patients with right ventricular failure, and helps the frontline physician in guiding both the diagnostic work-up and acute management.

Take Home Messages

- Right ventricular failure refers to a rapidly progressive syndrome with systemic congestion resulting from impaired right ventricular filling and/or reduced right ventricular flow output.
- Right ventricular failure develops in acute diseases which alter unfavorably right ventricular loading conditions and/or decrease right ventricular contractility.
- Right ventricular failure is frequently encountered in critically ill patients and results predominantly from an acute pulmonary hypertension, irrespective of its origin.
- In patients with circulatory failure and systemic venous congestion, basic critical echocardiography promptly rules out a tamponade and depicts right ventricular enlargement with congested IVC.
- The presence of a paradoxical septal motion ascribes right ventricular dilatation to a pressure overload.
- The presence of a hypertrophied right ventricular free wall reflects chronic and advanced pulmonary hypertension.
- Right ventricular dilatation associated with systolic dysfunction and systemic venous congestion suggest altered myocardial contractility, such as right ventricular infarction or septic cardiomyopathy.
- Basic critical care echocardiography helps the frontline physician in guiding both the diagnostic work-up and acute management in patients with right ventricular failure.

References

1. Lahm T, Douglas IS, Archer SL, et al. Assessment of right ventricular function in the research setting: knowledge gaps and pathways forward. An Official American Thoracic Society Research Statement. Am J Respir Crit Care Med. 2018;198(4):e15–43.
2. Harjola VP, Mebazaa A, Čelutkienė J, et al. Contemporary management of acute right ventricular failure: a statement from the Heart Failure Association and the Working Group on Pulmonary Circulation and Right Ventricular Function of the European Society of Cardiology. Eur J Heart Fail. 2016;18(3):226–41. https://doi.org/10.1002/ejhf.478.
3. Repessé X, Charron C, Vieillard-Baron A. Assessment of the effects of inspiratory load on right ventricular function. Curr Opin Crit Care. 2016;22(3):254–9.
4. Pellicori P, Carubelli V, Zhang J, Castiello T, Sherwi N, Clark AL, et al. IVC diameter in patients with chronic heart failure: relationships and prognostic significance. J Am Coll Cardiol Cardiovasc Imaging. 2013;6(1):16–28.

5. Dong D, Zong Y, Li Z, Wang Y, Jing C. Mortality of right ventricular dysfunction in patients with acute respiratory distress syndrome subjected to lung protective ventilation: a systematic review and meta-analysis. Heart Lung J Crit Care. 2021;50(5):730–5.
6. Evrard B, Goudelin M, Giraudeau B, François B, Vignon P. Right ventricular failure is strongly associated with mortality in patients with moderate-to-severe COVID-19-related ARDS and appears related to respiratory worsening. Intensive Care Med. 2022;48(6):765–7.
7. Robba C, Wong A, Poole D, Al Tayar A, Arntfield RT, Chew MS, Corradi F, Douflé G, Goffi A, Lamperti M, Mayo P, Messina A, Mongodi S, Narasimhan M, Puppo C, Sarwal A, Slama M, Taccone FS, Vignon P, Vieillard-Baron A. Basic ultrasound head-to-toe skills for intensivists in the general and neuro intensive care unit population: consensus and expert recommendations of the European Society of Intensive Care Medicine. European Society of Intensive Care Medicine task force for critical care ultrasonography. Intensive Care Med. 2021;47(12):1347–67.
8. Naeije R, Badagliacca R. The overloaded right heart and ventricular interdependence. Cardiovasc Res. 2017;113(12):1474–85.
9. Vonk Noordegraaf A, Westerhof BE, Westerhof N. The relationship between the right ventricle and its load in pulmonary hypertension. J Am Coll Cardiol. 2017;69(2):236–43.
10. Vieillard-Baron A, Naeije R, Haddad F, et al. Diagnostic workup, etiologies and management of acute right ventricle failure: a state-of-the-art paper. Intensive Care Med. 2018;44(6):774–90.
11. Vieillard-Baron A, Prigent A, Repessé X, et al. Right ventricular failure in septic shock: characterization, incidence and impact on fluid responsiveness. Crit Care. 2020;24(1):630.
12. Mayo PH, Beaulieu Y, Doelken P, et al. American College of Chest Physicians/La Société de Réanimation de Langue Française statement on competence in critical care ultrasonography. Chest. 2009;135(4):1050–60.
13. Rudski LG, Lai WW, Afilalo J, et al. Guidelines for the echocardiographic assessment of the right heart in adults: a report from the American Society of Echocardiography endorsed by the European Association of Echocardiography, a registered branch of the European Society of Cardiology, and the Canadian Society of Echocardiography. J Am Soc Echocardiogr. 2010;23(7):685–788.
14. Prakash R, Matsukubo H. Usefulness of echocardiographic right ventricular measurements in estimating right ventricular hypertrophy and right ventricular systolic pressure. Am J Cardiol. 1983;51(6):1036–40.
15. Weyman AE, editor. Principles and practice of echocardiography. 2nd ed. Lea and Febiger; 1994. p. 1295.
16. Haddad F, Doyle R, Murphy DJ, Hunt SA. Right ventricular function in cardiovascular disease, part II: pathophysiology, clinical importance, and management of right ventricular failure. Circulation. 2008;117(13):1717–31.
17. Vignon P, Dugard A, Abraham J, et al. Focused training for goal-oriented hand-held echocardiography performed by noncardiologist residents in the intensive care unit. Intensive Care Med. 2007;33(10):1795–9.
18. Vignon P, Mücke F, Bellec F, et al. Basic critical care echocardiography: validation of a curriculum dedicated to noncardiologist residents. Crit Care Med. 2011;39(4):636–42.
19. Kasper W, Meinertz T, Kersting F, Löllgen H, Limbourg P, Just H. Echocardiography in assessing acute pulmonary hypertension due to pulmonary embolism. Am J Cardiol. 1980;45(3):567–72.
20. Jardin F, Dubourg O, Bourdarias JP. Echocardiographic pattern of acute cor pulmonale. Chest. 1997;111(1):209–17.
21. Kusumoto FM, Muhiudeen IA, Kuecherer HF, Cahalan MK, Schiller NB. Response of the interatrial septum to transatrial pressure gradients and its potential for predicting pulmonary capillary wedge pressure: an intraoperative study using transesophageal echocardiography in patients during mechanical ventilation. J Am Coll Cardiol. 1993;21(3):721–8.
22. Vignon P, Weinert L, Mor-Avi V, Spencer KT, Bednarz J, Lang RM. Quantitative assessment of regional right ventricular function with color kinesis. Am J Respir Crit Care Med. 1999;159(6):1949–59.
23. Lang RM, Vignon P, Weinert L, et al. Echocardiographic quantification of regional left ventricular wall motion with color kinesis. Circulation. 1996;93(10):1877–85.
24. Vignon P, Mor-Avi V, Weinert L, Koch R, Spencer KT, Lang RM. Quantitative evaluation of global and regional left ventricular diastolic function with color kinesis. Circulation. 1998;97(11):1053–61.

25. Elzinga G, Piene H, de Jong JP. Left and right ventricular pump function and consequences of having two pumps in one heart. A study on the isolated cat heart. Circ Res. 1980;46(4):564–74.
26. Ryan T, Petrovic O, Dillon JC, Feigenbaum H, Conley MJ, Armstrong WF. An echocardiographic index for separation of right ventricular volume and pressure overload. J Am Coll Cardiol. 1985;5(4):918–27.
27. Jardin F, Dubourg O, Guéret P, Delorme G, Bourdarias JP. Quantitative two-dimensional echocardiography in massive pulmonary embolism: emphasis on ventricular interdependence and leftward septal displacement. J Am Coll Cardiol. 1987;10(6):1201–6.
28. Vignon P, Merz TM, Vieillard-Baron A. Ten reasons for performing hemodynamic monitoring using transesophageal echocardiography. Intensive Care Med. 2017;43(7):1048–51.
29. Mekontso Dessap A, Boissier F, Charron C, et al. Acute cor pulmonale during protective ventilation for acute respiratory distress syndrome: prevalence, predictors, and clinical impact. Intensive Care Med. 2016;42(5):862–70.
30. Kinch JW, Ryan TJ. Right ventricular infarction. N Engl J Med. 1994;330(17):1211–7.
31. Lanspa MJ, Cirulis MM, Wiley BM, et al. Right ventricular dysfunction in early sepsis and septic shock. Chest. 2021;159(3):1055–63.
32. Martin L, Derwall M, Al Zoubi S, et al. The septic heart: current understanding of molecular mechanisms and clinical implications. Chest. 2019;155(2):427–37.
33. Mercat A, Diehl JL, Meyer G, Teboul JL, Sors H. Hemodynamic effects of fluid loading in acute massive pulmonary embolism. Crit Care Med. 1999;27(3):540–4.
34. Vieillard-Baron A, Evrard B, Repessé X, et al. Limited value of end-expiratory inferior vena cava diameter to predict fluid responsiveness impact of intra-abdominal pressure. Intensive Care Med. 2018;44(2):197–203.

Evaluation of Haemodynamically Important Pericardial Effusion

Michelle S. Chew, Jonathan Aron and Meriam Åström Aneq

Contents

5.1 Introduction – 48

5.2 Anatomy – 48

5.3 Aetiology – 49

5.4 Classification and Physiology – 50

5.5 Evaluation of Pericardial Effusion – 51
5.5.1 Signs and Symptoms – 51

5.6 Echocardiographic Evaluation of Pericardial Collection – 52
5.6.1 Two-Dimensional Echocardiography Assessment – 52
5.6.2 Haemodynamic Assessment Using Spectral Doppler Analysis – 53

5.7 Confounders in Clinical and Echocardiographic Examination – 55

5.8 Clinical Decision-Making – 55

References – 57

Supplementary Information The online version contains supplementary material available at https://doi.org/10.1007/978-3-031-32462-8_5.

© The Author(s), under exclusive license to Springer Nature Switzerland AG 2023
C. Robba et al. (eds.), *Basic Ultrasound Skills "Head to Toe" for General Intensivists*, Lessons from the ICU,
https://doi.org/10.1007/978-3-031-32462-8_5

Learning Objectives

- To understand the relevant anatomy and pathophysiology related to pericardial collections and tamponade.
- To be able to describe the 2-dimensional echocardiographic appearances of a pericardial collection.
- To be able to identify features that suggest tamponade physiology or impending tamponade.
- To understand the limitations of using echocardiography to assess tamponade physiology.
- To describe how to use echocardiography to manage pericardial collections and tamponade.

5

5.1 Introduction

A pericardial collection is defined as a build-up of fluid within the pericardial sac. As the collection expands and pressure within the pericardial sac increases it begins to exert compressive effects on local structures, notably the cardiac chambers within the pericardium. This begins by affecting the lower pressure chambers during the part of the cardiac cycle when pressure within these chambers is at its lowest. As pericardial fluid accumulates, intrapericardial pressure increases. Equalization of intrapericardial pressure with intracavitary pressures limits intracardiac filling, causing a reduction in cardiac output and so called 'tamponade physiology'.

Identifying the point at which tamponade physiology is imminent is the goal of echocardiographic analysis. This analysis can be done using focused 2-dimension echocardiography and, combined with clinical data, may be sufficient to diagnose tamponade. Haemodynamic data obtained from echocardiography can also assist with timely clinical decision-making.

This chapter will discuss in detail the relevant anatomy, physiology and echocardiography features that will enable the clinician to describe and monitor pericardial collections as well as to identify impending tamponade. The combination of understanding physiology and echocardiography will enable the attending clinician to make nuanced, timely clinical decisions.

5.2 Anatomy

The pericardium is a fibroelastic sac that surrounds the heart and consists of an outer fibrous layer and an inner serous layer. The serous layer is further divided into the parietal and visceral pericardium. Together, they act to protect the heart and to reduce friction between the mobile cardiac and surrounding structures. The space between the parietal and visceral layers is the intrapericardial cavity. This cavity normally contains less than 50 mL of fluid [1–3]. Mesothelial cells line the serosal layer and play an active role in healing and regeneration after injury and inflammation [1].

5.3 Aetiology

Pericardial effusion may be caused by a wide variety of diseases (Table 5.1) and idiopathic aetiologies are common. It may be associated with inflammatory and non-inflammatory pathology, with viral infections, autoimmune diseases, malignancy and trauma among the most common underlying causes. In endemic countries,

Table 5.1 Causes of pericardial inflammation and effusion

Infectious	Bacterial, e.g. tuberculosis, pneumococcus
	Viral, e.g. coxsackie, herpes, HIV
	Fungal, e.g. histoplasma, aspergillus, candida
	Protozoal, e.g. trypanosoma, toxoplasma
Malignancy	Metastates
	Lymphoma
	Mesothelioma
	Angiosarcoma
Inflammatory	Rheumatoid Arthritis
	Systemic Lupus Erythematosus
Infiltrative	Amyloidosis
	Sarcoidosis
Trauma	Iatrogenic
	Blunt and sharp injuries
	Aortic dissection
Surgery and post-procedural	Post-pericardiotomy, post-cardiac intervention, post-radiation
Cardiovascular diseases	Myocardial infarction
	Congestive cardiac failure
	Pulmonary hypertension
	Aortic dissection
Metabolic	Uraemia
	Hypothyroidism
Drugs	Antineoplastic, e.g. doxorubicin, cyclophosphamide, 5-flurouracil
	Hydralazine
	Phenytoin
	Penicillin and sulpha-drugs
	Amiodarone
	Vaccines
Idiopathic	

tuberculosis is still a common cause [3]. Large (>20 mm) idiopathic chronic pericardial effusions are also not uncommon and are associated with a high incidence of tamponade [4].

5.4 Classification and Physiology

Pericardial effusion may be classified according to size, onset, composition, location and its haemodynamic effects (Table 5.2).

Central to the understanding of the haemodynamic effects of pericardial effusion is the concept of interventricular dependence. An increase in venous return and right ventricular size during spontaneous inspiration will induce a septal shift of the interventricular septum towards the left ventricle, resulting in decreased left ventricular dimension and output.

Cardiac tamponade occurs when increased intrapericardial volume causes the intrapericardial pressure to exceed cardiac intracavitary pressures. In the normal heart, intrapericardial pressure approximates pulmonary pressure and increases as the volume of intrapericardial fluid increases. In the early phases, pericardial fluid accumulation 'stiffens' the heart and impairs their relaxation [5]. Intraventricular pressure increases and remains higher than intrapericardial pressure. As right ventricular pressure increases, the interventricular septum is pushed towards the left ventricle. This interventricular dependence is exaggerated since expansion of both

Table 5.2 Classification of pericardial effusion

Onset	Acute
	Subacute
	Chronic (>3 months)
Size	Small (<10 mm)
	Moderate (10–20 mm)
	Large (>20 mm)
Location	Circumferential
	Loculated
Composition	Transudate
	Exudate
	Blood
	Air
Haemodynamic effect	None
	Low pressure tamponade
	Tamponade

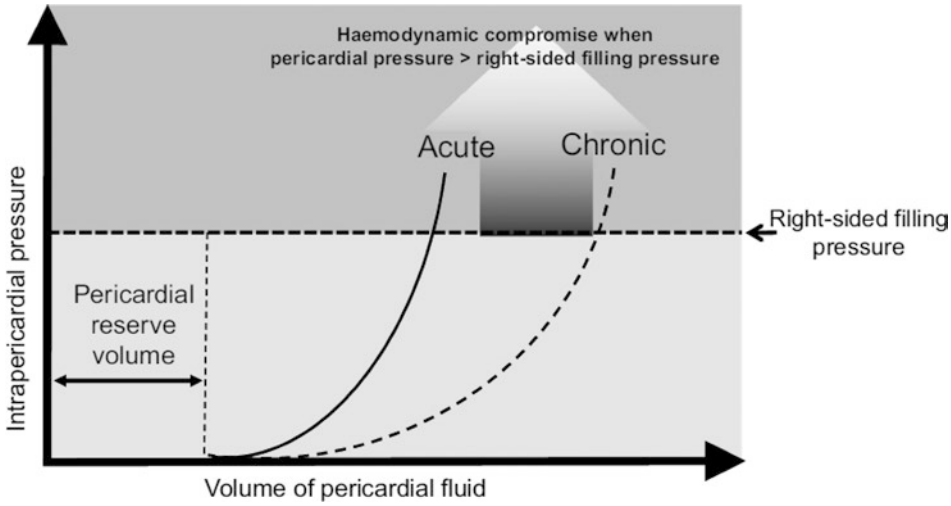

Fig. 5.1 Physiology of pericardial effusion and progression to cardiac tamponade. Footnote: Pericardial volume pressure relationship illustrating an initial slow rise followed by a steep rise in intrapericardial pressures. At the steep portion of the curve, only small additional volumes are required to precipitate tamponade. *Reproduced with permission from Mekontso-Dessap A and Chew MS. Intensive Care Medicine 2018;44:936–9*

ventricles are constrained by the effusion. Additionally, a compressive effect on the right atrium and then left atrium causes a decrease in cardiac output. With further increases, intrapericardial pressure will eventually equalize with left ventricular filling pressure, causing circulatory collapse [5–7].

Importantly, the rise in intrapericardial pressure is not necessarily related to the volume of pericardial fluid. The development of tamponade is more dependent on the rate of fluid accumulation. Large volumes of intrapericardial fluid may be tolerated if the intrapericardial pressure does not exceed right heart filling pressures. Similarly, acute accumulation of small volumes may cause tamponade due to a steep rise in intrapericardial pressure (Fig. 5.1). The relationship between intrapericardial pressure and volume also explains why withdrawal of modest amounts of pericardial fluid can dramatically reverse haemodynamic instability in an acute setting.

5.5 Evaluation of Pericardial Effusion

5.5.1 Signs and Symptoms

Classical symptoms and signs of pericardial effusion include tachycardia, tachypnoea, dyspnoea and chest pain that may progress to orthopnoea or even shock. Non-specific symptoms such as cough, hiccups, nausea, dysphagia and hoarseness may occur and reflect compression on contiguous structures such as the diaphragm, oesophagus and recurrent laryngeal nerve. In 1935, Beck described the classic triad of hypotension, increased jugular venous pressure and muffled heart sounds associ-

ated with acute tamponade [8]. Importantly, Beck also distinguished the physiologic differences between 'acute and chronic compressions'. These signs and symptoms may be accompanied by an enlargement of the cardiac silhouette on chest X-ray, although it should be noted that acute changes and smaller effusions may not produce any enlargement, and that the silhouette does not reflect the true size of the heart. A low voltage ECG and electrical alternans (alternating normal sized and small sized QRS complexes) may be present, and the combination of P and QRS alternation is highly specific for tamponade [6].

Another classical sign is pulsus paradoxus, defined as an inspiratory fall of systolic blood pressure of more than 10 mmHg during normal spontaneous breathing. Pulsus paradoxus is an important diagnostic finding in cardiac tamponade and reflects an exaggerated biventricular interdependence, although it can also be found during constrictive pericarditis, severe acute asthma, pneumothorax or exacerbations of chronic obstructive pulmonary disease [9–11]. The radial pulse may be intermittently impalpable and may be accompanied by an increase in the ▶ jugular venous pressure height (▶ Kussmaul's sign). Notably, pulsus paradoxus may not be present during positive pressure ventilation, hence its absence should not be synonymous with a lack of haemodynamic effect. Pulsus paradoxus can be visualized on echocardiography, so understanding its physiology is important.

5.6 Echocardiographic Evaluation of Pericardial Collection

Echocardiography is recommended as the first imaging technique for the evaluation of suspected cardiac tamponade. Added on to clinical evaluation, echocardiography may be used to evaluate the haemodynamic significance of the pericardial effusion and guide the timing of pericardiocentesis (◘ Table 5.3).

5.6.1 Two-Dimensional Echocardiography Assessment

Many focused protocols that can be learnt in 6–12 months focus on rapid 2-D assessment designed to identify treatable causes of shock, including pericardial collection. If a tamponade is a clinically likely cause of shock, an effusion is evident on focused echo and there is an absence of any other cause, immediate discussion regarding the possibility of drainage should commence. Pericardial collections can easily be identified, and the appearances can be described using the framework suggested above.

Echocardiographic evaluation should determine the location and size of the effusion. The size of the effusion should be measured when the separation between the pericardial layers is at a minimum to avoid falsely overstating the size of the effusion. In addition, the haemodynamic effects should be reported. Classically, this is described as chamber collapse. Right atrial collapse is an early sign that is highly sensitive, but poorly specific, for cardiac tamponade. Specificity is increased if the right atrial collapse is sustained for more than one-third of the cardiac cycle, or if

Table 5.3 Echocardiographic assessment of cardiac tamponade

Size	Small (<10 mm)
	Moderate (10–20 mm)
	Large (>20 mm)
Location	Circumferential
	Loculated
Chamber collapse	Right atrial systolic collapse >1/3 of cardiac cycle
	Right ventricular diastolic collapse
	Left atrial collapse
	Left ventricular diastolic collapse
Other findings	'Swinging heart' associated with alternating size of QRS complex on ECG
	Paradoxical septal movement
IVC plethora	Dilated IVC >20 mm with <50% respiratory collapse
	Diastolic flow reversal in hepatic veins
Doppler flows	Echocardiographic 'pulsus paradoxus', i.e. >40%increase in right-sided (transtricuspid/pulmonary) concomitantly with >25% decrease in left-sided (transmitral/aortic) flows in inspiration during *spontaneous breathing*

right ventricular diastolic collapse occurs [12, 13] (Fig. 5.2). The demonstration of 'IVC plethora' also supports the diagnosis of cardiac tamponade [14, 15] (Fig. 5.3).

Pulsus paradoxus may be visualized on 2-dimensional echocardiography if cardiac function is observed over the respiratory cycle. Changes in intrathoracic pressure over the respiratory cycle result in exaggerated variation in venous return, leading to clear variation in the end diastolic dimensions of the left ventricle and subsequently intermittently 'kissing' papillary muscles.

5.6.2 Haemodynamic Assessment Using Spectral Doppler Analysis

In more complicated cases in which the shock state is potentially multi-factorial, more advanced assessment using spectral doppler may be useful to help clinicians determine its haemodynamic significance. The operator should have an advanced accreditation and be confident in the measurement and interpretation (including limitations) of any data obtained.

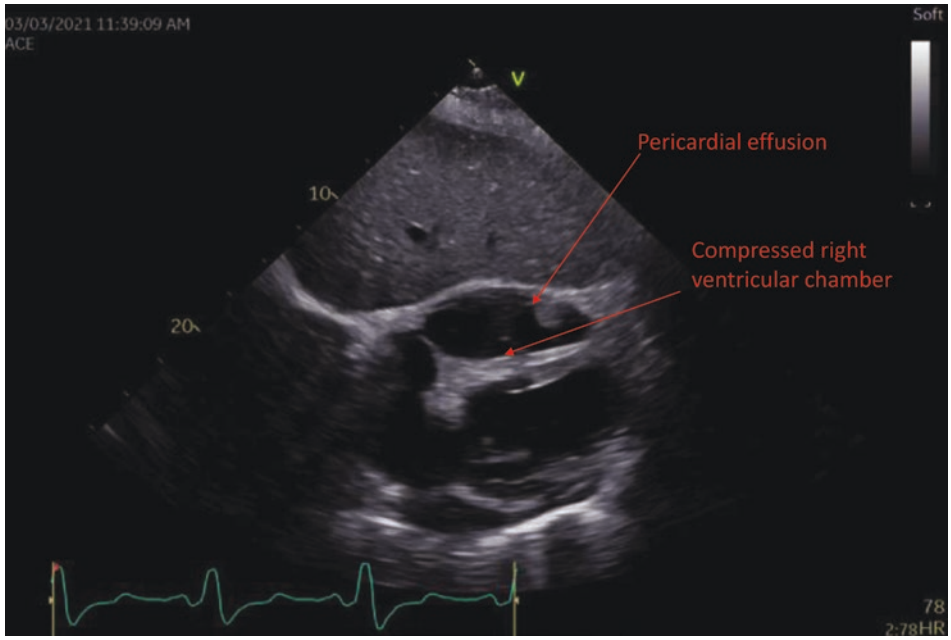

Fig. 5.2 Large, localized effusion over the right ventricular free wall compressing the ventricular chamber

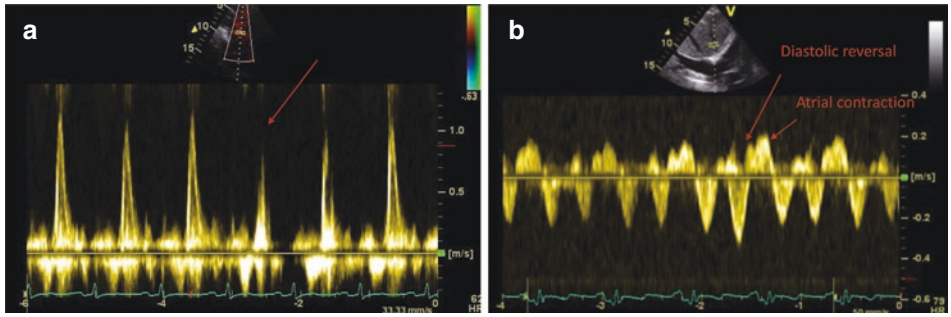

Fig. 5.3 (**a**) Transmitral flow decrease of >25% during early inspiration in a spontaneously breathing patient. (**b**) Hepatic vein diastolic flow reversal: peak flow normally occurs during systole (s wave larger than d wave, and there is no diastolic flow component). In tamponade, there is diastolic flow reversal

'Echocardiographic pulsus paradoxus', as demonstrated by a decrease (>25%) in the transmitral flow velocity or increase in the transtricuspid flow velocity during inspiration are classically associated with tamponade physiology [2, 14–18]. Hepatic venous diastolic flow reversal may also be demonstrated. However, these echocardiographic findings only apply to spontaneously breathing patients and respiratory transvalvular flow variations may be absent during positive pressure ventilation [19]. Further, patients with increased LV filling pressure, aortic regurgitation, loculated effusions or hypovolaemia may also have reduced or absent respiratory variations [20].

5.7 Confounders in Clinical and Echocardiographic Examination

Low pressure tamponade occurs when intrapericardial pressure exceeds right heart filling pressure in the setting of hypovolaemia. Many patients do not suffer from the typical physical findings of tamponade [21]. The low right ventricular filling pressure is normalized by volume loading, improving forward flow of blood allowing time for further investigations and management.

Acute or chronic cor pulmonale, which results in high right-sided filling pressures, may not present with chamber collapse, even if the pressure within the pericardium is high. Collapse occurs when pressure on one side of a divide exceeds the other. Therefore, the first signs of chamber compression may occur on left sided structures, without first causing right sided compression, as is the typical pattern.

Any increase in intra-abdominal pressure may compress the IVC and result in a small IVC, which is at first appearances, incongruous with the clinical presentation. Similarly, where tamponade and hypovolaemia coexist, for instance in the situation of trauma, the IVC may be small even though the pericardial collection is large.

5.8 Clinical Decision-Making

The decision to proceed to pericardiocentesis is guided by both clinical and echocardiographic features. A suggested triage strategy recommends a scoring system based on aetiology, clinical presentation and imaging findings; however, this score has not been validated or evaluated among critically ill patients [22]. The recognition that cardiac tamponade is not a binary phenomenon and necessarily involves both clinical and echocardiographic confirmation is an important first step in deciding the urgency of pericardiocentesis.

Although there is little doubt that large, symptomatic effusions require immediate drainage, concurrent conditions encountered among the critically ill, such as hypovolaemia, vasopressor and inotropic drug therapy, positive pressure ventilation and biventricular failure, complicates this decision and requires a careful consideration of risk vs benefits. For example, malignant effusions are generally associated with poor prognosis, and clinical management should be directed towards symptomatic relief and quality of life. Pericardiocentesis in the setting of myocardial rupture and aortic dissection may extend the underlying pathology [23] and low-pressure tamponade may be relieved by fluid therapy alone.

Summary

Pericardial tamponade is a reversible cause of shock caused by a collection within the pericardium compressing the heart, restricting its filling. Echocardiography can expedite the diagnosis and identification of impending tamponade physiology. Two-dimensional focused echocardiography, is often sufficient to be able to adequately describe the significance of a pericardial collection. Doppler echocardiography with concurrent respiratory tracking can assist in the management of more complex cases in which multiple conditions coexist.

Take-Home Messages

- The use of focused echocardiography can accelerate the diagnosis of pericardial effusion, identify impending tamponade physiology before the onset of clinically overt shock states and help to disentangle complicated clinical cases in which multiple pathologies coexist. Early identification and monitoring can result in a more measured, timely intervention whilst avoiding the consequences of prolonged shock.
- Most of the relevant information regarding the identification of a pericardial collection and an assessment of its significance can be obtained using a rapid, focused 2-D echocardiography protocol alone. For more challenging cases, advanced haemodynamic measurements can assist further, but caveats exist, especially in a sick, ventilated ICU patient. The advanced operator needs to understand the limitations of such an assessment and, if in doubt, always revert back to their clinical acumen to make a safe, balanced decision.

Questions

1. Classical ECG signs of tamponade include:
   (a) A low voltage ECG
   (b) Hanging (concave up) ST segment
   (c) Alternating low and high voltage QRS complex
   (d) Bradycardia
2. A large pericardial effusion
   (a) is defined as a fluid collection measuring >20 mm
   (b) is usually caused by malignancy
   (c) should be drained immediately
   (d) may not cause haemodynamic compromise
3. Low pressure tamponade
   (a) Usually occurs in young, healthy persons
   (b) Is not associated with haemodynamic compromise
   (c) Is said to occur when only right sided cardiac chambers are affected
   (d) Manifests as tamponade physiology in the setting of hypovolaemia
4. Highly specific echocardiographic signs indicating haemodynamically significant pericardial effusion/cardiac tamponade include:
   (a) a large effusion (>20 mm)
   (b) Systolic right atrial collapse extending more than one-third of the cardiac cycle
   (c) Systolic right ventricular collapse
   (d) Systolic left atrial collapse
5. Pulsus paradoxus
   (a) Is pathognomonic of cardiac tamponade
   (b) Is defined as an expiratory decrease in systolic blood pressure of <10 mmHg
   (c) Is exaggerated when the patient is fully mechanically ventilated
   (d) >20 mmHg drop indicates that pericardiac drainage should be expedited

Answers

1. (a) T (b) F (c) T (d) F
2. (a) T (b) F (c) F (d) T
3. (a) F (b) F (c) F (d) T
4. (a) F (b) T (c) F (d) T
5. (a) F (b) F (c) F (d) F

References

1. Jaworska-Wilczynska M, Trzaskoma P, Andrzej A, Szczepankiewicz AA, Tomasz Hryniewiecki T. Pericardium: structure and function in health and disease. Folia Histochem Cytobiol. 2016;54:121–5.
2. Mekontso-Dessap A, Chew MS. Cardiac tamponade. Intensive Care Med. 2018;44:936–9.
3. Adler Y, Charron P, Imazio M, et al. 2015 ESC Guidelines for the diagnosis and management of pericardial diseases: the Task Force for the Diagnosis and Management of Pericardial Diseases of the European Society of Cardiology (ESC) Endorsed by: The European Association for Cardio-Thoracic Surgery (EACTS). Eur Heart J. 2015;36:2921–64. https://doi.org/10.1093/eurheartj/ehv318.
4. Sagristà-Sauleda J, Angel J, Permanyer-Miralda G, Soler-Soler J. Long-term follow-up of idiopathic chronic pericardial effusion. N Engl J Med. 1999;341:2054–9.
5. Reddy PS, Curtiss EI, Uretsky BF. Spectrum of hemodynamic changes in cardiac tamponade. Am J Cardiol. 1990;66:1487–91.
6. Spodick DH. Acute cardiac tamponade. N Engl J Med. 2003;349:684–90.
7. Dragoi L, Teijeiro-Paradis R, Douflé G. When is tamponade an echocardiographic diagnosis….Or is it ever? Echocardiography. 2022:1–6.
8. Beck C. Two cardiac compression triads. JAMA. 1935;104:714–7.
9. Gauchat HW, Katz LN. Observations on pulsus paradoxus (with special reference to pericardial effusions): I. Clinical. Arch Intern Med. 1924;33:350–70. https://doi.org/10.1001/archinte.1924.00110270071008.
10. Argulian E, Messerli F. Misconceptions and facts about pericardial effusion and tamponade. Am J Med. 2013;126:858–61. https://doi.org/10.1016/j.amjmed.2013.03.022.
11. Hamzaoui O, Monnet X, Teboul JL. Pulsus paradoxus. Eur Respir J. 2013;42:1696–705.
12. Gillam LD, Guyer DE, Gibson TC, et al. Hydrodynamic compression of the right atrium: a new echocardiographic sign of cardiac tamponade. Circulation. 1983;68:294–301. https://doi.org/10.1161/01.CIR.68.2.294.
13. Armstrong WF, Schilt BF, Helper DJ, et al. Diastolic collapse of the right ventricle with cardiac tamponade: an echocardiographic study. Circulation. 1982;65:1491–6.
14. Perez-Casares A, Cesar S, Brunet-Garcia L, Sanchez de Toledo H. Echocardiographic evaluation of pericardial effusion and cardiac tamponade. Front Paed. 2017;5:79.
15. Alerhand S, Carter JM. What echocardiographic findings suggest a pericardial effusion is causing tamponade? Am J Emerg Med. 2019;37:321–6.
16. Appleton CP, Hatle LK, Popp RL. Cardiac tamponade and pericardial effusion: respiratory variation in transvalvular flow velocities studied by Doppler echocardiography. J Am Coll Cardiol. 1988;11:1020–30.
17. Leeman DE, Levine MJ, Come PC. Doppler echocardiography in cardiac tamponade: exaggerated respiratory variation in transvalvular blood flow velocity integrals. J Am Coll Cardiol. 1988;11:572–8.
18. Jensen JK, Hvidfeldt Poulsen S, Mölgaard H. Cardiac tamponade: a clinical challenge. E-J Cardiol Pract. 2017;15(17). https://www.escardio.org/Journals/E-Journal-of-Cardiology-Practice/Volume-15/Cardiac-tamponade-a-clinical-challenge#:~:text=Cardiac%20tamponade%20results%20from%20an,cardiac%20filling%20and%20haemodynamic%20compromise. Accessed 4 July 2022.

19. Faehnrich JA, Noone RB, White WD, et al. Effects of positive pressure ventilation, pericardial effusion, and cardiac tamponade on respiratory variation in transmitral flow velocities. J Cardiothorac Vasc Anesth. 2003;17:45–50. https://doi.org/10.1053/jcan.2003.9.
20. Fowler NO. Cardiac tamponade. a clinical or echocardiographic diagnosis? Circulation. 1993;87:1738–41.
21. Sagrista-Sauleda J, Angel J, Sambola A, et al. Low-pressure cardiac tamponade: clinical and hemodynamic profile. Circulation. 2006;114:945–52. https://doi.org/10.1161/CIRCULATIONAHA.106.634584.
22. Ristic AD, Imazio M, Adler Y, et al. Triage strategy for urgent management of cardiac tamponade: a position statement of the European Society of Cardiology Working Group on Myocardial and Pericardial Diseases. Eur Heart J. 2014;35:2279–84. https://doi.org/10.1093/eurheartj/ehu217.
23. Tsang TSM, Oh JK, Seward JB. Diagnosis and management of tamponade in the era of echocardiography. Clin Cardiol. 1999;22:446–52.

Evaluation for Severe Hypovolemia

Max Rosenthal and Paul Mayo

Contents

6.1 Introduction – 60
6.1.1 The Physiology of Absolute Hypovolemia – 60
6.1.2 Causes of Severe Hypovolemia – 60
6.1.3 Ultrasonography for Diagnosis of Severe Hypovolemia – 61

6.2 Basic Echocardiography for Identification of Severe Hypovolemia – 61
6.2.1 Inferior Vena Cava – 61
6.2.2 Left Ventricular End Diastolic Area – 64
6.2.3 Advanced Critical Care Echocardiography – 65

6.3 Identification of the Source of Severe Hypovolemia – 66

References – 73

Supplementary Information The online version contains supplementary material available at https://doi.org/10.1007/978-3-031-32462-8_6.

© The Author(s), under exclusive license to Springer Nature Switzerland AG 2023
C. Robba et al. (eds.), *Basic Ultrasound Skills "Head to Toe" for General Intensivists*, Lessons from the ICU,
https://doi.org/10.1007/978-3-031-32462-8_6

Learning Objectives

- Describe the use of bedside ultrasonography for the assessment of severe hypovolemia.
- Explain the utility and limitations of inferior vena cava measurement for the detection of severe hypovolemia.
- Review the utility of left-ventricular end diastolic area measurement for detection of severe hypovolemia.
- Describe the utility of ultrasonography to identify cryptic blood loss in the patient with severe hypovolemia.

6.1 Introduction

Ultrasonography is useful for identification of severe hypovolemia, of which there are two general subcategories: absolute hypovolemia and relative hypovolemia. This chapter will review the utility of ultrasonography for assessment of severe hypovolemic shock, which, by definition, occurs with absolute hypovolemia.

6.1.1 The Physiology of Absolute Hypovolemia

Absolute hypovolemia occurs when there is a reduction of total circulating blood volume resulting in a sufficient reduction of the stressed volume of the system to result in hemodynamic failure. By Guytonian principle, reduction of the stressed volume results in a lowering of mean systemic filling pressure and consequent reduction in venous return and cardiac output. For clinicians who prefer Starling principle, severe hypovolemia results in a small left ventricular end diastolic volume because of the reduction in venous return, that results in a diminished stroke volume and cardiac output. With either explanation, the presence of shock due to severe hypovolemia is remedied with volume resuscitation, so its identification is a priority for the frontline intensivist.

6.1.2 Causes of Severe Hypovolemia

Loss of blood is associated with combined reduction of both red cell mass and plasma volume. The resulting hypovolemia is hazardous, as it is associated with a reduction of both cardiac output and reduction in arterial oxygen content, the net result being a major reduction in peripheral oxygen delivery. Ultrasonography has value in identifying causes of hemorrhagic shock (*vide infra*). In the initial phase of hemorrhagic hypovolemia, the hemoglobin level may not be reduced; as the loss of red cell mass and plasma volume occurs in balanced fashion. Typically, the intensive care unit (ICU) team will be able to resuscitate the plasma volume with the immediate use of crystalloid; so, by dilutional effect, the hemoglobin level falls until red cell transfusion is initiated.

Plasma volume reduction without blood loss may occur with major fluid losses due to diarrhea, emesis, and transcutaneous or respiratory fluid losses related to envi-

ronmental exposure or excessive urinary losses in conjunction with inadequate volume repletion. It may be associated with hemoconcentration, unlike hemorrhagic shock. This type of hypovolemia is often associated with the inability of the patient to maintain volume status over some period as may occur in the neglected nursing home patient, the obtunded patient with diabetic ketoacidosis or hyperosmolar state, the victim of exposure to a hot environment with limited access to water or in remote and/or under-resourced environments.

6.1.3 Ultrasonography for Diagnosis of Severe Hypovolemia

In establishing the cause and therefore treatment of severe hypovolemia; the intensivist considers the history, physical examination, and laboratory values to be of primary importance with ultrasonography deployed as an imaging modality to confirm diagnosis, to exclude additional diagnosis, and to guide management. This reminds the clinician that critical care ultrasonography (CCUS) is not used in vacuo, but is integrated into the other aspects of clinical assessment. Unlike consultative ultrasonography or echocardiography, the intensivist is responsible for all aspects of image acquisition, image interpretation, and immediate application of the results at the point of care. Severe hypovolemic shock is an emergency, so the ultrasonography examination cannot be hampered by the inevitable delays associated with consultative imaging.

6.2 Basic Echocardiography for Identification of Severe Hypovolemia

Basic echocardiography (defined as 2-D imaging of the parasternal long axis, midventricular parasternal short axis, apical four chamber, subcostal long axis, and IVC long axis views) may be used to detect fluid responsiveness due to severe hypovolemia.

6.2.1 Inferior Vena Cava

Assessment of the inferior vena cava (IVC) may be helpful in identifying the patient who is fluid responsive, i.e., if volume is given to the patient who is fluid responsive, their cardiac output, by definition, will increase. Identification of fluid responsiveness does not necessarily mean that the patient is severely hypovolemic, but the patient who has severe hypovolemia will be volume responsive.

Initial studies focused on respirophasic variation of the IVC diameter as a marker of fluid responsiveness. They were performed on patients on mechanical ventilatory support without any spontaneous respiratory effort while on a tidal volume of at least 8 cc/kg ideal body weight. Depending on the formula used, respirophasic variation of IVC diameter of 12 or 18% were thresholds that predicted fluid responsiveness [1, 2]. More recently, Vignon et al. found that the IVC could be visualized in 78% of subjects and detected fluid responsiveness with a sensitivity of 55% and specificity

of 70% when using a cut off in respiratory variation of 8% [3]. In this study, the receiver operating characteristic curve area under the curve was an unimpressive value of 0.70. For spontaneously breathing patients, Airapetian et al. showed that a collapsibility of the IVC of >42% on inspiration had a high specificity of 97%, a positive predictive value of 90% but a low sensitivity of 31% [4].

Respirophasic variation of IVC diameter has problems associated with the measurement. The IVC is susceptible to respiratory translational artifact where the structure is moved through the tomographic plane when inspiratory movement of the diaphragm moves the underlying liver and IVC out of the tomographic plane. The examiner mistakes a change in diameter as a true change when, in fact, it is an artifact from the effect of ventilator cycling (Fig. 6.1, Video 6.1).

The measurement of the diameter change is problematic, as the numerical value of the change may be on the order of a few millimeters. This introduces the possibility of confirmation bias on the part of the operator who is making the measurement. Intrathoracic pressures are highly variable in the critically ill patient on ventilatory support and when breathing spontaneously, which will influence IVC variation independent of fluid responsiveness. The concept that there is a single cutoff point that defines fluid responsiveness is a simplistic notion that has no bearing on real life physiology, where values occur across a continuum.

Given the problems with respirophasic diameter variation of the IVC, the absolute size of the IVC measured at end exhalation may be a better alternative. Vieillard-Baron et al. reported that, if the absolute end expiratory diameter was less than 1.3 cm, there was an 80% chance of fluid responsiveness, while if the diameter was

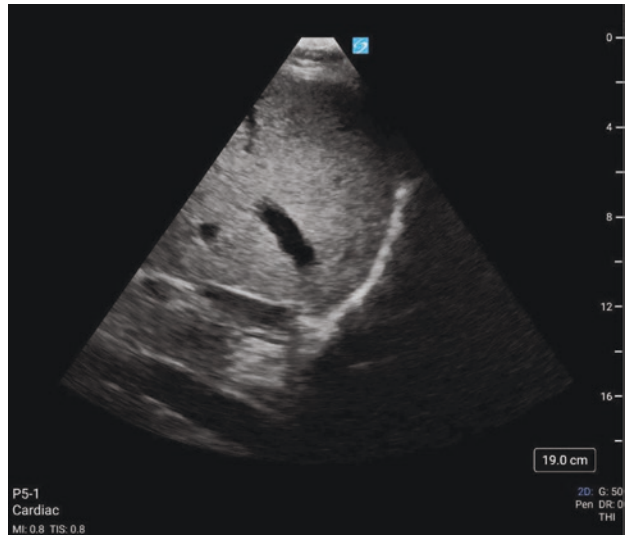

Fig. 6.1 Translational artifact of the IVC. This image was recorded with a 3.5 MHz phased array transducer in the cardiac preset. The apparent diameter change of the IVC is due to movement of the IVC lumen out of the tomographic plane. One could mistakenly assume a significant change in diameter of the IVC during the respiratory cycle

greater than 2.5 cm, there was an 80% chance of fluid non-responsiveness [5]. This conforms to the concept of "gray zone analysis" [6] where intermediate values of IVC diameter are considered indeterminate, but values outside of 1.3 and 2.5 cm become increasingly predictive. Elevation of intra-abdominal pressure invalidated the measurement of IVC diameter [5] (■ Figs. 6.2, 6.3, and 6.4).

Respirophasic variation of the superior vena cava is a well-validated method of detecting fluid responsiveness [7]. As this measurement requires insertion of a TEE probe, it is not within the definition of basic echocardiography. In summary, identification of a small diameter IVC in a hypotensive patient is consistent with severe hypovolemia and would indicate for volume resuscitation with serial follow up of IVC diameter to observe for response.

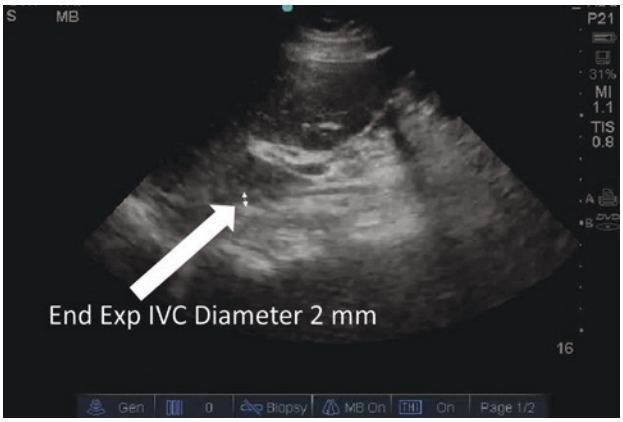

■ **Fig. 6.2** Small diameter IVC. This image was recorded using a 3.5 MHz phased array transducer in the cardiac preset. The diameter of the IVC is 2 mm, which is consistent with severe hypovolemia in the appropriate clinical setting

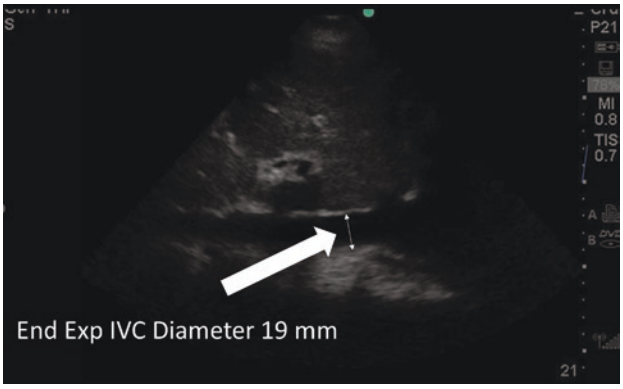

■ **Fig. 6.3** Indeterminate IVC. This image was recorded using a 3.5 MHz phased array transducer in the cardiac preset. The diameter of the IVC is 19 mm, which is in the indeterminate range for assessment of volume responsiveness

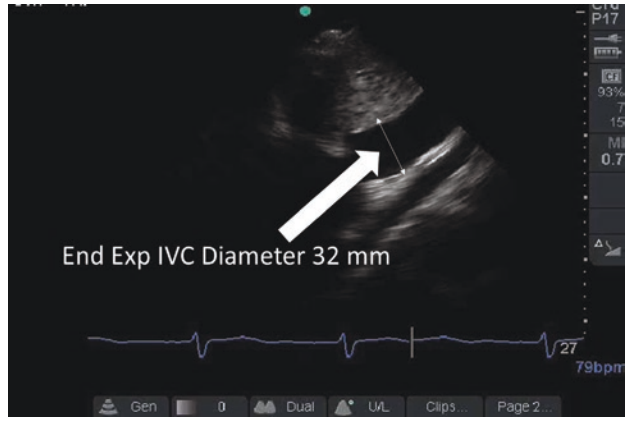

6

Fig. 6.4 Large diameter IVC. This image was recorded using a 3.5 MHz phased array transducer in the cardiac preset. The diameter of the IVC is 32 mm, which is not consistent with severe hypovolemia

6.2.2 Left Ventricular End Diastolic Area

A standard view of the basic echocardiography examination is the parasternal short-axis view at mid-ventricular level. If the operator freezes the image at end diastole, planimetry function allows an accurate measurement of the end diastolic area of the left ventricle (LVEDA). This area may have utility for identification of severe hypovolemia. Most studies of this parameter have been performed with TEE, but there is no a priori reason that a good quality transthoracic echocardiography image would not give equivalent results providing the endomyocardial border is well visualized. Serial measurement of LVEDA track left ventricular preload during graded blood removal and reinfusion [8, 9]. The reference value in adults for LVDEA is 23 ± 4 cm^2 [10]. However, in patients undergoing cardiac surgery or in patients with septic shock, the absolute value of LVEDA is not a good predictor of fluid responsiveness. The measurement may have relevance for identification of severe hypovolemia where the LVEDA is less than 10 cm^2 or less than 6 cm^2/m^2 [11]. A very small LVEDA should be regarded as specific for identification of severe hypovolemia, but not sensitive. End systolic effacement of the left ventricle in of itself should not be regarded as consistent with absolute hypovolemia, particularly if associated with a normal left LVEDA; as left ventricular afterload and contractility are factors that may influence the degree of ventricular emptying [12]. An end systolic left ventricular cavity obliteration in association with a small LVEDA would indicate a high probability of severe hypovolemia. In assessing LVEDA in the patient with hypotension, the intensivist checks for an alternate cause to reduced LVEDA such as severe dilation of the right ventricle with impairment of left ventricular diastolic filling due to ventricular interdependence. In this case, volume resuscitation is strongly contraindicated (Figs. 6.5 and 6.6, Videos 6.2 and 6.3).

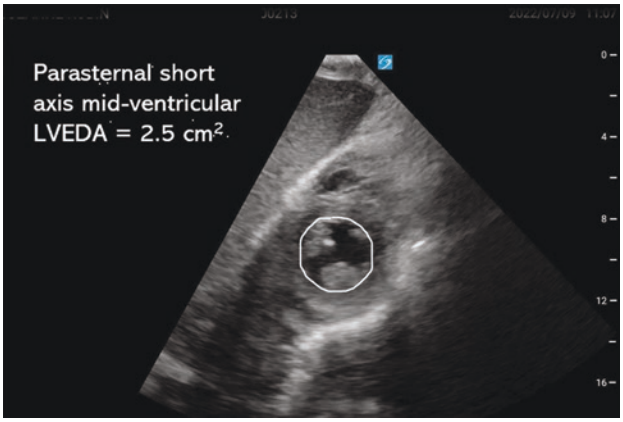

Fig. 6.5 Low LVEDA. This parasternal long-axis view was recorded using a 3.5 MHz phased array transducer in the cardiac preset. It demonstrates a low LVEDA which is consistent with severe hypovolemia. This LVEDA can be measured with planimetry off a frozen end diastolic image. The patient presented with a large upper gastrointestinal bleed. The study was performed before the patient had received volume resuscitation

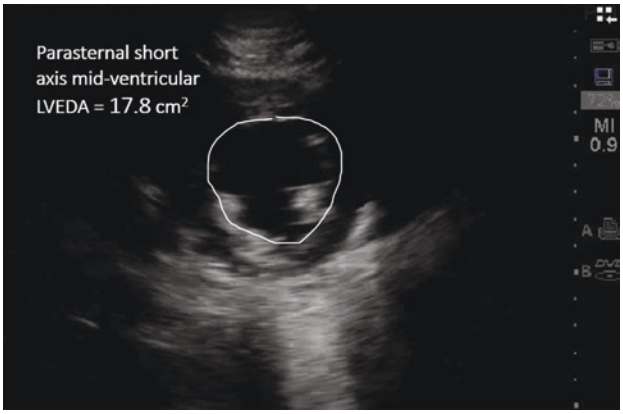

Fig. 6.6 Normal LVEDA. This parasternal long axis view was recorded using a 3.5 MHz phased array transducer in the cardiac preset. It demonstrates a normal LVEDA which is not consistent with severe hypovolemia. This LVEDA can be measured with planimetry off a frozen end diastolic image. In this case, the patient had septic shock with relative hypovolemia that was managed with early use of norepinephrine and limited volume resuscitation

6.2.3 Advanced Critical Care Echocardiography

Absolute hypovolemia with shock is a medical emergency. The combination of clinical assessment with measurement of end expiratory IVC diameter and LVEDA allows for rapid decision-making regarding volume resuscitation. The basic echocardiography examination also allows the intensivist to evaluate for the presence of

coexisting causes for shock that may complicate management. There are a variety of methods that can be used to identify fluid responsiveness that utilize advanced critical care echocardiography with transthoracic echocardiography and TEE. These include respirophasic variation of SVC diameter, respirophasic variation of left ventricular outflow tract velocity time integral, respirophasic variation of peripheral arterial Doppler signal, and a variety of methods that use the ventilator as a testing device. While these techniques are valuable for identification of fluid responsiveness, they are not immediately useful for identification of severe hypovolemia which requires immediate identification and treatment using basic echocardiography technique.

6.3 Identification of the Source of Severe Hypovolemia

The cause of severe hypovolemia may be apparent by simple history and physical examination. Profound hypovolemia due to environmental exposure without access to water, massive rectal bleeding, or major bleeding from lacerating or avulsing injury are readily diagnosed without need for immediate ultrasonography examination. Ultrasonography is useful where there is clinical evidence of severe hypovolemia supported by characteristic findings by the basic echocardiography examination, but where the cause of the hypovolemia is not immediately obvious to the intensivist. Ultrasonography is then used to search for cryptic sources of bleeding using a whole-body ultrasonography approach. Several sources are possible, with the examination sequence determined by the clinical presentation of the patient. Possible sources include the thoracic, peritoneal, retroperitoneal, bladder, gastrointestinal, and soft tissue compartment, all of which are feasible targets for rapid ultrasonography examination (see Images and Videos).

Blood within a body cavity has some characteristic features. Fresh blood may be relatively hypoechoic or exhibit a pattern of homogenous echogenicity. A mobile thrombus may be visible within the collection of anechoic fluid. A sedimentation effect may occur. Within the hematoma, red cells settle to a dependent position due to gravitational effect yielding a linear demarcation between the non-dependent plasma and the dependent red blood cells. This has been termed the "hematocrit sign" (◘ Fig. 6.7, ◘ Video 6.4). Gastric blood frequently appears as a heterogeneously echogenic collection within the fundus or the antrum. Early identification of major internal bleeding in the patient with severe hypovolemic shock allows the ICU team to consider therapeutic intervention while resuscitation is ongoing.

The reader is referred to the video collection for examples of blood collections that were associated with severe hypovolemia and identified with ultrasonography (◘ Figs. 6.8, 6.9, 6.10, 6.11, 6.12, 6.13, 6.14, 6.15, 6.16, 6.17, and 6.18. ◘ Videos 6.5, 6.6, 6.7, 6.8, 6.9, 6.10, 6.11, 6.12, 6.13, 6.14, and 6.15).

Fig. 6.7 Hemoperitoneum with hematocrit sign. This image was recorded using a 3.5 MHz phased array transducer in the abdominal preset with the probe placed in the right flank area with the tomographic plane in longitudinal orientation. There is a large intraperitoneal fluid collection with a distinct linear boundary between anechoic and echoic fluid that represents a sedimentation effect termed the "hematocrit sign" that is strongly suggestive of hemoperitoneum. This occurs in the patient who is immobile, as patients' movement disrupts sedimentation findings. The patient presented with undifferentiated hypotension. The bleeding occurred due to a spontaneous splenic rupture

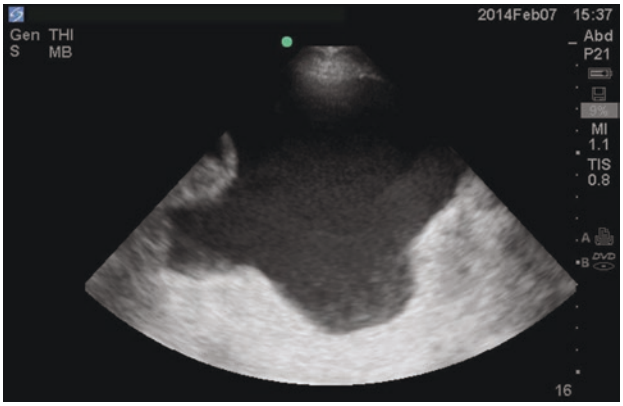

Fig. 6.8 Hemoperitoneum. This image was recorded using a 3.5 MHz phased array transducer in the abdominal preset with the probe placed in the left flank area. There is a large intraperitoneal fluid collection surrounded by loops of bowel. The fluid collection is anechoic in the near field and is more echoic in the dependent region due to a gravitational sedimentation effect consistent with a hemoperitoneum. The patient presented with hypotension several hours after a therapeutic paracentesis where the team had neglected to scan the proposed needle trajectory with a vascular probe. Following resuscitation and a successful interventional radiology procedure, a later scan showed an aberrantly positioned abdominal vessel at the site of the initial paracentesis

Fig. 6.9 Hemothorax. This image was recorded using a 3.5 MHz phased array transducer in the abdominal preset with the probe placed in the lower lateral thoracic right mid-axillary line with the tomographic plane in longitudinal orientation. There is a large homogenously echogenic pleural effusion that is consistent with a hemothorax. The patient presented with undifferentiated hypotension following a fall that resulted in several rib fractures. Chest tube insertion showed a hemothorax

Fig. 6.10 Hemothorax with stranding. This image was recorded using a 3.5 MHz phased array transducer in the abdominal preset with the probe placed in the lower lateral thoracic right mid-axillary line with the tomographic plane in longitudinal orientation. The patient presented with hypotension 24 h following an outpatient diagnostic thoracentesis. This delay may explain the presence of the stranding, which would not be typical of an acute hemothorax. Chest tube insertion showed a hemothorax

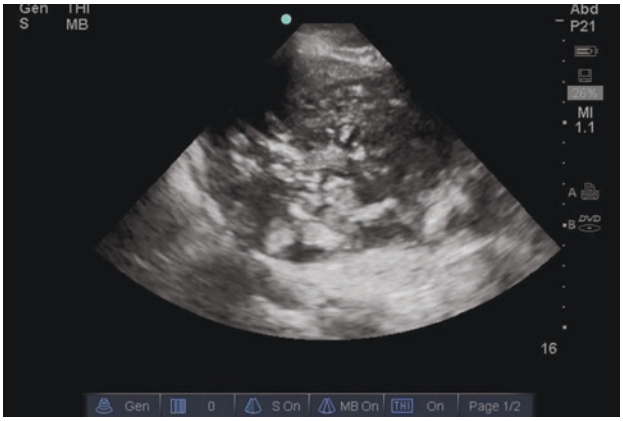

Fig. 6.11 Blood in gastric fundus. This image was recorded using a 3.5 MHz phased array transducer in the abdominal preset with the probe placed in the left lower lateral thoracic posterior axillary line with the tomographic plane in longitudinal orientation. With the spleen utilized as an ultrasonography window, there is a large heterogeneously echogenic collection within the stomach that is consistent but not diagnostic of gastric blood. In the author's experience, gastric blood is often heterogeneously echogenic compared to blood in other body compartments. This may be because of the digestive function of the stomach. The patient presented with undifferentiated hypotension. Endoscopy showed an esophageal variceal bleeding source

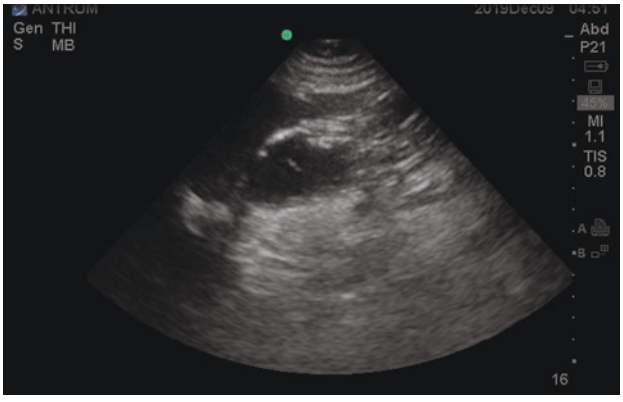

Fig. 6.12 Blood in gastric antrum. This image was recorded using a 3.5 MHz phased array transducer in the abdominal preset with the probe placed in the subcostal right paramedian area with the tomographic plane in longitudinal orientation. There is blood in the gastric antrum. The image is from the same patient as in Fig. 6.11

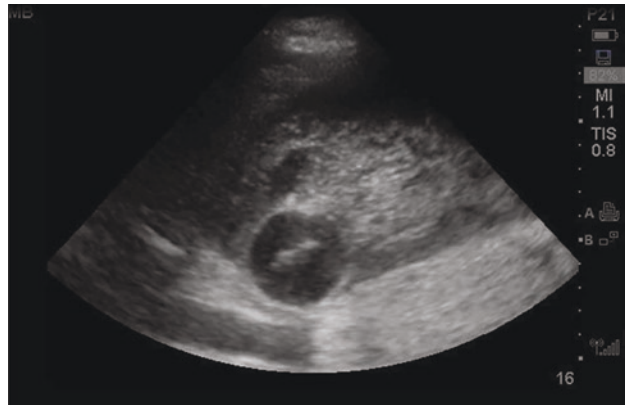

Fig. 6.13 Blocked Sengstaken-Blakemore tube with gastric blood. This image was recorded using a 3.5 MHz phased array transducer in the abdominal preset with the probe placed in the left lower lateral thoracic posterior axillary line with the tomographic plane in longitudinal orientation. The image is from the same patient as in fig. 6.11 and 6.12. There is gastric blood within the fundus with a well-positioned gastric tamponade balloon. Following initial placement of the esophageal tamponade device (Sengstaken-Blakemore tube), the esophageal bleeding stopped. Subsequently, the patient became hypotensive, but no blood was aspirated from the gastric drainage channel. Ultrasonography confirmed renewed esophageal bleeding that was not detected due to a blockage of the gastric aspiration channel

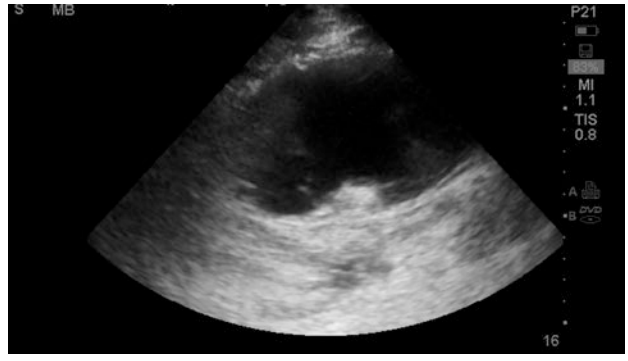

Fig. 6.14 Retroperitoneal hematoma. This image was recorded using a 3.5 MHz phased array transducer in the abdominal preset with the probe placed in the left lower posterolateral flank area with the tomographic plane in longitudinal orientation. There is a fluid collection which is primarily anechoic with areas of homogenous echogenicity consistent with a retroperitoneal hematoma. The patient presented with undifferentiated hypotension and history of chronic anticoagulation. Further evaluation confirmed the presence of a retroperitoneal hematoma that was controlled with a successful interventional radiology procedure

Fig. 6.15 Bladder hematoma. This image was recorded using a 3.5 MHz phased array transducer in the abdominal preset with the probe placed in the midline suprapubic area with the tomographic plane in transverse orientation. There is a large amount of heterogeneously echogenic material within the distended bladder consistent with a bladder hematoma. The inflated foley catheter balloon is seen within the hematoma. The patient presented with undifferentiated hypotension following renal biopsy. No hematuria was detected due to blockage of the bladder catheter. Bladder irrigation was performed under direct ultrasonography control with removal of the hematoma

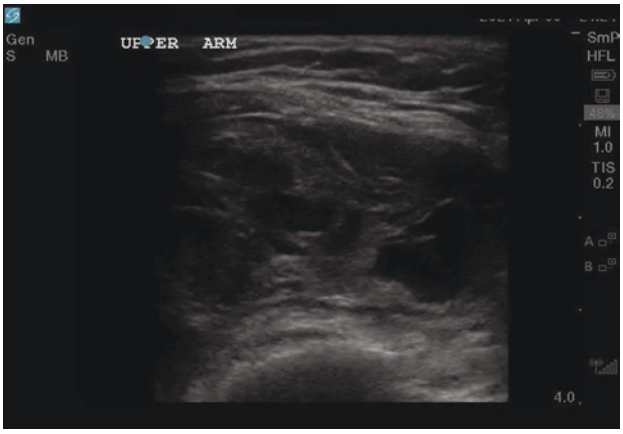

Fig. 6.16 Soft tissue hematoma. This image was recorded using a 7.5 MHz linear transducer over one of multiple ecchymotic areas on the extremities and torso. There is a heterogeneously echogenic area consistent with a subcutaneous hematoma. The patient presented with hypotension following a violent altercation. No other site of blood loss was identified and there was good response to blood transfusion

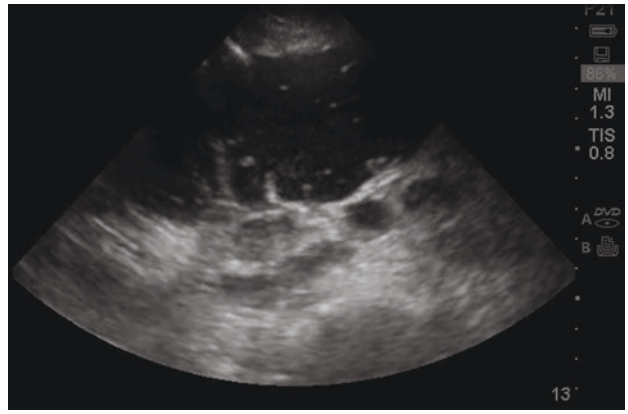

Fig. 6.17 Fluid in the lower GI tract. This image was recorded using a 3.5 MHz phased array transducer in the abdominal preset with the probe placed in the lateral left flank area with the tomographic plane in longitudinal orientation. There are multiple loops of fluid-filled bowel. The patient presented with unexplained hypotension. The final diagnosis was severe gastroenteritis

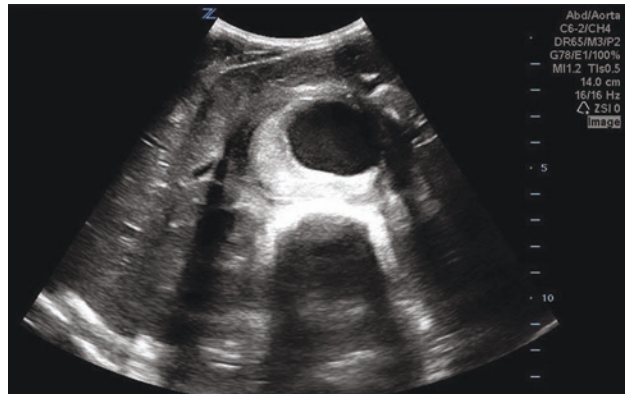

Fig. 6.18 Periaortic hematoma. This image was recorded using a 3.5 MHz curvilinear transducer with the probe placed in the mid-abdominal midline with the tomographic plane in transverse orientation. There is an aortic aneurysm with periaortic hematoma. The patient presented with undifferentiated hypotension. Emergency surgery was performed with successful aortic graft placement

Summary

Ultrasonography is useful for the identification of severe hypovolemia and for assessing hypovolemia due to cryptic blood loss.

Take-Home Messages

- Ultrasonography can be useful in detecting severe hypovolemia.
- In assessment of the patient with shock, a small IVC and a reduced end diastolic area of the left ventricle is consistent with severe hypovolemia.
- Identification of severe hypovolemia mandates fluid resuscitation and a search for the cause of hypovolemia.
- Ultrasonography has utility for the identification of cryptic blood loss in the patient with severe hypovolemia.

References

1. Vieillard-Baron A, Evrard B, Repessé X, et al. Limited value of end-expiratory inferior vena cava diameter to predict fluid responsiveness impact of intra-abdominal pressure. Intensive Care Med. 2018;44:197–203.
2. Leung JM, Levine EH. Left ventricular end-systolic cavity obliteration as an estimate of intraoperative hypovolemia. Anesthesiology. 1994;81:1102–9.
3. Vieillard-Baron A, Chergui K, Rabiller A, Peyrouset O, Page B, Beauchet A, Jardin F. Superior vena caval collapsibility as a gauge of volume status in ventilated septic patients. Intensive Care Med. 2004;30:1734–9.
4. Cheung AT, Savino JS, Weiss SJ, Aukburg SJ, Berlin JA. Echocardiographic and hemodynamic indexes of left ventricular preload in patients with normal and abnormal ventricular function. Anesthesiology. 1994;81:376–87.
5. van Daele ME, Trouwborst A, van Woerkens LC, Tenbrinck R, Fraser AG, Roelandt JR. Transesophageal echocardiographic monitoring of preoperative acute hypervolemic hemodilution. Anesthesiology. 1994;81:602–9.
6. Barbier C, Loubières Y, Schmit C, Hayon J, Ricôme J-L, Jardin F, Vieillard-Baron A. Respiratory changes in inferior vena cava diameter are helpful in predicting fluid responsiveness in ventilated septic patients. Intensive Care Med. 2004;30:1740–6.
7. Duwat A, Zogheib E, Guinot P, Levy F, Trojette F, Diouf M, Slama M, Dupont H. The gray zone of the qualitative assessment of respiratory changes in inferior vena cava diameter in ICU patients. Crit Care. 2014;18:R14.
8. Vignon P. Preload and fluid responsiveness. 2020. p. 141–151.
9. Vieillard-Baron A, Prin S, Chergui K, Dubourg O, Jardin F. Hemodynamic instability in sepsis: bedside assessment by doppler echocardiography. Am J Respir Crit Care Med. 2003;168:1270–6.
10. Vignon P, Repessé X, Bégot E, Léger J, Jacob C, Bouferrache K, Slama M, Prat G, Vieillard-Baron A. Comparison of echocardiographic indices used to predict fluid responsiveness in ventilated patients. Am J Respir Crit Care Med. 2017;195:1022–32.
11. Airapetian N, Maizel J, Alyamani O, et al. Does inferior vena cava respiratory variability predict fluid responsiveness in spontaneously breathing patients? Crit Care. 2015;19:400.
12. Feissel M, Michard F, Faller J-P, Teboul J-L. The respiratory variation in inferior vena cava diameter as a guide to fluid therapy. Intensive Care Med. 2004;30:1834–7.

Evaluation for Acute, Severe Left-Sided Valvulopathy

Alexander Astell, Erica Clarke Whalen and Robert T. Arntfield

Contents

7.1 Introduction – 76

7.2 General Considerations for Valve Interrogation – 76

7.3 Emergency Lesions – 78
7.3.1 Aortic Regurgitation – 78
7.3.2 Mitral Regurgitation – 80
7.3.3 Left Ventricular Outflow Tract Obstruction – 83

7.4 Stenotic Lesions – 85
7.4.1 Aortic Stenosis in the Critically Ill Patient – 85
7.4.2 Mitral Stenosis in the Critically Ill Patient – 86

References – 88

Supplementary Information The online version contains supplementary material available at https://doi.org/10.1007/978-3-031-32462-8_7.

© The Author(s), under exclusive license to Springer Nature Switzerland AG 2023
C. Robba et al. (eds.), *Basic Ultrasound Skills "Head to Toe" for General Intensivists*, Lessons from the ICU,
https://doi.org/10.1007/978-3-031-32462-8_7

Learning Objectives

- Develop a simplified approach to identifying clinically important valvular lesions.
- Understand the advantages and limitations of different ultrasound techniques in valvular assessment.
- Implement appropriate management strategies based on specific valvular pathologies.

7.1 Introduction

With critical care echocardiography (CCE) now standard of care for the assessment of critically ill patients [1, 2], it is incumbent on intensivists to have fluency in the assessment of acute, severe left-sided (aortic and mitral) valvulopathy. In addition to identifying the presence or absence of such pathology, the intensivist must also be able to integrate relevant findings into a hemodynamic management plan.

The importance of identifying left-sided regurgitant lesions is highlighted by the high mortality rate of patients with severe lesions, if left untreated [3, 4]. Accordingly, this chapter focuses primarily on the identification of acute regurgitant lesions and their management. It is worth noting that chronic left-sided valvular lesions can also impact the hemodynamic management of critically ill patients and we address the findings and management of those lesions here as well.

The primary lesions of importance for the intensivist are acute, severe aortic and mitral regurgitation and left ventricular outflow tract (LVOT) obstruction. Beyond the endorsed 2D and color Doppler techniques for basic CCE [2, 5], we have further included some practical spectral Doppler quantification methods for the motivated user, while excluding the more laborious quantitative measurements [6, 7] that rarely add to the management of critically ill patients [8].

There are many valvular scenarios that stretch beyond the knowledge of the general intensivist and we encourage consultation with specialists in echocardiography to help. In particular, patients with prosthetic valves and adult congenital valvular concerns generally benefit from specialist level knowledge [9].

7.2 General Considerations for Valve Interrogation

As incidental valvular pathology is quite common in the ICU setting, it is valuable to pose the question: "Is this patient critically-ill *because of* this specific valvular lesion or are they critically-ill *with* this valvular lesion?" This framework is helpful for many abnormalities in the ICU and we have found it particularly helpful for non-experts when identifying and managing valvular findings.

A descriptive framework for assigning hemodynamic importance can divide valvular pathology into devastating, important, and incidental (Fig. 7.1). Devastating lesions are those considered to be acute and likely the culprit of ongoing shock (i.e. acute mitral regurgitation secondary to papillary muscle rupture), where important

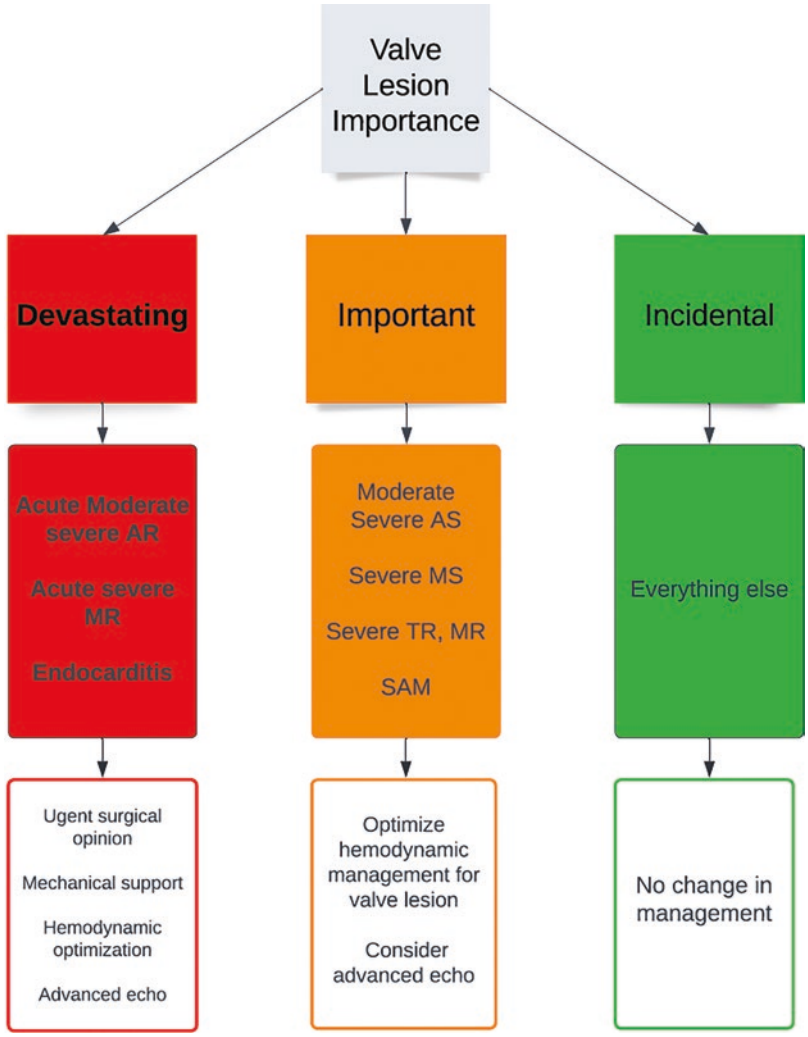

Fig. 7.1 Algorithm for assigning importance of valvular lesions. *SAM* systolic anterior motion (of the mitral valve leaflet); *AR* aortic regurgitation; *MR* mitral regurgitation; *AS* aortic stenosis; *TR* tricuspid regurgitation. (Original to authors)

lesions are those that may impact hemodynamic management of the critically ill, but are secondary to the admission pathology (i.e. chronic, severe aortic stenosis in the setting of septic shock). Incidental valvular lesions (i.e. mild aortic stenosis) rarely impact management within the ICU setting and therefore are not discussed in this chapter.

7.3 Emergency Lesions

7.3.1 Aortic Regurgitation

7.3.1.1 Etiology of Aortic Regurgitation

Aortic regurgitation (AR) arises from a pathology involving either the aortic valve or aortic root. Acute AR can be caused by leaflet perforation or prolapse (▣ Video 7.1) from infective endocarditis, flail leaflet due to blunt thoracic trauma, or acute aortic dissection. Chronic AR can be caused by aortic root dilation, age-related valvular degeneration, inflammatory states affecting the aorta or valve leaflets, congenitally acquired connective tissue disease, or a bicuspid aortic valve [6].

7.3.1.2 Detection of Aortic Regurgitation

Assessment for AR starts with a 2D examination of the aortic valve (AV) and root for obvious abnormalities in structure, as mentioned above. Vegetations can manifest on a spectrum, from areas of valve thickening to complete independent mobility, and are most typically found on the ventricular side of the valve [10]. Prolapse may be apparent and by itself usually denotes severe disease. In severe AR, M-mode of the mitral valve (MV) may illustrate decreased end point septal separation (EPSS) as the regurgitant aortic jet prevents opening of the anterior MV in diastole.

Color Doppler offers the most practical method for determination of AR at the bedside, demonstrating regurgitant flow in the LVOT during diastole. Color Doppler should maintain a Nyquist limit between 50 and 60 cm/s for all left-sided lesions to avoid overestimation of regurgitant flows. In the parasternal long-axis (PLAX) view, a regurgitant jet width/LVOT ratio >65% suggests severe disease (▣ Video 7.2). A PLAX view zoomed to the AV is the appropriate view to measure the vena contracta width, the narrowest point of the jet as the blood passes through the regurgitant orifice, with a measurement >6 mm being severe (▣ Fig. 7.2).

The apical 5-chamber (A5) and apical 3-chamber (A3) views allow for near parallel alignment with the regurgitant jet and are thus amenable to spectral Doppler interrogation with continuous-wave (CW) technique (as the speed of regurgitant jets are too fast for pulsed-wave). Pressure half time (PHT) is defined as the time interval between peak pressure in early-diastole to the time at which the pressure is half that amount. A PHT <200 m/s denotes severe disease (▣ Fig. 7.3). As the PHT is influenced by the transvalvular gradient and compliance of the LV, chronic, severe AR may have PHT measurements >200 m/s, reflecting the compensation of the LV over time. Similarly, patients receiving afterload reduction or with severe diastolic dysfunction (and consequent low LV compliance) may have a PHT that is not in keeping with their degree of valvular failure.

As the severity of the lesion increases, diastolic flow will diminish and then reverse in the aorta. Evidence of holodiastolic flow reversal in the proximal abdominal aorta, imaged from the subcostal window using pulsed-wave (PW) Doppler, is specific but insensitive of severe disease (▣ Fig. 7.4, ▣ Table 7.1).

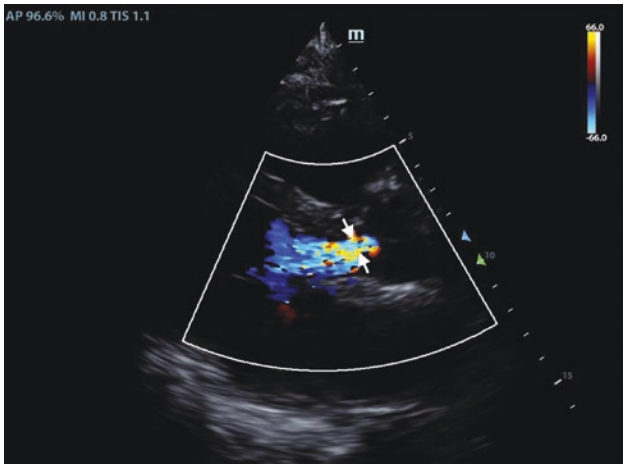

Fig. 7.2 Aortic regurgitation vena contracta measurement. The arrows highlight the outer edges of the regurgitant jet at its narrowest point. Measuring between determines the vena contracta. (Original to authors)

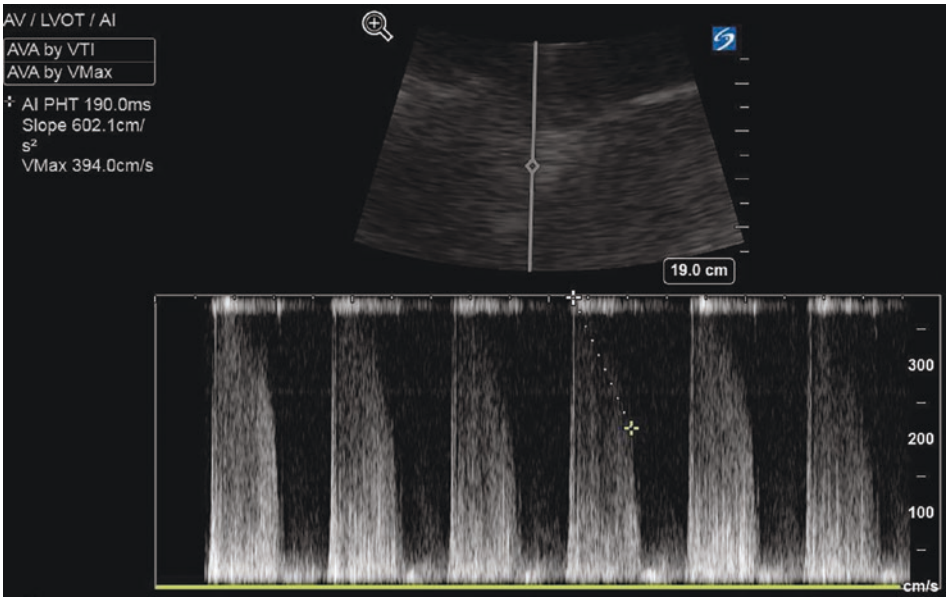

Fig. 7.3 Aortic regurgitation pressure half time. The slope of the regurgitant flow waveform is measured from just after its peak to the end of diastole. (Original to authors)

7.3.1.3 Management

Identification of acute, severe aortic regurgitation requires consultation with a cardiac surgeon to restore integrity to, or replace, the valve. The timing and operative approach will vary depending on the cause and other patient factors. Pending surgi-

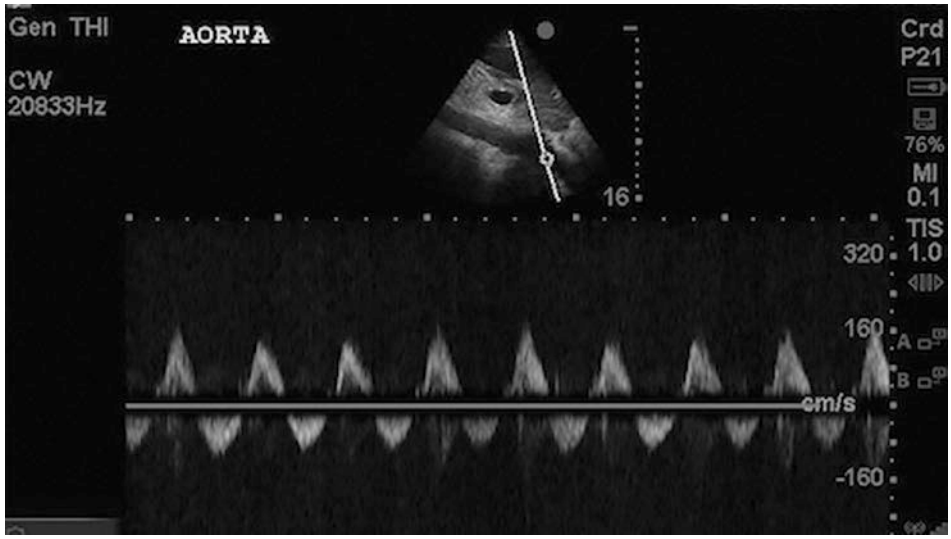

Fig. 7.4 Aortic regurgitation aortic flow reversal. Holodiastolic flow reversal captured in the proximal abdominal aorta is highly specific for severe aortic regurgitation. (Original to authors)

Table 7.1 Severe aortic regurgitation findings

Flail valve
Vena contracta width >0.6 cm
Central jet comprising >65% of LVOT
Pressure half time <200 ms
Prominent holodiastolic flow reversal in the descending aorta
(Original to authors)

cal or mechanical intervention, hemodynamic optimization of cardiac output can be achieved by maintaining a faster heart rate, while lowering afterload to reduce the time and gradient for the regurgitation.

7.3.2 Mitral Regurgitation

7.3.2.1 Etiology of Mitral Regurgitation

Acute severe mitral regurgitation (MR) most commonly arises from intrinsic valvular pathology, such as flail leaflet or perforation due to infective endocarditis, chest trauma leading to compromised valve integrity, and acute chordal rupture in the setting of fibrosed or calcified subvalvular disease (myxomatous disease, rheumatic disease, etc.) [10, 11]. Less commonly, severe MR can result from restricted leaflet movement from regional wall motion abnormalities in the setting of myocardial ischemia or Takotsubo cardiomyopathy [12]. In the ICU setting, papillary muscle rup-

ture is a rare but important consideration in unstable patients with right coronary artery (RCA) infarcts, given the single blood supply to the posteromedial papillary muscle and the associated high mortality from consequent cardiogenic shock [4, 13].

Secondary or "functional" MR, which is typically chronic in nature, results from the dilation of the LV and compromised coaptation of the anterior and posterior leaflets during systole.

7.3.2.2 Detection of Mitral Regurgitation

2D assessment of the mitral valve utilizes the PLAX, apical 4-chamber (A4), and subcostal views. Morphological assessment should assess the opening of the MV leaflets during diastole as well as the coaptation of the anterior and posterior leaflets during systole. The presence of flail segments, loss of coaptation, or tenting of the leaflets are specific for severe regurgitation [6] (▶ Video 7.3); however, these findings have a low sensitivity and their absence does not rule out mitral regurgitation. Other pathologic findings include leaflet thickening, restricted movement, calcification, and the presence of vegetations.

Assessment of left-sided chamber size is important in assessing the chronicity of MR. A dilated LV can cause functional MR through chordal stretch and apical leaflet tenting, which, when seen with a dilated LA, suggests that the regurgitation is chronic and unlikely the primary cause of shock in the critically ill [14]. Acute MR is usually associated with normal LV and LA size, on 2D assessment. This finding is associated with a sudden change in chamber pressures and lack of chamber compliance and results in pulmonary edema and cardiovascular collapse [15].

Color Doppler is the main method for rapid detection of mitral regurgitation at the bedside and, with optimal settings and technique, is highly specific and sensitive [10] (▶ Video 7.4). There are multiple semiquantitative color Doppler measurements that determine the severity of MR [6]. The origin and direction of the MR jet with color Doppler can provide insight into the mechanism of mitral regurgitation when used in conjunction with 2D findings. MR caused by excessive leaflet movement will cause a regurgitant jet that is opposite to the pathologic leaflet, while a restricted leaflet will create a jet in the same direction as the pathological leaflet.

Jet area determination can be done in the PLAX and A4 views. MR is deemed severe if the jet area occupies >50% of the left atrium (▶ Video 7.5). It is important to note that spatial mapping of the jet area in the left atrium has pitfalls associated with it and can be influenced by LA size, LV function, and the loading conditions of the heart. As with AR, the vena contracta can be utilized and is best measured in the PLAX view, though A4 views are acceptable if the PLAX views are inadequate [10]. A vena contracta that is ≥0.7 cm is considered severe (▶ Fig. 7.5). The presence of an eccentric jet that tracks along the side-wall of the LA, described by the Coanda effect (▶ Video 7.6), typically reflects severe MR.

Spectral Doppler assessment of MR includes both PW and CW Doppler and requires additional training in advanced critical care echocardiography [16]. For clinicians with understanding of spectral Doppler, the most practical application for determining severity of MR at the bedside is the use of CW Doppler comparing the density of retrograde signal in systole compared to the antegrade signal in diastole (▶ Fig. 7.6). The presence of systolic flow reversal in the pulmonary veins when interrogated by pulse wave Doppler is another quantitative measurement that classifies the MR as severe (▶ Table 7.2).

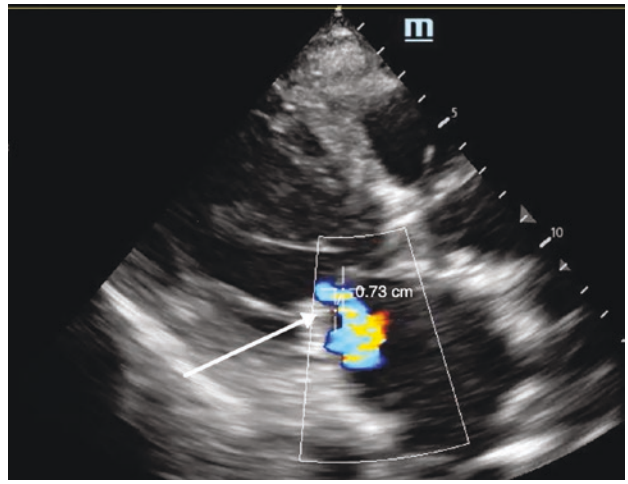

7

Fig. 7.5 Mitral regurgitation vena contracta measurement. The outer edges of the regurgitant jet are measured at their narrowest point to determine the vena contracta. (Original to authors)

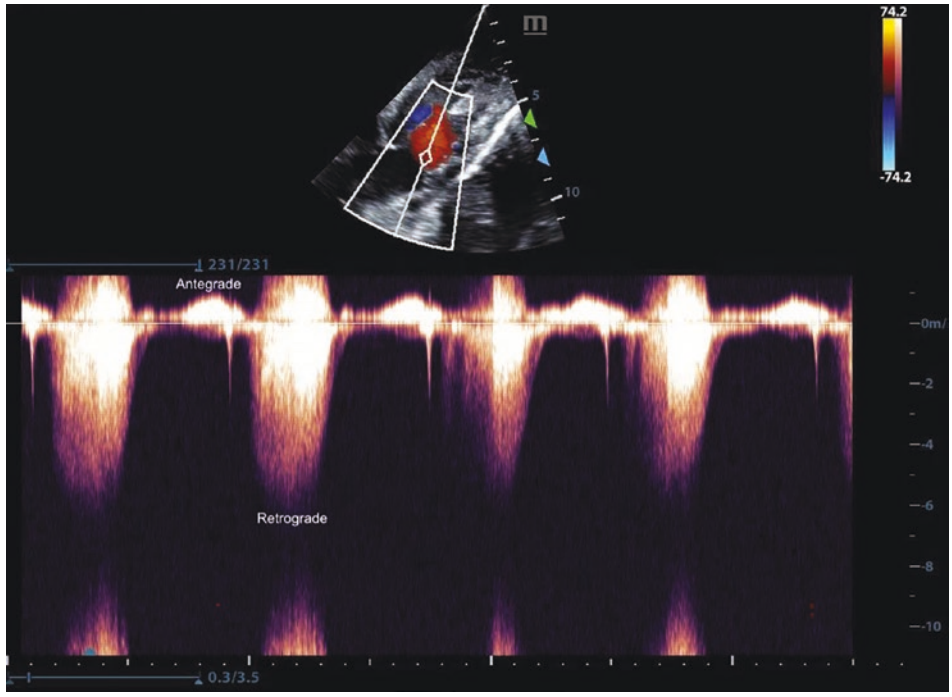

Fig. 7.6 Mitral regurgitation signal intensity analysis. Comparison of the antegrade and retrograde flow through the mitral valve demonstrates a similar signal intensity, suggestive of severe mitral regurgitation. (Original to authors)

Table 7.2 Severe mitral regurgitation findings

Severe structural abnormality (e.g., flail leaflet, ruptured papillary muscle, large perforation)
Vena contracta width >0.7 cm
Central jet area occupying >50% of LA
Eccentric jet wrapping the LA wall (Coanda Effect)
Systolic flow reversal in the pulmonary veins

(Original to authors)

7.3.2.3 Management

Hemodynamic management of severe MR depends upon whether it is acute and the cause of cardiogenic shock or whether it is chronic. Delineating these two clinical entities relies mostly on history and clinical exam as well as the sizes of the LA and LV (see above).

Acute severe MR is a surgical emergency that requires early involvement of cardiac surgery for consideration of mechanical support and/or surgical repair. Hemodynamic goals for both acute and chronic severe MR are to reduce afterload and minimize diastolic filling time by targeting relative tachycardia. Slow heart rates will increase LV filling during diastole worsening the MR by distending the MV annulus [17].

7.3.3 Left Ventricular Outflow Tract Obstruction

Certain anatomic features can predispose patients to LVOT obstruction (LVOTO) which can be exacerbated by the physiologic changes in the critical illness. Dynamic LVOTO differs from aortic stenosis (see below) as it is both inducible and modifiable.

Systolic anterior motion (SAM) of the mitral valve occurs when there is increased velocity of blood flow in the LVOT, which causes a Venturi effect that ultimately drags any protruding portion of the anterior MV leaflet into the LVOT during systole [18], causing an obstruction to flow (Video 7.7). This phenomenon can be exacerbated by an underfilled, hyperdynamic left ventricle (LV) and should be ruled out in all critically ill patients, particularly those who are thought to be hypovolemic or in distributive shock. It most commonly occurs in hypotensive, tachycardic patients with hypertrophic cardiomyopathy or basal hypertrophy. Patients with a distended right ventricle (RV) and elevated right-sided pressures are at increased risk for LVOT, as well as those who have recently undergone AV replacement.

2D interrogation of the MV can illustrate the motion of the anterior MV into the LVOT in both the PLAX and A5 view. Placing M-mode through the anterior MV leaflet in the PLAX provides excellent temporal resolution to assess the systolic motion of the leaflet throughout the cardiac cycle.

Color Doppler placed in the LVOT or mid-LV cavity will demonstrate aliasing from the narrowing and consequent flow acceleration at the level of the obstruction,

as seen in Video 7.8 (Video 7.8). PW Doppler at the level of the LVOT will often demonstrate aliasing (Fig. 7.7), reflecting the elevated velocity of flow at the point of the narrowing. Using PW Doppler along the length of the LVOT can help determine the exact level of obstruction. This is done by placing the sample gate at the level of the AV annulus and incrementally moving it towards the apex of the heart, resampling each time, until the aliased flow disappears. Placing CW Doppler through the LVOT in the A5 view will show the characteristic late peaking, concave, "dagger shaped," acceleration curve (Fig. 7.8) often with velocities upwards of 3 m/s. Velocities >2.7 m/s with peak pressure gradients >30 mmHg are considered clinically significant.

7.3.3.1 Management

Dynamic LVOTO can often be improved, if not corrected, with a targeted hemodynamic strategy. This strategy includes increasing LV filling with additional fluid volume, slowing the heart rate, limiting inotropy, and limiting afterload reduction. Switching vasopressors to primarily α-agonists (i.e. phenylephrine), adding β-blockade (i.e. esmolol), and avoiding hypovolemia are the main principles of management.

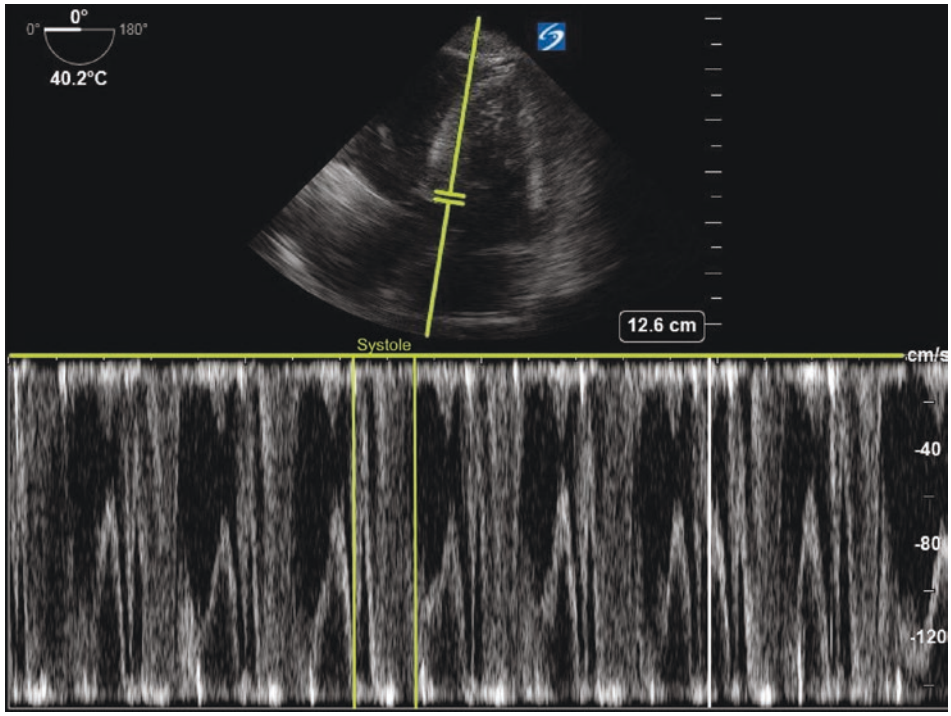

Fig. 7.7 LVOT obstruction with PW Doppler aliasing. The systolic outflow waveform extends beyond the upper limit of the pulse-wave Doppler's ability to measure, creating a band-like signal that cannot be resolved. *LVOT* left ventricular outflow tract; *PW* pulsed wave. (Original to authors)

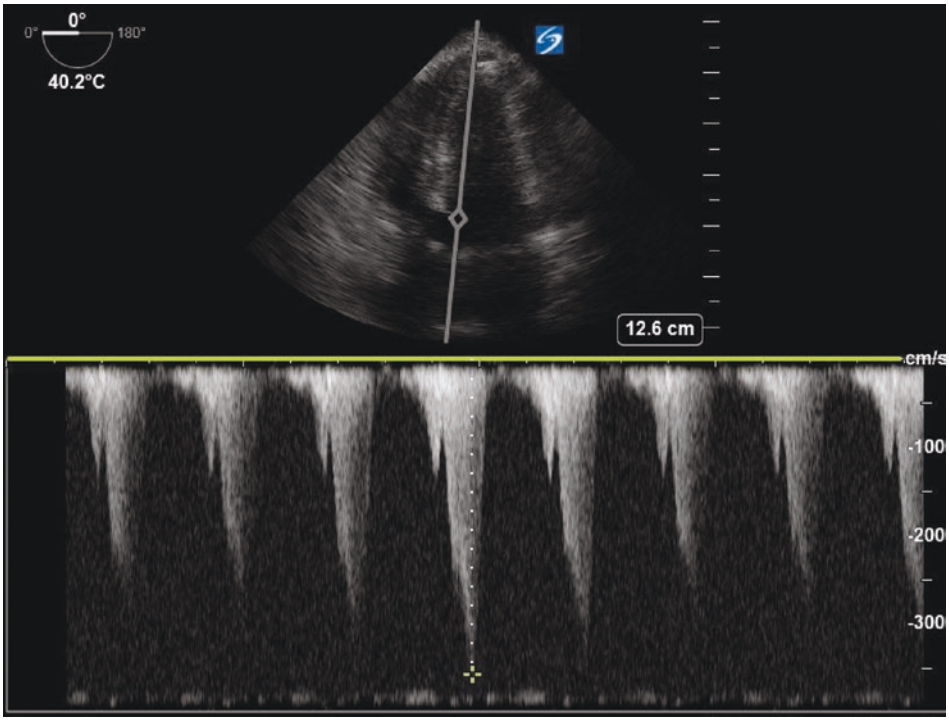

Fig. 7.8 LVOT obstruction with dagger-shaped CW Doppler signal. Use of continuous wave Doppler allows for resolution and measurement of the high velocities through the LVOT and demonstrates the classic "dagger-like," late-peaking outflow waveform. *LVOT* left ventricular outflow tract; *CW* continuous wave. (Original to authors)

7.4 Stenotic Lesions

7.4.1 Aortic Stenosis in the Critically Ill Patient

Aortic stenosis (AS) does not present acutely, but can complicate management of patients in shock for other reasons. The degree of stenosis provides an effective upper limit to cardiac output, which may complicate vasodilatory shock states commonly seen in the ICU setting. Common causes of aortic stenosis include age related calcific degeneration, particularly of bicuspid valves, and rheumatic disease.

A 2D examination will usually demonstrate a highly calcified valve with limited opening during systole (Video 7.9). This can be best appreciated in the PLAX and the parasternal short axis (PSAX) aortic-level views.

Color Doppler placed over the LVOT demonstrates aliased flow at the level of the obstruction, reflecting the high velocities required to pass through the narrowed valve.

CW Doppler from the A5 or A3 view allows for assessment of the degree of stenosis. A velocity time integral (VTI) can be measured by tracing the outer edge of the systolic outflow signal (Fig. 7.9). A peak velocity >4 m/s or a mean gradient

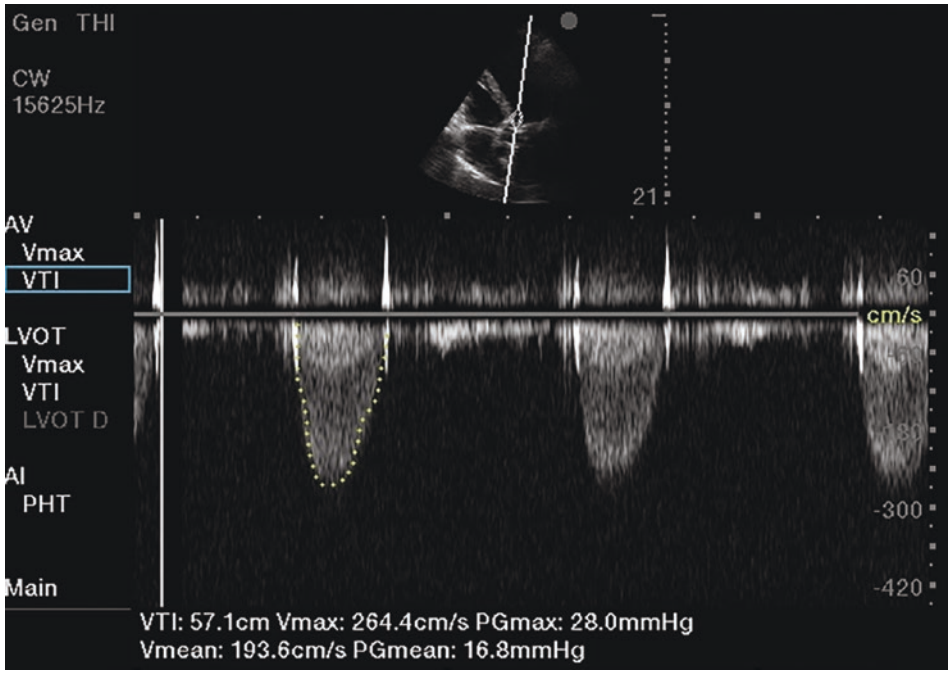

Fig. 7.9 Aortic stenosis outflow waveform. In this example, demonstrating mild stenosis, both the high-velocity, parabolic aortic stenosis waveform, as well as the lower-velocity LVOT outflow waveform can be seen superimposed upon one another. *LVOT* left ventricular outflow tract. (Original to authors)

>40 m/s signifies severe stenosis. With measurement of the LVOT diameter in the PLAX and LVOT VTI from the A5 or A3, the continuity equation can be applied to estimate the AV area, with an AV area of <1.0 cm^2 being severe.

$$\text{LVOT cross sectional area} \times \text{LVOT VTI} = \text{AV cross sectional area} \times \text{AV VTI}$$

A dimensionless index (LVOT VTI/AV VTI) <0.25 also denotes severe stenosis, which is a more useful marker in the setting of suspected AS and compromised LV systolic function.

7.4.1.1 Management

Though valve replacement is the definitive management for severe AS, hemodynamics can be optimized for the critically ill patient with this chronic valvulopathy. As the stenotic aortic valve provides a fixed opening for blood to leave the LV, prolonging systole by lowering heart rate and reducing afterload can both be helpful in improving forward flow.

7.4.2 Mitral Stenosis in the Critically Ill Patient

While severe mitral stenosis (MS) is not a pathology that occurs acutely, it may complicate the hemodynamic management for the critically ill patient.

A normal 2D appearance of the MV typically rules out any significant mitral stenosis [14]. A stenotic MV will have restricted leaflet opening, calcification, and thickening of both the MV leaflets and subvalvular apparatus (▣ Video 7.10). The most common etiology for MS is rheumatic heart disease, but it can also be seen in myxomatous disease and mitral annulus calcification (MAC).

Spectral Doppler is used to quantify the severity of MS by estimating the mean transvalvular gradient and mitral valve area (MVA) from the A4 view. The mean gradient is measured by aligning CW Doppler with the mitral inflow jet and tracing the outer edge of the inflow velocity signal. Higher gradients denote more significant stenosis, with mean gradients ≥10 mmHg considered severe. Mean gradients for MS are highly dependent on heart rate, with the longer period of diastolic filling translating to a lower gradient through the valve.

PHT is also measured by CW Doppler by the slope of the transmitral inflow velocity signal. A longer PHT denotes more severe stenosis, reflecting the increased time required for equalization of the pressure gradient between the left ventricle and left atrium [10]. PHT is used to estimate MVA with the following equation: MVA (cm^2) = 220/PHT. An MVA less than 1.0 cm^2 is considered severe MS [19].

7.4.2.1 Management

The principles for hemodynamic management include reducing the heart rate to achieve longer diastolic filling times, and lowering the mean gradient across the valve with afterload reduction. Atrial arrhythmias should be avoided as these patients have a higher dependence on their "atrial kick" for diastolic filling. Avoiding significant changes in preload and targeting a low-to-normal afterload will further optimize hemodynamics in patients with severe MS who are critically ill [20].

Summary

Bedside identification of devastating and important valvular lesions is an essential skill for an intensivist and can be quickly learned and applied using only 2D and color Doppler imaging techniques. Differentiating acute from chronic lesions influences management and relies on the patient's history in conjunction with signs of atrial and ventricular remodeling. Early recognition of these pathologies is critical to patients receiving appropriate hemodynamic support and surgical consultations when needed.

Take-Home Messages

- The scope of clinical practice for intensivists encompasses the use of basic critical care echocardiography to assess for severe, acute left sided valvular pathology.
- The primary lesions of importance for the intensivist are acute, severe aortic and mitral regurgitation, and left ventricular outflow tract obstruction.
- Performing 2D inspection of both the mitral and aortic valve is an essential first step in evaluating valvular pathology.
- There are several quantitative measurements to grade the severity of valvular lesions; however, color flow Doppler is the most basic and practical initial bedside technique.

- The hemodynamic impact of a valvular lesion may not match the valvular severity; therefore, it is important to distinguish acute from chronic valvulopathies in order to identify devastating lesions that are the primary cause of shock.
- While chronic valvular lesions such as severe aortic and mitral stenosis are not the primary pathology in acute hemodynamic instability, their presence may impact the approach to hemodynamic management.

References

1. Arntfield R, et al. Canadian recommendations for critical care ultrasound training and competency. Can Respir J. 2014;21:341–5.
2. Wong A, et al. Recommendations for core critical care ultrasound competencies as a part of specialist training in multidisciplinary intensive care: a framework proposed by the European Society of Intensive Care Medicine (ESICM). Crit Care. 2020;24:393.
3. Dujardin KS, et al. Mortality and morbidity of aortic regurgitation in clinical practice. Circulation. 1999;99:1851–7.
4. Güvenç RÇ, Güvenç TS. Clinical presentation, diagnosis and management of acute mitral regurgitation following acute myocardial infarction. J Acute Disease. 2016;5:96–101.
5. Mayo PH, et al. American College of Chest Physicians/La Société de Réanimation de Langue Française statement on competence in critical care ultrasonography. Chest. 2009;135:1050–60.
6. Zoghbi WA, et al. Recommendations for Noninvasive Evaluation of Native Valvular Regurgitation. J Am Soc Echocardiogr. 2017;30:303–71.
7. Vahanian A, Beyersdorf F, Milojevic M, et al. 2021 ESC/EACTS Guidelines for the management of valvular heart disease: Developed by the Task Force for the management of valvular heart disease of the European Society of Cardiology (ESC) and the European Association of Cardio-Thoracic Surgery (EACTS). European Heart Journal 2022; 43: 561–632.
8. Stout KK, Verrier ED. Acute valvular regurgitation. Circulation. 2009;119:3232–41.
9. Zoghbi WA, et al. Recommendations for evaluation of prosthetic valves with echocardiography and doppler ultrasound: a report From the American Society of Echocardiography's Guidelines and Standards Committee and the Task Force on Prosthetic Valves, developed in conjunction with the American College of Cardiology Cardiovascular Imaging Committee, Cardiac Imaging Committee of the American Heart Association, the European Association of Echocardiography, a registered branch of the European Society of Cardiology, the Japanese Society of Echocardiography and the Canadian Society of Echocardiography, endorsed by the American College of Cardiology Foundation, American Heart Association, European Association of Echocardiography, a registered branch of the European Society of Cardiology, the Japanese Society of Echocardiography, and Canadian Society of Echocardiography. J Am Soc Echocardiogr. 2009;22:975–1014; quiz 1082–4.
10. Otto CM. Textbook of clinical echocardiography. Elsevier Health Sciences; 2013.
11. Apostolidou E, Maslow AD, Poppas A. Primary mitral valve regurgitation: update and review. Glob Cardiol Sci Pract. 2017;2017:e201703.
12. Watanabe N. Acute mitral regurgitation. Heart. 2019;105:671–7.
13. Vazquez A, Osa A, Vicente R, Montero JA. Triple cardiac rupture. Interact Cardiovasc Thorac Surg. 2014;19:535–6.
14. Soni NJ, Arntfield R, Kory PD. Point of care ultrasound E-book. Elsevier Health Sciences; 2019.
15. Lancellotti P, et al. European Association of Echocardiography recommendations for the assessment of valvular regurgitation. Part 2: mitral and tricuspid regurgitation (native valve disease). Eur J Echocardiogr. 2010;11:307–32.

16. Millington SJ, Goffi A, Arntfield RT. Critical care echocardiography: a certification pathway for advanced users. Can J Anaesth. 2018;65:345–9.
17. Fontes, ML, Pellikka PA, Yeon, SB. Intraoperative hemodynamic management of aortic or mitral valve disease in adults. Up to Date 2023.
18. Evans JS, Huang SJ, McLean AS, Nalos M. Left ventricular outflow tract obstruction—be prepared! Anaesth Intensive Care. 2017;45:12–20.
19. Baumgartner H, et al. Echocardiographic assessment of valve stenosis: EAE/ASE recommendations for clinical practice. Eur J Echocardiogr. 2009;10:1–25.
20. Paul A, Das S. Valvular heart disease and anaesthesia. Indian J Anaesth. 2017;61:721–7.

Lung

Contents

Chapter 8 **Pneumothorax – 000**
Silvia Mongodi, Giulia Salve, and Francesco Mojoli

Chapter 9 **Pleural Effusion in Critically Ill Patients – 000**
Luigi Vetrugno, Fabrizio Tritapepe, Valentina Angelini, Salvatore Maurizio Maggiore, and Giovanni Volpicelli

Chapter 10 **Airway Ultrasound for the Intensivist – 000**
Ashraf Al-Tayar, Serene SP Ho, and Adrian V. K. Wong

Chapter 11 **Ultrasound Assessment of the Respiratory Muscles – 000**
Annemijn H. Jonkman, Nuttapol Rittayamai, Annia Schreiber, Laurent Brochard, and Alberto Goffi

Pneumothorax

Silvia Mongodi, Giulia Salve and Francesco Mojoli

Contents

8.1 Introduction – 94

8.2 Pathophysiology and Aetiology – 94

8.3 Diagnosis and Evaluation – 95
8.3.1 Scanning Technique and Probes – 96
8.3.2 Probe Positioning – 97
8.3.3 Ultrasound Features to Rule Out and Rule in Pneumothorax – 98
8.3.4 Validation with Other Imaging Techniques and Clinical Impact – 100
8.3.5 Lung Ultrasound Training for Pneumothorax Detection – 101
8.3.6 Limitations – 101
8.3.7 Pitfalls – 102

8.4 Treatment – 102

References – 103

© The Author(s), under exclusive license to Springer Nature Switzerland AG 2023
C. Robba et al. (eds.), *Basic Ultrasound Skills "Head to Toe" for General Intensivists*, Lessons from the ICU,
https://doi.org/10.1007/978-3-031-32462-8_8

Learning Objectives

- Discuss lung ultrasound advantages for pneumothorax identification.
- Describe types of ultrasound machine and probes to identify a pneumothorax.
- Describe probe positioning on the thorax to identify a pneumothorax.
- List ultrasound signs to rule out pneumothorax.
- List ultrasound sign to rule in pneumothorax.
- Describe methods for semi-quantification of air collection.
- Discuss lung ultrasound limits and pitfall in pneumothorax identification.

8.1 Introduction

Pneumothorax is defined as the presence of air in the pleural cavity. Clinical manifestations range from asymptomatic to life-threatening [1]. Pneumothorax is classified by aetiology and pathophysiology in spontaneous (primary or secondary), traumatic, and iatrogenic [2, 3]. Primary spontaneous pneumothorax has a recurrence rate between 17 and 54% [4]; traumatic pneumothorax can be seen in 40–50% of patients with thoracic injuries [5].

Acute onset with chest pain and dyspnoea is a common clinical presentation; diagnosis includes clinical examination with abolished murmur and chest imaging, i.e. traditional chest X-ray (CXR) and thoracic computed tomography (CT). Lung ultrasound (LUS) gained a leading position in this field in the last years [6], for diagnosis [7], semi-quantification [8], and as a guide to the treatment, which consists of pleural drainage.

8.2 Pathophysiology and Aetiology

Pneumothorax means presence of air in the pleural cavity, the space between the lung and the chest wall delimited by pleural sheets. The air can enter the pleural space for an abnormal connection with pulmonary alveoli/airways or for a chest wall traumatic injury that lets air enter the pleural cavity from the environment. When the air in the pleural cavity is sufficient to increase the pleural pressure, this acts as an external force, causing a partial or complete lung collapse, decreasing pulmonary vital capacity, and leading to a reduction in arterial oxygen tension [1, 3].

Pneumothorax is classified according to its aetiology into:

- **Spontaneous pneumothorax:** traditionally divided into primary and secondary based on the absence or presence of underlying lung diseases [9]. The most important risk factor for primary spontaneous pneumothorax is tobacco smoking, followed by male sex and height. This last can be explained either by the fact that in tall men pleural blebs may develop because of greater mechanical stretching of lung tissue in the apex during growth or because the apical lung tissue growth is faster than the accompanying vasculature growth and may outstrip its blood supply. Around 10% of individuals with primary spontaneous pneumothorax have a family history of mutation in the FLCN gene (Birt-Hogg-Dubé syndrome) or other hereditary disorders such as Marfan and Ehlers-Danlos syndromes [3]. Sec-

ondary pneumothorax typically occurs in presence of pre-existing lung diseases, such as chronic obstructive pulmonary disease, malignancy, cystic fibrosis, acute severe asthma, idiopathic fibrosis, rheumatic diseases (rheumatoid arthritis, ankylosing spondylitis, polymyositis, dermatomyositis, systemic sclerosis), or infectious diseases [2] (tuberculosis, pneumocystis carinii, Sars-Cov2 [10, 11], hydatid disease [12]). Catamenial pneumothorax is a recurrent spontaneous pneumothorax secondary to endometriosis: it occurs within one day before and three days after menstruation, probably associated to pleural localization of endometriosis [3].

- **Traumatic pneumothorax:** pneumothorax is a potentially severe consequence of blunt thoracic trauma and, if misdiagnosed, may quickly become life-threatening [13]. Traumatic pneumothorax affects 40–50% of patients with thoracic injury [5]. In this time-dependent scenario, it is particularly important to have a bedside reliable and repeatable tool to rapidly rule in or out a pneumothorax.
- **Iatrogenic pneumothorax:** in this case, the air collection is a complication of invasive procedures such as pulmonary needle biopsy (transthoracic or transbronchial), positive pressure ventilation, central venous line placement (subclavian or jugular).

8.3 Diagnosis and Evaluation

Acute onset with chest pain and dyspnoea is a common clinical presentation; ipsilateral decreased air entry, percussion hyperresonance, and decreased thoracic excursions/mobility are the most commonly reported chest examination findings in unilateral pneumothorax [14]. Tension pneumothorax also has a progressive impact on haemodynamics, impeding venous return and leading to an obstructive shock with dilated right ventricle and fixed inferior vena cava, with transient response to fluid challenge. The diagnosis requires the integration of clinical parameters and thoracic imaging [6].

1. **Traditional Imaging: CXR and CT**

   Lung imaging for pneumothorax diagnosis traditionally includes CXR or CT [1]. Bedside CXR has low sensitivity and high specificity for pneumothorax detection; in particular, when performed at the bedside on critically ill patients, the limited quality of the obtained images justifies an extremely low sensitivity. It has been shown that even under carefully controlled exposure conditions, more than 30% of the X-ray films are considered suboptimal [15]. In ICU, the film cassette is placed posterior to the thorax, the X-ray beam originates anterior, at a shorter distance than recommended and often not tangentially to the diaphragmatic cupola, preventing the correct interpretation of the silhouette sign. Finally, there is poor correlation between CXR and CT findings in acute patients, in particular for anterior air collections, where the overlapped image of the posterior lung may impede the visualization of anterior pneumothoraxes [15, 16] (Fig. 8.1). Finally, both CXR and CT are not immediately available at the bedside, making them poorly suitable to time-dependent scenarios, and imply irradiation, a major limitation in paediatrics and pregnant women. So, even if CT is considered the

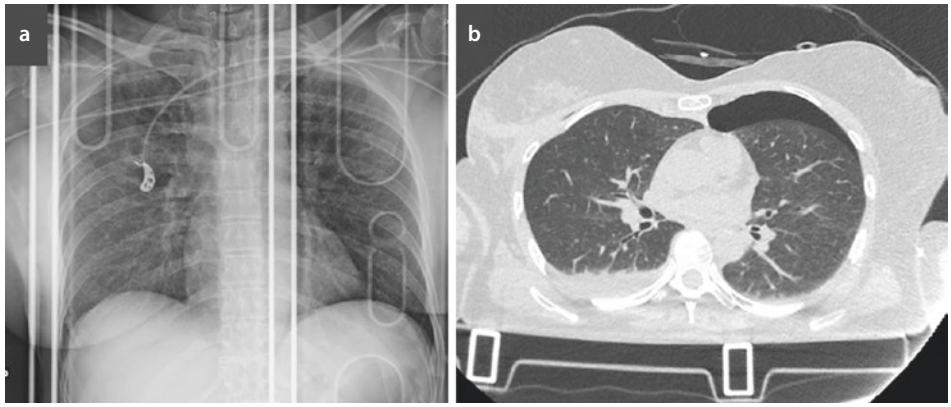

Fig. 8.1 Panel **a** Antero-posterior chest-X-ray in a patient admitted for thoracic blunt trauma to Emergency Department. Image quality is compromised by both mandatory supine position and by immobilization devices. The anterior left pneumothorax is hard to detect. Panel **b** The corresponding CT scan where left anterior pneumothorax is well visible; a lung point was also visualized in anterior axillary line

gold standard for lung imaging and for pneumothorax detection and quantification, it is not used on a routine basis for pneumothorax diagnosis; moreover, it requires patient transportation to radiology department, which can involve high risk for unstable, critically ill patients.

2. **Lung ultrasound**

Ultrasound has been described for a long time as unsuitable for the exploration of the thorax since the high difference in acoustic impedance between superficial tissues and air in the lung prevents the penetration of the beam beneath the visceral pleura. In fact, the lung is mostly not directly visible to ultrasound and LUS semiotic is mainly based on artefacts. However, in the last decades, literature demonstrated how LUS is a reliable tool for the assessment of lung diseases. In particular, it carries high sensitivity (88%) and specificity (100%) for pneumothorax with good correlation with the gold standard technique, i.e. CT scan [7]. Moreover, it can be performed at the bedside with any simple ultrasound machine and probe [17], is repeatable since not irradiating, and is easy to perform [18]. LUS also allows semi-quantification of pneumothorax [8] and may guide the procedure of thoracic drainage. LUS can also be used during invasive procedures such as pulmonary needle biopsy (transthoracic and transbronchial), recruitment manoeuvres, central venous line placement, or paravertebral nerve block to promptly identify an iatrogenic pneumothorax [19, 20].

8.3.1 Scanning Technique and Probes

LUS can be performed with any probe and with simple ultrasound machines [21]; however, a high frequency linear probe with one focus set on the pleural line allows the best visualization of the pleural surface and of the artefacts generated at the correspondent tissue–air interface.

8.3.2 Probe Positioning

A complete LUS examination includes 12 regions, six per hemithorax: upper and lower in anterior (regions 1 and 2), lateral (regions 3 and 4), and posterior fields (regions 5 and 6). Right regions are named R1–R6 and left regions L1–L6. Anterior, lateral, and posterior fields are defined by parasternal, anterior, and posterior axillary lines (Fig. 8.2a) [22]. A complete examination is performed for an overall lung assessment and monitoring, in particular of complex patients such as those critically ill and under mechanical ventilation. However, in time-dependent scenarios and to answer to a simple clinical question (pneumothorax yes/no), a quick examination focused on anterior fields is recommended to rule in/out free air collections. Such approach is now integrated in the extended-Focused Assessment with Sonography for Trauma (e-FAST), where LUS demonstrated its superiority when compared to standard supine CXR [23].

The probe is placed perpendicular to the thoracic surface and can be oriented longitudinally or transversally (Fig. 8.2b–d). To obtain a longitudinal scan, the probe is placed centred in the intercostal space with its major axis aligned with the cranio-caudal axis of the patient: this approach allows the visualization of the bat sign, i.e. the clear identification of the pleural line within the intercostal space delimited by the ribs' shadows [24]. Longitudinal scan is easier and is recommended to start the exam; this is particularly true for pneumothorax, where the presence of

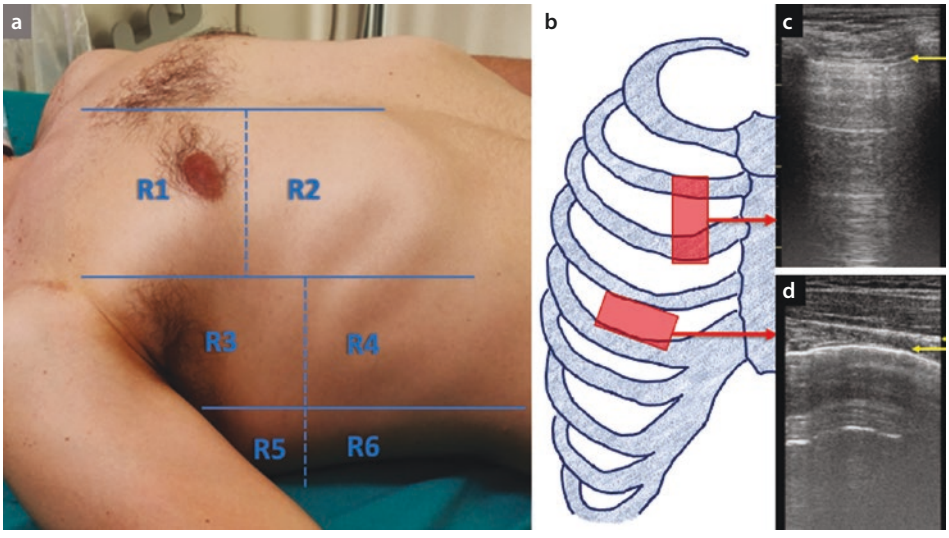

Fig. 8.2 Panel **a** A complete lung ultrasound examination includes six regions per hemithorax: upper and lower in anterior (regions 1 and 2), lateral (regions 3 and 4), and posterior fields (regions 5 and 6). Anterior, lateral, and posterior fields are limited parasternal, anterior, and posterior axillary lines. Panel **b** Position of the probe on the thorax in longitudinal (above) and transversal (below) scans. Panel **c** Ultrasound findings in longitudinal scan: the pleural line (yellow arrow) is visualized as a horizontal hyperechoic line around half a centimetre below the ribs; the intercostal space is well delimited by the ribs' acoustic shadows (bat sign). Panel **d** Ultrasound findings in transversal scan: the probe is aligned with the intercostal space: the entire length of the probe is used to visualize a wider pleural line and the ribs are not visible anymore

subcutaneous emphysema may generate artefacts—called E-lines—deriving from the air in the tissue, mimicking the B-lines and making difficult or even impossible the visualization of the pleural line. To obtain a transversal scan, the probe is aligned with the intercostal space: this approach avoids ribs' shadows (Fig. 8.2d) and allows the visualization of a larger portion of pleura [25].

8.3.3 Ultrasound Features to Rule Out and Rule in Pneumothorax

Normal lung appears at LUS as a horizontal hyperechoic line, visible in longitudinal scan around 0.5 cm below the ribs, that slides synchronously with tidal ventilation. The lung sliding corresponds to the visceral pleura sliding against the parietal one, which is fixed [26]. It can be confirmed in M-mode with the seashore sign, a helpful tool in case of limited sliding since the frame rate is higher (Fig. 8.3c) [27]. In absence of lung sliding, the pleura can be visualized as pulsing synchronously with heart beats: the lung pulse corresponds to the pulsing of the visceral pleura against the parietal one and indicates that the analysed region is still aerated but very poorly ventilated [27]. Beneath the pleural line, a normally aerated lung presents the A-lines [28], horizontal reverberation artefacts generated by the parietal pleura and air–tissue interface. A-lines are spaced by a constant distance, which corresponds to the distance between the probe and the pleural line. If lung aeration is impaired and lung density increased, B-lines appear: they are vertical hyperechoic artefacts generated by the visceral pleura, erasing the A-lines, reaching the bottom of the screen, and moving synchronously with the visceral pleura. Pneumothorax is characterized by air interposition between the two pleural sheets: this implies that the ultrasound beam cannot reach the visceral pleura. The visualization of any sign or artefact deriving from the visceral pleura allows therefore to rule out pneumothorax with 100% negative predictive value: in presence of lung sliding/seashore sign [26] or B-lines [29] pneumothorax can easily be excluded. This is also true for real images—i.e. tissue-like pattern and pleural effusion—visible only when there is no air within or around the lung impeding the ultrasound beam penetration.

The presence of A-lines without lung sliding, lung pulse, or any B-line (called A-pattern) strongly suggests pneumothorax, with high sensitivity and moderate context-dependent specificity, reaching particularly high accuracy in trauma patients (sensitivity 98.1%; specificity 99.2%) (Fig. 8.3a) [30, 31]. An abolished lung sliding with A-lines orients to pneumothorax, but is not sufficient to rule it in; in fact, it can also be associated to other factors reducing regional tidal ventilation, as hyperinflation [32] or emphysematous bullae. The specific sign to confirm a pneumothorax is the lung point. It corresponds to the limit of the pneumothorax, being the contact point between the collapsed lung and the air collection (Fig. 8.3b). The lung point confirms pneumothorax with 100% specificity [33]. Once identified, it is possible to quantify and monitor the pneumothorax extension mapping the lung point on the chest surface [8]. A lung point beneath the mid-axillary line in a presumed free collection—e.g., in trauma patients—indicates a collapse of at least 30% of the parenchyma. It must be underlined that in a completely collapsed lung the lung point

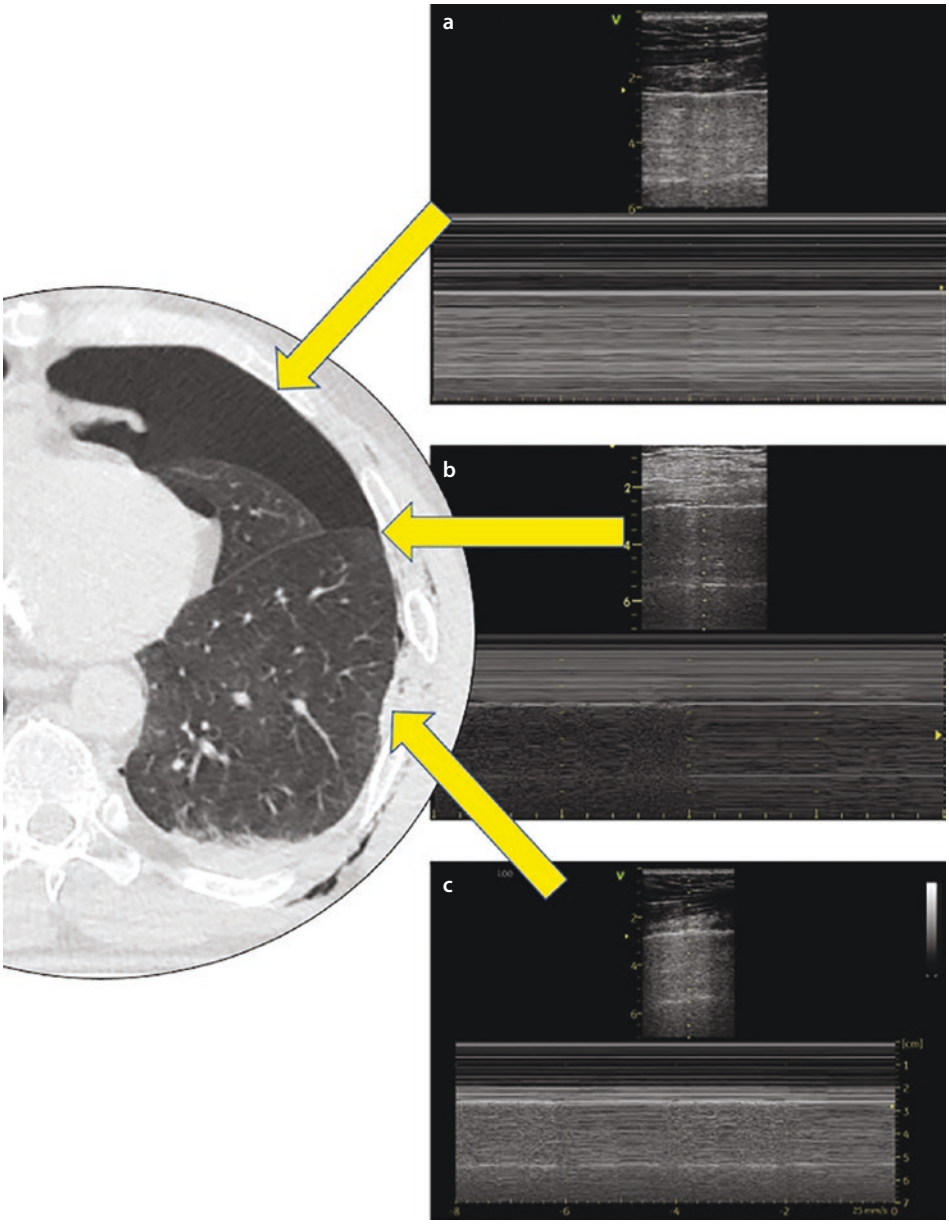

Fig. 8.3 CT scan of a patient with a left pneumothorax and corresponding ultrasound findings in different parts of the thorax. Panel **a** In anterior fields, where the air collection is visualized at CT scan, lung ultrasound shows A-lines with no lung sliding, as confirmed by the stratosphere sign in M-mode. Panel **b** The contact point between the air collection and the collapsed lung corresponds in lung ultrasound to the lung point: alternation of seashore and stratosphere sign synchronous with tidal ventilation. Panel **c** Where the visceral pleura is in contact with the parietal one, lung sliding with corresponding seashore sign at M-mode is visualized

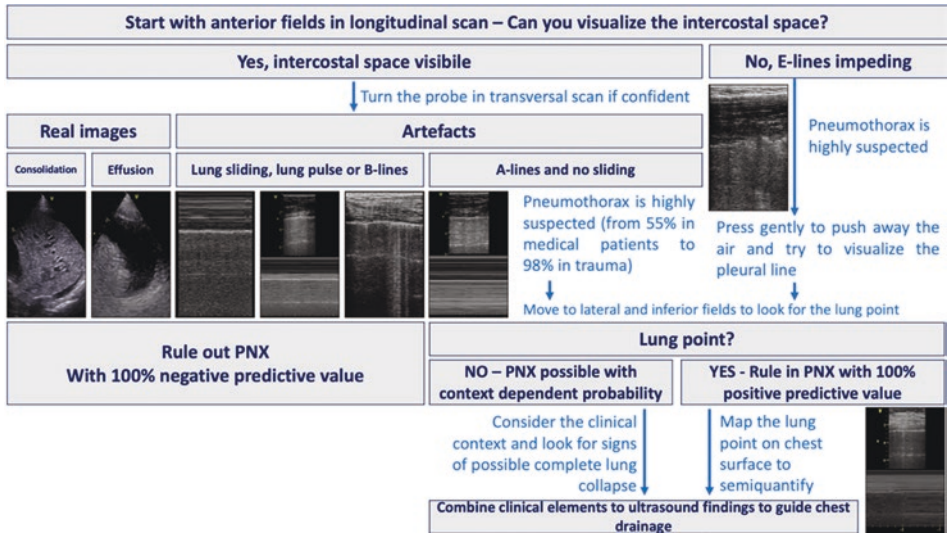
Start with anterior fields in longitudinal scan – Can you visualize the intercostal space?
Yes, intercostal space visibile
No, E-lines impeding
Turn the probe in transversal scan if confident
Real images
Artefacts
Consolidation
Effusion
Lung sliding, lung pulse or B-lines
A-lines and no sliding
Pneumothorax is highly suspected
Pneumothorax is highly suspected (from 55% in medical patients to 98% in trauma)
Press gently to push away the air and try to visualize the pleural line
Move to lateral and inferior fields to look for the lung point
Rule out PNX
With 100% negative predictive value
Lung point?
NO – PNX possible with context dependent probability
YES - Rule in PNX with 100% positive predictive value
Consider the clinical context and look for signs of possible complete lung collapse
Map the lung point on chest surface to semiquantify
Combine clinical elements to ultrasound findings to guide chest drainage

Fig. 8.4 Flow-chart for a systematic approach to rule in/out a pneumothorax. *PNX* pneumothorax

cannot be visualized; this further stresses the need to always integrate ultrasound findings to clinical evaluation. In this situation, the absence of lung sliding, lung pulse, and B-lines will strongly support the diagnosis of pneumothorax in a likely unstable patient with marked thoracic asymmetry and abolished murmur.

A systematic ultrasound approach allows quickly ruling in or out pneumothorax (Fig. 8.4).

Once confirmed the pneumothorax, LUS can be used to guide the choice of the best intercostal space for pleural drainage (i.e. where no lung sliding or other structures, included intercostal arteries, are visualized in any phase of the respiratory cycle), to check its efficacy with the immediate reappearance of the lung sliding in anterior fields and to rule out complications as haemothorax.

8.3.4 Validation with Other Imaging Techniques and Clinical Impact

LUS is a cost-effective and safe bedside method and performs better than CXR for pneumothorax [15, 34]. Its reliability and clinical impact, thanks to a quick bedside examination [35], has specifically been demonstrated in the context of trauma patients, where CXR marginally affects the management of patients [36]. Anteroposterior CXR may in fact not detect the presence of a small or medium pneumothorax in supine patients, while LUS showed higher sensitivity (Fig. 8.1). Furthermore, LUS allows to differentiate between small, medium, and large pneumothorax with good agreement with CT results [34] and represents a feasible and reliable diagnostic approach to the patient with dyspnoea [38].

In the emergency setting, it has been demonstrated how LUS significantly affects diagnostic and therapeutic practices [37]. It impacts on the management of hypox-

emic patients, with reduced time to diagnosis and treatment [39], better use of advanced thoracic imaging [39], and reduced need of traditional radiography, especially in intensive care unit [40, 41].

8.3.5 Lung Ultrasound Training for Pneumothorax Detection

A recent consensus and expert recommendations of the European Society of Intensive Care Medicine recommends that LUS semiotic should be part of basic core competences for all intensivists; this includes the identification of sonographic findings to rule in/out a pneumothorax [43] and to guide its management. However, training methods to acquire the appropriate skills for LUS measurement vary among centres and a formal certification is not available. A 25-examination training programme, supervised by an expert physician, demonstrated to be adequate to improve trainees' capability to recognize normal aeration, interstitial syndrome, alveolar oedema, and lung consolidation [18]. Simple skills can be easily acquired with a short training: anaesthesia residents were able to rule out pneumothorax after 5 min of online training [42].

8.3.6 Limitations

A common limitation to the use of ultrasound is the presence of anything that prevents the direct contact of the probe with the skin, as thoracic dressing, extensive burn, or wounds. Extreme obesity can also make ultrasound examination challenging. Subcutaneous emphysema is a major limitation, in particular for pneumothorax detection (◘ Fig. 8.5a): the interposition of air between the transducer and the

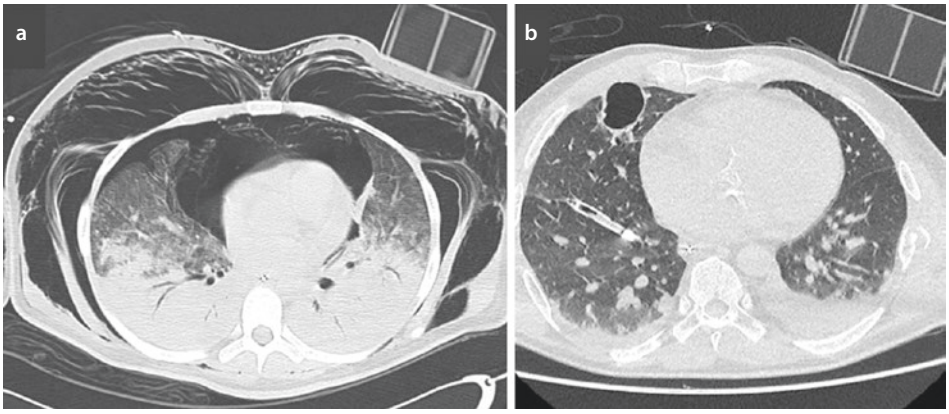

◘ **Fig. 8.5** Panel **a** The presence of subcutaneous emphysema prevents the possibility of lung ultrasound beam to reach the pleural line and to visualize the pneumothorax. Panel **b** A pleural bulla can mimic lung ultrasound findings of pneumothorax. However, an unusual shape of the air collection and a limited sliding of the surrounding lung can be visible to an expert eye

pleura impedes in fact the ultrasound beam penetration and can generate artefacts called E-lines mimicking the B-lines and leading to possible misinterpretation of ultrasound findings in non-adequately trained hands.

8.3.7 Pitfalls

Impaired regional ventilation due to an airway obstruction, hyperinflation, pleural adherence, or bullae (Fig. 8.5b) also limits or even abolishes the lung sliding [44, 45]. In mechanically ventilated patients, with the progressive increase of positive end expiratory pressure and hyperinflation, a progressive reduction of sliding has been observed [32]. In patients with asbestos-related pleural diseases, the image of absent lung sliding is frequent; in these cases, the past medical history can help in differential diagnosis [46]. Moreover, the abolished lung sliding is, in general, associated to artefacts as subpleural consolidations and B-lines. Pneumomediastinum can be confused with pneumothorax; when a pneumothorax pattern is visualized in parasternal fields only, pneumomediastinum should be considered for differential diagnosis. In this case, the integration with traditional imaging, included CXR, is useful [47].

8.4 Treatment

While conservative treatment and monitoring is the first choice for small pneumothorax without significant breathlessness, chest drainage should be considered for symptomatic patients, regardless the size of the air collection [48]. A chest drain is usually required for tension or bilateral pneumothorax. Ultrasound guidance reduces the complications associated with pleural procedures in the critical care setting and its routine use is recommended [49]: LUS can be used to guide the need of a safe drainage by semi-quantification of the air collection, to choose the most correct intercostal space where no lung sliding or other structures are visualized during the entire respiratory cycle and to avoid the intercostal artery, easily visible with colour Doppler. An ultrasound-assisted procedure is therefore recommended. Moreover, LUS can be used to monitor the efficacy of the drainage by the immediate visualization of lung sliding in previously collapsed regions and to rule out complications by the systematic search of pleural effusions.

Summary

Pneumothorax is a common and potentially severe respiratory disease that requires prompt identification and treatment. Lung ultrasound has high sensitivity and specificity for pneumothorax diagnosis, allows its quantification, and guides chest drainage positioning. Being a bedside non-irradiating and relatively easy-to-learn technique, lung ultrasound is the ideal tool in the hands of the intensivist to integrate the clinical evaluation in this context.

Take-Home Messages

- Lung ultrasound is a reliable method to identify a pneumothorax, with high sensitivity (88%) and specificity (100%).
- We suggest using a linear probe. Start your systematic approach with longitudinal scan in anterior fields.
- The presence of lung sliding, lung pulse, B-lines, or real images (consolidation, effusion) rules out pneumothorax with 100% negative predictive value.
- The absence of lung sliding, lung pulse, or B-lines strongly suggests pneumothorax, with high sensitivity and moderate context-dependent specificity.
- Pay attention to the pulmonary conditions that may limit the lung sliding: bullous lung diseases, pleural diseases, hyperinflation.
- The visualization of the lung point rules in pneumothorax with 100% positive predictive value.
- A lung point beneath the midaxillary line indicates a collapse of at least 30% of the parenchyma.
- The lung point cannot be visualized if the lung collapse is complete.
- Always combine ultrasound findings to clinical assessment in the decision to drain the air collection; use ultrasound to choose the best intercostal space and to monitor efficacy and complications of the procedure.

References

1. Huan NC, Sidhu C, Thomas R. Pneumothorax: classification and etiology. Clin Chest Med. 2021;42:711–27. https://doi.org/10.1016/j.ccm.2021.08.007.
2. Zarogoulidis P, Kioumis I, Pitsiou G, Porpodis K, Lampaki S, Papaiwannou A, et al. Pneumothorax: from definition to diagnosis and treatment. J Thorac Dis. 2014;6(Suppl 4):372–6. https://doi.org/10.3978/j.issn.2072-1439.2014.09.24.
3. Arshad H, Young M, Adurty R, Singh AC. Acute pneumothorax. Crit Care Nurs Q. 2016;39(2):176–89.
4. Tschopp JM, Bintcliffe O, Astoul P, Canalis E, Driesen P, Janssen J, et al. ERS task force statement: diagnosis and treatment of primary spontaneous pneumothorax. Eur Respir J. 2015;46:321–35. https://doi.org/10.1183/09031936.00219214.
5. Tran J, Haussner W, Shah K. Traumatic pneumothorax: a review of current diagnostic practices and evolving management. J Emerg Med. 2021;61(5):517–28. https://doi.org/10.1016/j.jemermed.2021.07.006.
6. Lee HJ, Yarmus L, Feller-Kopman D. Pneumothorax. In: Vincent JL, Abraham E, Moore FA, Kochanek PM, Fink MO, editors. Textbook of critical care. Elvisier; 2017. p. 461–3.
7. Lichtenstein DA, Mezière GA. Relevance of lung ultrasound in the diagnosis of acute respiratory failure: the BLUE protocol. Chest. 2008;134(1):117–25. https://doi.org/10.1378/chest.07-2800.
8. Volpicelli G, Boero E, Sverzellati N, Cardinale L, Busso M, Boccuzzi F, et al. Semi-quantification of pneumothorax volume by lung ultrasound. Intensive Care Med. 2014;40(10):1460–7. https://doi.org/10.1007/s00134-014-3402-9.
9. Bintcliffe OJ, Edey AJ, Arstrong L, Negus IS, Maskell NA. Lung parenchymal assessment in primary and secondary pneumothorax. Ann Am Thorac Soc. 2016;13(3):350–5. https://doi.org/10.1513/AnnalsATS.201509-584OC.
10. Agrafiotis AC, Rummens P, Lardinois I. Pneumothorax in otherwise healthy non-intubated patients suffering from COVID-19 pneumonia: a systematic review. J Thorac Dis. 2021;13(7):4519–29. https://doi.org/10.21037/jtd-21-208.

11. Afrazi A, Garcia Rodriguez S, Maloneya JD, Morgan CT. Cavitary lung lesions and pneumothorax in a healthy patient with active coronavirus-19 (COVID-19) viral pneumonia. Interact Cardiovasc Thorac Surg. 2021;32(1):150–2. https://doi.org/10.1093/icvts/ivaa238.
12. Acharya AB, Bhatta N, Mishra DR, Verma A, Shahi R. Rare cause of tension pneumothorax: hydatid disease of lung: a case report. J Nepal Med Assoc. 2020;58(224):265–8. https://doi.org/10.31729/jnma.4693.
13. Ianniello S, Di Giacomo V, Sessa B, Miele V. First-line sonographic diagnosis of pneumothorax in major trauma: accuracy of e-FAST and comparison with multidetector computed tomography. Radiol Med. 2014;119(9):674–80. https://doi.org/10.1007/s11547-014-0384-1.
14. Roberts DJ, Leigh-Smith S, Faris PD, Blackmore C, Ball CG, Lee Robertson H, et al. Clinical presentation of patients with tension pneumothorax a systematic review. Ann Surg. 2015;261(6):1068–78. https://doi.org/10.1097/SLA.0000000000001073.
15. Xirouchaki N, Magkanas E, Vaporidi K, Kondili E, Plataki M, Patrianakos A, et al. Lung ultrasound in critically ill patients: comparison with bedside chest radiography. Intensive Care Med. 2011;37(9):1488–93. https://doi.org/10.1007/s00134-011-2317-y.
16. Bouhemad B, Zhang M, Lu Q, Rouby JJ. Clinical review: bedside lung ultrasound in critical care practice. Crit Care. 2007;11(1):205. https://doi.org/10.1186/cc5668.
17. Gomond-Le Goff C, Vivalda L, Foligno S, Loi B, Yousef N, De Luca D. Effect of different probes and expertise on the interpretation reliability of point-of-care lung ultrasound. Chest. 2020;157(4):924–31. https://doi.org/10.1016/j.chest.2019.11.013.
18. Arbelot C, Dexheimer Neto FL, Gao Y, Brisson H, Chunyao W, et al. Lung ultrasound in emergency and critically ill patients: : Number of Supervised Exams to Reach Basic Competence. Anesthesiology. 2020;132(4):899–907. https://doi.org/10.1097/ALN.0000000000003096.
19. Rodriguez JAO, Hipskind JE. Pneumothorax, Iatrogenic. StatPearls; 2020. p. 1–6.
20. Blans MJ, Endeman H, Bosch FH. The use of ultrasound during and after central venous catheter insertion versus conventional chest X-ray after insertion of a central venous catheter. Neth J Med. 2016;74(8):353–7.
21. Gargani L, Volpicelli G. How I do it: lung ultrasound. Cardiovasc Ultrasound. 2014;12:25. https://doi.org/10.1186/1476-7120-12-25.
22. Bouhemad B, Mongodi S, Via G, Roquette I. Ultrasound for "lung monitoring" of ventilated patients. Anesthesiology. 2015;122:437–47. https://doi.org/10.1097/ALN.0000000000000558.
23. Heinz ER, Vincent A. Point-of-care ultrasound for the trauma anesthesiologist. Curr Anesthesiol Rep. 2022;12:217. https://doi.org/10.1007/s40140-021-00513-x.
24. Volpicelli G, Elbarbary M, Blaivas M, Lichtenstein DA, Mathis G, Kirkpatrick AW, et al. International evidence-based recommendations for point-of-care lung ultrasound. Intensive Care Med. 2012;38(4):577–91. https://doi.org/10.1007/s00134-012-2513-4.
25. Mongodi S, De Luca D, Colombo A, Stella A, Santangelo E, Corradi F, et al. Quantitative lung ultrasound: technical aspects and clinical applications. Anesthesiology. 2021;134(6):949–65. https://doi.org/10.1097/ALN.0000000000003757.
26. Lichtenstein DA, Menu Y. A bedside ultrasound sign ruling out pneumothorax in the critically ill: lung sliding. Chest. 1995;108(5):1345–8. https://doi.org/10.1378/chest.108.5.1345.
27. Lichtenstein DA, Lascols N, Prin S, Mezière G. The "lung pulse": an early ultrasound sign of complete atelectasis. Intensive Care Med. 2003;29(12):2187–92. https://doi.org/10.1007/s00134-003-1930-9.
28. Chiumello D, Umbrello M, Sferrazza Papa GF, Angileri A, Gurgitano M, Formenti P, et al. Global and regional diagnostic accuracy of lung ultrasound compared to CT in patients with acute respiratory distress syndrome. Crit Care Med. 2019;47(11):1599–606. https://doi.org/10.1097/CCM.0000000000003971.
29. Lichtenstein DA, Meziere G, Biderman P, Gepner A. The comet-tail artifact: an ultrasound sign ruling out pneumothorax. Intensive Care Med. 1999;25(4):383–8. https://doi.org/10.1007/s001340050862.
30. Soldati G, Testa A, Sher S, Pignataro G, La Sala M, Silveri NG. Occult traumatic pneumothorax: diagnostic accuracy of lung ultrasonography in the emergency department. Chest. 2008;133(1):204–11. https://doi.org/10.1378/chest.07-1595.
31. Mojoli F, Bouhemad B, Mongodi S, Lichtenstein D. Lung ultrasound for critically ill patients. Am J Respir Crit Care Med. 2019;199(6):701–14. https://doi.org/10.1164/rccm.201802-0236CI.

32. Markota A, Golub J, Stozer A, Fluher J, Prosen G, Bergauer A, et al. Absence of lung sliding is not a reliable sign of pneumothorax in patients with high positive end-expiratory pressure. Am J Emerg Med. 2016;34(10):2034–6. https://doi.org/10.1016/j.ajem.2016.07.032.
33. Lichtenstein DA, Meziere G, Biderman P, Gepner A. The "lung point": an ultrasound sign specific to pneumothorax. Intensive Care Med 2020;26:1434–1440. doi:https://doi.org/10.1007/s001340000627.
34. Blaivas M, Lyon M, Duggal S. A prospective comparison of supine chest radiography and bedside ultrasound for the diagnosis of traumatic pneumothorax. Acad Emerg Med. 2005;12(9):844–9. https://doi.org/10.1197/j.aem.2005.05.005.
35. Reissig A, Kroegel C. Accuracy of transthoracic sonography in excluding post-interventional pneumothorax and hydropneumothorax, comparison to chest radiography. Eur J Radiol. 2005;53(3):463–70. https://doi.org/10.1016/j.ejrad.2004.04.014.
36. Zieleskiewicz L, Fresco R, Duclos G, Antonini F, Mathieu C, Medam S, et al. Integrating extended focused assessment with sonography for trauma (eFAST) in the initial assessment of severe trauma: impact on the management of 756 patients. Injury. 2018;49(10):1774–80. https://doi.org/10.1016/j.injury.2018.07.002.
37. Bobbia X, Zieleskiewicz L, Pradeilles C, Hudson C, Muller L, Géraud Claret P, et al. The clinical impact and prevalence of emergency point-of-care ultrasound: a prospective multicenter study. Anesth Crit Care Pain Med. 2017;36(6):383–9. https://doi.org/10.1016/j.accpm.2017.02.008.
38. Zanobetti E, Scorpiniti M, Gigli C, Nazerian P, Vanni S, Innocenti F, Stefanone VT, et al. Point-of-care ultrasonography for evaluation of acute dyspnoea in the ED. Chest. 2017;151(6):1295–301. https://doi.org/10.1016/j.chest.2017.02.003.
39. Laursen CB, Sloth E, Touborg Lassen A, de Pont Christensen R, Lambrechtsen J, Henning Madsen P, et al. Point-of-care ultrasonography in patients admitted with respiratory symptoms: a single-blind, randomised controlled trial. Lancet Resp Med. 2014;2(8):638–46. https://doi.org/10.1016/S2213-2600(14)70135-3.
40. Mongodi S, Orlando A, Arisi E, Tavazzi G, Santangelo E, Caneva L, et al. Lung ultrasound in patients with acute respiratory failure reduces conventional imaging and health care provider exposure to COVID-19. Ultrasound Med Biol. 2020;46(8):2090–3. https://doi.org/10.1016/j.ultrasmedbio.2020.04.033.
41. Brogi E, Bignami E, Sidoti A, et al. Could the use of bedside lung ultrasound reduce the number of chest x-rays in the intensive care unit? Cardiovasc Ultrasound. 2017;15:23. https://doi.org/10.1186/s12947-017-0113-8.
42. Krishnan S, Kuhl T, Ahmed W, Togashi K, Ueda K. Efficacy of an online education program for ultrasound diagnosis of pneumothorax. Anesthesiology. 2013;118(3):715–21. https://doi.org/10.1097/ALN.0b013e31827f0979.
43. Robba C, Wong A, Poole D, Al Tayar A, Arntfield RT, Chew MS, et al. Basic ultrasound head-to-toe skills for intensivists in the general and neuro intensive care unit population: consensus and expert recommendations of the European Society of Intensive Care Medicine. Intensive Care Med. 2021;47(12):1347–67. https://doi.org/10.1007/s00134-021-06486-z.
44. Breitkopf R, Treml B, Rajsic S. Lung sonography in critical care medicine. Diagnostics. 2022;12:1405. https://doi.org/10.3390/diagnostics12061405.
45. Gelabert C, Nelson M. Bleb point: mimicker of pneumothorax in bullous lung disease. West J Emerg Med. 2015;16(3):447–9. https://doi.org/10.5811/westjem.2015.3.24809.
46. Steenvoorden TS, Hilderink B, Elbers PWG, Tuinman PR. Lung point in the absence of pneumothorax. Intensive Care Med. 2018;44(8):1329–30. https://doi.org/10.1007/s00134-018-5112-1.
47. Zachariah S, Gharahbaghian L, Perera P, Joshi N. Spontaneous Pneumomediastinum on bedside ultrasound: case report and review of the literature. West J Emerg Med. 2015;16(2):321–4. https://doi.org/10.5811/westjem.2015.1.24514.
48. MacDuff A, Arnold A, Harvey J, on behalf of the BTS Pleural Disease Guideline Group. Management of spontaneous pneumothorax: British Thoracic Society pleural disease guideline. Thorax. 2010;65:8–31. https://doi.org/10.1136/thx.2010.136986.
49. Havelockc T, Teoh R, Laws D, Gleeson F, On behalf of the BTS Pleural Disease Guideline Group. Pleural procedures and thoracic ultrasound: British Thoracic Society pleural disease guideline 2010. Thorax. 2010;65(2):61–76. https://doi.org/10.1136/thx.2010.137026.

Pleural Effusion in Critically Ill Patients

Luigi Vetrugno, Fabrizio Tritapepe, Valentina Angelini, Salvatore Maurizio Maggiore and Giovanni Volpicelli

Contents

9.1 Pleural Effusion in Intensive Care – 108

9.2 Mechanisms of PE Formation – 109

9.3 Ultrasound Diagnostic Criteria – 109

9.4 Comparison with Radiologic Tools – 112

9.5 Assessment of Fluid Volume – 112

9.6 Clinical Symptoms and Outcome – 114

9.7 Ultrasound Thoracocentesis and PE Drainage – 114

9.8 Procedure for Drainage of PE – 115

References – 117

© The Author(s), under exclusive license to Springer Nature Switzerland AG 2023
C. Robba et al. (eds.), *Basic Ultrasound Skills "Head to Toe" for General Intensivists*, Lessons from the ICU,
https://doi.org/10.1007/978-3-031-32462-8_9

Learning Objectives

The reader will learn the main etiology of pleural effusion in intensive care and the relevance and nature of this phenomenon. The sonographic signs with power and limitation of bedside thoracic ultrasound for pleural effusion are presented and discussed. Specific focus will be given to the techniques to estimate the volume of the effusion by thoracic ultrasound and how ultrasound guidance can be used for drainage.

9.1 Pleural Effusion in Intensive Care

Pleural effusion (PE) is a fluid collection between the two pleural layers, parietal and visceral. Many etiologies can lead to PE, but excluding traumatic or iatrogenic hemothorax, and, as a rare event, chylothorax and bilothorax, the main three causes of PE in the setting of general intensive care unit (ICU) are fluid overloads, heart failure, and pneumonia, this latter with or without the evolution in acute respiratory distress syndrome (ARDS) [1]. PE secondary to nephrosis and liver cirrhosis is less frequent [2]. Some studies reported PE with a high-frequency rate from 41 to 62% in ICU [3]. Liberal fluid resuscitation following the Early Goal-Directed Therapy (EGDT), considered the standard of care for patients with severe sepsis and septic shock since 2001, has been probably one cause of high prevalence of the condition in the ICU setting. Indeed, recent multicenter clinical trials (ProCESS, ARISE, and ProMISe) and a meta-analysis of EGDT has demonstrated that a liberal fluid approach does not improve the outcome of patients, and fluid administration has changed over time to a more conservative approach [4–6]. A recent prospective multicenter cohort study suggested a low prevalence of PE, and an incidence of around 26% seems more realistic for the general ICU [7]. Acute heart failure (AHF) remains the second most common cause of PE in general ICUs, and both systolic and diastolic heart dysfunction can represent the main pathogenesis. The widespread and ever-growing use of cardiac ultrasound in the ICU over the last 15 years and the advent of the critical care echocardiography (CCE) [8] allowed to determine more in detail the characteristics of heart failure in critically ill patients. For instance, the condition of impaired systolic function (i.e., a reduced left ventricular ejection fraction) is less frequently associated with decompensated heart failure than expected. Impaired diastolic function is a highly frequent condition found in patients who fail the spontaneous breathing trial for weaning from mechanical ventilation [9]. Therefore, recent literature placed more emphasis on the impact of diastolic dysfunction in the weaning process from mechanical ventilation in ICU patients [10]. The transition from mechanical to spontaneous ventilation seems to induce a negative intrathoracic pressure, increasing systemic venous return and left ventricle (LV) afterload, thus rising pulmonary artery occlusion pressure that may favor pulmonary edema and PE even in the presence of preserved LV function [11].

Moderate-to-large PE was also found in one-third of patients with normal systolic and diastolic cardiac function. Unexpectedly, reducing moderate-to-large pleural effusion either by aggressive depletion or drainage has never been demonstrated as being useful, even though the amount of PE is known to influence diaphragm force and is associated with worse outcomes [12].

The third most common cause of pleural effusion in ICU is pneumonia. Of those patients affected by pneumonia, 40–60% will develop PE on the ipsilateral lung infection, and 29% of parapneumonic PE in mechanically ventilated patients will progress to ARDS [13]. Complicated parapneumonic PE leads to pus and empyema formation in the pleural space. However, despite many parapneumonic effusions being complicated, less than 10% require pleural drainage during the ICU stay [14].

During the COVID-19 pandemic, the great majority of patients with interstitial pneumonia showed absence or very low quantity of PE. In the decision algorithm tree of patients with suspected COVID-19, visualization of large PE by ultrasound has been proposed as a diagnostic criterion alternative to the diagnosis of interstitial pneumonia [15].

9.2 Mechanisms of PE Formation

The main pathophysiological mechanisms of PE are increased hydrostatic and oncotic pressure imbalance across the lung capillaries (transudate or protein-poor fluid). These mechanisms lead to increased pleural membrane leakage overreaching the normal lymphatics absorptive capacity of the parietal pleura, which is reported to be 0.2 mL/kg/h. Although this lymphatic flow can increase up to 20-fold, demonstrating a large reserve capacity, this mechanism can be saturated when more than a usual amount of pleural fluid is produced. This phenomenon is responsible for most of the PE formation [1]. Effusion due to left heart failure is an exception because, in this case, PE originates from the visceral pleura. In cases of infection and cancer, the underlying pathophysiological mechanism of PE formation is different; it is due to the increased permeability of pleural membranes (exudate PE, protein-rich fluid) [16].

The study of Light et al., after 50 years, still provides the landmark criteria in distinguishing exudative from transudative PE by reporting that: (1) a PE with serum protein (P) ratio (R) > 0.5; (2) PE with serum lactate dehydrogenase (LDH) ratio >0.6; and (3) PE with LDH concentration greater than two-thirds of the upper limit for serum, rule-in the diagnosis of exudate [17]. Moreover, a high hematocrit value in the pleural fluid can confirm the presence of hemothorax (at least 50% of that in the peripheral blood). Cell count restricts the differential diagnoses, because presence of lymphocytes more frequently is associated with cancer, tuberculosis, and rheumatoid PE, while presence of neutrophils usually characterizes parapneumonic PE [18]. Most of the time, when thoracic ultrasound (TUS) for PE is applied, it is not possible to distinguish exudates from transudates. However, by TUS, it is possible to observe some characteristics that may guide the diagnostic process.

9.3 Ultrasound Diagnostic Criteria

Ultrasound examination for PE is a conventional imaging tool, well established from many years. TUS is well suited to visualize a fluid collection in the thorax, (◘ Fig. 9.1). However, during the last years, thanks to the advent of the modern consideration of bedside lung ultrasound in critical care and emergency, the topic of TUS diagnosis

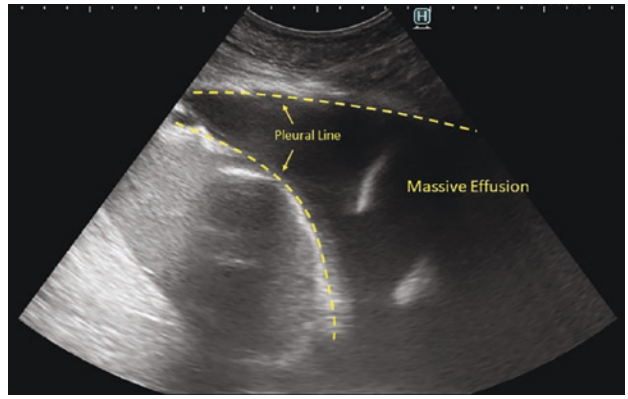

Fig. 9.1 Anechoic, fluid collection in the pleural space

and evaluation of PE has been enriched by more detailed signs and new procedures. The basic diagnostic criteria for the ultrasound diagnosis of PE should follow the recommendations of the first international consensus conference (ICC) on point-of-care lung ultrasound [19].

Technique for PE: the optimal site to visualize free PE is at the posterior axillary line, above the diaphragm. Patients should be placed in supine position and the initial evaluation should start from positioning the probe at the level of the bed, in the lateral regions to visualize the apposition between the diaphragm and the thorax. To optimize sensitivity, special attention should be given to positioning the probe in the most dependent area, directed toward the sky to visualize even the smallest amount of fluid. When the diaphragm apposition zone is visualized, but the probe is placed in the lateral chest not enough inferiorly, there is the possibility of false negative exams. Absence of fluid is demonstrated when the so-called "curtain sign" is visualized, that is the appearance of the artifactual ultrasound image of the lung opposed to the diaphragm and the liver (the spleen on the left side), moving like a curtain synchronously with respiratory acts. Any probe can be used to perform the exam for PE. Of course, the panoramic probes at low frequency (microconvex, phased array, convex) are more indicated to this scope than the linear high frequency probe.

Diagnostic criteria: the document of the ICC reports a clear explanation of the basic signs allowing the ultrasound diagnosis of PE. The main sign is defined as visualization of *a space between the pleural layers*. A second important criterion is visualization of a sinusoid movement of the lung inside the space (*sinusoid sign*). Indeed, when the parietal and visceral pleurae separated by a space move intermittently closer one to the other with respiration, it gives on the screen the image of a sinusoid movement that can be clearly displayed and demonstrated by M-mode. When a space is visualized, but in a condition of absence of the sinusoid respiratory movement, it is not possible to conclude that that space is fluid. Thus, to diagnose PE both signs must be present.

The spine sign: this sign was not considered in the ICC. However, it is worthy to be mentioned because it may be of some help especially for beginners [20]. When a low frequency panoramic probe is used in the examination of the abdomen, it is possible to visualize the vertebral bodies appearing at the bottom of the image as hyper-

echoic or brilliant white reflecting objects beneath the diaphragm. In a normal condition, the image of the vertebral spine abruptly disappears at the level of the diaphragm due to the interposition of the aerated lung. In presence of PE, the spine can be visualized even above the diaphragm, in the thorax. Thus, the appearance of the typical image of the vertebral bodies when the probe is placed in the thorax is an indirect sign that confirms PE.

Pitfalls: a frequent pitfall is represented by the visualization of an image that reproduces the echogenic liver reflected in the thorax, just above the diaphragm. This phenomenon is known as *mirror effect* and is a well-known artifact in ultrasonography. The mirroring of the liver may appear on the right side when the probe is placed in the lateral inferior chest, at the bottom of the screen below a regular curtain movement of the lung, and may mimic, especially to the eyes of a non-expert, the presence of a fluid collection. In this case, to avoid misinterpretation, particular attention should be given to the absence of a space between the pleural layers still visible in the upper part of the image at the pleura parietal level and the absence of the spine sign to rule out safely any PE. Moreover, changing the angle of insonation may be useful to a correct interpretation of mirroring.

Differential diagnosis: as said, the main principle for differential diagnosis of the nature of PE is performing the drainage and analyzing the fluid. However, TUS can be of help by following some basic rules. Again, this rule is clearly stated in the ICC document. A PE with internal echoes suggests that it is an exudate or hemorrhage, especially in acute conditions. Only very long-standing chronic transudates occasionally may show internal echoes. When echoic images inside the PE are very complex, like in form of multiple septations or intense sparkling echoic contrast or particles, the diagnosis of exudate or even clotted blood can be confirmed (■ Fig. 9.2). Indeed, in case of anechoic PE, it is not possible to arrive at any conclusion because transudate, exudate, and blood may be totally anechoic, especially in the acute phase [19, 21–23]. Of course, like for other common applications of point-of-care ultrasound, the combination with all the clinical information and patient condition may be helpful to settle dubious cases.

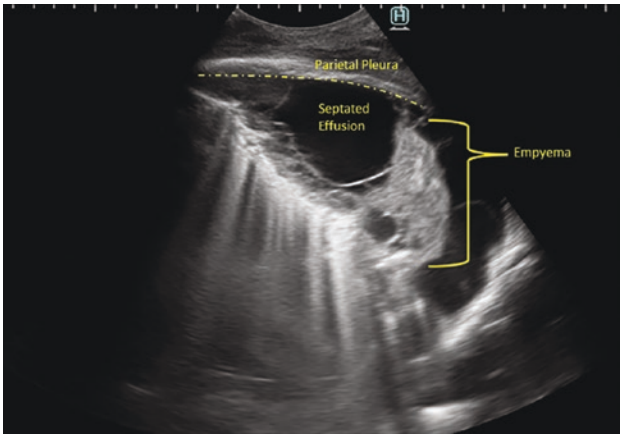

■ **Fig. 9.2** Pleural effusion with complex septation and empyema

9.4 Comparison with Radiologic Tools

In ICU, patients' physical examination with percussion and auscultation has shown low sensitivity and specificity in several trials when compared with imaging modalities such as chest radiography (CXR), TUS, and computed tomography (CT), due to the presence of many factors that can alter the intrathoracic transmission of sounds (i.e., mechanical ventilation, subcutaneous emphysema, uncooperative patients, presence of surgical drains) [1]. The evaluation of CT imaging is the gold standard. Indeed, CT shows a reference sensitivity for PE, far superior to CXR and close, but still superior, to TUS. However, the extensive use of CT is limited because it requires moving the patients to the radiology suite and exposure to ionizing radiations. Thus, the two main bedside options remain CXR and TUS. However, CXR's minimum sign that confirms the presence of PE, that is, an opacity obliterating the hemidiaphragmatic sinus, requires a volume of at least 200 or 500 mL to be viewed. Moreover, the possibility of coexisting parenchymal lung opacities and the supine position with anterior-posterior views, typical conditions of ICU patients, determine a further decrease in sensitivity due to poorer image quality. In 2008, Rocco et al. published a trial comparing bedside CXR and TUS for the diagnosis of PE in trauma patients. They found TUS more accurate than CXR [24]. Another study comparing the diagnostic accuracy of TUS and bedside CXR in ICU patients showed the excellent sensitivity, specificity, and accuracy of 100%, whereas CXR showed suboptimal corresponding values of 65%, 81%, and 69% [25]. Other studies confirmed the superiority of TUS [26]. Based on the existing evidence and the discussion among experts, the first ICC on point-of-care lung ultrasound stated that for the detection of effusion, TUS is more accurate than supine CXR [19].

9.5 Assessment of Fluid Volume

In the practical clinical activity, it is not common the necessity to quantify the PE. Sometimes, due to internal protocols or specific conditions, a qualitative semiquantification in small, medium, and large PE is clinically needed. Qualitative quantification may be based on a simple visual eyeball technique that, of course, is highly variable between operators. However, there is also the possibility to use TUS for a more precise volumetric quantification. To this purpose, many formulas exist that allow the estimation of the volume of a PE. The common element to all the formulas proposed is a measurement of the distance between the two pleurae separated by the effusion [27, 28]. Vignon et al. measured the maximal perpendicular interpleural distance (the distance between the lung and posterior chest wall) at the apex and the lung base and compared the maximal distance with the drained volume [29]. Roch et al. used the mean of 3 distances measured between lung and diaphragm, lung and posterior chest wall at the base, lung and posterior chest wall at the fifth intercostal space [30]. Balik et al. measured the maximal interpleural distance (D) at lung base during end-expiration and used the formula Volume (mL) = 16 × D (mm) [31]. Usta et al. measured the maximal distance between the mid-height of the diaphragm and the visceral pleura in the sitting position in spontaneously breathing patients after cardiac surgery [32]. Finally, Remérand et al. identified the lower and upper intercos-

tal spaces where PE was visible in supine patients; the distance between these two points was drawn on the patient's skin to establish pleural effusion paravertebral length (LUS) [33]. The pleural effusion cross-sectional area (AUS) was manually delineated at the halfway point of TUS. The volume of PE was obtained by multiplying LUS by AUS. All these authors found a good correlation between their formulas and measures with the volume of PE drained, showing no superiority of one formula over the others. However, in some studies, the patients were mechanically ventilated and in others TUS was performed during spontaneous breathing with supine mild torso elevation of 15°; in further studies, patients were in a semi-recumbent position (i.e., head and torso at an angle of 40–45°). As fluid follows the law of gravity, the maximal distance (diameter) between parietal and visceral pleura can be influenced by the patient's position and is overestimated when the patient is in the upright position [34]. Thus, in the literature on the topic, there is no standardization of the studies. Overall, the Balik formula—V(mL) = 20 × Sep (mm)—gained much popularity for its simplicity (■ Fig. 9.3). Thus, the simple distance between parietal and visceral pleura allows a gross estimation of PE volume. For example, 2 cm of diameter predicts a volume around 400 mL, 3 cm 600 mL and 4 cm 800 mL.

Some limitations of Balik's equation should be also highlighted. For the left hemithorax, our suggestion is to estimate PE by multiplying intrapleural distance × 15 because the heart occupies some volume, a phenomenon known as the "stone in a water effect" [35]. Moreover, the formula overestimates the volume on some conditions, like in tall males with large thoracic circumference, in cases of small effusions under 200 mL, and in the larger effusions above 1000 mL. The average error of the formula can be calculated in around 158–160 mL). Indeed, a standardization of the method is needed to assess PE volume by TUS . Volumetric CT scan studies enhanced by modern software to measure volumes of PE represent the gold standard [36].

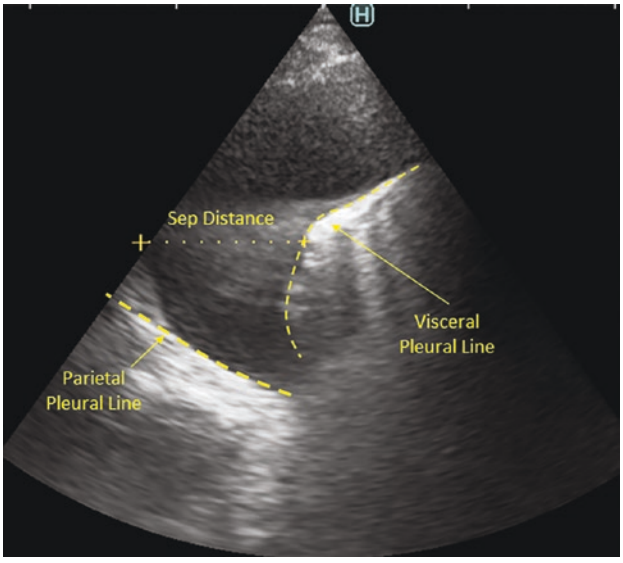

■ **Fig. 9.3** Ultrasound technique and Balik formula—V(mL) = 20 × Sep (mm) to measure the pleural effusion from chest wall to pulmonary parenchyma (dashed line)

9.6 Clinical Symptoms and Outcome

In most ICU patients, PE does not manifest specific symptoms. It is quite common that PE is diagnosed occasionally by CXR reading, performed for other reasons like for standard check of orotracheal intubation and for the post-procedural evaluation of central venous catheter. In non-intubated patients, the most common symptoms of PE are dyspnea with respiratory failure and acute chest pain. The severity of the consequence of PE correlates with the evolution of the underlying disease, the size of the effusion and its etiology. Usually, small PE is well tolerated. The effect of moderate PE depends on the patients' age and clinical condition, and the underlying pathology. Moreover, the timing of growth of the PE volume is also influencing the symptoms. A PE that increases slowly, leaves the time to the respiratory system to find a form of adaptation and larger volumes can be well tolerated by the patient [3]. Indeed, a faster increase of moderate or large PE inside the rib cage reduces the total lung volume and is less tolerated. It is thought that a volume of >500 mL significantly worsens the respiratory mechanics, the gas exchange, and the hemodynamic state, and is associated with high ICU mortality [1].

The size of PE and alteration in gas exchange may be the most important aspects that guide decisions on thoracic drainage. For small sized PE, the benefit of drainage, such as reaching a diagnosis, should be considered against the risks of complications, mainly pneumothorax and hemothorax. At the same time, drainage of moderate and large PE causing acute and severe respiratory symptoms at ICU admission may improve the clinical condition of the patient, improving the gas exchange and reducing the need for tracheal intubation in some patients [37]. Vetrugno et al. addressed the effectiveness of ultrasound-guided placement of a small-bore pleural drain for improving patient respiratory gas exchange demonstrated by the improvement of the PaO2/FiO2 ratio. However, this treatment does not correlate with maintenance of spontaneous breathing after weaning from mechanical ventilation, supporting the concept that PE does not represent the sole parameter that should be considered in the decisions of management [35, 38]. However, it is also important to consider that large PE expands the thoracic cage thus shifting the inspiratory muscles' length-tension curve to an unfavorable condition and contributing to the sensation of dyspnea [37]. Klecka et al. reported a case in which a patient experienced dyspnea relief after thoracentesis despite absence of perfusion in the affected lung [39].

9.7 Ultrasound Thoracocentesis and PE Drainage

The British Thoracic Society guideline on pleural diseases published in 2010 recommends the use of TUS for thoracocentesis or to position a chest tube, to improve the safety of the procedures, particularly in ventilated ICU patients and for small, loculated effusions [40]. Traditionally, large-bore chest tubes (24–32 F) have been used for PE drainage, but, more recently, smaller-bore tubes (<14 F) using the modified Seldinger technique have demonstrated to be as effective as larger devices with fewer related complications. Both drains may be attached to a water seal device and can be left in place until the lung expands and the PE is completely drained. The negative

pressure of −10 to −20 cm/H_2O is normally recommended to maintain drainage. However, the early application of suction should be avoided for the increased risk of re-expansion pulmonary edema.

Ultrasound can be of help in finding the appropriate time to remove the drainage. In recent years there has been a global trend toward increased use of small-bore chest drains. This is justified because the risk of serious complications associated with small-bore catheters is quite low, with an incidence of injury of about 0.2% and a mispositioning rate of 0.6% [40]. Small devices have several advantages: they are easier to insert and less painful during the procedure, better tolerated once placed, and have lower placement-related complication rates. In one study, analyzing chest drain complications, the incidence of injury with large bore versus small bore catheters was 1.4% versus 0.2%, the incidence of mispositioning was 6.5% versus 0.6%, and the incidence of empyema was 1.4% versus 0.2%, respectively [41]. Training programs using appropriate manikins should be encouraged to teach residents and clinicians how to use TUS to guide a pleural procedure.

9.8 Procedure for Drainage of PE

(a) *Dissecting procedure with large-bore drainage*: the optimal puncture site can be chosen by TUS and then putting a mark over the skin. In this case, particular attention should be given to avoid any movement of the patient after the maneuver, to maintain the anatomical reference obtained by TUS. Without the use of TUS, usually the fifth or sixth intercostal space along the mid-axillary line, in axis with the nipple, is applied as a blind anatomical mark. The needle should be inserted just above the rib to avoid injuries to the intercostal vessels and nerves that run below the inferior margin. In a semi-recumbent position of 40–45°, an open incision with a scalpel should be done using local anesthetic for a pain-free procedure. Then, a blunt dissection of deep tissues with forceps is applied, and the drainage introduced with the finger or with the help of a Kelly. The force of the insertion should be dosed because of the risk to injure intra-thoracic structures. Finally, a stitch and dressing are applied to keep the tube in place. The tube will be attached to a one-way drainage system that only allows air and fluid to flow out from the pleural space to obtain lung expansion.

(b) *Seldinger technique and small bore-drainage*: to estimate PE, it is possible to apply the Balik formula. The patient is placed in supine position with the trunk elevated at 15° and measures are taken. When the patient is hemodynamically stable without the need of high dose of amine, after measurements, the patient can be moved to semi-recumbent position at 40–45°. This position increases the margin for a safe maneuver because the fluid will follow the gravity and the lung will be pushed away. The homolateral patient's arm is elevated behind the head to facilitate access to the safety triangle. The safety triangle is bordered by the lateral edge of the pectoralis major, the lateral edge of the latissimus dorsi and a line along the fifth intercostal space at the level of the nipple (◘ Fig. 9.4). The Thoracic British Society has recommended this zone as the best puncture site [40].

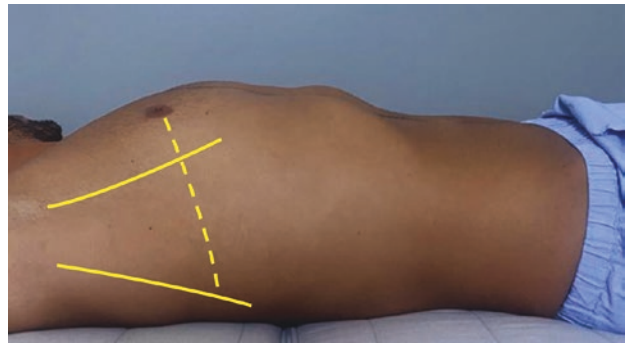

Fig. 9.4 The safety triangle, bordered by the lateral edge of the pectoralis major, the lateral edge of the latissimus dorsi, and a line along the fifth intercostal space at the level of the nipple

Scanning by TUS, this zone allows the operator to visualize the diaphragm, the lung, the PE, and intrabdominal organs. Of course, attention should be paid to perform a pain-free maneuver by using a local anesthetic, and to prevent infections by wearing sterile medical protections and skin antiseptics. Ultrasound can be used to choose the puncture site and mark the skin (ultrasound assist procedure) or for a real-time visualization and guidance of the needle (ultrasound guided procedure). This latter approach is technically more difficult but also safer [42]. A low frequency (3.5–5 MHz) ultrasound transducer (convex or phased array probe) can facilitate the panoramic view of the thorax, diaphragm, and upper abdomen. When real-time guidance is chosen, the high-frequency (7–15 MHz) ultrasound transducer (linear probe) is better used in a second step to obtain a better resolution imaging of the rib and the intercostal space. The probe should be oriented in a transverse scan between two ribs. The puncture site and the needle trajectory must be carefully designed with particular attention to the depth required to reach the pleural fluid and avoid lung injuries. The needle should be advanced slowly only under direct visualization of the tip. Aspiration of fluid with a syringe confirms the correct position and depth. At this point, the guidewire is inserted. It is useful to define the guidewire's final position using TUS before proceeding with dilation and introduction of the tube. Specific caution should be used on patients with coagulopathy and platelet count <50,000/μL, or those affected by pulmonary bullae, and pleural adhesions.

Complications: during the maneuver, there is the possibility to injure the lung, the heart, the liver, and other organs. Bleeding, pneumothorax, and infection are the main complications reported in the literature. At the end of the procedure, the operator should perform a complete bilateral TUS scan to exclude pneumothorax, by following the criteria recommended in the ICC [43]. TUS can rule in pneumothorax with 75% sensitivity, 93% specificity and 92% of diagnostic accuracy, while CXR shows similar specificity, but much less sensitivity [43].

During large PE drainage, caution is needed to avoid re-expansion edema (REE). It is the occurrence of monolateral pulmonary edema secondary to the maneuver. The etiopathogenesis of this condition is not fully known. It is supposed that the increased permeability of pulmonary blood vessels damaged by fast re-expansion of the lung parenchyma and the presence of free oxygen radicals generated by reperfusion of the ischemic lung, together with the increase of pulmonary hydrostatic pres-

sure caused by the improvement of the venous return and the pressure-induced disruption of the alveolar capillaries with altered lymphatic clearance, represent the etiologic cascade causing edema of the affected lung [44]. Mokotedi postulated that REE could be due to decreased pleural and intrathoracic pressure and increased left ventricular afterload occurring after PE drainage, negatively affecting left ventricle performance, especially in a pre-existing condition of moderate compromised systolic function [44]. The main risk factors for REE are: (1) young patients; (2) large volume pleural drainage (>3 L) or high negative pressure suction (more than −20 cm H_2O); (3) lung collapse for over seven days. Because the exact etiology of REE is unclear and a large PE is identified as a predisposing factor, most authors suggest draining no more than 1–1.5 L of fluid per maneuver and applying a device for pleural manometry. However, the incidence of REE has been reported to be from 0.2% up to 14%, and it seems not always to be related to the total amount of fluid removed [40].

Take-Home Messages

- Pleural effusion is less present than expected in ICU patients, but still frequently encountered.
- The examination of the fluid and application of the Light criteria are the landmarks in the differential diagnosis of PE between transudate and exudate.
- TUS is more accurate than supine CXR for the diagnosis of PE.
- Balik's formula, based on the TUS measure of the distance between the two pleural layers separated by fluid, is one of the most used methods allowing a simple assessment of PE volume.
- The volume estimation of PE and the changes in gas exchange are the most important aspects to decide drainage. However, drainage of small pleural effusions may be important to finalize the diagnostic process.
- TUS is recommended for thoracocentesis and to position a chest tube, because it improves the safety of the invasive maneuver in ventilated ICU patients.
- Smaller-bore tubes using the modified Seldinger technique are as effective as the bigger tubes to drain a PE, but give fewer complications.

References

1. Vetrugno L, Brogi E, Gargani L, Bignami E, Barbariol F, Marra A, Forfori F. Thoracic ultrasound for pleural effusion in the intensive care unit: a narrative review from diagnosis to treatment. Crit Care. 2017;21:325.
2. R. Krishna and M. Rudrappa, Pleural effusion., StatPearls, 2021.
3. Vetrugno L, Bignami E, Orso D, Vargas M, Guadagnin GM, Saglietti F, Servillo G, Volpicelli G, Navalesi P, Bove T. Utility of pleural effusion drainage in the ICU: an updated systematic review and META-analysis. J Crit Care. 2019;52:22–32.
4. Angus DC, Barnato AE, Eaton TL, Yealy DM. A randomized trial of protocol-based care for early septic shock. N Engl J Med. 2014:1683–93.
5. Peake S, Delaney A, Bailey M, Williams P. Goal-directed resuscitation for patients with early septic shock. N Engl J Med. 2014:1496–506.
6. Mouncey PR, Osborn TM, Power GS, Singer M. Trial of early, goal-directed resuscitation for septic shock. N Engl J Med. 2015;372:1301–11.

7. Fysh ET, Smallbone P, Mattock N, Gary Lee YC. Clinically significant pleural effusion in intensive care: a prospective multicenter cohort study. Crit Care Explor. 2020;2:e0070.
8. Vieillard-Baron A, Millington SJ, Sanfilippo F, Chew FN. A decade of progress in critical care echocardiography: a narrative review. Intensive Care Med. 2019;45:770–88.
9. Papanikolaou J, Makris D, Saranteas T, Zakynthinos E. New insights into weaning from mechanical ventilation: left ventricular diastolic dysfunction is a key player. Intensive Care Med. 2011;37:1976–85.
10. Feihl F, Broccard A. Interactions between respiration and systemic hemodynamics. Part II: practical implications in critical care. Intensive Care Med. 2008;35(2):198–205.
11. Teboul J-L, Xavier M, Richard C. Weaning failure of cardiac origin: recent advances. Crit Care. 2010;14(2):211.
12. Vetrugno L, Brussa A, Guadagnin GM, Bove T. Mechanical ventilation weaning issues can be counted on the fingers of just one hand.," The Ultrasoung journal, vol. 12; 2020.
13. Cilloniz C, Ferrer M, Liapikou A, Torres A. Acute respiratory distress syndrome in mechanically ventilated patients with community-acquired pneumonia. Eur Repirat J. 2018;51(3):51.
14. E. Shebl and M. Paul, "Parapneumonic pleural effusions and empyema Thoracis.," StatPearls, 2022.
15. Volpicelli G, Gargani L, Perlini S, Vetrugno G. Lung ultrasound for the early diagnosis of COVID-19 pneumonia: an international multicenter study. Intensive Care Med. 2021;47(4):444–54.
16. H. P. D'Agostino and M. A. Edens, "Physiology, pleural fluid.," StatsPearls, 2021.
17. Light RW, Macgregor MI, Luchsinger PC, Ball WC. Pleural effusion. Ann Intern Med. 1972;77(4):507–13.
18. Porcel MJ. Diagnostic approach to pleural effusion in adults. Am Fam Physician. 2006;73(7):1211–20.
19. Volpicelli G, Elbarbary M, International Liaison Committee on Lung Ultrasound (ILC-LUS) for the International Consensus Conference on Lung Ultrasound (ICC-LUS). International evidence-based recommendations for point-of-care lung ultrasound. Intensive Care Med. 2012;38:577–91.
20. Dickman E, Terentiev V, Likourezos A, Derman A, Haines L. Extension of the thoracic spine sign: a new sonographic marker of pleural effusion. J Ultrasound Med. 2015;34(9):1555–61. https://doi.org/10.7863/ultra.15.14.06013.
21. Yang PC, Luh KT, Chang DB, Kuo SH. Value of sonography in determining the nature of pleural effusion: analysis of 320 cases. Am J Roetengenol. 1992;1(159):29–33.
22. Sajadiejh H, Afzali F, Sajadieh V, Sajadieh A. Ultrasound as an alternative to aspiration for determining the nature of pleural effusion, especially in older people. A N Y Accad Sci. 2004;1019:585–92.
23. Qureshi NR, Rahman NM, Gleeson FV. Thoracic ultrasound in the diagnosis of malignant pleural effusion. Thorax. 2009;64(2):139–43.
24. Rocco M, Carbone I, Morelli A, Pietropaoli P. Diagnostic accuracy of bedside ultrasonography in the ICU: feasibility of detecting pulmonary effusion and lung contusion in patients on respiratory support after severe blunt thoracic trauma. Acta Anaesthesiol Scand. 2008;6(52):776–84.
25. Xirouchaki N, Magkanas E, Vaporidis K, Georgopoulos D. Lung ultrasound in critically ill patients: comparison with bedside chest radiography. Intensive Care Med. 2011;37:1488.
26. Seyyed Hossein OH, Adimi I, Vahdati SS, Khiavi RS. Ultrasonographic diagnosis of suspected Hemopneumothorax in trauma patients. Trauma Mon. 2014;19(4):e17498.
27. Mattison LE, Coppage L, Alderman D, Herlong JO, Sahn SA. Pleural effusions in the medical ICU: prevalence, causes, and clinical implications. Chest. 1997;111:1018–23.
28. Fartoukh M, Azoulay E, Galliot R, Schlemmer B. Clinically documented pleural effusions in medical ICU patients: how useful is routine thoracentesis? Chest. 2002;121(1):178–84.
29. Vignon P, Chastagner C, Berkane V, Gastinne H. Quantitative assessment of pleural effusion in critically ill patients by means of ultrasonography. Crit Care Med. 2005;33:1757–63.
30. Roch A, Bojan M, Michelet P, Auffray J. Usefulness of ultrasonography in predicting pleural effusions >500 mL in patients receiving mechanical ventilation. Chest. 2005;127:224–32.
31. Balik M, Plasil P, Waldauf P, Pachl J. Ultrasound estimation of volume of pleural fluid in mechanically ventilated patients. Intensive Care Med. 2006;2(32):318.
32. Usta E, Mustafi M, Ziemer G. Ultrasound estimation of volume of postoperative pleural effusion in cardiac surgery patients. Interact Cardiovasc Thorac Surg. 2010;2(10):204–7.

33. Remerand F, Dellamonica J, Mao Z, Rouby JJ. Multiplane ultrasound approach to quantify pleural effusion at the bedside. Intensive Care Med. 2010;4(36):656–64.
34. Vetrugno L, Bove T. Lung ultrasound estimation of pleural effusion fluid and the importance of patient position.," Ann Intensive Care, vol. 8; 2018. p. 125.
35. Vetrugno L, Volpicelli G, Guadagnin GM, Bove T. Assessment of pleural effusion and small pleural drain insertion by resident doctors in an intensive care unit: an observational study. Clin Med Insights Circ Respir Pulm Med. 2019;13:1–10.
36. Moy MP, Levsky JM, Berko NS, Haramati LB. A new, simple method for estimating pleural effusion size on CT scans. Chest. 2013;4(143):1054–9.
37. Estenne M, Yernault J-C, De Troyer A. Mechanism of relief of dyspnea after thoracocentesis in. Am J Med. 1983;74(5):813–9.
38. Chiao D, Hanley M, Olazagasti JM. CT volumetric analysis of pleural effusions: a comparison with thoracentesis volumes. Acad Radiol. 2015;22(9):1122–7.
39. Klecka EM, Maldonado F. Symptom relief after large-volume thoracentesis in the absence of lung perfusion. Chest. 2014;5(145):1141–3.
40. Havelock T, Teoh R, Laws D, BTS Pleural Disease Guideline Group. Pleural procedures and thoracic ultrasound: British Thoracic Society pleural disease guideline 2010. Thorax. 2010;2:61–76.
41. Mehra S, Heraganahally S, Sajkov D, Bowden J. The effectiveness of small-bore intercostal catheters versus large-bore chest tubes in the management of pleural disease with the systematic review of literature. Lung India. 2020;3(37):198–203.
42. Vetrugno L, Guadagnin GM, Orso D, Bove T. An easier and safe affair, pleural drainage with ultrasound in critical patient: a technical note. Crit Ultrasound J. 2018;10:10–8.
43. Lichtenstein D, Goldstein I, Mourgeon E, Rouby J-J. Comparative diagnostic performances of auscultation, chest radiography, and lung ultrasonography in acute respiratory distress syndrome. Anesthesiology. 2004;100:9–15.
44. Mkotedi CM, Balik M. Is the mechanism of re-expansion pulmonary oedema in a heart-lung interaction? BMJ Case Rep. 2017;2017:bcr2017219340.

Airway Ultrasound for the Intensivist

Ashraf Al-Tayar, Serene SP Ho and Adrian Wong

Contents

10.1 Introduction – 122

10.2 Ultrasound Probe Selection – 123

10.3 Focused Airway Sono-anatomy – 124

10.4 Fundamental Uses of Airway US in ICU – 128
10.4.1 Pre-intubation Assessment – 129
10.4.2 Confirming Endotracheal Intubation/Excluding Oesophageal Intubation – 129
10.4.3 Assessing Depth of ETT – 131
10.4.4 Identification of CTM and Cricothyroidotomy – 131
10.4.5 Percutaneous Dilatational Tracheostomy (PDT) – 132

10.5 Technique of US-Guided PDT – 132

10.6 Training – 133

References – 133

© The Author(s), under exclusive license to Springer Nature Switzerland AG 2023
C. Robba et al. (eds.), *Basic Ultrasound Skills "Head to Toe" for General Intensivists*, Lessons from the ICU,
https://doi.org/10.1007/978-3-031-32462-8_10

Learning Objectives

- Identification of airway anatomy using US
- Predicting a difficult airway
- Identifying the cricothyroid membrane (CTM) for possible cricothyroidotomy
- Confirmation of successful tracheal intubation/detection of oesophageal intubation
- Described the use of US in guiding percutaneous dilatational tracheostomy

10.1 Introduction

Difficult airway management is associated with increased risk of morbidity and mortality in acutely ill patients [1]. Bedside US has become common practice in many ICUs; it can be a valuable tool in many aspects of airway management, including [2]: identification of anatomical landmarks during elective intubation; guidance for elective tracheostomy; real-time identification of tracheal/oesophageal intubation; prediction of the optimal size of ET/tracheostomy tube; and identification of vocal cord palsy. Recently, the ESICM CCUS task force Group [3] identified two main airway US applications for the intensivist (among other more advanced skills): ET tube confirmation and identification of important airway landmarks in patients with potentially difficult airways prior to tracheostomy. The common landmarks that will be mentioned here include the thyroid cartilage, cricoid cartilage, CTM, tracheal cartilage, and oesophagus (Fig. 10.1).

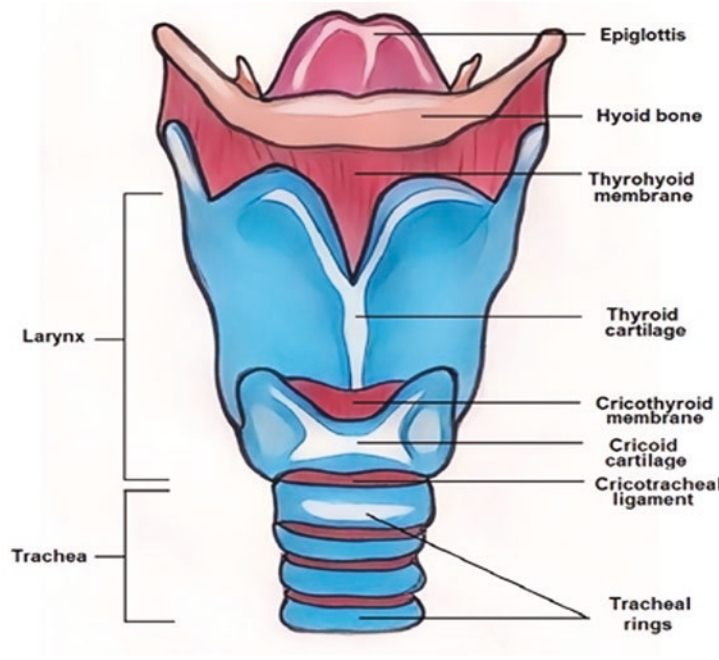

Fig. 10.1 Anatomy of the airway

10.2 Ultrasound Probe Selection

The high-frequency linear and low-frequency curvilinear probes can both be used to assess the airway, although the linear probe (with its high resolution and low penetration properties) may be preferable for superficial structures, e.g. cartilaginous structures, strap muscles, thyroid, as well as blood vessels crossing the neck anteriorly [2]. The probe can be applied in the transverse (Fig. 10.2) and longitudinal planes (Fig. 10.3), and either side of the midline (parasagittal). With the neck in slight extension, it can also be positioned just above the suprasternal notch and angled cephalad.

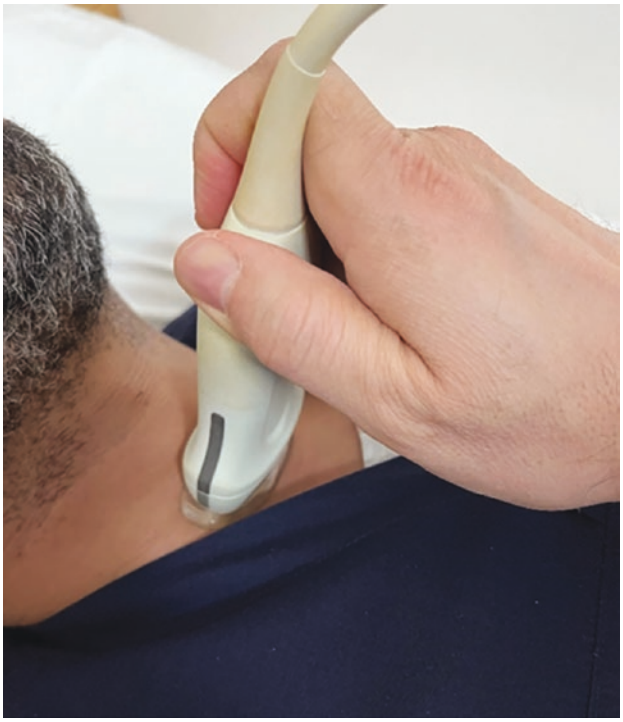

Fig. 10.2 Linear probe above suprasternal notch in transverse plane

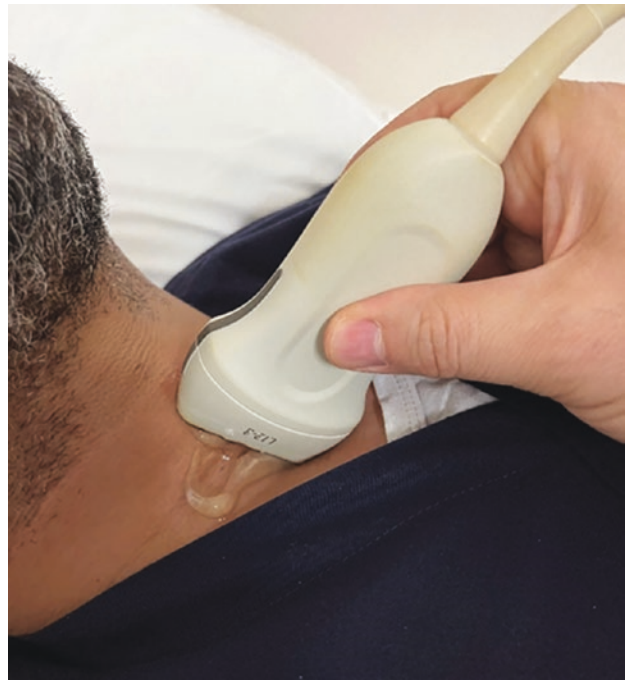

Fig. 10.3 Linear probe in longitudinal/sagittal plane

10.3 Focused Airway Sono-anatomy

The relevant anatomical landmarks for airway management are shown in Fig. 10.1.

Cartilaginous structures appear hypoechoic unless there are calcific changes (which appear as echogenic foci); they are bordered posteriorly by the air-mucosal interface (AMI) which appears as a hyperechoic line (in the transverse [Fig. 10.4] and longitudinal planes [Figs. 10.5 and 10.8]).

The thyroid cartilage forms a triangular or inverted 'v' shape, and can be visualized as the probe is moved cephalad from the suprasternal notch. Vocal cord structures (true cord, false cord, and arytenoids) appear as inverted 'v' shapes through the thyroid cartilage (Fig. 10.6). The triangular appearance of the thyroid cartilage and vocal cords may be lost following endotracheal intubation (Fig. 10.7).

As the probe is moved caudally, the cricoid cartilage appears as a hypoechoic arch in the transverse plane. Rotation of the probe to the longitudinal plane enables visualization of the airway cartilage structures and membranes (Fig. 10.3). The CTM forms a hyperechoic band connecting the thyroid cartilage inferiorly to the superior aspect of the cricoid cartilage, with reverberation artefact of the air-mucosal interface posteriorly (Figs. 10.5 and 10.8). In this plane, the cricoid cartilage forms a large hypoechoic landmark to identify the start of tracheal rings (Fig. 10.8).

The trachea is composed of six cartilaginous rings inferior to the cricoid cartilage, covered by skin, subcutaneous fat, and strap muscles. The thyroid isthmus overlies the second and third tracheal rings. The tracheal rings appear as hypoechoic inverted 'u' shaped structures in transverse plane (Fig. 10.9), or a string of beads if scan-

Fig. 10.4 Air-mucosal interface (AMI) and 'double tract' sign of endotracheal tube (ETT) in situ

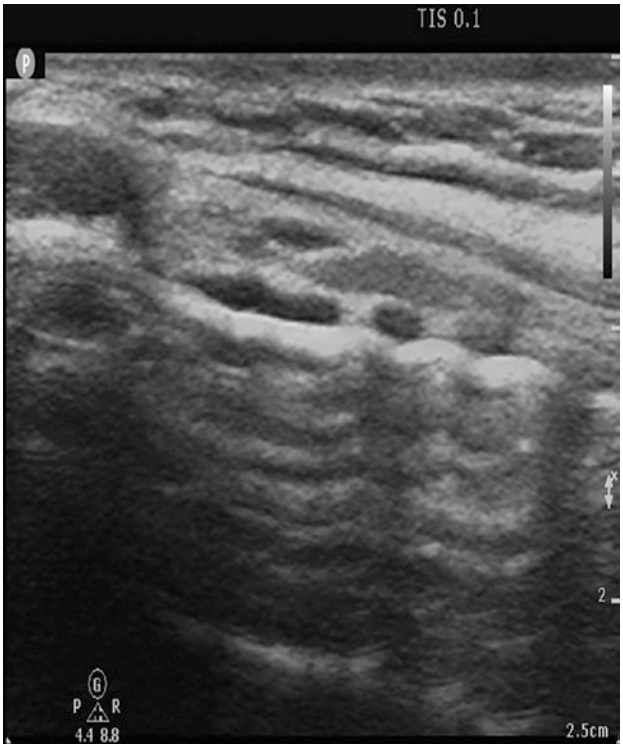

Fig. 10.5 Longitudinal section of cartilaginous structures of airway

Fig. 10.6 Normal inverted 'v' shape of the thyroid cartilage and vocal cords

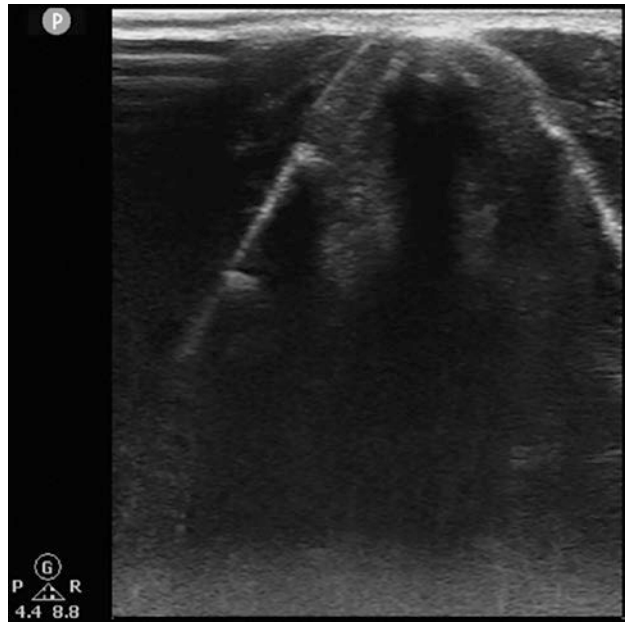

Fig. 10.7 Loss of inverted 'v' shape in the thyroid cartilage and vocal cords following intubation, also known as the 'bullet' sign. Increased echogenicity of the thyroid cartilage is due to calcification

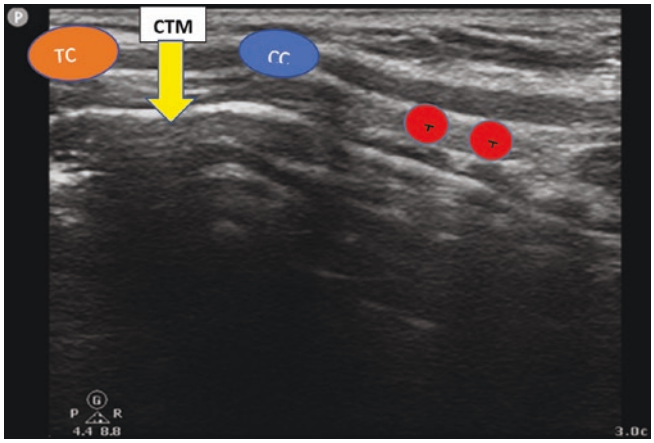

Fig. 10.8 Sagittal (longitudinal) view of the airway. *TC* thyroid cartilage (orange); *CC* cricoid cartilage (blue); *CTM* cricothyroid membrane (white); and *T* tracheal cartilage rings (red)

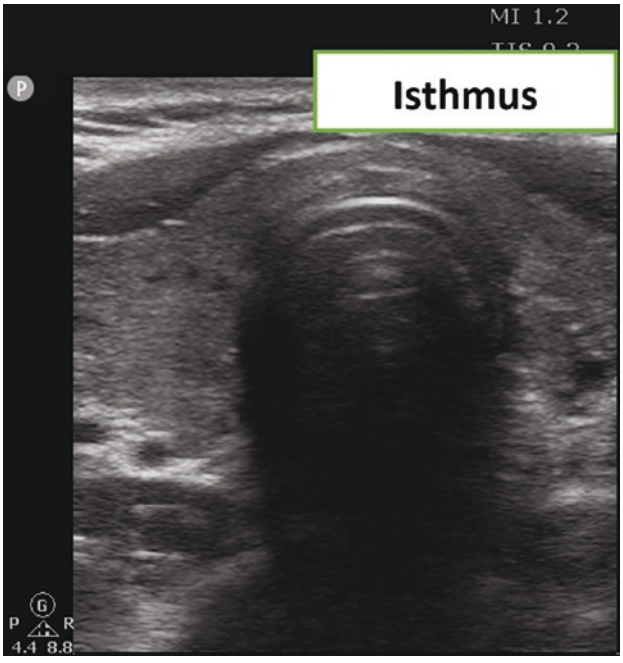

Fig. 10.9 Thyroid overlying tracheal cartilage ring, in the transverse plane

ning longitudinally (Fig. 10.8). The posterior aspects of the tracheal rings are obscured by artefacts due to intraluminal air.

Whilst it is not an airway structure, identification of the oesophagus is important in airway management, if only to exclude erroneous oesophageal intubation. The oesophagus is located on either side of the trachea and has a characteristic bull's eye appearance, when the head is rotated contralaterally at a 45° incline (Figs. 10.10 and 10.11), with the probe transverse at the level of the suprasternal notch.

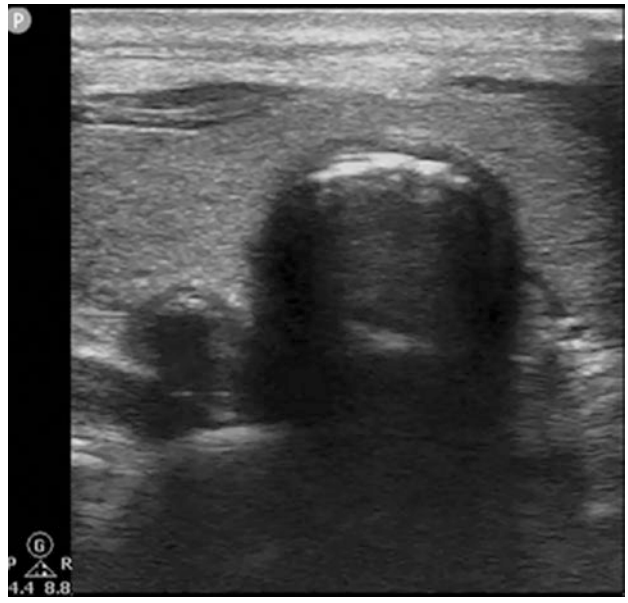

Fig. 10.10 The oesophagus is lateral to the trachea

Fig. 10.11 'Double tract' signs are visible in both trachea and oesophagus, indicative of endotracheal tube (ETT) and nasogastric tube in situ

10.4 Fundamental Uses of Airway US in ICU

The common applications of airway US in ICU practice are summarized in Table 10.1.

Table 10.1 Applications of airway US in ICU

Application	Brief description
Pre-intubation assessment	– Delineate airway anatomy by identifying the thyroid cartilage, cricoid, and tracheal rings – Identify CTM in preparation for emergency cricothyroidotomy) – Identify patients with potentially difficult airway
During and after intubation	– To visualize ETT passing through vocal cords into trachea – Exclude oesophageal intubation – Check tip of ETT lies above carina
Guide percutaneous dilatational tracheostomy (PDT)	– Identify ideal position for needle insertion – Identify expected difficult cases, e.g. thyroid goitre – Locate blood vessels which should be avoided – Exclude pneumothorax after procedure

10.4.1 Pre-intubation Assessment

Difficult intubation in ICU was reported to be in up to 13% of cases [4] and the most used clinical score, through Mallampati assessment was found to be 53% sensitive only in predicting difficult laryngoscopy in the critically ill and this may be found to be even worse in obese and anatomically distorted neck [5]. There are several soft tissue depth measurements on airway US that can predict difficulty in intubation, e.g. skin-hyoid depth of 1.51 cm was associated with difficult intubation in general ICU and trauma patients [6]; this was also noted in patients with skin-vocal cord depth of 1.75 cm and skin-thyrohyoid membrane depth of >2.8 cm [6–8]. Airway US in trauma patients can help identify tracheal injury and paratracheal haematoma; however, it must not delay intubation in urgent cases [9].

US can be used to diagnose subglottic stenosis by measuring the inner diameter of cricoid cartilage in the transverse plane (Fig. 10.12). This can guide the choice of ETT size especially in the paediatric age group [10]; it has been found to be more accurate than the age-based calculations and is comparable to CT/MRI assessment.

10.4.2 Confirming Endotracheal Intubation/Excluding Oesophageal Intubation

Oesophageal ETT displacement occurs in a minority of emergency intubations (approximately 3.3%) and is linked to increased morbidity and mortality [11]. Conventional methods of confirming ETT placement include direct visualization of the tube passing between the vocal cords, misting in ETT, as well as symmetrical air entry on chest auscultation, none of which is fully reliable [12]. Quantitative and qualitative capnography may also be misleading, particularly in situations involving

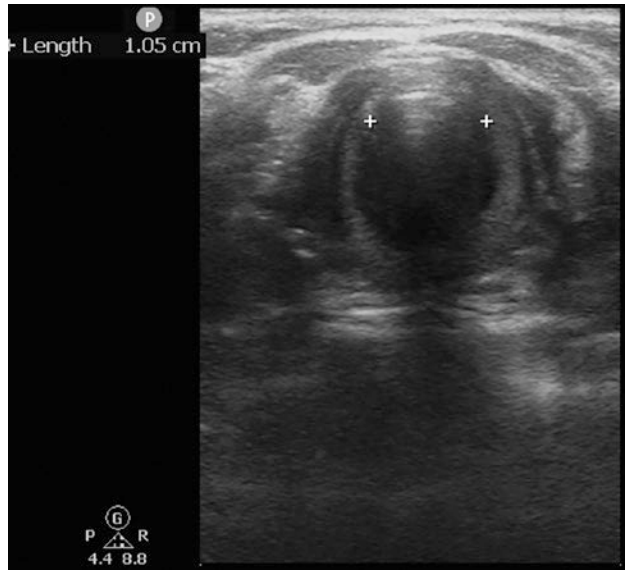

Fig. 10.12 Cricoid cartilage. The distance between '+' symbols is the inner cricoid diameter, which can be used to predict ETT size in paediatric patients

prior bag-mask ventilation, ingestion of carbonated materials as well as in cases of low or no cardiac output (e.g. pulmonary embolism and cardiac arrest).

Furthermore, they require at least five breath cycles to be conclusive, which may be sufficient to cause significant gastric distension and related complications [13, 14]. According to several recent meta-analyses, US is more reliable in confirming ETT placement with excellent sensitivity and specificity [15]; however, in most developed countries, capnography remains the accepted gold-standard for confirming ETT placement. The diagnostic accuracy of US was not affected by the size of ETT. In addition, the time needed to confirm was 12–14 s [15], with a short learning curve for this skill [16]. US was found to be quicker and more efficient in confirming endotracheal intubation during emergency rapid sequence intubation when compared to both auscultation and capnography [9].

Studies showed no difference between linear and curvilinear probes [2, 15], although linear probes are usually recommended for their resolution and smaller footprint in the limited space of the anterior neck.

10.4.2.1 Signs in Airway US (Table 10.2)

With the probe transversely just above the suprasternal notch, identify the trachea and oesophagus. ETT positioning can be checked during intubation (dynamic) or afterwards (static). Studies showed no difference between these two techniques, although the static technique does not apply pressure on the neck during intubation, and is the only option in the absence of an operator to perform real-time US [17, 18]. Endotracheal intubation can be confirmed using several methods on US. Passage of the ET tube into the trachea is seen as fluttering hyperechoic artefacts ('snowstorm sign'). Endotracheal location of the ET tube is confirmed by the presence of two hyperechoic artefacts in the trachea ('double tract' sign, Figs. 10.4 and 10.11) rep-

Table 10.2 US signs to confirm endotracheal intubation

Sonographic sign	Description
'Snowstorm'	Seen as ETT passes through vocal cords into trachea, this provides dynamic confirmation of endotracheal intubation. Cautious back and forth movement of ETT produces a fluttering hyperechoic shadow
'Double tract' (Figs. 10.4 and 10.11)	Two hyperechoic shadows in trachea representing AMI and ETT
'Bullet' (Fig. 10.7)	Thyroid cartilage and vocal cords lose their inverted 'v' shape when there is an ETT in situ, becoming rounded/bullet-shaped

resenting the air–mucosal interface and the ETT; the 'double tract' sign will be seen in the oesophagus in oesophageal intubation (Fig. 10.11). Endotracheal location of ET tube changes the inverted 'v' shape of the vocal cords and thyroid cartilage into a rounded shape ('bullet' sign) [17] (Fig. 10.7).

10.4.3 Assessing Depth of ETT

Right main bronchus intubation is a known complication occurring in around 8% of intubations [19] and can result in hypoxia, atelectasis of the contralateral lung side, and barotrauma if not promptly rectified. US is more accurate than auscultation [20] in confirming the location of the ETT tip above the carina, and maybe comparable to chest X-ray (CXR) [21] which takes an average of 20 min to perform and interpret CXR in ICU.

The presence of bilateral pleural line sliding can be considered an indirect sign of ET intubation and correct ETT position. Absent left-sided pleural sliding in the presence of left lung pulsation (due to transmitted cardiac motion) is indicative of left lung collapse, suggestive of right main bronchial intubation. By the same token, reappearance of left pleural line sliding and disappearance of left lung pulsation upon progressive ETT withdrawal are markers of good ETT position, and have been found to be quicker and better than auscultation and capnography combined [22, 23].

10.4.4 Identification of CTM and Cricothyroidotomy

Cricothyroidotomy is potentially lifesaving in 'can't intubate, can't ventilate' emergency situations. Traditional landmark technique for CTM identification was found to be successful in only 36% of cases, even lower patients with obesity and/or distorted neck anatomy [24, 25]. Airway US increased the success rate for CTM identification fivefold, as well as the rate of successful cricothyroidotomy even in non-straightforward cases (8% versus 81% for landmark and US techniques, respectively [26–28]).

CTM identification using the US has been described above (Fig. 10.8). US guidance for the cricothyroidotomy procedure can be either dynamic or static. Dynamic guidance was associated with a higher success rate (87%) than the landmark technique (58%) [29].

10.4.5 Percutaneous Dilatational Tracheostomy (PDT)

PDT is commonly practiced in ICU, and it is generally preferred over a surgical open tracheostomy. Airway US has several advantages over bronchoscopy, including the ability to visualize the tracheal rings, anterior tracheal wall, and lumen. Assessment of skin-trachea distance can guide choice of puncture cannula (minimize risk of posterior tracheal wall injury) and tracheostomy tube size. The use of colour Doppler can highlight any blood vessels within the field, e.g. high-riding innominate artery, thereby reducing the risk of serious bleeding during and/or after PDT [30]. (v) Selecting the proper site for PDT by avoiding being too caudal will also decrease the risk of injuries to surrounding vessels and hence subsequent bleeding. Airway US does not result in hypercapnia or hypoxia, which can occur during bronchoscopic guidance through air leaks and loss of PEEP [31].

Early identification of cases that need a surgical approach, e.g. thyroid enlargement is possible with airway US [15]. When US and bronchoscopy were used in combination in a prospective series of 72 cases, almost a quarter of cases had a change in puncture site, with one case referred for surgical tracheostomy, based on US identification of thyroid goitre and extensive vessels prior to PDT [32]. Randomized controlled trials have shown that dynamic US guidance significantly improves the first pass rate and puncture accuracy in PDT, while reducing the post-procedure complication rate, as compared to anatomical landmark technique [29].

10.5 Technique of US-Guided PDT

A sterile linear probe positioned transversely in the suprasternal notch allows visualization of the tracheal rings. Colour Doppler is used to identify blood vessels at/near the incision site [33, 34]. Rotation of the probe provides a sagittal view of the first to fourth tracheal rings as a row of hypoechoic shadows above the echogenic AMI (Figs. 10.5 and 10.8).

The thyroid cartilage and cricoid are identified by moving the probe caudally over the first (T1) or second (T2) tracheal ring. The introducer cannula is inserted immediately caudal to the transversely positioned probe at its midpoint, enabling entry in the T1–T2 or T2–T3 space. Advancement of the cannula tip can be followed using soft tissue movement and indentation of the AMI as it enters the trachea, supported by the 'give' that is felt by the operator. The needle, guidewire, dilator, and then tracheostomy tube can all be passed into the targeted intercartilaginous tracheal space.

Following PDT, US can be used to look for bilateral pleural line sliding, the presence of which excludes pneumothorax as a complication (See lung, pneumothorax chapter).

10.6 Training

Significant variations in airway US training exist in the literature. For example, studies exploring its use for real-time identification of tracheal/oesophageal intubation have reported training ranging from a 30-min lecture followed by a single hands-on session to three months of US training as well as variable minimum experience of US-assisted intubations, etc. [17]. Furthermore, prior experience in point-of-care US is likely to affect training requirements in these studies, but has not been consistently reported. In a recent cadaver study involving military flight medic trainees with no previous US experience, a short period of training in the technique resulted in only moderate accuracy for the identification of oesophageal intubation, which is significantly lower than other studies involving personnel with previous US experience [35].

Limitations

- Subcutaneous emphysema may significantly limit visualization of anatomical structures.
- If the cervical oesophagus cannot be identified, airway US cannot be used to identify oesophageal intubation; artefacts from air in the trachea and ETT will prevent visualization of the oesophagus.
- Large diameter nasogastric tubes can mimic the US features of the ETT.
- Selective intubation cannot be detected.

Take-Home Messages

- Airway US is part of the CCUS skill set that can be of benefit to the practitioner; there is no consensus yet to support airway US as an essential basic skill for intensivists.
- Confirmation of ETT position and depth can be performed using US.
- There are many advantages to using US to guide PDT, as compared to traditional techniques, including bronchoscopy.

References

1. Brown CA, Bair AE, Pallin DJ, et al. Techniques, success, and adverse events of emergency department adult intubations. Ann Emerg Med. 2015;65:363–70.
2. You-Ten KE, Siddiqui N, Teoh WH, Kristensen MS. Point-of-care ultrasound (POCUS) of the upper airway. Can J Anaesth. 2018;65(4):473–84. https://doi.org/10.1007/s12630-018-1064-8. Epub 2018 Jan 18.
3. Robba C, Wong A, Al Poole D, Tayar A, et al. Basic ultrasound head-to-toe skills for intensivists in the general and neurointensive care unit population: consensus and expert recommendations of the European Society of Intensive Care Medicine. Intensive Care Med. 2021;47:1347–67.
4. Natt BS, Malo J, Hypes CD, Sakles JC, Mosier JM. Strategies to improve first attempt success at intubation in critically ill patients. Br J Anaesth. 2016;117(suppl_1):i60–8.
5. Green SM, Roback MK. Is the Mallampati score useful for emergency department airway management or procedural sedation? Ann Emerg Med. 2019;74(2):251–9.

6. Srinivasarangan M, Akkamahadevi P, Balkal VC, Javali RH. Diagnostic accuracy of ultrasound measurements of anterior neck soft tissue in determining a difficult airway. J Emerg Trauma Shock. 2021;14(1):33–7.
7. Wu J, Dong J, Ding Y, Zheng J. Role of anterior neck soft tissue quantifications by ultrasound in predicting difficult laryngoscopy. Med Sci Monit. 2014;20:2343–50.
8. Ezri T, Gewürtz G, Sessler DI, et al. Prediction of difficult laryngoscopy in obese patients by ultrasound quantification of anterior neck soft tissue. Anesthesia. 2003;58(11):1111–4.
9. Mishra PR, Bhoi S, Sinha TP. Integration of point-of-care ultrasound during rapid sequence intubation in trauma resuscitation. J Emerg Trauma Shock. 2018;11(2):92.
10. Pillai R, Kumaran S, Jeyaseelan L, George SP, Sahajanandan R. Usefulness of ultrasound-guided measurement of the minimal transverse diameter of subglottic airway in determining the endotracheal tube size in children with congenital heart disease: a prospective observational study. Ann Card Anaesth. 2018;21(4):382–7.
11. Clyburn P, Rosen M. Accidental esophageal intubation. Br J Anaesth. 1994;73:55–63.
12. Takeda T, Tanigawa K, Tanaka H, et al. The assessment of three methods to verify tracheal tube placement in the emergency setting. Resuscitation. 2003;56:153–7.
13. Tanigawa K, Takeda T, Goto E, et al. Accuracy and reliability of the self-inflating bulb to verify tracheal intubation in out-of-hospital cardiac arrest patients. Anesthesiology. 2000;93:1432–6.
14. Li J. Capnography alone is imperfect for endotracheal tube placement confirmation during emergency intubation. J Emerg Med. 2001;20(3):223–9.
15. Gobatto ALN, Besen BAMP, Tierno PFGMM, et al. Ultrasound-guided percutaneous dilational tracheostomy versus bronchoscopy-guided percutaneous dilational tracheostomy in critically ill patients (TRACHUS): a randomized no inferiority controlled trial. Intensive Care Med. 2016;42:342–51.
16. Chenkin J, McCartney CJ, Jelic T, et al. Defining the learning curve of point-of-care ultrasound for confirming endotracheal tube placement by emergency physicians. Crit Ultrasound J. 2015;7(1):14.
17. Gottlieb M, Nakitende D, Sundaram T, et al. Comparison of static versus dynamic ultrasound for the detection of endotracheal intubation. West J Emerg Med. 2018;19(2):412–6.
18. Gottlieb M, Holladay D, Burns KM, Nakitende D, Bailitz J. Ultrasound for airway management: an evidence-based review for the emergency clinician. Am J Emerg Med. 2020;38(5):1007–13.
19. Geisser W, Maybauer DM, Wolff H, Pfenninger E, Maybauer MO. Radiological validation of tracheal tube insertion depth in out-of-hospital and in-hospital emergency patients. Anesthesia. 2009;64(9):973–7.
20. Ramsingh D, Frank E, Haughton R, et al. Auscultation versus point-of-care ultrasound to determine endotracheal versus bronchial intubation: a diagnostic accuracy study. Anesthesiology. 2016;124(5):1012–20.
21. Butcher CH, Levitov A. A comparison of CXR versus a specific ultrasound protocol to ascertain endotracheal tube position after intubation in the ICU: a pilot study. Chest. 2009;136(4):69S.
22. Weaver B, Lyon M, Blaivas M. Confirmation of endotracheal tube placement after intubation using the ultrasound sliding lung sign. Acad Emerg Med. 2006;13(3):239–44.
23. Kerrey BT, Geis GL, Quinn AM, et al. A prospective comparison of diaphragmatic ultrasound and chest radiography to determine endotracheal tube position in a pediatric emergency department. Pediatrics. 2009;123(6):e1039–44.
24. Cook T, Woodall N, Frerk C. Major complications of airway management in the UK: results of the Fourth National Audit Project of the Royal College of Anaesthetists and the Difficult Airway Society. Part 1: anesthesia. Br J Anaesth. 2011;106(5):617–31.
25. Schaumann N, Lorenz V, Schellongowski P, et al. Evaluation of Seldinger technique emergency cricothyroidotomy versus standard surgical cricothyroidotomy in 200 cadavers. Anesthesiology. 2005;102:7–11.
26. Kristensen MS, Teoh WH, Rudolph SS. Ultrasonographic identification of the cricothyroid membrane: best evidence, techniques, and clinical impact. Br J Anaesth. 2016;117(1):39–48.
27. You-Ten KE, Desai D, Postonogova T, Siddiqui N. Accuracy of conventional digital palpation and ultrasound of the cricothyroid membrane in obese women in labour. Anaesthesia. 2015;70:1230–4.

28. Siddiqui N, Arzola C, Friedman Z, Guerina L, You-Ten KE. Ultrasound improves cricothyrotomy success in cadavers with poorly defined neck anatomy: a randomized control trial. Anesthesiology. 2015;123(5):1033–41.
29. Rudas M, Seppelt I, Herkes R, Hislop R, Rajbhandari D, Weisbrodt L. Traditional landmark versus ultrasound-guided tracheal puncture during percutaneous dilatational tracheostomy in adult intensive care patients: a randomized controlled trial. Crit Care. 2014;18(5):514. https://doi.org/10.1186/s13054-014-0514-0.
30. Hatfield A, Bodenham A. Portable ultrasonic scanning of the anterior neck before percutaneous dilatational tracheostomy. Anaesthesia. 1999;54:660–3.
31. Reilly PM, Sing RF, Giberson FA, Anderson HL, Rotondo MF, Tinkoff GH, Schwab CW. Hypercarbia during tracheostomy: a comparison of percutaneous endoscopic, percutaneous Doppler, and standard surgical tracheostomy. Intensive Care Med. 1997;23:859–64.
32. Kollig E, Heydenreich U, Roetman B, Hopf F, Muhr G. Ultrasound and bronchoscopic controlled percutaneous tracheostomy on trauma ICU. Injury. 2000;31:663–8.
33. Chacko J, Nikahat J, Gagan B, et al. Real-time ultrasound-guided percutaneous dilatational tracheostomy. Intensive Care Med. 2012;38:920–1.
34. Sustić A, Zupan Z, Antoncić I. Ultrasound-guided percutaneous dilatational tracheostomy with laryngeal mask airway control in a morbidly obese patient. J Clin Anesth. 2004;16:121–3.
35. Hanlin ER, Zelenak J, Barakat M, Anderson KL. Airway ultrasound for the confirmation of endotracheal tube placement in cadavers by military flight medic trainees—a pilot study. Am J Emerg Med. 2018;36(9):1711–4. https://doi.org/10.1016/j.ajem.2018.01.074. Epub 2018 Feb 2

Ultrasound Assessment of the Respiratory Muscles

Annemijn H. Jonkman, Nuttapol Rittayamai, Annia Schreiber, Laurent Brochard, and Alberto Goffi

Contents

11.1 Introduction – 139

11.2 Anatomy of the Respiratory Muscles – 139
11.2.1 Diaphragm – 140
11.2.2 Intercostal Muscles – 141
11.2.3 Abdominal Muscles – 142

11.3 Diaphragm Ultrasound – 142
11.3.1 Diaphragm Excursion – 143
11.3.2 Diaphragm Thickness and Thickening Fraction – 145

11.4 Extra-diaphragmatic Muscle Ultrasound – 148
11.4.1 Parasternal Intercostal Muscle Ultrasonography – 148
11.4.2 Abdominal Muscle Ultrasonography – 149

11.5 Clinical Applications – 151
11.5.1 Identification of Diaphragm Dysfunction – 151
11.5.2 Prediction of Weaning Outcomes – 153
11.5.3 Assessment of Breathing Effort – 155
11.5.4 Muscle Ultrasonography in Neuromuscular Diseases – 155
11.5.5 Assessment of Patient-Ventilator Asynchronies – 157

11.6 Pitfalls and Limitations – 158

© The Author(s), under exclusive license to Springer Nature Switzerland AG 2023
C. Robba et al. (eds.), *Basic Ultrasound Skills "Head to Toe" for General Intensivists*, Lessons from the ICU,
https://doi.org/10.1007/978-3-031-32462-8_11

11.7 Emerging and Future Developments – 158
11.7.1 Tissue Doppler Imaging – 159
11.7.2 Strain Imaging – 159
11.7.3 Shear Wave Elastography – 159
11.7.4 Echogenicity – 160

References – 162

Learning Objectives

- To describe sonographic assessment of respiratory muscles (diaphragm and extra-diaphragmatic respiratory muscles)
- To describe main clinical and research applications of respiratory muscle ultrasonography
- To identify limitations and pitfalls of respiratory muscle ultrasonography
- To introduce emerging applications and discuss possible future directions of respiratory muscle ultrasonography

11.1 Introduction

The various muscles that closely work together to maintain alveolar ventilation are commonly called "respiratory muscles." Dysfunction of these respiratory muscles is exceedingly common in mechanically ventilated critically ill patients (>60% of patients [1]) and often results in difficult ventilator liberation [2, 3]. Respiratory muscle dysfunction is associated with poor clinical outcomes, including prolonged intensive care unit (ICU) stay, a higher risk of complications and increased mortality [1, 3, 4]. Although a range of factors could impair respiratory muscle function in the critically ill, mechanical ventilation itself plays a crucial role. Excessive ventilator unloading resulting in low respiratory drive and muscle inactivity is associated with atrophy and alterations in respiratory contractile properties [5–9], whereas excessive breathing efforts due to insufficient ventilator assist or excessive respiratory drive may result in diaphragm injury [10, 11], but strong clinical evidence for the latter is still lacking.

Monitoring the respiratory muscle function is important to limit the detrimental consequences of mechanical ventilation on the respiratory muscles [12, 13]. The use of ultrasound for this purpose is relatively new, but it is becoming increasingly popular in the Intensive Care Unit (ICU) due to its non-invasive nature, real-time visualization, relatively fast learning curve, and bedside availability. Examination of the respiratory muscles by ultrasound could (1) detect respiratory muscle dysfunction either pre-existing or that has developed during mechanical ventilation; (2) quantify the degree of muscle activation during patient effort; and (3) help to identify patients at risks of weaning failure [14]. Diaphragm ultrasound has become a well-established tool to be used at the bedside and the technique and its reproducibility have now been extensively evaluated in healthy subjects, ambulatory patients, and critically ill patients. In contrast, ultrasound of the extra-diaphragmatic inspiratory and expiratory muscles is still in its infancy and has been mostly used as a research tool.

In this chapter, we provide an overview of the principles of respiratory muscle ultrasound and its clinical applications. We also describe key pitfalls and limitations and introduce future directions.

11.2 Anatomy of the Respiratory Muscles

The respiratory muscles are skeletal muscles whose primary task is to displace the chest wall rhythmically to allow effective alveolar ventilation and therefore gas exchange [15, 16]. As the chest wall consists of two compartments, the rib cage and

the abdomen, muscles of both compartments are involved in different tasks of breathing [17]. These two compartments are mechanically arranged in parallel; therefore, lung inflation/deflation can occur by volume changes in either the rib cage or the abdomen or in both compartments concurrently. Principal inspiratory muscles are the diaphragm, followed by external intercostal and parasternal intercostal muscles; accessory inspiratory muscles are traditionally considered the scalene, sternocleidomastoids, *pectoralis major* and *minor*, *serratus anterior*, *serratus posterior superior*, *elevator scapulae*, and *trapezius*. Expiratory muscles include the abdominal wall muscles (external and internal oblique, *transverse abdominis*, and rectus abdominis), internal intercostal muscles and *triangularis sterni.* The diaphragm is the main inspiratory muscle, whereas accessory inspiratory muscles are activated in conditions of high respiratory loading or low diaphragm capacity [18]. In normal conditions, expiration is passive and does not involve activation of expiratory muscles. When the (relative) load imposed on the inspiratory muscles significantly increases (e.g., during exercise, low inspiratory muscle capacity, or intrinsic positive end-expiratory pressure - PEEP), the expiratory muscles are frequently activated [16–19], as well as in situations when forced exhalation is needed, such as with coughing. In addition, expiratory muscles contribute to respiration by (1) acting as a fulcrum against which the diaphragm can contract (intercostal and abdominal muscles); (2) stabilizing the rib cage, preventing its inward collapse during diaphragmatic contraction (intercostal muscles); (3) maintaining a steep functionally efficient dome-shape of the diaphragm by preventing caudal relocation of abdominal content (abdominal muscles).

11

11.2.1 Diaphragm

The diaphragm is a thin musculotendinous structure whose muscle fibers diverge from a central tendinous structure (central tendon) toward their insertion points at the level of (1) the xiphoid process of the sternum (sternal portion); (2) the internal surface and the superior margin of the last six ribs (costal portion); and (3) the first three lumbar vertebrae and the aponeurotic arcuate ligaments (crural or vertebral portion) [17, 20]. From a functional perspective, the crural and costal regions are involved in different processes, with the costal fibers involved in respiration and the crural ones in prevention of gastroesophageal reflux [20]. From their insertion to the ribs, the costal fibers run obliquely in a cranial–dorsal direction, directly apposed to the internal aspect of the lower rib cage ("zone of apposition"). At resting condition (i.e., at functional residual capacity), the zone of apposition represents a significant portion of both the diaphragmatic surface (60–65% of the total surface area) and the rib cage surface (25–40%) [21]. This specific anatomic organization can be represented as an elliptical cylindroid (the zone of apposition) capped by a dome (primarily the central tendon) (◘ Fig. 11.1a). During inspiration, the contraction of muscle fibers leads to shortening of the apposed diaphragm in the cranio-caudal length and subsequent descent of the dome of the diaphragm relative to its costal insertions. Basically, the diaphragm can be imagined as a piston that produces both an expansion of the pleural cavity in its cranio-caudal axis and a displacement of the abdominal viscera. In addition, the costal fibers, due to their point of insertion on the lower six ribs, cause their lift and rotation outward [22].

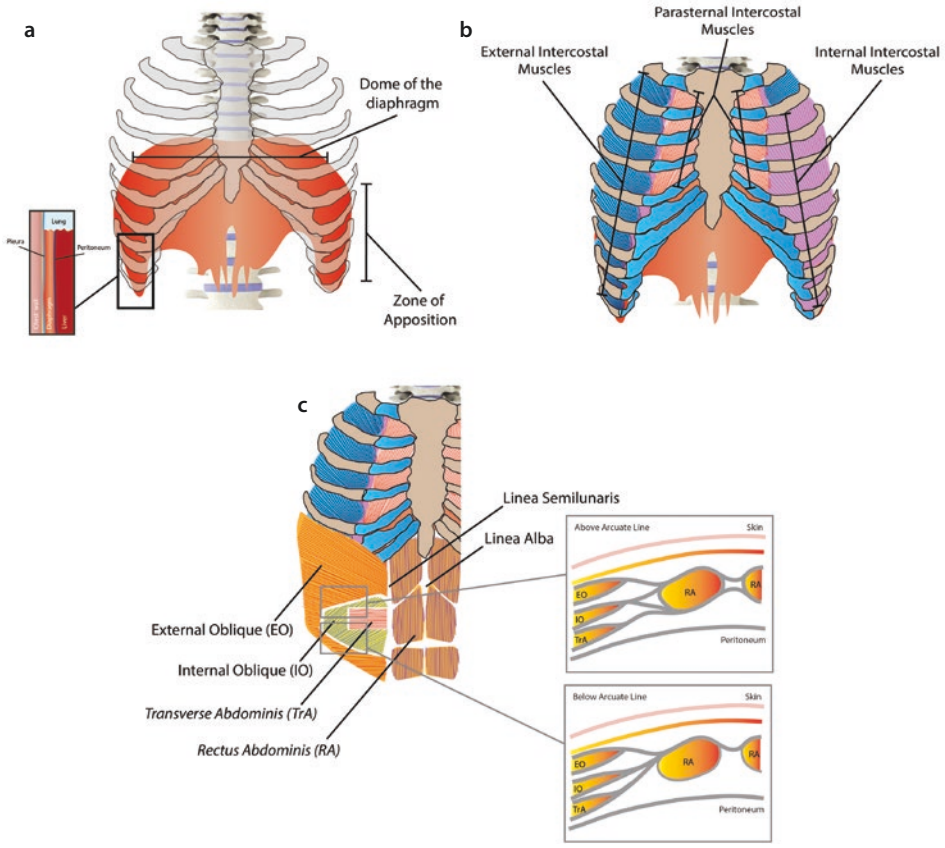

Fig. 11.1 **a** Schematic of diaphragm and its zone of apposition. **b** Schematic of Intercostal muscles. **c** Schematic of abdominal expiratory muscles

11.2.2 Intercostal Muscles

The intercostal muscles are two thin muscular layers that occupy each intercostal space (Fig. 11.1b).

- The **external intercostal muscles** (i.e., more superficial) stretch obliquely and caudally from the tubercle of the superior ribs to the chondrocostal junction of the inferior ribs (i.e., the fibers run in a caudal-ventral direction).
- The **internal intercostal muscles** (i.e., deeper layer) stretch obliquely from the chondro-sternal junctions of the superior ribs to near the tubercle of the inferior ribs (i.e., the fibers run in a caudal-dorsal direction).
- Because of these different anatomical insertions, the intercostal spaces contain two layers of muscles only in the lateral portion of the chest, whereas in the anterior and dorsal portions, there is only one layer of muscle. In particular, only the internal intercostals are present ventrally between the sternum and the chondrocostal junctions and the external intercostals are replaced by a fibrous aponeurosis (anterior intercostal membrane). The internal intercostals at this level are called "**parasternal intercostal muscles**" and functionally acts as inspiratory muscles.

The effect of the intercostal muscles on the ribs is quite complex and even nowadays not completely elucidated. For a more comprehensive description, we refer to previously published reviews on the topic [15–17, 21, 23–25]. For simplicity, we could consider the parasternal and external intercostal muscles as inspiratory muscles, whereas the internal interosseous intercostals have expiratory effects.

11.2.3 Abdominal Muscles

Four muscles of the abdominal wall are involved as expiratory muscles: *rectus abdominis* (medial abdominal muscle), external and internal obliques, and *transverse abdominis* (collectively called lateral abdominal muscles) (Fig. 11.1c). Contraction of these muscles: (1) draws the abdominal wall inward, leading to cranial displacement of the diaphragm into the thoracic cavity; (2) pulls the lower ribs caudally, causing rib cage deflation [17]. The *rectus abdominis* is least involved in active expiration and mainly provides stability to the trunk.

- The **rectus abdominis muscle** is a long, paired muscle located on either side of the midline that runs vertically from the sternum and fifth–seventh costal cartilages to the pubis. Its primary function is non-respiratory, flexion of the thoracic and lumbar spine. The linea alba is a midline fibrous structure that separates the right and left rectus abdominis muscles. The linea semilunaris is a vertical, curved tendinous structure that runs along the lateral border of the rectus abdominis; at its level, the tendons of the lateral abdominal muscles meet the rectus sheath, which either surrounds (above the arcuate line) or anteriorly covers (below the arcuate line) the rectus abdominis muscle.
- The oblique muscles are located laterally to the rectus abdominis muscle. The **external abdominal oblique muscle** is the most superficial and the largest of the lateral abdominal muscles. It originates from the lower eight ribs and covers the lower ribs and the intercostal muscles; its fibers run caudally and insert into the iliac crest, the inguinal ligament and the linea alba. The **internal abdominal oblique muscle** lies deep to the external oblique. It originates from the inguinal ligament in the iliac crest and inserts into the anterolateral aspect of the cartilages of the last three ribs and into the linea alba.
- The **transverse abdominis muscle** is the deepest among the lateral abdominal muscles. It originates from the inner surface of the lower six ribs, the lumbar fascia, the iliac crest and the inguinal ligament and runs medially into the rectus sheath.

11.3 Diaphragm Ultrasound

Ultrasound can be used to assess the muscular structure, mobility, activity, and function of the diaphragm. Common sonographic assessments of the diaphragm are (1) diaphragm excursion, (2) diaphragm thickness, and (3) diaphragm thickening fraction. A consensus statement on these measurement techniques was recently published [26].

11.3.1 Diaphragm Excursion

11.3.1.1 Image Acquisition and Parameters

Low frequency (2–5 MHz) phased array (cardiac) or curvilinear (abdominal) transducers can be used to measure diaphragm excursion. A subcostal approach is preferred, and the patient should be in supine or semi-recumbent position. Diaphragm excursion should be assessed without any ventilator support (T-piece trial or lowest CPAP level possible), since positive pressure provided by ventilator insufflation will also result in caudal diaphragm displacement that cannot be distinguished from displacement owing to true patient effort. In addition, the PEEP level should be as low as feasible and safe, since PEEP results in a more caudal diaphragm position and may affect the capacity of the muscle to generate excursion. Both hemidiaphragms can be visualized with ultrasound; however, the left hemidiaphragm is more difficult to evaluate due to the poor acoustic window of the spleen.

The ultrasound transducer is placed at the (right) subcostal area, just below the costal margin, between the anterior axillary and the midclavicular lines (◘ Fig. 11.2a). To allow the ultrasound beam to insonate perpendicularly the posterior part of the dome of the right hemidiaphragm, the ultrasound probe should be angled as much as possible cranially, medially, and dorsally. The (right) hemidiaphragm is identified as a bright echogenic line attached to the liver (◘ Fig. 11.2b). This bright echogenic line is generated by the pleural and peritoneal layers surrounding the diaphragm; at this depth and with a low frequency transducer, these two layers are not clearly separated, and the diaphragm cannot be clearly identified.

Initially, the B-mode is used to identify the best position of the ultrasound probe; then, M-mode is activated to measure diaphragm excursion by placing the M-line perpendicular to the diaphragm and in line with its movement [26]. As during inspiration the diaphragm moves caudally, the bright echogenic line moves toward the transducer. Diaphragm excursion is quantified as the amplitude of diaphragmatic movement during respiration (the perpendicular distance between the end of expiration and the end of inspiration). Maximum depth of the ultrasound beam should be adjusted to obtain the maximum excursion and the sweep speed should be adjusted to the lowest possible speed to capture a minimum of three breaths in the same ultrasound image (◘ Fig. 11.2c). Due to breath-by-breath variability, the average value of diaphragm excursion from three to five breaths should be taken.

When the diaphragm is difficult to visualize in the subcostal window, the movement of the liver and spleen, as assessed in the posterolateral area on the chest wall, is a good alternative (◘ Fig. 11.2d). This allows assessing the direction of diaphragm movement, but not its quantification (the M-mode line cannot be placed in line with the direction of diaphragm movement).

11.3.1.2 Interpretation

Diaphragm excursion can be measured during quiet breathing—a measure associated with tidal inspiratory effort—or during a maximum inspiratory effort (deep breathing or sniff maneuver)—a measure associated with diaphragm function (◘ Fig. 11.3a–c). Normal values of right diaphragm excursion in healthy subjects during quiet breathing, deep breathing, and voluntary sniffing have been reported to be 1.8 ± 0.3, 7.0 ± 1.1, and 2.9 ± 0.6 cm in men and 1.6 ± 0.3, 5.7 ± 1.0, and

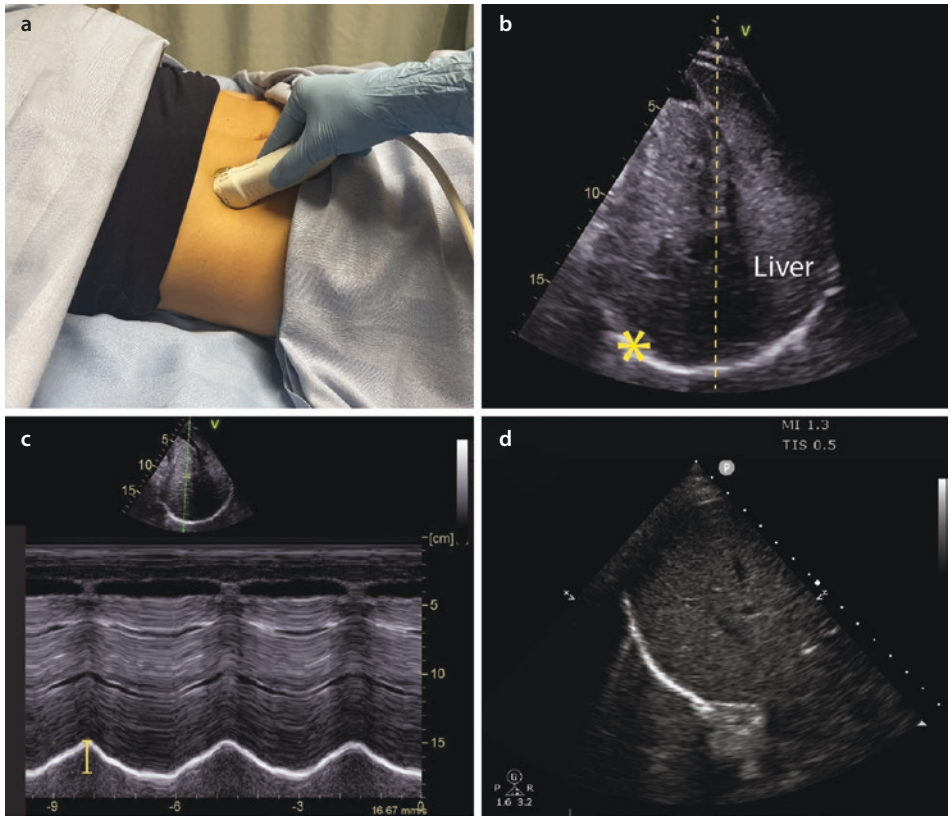

Fig. 11.2 **a** Diaphragm excursion—transducer position. The ultrasound transducer is placed at the (right) subcostal area, just below the costal margin, between the anterior axillary and the midclavicular lines. **b** Diaphragm excursion—ultrasound 2D. The hemidiaphragm is identified as a bright echogenic line (*) attached to the liver. **c** Diaphragm excursion—ultrasound M-mode. M-mode is used to measure diaphragm excursion by placing the M-line perpendicular to the diaphragm and in line with its movement. As during inspiration the diaphragm moves caudally, the bright echogenic line moves toward the transducer. Diaphragm excursion is quantified as the amplitude of diaphragmatic movement during respiration (the perpendicular distance between the end of expiration and the end of inspiration—yellow line). Due to breath-by-breath variability, the average value of diaphragm excursion from three to five breaths should be taken. **d** Diaphragm excursion—posterolateral approach. When the diaphragm is difficult to visualize in the subcostal window, the movement of the liver and spleen in the posterolateral area on the chest wall is a good alternative. This allows assessing the direction of diaphragm movement, but not its quantification (the M-mode line cannot be placed in line with the direction of diaphragm movement)

2.6 ± 0.5 cm in women, respectively [27]. The lower limit of normal diaphragm excursion for women and men was 0.9 cm and 1 cm during quiet breathing, 3.7 cm and 4.7 cm during deep breathing, and 1.6 cm and 1.8 cm during a sniff maneuver, respectively [28].

In critically ill patients, diaphragm excursion <1.1 cm during quiet breathing [27] and <2.5 cm at maximal inspiratory effort [29] has been used to diagnose diaphragm dysfunction. Furthermore, paradoxical motion (i.e., cranial displacement during

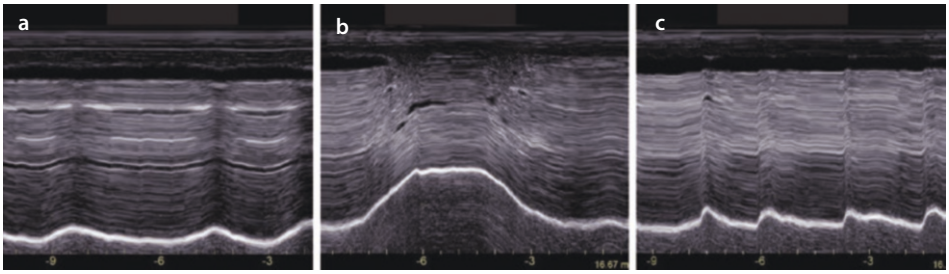

Fig. 11.3 Diaphragm excursion can be measured during quiet breathing (panel **a**), a measure associated with tidal inspiratory effort, or during a maximum inspiratory effort, either deep breathing (panel **b**) or sniff maneuver (panel **c**), measures associated with diaphragm function. Normal values of right diaphragm excursion in healthy subjects during quiet breathing, deep breathing, and voluntary sniffing have been reported to be 1.8 ± 0.3, 7.0 ± 1.1, and 2.9 ± 0.6 cm in men and 1.6 ± 0.3, 5.7 ± 1.0, and 2.6 ± 0.5 cm in women, respectively [27]

inspiration) indicates severe paralysis. In addition, measurement of diaphragm excursion during spontaneous breathing trial has been shown to predict weaning outcome [30, 31]. Although excursion of the left hemidiaphragm is more challenging to assess, it is recommended to compare both sides to look for symmetry and to identify unilateral weakness or paralysis.

11.3.2 Diaphragm Thickness and Thickening Fraction

11.3.2.1 Image Acquisition and Parameters

Diaphragm thickness can be measured using an intercostal approach at the zone of apposition (i.e., the location where the diaphragm attaches to the rib cage), usually between the eighth and tenth intercostal space and at the anterior to mid-axillary line. The patient should be in supine or semi-recumbent position (Fig. 11.4a). In contrast to the assessment of diaphragm excursion, diaphragm thickness can be measured both under mechanical ventilation assist and during spontaneous breathing. The diaphragm at the zone of apposition is a very thin and superficial structure, therefore requiring a high frequency linear probe (10–15 MHz) for its identification. The diaphragm is identified as a three-layered structure with a low echogenic structure located between the parietal pleura and the peritoneum at a depth of 2–4 cm from the skin (Fig. 11.4b). A third bright echogenic line is frequently identified in the middle of the low echogenic structure which corresponds to the fibrous layer of the diaphragm. To evaluate diaphragm thickness, either B-mode or M-mode can be used to measure the thickness by placing the probe perpendicular to the diaphragm [26]. Diaphragm thickness is measured as the distance between the two bright echogenic lines at the end of expiration (baseline thickness) and at the end of inspiration (Fig. 11.4c); as per the recent consensus document [26], the pleura and peritoneum should not be included with the measurement. The average value of diaphragm thickness from three to five breaths is usually taken due to breath-by-breath variability.

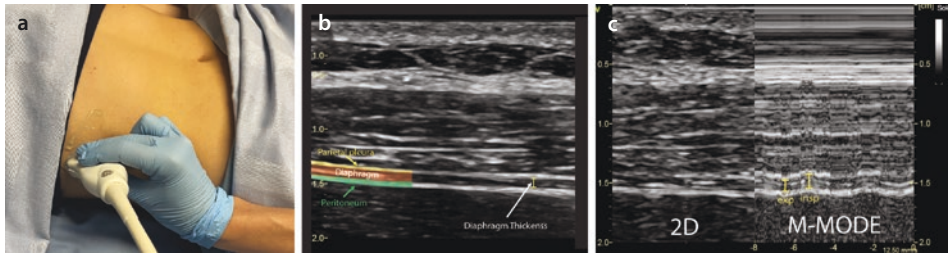

Fig. 11.4 **a** Diaphragm thickness and thickening fraction—transducer position. Diaphragm thickness can be measured using an intercostal approach at the zone of apposition, usually between the eighth and tenth intercostal space and at the anterior to mid-axillary line. The patient should be in supine or semi-recumbent position. **b** Diaphragm thickness and thickening fraction—ultrasound 2D. The diaphragm at the zone of apposition is a very thin and superficial structure, therefore requiring a high frequency linear probe (10–15 MHz) for its identification. The diaphragm is identified as a three-layered structure with a low echogenic structure located between the parietal pleura and the peritoneum at a depth of 1–4 cm from the skin. **c** Diaphragm thickness and thickening fraction—ultrasound M-mode. Diaphragm thickness is measured as the distance between the two bright echogenic lines at the end of expiration (baseline thickness) and at the end of inspiration; the pleura and peritoneum should not be included with the measurement. The average value of diaphragm thickness from three to five breaths is usually taken due to breath-by-breath variability

During inspiration, the increase in diaphragm thickness is observed due to diaphragm contraction and active muscle fiber shortening. The percentage increase in thickness during the respiratory cycle can be reported as diaphragm thickening fraction (TFdi) using the following equation:

$$\text{Thickening fraction}(\text{TFdi}) = \frac{\left[\text{Thickness end inspiration}(\text{Tei}) - \text{Thickness end expiration}(\text{Tee})\right]}{\text{Thickness end expiration}(\text{Tee})} \times 100\%$$

11

11.3.2.2 Interpretation

Measurement of diaphragm thickness using ultrasound is accurate and reproducible in healthy subjects and critically ill patients [32–34]. A high relationship with direct measurements by ruler in cadavers has been shown [35]. Normal value of diaphragm thickness at end of expiration (functional residual capacity) was reported varying between 2.2 and 3.3 mm and the lower limit of normal diaphragm thickness at the end of expiration was 1.5 mm [32, 36]; however, these values should be interpreted with some level of caution because earlier studies often did not report whether the fascia boundaries were included in the measurement of thickness—this may result in a slight overestimation of true muscle thickness. For instance, a recent work in healthy volunteers demonstrated median values of 1.27 mm for end-expiratory diaphragm thickness as measured in the mid-axillary line [37]. Diaphragm thickness reflects primarily the macroscopic structure and trophism of the muscle, and greatly varies across individuals, gender, and age, although remaining in the range of normality [14]. Therefore, a definition of dysfunction *only* based on the absolute thickness in comparison to some reported standard values might not be useful in clinical

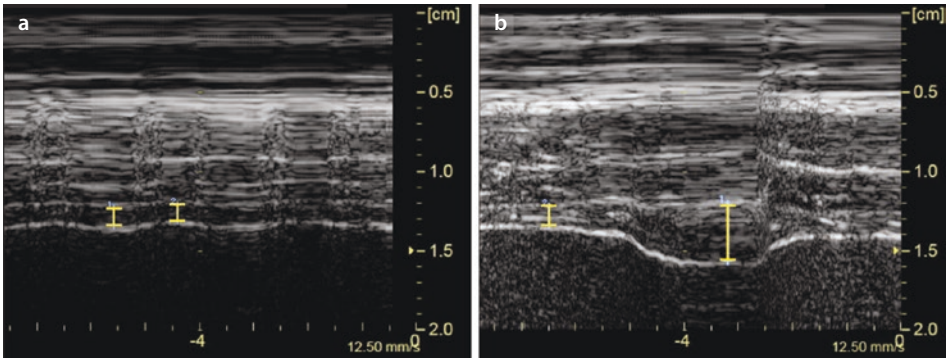

Fig. 11.5 Diaphragm thickening fraction can be measured during quiet breathing (panel **a**) and during a maximal inspiratory effort, such as deep breathing (panel **b**). In healthy subjects, normal diaphragm thickening fraction during quiet breathing of 32 ± 15% for men and 35 ± 16% for women and during deep breathing of 106 ± 34% for men and 116 ± 40% for women were reported [41]

practice. Conversely, monitoring the evolution of diaphragm thickness over the course of mechanical ventilation can be used to detect diaphragm atrophy and to presume changes in function. A cut-off value of >10% decrease from baseline thickness has been used in literature [3, 26]. In addition, a left-right ratio for thickness of <0.5 or >1.6 should be considered abnormal [14].

Diaphragm thickening fraction can be measured during quiet breathing (Fig. 11.5a) and during a maximal inspiratory effort. At quiet breathing, TFdi represents contractile activity of the diaphragm that has been shown to be related to the inspiratory effort in some studies [38, 39]; however, individual values of TFdi poorly correlate with the transdiaphragmatic pressure in healthy volunteers as well as in critically ill patients [40]. Conversely, measurement of diaphragm thickening fraction during maximum inspiratory effort such as deep breathing or a sniff maneuver are associated with diaphragm function (Fig. 11.5b). In healthy subjects, normal diaphragm thickening fraction during quiet breathing of 32 ± 15% for men and 35 ± 16% for women and during deep breathing of 106 ± 34% for men and 116 ± 40% for women were reported [41]. TFdi <20% is usually used as a cut-off for detection of diaphragm dysfunction [42], and should be assessed during a maximal effort. In fact, values of TFdi around 20–30% are also reported during resting quiet breathing in healthy adults [3, 43]. A low TFdi during assisted breathing may therefore also reflect a minimal level of effort performed by the muscle in the absence of any reduction in function. In patients on assisted ventilation, this could, for instance, be caused by ventilator over-assistance. It is then recommended to lower ventilator inspiratory support (with close monitoring of other respiratory parameters) and look for an increase in TFdi.

In mechanically ventilated patients, diaphragm thickening fraction can be used to evaluate diaphragm dysfunction [44]; the measurement of diaphragm thickening fraction during spontaneous breathing trials has been used to predict weaning outcome with a threshold value between 30 and 36% [45, 46]; the role of diaphragm ultrasound in these clinical scenarios is further detailed below.

11.4 Extra-diaphragmatic Muscle Ultrasound

11.4.1 Parasternal Intercostal Muscle Ultrasonography

11.4.1.1 Image Acquisition and Parameters

Parasternal intercostal muscles can be visualized with a linear high frequency (10–15 MHz) transducer placed at the level of the second and third intercostal space and positioned in cranio-caudal direction 3–5 cm laterally from the sternum [14, 47, 48]. The patient should be in a supine or semi-seated position (Fig. 11.6a). In B-mode, the muscle can be identified as a biconcave muscular structure in between two ribs and covered by fascia (Fig. 11.6b). Beneath the parasternal intercostal muscle, the pleural line is visible.

Muscle thickness can be measured in both B-mode and in M-mode, with the calipers placed within the inner hyperechoic borders of the fascia. Similar to the diaphragm, when measuring the thickness at end-expiration (Tee) and end-inspiration (Tei), the intercostal muscle thickening fraction (TFic) can be computed as the percentage increase in muscle thickness during inspiration: TFic = ((Tei − Tee)/Tee) × 100%. It is recommended to take an average value of at least three to five breaths to limit variability.

11.4.1.2 Interpretation

During normal resting breathing in healthy volunteers, TFic of 3% [interquartile range, 2–5%] have been reported, whereas the TFic was found to be 5% [3–8%] vs. 17% [10–25%] in ICU patients without (n = 21) and with (n = 33) diaphragm dysfunction, respectively [48]. In healthy volunteers, reproducibility of thickness [48–50] and TFic [48] measurements have been reported from fair to excellent and good, respectively. In the same report [48], in 16 patients undergoing assisted breathing, a progressive

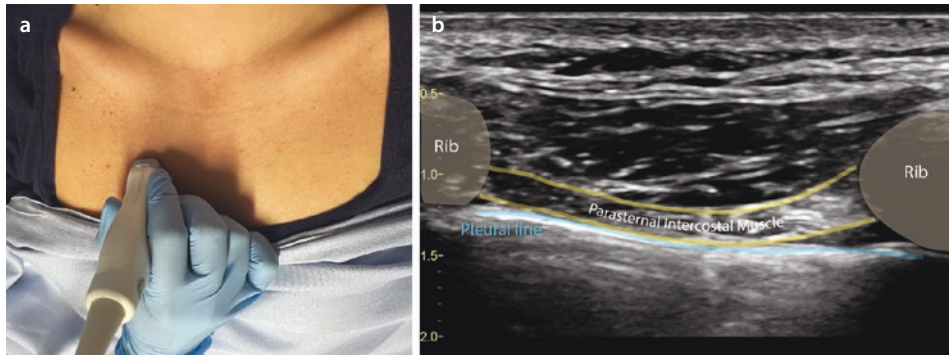

Fig. 11.6 **a** Parasternal intercostal muscles—transducer position. Parasternal intercostal muscles can be visualized with a linear high frequency (10–15 MHz) transducer placed at the level of the second and third intercostal space and positioned in cranio-caudal direction 3–5 cm laterally from the sternum. The patient should be in a supine or semi-seated position. **b** Parasternal intercostal muscles—ultrasound 2D. In B-mode, the muscle can be identified as a biconcave muscular structure in between two ribs and covered by fascia. Beneath the parasternal intercostal muscle, the pleural line is visible

decrease in TFic was described when increasing levels of ventilator assistance were applied (Spearman $\rho = -0.61$ [95% CI, −0.74 to −0.44]; $P < 0.001$). The higher TFic in patients with diaphragm dysfunction may therefore indicate a compensatory mechanism of extra-diaphragmatic inspiratory muscles [18], which was also suggested by the inverse correlation between TFic and the pressure-generating capacity of the diaphragm that was reported (Spearman $\rho = -0.79$ [95% CI, −0.87 to −0.66]; $P < 0.001$) [48]. In line with this reasoning, the TFic and its ratio with diaphragm thickening fraction (TFdi) was found to be a predictor for extubation failure (AUROC 0.81) [51].

11.4.2 Abdominal Muscle Ultrasonography

11.4.2.1 Image Acquisition and Parameters

Ultrasound of the abdominal wall muscles should be performed with the patient in supine position and with a linear high frequency (10–15 MHz) transducer [14, 52, 53]. The operator should not apply any pressure with the probe to the skin to prevent that compression of the abdominal wall alters the shape/thickness of the expiratory muscles. Using B-mode, the external oblique (EO), internal oblique (IO), and transversus abdominis (TrA) muscles can be best visualized with the probe positioned in transverse orientation on the anterior axillary line, midway between the last rib and the iliac crest (◘ Fig. 11.7). For optimal orientation, it is recommended to start with visualization of the rectus abdominis (RA) muscle. The RA muscle can be imaged by positioning the probe 2–3 cm above the umbilicus (to identify the linea alba) and then sliding the probe 2–3 cm away from this midline. The probe should be moved in the cranio-caudal direction to obtain maximal RA muscle thickness. Then, slow sliding of the probe laterally will visualize the semilunar line. This is a thick echogenic fascia that blends lateral to the RA muscle and medial to the oblique muscles. The EO, IO, and TrA muscles can then be identified as three muscular layers running in parallel [14].

Using M-mode imaging or a B-mode frames/video of the respiratory cycle, the thickness at end-inspiration (Tei) and end-expiration (Tee) can be measured by placing the calipers within the inner borders of each fascia. Again, it is recommended to measure an average value of three to five separate breaths. Studies have also used the total thickness of the lateral expiratory muscles as measured from the lower TrA fascia till the upper EO fascia, but it should be noted that this thus includes the fascia surrounding the IO muscle [53–55]. During active expiration, the thickening fraction of the abdominal wall muscles (TFab) can be determined as: $TFab = ((Tee - Tei)/Tei) \times 100\%$. Note that in contrast to the diaphragm and parasternal intercostal muscle, the TFab measures the increase in thickness during expiration, with Tei as resting thickness.

11.4.2.2 Interpretation

In mechanically ventilated patients, reproducibility of thickness [53] and TFab [56] measurements were reported as excellent and moderate, respectively. Normal values for the expiratory muscles have been reported previously [14]. Generally, the RA muscle is the thickest structure, followed by IO, EO, and TrA muscles [57]. Changes in total lateral abdominal wall muscle thickness were described in 77 ICU patients dur-

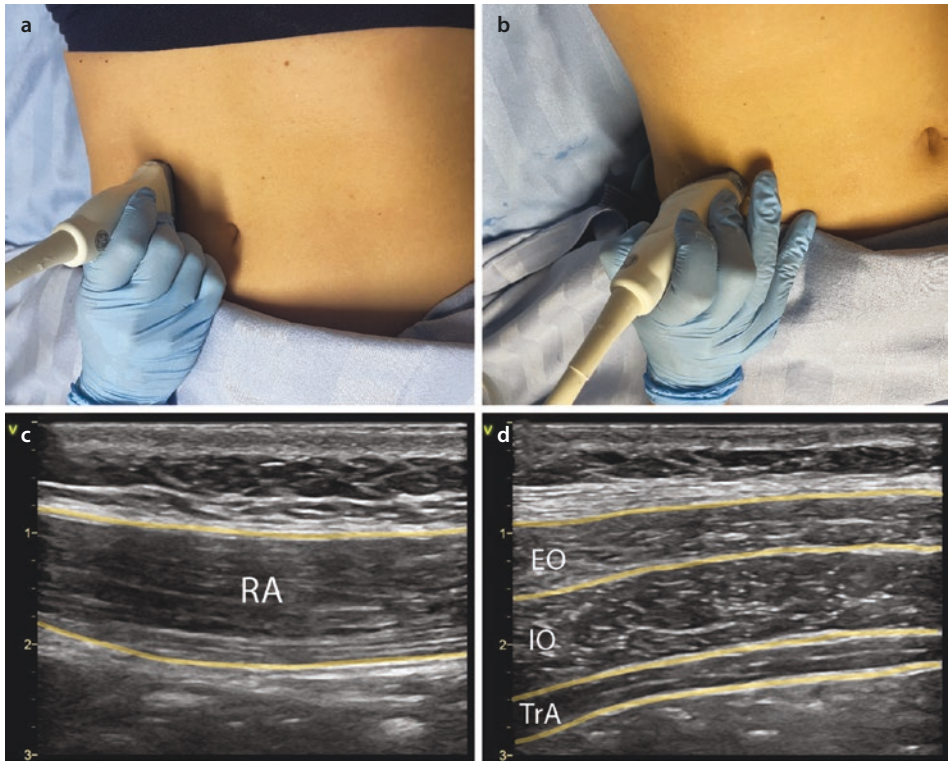

11

Fig. 11.7 Expiratory abdominal muscles. Image acquisition should be performed with the patient in supine position and with a linear high frequency (10–15 MHz) transducer. The operator should not apply any pressure with the probe to the skin to prevent that compression of the abdominal wall alters the shape/thickness of the expiratory muscles. For optimal orientation, it is recommended to start with visualization of the rectus abdominis (RA) muscle. The RA muscle can be imaged by positioning the probe 2–3 cm above the umbilicus (to identify the linea alba) and then sliding the probe 2–3 cm away from this midline (panel **a**). The probe should be moved in the cranio-caudal direction to obtain maximal RA muscle thickness (panel **c**). Then, slow sliding of the probe laterally allows visualization of the semilunar line. This is a thick echogenic fascia that blends lateral to the RA muscle and medial to the oblique muscles. The external oblique (EO), internal oblique (IO), and transversus abdominis (TrA) muscles can be best visualized with the probe positioned in transverse orientation on the anterior axillary line, midway between the last rib and the iliac crest (panel **b**). They are identified as three muscular layers running in parallel (panel **d**)

ing the first week of mechanical ventilation; atrophy developed in 22% of patients and was attributed to a loss in muscle tissue, whereas increases in thickness developed in 12% of patients and was related to the increased thickness of the interparietal fascia surrounding the IO muscle [53]. The latter stresses the importance of not including the fascia for following changes in any respiratory muscle thickness over time.

Interpreting the TFab is complex, since the expiratory muscles have more degrees of freedom as compared to the diaphragm and parasternal intercostal muscles: active contraction of one layer may directly affect the position and thickness of the adjacent muscle layers [52]. Therefore, TFab is suggested to be a screening parameter to identify active expiratory muscle use under assisted mechanical ventilation until more clinical data is available for interpretation of absolute values. In patients failing

a spontaneous breathing trial, the combined TFab of the TrA, IO, and RA muscles measured during cough was associated with an increased risk of reintubation or reconnection to the ventilator after a liberation attempt (OR 2.1; 95% CI, 1.1–4.4 per 10% decrease in thickening fraction) [56].

11.5 Clinical Applications

11.5.1 Identification of Diaphragm Dysfunction

Diaphragm dysfunction is highly prevalent in mechanically ventilated patients and it is associated with worse outcomes, including extubation failure, prolonged mechanical ventilation, and higher in-hospital and 1-year mortality [1, 3, 30, 58, 59]. From a physiological standpoint, diaphragm dysfunction can be defined as a decrease in its capacity to generate pressure. Different methods have been used in clinical practice and in research to assess and monitor diaphragmatic function, including diaphragm electromyography (through surface or transesophageal approach), and measurements of esophageal (Pes) and gastric (Pga) (and resulting transdiaphragmatic—Pdi) pressures during maximal inspiratory effort (Pdi,max) or during supramaximal bilateral magnetic stimulation of the phrenic nerve (Pdi,twitch) [60]. Changes in tracheal pressure during magnetic phrenic stimulation (Ptr,stim) can be used as a less invasive alternative to Pdi,twitch. Although magnetic phrenic nerve stimulation is considered the reference method for diaphragm function assessment in ICU, this technique is not widely available and requires high technical expertise. Similar considerations are also true for electromyography, that, additively, shows high inter-patient variability and normal values are not defined [61].

Contrasting with these complex methods, ultrasound has been proposed as a promising diagnostic technique for a non-invasive and rapid estimation of diaphragm function [6, 30, 44, 45].

Early reports of the use of diaphragm ultrasound to diagnose paralysis date back to the late 1980s [62] and, over the last two decades, numerous studies have reported the advantage of ultrasound in the assessment of diaphragmatic function, particularly in ICU settings.

In analogy with measurements of Pdi,max or Pdi,twitch, ultrasound measurements (either of caudal displacement/excursion or of inspiratory thickening) theoretically provide a more correct and accurate information about diaphragm functionality when performed during maximum inspiratory effort, compared to measurements performed during quiet breathing [63]. However, there are still concerns about potential variability in eliciting maximum effort (especially in ICU patients) and in estimating if a real maximum effort is achieved. Moreover, the cut-off values that should be considered for diaphragm dysfunction assessed by maximal thickening fraction are still under debate [63]. Finally, literature is quite heterogeneous, as it provides several examples where diaphragm dysfunction is assessed or defined based on measurements not performed during maximum effort. Diaphragmatic dysfunction is often associated with reduced thickness, and reduced excursion and thickening fraction at rest. However, these findings should not be considered as synonymous of dysfunction, nor should be used to make its diagnosis; instead, ultrasound (thickness

and thickening fraction) at rest should be considered a useful tool to sceen for diaphragm dysfunction, while ultrasound performed during maximum effort and more invasive techniques should be used for further quantification.

11.5.1.1 Diaphragmatic Excursion in Diaphragm Dysfunction

Diaphragm excursion measurements could screen for dysfunction. Paradoxical movement (e.g., cranial displacement) during inspiratory effort suggests severe/complete paralysis. In the presence of unilateral paralysis, the unaffected hemidiaphragm may demonstrate large caudal excursion as compensatory mechanism to generate sufficient tidal volume; it is therefore always important to look for symmetry between left and right diaphragm excursions. Cut-off values of diaphragmatic dysfunction, using caudal displacement of the diaphragm during inspiration, vary across studies [58, 64–67]. In patients who underwent cardiac surgery and needed prolonged mechanical ventilation during the postoperative course, Lerolle et al., in order to find a quantitative cut-off value for the diagnosis of diaphragmatic dysfunction, used Pdi as a reference method [64]. The excursion at maximum inspiratory effort, called Best E, correlated significantly with the Gilbert index ($\rho = 0.64$, $p = 0.001$), an index reflecting the contribution of the diaphragm to inspiratory effort (computed from the ratio ΔPga/ΔPdi). A Best E <25 mm was the cut-off point with the highest accuracy for predicting severe diaphragmatic dysfunction.

A few further studies [65, 66, 68] defined the presence of diaphragm dysfunction and/or paralysis *a priori*, mainly based on lower limits of excursion described in previous physiological studies performed in healthy subjects [28], with small variability in terms of the way of assessment (M-mode, B-mode, both), type of breathing (during maximal inspiratory effort or breathing at rest), observed prevalence, and correlation with outcomes [69]. Valette et al., in ICU patients hospitalized for acute respiratory failure of unknown etiology, defined the presence of diaphragmatic dysfunction as an excursion of less than 10 mm in M-mode during unassisted deep breathing, and reported an enhanced ultrasonographic ability to detect diaphragmatic dysfunction (of either side) when compared to clinical and radiological criteria [65]. In Mariani et al., the same cut-off was chosen to define diaphragmatic dysfunction, but assessed during quiet breathing and both in M- and B-modes [66].

Other studies defined diaphragm function based on a semiquantitative assessment. Normal, hypokinetic, akinetic, and paradoxical diaphragmatic excursions during quiet breathing (assessed after a disconnection of the patients from the ventilator) were found to have in infants a great sensitivity and specificity in diagnosing abnormal diaphragm motion as detected at the fluoroscopy [69, 70]. However, no clear cut-off values distinguishing hypokinesia from akinesia and no criteria for identification of a paradoxical or a normal motion were provided.

11.5.1.2 Thickening Fraction in Diaphragm Dysfunction

The measurement of diaphragm thickness and inspiratory thickening has also been proposed for assessing diaphragmatic function. Gottesman et al. [42], in patients referred for possible diaphragmatic dysfunction, based either on the presence of evocative symptoms or on radiological diaphragm elevation, reported a significant reduction both in diaphragmatic thickening fraction (TFdi) (−8 ± 13% with a range of −35 to 5% versus 65 ± 26% with a range of 28 to 96%, $p < 0.001$) and in thickness (1.7 ± 0.2 mm with a range of 1.3–1.9 mm, versus 2.7 ± 0.5 mm with a range of

2.0–3.9 mm, $p < 0.01$). In a few cases, the TFdi was reported as negative (decrease in thickness during inspiration), reflecting a probable passive stretching of the diaphragm during inspiration [42].

More recently, the TFdi as a marker of diaphragmatic function was assessed in relationship with the Ptr,stim. The TFdi was able to reliably identify diaphragmatic dysfunction, defined as a Ptr,stim <11 cm H2O, at switch to pressure support ventilation (AUCROC 0.91, 95%CI 0.85–0.97, $p < 0.001$), but not at initiation of mechanical ventilation. Values of TFdi <29% (bootstrapped 95%CI 25–30%) could distinguish diaphragm dysfunction with 85% sensitivity and 88% specificity [1]. The correlation between TFdi and Ptr,stim was also found during unassisted spontaneous breathing [58]. Conversely, thickness and pressure generation ability of the diaphragm appeared to be unrelated, regardless of the mode of ventilation [1].

The simultaneous assessment of extra-diaphragmatic respiratory muscle activity can support the diagnosis of diaphragmatic dysfunction in the presence of a reduced TFdi. In critically ill intubated patients with diaphragmatic dysfunction (defined as the presence of a negative Gilbert index), TFdi was lower (13.2 ± 9.2% vs. 33.6 ± 18.2%) and TF of the parasternal intercostal muscles was higher (12.7 ± 9.1% vs. 2.1 ± 1.7%) when compared with patients without diaphragmatic dysfunction. This finding suggests recruitment of extra-diaphragmatic respiratory muscles in the presence of diaphragmatic dysfunction and increased respiratory workload [71]. An increase in thickening fraction of the parasternal intercostals in patients with vs. without diaphragm dysfunction (17% vs. 5%, $p < 0.0001$) was also found in a recent study by Dres et al. [48].

11.5.2 Prediction of Weaning Outcomes

Focusing on the diaphragm function at the time of weaning was proven to be particularly relevant to predict weaning outcomes. Two systematic reviews and meta-analyses were recently published on the topic [72, 73]. The first one, including 19 studies (1071 patients), suggested that TFdi was consistently a good predictor of weaning outcome (AUC 0.87); while diaphragm excursion showed a lower accuracy and high heterogeneity across the studies [73]. The most recent one included 28 studies in the qualitative analysis, of which 16 in the quantitative analysis (816 patients) [72]. Both TFdi and diaphragmatic excursion were accurate in predicting weaning failure when reduced; however, the presence of normal ultrasound findings did not exclude subsequent weaning failure (pooled sensitivity were 0.70 and 0.71 for TFdi and excursion, respectively; pooled specificity 0.84 and 0.80). TFdi cut-off values ranged between 20 and 36%, with most consistent values around 30–35% [45, 74–76]; excursion threshold values were all around 1–2 cm [30, 75–77]. The wide variability across the studies in patient selection, definition of weaning success (and even more of weaning failure), ventilator settings, timing of and body positioning during ultrasound measurements affect final conclusions on the accuracy of diaphragmatic ultrasound as single predictor of weaning outcome.

To predict successful spontaneous breathing >48 h after extubation, Spadaro et al. combined the assessment of diaphragmatic excursion with the rapid shallow breathing index [78] (the resulting D-RSBI was derived from the ratio between respiratory rate and diaphragmatic excursion) during a T-tube SBT, and showed a greater

discriminative ability of this latter index compared to the standard RSBI (AUROC D-RSBI 0.89 vs. RSBI 0.72, $p = 0.006$). More recently, another study integrated diaphragmatic excursion and inspiratory time evaluation [67]; however, the resulting diaphragm contraction velocity was a weaker predictor of extubation outcome than diaphragmatic excursion alone. The same authors proposed the sequential assessment of diaphragm excursion during assisted/controlled ventilation and during the SBT and found the ability to maintain a consistent excursion between the two conditions to be a better predictor of extubation success than the excursion alone measured during the SBT.

In contrast with most of the studies performed and with the overall results of the two meta-analyses, a large multicenter trial of patients at risk of reintubation (>65 years of age, ventilated for more than seven days or with underlying cardiac or respiratory disease) and extubated after a successful weaning trial [79], showed that TFdi was not significantly different between patients who ultimately failed and patients who succeed extubation ($p = 0.67$). The same was also true for diaphragmatic excursion. The only variable independently associated with extubation success at the multivariable logistic regression analysis was the presence of effective cough, clinically assessed by respiratory therapists.

Consistently with Vivier's multicentric trial [79], a more recent bicentric study showed how a reduced cough function, assessed sonographically as the sum of internal oblique, transversus abdominis, and rectus abdominis TF during coughing (called coughTFabs), was associated with an increased risk of post-extubation failure in patients who passed an SBT (OR for failed extubation 2.1 [95% CI 1.1–4.4] per 10% decrease in coughTFabs) [56]. CoughTFabs discriminative ability outperformed the one of the TFdi measured during the SBT (AUC ROC 82% [95% CI, 59–100]) vs. 70% [95% CI, 49–91]), $p < 0.001$) [56].

11.5.2.1 Integrated Approaches

Given the multifactorial pathophysiology of weaning failure, in the attempt to improve accuracy in predicting weaning outcomes, the concomitant ultrasonographic assessment of extra-diaphragmatic respiratory muscles [48] and other integrated approaches, combining ultrasonographic, clinical and laboratory measurements [14, 47, 80], have been proposed.

In Dres et al., a high TF of the parasternal intercostals (17% [10–25%]), together with a reduced TFdi (19% [16–23%] vs. 39% [34–44%]), was associated with diaphragmatic dysfunction and a higher likelihood of SBT failure [47]. More specifically, a TF of the parasternal intercostals greater than 10% was able to predict weaning failure. Subjects who ultimately passed the SBT showed very low values of parasternal intercostal thickening, similarly to healthy subjects at rest (5% [3–8%]). In the recently published review by Formenti et al., a practical flow chart involving a simultaneous ultrasound assessment of the diaphragm and of the parasternal intercostals has been proposed in patients who failed a first SBT [47]. A TFdi >20% associated with a TF of the parasternal intercostals <10% was presented as a suggestive index of successful SBT, and an integration with other predictive parameters of weaning outcomes (including P0.1, RSBI, forced vital capacity and gas exchanges) was proposed to guide the weaning phase and potential optimization of muscular load.

Mayo et al. earlier [80], and Tuinman more recently [14] and in a more standardized way, proposed holistic ultrasonographic approaches to the weaning process. The

ABCDE approach in particular [14], refers to the evaluation of different organs, each relevant for the outcome of the weaning process and each represented by a letter: (A) Aeration score and pleural effusion [81], including the assessment of the lung and of the pleural space; (B) Below the diaphragm, assessing the presence of ascites and abdominal abnormalities potentially interfering with respiratory mechanics; (C) Cardiac; (D) Diaphragm; (E) Extra-diaphragmatic respiratory muscles, including the parasternal intercostals and the abdominals. The benefits of implementing such approaches in clinical practice needs further evaluation, as preliminary results are neither conclusive nor promising [82].

11.5.3 Assessment of Breathing Effort

Following the hypothesis that the contractile activity of the diaphragm could reflect the magnitude of diaphragmatic work, a few studies assessed the performance of diaphragm ultrasound as an index of respiratory effort in mechanically ventilated patients using reference methods to evaluate its accuracy [34, 38, 64, 83]. A preliminary physiological study was performed in 12 patients requiring non-invasive ventilation after extubation [38]. With increasing levels of pressure support, a parallel decrease in both diaphragmatic pressure-time product (PTPdi) and TFdi was found. TFdi was significantly correlated with the PTPdi/breath ($\rho = 0.74$, $p < 0.001$) and, to a lesser extent, to the PTPdi/minute ($\rho = 0.52$, $p < 0.001$), but not with the expired tidal volume (as expected, being this also determined by the support provided by the ventilator). Consistent results were found a few years later in post-surgical intubated patients, where esophageal pressure-time product (PTPes) and PTPdi were both significantly correlated with TFdi. However, recent work by Poulard et al. demonstrated, in 14 healthy volunteers and 25 ICU patients, that TFdi was only weakly related to the transdiaphragmatic pressure and should therefore not be used to quantify its function [40]. Similarly, no correlation was found between muscle effort and diaphragmatic excursion, confirming its scarce utility when assessed during mechanical ventilation [83].

A couple of considerations should be made about the use of TFdi as an index of diaphragmatic effort. First, the degree of diaphragmatic thickening varies considerably across subjects exposed to the same level of inspiratory effort, as shown in healthy subjects [34]. This limits the utility of this measurement for quantitative between-subjects comparisons; however, it still remains useful for within-subject assessments. Second, the presence of diaphragmatic dysfunction could limit the use of TFdi as an index of patient effort, as showed by Umbrello et al. [71]. In fact, despite an increase in global inspiratory effort (PTPes) the dysfunctional diaphragm could not be able to simultaneously increase its TF. The concomitant assessment of the TF of the parasternal intercostals could be helpful in identifying these cases.

11.5.4 Muscle Ultrasonography in Neuromuscular Diseases

In addition to the more standardized and traditional techniques (such as maximal inspiratory pressure MIP measurements, forced vital capacity—FVC, sniff nasal inspiratory pressure and peak cough flow), diaphragmatic ultrasound has emerged as

a non-invasive tool for the assessment and monitoring of respiratory muscle strength in patients with neuromuscular disorders. Regardless of the original involvement, either the motor nerve (e.g., amyotrophic lateral sclerosis, Guillain–Barré syndrome, critical illness neuropathy), the neuromuscular junction (e.g., myasthenia gravis), or directly the muscle (e.g., late-onset Pompe disease—LOPD, Steinert disease, Duchenne muscular dystrophy), and regardless of the speed of the evolution and the amount of muscle compromise, respiratory muscle weakness is a common feature in neuromuscular diseases (NMDs). In this context, ultrasound may be utilized to characterize respiratory muscles, enabling an early detection of diaphragmatic weakness (with a possible early discrimination of a subpopulation who may eventually need mechanical ventilation), a progressive alteration in the macroscopic structure of the muscle, and a change in contractile activity over time and dependent on body position. The nature of ultrasound examination allows its execution even when pulmonary function tests cannot be performed due to severe muscle impairment, dyspnea [84], or weakness of the facial muscles (e.g., bulbar patients with amyotrophic lateral sclerosis), or when other measurements would result less feasible due to the young age of the patients (e.g., Duchenne muscular dystrophy or spinal muscular atrophies).

In *amyotrophic lateral sclerosis (ALS)*, diaphragm thickness and TF were found to be decreased when compared to age-matched healthy controls [85, 86], with no differences between patients with bulbar or spinal onset [87]. Diaphragm thickness at full inspiration was also found to correlate with the amplitude of the motor response induced by electrical phrenic nerve stimulation ($r = 0.60$, $p < 0.001$) [87]. Thickness at end expiration, thickness at maximal effort, and the ratio of the two were found to be significantly correlated with the vital capacity expressed as percentage of the predicted value [85, 86]. This is particularly relevant as the indication for ventilator support in ALS patients is usually based on impaired pulmonary function tests [88]. Moreover, maximal TFdi as well as end-expiratory thickness were found to be correlated with clinical scores, particularly in bulbar patients, possibly predicting disease evolution over time [89]. In a small case series, Yoshioka et al. described no change in diaphragmatic excursion between quiet breathing and maximal inspiratory effort, and no thickening during deep inspiration, suggesting a severe diaphragm impairment [84].

In children with *Duchenne muscular dystrophy*, despite a greater diaphragmatic thickness at functional residual capacity, TFdi was reduced as compared to healthy peer controls during maximum inspiratory effort [90, 91]. The diaphragm increase in thickness is consistent with the pseudo-hypertrophy described early in other muscular districts of patients with this type of dystrophy. With the progression of the disease and age advance, both minimal and maximal thickness and their ratio during quiet breathing were reported to be all decreased [90]. In a cohort of neuromuscular patients, where Duchenne muscular dystrophy represented the majority of patients, excursion amplitude during both deep breathing and sniff maneuvers, as well as excursion velocity at tissue doppler imaging during sniff maneuvers were reported to be decreased compared to healthy controls [92]. Reported abilities for predicting a forced vital capacity <60%, expressed as area under curves, were 0.93 ($p < 0.0001$) for the right diaphragm excursion during sniff, and 0.86 ($p < 0.001$) for right peak diaphragm velocity on tissue doppler imaging during sniff, respectively. Fat infiltration of the diaphragm, progressively increasing with age, as reported by magnetic reso-

nance (MRI) studies, were found to match with the reduced diaphragm excursion [93]. As expiratory muscles, and particularly the internal oblique, were described to have an elevated fat fraction [94], it can be speculated that the cumulative ultrasonographic measurement of abdominal muscle function during cough (coughTFabs) could be a suitable tool to monitor cough efficacy over time in these patients [56].

Similar ultrasonographic alterations of diaphragm excursion, thickness, and TF versus age- and gender-matched healthy controls were also described in *late-onset Pompe disease* [95]. Static and dynamic MRI studies also showed a less pronounced intercostal muscle atrophy (as compared to diaphragm and abdominal) and an increased ribcage expansion (as compared to abdominal) [96]. Therefore, an assessment of the TF of the parasternal intercostals (together with TFdi) could be particularly useful in these patients to detect diaphragmatic dysfunction when pulmonary function tests are still relatively normal [71].

In patients suffering from *stroke*, significant reduction in diaphragmatic excursion on the hemiplegic side has been reported [97]. Diaphragm was also described to be thinner on the affected side in patients with chronic stroke [98]. Interestingly, in patients with right-hemiplegia the excursion could be reduced bilaterally as compared to healthy subjects [97].

11.5.5 Assessment of Patient-Ventilator Asynchronies

Ultrasonographic evaluation of the diaphragm might be a useful non-invasive tool to detect the different types of patient-ventilator asynchronies. [14]. A rationale for its use has been provided by a described concordance between esophageal pressure and M-mode diaphragmatic displacement tracings [99]. A recently published study performed on healthy subjects placed under non-invasive ventilation reported a greater performance of excursion and thickening in detecting auto-triggering and delayed cycling when compared with the assessment of flow/pressure tracings [100]. However, it requires optimal timing and synchronization with ventilator waveforms. Furthermore, more studies are needed to better validate the technique and its application in detecting asynchronies.

Ineffective efforts can be detected visualizing a diaphragmatic thickening and/or a small displacement in the absence of a breath delivered by the ventilator. The ultrasonographic tracings will be characterized by thickening, both when the breath is delivered and when the effort is missed; while a larger excursion (when the effort triggers the ventilator) will be alternated by a minimal one (when the effort is missed, and the breath is not delivered by the ventilator) [99]. In case of *auto-triggering*, no thickening will be evident, as the patient is not actively triggering the ventilator, but a small (passive) displacement could still be visible, as the breath is delivered by the ventilator. *Double triggering* can be visualized as a diaphragmatic thickening (reflecting the inspiratory effort) extended beyond the duration of the first breath delivered by the ventilator. Therefore, a second consecutive breath is delivered by the ventilator during the same thickening (and same effort). A single excursion can be evident during the two delivered breaths [99]. *Delayed triggering* can be characterized by diaphragmatic thickening, only later followed by a rise in airway pressure delivered by the ventilator and a corresponding increase in diaphragmatic excursion; *delayed cycling* by a pressurization prolonged after the end of diaphragm thickening. During

the first mandatory breath of *reverse triggering*, no thickening will be seen, while during the following triggered breath, thickening will be manifest. Passive displacement (induced by mechanical insufflation) will be followed by an active diaphragm excursion (triggered by the preceding mandatory breath), sometimes molten in the same diaphragm movement, but with a different displacement steepness.

11.6 Pitfalls and Limitations

Although ultrasound of the respiratory muscles is clinically useful, easy to perform, and radiation-free, some limitations should be considered:

- Although diaphragm ultrasound has shown good intra- and inter-observer reproducibility, the technique is significantly operator-dependent. Proper supervision during training is needed, especially when practicing diaphragm thickness measurement. Recent expert consensus document recommends a minimum of 40 supervised examinations before independent use in clinical practice [26].
- Measurement of diaphragm excursion and thickening fraction during a maximum inspiratory effort requires patient cooperation which can be challenging in poorly cooperative or mechanically ventilated patients.
- In mechanically ventilated patients, diaphragm excursion is influenced by positive pressure ventilation. During passive ventilation, diaphragm excursion solely depends on tidal volume because of no diaphragm contraction; whereas during assisted mechanical ventilation such as pressure support ventilation, diaphragm excursion is the sum of patient's inspiratory effort and the effect of positive pressure produced by mechanical ventilator. Furthermore, PEEP lowers the resting position of the diaphragm and reduces diaphragm excursion [101].
- Several factors also affect diaphragm thickness and thickening fraction in mechanically ventilated patients. For example, a strong relationship between lung volume and diaphragm thickness has been described [35]. Lung volume changes caused by PEEP significantly impact diaphragm geometry and diaphragm resting position; these changes lead to increase in diaphragm thickness due to shortening of the muscle fiber [101]. Increased levels of pressure augmentation may also reduce patient inspiratory effort and diaphragm thickening fraction. Furthermore, systemic inflammation and excessive fluid accumulation in critically ill patients may spuriously increase diaphragm thickness due to edematous change of the diaphragm.

11.7 Emerging and Future Developments

In the last decade, a wealth of novel ultrasound techniques has been released to the market. The most important developments are advanced ultrasound techniques for quantification of functional and elastic properties of tissues. In this section, we will address the potential role of strain imaging/speckle tracking, shear wave elastography, tissue Doppler imaging, and echogenicity assessment on diaphragm ultrasound (no studies applying these techniques to other respiratory muscles exist). None of these techniques has reached clinical implementation when related to diaphragm assessment and they should be considered only in the context of research protocols.

Other emerging developments in the ultrasound field include advances in image processing with artificial intelligence, and the use of wearable (and three-dimensional) ultrasound systems, but this is beyond the scope of this chapter.

11.7.1 Tissue Doppler Imaging

Tissue Doppler imaging is a technique that can quantify the velocity of moving structures in two dimensions. As all Doppler imaging modalities, also tissue Doppler imaging is dependent on the angle between the insonated tissue and the transmitted ultrasound beams. Theoretically, tissue Doppler imaging could be an interesting modality to quantify diaphragm kinetics when superimposed over B-mode diaphragm excursion images. Potential applications for tissue Doppler imaging in critically ill patients are the assessment of regional diaphragm contractile function at rest and with stress, and measurement of diaphragm relaxation velocity. Tissue Doppler imaging for the assessment of diaphragm mobility and function in healthy volunteers and ICU patients undergoing a weaning trial was recently proposed [102], and it was reported that weaning failure patients exhibited higher diaphragm contraction and relaxation velocities compared to succeeding patients. In line with these findings, another study found a greater diaphragmatic activation at the end of a spontaneous breathing trial in patients who failed extubation (at 48 h after extubation) as compared to successfully extubated patients [103]. These pilot results should be validated in larger multicenter studies. As ultrasound settings (e.g., gain, smoothing) and probe position directly affect the velocity profile and thus tissue Doppler imaging-derived parameters, further standardization of the technique is needed before the use in routine clinical practice [104].

11.7.2 Strain Imaging

Strain imaging is widely applied in cardiac imaging and initial studies applying this technique on the diaphragm were recently performed. Strain imaging is based on tracking sonographic speckles over time. Although seen as noise in conventional echograms, speckles are an excellent feature for quantifying the motion, velocity, and deformation of tissue in two directions. In contrast to techniques such as tissue Doppler imaging, strain imaging is not affected by the angle between ultrasound beam and tissue motion. Oppersma et al. demonstrated that strain and strain rate are highly correlated to transdiaphragmatic pressure in healthy subjects [105]. In addition, two groups [106, 107] developed a speckle tracking method for evaluating true diaphragm displacement in two directions, which is not affected by the imaging plane and is considered a more accurate measure of displacement as compared to diaphragm motion along the M-mode line.

11.7.3 Shear Wave Elastography

Besides functional imaging, quantification of the elastic properties of tissues may provide an additional diagnostic tool. Shear wave elastography is a technique that

allows quantification of the elastic modulus of tissue. A shear wave is generated by the acoustic radiation force from a focused ultrasound beam, and it propagates orthogonal to the ultrasound beam. Measurement of shear wave speed (v) allows quantification of the directly related shear modulus (i.e., SM = p v^2, with p the density of the tissue). A higher shear modulus indicates a stiffer tissue. Application of this technique to the diaphragm could be of clinical importance since changes in muscle stiffness may reflect alterations in muscle physiology due to fibrosis or injury, for instance. Reliability of assessment of diaphragm shear modulus with ultrasound was recently described in healthy controls and ICU patients [108]. However, it should be noted that shear wave speed is challenging to reliably measure in a thin muscle such as the diaphragm, and that values are affected by probe position, lung volume, the timing of measurement within the breathing cycle, and the presence of the hyperechoic tendinous layer within the diaphragm [109]. Initial application of the technique as a potential non-invasive tool to assess diaphragm contractile activity has been recently performed by Bachasson and coworkers [110]; they demonstrated in healthy volunteers that changes in diaphragm stiffness throughout inspiratory efforts reflected changes in transdiaphragmatic pressure. A pilot study in ICU patients also reported correlations between transdiaphragmatic pressure and changes in diaphragm shear modulus; however, only moderate associations were present in a small subset (8 out of 25) of patients [111]. In contrast to the application during inspiratory efforts, measurements of diaphragm shear modulus at end-expiration throughout the course of mechanical ventilation could provide clinically important insights in the development of structural alterations in diaphragm muscle quality. This is an important emerging area of research, as it could contribute to a better understanding of the development of diaphragm dysfunction due to critical illness and mechanical ventilation that can be assessed noninvasively. Recent work by Aarab and colleagues [112] demonstrated in 102 patients that changes in diaphragm shear modulus occurred during the first week of invasive mechanical ventilation: shear modulus increased in 51%, decreased in 41% and did not change in 8% of patients. Interpretation of these findings is complex in the context of simultaneous changes in diaphragm thickness, but they definitively indicate the presence of changes in tissue quality and stimulates the design of future studies.

11.7.4 Echogenicity

Assessment of echogenicity (also known as echodensity, or ultrasound intensity) can potentially quantify muscle quality. In general, it is assumed that lower echogenicity values (e.g., darker pixels on the image) indicate good muscle quality. Coiffard et al. reported a higher median diaphragm echogenicity in mechanically ventilated patients compared to healthy subjects [113]. However, standardizing this technique is key since changes in ultrasound settings directly influence the gray values of the image and thus echogenicity results. Moreover, it was recently described that demographic factors such as age, sex, and body mass index affect echogenicity values even in healthy volunteers when using a standardized ultrasound echogenicity assessment protocol [114]. This stresses the need for properly matched controls before interpreting findings in critically ill patients.

Summary

The use of ultrasound to assess and monitor the respiratory muscles is becoming increasingly popular in the ICU due to its non-invasive nature, real-time visualization, fast learning curve, and bedside availability. Several sonographic techniques are currently used to assess structure, activity, and function of diaphragm (excursion and thickness/thickening fraction) and extra-diaphragmatic respiratory muscles (parasternal intercostal muscles and expiratory abdominal muscles). Respiratory muscle ultrasonography allows detection of respiratory muscle dysfunction and quantification of the degree of muscle activation during patient effort. It can also assist with the identification of patients at risks for weaning failure and is used for the assessment of patient-ventilator asynchronies. More evidence is currently needed to support its widespread use in the ICU, especially for extra-diaphragmatic respiratory muscles.

Take-Home Messages

- The various muscles that closely work together to maintain alveolar ventilation are commonly called "respiratory muscles." Dysfunction of these respiratory muscle is common in mechanically ventilated critically ill patients. Respiratory muscle dysfunction is associated with poor clinical outcomes, including prolonged intensive care unit (ICU) stay, a higher risk of complications and increased mortality.
- The chest wall consists of two compartments, the rib cage and the abdomen. These two compartments are mechanically arranged in parallel; lung inflation/deflation can occur by volume changes in either the rib cage or the abdomen or of both compartments concurrently. Principal inspiratory muscles are diaphragm, external intercostal, and parasternal intercostal muscles. Expiratory muscles include internal intercostal muscles and abdominal wall muscles (rectus abdominis, external and internal oblique, and transverse abdominis muscles).
- Monitoring the respiratory muscle function is important to limit the detrimental consequences of mechanical ventilation on the respiratory muscles. The use of ultrasound is becoming increasingly popular in the ICU due to its non-invasive nature, real-time visualization, fast learning curve, and bedside availability.
- Diaphragm ultrasound has become a well-established tool to be used at the bedside and the technique and its reproducibility have now been extensively evaluated in healthy subjects, ambulatory patients, and critically ill patients. In contrast, ultrasound of the extra-diaphragmatic inspiratory and expiratory muscles is still in its infancy and has been mostly used as a research tool.
- Respiratory muscle ultrasonography can (1) detect respiratory muscle dysfunction either pre-existing or that has developed during mechanical ventilation; (2) quantify the degree of muscle activation during patient effort; (3) support the identification of patients at risks for weaning failure; (4) help in the assessment of patients with neuromuscular disease; and (5) provide information on patient-ventilator asynchronies.
- Common sonographic assessments of the diaphragm are (1) diaphragm excursion, (2) diaphragm thickness, and (3) diaphragm thickening fraction (TFdi). Diaphragm thickness reflects primarily the macroscopic structure and trophism of the muscle, and greatly varies across individuals, gender, and age. Monitoring the evo-

lution of diaphragm thickness over the course of mechanical ventilation can be used to detect diaphragm atrophy and to presume changes in function. Both diaphragm excursion and diaphragm thickening fraction (TFdi) can be measured during quiet breathing and during a maximal inspiratory effort (e.g., deep breathing or a sniff maneuver). During quiet breathing, they are related to inspiratory effort, whereas during a maximum inspiratory effort, they are associated with diaphragm function.

- Sonographic assessments of the parasternal intercostal muscles are (1) intercostal muscle thickness, and (2) intercostal muscle thickening fraction (TFic). Higher TFic in patients with diaphragm dysfunction seems to indicate a compensatory mechanism of extra-diaphragmatic inspiratory muscles.
- Sonography assessments of the expiratory abdominal muscles are (1) abdominal wall muscles thickness; and (2) abdominal wall muscles thickening fraction (TFab). Interpreting the TFab is complex, since the abdominal muscles have more degrees of freedom as compared to the diaphragm and parasternal intercostal muscles. Therefore, TFab is currently considered to be a screening parameter to identify active expiratory muscle use.
- The concomitant ultrasonographic assessment of diaphragm and extra-diaphragmatic respiratory muscles with other sonographic, clinical, and laboratory measurements has been proposed as method to increase accuracy in the assessment of weaning process.
- Although ultrasound of the respiratory muscles is clinically useful, easy to perform, and radiation-free, several limitations and pitfalls have been described (e.g., operator-dependency, learning curve, patient characteristics and ability to cooperate, influence of positive pressure ventilation and PEEP, presence of systemic inflammation, and excessive fluid accumulation).

References

1. Dres M, Dube BP, Mayaux J, Delemazure J, Reuter D, Brochard L, et al. Coexistence and impact of limb muscle and diaphragm weakness at time of liberation from mechanical ventilation in medical intensive care unit patients. Am J Respir Crit Care Med. 2017;195(1):57–66.
2. Dres M, Demoule A. Diaphragm dysfunction during weaning from mechanical ventilation: an underestimated phenomenon with clinical implications. Crit Care. 2018;22(1):73.
3. Goligher EC, Dres M, Fan E, Rubenfeld GD, Scales DC, Herridge MS, et al. Mechanical ventilation-induced diaphragm atrophy strongly impacts clinical outcomes. Am J Respir Crit Care Med. 2018;197(2):204–13.
4. Adler D, Dupuis-Lozeron E, Richard JC, Janssens JP, Brochard L. Does inspiratory muscle dysfunction predict readmission after intensive care unit discharge? Am J Respir Crit Care Med. 2014;190(3):347–50.
5. Jaber S, Petrof BJ, Jung B, Chanques G, Berthet JP, Rabuel C, et al. Rapidly progressive diaphragmatic weakness and injury during mechanical ventilation in humans. Am J Respir Crit Care Med. 2011;183(3):364–71.
6. Goligher EC, Fan E, Herridge MS, Murray A, Vorona S, Brace D, et al. Evolution of diaphragm thickness during mechanical ventilation: impact of inspiratory effort. Am J Respir Crit Care Med. 2015;192(9):1080–8.

7. Hussain SNA, Mofarrahi M, Sigala I, Kim HC, Vassilakopoulos T, Maltais F, et al. Mechanical ventilation–induced diaphragm disuse in humans triggers autophagy. Am J Respir Crit Care Med. 2010;182(11):1377–86.
8. Hooijman PE, Beishuizen A, Witt CC, de Waard MC, Girbes ARJ, Spoelstra-de Man AME, et al. Diaphragm muscle fiber weakness and ubiquitin–proteasome activation in critically ill patients. Am J Respir Crit Care Med. 2015;191(10):1126–38.
9. Levine S, Budak MT, Sonnad S, Shrager JB. Rapid disuse atrophy of diaphragm fibers in mechanically ventilated humans. N Engl J Med. 2008;9:1327.
10. Orozco-Levi M, Lloreta J, Minguella J, Serrano S, Broquetas JM, Gea J. Injury of the human diaphragm associated with exertion and chronic obstructive pulmonary disease. Am J Respir Crit Care Med. 2001;164(9):1734–9.
11. Ebihara S, Hussain SNA, Danialou G, Cho WK, Gottfried SB, Petrof BJ. Mechanical ventilation protects against diaphragm injury in sepsis: interaction of oxidative and mechanical stresses. Am J Respir Crit Care Med. 2002;165(2):221–8.
12. Goligher EC, Dres M, Patel BK, Sahetya SK, Beitler JR, Telias I, et al. Lung and diaphragm-protective ventilation. Am J Respir Crit Care Med. 2020;202(7):950–61.
13. Goligher EC. Clinical strategies for implementing lung and diaphragm-protective ventilation: avoiding insufficient and excessive effort. Intensive Care Med. 2020;46:2314–26.
14. Tuinman PR, Jonkman AH, Dres M, Shi ZH, Goligher EC, Goffi A, et al. Respiratory muscle ultrasonography: methodology, basic and advanced principles and clinical applications in ICU and ED patients—a narrative review. Intensive Care Med. 2020;46(4):594–605.
15. De Troyer A, Estenne M. Functional anatomy of the respiratory muscles. Clin Chest Med. 1988;9(2):175–93.
16. Derenne JP, Macklem PT, Roussos C. The respiratory muscles: mechanics, control, and pathophysiology. Am Rev Respir Dis. 1978;118(1):119–33.
17. Ratnovsky A, Elad D, Halpern P. Mechanics of respiratory muscles. Respir Physiol Neurobiol. 2008;163(1–3):82–9.
18. Parthasarathy S, Jubran A, Laghi F, Tobin MJ. Sternomastoid, rib cage, and expiratory muscle activity during weaning failure. J Appl Physiol. 2007;103:140–7.
19. Doorduin J. Respiratory muscle effort during expiration in successful and failed weaning from mechanical ventilation. Anesthesiology. 2018;129(3):490–501.
20. Bordoni B, Zanier E. Anatomic connections of the diaphragm: influence of respiration on the body system. J Multidiscip Healthc. 2013;6:281–91.
21. De Troyer A, Boriek AM. Mechanics of the respiratory muscles. Compr Physiol. 2011;1(3):1273–300.
22. DeTroyer A. The respiratory muscles. In: Crystal RG, editor. The lung: scientific foundation. Philadelphia: Lippincott Raven; 1997. p. 1203–15.
23. Derenne JP, Macklem PT, Roussos C. The respiratory muscles: mechanics, control, and pathophysiology. Part 2. Am Rev Respir Dis. 1978;118(2):373–90.
24. Derenne JP, Macklem PT, Roussos C. The respiratory muscles: mechanics, control, and pathophysiology. Part III. Am Rev Respir Dis. 1978;118(3):581–601.
25. De Troyer A, Kirkwood PA, Wilson TA. Respiratory action of the intercostal muscles. Physiol Rev. 2005;85(2):717–56.
26. Haaksma ME, Smit JM, Boussuges A, Demoule A, Dres M, Ferrari G, et al. EXpert consensus On Diaphragm UltraSonography in the critically ill (EXODUS): a Delphi consensus statement on the measurement of diaphragm ultrasound-derived parameters in a critical care setting. Crit Care. 2022;26(1):99.
27. Mariani LF, Bedel J, Gros A, Lerolle N, Milojevic K, Laurent V, et al. Ultrasonography for screening and follow-up of diaphragmatic dysfunction in the ICU: a pilot study. J Intensive Care Med. 2016;31(5):338–43.
28. Boussuges A, Gole Y, Blanc P. Diaphragmatic motion studied by m-mode ultrasonography: methods, reproducibility, and normal values. Chest. 2009;135(2):391–400.
29. Lerolle N, Guérot E, Dimassi S, Zegdi R, Faisy C, Fagon JY, et al. Ultrasonographic diagnostic criterion for severe diaphragmatic dysfunction after cardiac surgery. Chest. 2009;135(2):401–7.
30. Kim WY, Suh HJ, Hong SB, Koh Y, Lim CM. Diaphragm dysfunction assessed by ultrasonography: influence on weaning from mechanical ventilation. Crit Care Med. 2011;39(12):2627–30.

31. Jiang JR, Tsai TH, Jerng JS, Yu CJ, Wu HD, Yang PC. Ultrasonographic evaluation of liver/spleen movements and extubation outcome. Chest. 2004;126(1):179–85.
32. Boon AJ, Harper CJ, Ghahfarokhi LS, Strommen JA, Watson JC, Sorenson EJ. Two-dimensional ultrasound imaging of the diaphragm: quantitative values in normal subjects. Muscle Nerve. 2013;47(6):884–9.
33. Baldwin CE, Paratz JD, Bersten AD. Diaphragm and peripheral muscle thickness on ultrasound: intra-rater reliability and variability of a methodology using non-standard recumbent positions. Respirology. 2011;16(7):1136–43.
34. Goligher EC, Laghi F, Detsky ME, Farias P, Murray A, Brace D, et al. Measuring diaphragm thickness with ultrasound in mechanically ventilated patients: feasibility, reproducibility and validity. Intensive Care Med. 2015;41(4):642–9.
35. Cohn D, Benditt JO, Eveloff S, McCool FD. Diaphragm thickening during inspiration. J Appl Physiol (1985). 1997;83(1):291–296.
36. Wait JL, Nahormek PA, Yost WT, Rochester DP. Diaphragmatic thickness-lung volume relationship in vivo. J Appl Physiol (1985). 1989;67(4):1560–1568.
37. Haaksma ME, van Tienhoven AJ, Smit JM, Heldeweg MLA, Lissenberg-Witte BI, Wennen M, et al. Anatomical variation in diaphragm thickness assessed with ultrasound in healthy volunteers. Ultrasound Med Biol. 2022;48(9):1833–9.
38. Vivier E, Mekontso Dessap A, Dimassi S, Vargas F, Lyazidi A, Thille AW, et al. Diaphragm ultrasonography to estimate the work of breathing during non-invasive ventilation. Intensive Care Med. 2012;38(5):796–803.
39. Umbrello M, Formenti P, Longhi D, Galimberti A, Piva I, Pezzi A, et al. Diaphragm ultrasound as indicator of respiratory effort in critically ill patients undergoing assisted mechanical ventilation: a pilot clinical study. Crit Care. 2015;19:161.
40. Poulard T, Bachasson D, Fossé Q, Niérat MC, Hogrel JY, Demoule A, et al. Poor correlation between diaphragm thickening fraction and transdiaphragmatic pressure in mechanically ventilated patients and healthy subjects. Anesthesiology. 2022;136(1):162–75.
41. Boussuges A, Rives S, Finance J, Chaumet G, Vallée N, Risso JJ, et al. Ultrasound assessment of diaphragm thickness and thickening: reference values and limits of normality when in a seated position. Front Med (Lausanne). 2021;8:742703.
42. Gottesman E, McCool FD. Ultrasound evaluation of the paralyzed diaphragm. Am J Respir Crit Care Med. 1997;155(5):1570–4.
43. Harper CJ, Shahgholi L, Cieslak K, Hellyer NJ, Strommen JA, Boon AJ. Variability in diaphragm motion during Normal breathing, assessed with B-mode ultrasound. J Orthop Sports Phys Ther. 2013;43(12):927–31.
44. Dubé BP, Dres M, Mayaux J, Demiri S, Similowski T, Demoule A. Ultrasound evaluation of diaphragm function in mechanically ventilated patients: comparison to phrenic stimulation and prognostic implications. Thorax. 2017;72(9):811–8.
45. DiNino E, Gartman EJ, Sethi JM, McCool FD. Diaphragm ultrasound as a predictor of successful extubation from mechanical ventilation. Thorax. 2014;69(5):423–7.
46. Ferrari G, De Filippi G, Elia F, Panero F, Volpicelli G, Aprà F. Diaphragm ultrasound as a new index of discontinuation from mechanical ventilation. Crit Ultrasound J. 2014;6(1):8.
47. Formenti P, Umbrello M, Dres M, Chiumello D. Ultrasonographic assessment of parasternal intercostal muscles during mechanical ventilation. Ann Intensive Care. 2020;10(1):120.
48. Dres M, Dubé BP, Goligher E, Vorona S, Demiri S, Morawiec E, et al. Usefulness of parasternal intercostal muscle ultrasound during weaning from mechanical ventilation. Anesthesiology. 2020;132(5):1114–25.
49. Wallbridge P, Parry SM, Das S, Law C, Hammerschlag G, Irving L, et al. Parasternal intercostal muscle ultrasound in chronic obstructive pulmonary disease correlates with spirometric severity. Sci Rep. 2018;8(1):15274.
50. Yoshida R, Tomita K, Kawamura K, Nozaki T, Setaka Y, Monma M, et al. Measurement of intercostal muscle thickness with ultrasound imaging during maximal breathing. J Phys Ther Sci. 2019;31(4):340–3.
51. Dres M, Similowski T, Goligher EC, Pham T, Sergenyuk L, Telias I, et al. Dyspnoea and respiratory muscle ultrasound to predict extubation failure. Eur Respir J. 2021;58(5):2100002.

52. Shi ZH, Jonkman A, de Vries H, Jansen D, Ottenheijm C, Girbes A, et al. Expiratory muscle dysfunction in critically ill patients: towards improved understanding. Intensive Care Med. 2019;45(8):1061–71.
53. Shi ZH, de Vries H, de Grooth HJ, Jonkman AH, Zhang Y, Haaksma M, et al. Changes in respiratory muscle thickness during mechanical ventilation: focus on expiratory muscles. Anesthesiology. 2021;134:748–59.
54. Jonkman AH, Frenzel T, McCaughey EJ, McLachlan AJ, Boswell-Ruys CL, Collins DW, et al. Breath-synchronized electrical stimulation of the expiratory muscles in mechanically ventilated patients: a randomized controlled feasibility study and pooled analysis. Crit Care. 2020;24(1). http://www.scopus.com/inward/record.url?scp=85094661914&partnerID=8YFLogxK.
55. McCaughey EJ, Jonkman AH, Boswell-Ruys CL, McBain RA, Bye EA, Hudson AL, et al. Abdominal functional electrical stimulation to assist ventilator weaning in critical illness: a double-blinded, randomised, sham-controlled pilot study. Crit Care. 2019;23(1):261.
56. Schreiber AF, Bertoni M, Coiffard B, Fard S, Wong J, Reid WD, et al. Abdominal muscle use during spontaneous breathing and cough in patients who are mechanically ventilated. Chest. 2021;160(4):1316–25.
57. Tahan N, Khademi-Kalantari K, Mohseni-Bandpei MA, Mikaili S, Baghban AA, Jaberzadeh S. Measurement of superficial and deep abdominal muscle thickness: an ultrasonography study. J Physiol Anthropol. 2016;35(1):17.
58. Jung B, Moury PH, Mahul M, de Jong A, Prades A. Diaphragmatic dysfunction in patients with ICU-acquired weakness and its impact on extubation failure. Intensive Care Med. 2016;42(5):853–61.
59. Medrinal C, Prieur G, Frenoy É, Robledo Quesada A, Poncet A, Bonnevie T, et al. Respiratory weakness after mechanical ventilation is associated with one-year mortality—a prospective study. Crit Care. 2016;20(1):1–7.
60. Gibson GJ, Whitelaw W, Siafakas N, Supinski GS, Fitting JW, Bellemare F, et al. ATS/ERS statement on respiratory muscle testing. Am J Respir Crit Care Med. 2002;166(4):518–624.
61. Dres M, Demoule A. Monitoring diaphragm function in the ICU. Curr Opin Crit Care. 2020;26(1):18–25.
62. Wait JL, Nahormek PA, Yost WT, Rochester DP. Diaphragmatic thickness-lung volume relationship in vivo. J Appl Physiol. 1989;67(4):1560–8.
63. Haaksma ME, Smit JM, Boussuges A, Demoule A, Dres M, Ferrari G, et al. EXpert consensus On Diaphragm UltraSonography in the critically ill (EXODUS): a Delphi consensus statement on the measurement of diaphragm ultrasound-derived parameters in a critical care setting. Crit Care. 2022;26(1):1–9.
64. Lerolle N, Guerot E, Dimassi S, Zegdi R, Faisy C, Fagon JY, et al. Ultrasonographic diagnostic criterion for severe diaphragmatic dysfunction after cardiac surgery. Chest. 2009;135(2):401–7.
65. Valette X, Seguin A, Daubin C, Brunet J, Sauneuf B, Terzi N, et al. Diaphragmatic dysfunction at admission in intensive care unit: the value of diaphragmatic ultrasonography. Intensive Care Med. 2015;41(3):557–9.
66. Mariani LF, Bedel J, Gros A, Lerolle N, et al. Ultrasonography for screening and follow-up of diaphragmatic dysfunction in the ICU: a pilot study. J Intensive Care Med. 2016;31(5):338–43.
67. Palkar A, Narasimhan M, Greenberg H, Singh K, Koenig S, Mayo P, et al. Diaphragm excursion-time index: a new parameter using ultrasonography to predict extubation outcome. Chest. 2018.;Accepted f;153:1213.
68. Kim SH, Na S, Choi JS, Na SH, Shin S, Koh SO. An evaluation of diaphragmatic movement by M-mode sonography as a predictor of pulmonary dysfunction after upper abdominal surgery. Anesth Analg. 2010;110(5):1349–54.
69. Zambon M, Greco M, Bocchino S, Cabrini L, Beccaria PF, Zangrillo A. Assessment of diaphragmatic dysfunction in the critically ill patient with ultrasound: a systematic review. Intensive Care Med. 2017;43(1):29–38.
70. Sanchez De Toledo J, Munoz R, Landsittel D, Shiderly D, Yoshida M, Komarlu R, et al. Diagnosis of abnormal diaphragm motion after cardiothoracic surgery: ultrasound performed by a cardiac intensivist vs. fluoroscopy. Congenit Heart Dis. 2010;5(6):565–72.

71. Umbrello M, Formenti P, Lusardi AC, Guanziroli M, Caccioppola A, Coppola S, et al. Oesophageal pressure and respiratory muscle ultrasonographic measurements indicate inspiratory effort during pressure support ventilation. Br J Anaesth. 2020;125(1):e148–57.
72. Le Neindre A, Philippart F, Luperto M, Wormser J, Morel-Sapene J, Aho SL, et al. Diagnostic accuracy of diaphragm ultrasound to predict weaning outcome: a systematic review and meta-analysis. Int J Nurs Stud. 2021;117:103890.
73. Llamas-Álvarez AM, Tenza-Lozano EM, Latour-Pérez J. Diaphragm and lung ultrasound to predict weaning outcome: systematic review and meta-analysis. Chest. 2017;152(6):1140–50.
74. Abdelwahed WM, Abd Elghafar MS, Amr YM, Alsherif SE, din I, Eltomey MA. Prospective study: diaphragmatic thickness as a predictor index for weaning from mechanical ventilation. J Crit Care. 2019;52:10–5.
75. Ali ER, Mohamad AM. Diaphragm ultrasound as a new functional and morphological index of outcome, prognosis and discontinuation from mechanical ventilation in critically ill patients and evaluating the possible protective indices against VIDD. Egypt J Chest Dis Tuberc. 2017;66(2):339–51.
76. Baess A, Abdallah T, Emara D, Hassan M. Diaphragmatic ultrasound as a predictor of successful extubation from mechanical ventilation: thickness, displacement, or both? Egypt J Bronchol. 2016;10(2):162.
77. Farghaly S, Hasan AA. Australian critical care diaphragm ultrasound as a new method to predict extubation outcome in mechanically ventilated patients. Aust Crit Care. 2017;30(1):37–43.
78. Spadaro S, Grasso S, Mauri T, Dalla Corte F, Alvisi V, Ragazzi R, et al. Can diaphragmatic ultrasonography performed during the T-tube trial predict weaning failure? The role of diaphragmatic rapid shallow breathing index. Crit Care. 2016;20:305.
79. Vivier E, Muller M, Putegnat JB, Steyer J, Barrau S, Boissier F, et al. Inability of diaphragm ultrasound to predict extubation failure a multicenter study. Chest. 2019;155:1131–9.
80. Mayo P, Volpicelli G, Lerolle N, Schreiber A, Doelken P, Vieillard-Baron A. Ultrasonography evaluation during the weaning process: the heart, the diaphragm, the pleura and the lung. Intensive Care Med. 2016;42:1107.
81. Soummer A, Perbet S, Brisson H, Arbelot C, Constantin JM, Lu Q, et al. Ultrasound assessment of lung aeration loss during a successful weaning trial predicts postextubation distress. Crit Care Med. 2012;40(7):2064–72.
82. Haaksma ME, Smit JM, Heldeweg MLA, Nooitgedacht JS, Atmowihardjo LN, Jonkman AH, et al. Holistic ultrasound to predict extubation failure in clinical practice. Respir Care. 2021;66(6):994–1003.
83. Umbrello M, Formenti P, Longhi D, Galimberti A, Piva I, Pezzi A, et al. Diaphragm ultrasound as indicator of respiratory effort in critically ill patients undergoing assisted mechanical ventilation: a pilot clinical study. Crit Care. 2015;19(1):1–10.
84. Yoshioka Y, Ohwada A, Sekiya M, Takahashi F, Ueki J, Fukuchi Y. Ultrasonographic evaluation of the diaphragm in patients with amyotrophic lateral sclerosis. Respirology. 2007;12(2):304–7.
85. Hiwatani Y, Sakata M, Miwa H. Ultrasonography of the diaphragm in amyotrophic lateral sclerosis: clinical significance in assessment of respiratory functions. Amyotrophic Lateral Scler Frontotemporal Degener. 2013;14(2):127–31.
86. Fantini R, Mandrioli J, Zona S, Antenora F, Iattoni A, Monelli M, et al. Ultrasound assessment of diaphragmatic function in patients with amyotrophic lateral sclerosis. Respirology. 2016;21(5):932–8.
87. Pinto S, Alves P, Pimentel B, Swash M, de Carvalho M. Ultrasound for assessment of diaphragm in ALS. Clin Neurophysiol. 2016;127(1):892.
88. Miller RG, Jackson CE, Kasarskis EJ, England JD, Forshew D, Johnston W, et al. Practice parameter update: the care of the patient with amyotrophic lateral sclerosis: drug, nutritional, and respiratory therapies (an evidence-based review). Neurology. 2016;73(15):1218–26.
89. Sartucci F, Pelagatti A, Santin M, Bocci T, Dolciotti C, Bongioanni P. Diaphragm ultrasonography in amyotrophic lateral sclerosis: a diagnostic tool to assess ventilatory dysfunction and disease severity. Neurol Sci. 2019;40(10):2065–71.
90. Laviola M, Priori R, D'Angelo MG, Aliverti A. Assessment of diaphragmatic thickness by ultrasonography in Duchenne muscular dystrophy (DMD) patients. PLoS One. 2018;13(7):e0200582.

91. De Bruin PF, Ueki J, Bush A, Khan Y, Watson A, Pride NB. Diaphragm thickness and inspiratory strength in patients with Duchenne muscular dystrophy. Thorax. 1997;52:472–5.
92. Fayssoil A, Nguyen LS, Ogna A, Stojkovic T, Meng P, Mompoint D, et al. Diaphragm sniff ultrasound: normal values, relationship with sniff nasal pressure and accuracy for predicting respiratory involvement in patients with neuromuscular disorders. PLoS One. 2019;14(4):1–17.
93. Pennati F, Arrigoni F, LoMauro A, Gandossini S, Russo A, D'Angelo MG, et al. Diaphragm involvement in Duchenne muscular dystrophy (DMD): an MRI study. J Magn Reson Imaging. 2020;51(2):461–71.
94. Barnard AM, Lott DJ, Batra A, Triplett WT, Forbes SC, Riehl SL, et al. Imaging respiratory muscle quality and function in Duchenne muscular dystrophy. J Neurol. 2019;266(11):2752–63.
95. Ruggeri P, Lo Monaco L, Musumeci O, Tavilla G, Gaeta M, Caramori G, et al. Ultrasound assessment of diaphragm function in patients with late-onset Pompe disease. Neurol Sci. 2020;41(8):2175–84.
96. Gaeta M, Barca E, Ruggeri P, Minutoli F, Rodolico C, Mazziotti S, et al. Late-onset Pompe disease (LOPD): correlations between respiratory muscles CT and MRI features and pulmonary function. Mol Genet Metab. 2013;110(3):290–6.
97. Jung KJ, Park JY, Hwang DW, Kim JH, Kim JH. Ultrasonographic diaphragmatic motion analysis and its correlation with pulmonary function in hemiplegic stroke patients. Ann Rehabil Med. 2014;38(1):29–37.
98. Kim MK, Lee KB, Cho J, Lee WH. Diaphragm thickness and inspiratory muscle functions in chronic stroke patients. Med Sci Monit. 2017;23:1247–53.
99. Soilemezi E, Vasileiou M, Spyridonidou C, Tsagourias M, Matamis D. Understanding patient-ventilator asynchrony using diaphragmatic ultrasonography. Am J Respir Crit Care Med. 2019;200(4):E27–8.
100. Vivier E, Haudebourg AF, Le Corvoisier P, Mekontso Dessap A, Carteaux G. Diagnostic accuracy of diaphragm ultrasound in detecting and characterizing patient-ventilator asynchronies during noninvasive ventilation. Anesthesiology. 2020;6:1494–502.
101. Jansen D, Jonkman AH, de Vries HJ, Wennen M, Elshof J, Hoofs MA, et al. Positive end-expiratory pressure affects geometry and function of the human diaphragm. J Appl Physiol (1985). 2021;131(4):1328–1339.
102. Soilemezi E, Savvidou S, Sotiriou P, Smyrniotis D, Tsagourias M, Matamis D. Tissue doppler imaging of the diaphragm in healthy subjects and critically ill patients. Am J Respir Crit Care Med. 2020;202(7):1005–12.
103. Cammarota G, Boniolo E, Santangelo E, De Vita N, Verdina F, Crudo S, et al. Diaphragmatic kinetics assessment by tissue Doppler imaging and Extubation outcome. Respir Care. 2021;66(6):983–93.
104. Jonkman AH, Wennen M, Sklar MC, de Korte C, Tuinman PR. Tissue Doppler imaging of the diaphragm. Am J Respir Crit Care Med. 2020;202(12):1741–2.
105. Oppersma E, Hatam N, Doorduin J, van der Hoeven JG, Marx G, Goetzenich A, et al. Functional assessment of the diaphragm by speckle tracking ultrasound during inspiratory loading. J Appl Physiol. 2017;123(5):1063–70.
106. Goutman SA, Hamilton JD, Swihart B, Foerster B, Feldman EL, Rubin JM. Speckle tracking as a method to measure hemidiaphragm excursion. Muscle Nerve. 2017;55(1):125–7.
107. Ye X, Liu Z, Ma Y, Song Y, Hu L, Luo J, et al. A novel normalized cross-correlation speckle-tracking ultrasound algorithm for the evaluation of diaphragm deformation. Front Med. 2021;8:612933.
108. Flatres A, Aarab Y, Nougaret S, Garnier F, Larcher R, Amalric M, et al. Real-time shear wave ultrasound elastography: a new tool for the evaluation of diaphragm and limb muscle stiffness in critically ill patients. Crit Care. 2020;24(1):34.
109. Jonkman AH, de Korte CL. Shear wave Elastography of the diaphragm: good vibrations? Am J Respir Crit Care Med. 2021;204(7):748–50.
110. Bachasson D, Dres M, Niérat MC, Gennisson JL, Hogrel JY, Doorduin J, et al. Diaphragm shear modulus reflects transdiaphragmatic pressure during isovolumetric inspiratory efforts and ventilation against inspiratory loading. J Appl Physiol. 2019;126(3):699–707.

111. Fossé Q, Poulard T, Niérat MC, Virolle S, Morawiec E, Hogrel JY, et al. Ultrasound shear wave elastography for assessing diaphragm function in mechanically ventilated patients: a breath-by-breath analysis. Crit Care. 2020;24(1):669.
112. Aarab Y, Flatres A, Garnier F, Capdevila M. Shear wave elastography, a new tool for diaphragmatic qualitative assessment. A translational study. Am J Respir Crit Care Med. 2021;204:797.
113. Coiffard B, Riegler S, Sklar MC, Dres M, Vorona S, Reid WD, et al. Diaphragm echodensity in mechanically ventilated patients: a description of technique and outcomes. Crit Care. 2021;25(1):64.
114. van Doorn JLM, Wijntjes J, Saris CGJ, Ottenheijm CAC, van Alfen N, Doorduin J. Association of diaphragm thickness and echogenicity with age, sex, and body mass index in healthy subjects. Muscle Nerve. 2022;66(2):197–202.

Abdomen

Contents

Chapter 12 **Triage or Clinical Suspicion for Aortic Syndromes – 000**
Federico Dazzi, Francesco Corradi, Erika Taddei, Giada Cucciolini, and Francesco Forfori

Chapter 13 **Assessment of Kidneys and Urinary Tract – 000**
Adrian V. K. Wong and Serene SP Ho

Chapter 14 **Assessment of Traumatic Acute Abdomen – 000**
Kelvin Wong, Dae Hyeon Kim, and Mangala Narasimhan

Chapter 15 **Ecographic Assessment of Nontraumatic Acute Abdomen – 000**
Martina Fregonese, Beatrice Vigna, Edoardo De Robertis, and Gianmaria Cammarota

Triage or Clinical Suspicion for Aortic Syndromes

Federico Dazzi, Francesco Corradi, Erika Taddei, Giada Cucciolini, and Francesco Forfori

Contents

12.1 Normal Aortic Anatomy – 172

12.2 How to Evaluate the Abdominal Aorta by US – 172
12.2.1 Patient Position – 172
12.2.2 US Device Settings – 172
12.2.3 US Scans of Visualization – 173
12.2.4 Ultrasonographic Examination – 173

12.3 Role of US in Acute Aortic Syndromes – 178
12.3.1 Abdominal Aortic Aneurysm – 178
12.3.2 Ruptured Abdominal Aortic Aneurysm – 180
12.3.3 Acute Aortic Dissection – 181
12.3.4 Traumatic Aortic Injury (TAI) – 184

References – 184

Supplementary Information The online version contains supplementary material available at https://doi.org/10.1007/978-3-031-32462-8_12.

© The Author(s), under exclusive license to Springer Nature Switzerland AG 2023
C. Robba et al. (eds.), *Basic Ultrasound Skills "Head to Toe" for General Intensivists*, Lessons from the ICU,
https://doi.org/10.1007/978-3-031-32462-8_12

Learning Objectives

- Knowledge of normal aortic anatomy
- Perform an US exam for detection of Aortic Aneurysms
- Establish the Role of Echo in Aortic syndromes
  - Abdominal Aortic Aneurysm (AAA)
  - Ruptured AAA
  - Acute Aortic Dissection (AAD)
  - Traumatic aortic injury and iatrogenic aortic injury

12.1 Normal Aortic Anatomy

The aorta is divided anatomically into thoracic and abdominal portions, each one subdivided into three sections.

The Thoracic Aorta, which spans from T3 to T12 spinal levels, above the diaphragm and can be subdivided into:

- ***Ascending aorta:*** from the sternal angle to T4–T5
- ***Aortic arch:*** from T4–T5 up to T3 and down to T4
- ***Descending thoracic aorta:*** from T4–T5 to T12, where it becomes abdominal aorta after passing through the aortic hiatus of the diaphragm

Transthoracic echocardiographic ultrasound (TTE) allows visualization of the ascending aorta via left parasternal view, the aortic arch via suprasternal view, and the descending thoracic aorta via cardiac apical window.

The Abdominal Aorta (AA), which spans from T12 to L4 spinal levels below the diaphragm, can be subdivided into:

- ***Proximal Abdominal Aorta:*** from the diaphragm, celiac trunk to the superior mesenteric artery (SMA)
- ***Mid-Abdominal Aorta:*** from SMA to the level of the renal arteries
- ***Distal Abdominal Aorta:*** from the level of the renal arteries to the iliac bifurcation

Proximal and mid-abdominal aorta together are also defined as suprarenal aorta and the distal abdominal aorta as infrarenal abdominal aorta.

12.2 How to Evaluate the Abdominal Aorta by US

12.2.1 Patient Position

The patient is usually examined in a supine position with the head raised at 30°.

12.2.2 US Device Settings

The ultrasonographic assessment of the abdominal aorta should be performed with a 2.5 to 3.5 MHz transducer to maintain adequate resolution and penetration. For

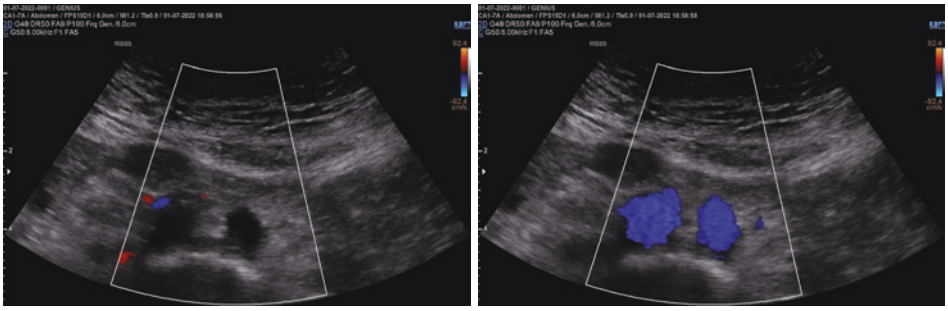

Fig. 12.1 Color Doppler imaging may be useful to identify the common iliac arteries and assess the lumen patency or demonstrate the presence of mural thrombus

proper visualization, the abdominal preset must be set at an initial depth of 10–15 cm. B-Mode imaging is used to obtain aortic measures, such as the aortic diameter. Color Doppler imaging may be useful to identify the common iliac arteries and assess the lumen patency or demonstrate the presence of mural thrombi (Fig. 12.1). An ECG trace should be acquired to distinguish systolic and diastolic phases.

12.2.3 US Scans of Visualization

US allows visualization of abdominal aorta on transverse, sagittal, and coronal planes by using a convex transducer (2.5–5 MHz).

A transverse scan of the proximal aorta can be obtained by placing the probe just below the xiphoid process, slightly to the left of the midline, with the pointer indicator facing the patient's right ("9 o'clock"). The depth must be adjusted until the hyperechoic vertebral body and its dense shadow are visible at the bottom of the screen. The probe must be kept perpendicular to the abdominal wall for the best short-axis view and accurate subsequent measurements.

The sagittal plane can be obtained by 90° rotation of the probe related to the short-axis view, with the probe indicator at 12 o'clock.

The coronal plane is possible by placing the probe at the patient's right side (Fig. 12.2) with the indicator facing patient's head, in the right mid-axillary line between 10th and 11th intercostal spaces [1, 2].

12.2.4 Ultrasonographic Examination

The assessment of the proximal abdominal aorta has the following objectives:

- Distinguishing aorta from inferior cava vein (ICV)
- Visualizing celiac trunk, superior mesenteric artery, and renal arteries
- Measuring the aortic diameter

Fig. 12.2 The coronal scan at the patient's right side allows to obtain long-axis views of the aorta, above the spine and below the inferior cava vein. Suvrahepatic vein (SHV)

Fig. 12.3 In the transverse section, the aorta appears as a round echo-free area in front of the spine, whereas the inferior vena cava (ICV) lies to the right of the spine

12

12.2.4.1 Distinguishing Aorta from ICV

On transverse scan, the Aorta appears as a thick-walled, hypoechoic, pulsatile circle just above the vertebral body, slightly to the right of midline on the screen (patient's left) (Fig. 12.3). The ICV is not as circular as the aorta and lies to the left of the midline on the screen (patient's right); it is usually collapsible during inspiration. The inferior boundary of the mid-abdominal aorta is in the correspondence of renal arteries emergence, which can be seen near the umbilicus region (Fig. 12.4). At this point, the aorta is more superficial and a reduction in depth may be necessary.

On a sagittal scanning plane, the aorta is shown as a tubular echo-free structure situated in front of the spine and slightly to the left of the mid-line compared with ICV (Fig. 12.5). Its proximal part is more posterior than its distal part due to the normal lumbar lordosis (Fig. 12.6). It is easily distinguished from the IVC, which curves forward to enter into the right atrium.

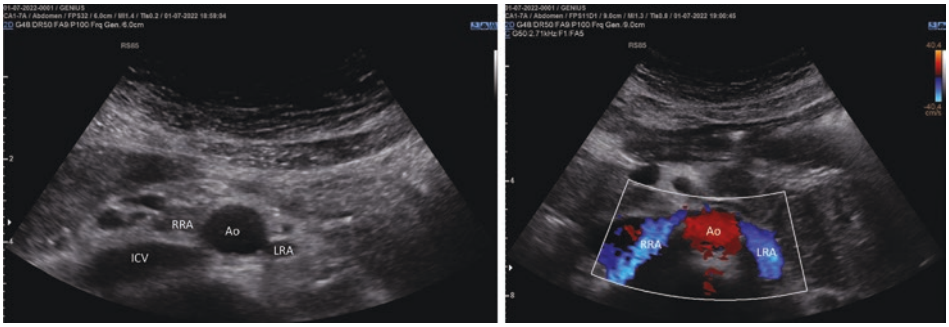

Fig. 12.4 Near the umbilical region, it's possible to locate the emergence of renal arteries from the aorta. Aorta (Ao); left renal artery (LRA); right renal artery (RRA); inferior cava vein (ICV)

Fig. 12.5 In a longitudinal section, the aorta is shown as a tubular echo-free structure situated in front of the spine and slightly to the left of the mid-line

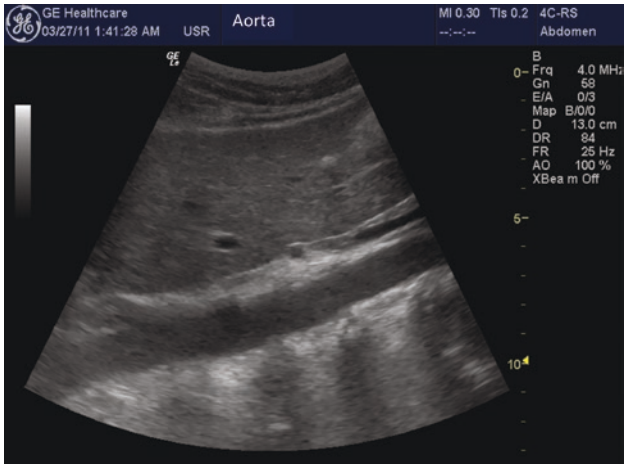

Fig. 12.6 The proximal part of the aorta is more posterior than its distal part due to the normal lumbar lordosis

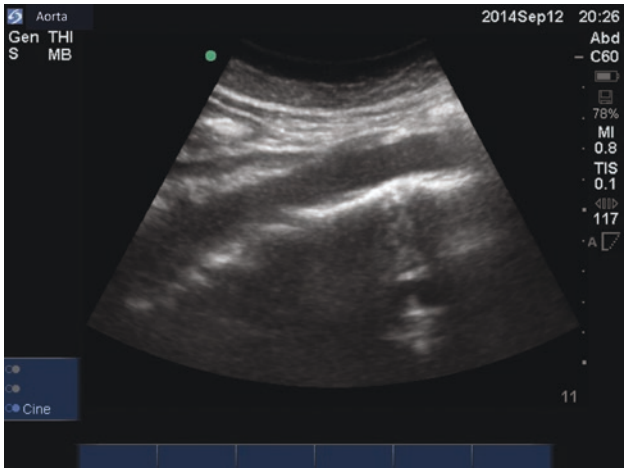

12.2.4.2 Identifiying Celiac Trunk, Superior Mesenteric Artery, and Renal Arteries

The origin of the celiac trunk from the aorta appears in transverse section as a "slit" defect on the anterior surface of the aorta. On a longitudinal section, it can be seen to arise from the anterior surface of the aorta running anteriorly or slightly cephalad. The celiac artery comes off first and then the superior mesenteric artery (SMA) is visualized parallel to the aorta.

The origin of the superior mesenteric artery from the anterior surface of the aorta appears in transverse section as an echo-free ring in front of the aorta. In longitudinal section, SMA can be seen to originate fron the anterior surface of the aorta and pass downwards—the average diameter of the SMA is 7 mm.

The renal arteries (RA) are located 1–3 cm distal to the SMA, which can be easily seen in a transverse section. The right RA runs around the anterior surface of the vertebral body and behind the ICV. The left RA originates from the posterior part of the left-side of the aorta, traveling downward parallel to the spine.

12.2.4.3 Measuring Aortic Diameter

Maximum diameter is an important parameter in the definition of AAA and is also used to predict the risk of rupture. The process of measurement in clinical practice is based on four steps: plane of acquisition, axis of measurement, caliper placement, and selection of the maximum diameter.

Diameter measurement of the abdominal aorta is performed along a pre-defined axis on the selected aortic section by positioning two calipers.

- On *Axial plane,* anteroposterior and transverse diameters are measured along the sagittal and transverse axes, respectively.
- On *Sagittal plane*, only the anteroposterior diameter is measured.

Caliper position is another discussed issue for US measurements, and the position chosen depends on the imaging resolution of AAA walls.

The three most widely recognized techniques for measuring the aorta diameter by US are:

- *Inner-to-Inner (ITI)*, where calipers are placed on the inner layer of the aortic wall.
- *Outer-to-Outer (OTO)*, where calipers are placed on the outer layer of the aortic wall.
- *Leading Edge-to-Leading Edge (LELE)*, where calipers are placed on the outer layer of the anterior wall and the inner layer of posterior wall.

Clinical trials have used different measurement methods [3–5]. Long et al. reviewed the methods used to measure AAA maximum diameter by US or Computed Tomography (CT) and found a wide range of definitions and practices, depending on the clinical setting in which measurements were obtained. They concluded that a comparison between the various methods is very difficult and that a standardized method should be recommended [6]. In a prospective study, Harthsorne et al. reported an inter-observer variability of 0.3 cm for ITI and 0.42 cm for OTO and intra-observer variability of 0.16 for ITI and 0.20 for OTO. For AAAs >5 cm, repeatability was significantly better with ITI than OTO (0.14 vs. 0.21; p 0.016) [7]. In 127 patients with

small AAA, Gurtelschmid et al. evaluated the maximum anteroposterior diameter taken on axial plane by ITI or OTO or LELE methods. Although LELE was the most reproducible method, all methods showed a high degree of variability [8]. The Tromso study by Singhl et al. was designed to evaluate the variability in aortic measurements between sonographers (different sonographers on the same occasion) and within sonographers (the same sonographer on two separate occasions) at the beginning and at the end of a survey period. For maximal aortic diameter on the anterior–posterior plane, the absolute intra-observer difference was 2 mm or less in 82%, 3 mm or less in 93%, and 4 mm or less in 97% of cases. The inter-observer differences were generally small and not statistically significant [4]. However, it is not yet clear which method of aortic caliber measurement is the best for the different clinical settings [9].

The final step in the measurement process is to define which value will be selected to quantify the maximum diameter. In most studies, more than one diameter was measured, and then the maximum diameter was chosen; this could be either the highest value obtained, an average of several measures, or the diameter obtained on a pre-defined axis, most often the anteroposterior one [6].

In the review by Beales et al., the intra-observer repeatability for anteroposterior diameter was below the 5 mm level regarded as acceptable by the United Kingdom and North Americans AAA screening programs in six of the nine studies examined. The inter-observer reproducibility was below the 5 mm level for anteroposterior diameter in five of the nine studies. However, the authors did not come to a definitive conclusion regarding the superiority of one method over another for the measurement of AAA diameters [10]. Bredahl et al. presented a validated ECG-gated method for US measurements of AAA, showing reproducibility within 3 mm and recommended measures from leading edge adventitia of AA anterior wall to leading edge adventitia of AA posterior wall be taken during peak systole [11].

Since patients may undergo subsequent explorations with both US and CT, their agreement between measures of diameter should be documented and validated for clinical practice. Sprouse et al. [12] retrospectively studied a cohort of patients with concomitant CT and US measurements available and found significant differences in measurements between the two techniques, which may have different explanations. First, CT measurements, unlike US measurements, most commonly include the full thickness of the AAA wall. Second, the maximal diameter obtained by CT is often defined as the maximal cross-sectional AAA diameter in any directions, while the diameter obtained by US in defined as the largest anteroposterior or transverse diameter. Thus, CT and US do not measure the same diameter. Finally, axial CT sections may represent an oblique cut of an AAA if the aneurysm is angulated, leading to overestimation of its size. As suggested by Lederle et al. [13], US measurements are less affected by tortuosity, because the US probe can be positioned to obtain a true cross-section or orthogonal view of the AAA and, in this situation, yields a more accurate measurement of diameter.

Another important point concerns the diagnostic accuracy of ultrasound when not performed by radiologists. Ultrasonography is increasingly used by clinicians to identify AAA; in ICU and emergency settings, the screening of abdominal aorta from the epigastrium up to the mesogastrium is considered a basic skill in case of unexplained shock, abdominal pain, pulsatile mass palpation, and presence of emboli [14]. In a systematic review and metanalysis, Concannon et al. compared the

accuracy of US performed by non-radiologist for detection of AAA disease with the "gold standard" of aortic imaging (US, CT, RMN, Angiography) by radiologists. They found that US by non-radiologists achieved acceptable sensitivity and specificity for the diagnosis of AAA [15], although there was high variability in US training and level of experience among non-radiologists. This points to the need of defining the basic skills for head-to-toe ultrasonography in the intensive care setting, also for the detection of acute aortic syndromes [14].

12.2.4.4 Limitations

There are limitations to the use of US for the examination of abdominal aorta in certain types of patients. First, a tortuous aorta may be difficult to visualize and track with the US probe, thus yielding inaccurate measurements. Patient's characteristics such as obesity and bowel gas may not allow an adequate window for visualization. Second, aortic branch aneurysms confined to the iliac vessels or renal arteries may not be visualized on US. Third, on sagittal plane, US may underestimate the size of aorta because of the cylinder tangent effect, so the maximum diameter is not captured by the US probe. If the US beam is off center, then the diameter measured will not be the maximal one. Finally, the US is accurate for detecting the size of the aorta, but is not able to detect the presence or absence of rupture.

12.3 Role of US in Acute Aortic Syndromes

In this section, we will discuss the specific role of the ultrasound examination in the recognition of the aortic syndromes most frequently encountered in the ICU and emergency setting.

12.3.1 Abdominal Aortic Aneurysm

The aneurysm of abdominal aorta is a segmental, full-thickness dilatation of the abdominal aorta exceeding the normal vessel diameter by 50%. Usually, the diameter of 3.0 cm is commonly regarded as the threshold for the diagnosis of aneurysm.

Non-modifiable risk factors for abdominal aortic aneurysm include age >65 years, male sex, and a family history of the disorder; smoking is the strongest modifiable risk factor. Aneurysms are usually asymptomatic until they rupture. The best-known predictor of rupture of abdominal aortic aneurysms is its size. Rupture is often lethal with a mortality rate ranging between 85 and 90%. Of those persons who reach the hospital, only 50 to 70% survive [16].

Abdominal aortic aneurysms can be classified according to their relationship to the renal arteries [17]. However, visualization of the renal arteries is not always easy and requires advanced training; the renal arteries are located 1–3 cm distal to the mesenteric artery branch, which can be easily localized on axial plane.

Abdominal color Doppler ultrasonography is the first-line imaging tool for detection and management of AAA, with high diagnostic accuracy. The role of abdominal US in screening and surveillance of abdominal aortic aneurysms is supported by robust scientific literature [5, 17–20]. In a review by Ferket et al., abdominal ultraso-

nography was unanimously advocated as the primary screening modality in elective conditions [21]. US plays an important role also in the decision-making for AAA elective repair [9], but its role in emergency and intensive care setting is still debated.

Patients with AAAs arrive at the emergency department with a myriad of clinical presentations. Symptoms are caused by rupture or rapid expansion of the aneurysm. In the first case, the patient may present with overt hypotension with or without shock, associated with intense abdominal pain radiating to different areas (legs, chest, genitals, flank, or groin). The classic triad of hypotension, back pain, and pulsatile abdominal mass is present only in 50% of cases [22]. However, the patients coming to the emergency department most frequently have a posterior rupture of the aneurysm sac at the level of the retroperitoneum, while anterior ruptures in the intraperitoneal cavity are often fatal. Retroperitoneal rupture may be contained within the retroperitoneal space; the resulting tamponade effect will limit the extent of bleeding and patients may be normotensive [1]. In addition, the aneurysm, especially if large, can compress the surrounding abdominal structures causing nausea, vomiting, hydronephrosis, and urinary retention.

Delay in diagnosis of an AAA can be fatal, whereas early recognition and surgical intervention may prevent morbidity and mortality. Physical examination is notoriously unreliable in detecting AAAs, with 68% sensitivity and 75% specificity [23]. The accuracy of physical examination improves with increasing size of AAA even if making diagnosis of a life-threatening condition in case of smaller abdominal girth is still not satisfactory. In this context, US can play a fundamental role for its high diagnostic accuracy (96.3% sensitivity and 100% specificity) to detect abnormal abdominal aorta dimension, also at the hands of emergency physicians with relatively limited training [24, 25].

In a retrospective study done in Emergency Department, Reed and Cheung found an important, albeit non-significant, trend toward a shorter time to diagnosis (51 min) in patients who underwent Emergency Ultrasound than in those who did not (111 min). However, they did not find an improvement in survival or ICU length of stay [26].

In patients who presented to the emergency department with symptoms characteristic of AAA (abdominal pain, flank pain, back pain, or other characteristic signs and symptoms), US showed 100% sensitivity, 98% specificity, 93% positive predictive value, and 100% negative predictive value [27] and can be used to rule in or rule out the need for an emergent CT and/or vascular surgery consultation. In patients arriving at ED with symptoms typical for an abdominal aortic syndrome, the expected US signs are represented by an enlarged abdominal aorta (diameter greater than 3 cm or increased by more than 50%) or focal dilatation of the aorta.

The entire aorta, from the xiphoid process to the bifurcation of the iliac vessels should be visualized and measured at the maximum diameter. It is critical to explore the entire extent of the aorta down to the bifurcation because 95% of AAAs are infrarenal. In patients with intraperitoneal rupture, fluid will be seen in Morrison's pouch, splenorenal place, or in Douglas space. US is insensitive for retroperitoneal bleeding, so it should not be used to detect the presence of posterior rupture [1]. Occasionally, an intramural thrombus will appear as an echoic pattern within the aorta lumen (◘ Fig. 12.7).

Fig. 12.7 Transverse axial scan of the aorta showing an intramural thrombus as an isoechoic pattern within the lumen of the aorta

12.3.2 Ruptured Abdominal Aortic Aneurysm

Aneurysm size is the best-known predictor for the rupture of abdominal aortic aneurysm. In accordance with Laplace's law, the larger the aneurysm, the higher the rate of expansion. The annual risk of rupture for aneurysms that are less than 5.5 cm in diameter is 1% or lower, whereas the risk increases significantly for aneurysms above this threshold [16]. In a cohort of 2257 patients with a known AAA kept under US surveillance, the risk of rupture was independently and significantly associated with female sex, larger initial aneurysm diameter, lower forced expiratory volume in 1 s by spirometry (FEV_1), current smoking, and higher mean blood pressure [28].

Abdominal ultrasound cannot reliably detect retroperitoneal bleeding and CT represents the gold standard for the diagnosis due to its higher diagnostic accuracy in detecting both an AAA and retroperitoneal hemorrhage. Contrast medium extravasation may eventually confirm the rupture and its location [29]. Although CT is the gold standard for diagnosing ruptured abdominal aortic aneurysm, it is time-consuming and often requires movement of the patient out of the ED.

12.3.2.1 Ultrasonographic Characteristic Patterns of Ruptured Aortic Aneurysm

Some ultrasonographic findings have been described as suggestive for ruptured abdominal aortic aneurysm (Fig. 12.8) [30, 31]:

- AAA deformation (defined as clear irregularity of aneurysm shape)
- Luminal thrombus inhomogeneity (defined as heterogeneous echogenicity of eventual peripheral thrombosis)
- Luminal thrombus interruption (defined as clear focal discontinuity of eventual peripheral thrombosis at the lumen-to-thrombus interface)

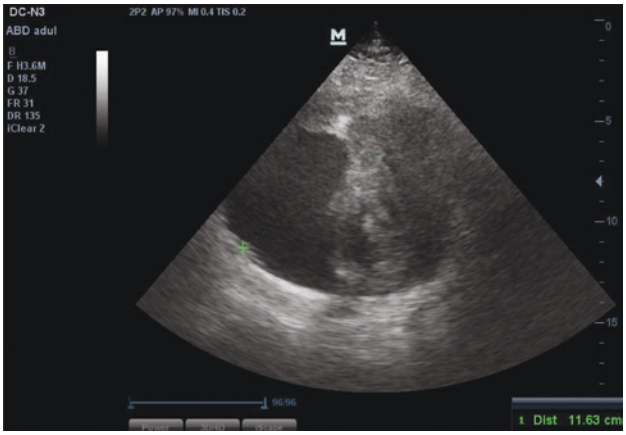

Fig. 12.8 Transverse scan of the abdominal aorta showing some ultrasonographic findings suggestive of ruptured abdominal aortic aneurysm: irregularity of aneurysm shape, heterogeneous echogenicity of the thrombus, luminal thrombus interruption, focal parietal interruption

- Thrombus floating layer (defined as a thrombus layer attached on 1 side and freely floating within the lumen on the other side)
- Focal parietal interruption (defined as clear focal discontinuity of the outer aneurysm wall)
- Para-aortic hypoechoic focus (defined as a small hypoechoic area adjacent to the aneurysm wall and surrounded on the opposite side by echoic, heterogeneous hematoma)
- Retroperitoneal hematoma (defined as fluidlike or mass-like obliteration of retroperitoneal spaces adjacent to the AAA)
- Hemoperitoneum (defined as free fluid filling peritoneal spaces)

12.3.3 Acute Aortic Dissection

Aortic dissection is defined as disruption of the middle layer caused by intramural bleeding; this results in separation of the aortic wall layers and subsequent formation of true and false lumens with or without communication between each other. In most cases, an intimal tear is the initiating condition, resulting in tracking of the blood in a dissection plane within the media [32]. This process is followed either by an aortic rupture in the case of adventitial disruption or by a re-entering into the aortic lumen through a second intimal tear.

Aortic dissection can be classified according to the Stanford classification (Type A or Type B) or the De Backey classification; the former is the most frequently used in clinical practice. In the Stanford classification, type A dissection involves the ascending aorta, regardless of the site of origin, and type B dissection includes all dissections not involving the ascending aorta.

Aortic dissection has an annual prevalence of 0.5–2.95 per 100,000 with very high mortality in the acute stage (48 h mortality reported to be near 50%) [33]. Symptoms and clinical signs may vary according to the classification (Stanford A or B) and extension. Chest pain is the most frequent symptom of acute Aortic Dissection, and abrupt onset of severe chest and/or back pain is the most typical feature. The pain may be sharp, ripping, tearing, knife-like, and typically different from other causes of chest

pain. Stanford type A dissections can present with cardiac tamponade, myocardial infarction, congestive heart failure, or symptoms of cerebral hypoperfusion [33, 34]. Physical examination can provide important clues as to the presence and origin of the aortic dissection, though clinical signs such as absence or asymmetry of the wrists are present in only in 20–30% of patients presenting with acute aortic dissection [35]. The multitude of clinical pictures with which an aortic dissection may occur requires the rapid use of additional instrumental tests to confirm or exclude the diagnosis.

The role of transthoracic echocardiography (TTE) and transesophageal echocardiography (TEE) for the evaluation of thoracic aorta has been extensively studied [35–38]. In the large international registry of aortic dissection (IRAD), the first diagnostic steps were transthoracic echocardiography (TTE) and transesophageal echocardiography (TEE) [34]. Echocardiography, mostly TTE, can be obtained at bedside in the general ward or in any other hospital department (emergency, intensive care unit, operating room); this is particularly advantageous when the patient has unstable hemodynamics, for it does not necessitate patient's transfer. Although considered as a reference technique for the diagnosis of aortic dissection, TEE is a semi-invasive exam which often requires sedation; furthermore, compared to TTE, TEE requires greater knowledge, experience, and a more specific training [38].

TTE permits adequate assessment of several aortic segments, particularly the aortic root and proximal ascending aorta and, in most cases, the aortic arch, proximal descending aorta and abdominal aorta. All scanning planes should be used, including the left and right parasternal long-axis views, the suprasternal (◘ Fig. 12.9), two-chamber, subcostal views and the coronal scans at the patient's left side in the right mid-axillary line around the 10th–11th intercostal space (◘ Fig. 12.10, ◘ Video 12.1) [38, 39]. Classically, TTE has been considered limited in the diagnosis of aortic dissection. The sensitivity for detecting an ascending aortic dissection ranges from 70 to 90%, while it is only 30–50% in descending aortic dissections [39]. However, harmonic imaging and use of contrast enhancement have been recently shown to improve the sensitivity and specificity of TTE in the diagnosis of aortic dissection [40]. CT plus TTE is the best combination for diagnosing Acute Aortic Syndrome (AAS) and

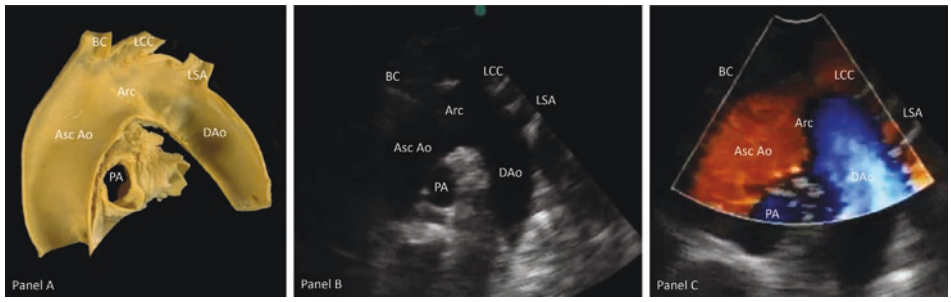

◘ **Fig. 12.9** Suprasternal scan by transthoracic echocardiography showing the proximal ascending aorta, the aortic arch, and the proximal descending aorta. Pulmonary artery (PA); ascending Aorta (Asc Ao); aortic arch (Arch); descending Aorta (DAo), left subclavian artery (LSA), left common carotid artery (LCC); brachiocephalic trunk (BC). Panel **a**: Anatomical dissection; Panel **b**: B-mode ultrasonography; Panel **c**: color Doppler ultrasonography

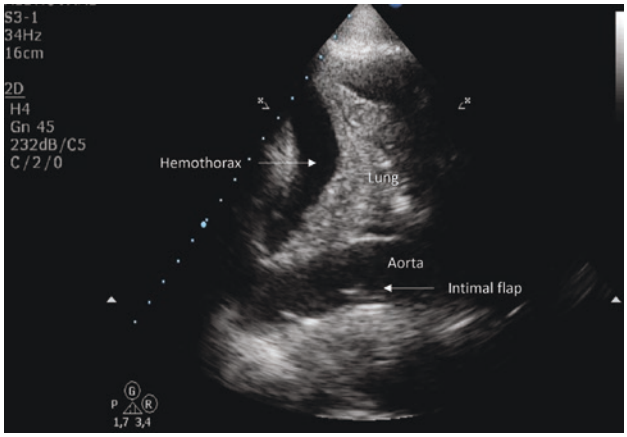

Fig. 12.10 Coronal scan of the thoracic descending aorta at the patient's left side in the right mid-axillary line around the 10th–11th intercostal space showing an aortic dissection depicted by an hyperechoic layer corresponding to the intimal flap within the lumen of the aorta with associated hemothorax

its complications and allows important morphological and dynamic aspects of AAS to be assessed and appropriately managed [41].

The low negative predictive value of TTE does not permit to rule out dissection, and further tests are required if the TTE exam is negative [39]. The value of TTE is limited in patients with abnormal chest wall configuration, narrow intercostal spaces, obesity, pulmonary emphysema, and in patients on mechanical ventilation [39]. In patients with acute chest pain, special attention should be paid during TTE to aortic root dilatation, aortic regurgitation, or pericardial effusion, since these findings should raise the suspicion of acute aortic syndrome. If a dissection cannot be directly visualized, other imaging techniques are mandatory.

The above limitations prevent adequate decision-making, but have been overcome by transesophageal echocardiography [42]. TEE, in addition to TTE, can be used for decision-making in the emergency room or even operating theater in acute aortic dissection with high accuracy. The most important transesophageal views of the ascending aorta, aortic root, and aortic valve are the high transesophageal long axis (at 120°–150°) and short axis (at 30°–60°). A short segment of the distal ascending aorta, just before the innominate artery, cannot be visualized, owing to interposition of the right bronchus and trachea (blind spot). The descending aorta is easily visualized in short-axis (0°) and long-axis (90°) views [39].

The diagnosis of classical aortic dissection is based on the demonstration of the presence of an intimal flap that divides the aorta into two, true and false, lumina. If the false lumen is completely thrombosed, central displacement of the intimal flap, calcification, or separation of intimal layers can be regarded as a definitive sign of aortic dissection. The differentiation between true and false lumen is based on M-mode, two-dimensional, and Doppler US signs. Criteria for identifying the true lumen are the following:

- Size: true lumen < false lumen
- Pulsation: systolic expansion and diastolic collapse (Video 12.2)
- Flow direction: systolic antegrade flow
- Communication flow: from true to false lumen in systole (Video 12.3)

Flow signals within the false lumen represent signs of communication, whereas the absence of flow signals in multiple cross-sections means no communication [41]. A thrombus is diagnosed when a mass separate from the intimal flap and the aortic wall is imaged in the free space of the false, or rarely the true, lumen. Because thrombus formation depends on flow velocity, it may be graded to provide an estimate of the degree of communication [42].

12.3.4 Traumatic Aortic Injury (TAI)

Blunt thoracic aortic injury, a life-threatening concern, may be fatal if not diagnosed and treated expeditiously. Free rupture of thoracic aorta can lead to left hemothorax (Fig. 12.10) and/or pericardial effusion leading to tamponade (Video 12.4), eventually detected and monitored by the extended Focused Assessment with Sonography for Trauma (e-FAST) [43, 44]. However, these findings have a low specificity and might be late signs of the disease process. After the initial stabilization phase and appropriate treatment, the adequacy of splanchnic perfusion and resuscitation targets can be non-invasively monitored at the bedside in the ICU by echo-color Doppler [45–50].

Transesophageal echocardiography is a valid option to diagnose a traumatic aortic rupture in the unstable polytrauma patient that cannot be moved to radiology for CT. Indeed, TEE can detect an intimal flap, aortic valve regurgitation, an intramural hematoma, or signs of a free rupture [51].

Take-Home Messages

- Emergency bedside ultrasound can be used to detect the presence of abdominal aortic aneurysm in symptomatic patients.
- Abdominal US should be recommended as a first-level examination in case of clinical suspicion of an abdominal aortic aneurysm.
- Abdominal ultrasound is burdened by a low diagnostic accuracy in the detection of retroperitoneal bleeding.
- Computer tomography represents the gold standard for the diagnosis of acute aortic syndromes.
- The low negative predictive value of transthoracic echocardiography does not allow to rule-out acute aortic dissection.
- Transesophageal echocardiography can be used for decision-making in the emergency room or in the operating theater in case of suspected acute aortic dissection.

References

1. Barkin AZ, Rosen CL. Ultrasound detection of abdominal aortic aneurysm. Emerg Med Clin North Am. 2004;22:675–82.
2. Watson JDB, Gifford SM, Bandyk DF. Aortic aneurysm screening using duplex ultrasound: choosing wisely who to examine. Semin Vasc Surg. 2020;33:54–9.
3. The U.K. Small Aneurysm Trial: design, methods and progress. The UK Small Aneurysm Trial participants. Eur J Vasc Endovasc Surg. 1995;9:42–48.

4. Singh K, Bønaa KH, Solberg S, Sørlie DG, Bjørk L. Intra- and interobserver variability in ultrasound measurements of abdominal aortic diameter. The Tromsø study. Eur J Vasc Endovasc Surg. 1998;15:497–504.
5. Ashton HA, Buxton MJ, Day NE, Kim LG, Marteau TM, Scott RP, Thompson SG, Walker NM, Multicentre Aneurysm Screening Study Group. The Multicentre Aneurysm Screening Study (MASS) into the effect of abdominal aortic aneurysm screening on mortality in men: a randomised controlled trial. Lancet. 2002;360:1531–9.
6. Long A, Rouet L, Lindholt JS, Allaire E. Measuring the maximum diameter of native abdominal aortic aneurysms: review and critical analysis. Eur J Vasc Endovasc Surg. 2012;43:515–24.
7. Hartshorne TC, McCollum CN, Earnshaw JJ, Morris J, Nasim A. Ultrasound measurement of aortic diameter in a national screening programme. Eur J Vasc Endovasc Surg. 2011;42:195–9.
8. Gürtelschmid M, Björck M, Wanhainen A. Comparison of three ultrasound methods of measuring the diameter of the abdominal aorta. Br J Surg. 2014;101:633–6.
9. Moll FL, Powell JT, Fraedrich G, et al. Management of abdominal aortic aneurysms clinical practice guidelines of the European society for vascular surgery. Eur J Vasc Endovasc Surg. 2011;41(Suppl 1):S1–S58.
10. Beales L, Wolstenhulme S, Evans JA, West R, Scott DJA. Reproducibility of ultrasound measurement of the abdominal aorta. Br J Surg. 2011;98:1517–25.
11. Bredahl K, Eldrup N, Meyer C, Eiberg JE, Sillesen H. Reproducibility of ECG-gated ultrasound diameter assessment of small abdominal aortic aneurysms. Eur J Vasc Endovasc Surg. 2013;45:235–40.
12. Sprouse LR, Meier GH, Lesar CJ, Demasi RJ, Sood J, Parent FN, Marcinzyck MJ, Gayle RG. Comparison of abdominal aortic aneurysm diameter measurements obtained with ultrasound and computed tomography: is there a difference? J Vasc Surg. 2003;38:466–71; discussion 471–472.
13. Lederle FA, Wilson SE, Johnson GR, Reinke DB, Littooy FN, Acher CW, Messina LM, Ballard DJ, Ansel HJ. Variability in measurement of abdominal aortic aneurysms. Abdominal Aortic Aneurysm Detection and Management Veterans Administration Cooperative Study Group. J Vasc Surg. 1995;21:945–52.
14. Robba C, Wong A, Poole D, et al. Basic ultrasound head-to-toe skills for intensivists in the general and neuro intensive care unit population: consensus and expert recommendations of the European Society of Intensive Care Medicine. Intensive Care Med. 2021;47:1347–67.
15. Concannon E, McHugh S, Healy DA, Kavanagh E, Burke P, Clarke Moloney M, Walsh SR. Diagnostic accuracy of non-radiologist performed ultrasound for abdominal aortic aneurysm: systematic review and meta-analysis. Int J Clin Pract. 2014;68:1122–9.
16. Kent KC. Clinical practice. Abdominal aortic aneurysms. N Engl J Med. 2014;371:2101–8.
17. Wanhainen A, Verzini F, Van Herzeele I, et al. Editor's choice—European Society for Vascular Surgery (ESVS) 2019 clinical practice guidelines on the Management of Abdominal Aorto-iliac Artery Aneurysms. Eur J Vasc Endovasc Surg. 2019;57:8–93.
18. Chaikof EL, Dalman RL, Eskandari MK, et al. The Society for Vascular Surgery practice guidelines on the care of patients with an abdominal aortic aneurysm. J Vasc Surg. 2018;67:2–77.e2.
19. Guirguis-Blake JM, Beil TL, Senger CA, Coppola EL. Primary care screening for abdominal aortic aneurysm: updated evidence report and systematic review for the US Preventive Services Task Force. JAMA. 2019;322:2219–38.
20. Sprynger M, Willems M, Van Damme H, Drieghe B, Wautrecht JC, Moonen M. Screening program of abdominal aortic aneurysm. Angiology. 2019;70:407–13.
21. Ferket BS, Grootenboer N, Colkesen EB, Visser JJ, van Sambeek MRHM, Spronk S, Steyerberg EW, Hunink MGM. Systematic review of guidelines on abdominal aortic aneurysm screening. J Vasc Surg. 2012;55:1296–304.
22. Rohrer MJ, Cutler BS, Wheeler HB. Long-term survival and quality of life following ruptured abdominal aortic aneurysm. Arch Surg. 1988;123:1213–7.
23. Fink HA, Lederle FA, Roth CS, Bowles CA, Nelson DB, Haas MA. The accuracy of physical examination to detect abdominal aortic aneurysm. Arch Intern Med. 2000;160:833–6.
24. Kuhn M, Bonnin RL, Davey MJ, Rowland JL, Langlois SL. Emergency department ultrasound scanning for abdominal aortic aneurysm: accessible, accurate, and advantageous. Ann Emerg Med. 2000;36:219–23.

25. Dent B, Kendall RJ, Boyle AA, Atkinson PRT. Emergency ultrasound of the abdominal aorta by UK emergency physicians: a prospective cohort study. Emerg Med J. 2007;24:547–9.
26. Reed MJ, Cheung L-T. Emergency department led emergency ultrasound may improve the time to diagnosis in patients presenting with a ruptured abdominal aortic aneurysm. Eur J Emerg Med. 2014;21:272–5.
27. Tayal VS, Graf CD, Gibbs MA. Prospective study of accuracy and outcome of emergency ultrasound for abdominal aortic aneurysm over two years. Acad Emerg Med. 2003;10:867–71.
28. Brown LC, Powell JT. Risk factors for aneurysm rupture in patients kept under ultrasound surveillance. UK small aneurysm trial participants. Ann Surg. 1999;230:289–96; discussion 296–297.
29. Rakita D, Newatia A, Hines JJ, Siegel DN, Friedman B. Spectrum of CT findings in rupture and impending rupture of abdominal aortic aneurysms. Radiographics. 2007;27:497–507.
30. Catalano O, Siani A. Ruptured abdominal aortic aneurysm: categorization of sonographic findings and report of 3 new signs. J Ultrasound Med. 2005;24:1077–83.
31. Diaz O, Eilbert W. Ruptured abdominal aortic aneurysm identified on point-of-care ultrasound in the emergency department. Int J Emerg Med. 2020;13:25.
32. Erbel R, Aboyans V, Boileau C, et al. 2014 ESC guidelines on the diagnosis and treatment of aortic diseases. Kardiol Pol. 2014;72:1169–252.
33. Alli O, Jacobs L, Amanullah AM. Acute aortic syndromes: pathophysiology and management. Rev Cardiovasc Med. 2008;9:111–24.
34. Hagan PG, Nienaber CA, Isselbacher EM, et al. The International Registry of Acute Aortic Dissection (IRAD): new insights into an old disease. JAMA. 2000;283:897–903.
35. Erbel R, Alfonso F, Boileau C, et al. Diagnosis and management of aortic dissection. Eur Heart J. 2001;22:1642–81.
36. Liu F, Huang L. Usefulness of ultrasound in the management of aortic dissection. Rev Cardiovasc Med. 2018;19:103–9.
37. Shiga T, Wajima Z, Apfel CC, Inoue T, Ohe Y. Diagnostic accuracy of transesophageal echocardiography, helical computed tomography, and magnetic resonance imaging for suspected thoracic aortic dissection: systematic review and meta-analysis. Arch Intern Med. 2006;166:1350–6.
38. Evangelista A, Maldonado G, Gruosso D, Gutiérrez L, Granato C, Villalva N, Galian L, González-Alujas T, Teixido G, Rodríguez-Palomares J. The current role of echocardiography in acute aortic syndrome. Echo Res Pract. 2019;6:R53–63.
39. Evangelista A, Flachskampf FA, Erbel R, et al. Echocardiography in aortic diseases: EAE recommendations for clinical practice. Eur J Echocardiogr. 2010;11:645–58.
40. Evangelista A, Avegliano G, Aguilar R, Cuellar H, Igual A, González-Alujas T, Rodríguez-Palomares J, Mahia P, García-Dorado D. Impact of contrast-enhanced echocardiography on the diagnostic algorithm of acute aortic dissection. Eur Heart J. 2010;31:472–9.
41. Evangelista A, Carro A, Moral S, Teixido-Tura G, Rodríguez-Palomares JF, Cuéllar H, García-Dorado D. Imaging modalities for the early diagnosis of acute aortic syndrome. Nat Rev Cardiol. 2013;10:477–86.
42. Erbel R, Oelert H, Meyer J, Puth M, Mohr-Katoly S, Hausmann D, Daniel W, Maffei S, Caruso A, Covino FE. Effect of medical and surgical therapy on aortic dissection evaluated by transesophageal echocardiography. Implications for prognosis and therapy. The European Cooperative Study Group on Echocardiography. Circulation. 1993;87:1604–15.
43. Pelosi P, Corradi F. Ultrasonography in the intensive care unit: looking at the world through colored glasses. Anesthesiology. 2012;117:696–8.
44. Vezzani A, Manca T, Brusasco C, Santori G, Valentino M, Nicolini F, Molardi A, Gherli T, Corradi F. Diagnostic value of chest ultrasound after cardiac surgery: a comparison with chest X-ray and auscultation. J Cardiothorac Vasc Anesth. 2014;28:1527–32.
45. Corradi F, Brusasco C, Via G, Tavazzi G, Forfori F. Renal Doppler-based assessment of regional organ perfusion in the critically ill patient. Shock. 2021;55:842–3.
46. Corradi F, Via G, Tavazzi G. What's new in ultrasound-based assessment of organ perfusion in the critically ill: expanding the bedside clinical monitoring window for hypoperfusion in shock. Intensive Care Med. 2020;46:775–9.
47. Brusasco C, Tavazzi G, Robba C, Santori G, Vezzani A, Manca T, Corradi F. Splenic Doppler resistive index variation mirrors cardiac responsiveness and systemic hemodynamics upon fluid challenge resuscitation in postoperative mechanically ventilated patients. Biomed Res Int. 2018;2018:1978968.

48. Corradi F, Brusasco C, Vezzani A, Palermo S, Altomonte F, Moscatelli P, Pelosi P. Hemorrhagic shock in polytrauma patients: early detection with renal Doppler resistive index measurements. Radiology. 2011;260:112–8.
49. Corradi F, Brusasco C, Garlaschi A, Santori G, Vezzani A, Moscatelli P, Pelosi P. Splenic Doppler resistive index for early detection of occult hemorrhagic shock after polytrauma in adult patients. Shock. 2012;38:466–73.
50. Corradi F, Brusasco C, Paparo F, et al. Renal Doppler resistive index as a marker of oxygen supply and demand mismatch in postoperative cardiac surgery patients. Biomed Res Int. 2015;2015:763940.
51. Mouawad NJ, Paulisin J, Hofmeister S, Thomas MB. Blunt thoracic aortic injury—concepts and management. J Cardiothorac Surg. 2020;15:62.

Assessment of Kidneys and Urinary Tract

Adrian Wong and Serene SP Ho

Contents

13.1 Introduction – 190

13.2 General Appearance – 191

13.3 Renal Size and Symmetry – 192

13.4 Vascularity – 193

13.5 Common Abnormalities – 194

13.5.1 Hydronephrosis – 194

13.5.2 Cysts/Abscesses – 195

13.6 Transplant Ultrasound – 196

13.7 Conclusion – 196

References – 197

© The Author(s), under exclusive license to Springer Nature Switzerland AG 2023
C. Robba et al. (eds.), *Basic Ultrasound Skills "Head to Toe" for General Intensivists*, Lessons from the ICU,
https://doi.org/10.1007/978-3-031-32462-8_13

Learning Objectives

- Identify the normal ultrasonographic appearance of the kidneys, ureters, and bladder.
- Measure the size of the kidneys, including cortical thickness.
- Measure the size of the bladder.
- Describe the ultrasonographic appearance of chronic kidney disease.
- Identify mild, moderate and severe hydronephrosis.
- Describe the ultrasonographic appearance of renal cysts.
- Recognise the appearance of stones and renal tract obstruction.

13.1 Introduction

There are several imaging options available for assessing the renal tract, each with their strengths and drawbacks; US remains the most widely used imaging modality in the first instance. It is safe, accessible and inexpensive to perform, with a number of practical advantages over plain radiographs, CT and MRI, particularly in the acute setting. Primarily, it is a bedside examination which does not significantly disrupt patient care; the absence of ionising radiation allows repeated examinations to monitor progress if required. Indeed, renal tract US is recommended by several international guidelines in the context of acute- and acute-on-chronic renal injury [1, 2, 3].

The formal renal tract US of a patient in the intensive care unit (ICU), whilst it has its place, can be time-consuming and complex to organise. Intensivists, as well as other non-radiologists, have developed US guidelines and competencies to support their workflow and improve the quality of patient care; focused renal tract US is now within the capabilities of a point-of-care US (POCUS)-trained intensivist. The purpose of a focused US scan is not a general examination of the entire renal tract, but rather to answer specific questions. In AKI, these questions usually include:

- Are the kidneys normal or abnormal; does the patient have one or two kidneys?
- Is there an obstructed system that needs urgent intervention; is there an identifiable level or cause for the obstruction?
- Are there any other obvious abnormalities within the renal tract?

Incidental findings beyond the remit of a POCUS examination must be referred for further investigation.

Whilst renal tract US is often unremarkable in the majority of patients with AKI, early detection of an abnormality can improve clinical outcomes, including mortality. US can rapidly detect renal tract obstruction and suggest a level and/or possible cause of obstruction, for which timely intervention may significantly improve renal function. It can also identify patients with solitary kidneys/single-functioning kidneys/long-standing renal dysfunction, for which intervention may not improve outcome but can guide ongoing management and prognostication. Following renal tract intervention, e.g. nephrostomy/ureteric stents, repeat US imaging can confirm the relief of renal tract obstruction and monitor subsequent changes. Baseline renal measurements can also be documented in those patients presenting with AKI without prior diagnoses.

13.2 General Appearance

The retroperitoneal kidneys are characteristically bean-shaped in appearance; the right kidney lies slightly more inferiorly than the left.

Sonographically, the normal kidney can be divided into the parenchyma and renal sinus. The parenchyma consists of the outer cortex (which has a smooth contour and is slightly hypoechoic as compared to the liver) and the less echogenic medullary pyramids. The hyperechoic renal sinus contains the calyces, renal pelvis, fat and major intrarenal vessels (Fig. 13.1).

The normal renal collecting system is not visible until it is distended. The ureters are visible at the pelvi-ureteric junction (PUJ) and at their insertion into the postero-basal aspect of the bladder as small para-midline protrusions. Bilateral ureteric jets may intermittently cause turbulence within the bladder as part of normal ureteric peristalsis (easily demonstrated on colour Doppler).

The bladder can be inspected in both long- and short-axes. The bladder wall is hyperechoic; delineating this is crucial in differentiating between urine in the bladder and free fluid in the pelvis. Urine volume can be estimated by measuring bladder dimensions, although in the ICU setting, the bladder is usually empty due to the presence of a urinary catheter (Fig. 13.2).

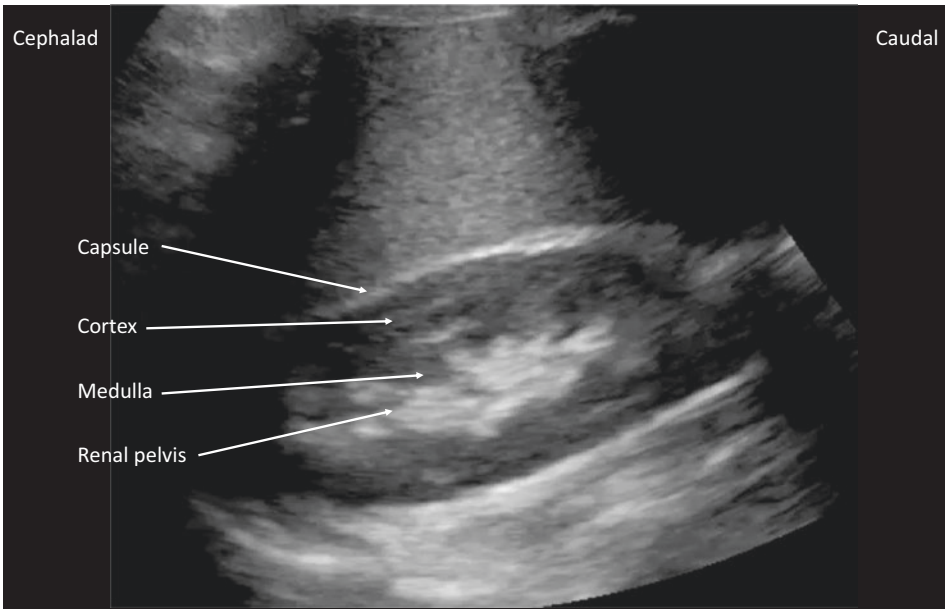

Fig. 13.1 Normal kidney with parts labelled

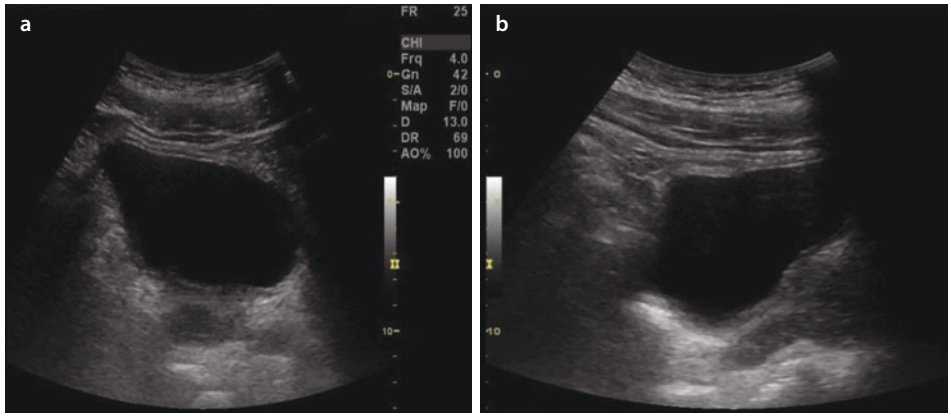

Fig. 13.2 Normal bladder. **a** Short-axis, **b** long-axis

13.3 Renal Size and Symmetry

Normal adult renal craniocaudal length ranges from 10 to 14 cm in males and 9 to 13 cm in females [4], with the left kidney usually 0.5 cm longer than the right [5]. Comparison with the contralateral kidney for symmetry is useful in patients at either end of the height spectrum. The transverse diameter (usually between 5 and 6 cm) is rarely used in the ICU setting.

Reduced renal length US may detect previously undiagnosed CKD. The kidneys in CKD are reduced in length and in cortical thickness (<6 mm) [6]. The cortex is often echogenic, with loss of the smooth renal outline and decreased visibility of the renal pyramids. Cysts may be present. These abnormalities become more pronounced with the increasing severity of CKD.

Increased renal length In the absence of outflow obstruction, the causes of renal enlargement include intrinsic conditions, e.g. ATN, acute interstitial nephritis (drug reactions/autoimmune diseases), renal vein thrombosis and infiltrative conditions, e.g. lymphoma, sarcoidosis and amyloidosis (differentiation usually requires biopsy). Transitional cell carcinoma can occasionally infiltrate while causing a degree of obstruction. In the aforementioned conditions, the kidneys may be enlarged and echogenic, although they often appear normal; in isolation, renal length is only of value where there is a baseline measurement for comparison.

In patients with a single functioning kidney due to unilateral renal agenesis, unilateral renal atrophy or nephrectomy, there is commonly compensatory hypertrophy in the functioning kidney.

Grossly enlarged and abnormal kidneys are seen in autosomal dominant polycystic kidney disease. The autosomal dominant form manifests itself around the age of 30 years and whilst it can occur spontaneously, most cases will have a known family history.

Renal cortical thickness is measured from the base of a medullary pyramid at the level of the mid-kidney to the outer margin of the kidney [7]. Normal cortical thickness is between 7 and 10 mm and slightly increased at the renal poles. Renal cortical

thickness is helpful in distinguishing acute kidney injury from long-standing renal dysfunction, where cortical thinning is expected.

Age-related changes With normal ageing, there is increased sinus fat and a gradual decrease in renal length, cortical thickness and GFR [8, 9]; the normal changes of senescence should not be labelled as CKD. Equally, ageing is associated with a reduced functional reserve and increased susceptibility to renal injury and its sequelae, so perhaps the appearance of the senescent kidney should serve as a reminder that mild insults can have pronounced consequences in the elderly. Other age-related changes include increased number and size of renal cysts and focal scarring.

Perception of renal echogenicity is subject to observer variability and should therefore be assessed through comparison with adjacent organs. The renal cortex of the right kidney should be of equal or decreased echogenicity compared to the liver; that of the left kidney is hypoechoic compared to the spleen [10]. In the absence of hepatic pathology, an echogenic right kidney (in comparison to the liver) may indicate underlying renal abnormality provided the liver is normal, e.g. glomerulonephritis, drug-induced toxicity or chronic kidney disease. Alternatively, this appearance could also represent a relatively normal right kidney in the presence of generalised reduced liver echogenicity, e.g. in acute hepatitis or diffuse malignant hepatic infiltration. Clinical context is important in the interpretation of these findings.

13.4 Vascularity

The renal arterial resistive index (RI) is a sonographic index of intrarenal arteries defined as (peak systolic velocity − end-diastolic velocity)/peak systolic velocity. The RI is considered a reflection of central haemodynamic characteristics (cardiac/aortic) rather than the inherent properties of the kidney [11, 12] (Fig. 13.3).

It is a nonspecific prognostic marker in vascular diseases that affect the kidney. The normal range is 0.50–0.70. High RI values (>0.8) in native kidneys are associated with renal dysfunction and adverse cardiovascular events [13]. High RI values (>0.8) in renal transplant patients are associated with an increased risk of allograft failure and death [14]. While some studies have found little correlation between RIs

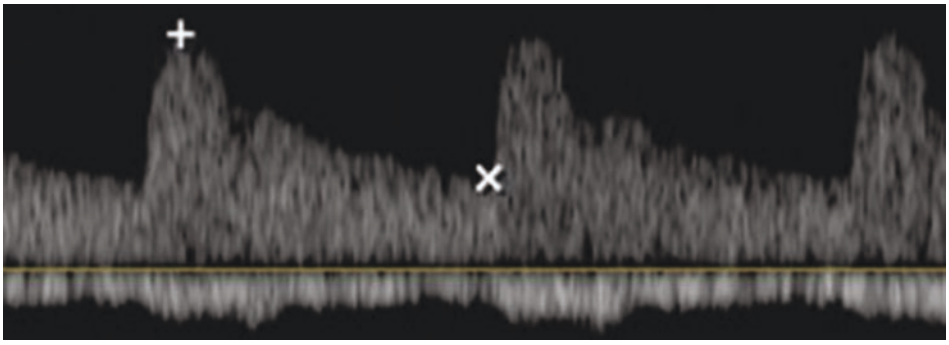

Fig. 13.3 Renal resistive index

and the quantitative extent of renal dysfunction (as measured by serum creatinine) [15], others suggest that RI > 0.70 in patients with CKD was independently associated with deterioration in renal function at 2- and 4-years follow-up [16, 17].

13.5 Common Abnormalities

13.5.1 Hydronephrosis

Hydronephrosis appears as branching connected anechoic areas starting at the renal pelvis and calyces. With increasing severity, there is loss of the normal pelvicalyceal pattern and cortical thinning; the hydronephrotic kidney can appear larger than normal. Grading of hydronephrosis is often subjective.

In obstructive hydronephrosis, the level of obstruction can occur at the PUJ, ureter, bladder or urethra. Obstruction can be intrinsic, e.g. mass/clot/stone/stricture, or external, e.g. compression from retroperitoneal masses or retroperitoneal fibrosis. Hydronephrosis alone with a normal ureter suggests PUJ obstruction. Beyond the PUJ, ureteric width >3 mm is considered abnormal (hydroureter). Ureteric dilation at the vesicoureteric junction (VUJ) suggests a VUJ or bladder cause of obstruction. Depending on the underlying cause, US may be able to identify the aetiology. Renal calculi are visible as hyperechoic lesions, with posterior acoustic shadowing.

The incidence of hydronephrosis is significantly increased in patients with AKI, in the presence of risk factors including renal colic, urosepsis, pelvic tumour or surgery and bladder outlet obstruction. In contrast, hydronephrosis is seen in a minority of patients presenting with AKI without the aforementioned risk factors [18] (Fig. 13.4).

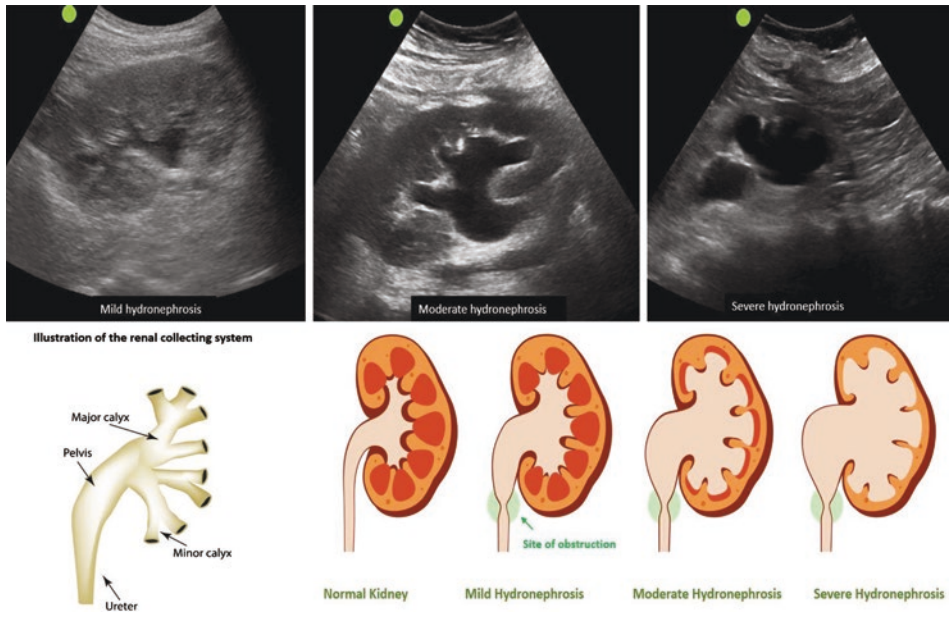

Fig. 13.4 Grading of hydronephrosis

13.5.1.1 Grading of Hydronephrosis

Several grading systems for hydronephrosis exist, with varying degrees of intra- and interobserver reliability [19]. The most common grading system in use (developed by the Society for Fetal Urology (SFU)) is shown below.

- Grade 0
  - No dilatation
- Grade 1 (mild)
  - Dilatation of the renal pelvis only (can also occur in the extrarenal pelvis)
  - No parenchymal atrophy
- Grade 2 (mild)
  - Dilatation of the renal pelvis (mild) and calyces (pelvicalyceal pattern is retained)
  - No parenchymal atrophy
- Grade 3 (moderate)
  - Moderate dilatation of the renal pelvis and all calyces
  - Blunted fornices and flat papillae
  - Mild cortical thinning may be seen
- Grade 4 (severe)
  - Gross dilatation of the renal pelvis and calyces
  - Loss of borders between pelvis and calyces
  - Cortical thinning

13.5.2 Cysts/Abscesses

Distortion of the normal renal architecture can be caused by soft tissue masses or cystic lesions.

Renal cysts are common and usually benign. Simple cysts (round, thin-walled and anechoic) do not require further evaluation. Complex cysts exhibit concerning features such as irregular walls, internal echoes and septations, particularly thicker septations that demonstrate vascularity. Short segments of thin mural calcifications are not of concern, but coarse calcifications should not be dismissed as normal. Complex cysts require further characterization. Any obvious soft-tissue components within a cyst require prompt referral for CT for further assessment.

Renal abscesses can appear as well-defined hypoechoic areas within the renal parenchyma containing internal echoes. These typically do not demonstrate any vascularity on Doppler and have no obvious connection to the collecting system. Perinephric collections may be present in acute pyelonephritis, although they can arise for a variety of other reasons; US-guided aspiration will help differentiate between urine, blood, pus, lymph, transudate or exudate [20] (◘ Fig. 13.5).

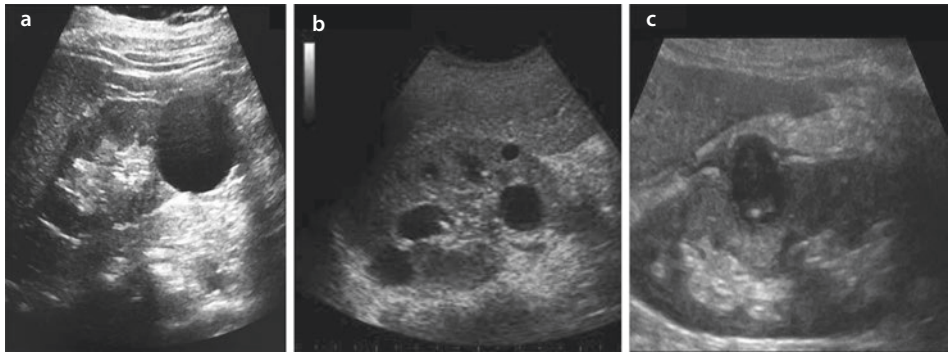

Fig. 13.5 **a** Simple solitary renal cyst. **b** Polycystic kidney disease. **c** Renal abscess

13.6 Transplant Ultrasound

Patients with renal transplants are a special subset warranting a separate mention here. These are patients who have undergone a significant surgical procedure with curative intent and whose renal function relies solely on the transplanted kidney. Renal transplant patients are admitted to ICU post-operatively, where they will undergo a baseline transplant US evaluation by a radiologist within the first 24–48 h in straightforward cases [21]. Those with a more complicated surgical course may already have had US evaluations intra-operatively or much earlier in the postoperative period.

The baseline US is a detailed examination to document renal size, echogenicity, collecting system, presence and size of perinephric collections. Vascular flow is assessed and quantified. This serves as a baseline with which future monitoring scans are compared and also to detect any early complications that require intervention.

In live transplants, the graft is expected to function immediately. Urine production may be delayed/sluggish in cadaveric donor transplants but none should develop sudden anuria—this could indicate vascular issues, e.g. kink/thrombosis, ureteric obstruction and urine leak.

Worrying signs or symptoms in a transplant patient particularly out of hours include anuria, pain/tenderness/swelling and pyrexia, perhaps even before biochemistry becomes deranged.

Conditions relevant to the POCUS practitioner include renal infarction, renal vein thrombosis, urinary obstruction (mild dilatation is acceptable—this results from loss of tonicity following denervation and increased flow through a single functioning kidney) and peri-graft collections, e.g. blood/urine/infective, which can cause compression of transplant.

13.7 Conclusion

US has become the first-choice imaging modality in the assessment of patients with acute or acute-on-chronic kidney injuries. Current guidelines and recommendations for the intensivist practising POCUS tend to be clinically focused, with emphasis on anatomical assessments, e.g. the presence/absence of hydronephrosis.

However, there is an evolving field involving the use of Doppler techniques of various blood vessels including renal vasculature as part of haemodynamic management in ICU. This is a departure from assessing renal perfusion in isolation and represents a move towards the holistic assessment of the critically ill patient using US.

Summary

This chapter describes some of the key points when imaging the kidney in critically ill patients. Whilst focusing on anatomical assessment, it is recognised that the use of Doppler-based techniques is evolving as part of a more holistic approach as part of the haemodynamic assessment.

Take-Home Message

- Ultrasound is the key modality of choice when evaluating patients who present with kidney injury.

Acknowledgements The author would like to thank Dr. Serene Ho for proofreading and language editing.

References

1. Acute kidney injury: prevention, detection and management. 2019. https://www.nice.org.uk/guidance/ng148/chapter/Recommendations.
2. KDIGO. KDIGO Clinical practice guideline for acute kidney injury. Kidney Int. 2012;2(Supp 1).
3. American College of Radiology (ACR) Appropriateness Criteria. http://www.acr.org/Quality-Safety/Appropriateness-Criteria.
4. Knipe A, Hacking C, Hacking C, et al. Kidneys. Radiopedia. 2013; https://doi.org/10.53347/rID-25813.
5. Moell H. Size of normal kidneys. Acta Radiol. 1956;46(5):640–5.
6. Beland M, Walle N, Machan J, et al. Renal cortical thickness measured at ultrasound: is it better than renal length as an indicator of renal function in chronic kidney disease? AJR Am J Roentgenol. 2010;195:W146–9.
7. Moghazi S, Jones E, Schroepple J, et al. Correlation of renal histopathology with sonographic findings. Kidney Int. 2005;67:1515–20.
8. Emamian S, Nielsen J, Pedersen L, et al. Kidney dimensions at sonography: correlation with age, sex and habitus in 665 adult volunteers. AJR Am J Roentgenol. 1993;160:83–6.
9. Wang X, Vrtiska T, Avula R, et al. Age, kidney function and risk factors associate differently with cortical and medullary volumes of the kidney. Kidney Int. 2014;85:677–85.
10. Faubel S, Patel N, Lockhart M, et al. Renal relevant radiology: use of ultrasonography in patients with AKI. Clin J Am Soc Nephrol. 2014;9(2):382–94.
11. Naesens M, Heylen L, Lerut E, et al. Intrarenal resistive index after renal transplantation. NEJM. 2013;369(19):1797–806.
12. O'Neill WC. Renal resistive index: a case of mistaken identity. Hypertension. 2014;64(5):915–7.
13. Pearce J, Craven T, Edwards M, et al. Associations between renal duplex parameters and adverse cardiovascular events in the elderly: a prospective cohort study. Am J Kidney Dis. 2010;55(2):281–90.
14. Radermacher J, Mengel M, Ellis S, et al. The renal arterial resistance index and allograft survival. NEJM. 2003;349(2):115–24.
15. Tublin M, Bude R, Platt J. The resistive index in renal doppler sonography: where do we stand? AJR Am J Roentgenol. 2003;180:885–92.

16. Sugiura T, Wada A. Resistive index predicts renal prognosis in chronic kidney disease. Nephrol Dial Transplant. 2009;24:2780–5.
17. Sugiura T, Wada A. Resistive index predicts renal prognosis in chronic kidney disease: results of a 4-year follow up. Clin Exp Nephrol. 2011;15:114–20.
18. Tummalapalli S, Zech J, Cho H, et al. Risk stratification for hydronephrosis in the evaluation of acute kidney injury: a cross-sectional analysis. BMJ Open. 2021;11(8):e046761.
19. Onen A. Grading of hydronephrosis: an ongoing challenge. Front Pediatr. 2020;8:458. https://doi.org/10.3389/fped.2020.00458.
20. Tsao T, Liang K, Huang H, et al. Sonography of perinephric fluid collections: a pictorial essay. J Clin Ultrasound. 2019;47:150–60.
21. Kolofousi C, Stefanidis K, Cokkinos D, et al. Ultrasonographic features of renal transplants and their complications: an imaging review. ISRN Radiol. 2013;2013:480862. https://doi.org/10.5402/2013/480862.

Assessment of Traumatic Acute Abdomen

Kelvin Wong, Dae Hyeon Kim and Mangala Narasimhan

Contents

14.1 Introduction – 200

14.2 Equipment and Supplies – 200

14.3 Examination Basics/Patient and Probe Orientation – 200

14.4 Limitations – 201

14.5 FAST Exam – 201
14.5.1 Right Flank – 202
14.5.2 Left Flank – 202
14.5.3 Pelvic – 202
14.5.4 Fluid Location – 203
14.5.5 Fluid Characterization – 204
14.5.6 Limitations of FAST – 205

14.6 Pneumoperitoneum – 205

14.7 Vascular Injury – 205
14.7.1 Traumatic Aortic Injury – 205
14.7.2 Vascular Pelvic Trauma – 206

14.8 Abdominal Compartment Syndrome – 207

References – 208

© The Author(s), under exclusive license to Springer Nature Switzerland AG 2023
C. Robba et al. (eds.), *Basic Ultrasound Skills "Head to Toe" for General Intensivists*, Lessons from the ICU,
https://doi.org/10.1007/978-3-031-32462-8_14

Learning Objectives

- Learning which probes to use for an abdominal ultrasound and how to hold the transducer for optimal imaging of the abdomen.
- Know the limitations of abdominal ultrasound and that patient factors, such as obesity, abdominal air, and dressings on the abdomen, can limit visualization in the abdomen.
- Understand the components of the FAST exam and how to perform them.
- Understand the limitations of the FAST exam and how to look for other key pathology.

14.1 Introduction

Abdominal pathology is encountered commonly in the intensive care unit. The presentation, management, or deterioration of a patient often leads one to consider abdominal pathology to be the differential diagnosis. Often, imaging is necessary to hone one's clinical decision-making and management. For the critically ill patient, time and accessibility are of the utmost importance which has resulted in ultrasonography becoming an exceedingly important and commonplace tool for the bedside intensivist. This chapter reviews an important and often overlooked and underutilized component of critical care ultrasonography: the assessment of traumatic acute abdomen.

14.2 Equipment and Supplies

Intensivists will most commonly have access to a phased array transducer probe (1.0–5.0) MHz as well as a linear probe (3.0–12.0 MHz). The low-frequency phased array transducer is versatile in the intensive care unit and is the tool of choice for lung and cardiac ultrasound. Its excellent penetration also makes it suitable for abdominal ultrasonography. An exceptionally well-equipped intensive care unit may also have a curvilinear/convex probe (1.0–5.0 MHz) as well, which provides the same penetration but also provides a larger far-field for better examination. Most Intensive care units (ICUs) will have portable handheld machines or laptop-style machines that sit on carts. All these machines are now capable and have enough Image resolution to evaluate the acute abdomen for common pathologies.

14.3 Examination Basics/Patient and Probe Orientation

Abdominal ultrasound is performed with the patient in a supine or slightly Trendelenburg position. This practice is borne out of the focused assessment with sonography for trauma (FAST) examination protocol which will be discussed in greater detail later. The FAST protocol originated as a rapid bedside noninvasive assessment for abdominal free fluid, the presence of which may be indicative of traumatic injury. Supine patient positioning provides high sensitivity for the detection of free fluid which can be further increased by placing the patient in Trendelenburg.

The ultrasound should be set to the "abdomen" preset with appropriate depth and gain. A low-frequency probe (phased array or curvilinear/convex) is generally held in a longitudinal plane with the indicator of the probe in the cephalad direction. However, as the focus is directed to specific organs and structures, the probe can be adjusted to view each structure on its own transverse and longitudinal axes.

14.4 Limitations

There are inherent limitations of ultrasonography that should be kept in mind. Ultrasound imaging may be suboptimal in certain groups of patients. Morbid obesity, significant body hair, patient agitation, abdominal dressings, large amounts of bowel gas, and subcutaneous emphysema are all factors that would negatively impact an exam. Evaluation of solid organ injuries, bowel perforation, and the retroperitoneal space is also limited with ultrasound. In these circumstances, a different imaging modality may be more appropriate such as CT imaging.

14.5 FAST Exam

It would be difficult to review the ultrasound assessment of the traumatic acute abdomen without first reviewing the FAST exam. The FAST exam was first coined in 1996, originally standing for focused abdominal sonography for trauma. It described a standard set of ultrasound examinations for the evaluation of trauma patients. It was later changed to stand for focused assessment with sonography for trauma in order to broaden its scope. Over time, multiple modifications and iterations have been made in order to expand its utility. The extended FAST exam (EFAST) included sonographic assessment for pneumothorax and more recently, r-EFAST was proposed to also include a focused assessment of the retroperitoneal space [1].

The order of assessment of the standard FAST is:
1. Pericardial
2. Right flank
3. Left flank
4. Pelvic
5. Thoracic (in EFAST)

While FAST has now extended beyond the abdomen, it provides a good framework for understanding how to perform and how to interpret ultrasound of the traumatic acute abdomen. The discussion here will touch upon the abdominal components of FAST (right flank, left flank, pelvic) as pericardial and thoracic ultrasound are discussed in different chapters of this book.

14.5.1 Right Flank

The ultrasound probe should be placed at the right mid-axillary line at the level of the xiphoid process. By convention, the index marker of the probe is in the cephalad direction. The probe should be aimed slightly posteriorly in order to obtain a coronal view of the right hemidiaphragm, liver, right kidney, and hepatorenal recess (Morison's pouch). The probe can be "fanned" anteriorly and posteriorly to locate any potential fluid (Image 14.1).

14.5.2 Left Flank

The imaging technique is similar for the left flank except the probe is placed at the left mid-axillary line at the same level of the xiphoid process. This provides a coronal view of the left hemidiaphragm, spleen, left kidney, and splenorenal recess (Image 14.2).

14.5.3 Pelvic

The probe is placed in the midline superior to the pubic symphysis. A long-axis view is obtained with the probe oriented with the index marker cephalad. A short-axis view is obtained with the probe oriented with the index marker to the patient's right. Depth should be adjusted to look for free fluid deep into the bladder (rectovesical pouch in men and vesicouterine pouch in women) and the uterus (pouch of Douglas) in women. Fluid can also be found lateral to the bladder walls (Image 14.3).

Image 14.1 Hepatorenal recess

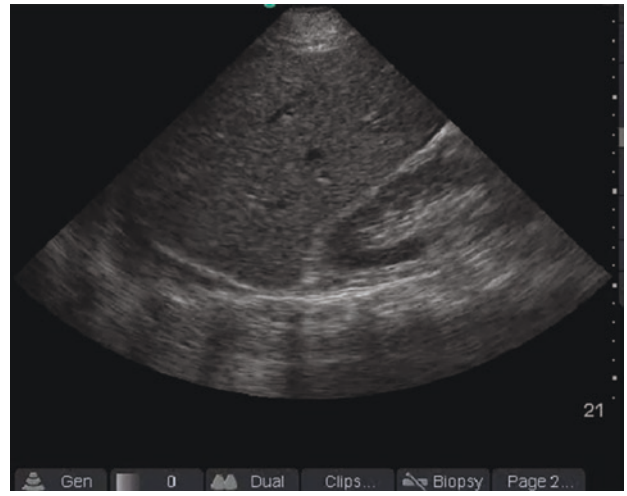

Image 14.2 Splenorenal recess

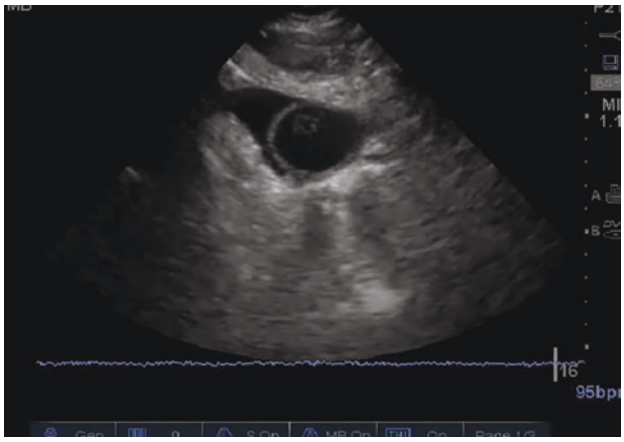

Image 14.3 Bladder

14.5.4 Fluid Location

The primary purpose of the FAST exam is the detection of intraperitoneal or intrathoracic free fluid and pericardial effusion, all of which may be indicative of trauma due to hemorrhage or bowel contents. The overall sensitivity of FAST for detecting free fluid in trauma has been shown to range from 46% to 88%, with specificity ranging from 74% to 100% [2–5]. It has been demonstrated that as little as 100 cc of free fluid can be detectable on FAST [6].

Free fluid accumulates in the most gravity-dependent spaces of the body and this holds true for the abdomen as well. It is important to be cognizant of the fact that the most gravity-dependent spaces will change with patient positioning. In a supine patient, the most dependent area is the pelvic space where the volume threshold for

fluid detection is lowest. However, as the bladder provides the sonographic window for evaluation of the pelvic space, an empty bladder may limit the evaluation of free fluid in this area.

Equally important is an understanding of normal abdominal anatomy and how this affects the flow of free fluid. For instance, the phrenicocolic ligament is a strong peritoneal fold extending from the anatomic splenic flexure of the colon to the diaphragm. This presence of the phrenicocolic ligament prevents the flow of fluid from the upper to lower peritoneum via the left pericolic gutter, ensuring that any flow of fluid between the two areas only occurs via the right side. The converse also holds true.

This is the anatomical basis for the RUQ, more specifically the superior paracolic gutter area around the caudal liver edge, being the next most sensitive area for free fluid detection [7]. If the focus is on the RUQ, the Trendelenburg position has been shown to lower the threshold of detection of free fluid, from approximately 700 to 400 cc [8].

14.5.5 Fluid Characterization

Simple fluid on ultrasound will have a black or anechoic appearance. Simple abdominal fluid on exam is more likely to be due to preexisting nontraumatic etiologies such as liver cirrhosis, heart failure, and end-stage renal disease. The presence of echogenic elements within fluid suggests an exudative process which may be the result of trauma, bleeding, or infection (Image 14.4).

The "plankton sign" refers to the presence of punctiform internal echoes swirling around in anechoic space. The "hematocrit sign" refers to the presence of layering echogenicity that increases with depth. It is important to recognize that ultrasound characterization of blood will change over time. Fresh blood will appear relatively homogenously anechoic with an increasing degree of heterogeneity and echogenicity as clots begin to develop. The presence of septations also suggests an exudative process and in the correct clinical context (peritoneal signs) could be seen in bowel perforation.

Image 14.4 Complex ascites

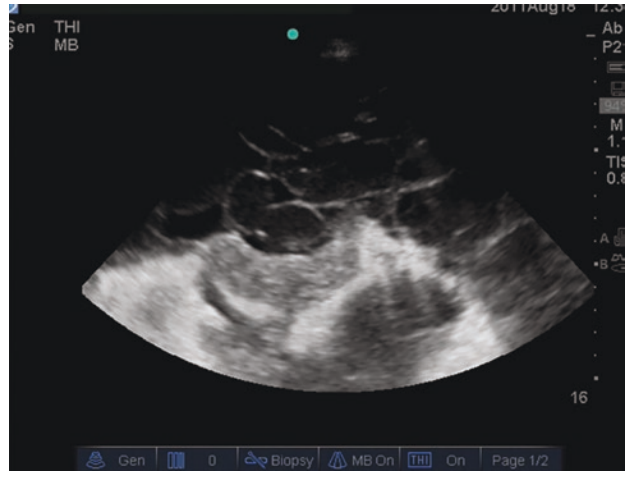

14.5.6 Limitations of FAST

A major limitation of FAST is its variable sensitivity and the possibility of false negatives. As previously mentioned, small amounts of free fluid below the detection threshold (100–200 cc) may be missed. Studies have also shown a false negative rate ranging from 2% to 17%.

It is also important to be cognizant of the fact that free fluid is not the only manifestation of abdominal trauma. In a complete assessment of the traumatic abdomen, an experienced scanner should be able to look for, or recognize incidentally, the following findings.

14.6 Pneumoperitoneum

Pneumoperitoneum may be present in cases of bowel and hollow viscus perforation. While CT imaging is most sensitive for this finding, ultrasound has been demonstrated to be a suitable point-of-care screening tool. Studies have demonstrated a sensitivity of 92%, competitive to those of plain radiography [9–11].

Evaluation for pneumoperitoneum can be performed with the phased array or curvilinear probes. However, a higher frequency linear probe can provide better resolution as the area of interest will be relatively shallow in depth.

On normal abdominal ultrasound imaging, the parietal peritoneum can be visualized as a discrete, thin, smooth, single echogenic line in the deepest layer of the abdominal wall. In the pneumoperitoneum, air accumulates underneath the parietal peritoneum in an antigravity-dependent manner. This results in a more reflective air-soft tissue interface and increased scattering of ultrasound waves, resulting in enhanced echogenicity/thickening of the peritoneal stripe. With the accumulation of large amounts of air, reverberation artifacts may also be visualized. These resemble the well-known "A lines" in lung ultrasonography (◘ Image 14.6).

A common pitfall lies in mistaking intraluminal bowel gas for pneumoperitoneum and vice versa. Identification of movement of air (or its shadowing) with concomitant peristalsis ensures intraluminal bowel gas. The head of the bed can also be raised 10°–20° from the supine position to improve the specificity of any concerning findings. This simple maneuver promotes the movement of any accumulation of air to the anterior prehepatic space between the liver and abdominal wall, where there are generally no confounding bowel loops [12].

14.7 Vascular Injury

14.7.1 Traumatic Aortic Injury

Aortic injury following non-penetrating trauma can be life-threatening with a high mortality rate. The majority of these injuries involve the thoracic aorta with thoracic involvement being about 15 times more common than abdominal [13, 14]. This thoracic predisposition is due in part to the greater effect of shearing forces acting on the

transition zone between the more mobile ascending aorta and relatively fixed descending thoracic aorta. Additionally, the abdominal aorta is better protected by its retroperitoneal position, cushioned by the anterior abdominal wall, visceral organs, vertebrae, and paravertebral musculature.

However, blunt aortic abdominal injury is still an entity experienced scanners should be able to recognize as incidence in fatal blunt trauma has been demonstrated to range from 12% to 15% in autopsy series [13]. Injury is most commonly due to motor vehicle accidents with other etiologies including hard blows to the abdomen, mining accidents, falls from a height, and explosions.

14.7.2 Vascular Pelvic Trauma

Major pelvic vascular injuries to the iliac artery and vein can occur in patients who suffer blunt pelvic trauma and displaced fractures. Systematic reviews have shown mortality related to intrapelvic bleeding to be as high as 25%, with early mortality being predominantly due to the inability to control hemorrhage [13]. While computed tomographic angiography remains the most sensitive initial screening imaging modality for abdominal vascular injury, ultrasonography still can play an important role in patients thought to be too unstable to transport for CT imaging or recognized as an incidental finding at the bedside.

Ultrasound evaluation of the abdominopelvic vessels can be easily incorporated into the abdominal exam if clinically indicated. The study begins at the proximal abdominal aorta with a phased array or curvilinear probe in the midline epigastrium. Image quality can be improved by applying dosed pressure with the probe to compress intra-abdominal air and reduce penetration depth. After the abdominal aorta is identified, the probe is moved distally to the inguinal ligament, following the course of the iliac arteries. The bifurcation point is generally at the point of the umbilicus. The aortoiliac vessels can be examined in both transverse and longitudinal planes with the application of color-flow imaging to add additional information.

Normal arteries appear as echogenic tubular structures with an anechoic lumen. With high-frequency ultrasound, the three layers of the arterial wall are sonographically distinct, appearing as two hyperechoic layers with a hypoechoic layer in between. The abdominal aorta is normally less than 3 cm in diameter, gradually tapering in size until the bifurcation into the iliac arteries.

In arterial dissection, an intimal flap may be visualized as a hyperechoic linear structure in the lumen with undulating motion. Alternatively, there may be a marked widening of an arterial wall. Color Doppler may show flow in one or both lumens. If the flow is detected in both lumens, they may be bidirectional or unidirectional with differing color intensities indicating differing velocities. Thrombus may be seen as well as a heterogeneously echogenic material within the lumen (Image 14.5).

A pseudoaneurysm, essentially a contained vascular rupture, may be seen following trauma as well. It appears as a pulsatile anechoic saccular lesion with variable echogenicity, depending on the presence and age of any potential intraluminal thrombus. Color Doppler is notable for a characteristic “yin and yang” sign which refers to a bidirectional, turbulent, swirling blood-flow pattern within the pseudoaneurysm.

Image 14.5 Aortic dissection with thrombus

Vascular rupture or leak will be evident on ultrasound with findings of free abdominal fluid with progressive echogenicity and heterogeneity as mentioned previously.

14.8 Abdominal Compartment Syndrome

A feared and potentially devastating complication of abdominal trauma is abdominal compartment syndrome (ACS), the presence of intra-abdominal hypertension (IAH) with resultant organ dysfunction. IAH is defined as intra-abdominal pressure (IAP) between 12 and 20 mmHg, whereas ACS refers to intra-abdominal pressure >20 mmHg with associated new organ dysfunction. Etiology/risk factors include trauma with aggressive fluid resuscitation, intraperitoneal hemorrhage, ruptured abdominal aortic aneurysm, pelvic fracture with bleeding, and various nontraumatic conditions such as acute pancreatitis.

In the most recent guidelines for the management of ACS, published by the World Society of the Abdominal Compartment Syndrome (WSACS), abdominal ultrasonography is mentioned only for the evaluation of any potential space-occupying lesions that may be evacuated. However, its potential role in diagnosis and management is larger [15].

While the gold standard method for measuring intra-abdominal pressures as recommended by WSACS is measurement from the urinary bladder, this method has certain drawbacks. It requires regular and repeated instillation of saline into the bladder which presents an elevated infection risk. It may also not be a reliable measure in certain patients such as those with neurogenic bladder or urinary system trauma.

Noninvasive measurements of the renal resistive index (RRI) have been shown to significantly correlate with IAP. A phased array or convex transducer probe can be utilized for pulsed-wave Doppler evaluation of the intrarenal arteries, adjacent to the

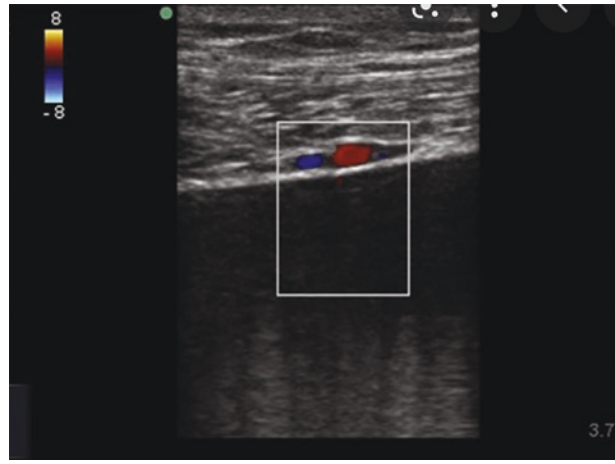

Image 14.6 Doppler-guided paracentesis

medullary pyramids. Measurements of peak systolic and end-diastolic peak velocities are made and an RRI is calculated with the following formula: (peak systolic velocity − end-diastolic velocity)/peak systolic velocity. The normal range of RI is 0.5–0.7 with greater values being correlated to greater IAP. This can be easily incorporated into the abdominal ultrasound examination for screening if there is clinical concern for IAH as well as for interval monitoring to determine clinical progression or response to intervention [16].

Additionally, ultrasonography should be utilized to guide therapeutic and diagnostic paracentesis in a patient with IAH/ACS who has a significant fluid collection. When performing paracentesis, color Doppler ultrasound can be used to identify significant vessels in the path of the needle to avoid a hemoperitoneum post-procedure [16] (Image 14.6).

Take-Home Messages

- Use the correct equipment and technique to perform an abdominal exam.
- A FAST exam is composed of views of the pericardium, the right flank, the left flank, the pelvis, and in the case of the EFAST exam a thoracic view as well.
- Fluid characteristics are important to distinguish between simple and complex fluid.
- A safe site for paracentesis should be identified with ultrasound and the path examined for rogue vessels.

References

1. Vázquez Martínez JL, Quiñones Coneo KL, Villegas TV, Sánchez Porras M, Macarrón CP, Pérez AC, et al. Applicability of a modified EFAST protocol (r-EFAST) to evaluate hemodynamically unstable patients after percutaneous cardiac intervention. Crit Ultrasound J. 2017;9(1):12.
2. Kumar S, Bansal VK, Muduly DK, Sharma P, Misra MC, Chumber S, et al. Accuracy of focused assessment with sonography for trauma (FAST) in blunt trauma abdomen-a prospective study. Indian J Surg. 2015;77(Suppl 2):393–7.

3. Levitov A, Slonim AD, Mayo PH. Critical care ultrasonography. 2nd ed. New York: McGraw-Hill Education Medical; 2014.
4. Lichtenstein D. General ultrasound in the critically ill. Berlin: Springer; 2005. ix, 199 p
5. Lichtenstein DA. Whole-body ultrasound in the ICU. A visual approach to the critically ill. Bull Acad Natl Med. 2007;191(3):495–516; discussion –7.
6. Von Kuenssberg JD, Stiller G, Wagner D. Sensitivity in detecting free intraperitoneal fluid with the pelvic views of the FAST exam. Am J Emerg Med. 2003;21(6):476–8.
7. Lobo V, Hunter-Behrend M, Cullnan E, Higbee R, Phillips C, Williams S, et al. Caudal edge of the liver in the right upper quadrant (RUQ) view is the most sensitive area for free fluid on the FAST exam. West J Emerg Med. 2017;18(2):270–80.
8. Abrams BJ, Sukumvanich P, Seibel R, Moscati R, Jehle D. Ultrasound for the detection of intraperitoneal fluid: the role of Trendelenburg positioning. Am J Emerg Med. 1999;17(2):117–20.
9. Asrani A. Sonographic diagnosis of pneumoperitoneum using the 'enhancement of the peritoneal stripe sign'. A prospective study. Emerg Radiol. 2007;14(1):29–39.
10. Nazerian P, Tozzetti C, Vanni S, Bartolucci M, Gualtieri S, Trausi F, et al. Accuracy of abdominal ultrasound for the diagnosis of pneumoperitoneum in patients with acute abdominal pain: a pilot study. Crit Ultrasound J. 2015;7(1):15.
11. Romero JA, Castaño N. Ultrasonography is superior to plain radiography in the diagnosis of pneumoperitoneum (Br J Surg 2002; 89: 351–4). Br J Surg. 2002;89(9):1194–5; author reply 5.
12. Boniface KS, Calabrese KY. Intensive care ultrasound: IV. Abdominal ultrasound in critical care. Ann Am Thorac Soc. 2013;10(6):713–24.
13. Genovese EA, Fonio P, Floridi C, Macchi M, Maccaferri A, Ianora AA, et al. Abdominal vascular emergencies: US and CT assessment. Crit Ultrasound J. 2013;5(Suppl 1):S10.
14. Naude GP, Back M, Perry MO, Bongard FS. Blunt disruption of the abdominal aorta: report of a case and review of the literature. J Vasc Surg. 1997;25(5):931–5.
15. Kirkpatrick AW, Sugrue M, McKee JL, Pereira BM, Roberts DJ, De Waele JJ, et al. Update from the Abdominal Compartment Society (WSACS) on intra-abdominal hypertension and abdominal compartment syndrome: past, present, and future beyond Banff 2017. Anaesthesiol Intensive Ther. 2017;49(2):83–7.
16. Smereczyński A, Kołaczyk K, Bernatowicz E. Ultrasonography in the diagnosis and monitoring of intra-abdominal hypertension and abdominal compartment syndrome: Ultrasonografia a nadciśnienie wewnątrzbrzuszne i zespół przedziału brzusznego. J Ultrason. 2020;20(82):e201–4.

Ecographic Assessment of Nontraumatic Acute Abdomen

Martina Fregonese, Beatrice Vigna, Edoardo De Robertis and Gianmaria Cammarota

Contents

15.1 Introduction – 212

15.2 Abdominal Ultrasound in Emergency Settings – 213
15.2.1 Pros and Cons – 213
15.2.2 Technical Aspects of the Echographic Evaluation of the Abdomen – 213
15.2.3 Scanning Approach – 214

15.3 Nontraumatic Acute Abdomen: Topographic Assessment – 215
15.3.1 Epigastium (Stomach and Pancreas) – 215
15.3.2 Right Upper Quadrant (Liver, Gallbladder, Right Kidney) – 216
15.3.3 Left Upper Quadrant (Spleen, Subphrenic Space, Right Kidney) – 219
15.3.4 Mesogastrium (Aorta) – 220
15.3.5 Hypogastrium (Bladder, Uterus, Ovaries, Rectovescical/Rectouterine Pouch) – 221
15.3.6 Right to Left Iliac Fossa (Appendix, Large and Small Intestine) – 223

15.4 Etiological Approach to Acute Abdominal Pain (ALFA Or BETA) – 224

References – 226

© The Author(s), under exclusive license to Springer Nature Switzerland AG 2023
C. Robba et al. (eds.), *Basic Ultrasound Skills "Head to Toe" for General Intensivists*, Lessons from the ICU,
https://doi.org/10.1007/978-3-031-32462-8_15

Learning Objectives

- List advantages and limits of echographic abdominal assessment over other imaging methodologies such as computed tomography scan, magnetic resonance imaging, and conventional radiological examination.
- Discuss about technical aspects of an echographic examination of the abdomen and pelvis.
- Outline different systematic approaches investigating acute abdominal pain by ultrasound.
- Describe physiological and pathological findings in the examination of each abdominal echographic window.
- Point out the principal causes of acute nontraumatic abdominal pain through the acronym "ALFA Or BETA."

15.1 Introduction

Acute abdomen is defined as a sudden and severe abdominal pain commonly associated with abdominal tenderness, guarding, and wall rigidity [1]. Gastrointestinal or systemic symptoms such as fever, nausea, vomiting, diarrhea, and hypotension can also be present. The acute abdomen includes a wide range of medical and surgical conditions often requiring urgent surgical therapy [2]. A prompt and accurate diagnosis is therefore imperative although it might pose a challenge for the clinician. Careful acquisition of patient history, clinical examination, and laboratory results are of pivotal importance in guiding the physician toward a possible diagnosis. However, the poor specificity of the associated clinical symptoms and laboratory test findings along with an atypical clinical presentation may further complicate the diagnosis of acute abdomen [3, 4]. For this reason, imaging techniques such as conventional ultrasound (US) and computed tomography (CT) are routinely used to speed up the diagnostic process and subsequent clinical decision-making [5–9]. Among the different methodologies, CT and/or magnetic resonance imaging (MRI) scans are widely considered the gold standard in detecting the causes of acute abdomen due to their high diagnostic accuracy [10, 11]. Nevertheless, both techniques have their drawbacks, including the administration of a radiation to the patient in the case of a CT scan, long image acquisition times and claustrophobia for MRI, and the potential for renal and anaphylactic complications from the use of MRI and CT contrast [12].

The conventional radiography examination has progressively lost its application due to the paucity of information provided, maintaining only a possible role as a first-line examination in the setting of bowel obstruction and perforation [13]. US, on the other hand, is becoming a diffuse tool, mainly for practical first-line assessment in emergency settings [13–18].

15.2 Abdominal Ultrasound in Emergency Settings

15.2.1 Pros and Cons

US offers several interesting advantages compared to CT scan, being a noninvasive and radiation-free examination applicable at bedside. Additionally, high-frequency US shows a spatial resolution even higher than that of a CT scan if a small organ-transducer distance is assured as observed in thin patients using a graded compression [19]. US is also unique in providing a dynamic and real-time examination which becomes very useful when assessing peristalsis, blood flow, the compressibility of tissue, or in case of US-guided puncture of a fluid collection. Another advantage of being a real-time examination is the direct patient-ultrasound assessor interaction that allows the precise correlation between US findings and the area of maximum tenderness or palpable mass.

On the contrary, the impossibility to provide a panoramic view, the inter-operator variability, and the impairment given by the presence of enteral gases and abdominal fat result in a limitation of this methodology in certain clinical situations [20].

Given all its pros and cons, abdominal US still remains a valid first assessment tool, especially in emergency settings or in critically ill patients that cannot undergo CT scans. Probably, the most efficient diagnostic pathway relies on US used as the first imaging tool in a conditioned US-CT strategy where patients with US positive exams for urgent surgical procedures are sent directly to surgery, avoiding CT, while those with inconclusive or negative sonographic results are submitted to CT after clinical stabilization. This strategy has been proven to be as effective as immediate CT for all patients, and, although potentially burdened by more false positive results, it halves the number of CTs needed, saving radiation exposures and costs [21, 22].

15.2.2 Technical Aspects of the Echographic Evaluation of the Abdomen

Humans can generally hear from 20 Hz to 20 kHz. US differs from audible sound only in its higher frequency, hence the name *ultrasound* (i.e., >20 kHz).

Diagnostic sonography generally operates at frequencies ranging from 1 to 20 MHz [23]. Curved (3.5–5.0 MHz) and linear (5.0–12.0 MHz) transducers are most commonly used, with frequencies depending on the application and the patient's stature [13]. Since the thickness of the bowel wall layers usually is less than 1 mm, the frequency of a transducer must be at least 5 MHz for the wall layers to be well discriminated [24]. Most mid-frequency range transducers offer a good compromise between resolution and depth penetration, usually around 8–10 cm. Nevertheless, a low-frequency range transducer might still be needed to reach deeper-lying bowel segments, such as the rectum and in obese patients. Harmonic imaging should be activated when available as this may improve the delineation of bowel wall layers.

Color or power Doppler can both be used to evaluate bowel wall vascularity paying attention to adjust flow parameters to maximize the sensitivity for the detection of vessels with low-velocity flow in the bowel wall. In general, it is recommended to set color persistence at "medium," adopt the lowest wall filter, and assure a combination of the lowest velocity scale with a high color sensitivity to maximize visualization of vessels in the absence of color blooming. The information obtained from color Doppler images is semiquantitative and it is recommended to grade bowel wall vascularization according to the number of vessels detected per square centimeter [22].

Contrast-enhanced ultrasound (CEUS) plays an increasingly interesting role in the assessment of nontraumatic abdominal emergencies [25]. This methodology consists of the injection of stabilized microbubbles with gas content into the bloodstream enhancing the definition of anatomical structures through the visualization of small vessels and microcirculation; as it has a high temporal resolution, the operator can detect the contrast transit in the arterial, portal-venous, and late phase [26]. CEUS is employed in a deep analysis of infarctions, abscesses, and hemorrhages. One of the advantages of this application is that contrast agents usually employed are tolerated and can be injected despite hemodynamic instability, renal failure, and other acute conditions, without any need for fasting or preliminary laboratory testing [27]. On the downside, there are not yet enough studies focused on CEUS, making it rather difficult to strictly categorize the clinical indications for its application in emergency abdominal pain. Thus, the decision to proceed with CEUS is in charge of the expert radiologist who decides to inject the contrast whenever they feel that the microbubbles may help in solving unclear or indeterminate findings at baseline US [22, 28].

15.2.3 Scanning Approach

The most common US technique used to examine patients with acute abdominal pain is the graded-compression procedure [14]. With this technique, interposing fat and bowel can be displaced or flattened by means of gradual compression to show underlying structures reducing the distance from the transducer to the target structure. Furthermore, if the bowel cannot be compressed, the non-compressibility itself is a sign of inflammation [13, 29]. In order to avoid pain, the compression should be applied slowly and gently, similar to the classic palpation of the abdominal wall [19].

Another technique used for a systematic study of the small and large bowel consists in sweeping with the probe up and down the abdomen on parallel overlapping lanes in order to survey the entire gut. This technique is referred to as "mowing the lawn" due to the up-down movement that resembles that of the lawnmower [19, 30, 31].

Data on the methodological approach for an US-focused evaluation of the acute abdomen are scarce. However, here we propose two different methodologies of examination, an anatomical approach and an etiological one, respectively.

15.3 Nontraumatic Acute Abdomen: Topographic Assessment

15.3.1 Epigastium (Stomach and Pancreas)

By positioning a curvilinear probe under the xiphoid process, the operator can visualize the stomach and the different portions of the pancreas (head, body, tail, uncinate process).

Stomach wall thickness and its physiologic five layers structure can be evaluated with US. However, this is certainly not the most accurate technique to assess viscus wall pathology since US does not provide a panoramic view. Thus, wall diseases such as ulcers or perforations are not always easily recognized by an inexperienced operator. In the case of acute abdominal pain, another echographic finding in the study of the epigastric region could be an overdistended stomach, often a sign of gastroparesis or distal bowel obstruction. On this window it is also possible to explore the pancreas and the presence of intraperitoneal free air (IFA) and free fluid, both signs of viscus perforation [32–34]. Echographically, IFA appears as increased echogenicity of a peritoneal stripe, accompanied by posterior artifactual reverberation echoes with characteristic comet-tail appearance. The free air distribution inside the abdominal cavity changes with patient mobilization in opposition to intraluminal bowel gas. In a left decubitus position, free air will collect between the liver and the lateral abdominal wall while, in a supine position, the air reverberations will be stronger in the midline. When suspecting IFA, the use of a linear transducer allows a better spatial resolution and could also help in detecting the so-called gut point which, similarly to the "lung point" in the case of pneumothorax, is defined as the contemporary presence of abdominal wall sliding and abdominal wall palsy in the same echographic window [35]. A sensitivity between 95% and 92% and a specificity varying from 53% to 81.8%, depending on the different studies, have been reported for US detection of perforation, with an overall accuracy of around 88% [36, 37]. US can therefore be considered a valid diagnostic tool to rule out bowel perforation.

Abdominal free fluid can also be visualized in US scanning of the upper peritoneal cavity in cases of peptic or duodenal perforated ulcer [19]. Nevertheless, it is important to note that establishing the cause and location of the perforation is extremely difficult with US and a CT study is always recommended in the suspect of gastroenteric perforation [4].

Because of its size, retroperitoneal location, and echogenicity, the pancreas is one of the most difficult abdominal organs to scan by US; for this reason, adjacent vascular landmarks are mandatory in its localization. In most patients, the body of the pancreas is well detected by an anterior subxiphoid approach across the acoustic window of the left lobe of the liver [16, 38]. The head of the pancreas is located immediately anterior to the inferior vena cava, while the body of the pancreas is located anterior to the splenic vein and the portal splenic confluence. The tail of the pancreas is located in the splenic hilum, immediately anterior to the left kidney and inferior to the splenic vein (◘ Fig. 15.1). Pancreatic echogenicity is variable, depend-

Fig. 15.1 Pancreas. Epigastric window, transverse plane. In this scanning the left lobe of the liver (*L*), the different portions of the pancreas (*head*, *body,* and *tail*), and its vascular anatomical landmarks are visualized: the aorta (*Ao*), the inferior vena cava (*IVC*) and the confluent left renal vein (*LRV*), the splenic vein (*Splenic vein*), the superior mesenteric artery (*SMA*), and the porto-splenic confluence (asterisk)

ing on the amount of fatty replacement which increases with age. The normal pancreas is equal to, or more echogenic than, the normal liver [39]. Abnormally enlarged pancreas (thickness of the head, body, and tail are reported as equal to or greater than 3.0, 2.5, and 2.0 cm, respectively) along with a decreased or heterogeneous pancreatic echogenicity are the sonographic hallmarks of acute pancreatitis. The vast majority of cases of acute pancreatitis are due to gallstones or alcohol abuse; hence it is important to look for gallstones and biliary obstruction in patients admitted with acute pancreatitis [2, 40].

15.3.2 Right Upper Quadrant (Liver, Gallbladder, Right Kidney)

US is a first-line imaging modality for evaluating the gallbladder, the biliary tree, and the liver in an emergency situation [41]. Two windows can be used, the intercostal view and the right subcostal view. Across these acoustic windows, the right hemiliver, the gallbladder, the right kidney, and the hepatorenal recess (Morrison's pouch) are evaluable (Fig. 15.2). The right subcostal view is the window of choice to explore the left hemiliver, the gallblader, the portal veins, and the inferior vena cava (Figs. 15.3 and 15.4).

Pain from gallstones, particularly acute cholecystitis, is by far the most common group of disorders that present with acute right upper quadrant (RUQ) pain. Other differential diagnoses for RUQ pain include hepatitis of all etiologies, liver abscess, and, rarely, a ruptured liver mass, due to hepatocellular adenoma or carcinoma [42].

US has gained an important role in evaluating the gallbladder since it is one of the most sensitive methodologies for detecting gallstones, even in obese patients. US focuses on the cholecystitis assessment which has reported a sensitivity of approximately 81% and a specificity of approximately 83% [43, 44]. Various sonographic findings support the diagnosis of acute cholecystitis including the presence of gall-

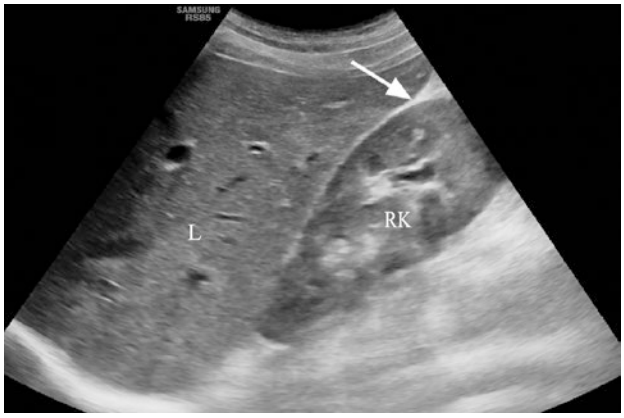

Fig. 15.2 Liver (*L*), right kidney (*RK*), and Morrison's pouch (arrow). Right intercostal window

Fig. 15.3 Portal axis. Right intercostal view. In this scanning the liver (*L*) with the portal vein (*PV*) and the inferior vena cava (*IVC*) can be visualized

Fig. 15.4 Gallbladder partially distended (*GB*). Right intercostal view

stones, increased thickness of gallbladder wall (>3 mm), enlargement (transverse diameter >5 cm), and non-compressibility of the gallbladder, pericholecystic fluid, and a focal tenderness directly over the gallbladder, also known as sonographic Murphy's sign [32]. By themselves, none of these findings is pathognomonic for acute cholecystitis, but their presence in the appropriate clinical setting makes the diagnosis more likely. Between all these findings, pericholecystic fluid usually indicates more advanced cholecystitis and thus the need for more urgent intervention [23, 45].

As concerns the liver, US evaluation should focus on the dimension and homogeneity of liver parenchyma, presence of free fluid, and portal-venous axis evaluation.

Acute hepatitis, both infective and secondary to intoxication, usually results in no characteristic sonographic abnormalities. Hepatomegaly (diameter > 15 cm at the midclavicular line) and gallbladder wall thickening may be present, along with a "starry sky," a so-called aspect of the liver consisting of relative hyperechogenic portal triads in the context of decreased liver echogenicity. Nevertheless, this last sign has shown very poor sensitivity and specificity and has limited clinical importance [46, 47].

Focal hepatic infections, including liver abscesses, can be easily diagnosed by US. Hepatic abscesses typically appear as complex fluid collections with mixed echogenicity, thick-walled cystic lesions, or cysts with fluid-fluid levels. However, it is important to realize that abscesses in the liver may mimic solid hepatic masses, and, therefore, a more in-depth investigation using MRI or CT is often recommended.

Capsular infiltration or spontaneous rupture of a primary or secondary hepatic tumor is a rare cause of acute abdomen in the Western world, but must be kept in mind when considering acute causes of nontraumatic hemoperitoneum.

Acute portal vein thrombosis is also an uncommon condition of acute abdominal pain, but it may be present, apart from cirrhotic patients, also in a wide variety of hypercoagulable states such as sepsis, abdominal infections, infiltrative tumors, and local injury to portal venous axis following surgery or trauma. US can be a valid tool since the overall accuracy of color Doppler in diagnosing portal vein thrombosis is high, with a sensitivity and specificity of approximately 90%. False negatives are very uncommon, and the negative predictive value is close to 98% [48]. On the grayscale US, heterogeneously hypoechoic thrombus within the vein lumen is the main finding of portal vein thrombosis, but this must always be combined with a color Doppler imaging showing the absence of detectable blood flow or the presence of intraluminal filling defects [49].

In the study of the genitourinary system, US allows to detect significant abnormalities that could be associated with acute abdominal pain such as hydronephrosis, renal abscess, and emphysematous pyelonephritis [50]. Hydronephrosis and fluid collections represent the most common findings of complicated renal pathologies and intensive care and emergency clinicians should focus on their detection. The echographic assessment of the parenchyma requires robust expertise and can be tricky for a naive hand.

Renal calculi are not always seen echographically, but generally they present as echogenic foci with sharp distal acoustic shadowing. When they determine a complete obstruction of the ureters, hydronephrosis can be detected as an anechoic space in the shape of the renal calyces and pelvis [32]. Usually, the more distended the renal collecting system is, the more likely it is due to a clinically significant obstruction. Nevertheless, sometimes obstruction can be detected in the presence of mild or no

hydronephrosis. Therefore, in case of a strong clinical suspect of renal obstruction, or whenever the cause of the obstruction is not easily visible by US, the use of CT or MRI is required.

US is insensitive to the parenchymal changes of acute pyelonephritis. Most patients have "normal" scans and abnormalities are identified in only 25% of cases of acute pyelonephritis. Pyelonephritis-associated complications, therefore, should be looked for. These include fluid collections around the kidney due to pericalyceal rupture or abscess, reduced areas of cortical vascularity using power Doppler, and the presence of gas that is highly suggestive of emphysematous pyelitis or pyelonephritis [51].

A renal or adrenal gland mass or complex cyst, often incidentally detected, may also be associated with pain if a complication (necrosis, hemorrhage, or rupture) occurs, but these lesions are usually studied with CT or MRI rather than US [32].

15.3.3 Left Upper Quadrant (Spleen, Subphrenic Space, Right Kidney)

Acute pain in the left upper quadrant is most often caused by splenic infarction or splenic abscess (e.g., secondary to septic emboli in the spleen). Left renal pathologies can also be the cause of acute pain in this area and the examination, as mentioned above, should focus on the identification of renal calculi, hydronephrosis, or fluid collections.

The spleen is generally best visualized through a high posterolateral intercostal approach with the patient laying in the supine position. With this methodology, tilting the probe, the left kidney is also evaluable (◘ Figs. 15.5 and 15.6).

Splenic infarctions are the consequences of an embolic phenomenon or thrombosis of the splenic artery, splenic vein, and its branches. Other etiologies of splenic infarction include marked splenomegaly, with the outgrowth of the splenic blood supply, and pancreatitis [52]. Often, multiple splenic infarctions are visualized. Their overall appearance is that of a wedge-shaped lesion usually located in the peripheral

◘ **Fig. 15.5** Spleen. Left intercostal window, long axis

Fig. 15.6 Left kidney. Left intercostal window, long axis

regions. Complete infarction of the spleen can be more difficult to be detected due to its homogenous pattern at US evaluation. However, as with focal infarctions, in the presence of alterations of splenic echogenic structure, an underlying ischemic injury must be ruled out. A splenic torsion can be suspected as the cause of the infarction when the spleen is hypermobile (wondering spleen) and ectopically located, usually in the lower abdomen [53]. Most splenic abscesses are secondary to hematogenous dissemination of infection and are seen primarily in immunocompromised subjects and in intravenous drug abusers [42]. Splenic abscesses share the sonographic characteristics of the common abscesses elsewhere located in the body, appearing as solid masses or fluid collections [23]. Although a rare event, spontaneous splenic rupture can occur in patients with splenomegaly caused by hematologic malignancy or viral infection (e.g., mononucleosis) resulting in hemoperitoneum and free fluids in the left subphrenic space, usually between the diaphragm and the spleen [2].

15

15.3.4 Mesogastrium (Aorta)

Acute diseases of the aorta, such as dissection and aneurysm rupture, are life-threatening causes of acute abdominal pain that have to be quickly identified and treated. US is commonly performed in the emergency department for a rapid assessment, with a sensitivity of 70–80% and a specificity of 100% for aortic disease; accuracy, however, depends on operator experience and patient characteristics such as body habitus [54].

The aorta is visualized in the mesogastrium, slightly on the left with respect to the midline. An aortic aneurysm is considered in the presence of a focal dilatation of the infrarenal aorta larger than 3 cm; anteroposterior measurements are obtained both from a sagittal and a transverse view (Fig. 15.7).

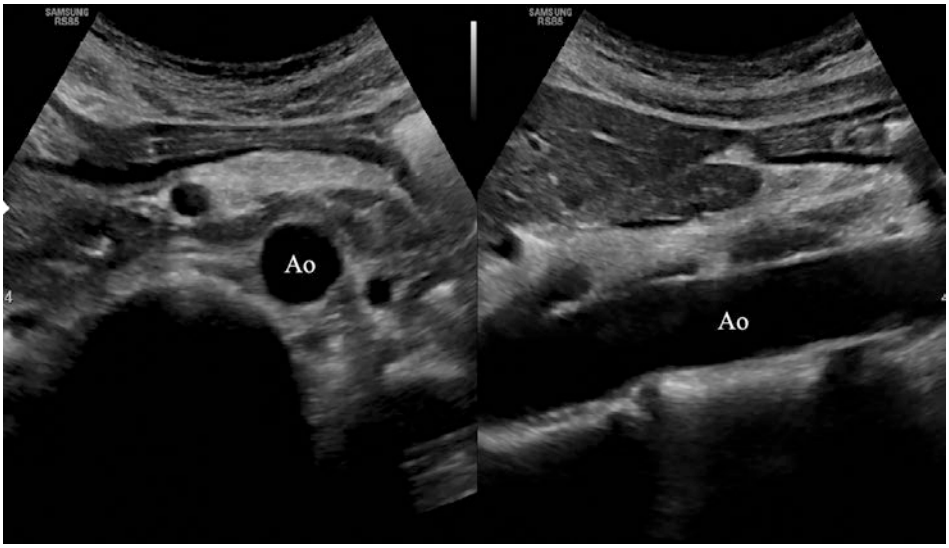

Fig. 15.7 Aorta (*Ao*). On the left: mesogastrium, transverse plane, short axis. On the right: mesogastrium, sagittal plane, long axis

An intramural thrombus is often present, especially in larger aneurysms. Occasionally, the thrombus will contain crescent-shaped areas of reduced echogenicity that should not be confused with dissection, rupture, or impending rupture.

Concerning aortic dissection, using grayscale scanning, the intimal flap can be evaluated by optimizing the sound beam perpendicularly to the flap. Despite blooming artifacts often obscuring the flap, the differential flow may be visualized in the two lumens at the color Doppler examination. The aorta should be scanned along its entire abdominal path from the epigastrium to the iliac bifurcation. If a significant dilation is found in the presence of hemodynamic instability and free intraperitoneal fluid, then the diagnosis of acute aortic aneurysm rupture should be made promptly.

15.3.5 Hypogastrium (Bladder, Uterus, Ovaries, Rectovescical/Rectouterine Pouch)

In the study of the pelvis, the main structures identified (bladder, uterus, annexa) must be visualized both in a transversal and a sagittal plane (Fig. 15.8).

The bladder wall thickening is the most common abnormality seen on pelvic sonography examination; usually, it is considered an upper limit of 3 mm for a well-distended bladder and an upper limit of 5 mm for a poorly distended bladder. In most cases, this thickness increase is caused by a bladder outlet obstruction but other etiologies must be considered such as neurogenic bladder, cystitis, edema from adjacent inflammatory processes, and tumors.

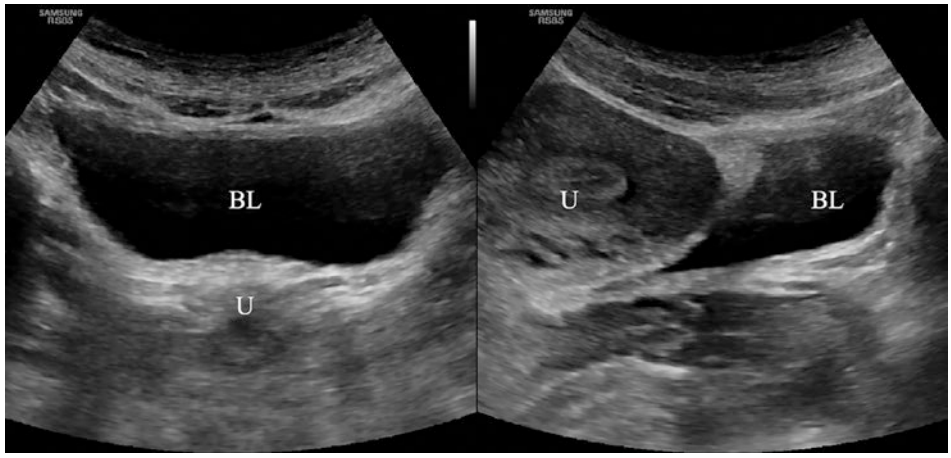

Fig. 15.8 Bladder. On the left: suprapubic window, transverse plane, short axis. On the right: suprapubic window sagittal plane long axis. In both scanning the bladder (*BL*) and the uterus (*U*)

Bladder stones occur usually in the setting of bladder outflow obstruction. They are similar in composition to renal stones and are easily distinguished from other abnormalities by the combination of shadowing and mobility.

In the transabdominal examination of the uterus, a distended urinary bladder aids in the visualization of pelvic structures, displacing gas-filled bowel loops out of the scanned window and enhancing the quality of the examination. It is important to accurately identify the urinary bladder because sometimes a midline cyst, interposed between the uterus and abdominal wall, can be mistaken for the bladder. A distended urinary bladder typically has an elongated or pear-shaped configuration on midline sagittal scans, with a distinct posterior impression from the uterus, whereas a cystic ovarian mass exhibits a more rounded contour [55]. In addition, the identification of the bladder is allowed by its emptying or filling through a urinary catheter.

The ovaries are ovoid or teardrop in shape. They are laterally located with respect to the uterus and anteromedially located to the internal iliac blood vessels. Follicles are depicted as rounded, thin-walled anechoic cystic structures in the ovary, and their identification distinguishes the ovary from adjacent structures such as bowel loops and uterine masses [11]. It is worth pointing out that, at the time of ovulation, the fluid that drains from the dominant follicle can often result in a small amount of free fluid in the pelvis. This must be considered as a physiological finding in fertile women.

During reproductive age, in the presence of acute abdominal pain and hemoperitoneum, ectopic pregnancy should be ruled out. If a gestational sac is found at US examination, the diagnosis of ectopic pregnancy can be rapidly made; otherwise, CT or MRI should be ordered.

Ovarian torsion causes congestion due to impaired venous and lymphatic drainage, resulting in unilateral ovarian enlargement on the side of pain. The injured ovarian is described at US assessment as a heterogeneous structure.

Associated edema, hemorrhage, ischemia, or necrosis may also be present. A more specific but less commonly appreciated sign of ovarian torsion is a direct demonstration of the torsed pedicle appearing as a twisted elongated mass with multiple concentric circular bands adjacent to the ovary, resulting in a target image [23]. The Doppler identification of twisted blood vessels in the pedicle has been termed as the "whirlpool sign" [56, 57]. Nevertheless, the Doppler demonstration of ovarian blood flow does not exclude torsion since both arterial and venous flow has been identified in surgically confirmed torsed ovaries. Also, flow is frequently not identified in the normal ovary [58], making it mandatory to interpret the Doppler findings in conjunction with ovarian size, morphologic appearance, and clinical presentation.

US can also be used in the evaluation of testicular torsion, particularly in identifying the twisted cord and determining the direction of the twist which may support clinicians in the manual detorsion maneuvers. Color Doppler is an effective US application to detect testicular ischemia by comparing the vascularity of the normal and abnormal testes: usually, the torsed testis shows no or markedly reduced blood flow. On the other hand, grayscale scanning may be useful in determining the severity of the ischemic injury in the torsed testis: a hypoechoic or heterogeneous testis is likely to be infarcted and irreversibly injured [59].

15.3.6 Right to Left Iliac Fossa (Appendix, Large and Small Intestine)

The scanning of the lower gastrointestinal tract must include a systematic approach, starting from the right or left iliac fossa. Usually the "mowing the lawn" technique, described in ▶ Sect. 15.2.3, is used. Starting from the right iliac region, the ileocecal valve and the terminal ileum are often found lying over the iliopsoas muscle. This is the best location to start the scan of both the large and small bowel [22]. A graded compression helps in displacing the endoluminal gas to obtain a better visualization of the deepest structures.

Appendicitis is the main cause of acute pain referred to in the right lower abdominal quadrant. Other disorders include Crohn's disease riacutization, right-sided colitis or diverticulitis, and, in women, pelvic inflammatory disease, ovarian cysts, and its complications.

Systematic reviews and meta-analyses have shown that US is highly accurate in detecting acute appendicitis, suggesting US to be a valid first-step tool to assess patients admitted for acute pain in the right iliac fossa [60–63]. US examination can confirm the diagnosis of appendicitis by visualizing the inflamed appendix (successful in 90% of cases) or exclude appendicitis, either by visualization of the normal appendix (successful in 50% of cases) or by demonstrating an alternative condition (possible in 20% of cases) [19]. In any case, it is important to point out that the normal appendix is not easily detected by inexperienced sonographers. Therefore, when US is not diriment in the assessment of the appendix (often the case in obese and pregnant patients), further radiological examinations are required to support the diagnosis.

Sonographically, the typical appearance of an inflamed appendix is that of a concentrically layered, noncompressible cylindric structure laying in a fixed position at the site of maximum tenderness. The average maximum diameter ranges from 7 to 17 mm. When the appendicular inflammation increase, the adjacent fat increase swells becoming more hyperechoic and less compressible. Vascularization of the appendix wall is either markedly increased or absent due to high intraluminal pressure with concomitant ischemic necrosis. However, there is always increased vascularization in the directly surrounding fat tissue. A large quantity of free fluid in the presence of an inflamed appendix is an echographic sign of perforated appendicitis.

Colon diverticular disease is a common pathological condition, primarily diagnosed in the elderly and in the Western patient population. Diverticula involves the sigmoid and the left colon more frequently, but the right colon and the cecum can be implicated as well. In the suspect of diverticulitis, the scanning can start at the point of maximum tenderness or by locating the sigmoid colon, ventrally to the left iliac artery.

Ultrasound images of diverticulitis include thickening of the colon wall >5 mm, a hyperechoic inflammatory surrounding fat, and probe tenderness. Sometimes, in an inflamed diverticulum, intraluminal coproliths can be detected. Abscess and developing phlegmon can also be visible [12].

Other conditions characterized by low quadrant pain are inflammatory diseases of the bowel presenting as a diffuse and concentric thickening of the bowel wall at US examination. Commonly encountered causes include diverticulitis, Crohn's disease, ischemia, infectious colitis, and ulcerative colitis. Although the sonographic findings are typically nonspecific, the combination of US findings with the clinical syndrome is often enough to suggest the diagnosis.

Bowel obstruction and its complications can also be a common cause of abdominal pain. Small bowel obstruction usually is due to adherences, mainly in patients with previous surgery, hernia, obstructing tumor, perforated appendicitis, inflammatory bowel disease, and complicated diverticulitis. Large bowel obstruction is most commonly ascribed to colorectal carcinoma, but diverticulitis and sigmoid or cecal volvulus also are important etiologies [2]. Sonographically, distended, fluid-filled, peristaltic loops are the hallmarks of bowel obstruction and the clues to switch toward CT examination.

15.4 Etiological Approach to Acute Abdominal Pain (ALFA Or BETA)

While assessing a patient with acute abdominal pain, the clinical presentation and the pain localization should guide the clinician in the diagnosis process. Here we present a mnemonic acronym "ALFA Or BETA" to speed up the US assessment in dealing with acute abdominal pain (Table 15.1):

Table 15.1 Acronym "ALFA Or BETA" protocol

Acronym		Corresponding disease
A	Air	– Viscus perforation
L	Lithiasis	– Renal lithiasis – Cholelithiasis – Bladder lithiasis
F	Fluid	– Hemoperitoneum – Ascitis – Viscus perforation
A	Aorta	– Aortic aneurysm rupture – Aortic dissection
Or	Other inflammatory conditions	– Nephritis/pyelonephritis – Inflammatory bowel diseases – Infectious/toxic colitis – Cholecystitis – Hepatitis – Pancreatitis – Cystitis
B	Bowel	– Bowel obstruction
E	Ectopic pregnancy	
T	Torsion/tumor	– Ovarian torsion – Testicular torsion – Abdominal masses
A	Appendix	– Appendicitis

Box

Air: in the presence of important air artifacts, especially if they change location with mobilization of the patient, pneumoperitoneum, as a sign of viscus perforation, must be suspected.

Lithiasis (cholelithiasis, renal, and bladder lithiasis): lithiasis is one of the most common causes of acute abdominal pain and can be often associated with inflammation and distention of the structures proximal to the obstruction.

Fluid: free abdominal fluid should be looked for using the extended FAST examination which may be an option for rapid detection of hemoperitoneum or free fluids also in non-trauma patients [50].

Aorta (aneurism, dissection): in the suspect of an aneurismatic lesion or dissection of the abdominal aorta, POCUS can rapidly detect those patients who need prompt intervention.

Or (Other causes of inflammation: cholecystitis, pancreatitis, enteritis, hepatitis, pyelonephritis): US is a useful tool to identify edema and hypervascularization which are the most common echographic findings in the presence of any inflammatory disease.

Bowel: given its unique dynamic features, US is a valid first-line tool to investigate bowel peristalsis and different kind of obstructive pathologies across small and large intestines.

Ectopic pregnancy: this eventuality must always be suspected in the fertile female presenting with acute abdominal pain.

Torsion (ovaries/testis)/tumor: injured gonads cause acute abdomen usually in the case of acute ischemia due to torsion or in the presence of a complicated cyst. The letter T can also stand for "tumor" which, even if is not an acute pathology, can always evolve in infectious complications or bleeding.

Appendicitis is the most common cause of acute abdomen pain located in the right lower quadrant, and US has proven to be a sensitive and specific first-line technique in experienced hands.

Take-Home Messages

- POCUS is a tool of great impact, especially in time-dependent pathologies and in emergency settings. In case of acute abdominal pain, a systematic echographic evaluation of the abdomen is recommended. When possible, organs and viscera must be scanned both in a sagittal and transverse plane.
- The use of the graded compression technique is recommended in order to get a better image resolution and to localize the point of maximum abdominal tenderness.
- The acronym "ALFA Or BETA" (A, air; L, lithiasis; F, fluid; A, Aorta; Or, other inflammatory diseases; B, bowel; E, ectopic pregnancy; A: appendicitis) can be used to speed up the US assessment of patients admitted with acute abdominal pain.

References

1. Patterson JW, Kashyap S, Dominique E. Acute abdomen. Treasure Island, FL: StatPearls Publishing LLC; 2022.
2. Heiken JP, Katz DS. Emergency radiology of the abdomen and pelvis: imaging of the nontraumatic and traumatic acute abdomen. Dis Abdomen Pelvis. 2014;2014–2017:3–20.
3. Kendall JL, Moreira MM. Evaluation of the adult with abdominal pain in the emergency department. Uptodate.com. 2022. https://www.uptodate.com/contents/evaluation-of-the-adult-with-abdominal-pain-in-the-emergency-department?search=acute-abdomen. Accessed 25 Jun 2022.
4. Gans SL, Pols MA, Stoker J, Boermeester MA. Guideline for the diagnostic pathway in patients with acute abdominal pain. Dig Surg. 2015;32:23–31.
5. Smyth L, Bendinelli C, Lee N, et al. WSES guidelines on blunt and penetrating bowel injury: diagnosis, investigations, and treatment. World J Emerg Surg. 2022;17:13.
6. National Insitute for Health and Care Excellence. Major trauma: assessment and initial management. Natl Clin Guidel Cent; 2016.
7. ACS TQIP. Best practices guidelines in imaging. Am Coll Surg. 2018:56–9.
8. Reimer RP, Heneweer C, Juchems M, Persigehl TT. Imaging in the acute abdomen – Part 1: Case examples of frequent organ-specific causes: liver, gallbladder, pancreas, spleen and vessels. Radiologe. 2021;61:497–510.

9. Reimer RP, Heneweer C, Juchems M, Persigehl TT. Imaging in the acute abdomen—Part 2: Case examples of frequent organ-specific causes: gastrointestinal tract and urogenital system. Radiologe. 2021;61:677–88.
10. De Muzio F, Cutolo C, Granata V, et al. CT study protocol optimization in acute non-traumatic abdominal settings. Eur Rev Med Pharmacol Sci. 2022;26:860–78.
11. Cartwright SL, Knudson MP. Diagnostic imaging of acute abdominal pain in adults. Am Fam Physician. 2015;91:452–9.
12. Gangadhar K, Kielar A, Dighe MK, O'Malley R, Wang C, Gross JA, Itani M, Lalwani N. Multimodality approach for imaging of non-traumatic acute abdominal emergencies. Abdom Radiol. 2016;41:136–48.
13. Stoker J, Van Randen A, Laméris W, Boermeester MA. Imaging patients with acute abdominal pain. Radiology. 2009;253:31–46.
14. Mazzei MA, Guerrini S, Cioffi Squitieri N, Cagini L, Macarini L, Coppolino F, Giganti M, Volterrani L. The role of US examination in the management of acute abdomen. Crit Ultrasound J. 2013;5(Suppl 1):S6.
15. Mosier JM, Stolz U, Milligan R, Roy-Chaudhury A, Lutrick K, Hypes CD, Billheimer D, Cairns CB. Impact of point-of-care ultrasound in the emergency department on care processes and outcomes in critically ill nontraumatic patients. Crit Care Explor. 2019;1:e0019.
16. Mattson B, Dulaimy K. The 4 quadrants: acute pathology in the abdomen and current imaging guidelines. Semin Ultrasound CT MRI. 2017;38:414–23.
17. Whitson MR, Mayo PH. Ultrasonography in the emergency department. Crit Care. 2016;20:227.
18. Berg I, Walpot K, Lamprecht H, Valois M, Lanctôt J-F, Srour N, van den Brand C. A systemic review on the diagnostic accuracy of point-of-care ultrasound in patients with undifferentiated shock in the emergency department. Cureus. 2022;14:e23188.
19. Puylaert J. Ultrasound in acute abdomen. 2007. https://radiologyassistant.nl/abdomen/acute-abdomen/role-of-ultrasound-in-acute-abdomen. Accessed 25 Jun 2022.
20. Van Randen A, Laméris W, Van Es HW, et al. A comparison of the accuracy of ultrasound and computed tomography in common diagnoses causing acute abdominal pain. Eur Radiol. 2011;21:1535–45.
21. de Burlet KJ, Ing AJ, Larsen PD, Dennett ER. Systematic review of diagnostic pathways for patients presenting with acute abdominal pain. Int J Qual Health Care. 2018;30:678–83.
22. Nylund K, Maconi G, Hollerweger A, et al. EFSUMB recommendations and guidelines for gastrointestinal ultrasound - Part 1: Examination techniques and normal findings (long version). Ultraschall Med. 2017;38:e1–e15.
23. Hertzberg BS, Middelton WD. ULTRASOUND: the requisites. 3rd ed. Philadelphia: Elsevier Inc.; 2016.
24. Hefny AF, Corr P, Abu-Zidan FM. The role of ultrasound in the management of intestinal obstruction. J Emerg Trauma Shock. 2012;5:84–6.
25. Wong A, Yusuf GT, Malbrain MLNG. Future developments in the imaging of the gastrointestinal tract: the role of ultrasound. Curr Opin Crit Care. 2021;27:147–56.
26. Trinci M, Ianniello S, Galluzzo M, Giangregorio C, Palliola R, Briganti V, Tursini S, Miele V. A rare case of accessory spleen torsion in a child diagnosed by ultrasound (US) and contrast-enhanced ultrasound (CEUS). J Ultrasound. 2019;22:99–102.
27. Cozzi D, Agostini S, Bertelli E, Galluzzo M, Papa E, Scevola G. Contrast-enhanced ultrasound (CEUS) in non-traumatic abdominal emergencies. Ultrasound Int Open. 2021;7:76–86.
28. Farina R, Catalano O, Stavolo C, Sandomenico F, Petrillo A, Romano L. Emergency radiology. Radiol Med. 2015;120:73–84.
29. Winnenden R, Mergentheim B, Ireland N, Sciences C, Specialties M, Universitario H, Peset D. EFSUMB position paper: recommendations for gastrointestinal ultrasound (GIUS) in acute appendicitis and diverticulitis EFSUMB-Positionspapier: Empfehlungen für den gastrointestinalen Ultraschall (GIUS) bei akuter Appendizitis und Divertikulitis. Utraschall Med. 2019;40:163. https://doi.org/10.1055/a-0824-6952.
30. Atkinson NSS, Bryant RV, Dong Y, et al. How to perform gastrointestinal ultrasound: anatomy and normal findings. World J Gastroenterol. 2017;23:6931–41.
31. Caton R, McCaffrey P, Zahn J, Colla J. Point of care ultrasound (POCUS) for small bowel obstruction in the ED. Emerg Med. 2018;50:1–4.

32. Testa A, Lauritano EC, Giannuzzi R, Pignataro G, Casagranda I, Gentiloni Silveri N. The role of emergency ultrasound in the diagnosis of acute non-traumatic epigastric pain. Intern Emerg Med. 2010;5:401–9.
33. Hefny AF, Abu-Zidan FM. Sonographic diagnosis of intraperitoneal free air. J Emerg Trauma Shock. 2011;4:511–3.
34. Hoffmann B, Nürnberg D, Westergaard MC. Focus on abnormal air: diagnostic ultrasonography for the acute abdomen. Eur J Emerg Med. 2012;19:284–91.
35. Taylor MA, Merritt CH, Riddle PJJ, DeGennaro CJ, Barron KR. Diagnosis at gut point: rapid identification of pneumoperitoneum via point-of-care ultrasound. Ultrasound J. 2020;12:52.
36. Chen S-C, Wang H-P, Chen W-J, Lin F-Y, Hsu C-Y, Chang K-J, Chen W-J. Selective use of ultrasonography for the detection of pneumoperitoneum. Acad Emerg Med. 2002;9:643–5.
37. Nazerian P, Tozzetti C, Vanni S, Bartolucci M, Gualtieri S, Trausi F, Vittorini M, Catini E, Cibinel GA, Grifoni S. Accuracy of abdominal ultrasound for the diagnosis of pneumoperitoneum in patients with acute abdominal pain: a pilot study. Crit Ultrasound J. 2015;7:15.
38. Türkvatan A, Erden A, Türkoğlu MA, Seçil M, Yener Ö. Imaging of acute pancreatitis and its complications. Part 1: Acute pancreatitis. Diagn Interv Imaging. 2015;96:151–60.
39. Pach R, Kulig P, Kołodziejczyk P, Szczepanik A. Ultrasonopraphy in the diagnosis of acute abdominal disorders. Pol Przegl Chir. 2012;84:590–600.
40. Mederos MA, Reber HA, Girgis MD. Acute pancreatitis: a review. JAMA. 2021;325:382–90.
41. Hanbidge AE, Buckler PM, O'Malley ME, Wilson SR. From the RSNA refresher courses: imaging evaluation for acute pain in the right upper quadrant. Radiographics. 2004;24:1117–35.
42. Heiken JP, Katz DS, Menu Y. Emergency radiology of the abdomen and pelvis: imaging of the non-traumatic and traumatic acute abdomen. In: Hodler J, Kubik-Huch RA, von Schulthess GK, editors. Diseases of the abdomen and pelvis 2018–2021: diagnostic imaging. Cham: Springer; 2018. p. 123–43.
43. Kiewiet JJS, Leeuwenburgh MMN, Bipat S, Bossuyt PMM, Stoker J, Boermeester MA. A systematic review and meta-analysis of diagnostic performance of imaging in acute cholecystitis. Radiology. 2012;264:708–20.
44. Gallaher JR, Charles A. Acute cholecystitis: a review. JAMA. 2022;327:965–75.
45. Gupta P, Marodia Y, Bansal A, Kalra N, Kumar MP, Sharma V, Dutta U, Sandhu MS. Imaging-based algorithmic approach to gallbladder wall thickening. World J Gastroenterol. 2020;26:6163–81.
46. Needleman L, Kurtz AB, Rifkin MD, Cooper HS, Pasto ME, Goldberg BB. Sonography of diffuse benign liver disease: accuracy of pattern recognition and grading. AJR Am J Roentgenol. 1986;146:1011–5.
47. Tchelepi H, Ralls PW, Radin R, Grant E. Sonography of diffuse liver disease. J Ultrasound Med. 2002;21:1023–32.
48. Riva N, Ageno W. Clinical manifestations and imaging tools in the diagnosis of splanchnic and cerebral vein thromboses. Thromb Res. 2018;163:252–9.
49. Karaosmanoglu AD, Uysal A, Akata D, Ozmen MN, Karcaaltincaba M. Role of imaging in visceral vascular emergencies. Insights Imaging. 2020;11:112. https://doi.org/10.1186/s13244-020-00913-3.
50. Kameda T. Overview of point-of-care abdominal ultrasound in emergency and critical care. J Intensive Care. 2016;4:1–9.
51. Gaillard F, Bell D. Acute pyelonephritis. 2022. Radiopedia.org.
52. Chapman J, Helm TA, Kahwaji CI. Splenic infarcts. Treasure Island, FL: StatPearls; 2022.
53. Bough GM, Gargan KE, Cleeve SJ, Farrell S. Diagnosis, management and outcome of splenic torsion; a systematic review of published studies. Surgeon. 2021;20:e296. https://doi.org/10.1016/j.surge.2021.08.006.
54. Patel TV, Canario DAH, Isaacson AJ, Mauro DM. Vascular etiologies of the acute abdomen. Semin Roentgenol. 2020;55:417–26.
55. Zucchini S, Marra E. Diagnosis of emergencies/urgencies in gynecology and during the first trimester of pregnancy. J Ultrasound. 2014;17:41–6.
56. Vijayaraghavan SB. Sonographic whirlpool sign in ovarian torsion. J Ultrasound Med. 2004;23:1641–3.
57. Lee EJ, Kwon HC, Joo HJ, Suh JH, Fleischer AC. Diagnosis of ovarian torsion with color Doppler sonography: depiction of twisted vascular pedicle. J Ultrasound Med. 1998;17:83–9.

58. Yang H, Wang R, Zhao L, Ye J, Li N, Kong L. Diagnosis and analysis of transabdominal and intracavitary ultrasound in gynecological acute abdomen. Comput Math Methods Med. 2021;2021:9508838.
59. Al Ali M, Jabbour S, Alrajaby S. ACUTE ABDOMEN systemic sonographic approach to acute abdomen in emergency department: a case series. Ultrasound J. 2019;11:4–9.
60. Fu J, Zhou X, Chen L, Lu S. Abdominal ultrasound and its diagnostic accuracy in diagnosing acute appendicitis: a meta-analysis. Front Surg. 2021;8:707160.
61. Terasawa T, Blackmore CC, Bent S, Kohlwes RJ. Systematic review: computed tomography and ultrasonography to detect acute appendicitis in adults and adolescents. Ann Intern Med. 2004;141:537–46.
62. Téoule P, de Laffolie J, Rolle U, Reissfelder C. Acute appendicitis in childhood and adulthood. Dtsch Arztebl Int. 2020;117:764–74.
63. Benabbas R, Hanna M, Shah J, Sinert R. Diagnostic accuracy of history, physical examination, laboratory tests, and point-of-care ultrasound for pediatric acute appendicitis in the emergency department: a systematic review and meta-analysis. Acad Emerg Med. 2017;24:523–51.

Vessels

Contents

Chapter 16 **Ultrasound-Guided Cannulation – 000**
Michel Slama, Yoann Zerbib, Clément Brault, and Julien Maizel

Chapter 17 **Deep Venous Thrombosis – 000**
Massimo Lamperti, Boris Tufegdzic, and Amit Jain

Ultrasound-Guided Cannulation

Michel Slama, Yoann Zerbib, Clément Brault, and Julien Maizel

Contents

16.1 Introduction – 234

16.2 Central Veins – 234
16.2.1 The Internal Jugular Vein – 234
16.2.2 The Subclavian Vein – 239
16.2.3 The Femoral Vein – 240
16.2.4 Peripheral Veins – 241

16.3 Arteries – 241
16.3.1 The Radial Artery – 241
16.3.2 The Femoral Artery – 242

16.4 Peripherally Inserted Central Catheters (PICCs) – 242

16.5 Catheter Infections and Ultrasound Guidance – 243

16.6 Training – 243

16.7 Nurses – 243

16.8 Conclusion – 244

References – 245

© The Author(s), under exclusive license to Springer Nature Switzerland AG 2023
C. Robba et al. (eds.), *Basic Ultrasound Skills "Head to Toe" for General Intensivists*, Lessons from the ICU,
https://doi.org/10.1007/978-3-031-32462-8_16

Learning Objectives

After reading this chapter, the reader should:

- Know that ultrasound-guided cannulation of both veins and arteries is possible.
- Be familiar with the technique for the ultrasound-guided cannulation of veins and arteries in adult and pediatric patients.
- Be aware of the levels of evidence and the various approaches, complications, and tricks concerning ultrasound-guided cannulation.

16.1 Introduction

The insertion of arterial and venous catheters is a routine practice in many fields of medicine. Ultrasound-guided catheterization techniques have become the gold standard and are now recommended by almost all medical societies and associations worldwide. In this chapter, we review the various vessel types and catheterization sites and then detail the levels of evidence for the use of this technique at the bedside.

16.2 Central Veins

Central venous catheter (CVC) insertion is a routine procedure in intensive care units (ICUs) and anesthesiology departments, and CVCs are very useful for infusing drugs and measuring central venous pressure. Approximately six million central venous catheterizations are performed each year in Europe and the USA [1–4]. The first prospective studies of ultrasound-guided catheterization were performed in cardiology departments and ICUs and concerned the internal jugular vein (IJV) [5, 6]. Subsequently, a large number of research articles, meta-analyses, reviews, consensus statements, and guidelines have focused on the value of ultrasound-guided CVC insertion.

16.2.1 The Internal Jugular Vein

16.2.1.1 Techniques (Figs. 16.1, 16.2, 16.3, and 16.4)

Customarily, jugular vein puncture was performed using a landmark technique. The insertion was orientated with regard to (1) the known basic anatomy of the neck and (2) palpation of the carotid artery. Although posterior or anterior approaches were possible, an anatomical evaluation concluded that the posterior approach was better than the anterior approach [7]. In one prospective clinical study, the posterior approach was associated with a higher proportion of successful catheterizations and a lower incidence of pneumothorax [8] and thus confirmed the results of an older prospective study [9]. The position of the head during IJV puncture also appears to be important. In a prospective study comparing head rotation to the side and a neutral position, the latter was associated with higher failure and complication rates [10]. However, another study concluded that 45° head rotation and a neutral position gave similar insertion times, success rates, and complication rates [11]. Ultrasound was used to analyze the effect of head rotation on the IJV's position; the vein was found

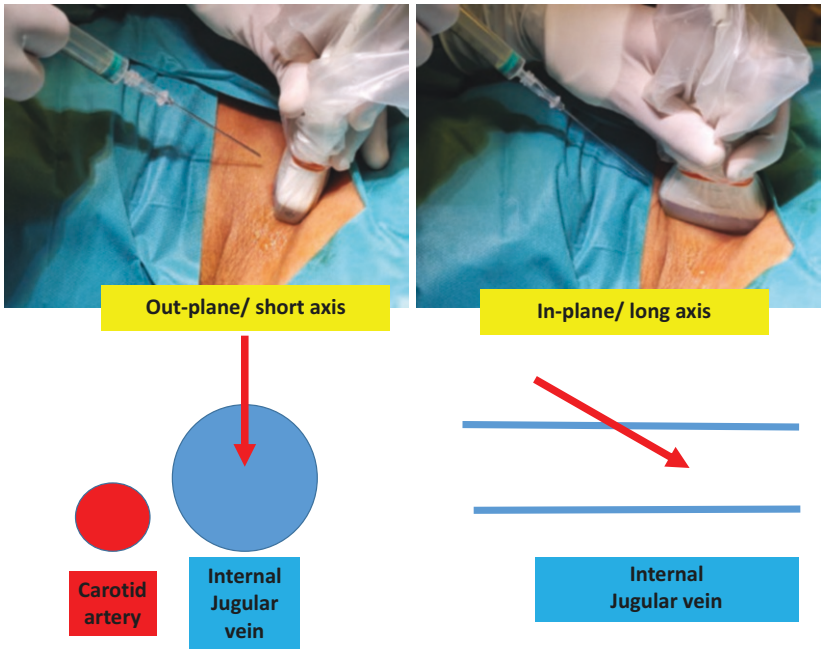

Fig. 16.1 Out-of-plane and in-plane views for ultrasound-guided cannulation techniques

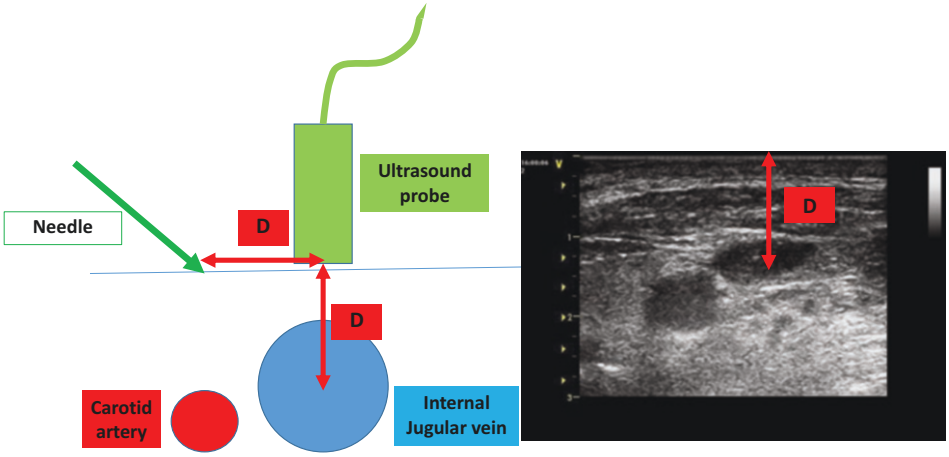

Fig. 16.2 The distance between the skin puncture point and the center of the probe should be equal to the distance between the center of the probe and the middle of the vessel's lumen

more frequently in the anterolateral segment than in the anterior segment, and the position changed with head rotation [12]. Given the effect of head rotation and the fact that the IJV's position is not predictable, it is best to check the IJV's position and the best head position prior to catheterization; this should increase the success rate and avoid complications like carotid artery puncture and pneumothorax. The results of our prospective study showed that the vein was small (lumen <5 mm) or thrombosed in 13% of left IJVs and 22% of right IJVs [13]. It is therefore very important to

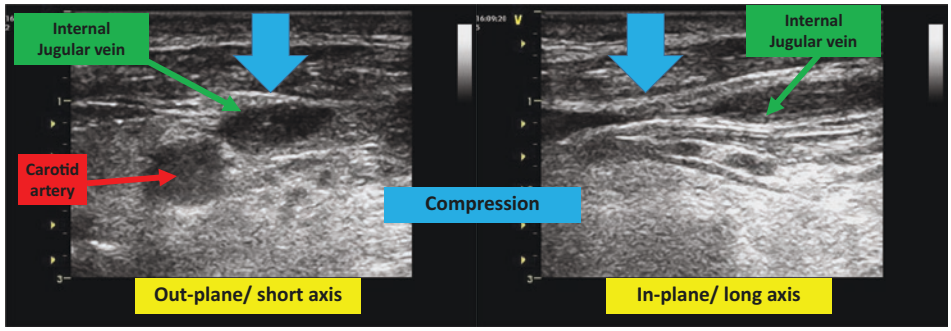

Fig. 16.3 Compression of the vein before cannulation (to check for the absence of thrombosis) is mandatory

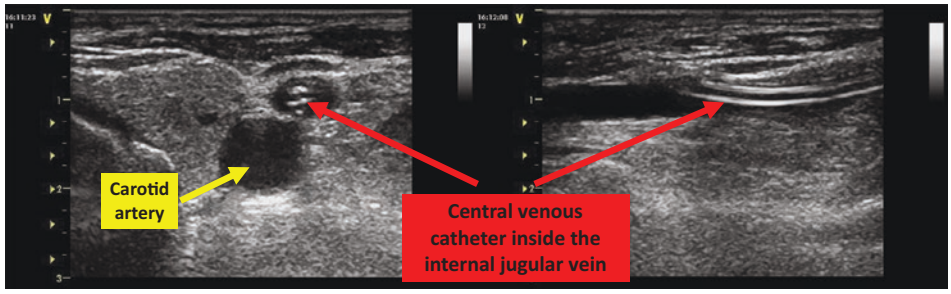

Fig. 16.4 The catheter's position can be checked with ultrasound. Left: the short-axis view; right: the long-axis view

evaluate the IJV before starting the catheterization procedure. For a very small IJV or a large change in lumen diameter during the respiratory cycle, a Trendelenburg position of 5° was found to increase the vein's diameter and thus facilitate puncture [13, 14]. Going above 5° did not result in a further increase in size [14]. The right IJV should be preferred for catheter insertion because it is larger than the left and give direct, straight access to the superior vena cava [13, 15].

The technical aspects can be summarized as follows. The operator wears a gown, cap, mask, and sterile gloves. He/she uses ultrasound to check the best jugular vein and the best head position and positions the patient in the reverse Trendelenburg position, if necessary. The skin is cleaned before sterile drapes are applied. A 1% lidocaine solution is then injected. The ultrasound device is covered with a sterile drape, and a two-dimensional image is displayed. This enables the carotid artery and IJV to be identified with regard to their relative positions, compressibility (for the vein), expansion during inspiration (for the vein), and visible pulsation (for the artery). The skin is swabbed with sterile saline solution, the transducer is positioned under sterile conditions over the thyroid cartilage, and the IJV is identified. A 19-gauge, 10 cm needle connected to a 10 mL syringe is advanced through the skin. The placement and direction of the cannulating needle are determined from the ultrasound image. The needle's progression is monitored in real time, with the image

showing the compression of the surrounding structures until blood (in black) is aspirated into the syringe. Piton et al. suggested using the geometry of a schematic isosceles triangle to determine the IJV's puncture point when using an ultrasound-guided technique [16]. With the probe held perpendicular to the skin and a needle held at 45° relative to the skin, the distance between the needle's skin entry point and the probe should be the same as the distance between the skin surface and the center of the vessel's lumen. A high-frequency (vascular) probe is usually used for this procedure, although probes with a lower frequency can also be used (albeit with a loss of imaging quality).

16.2.1.2 Level of Evidence

Many studies and meta-analyses have demonstrated that ultrasound-guided techniques are better than the landmark method when cannulating the IJV [17]. A Cochrane Collaboration analysis showed that ultrasound-guided techniques are associated with a lower incidence of all-cause complications (risk ratio (RR) 0.29), arterial puncture (RR: 0.34), and complications other than arterial puncture (thrombosis, embolism, hemothorax, pneumothorax, subcutaneous emphysema, and nerve injury; RR: 0.34), a lower time to successful cannulation, a lower number of attempts until success, and a higher overall success rate (RR: 1.12) and first-attempt success rate (RR: 1.57). The results of this Cochrane Collaboration analysis and other studies constitute evidence in favor of the use of ultrasound-guided IJV catheterization. All the national and international guidelines and expert consensus statements in this field have confirmed the high level of evidence for ultrasound-guided techniques [18–25].

The long (in-plane) axis, the short (out-of-plane) axis, and the oblique axis (◘ Figs. 16.1, 16.2, 16.3, and 16.4)

Short, long, and oblique views have been used for the ultrasound-guided catheterization of the IJV [26–32]. The short axis (also referred to as the out-of-plane axis) is the view that has been most frequently used in published studies. It is clearly safe and associated with a high success rate and a very low complication rate. However, the view has some disadvantages because it prevents the operator from monitoring the needle's trajectory in one plane. In contrast, the operator can simultaneously visualize the IJV and the carotid artery and will therefore know when the needle is located above the artery. This view tends to be used for posterior approaches to the IJV, which are frequent in hypovolemic patients when the vein collapses during the procedure; the incidence of hematoma was no greater for posterior puncture with an out-of-plane view than with other views [26]. The long-axis view (also known as the in-plane view) enables the operator to track the needle's trajectory and, in principle, helps to avoid posterior wall perforation. The in-plane view's main disadvantage is its inability to visualize the IJV, the needle, and the carotid artery on the same screen. The oblique view might combine the advantages of the in-plane and out-of-plane views. However, a meta-analysis has shown that none of the scanning axes has unique, outstanding features that make it suitable for IJV catheterization; hence, the scanning axis should be selected as a function of various factors, such as ease of application, the patient's characteristics, and the clinician's level of expertise.

16.2.1.3 Dynamic vs. Static Puncture

Few studies have compared quick-look (static) ultrasound with landmark-based techniques and dynamic ultrasound-guided techniques [33]. Quick-look ultrasound enables the operator to check the position of the IJV, mark the skin puncture point, and thus facilitate cannulation; it was found to be similar to the landmark method in terms of the success and complication rate and so should be avoided [33]. However, as mentioned above, quick-look ultrasound can be used to evaluate the position and size of the IJV and check for the absence of thrombosis before starting the cannulation procedure.

16.2.1.4 Pediatric Patients

Fewer data are available for pediatric patients. Ultrasound guidance appears to be associated with a lower number of attempts for success and a lower complication rate, as confirmed by a recent meta-analysis [34].

16.2.1.5 Experienced vs. Inexperienced Operators

Ultrasound-guided IJV cannulation was associated with higher success rates and lower complication rates with both experienced and inexperienced operators—prompting a recommendation for the systematic use of this technique [5, 33].

16.2.1.6 Misplacement and Complications (◘ Fig. 16.4)

In Chui et al.'s retrospective study of 6875 patients with ultrasound-guided CVC insertion, the overall incidences of pneumothorax and catheter misplacement were 0.33% (95% confidence interval (CI): 0.22–0.5; n = 23 patients) and 1.91% (95% CI, 1.61–2.26; n = 131 patients), respectively [35]. The catheterization site was the prime determinant of pneumothorax and catheter misplacement, and the risk of catheter misplacement was higher for the right IJV. Smit et al.'s meta-analysis [36] included 25 studies with a total of 2548 patients and 2602 CVC placements; the pooled specificity for either misplacement or pneumothorax was 98.9% (95% confidence interval (CI): 97.8–99.5%), and the sensitivity was 68.2% (95% CI: 54.4–79.4%). An ultrasound examination was feasible in 96.8% of cases. The prevalence of CVC misplacement and pneumothorax were 6.8% and 1.1%, respectively. Smit et al.'s meta-analysis considered various methods for the diagnosis of misplacement. After the injection of 10 mL of saline into the CVC's distal port, a rapid atrial swirl sign (RASS, i.e., the appearance of turbulence in the right atrium via superior vena cava less than 2 s after injection) is a very accurate indicator of correct CVC positioning [37, 38].

Regarding pneumothorax, ultrasound is a better diagnostic technique than a chest X-ray with the absence of the sliding lung sign and the lung point sign. In contrast, the presence of the sliding lung sign rules out a diagnosis of pneumothorax [39, 40].

Furthermore, misplacement and pneumothorax can be diagnosed in 2 or 3 min with ultrasound vs. typically more than 30 min with a chest X-ray.

Transesophageal echocardiography can also be used to assess the correct placement of the end of the CVC in the IVJ in mechanically ventilated patients but is rarely applied for this indication alone.

16.2.2 The Subclavian Vein

The subclavian vein is usually the recommended route for CVC cannulation in ICU patients because it is associated with a low incidence of nosocomial infection [20]. However, subclavian vein cannulation is associated with a higher incidence of pneumothorax and is not recommended in patients with a high risk of chronic kidney failure.

16.2.2.1 Technical Aspects

The probe is placed in the subclavian position or, less frequently, in a more lateral, axillary position. The cannulation is monitored with an in-plane view. The needle is held at an angle of 45° to the skin and, with ultrasound guidance, is then moved forward toward the opposite shoulder. The position can be more or less lateral. When the probe is positioned too laterally, the needle may puncture the axillary vein and not the subclavian vein.

16.2.2.2 Level of Evidence

In one of the first large, randomized studies (of 463 patients in the ICU), Fragou et al. [41] suggested that ultrasound-guided cannulation of the subclavian vein is superior to the landmark method and should be the method of choice in critical care patients. Other studies have confirmed that the ultrasound-guided technique should be preferred [42, 43]. In the Cochrane Collaboration meta-analysis, ultrasound-guided techniques were associated with (1) a lower complication rate, a lower number of attempts, and fewer arterial punctures and (2) a higher success rate and a higher first-attempt success rate, relative to the landmark method [44].

A subclavicular view can easily visualize the axillary vein, and so few studies have assessed ultrasound-guided insertion using this view [45–47]. The axillary vein might be an alternative to the subclavian vein and the IJV because it is outside the thorax, more distal to the pleural space and more comfortable for the patient [45], and is associated with a high success rate and a very low complication rate. Distal or proximal approaches are possible; Buzançais et al. concluded that the distal approach was not inferior to the proximal approach, although Wang et al. demonstrated that the proximal approach was better than the distal approach [46, 47].

16.2.2.3 The Short-Axis View vs. the Long-Axis View

Both short and long axis can be used to view the subclavian vein during cannulation. In a prospective, randomized study of 190 patients, Vezzani et al. found that the short-axis view was associated with a shorter mean insertion time, a higher success rate, a higher first puncture rate, and fewer redirections and complications [43]. The use of the oblique plane has also been suggested but there are no published data on the value of this plane [48]. Hence, any view could potentially be used. In our experience, however, the long-axis view is better for monitoring the cannulation.

16.2.2.4 Position of the Head and Shoulder

Ipsilateral 30° head rotation, a neutral shoulder position, and the Trendelenburg position significantly enhanced the size of the SCV in obese participants and should be applied as the standard position for subclavian cannulation in all patients [49].

16.2.2.5 Supraclavicular vs. Infraclavicular Approaches

Both infraclavicular and supraclavicular approaches have been used for catheterization of the subclavian vein [50–53] and have been evaluated in prospective studies. Kim et al. randomized 401 patients to supraclavicular vs. subclavicular cannulation with an ultrasound-guided technique. The complication and misplacement rates were lower in the supraclavicular group [54]. In another prospective study of 90 patients, Mageshwaran et al. demonstrated that the supraclavicular approach was better than the subclavicular approach [50]. In a meta-analysis of data from studies of supraclavicular access, the overall success rate ranged from 79% and 100%, and the overall complication rate ranged from 0% to 24.24% (Mean: 4.27%). The most prevalent complication was arterial puncture (1.39%), followed by catheter misplacement (0.42%) [51]. The meta-analysis's conclusion was confirmed by Chen et al., who observed a lower incidence of failure and misplacement with the supraclavicular approach [52].

16.2.2.6 The Location of the Tip of the CVC

Central venous catheter misplacement after right subclavian vein catheterization is observed in approximately 7% of cases. To avoid misplacement, ultrasound-guided tip navigation during the catheterization helps to direct the guidewire toward the lower superior vena cava. In a study of infraclavicular right subclavian vein catheterization, Adrian et al. demonstrated the utility of the right supraclavicular fossa ultrasound view for real-time confirmation and correction of the guidewire position [54]. Tarbiat et al. proved that the left subclavian vein should be preferred to the right vein because the former was associated with a lower misplacement rate and same the success and complication rates [55].

16.2.2.7 Pediatric Patients

Central venous cannulation in pediatric patients is challenging; this is particularly the case in infants. The subclavian vein is often the preferred site, and ultrasound-guided methods have become the standard for CVC cannulation [56–59]. Subclavicular and supraclavicular approaches have been suggested [56–59]. Pirrote et al. used the supraclavicular site in a study of 25 children (body weight: 2.2–27 kg) and reported a success rate of 84% after one attempt and 100% after two attempts [59]. Furthermore, ultrasound enabled the diagnosis of asymptomatic venous thrombosis. In Nardi et al.'s comparison of subclavicular and supraclavicular approach, the latter gave higher overall success and first-attempt success rates; only five cases of arterial puncture and no cases of pneumothorax were reported [56]. Byon et al. confirmed these findings: guidewire misplacement was less frequent with the supraclavicular approach [57].

16.2.3 The Femoral Vein

The femoral artery and femoral vein frequently overlap, which complicates cannulation. Ultrasound can be used to determine the best position for central venous cannulation. Many studies have demonstrated that ultrasound-guided cannulation of the femoral vein is effective, safe, and accurate [60–65]. However, there is less evi-

dence for femoral cannulation than for jugular or subclavian cannulation, and prospective randomized studies in ICUs are lacking. A recent meta-analysis of studies of cardiological and nephrology procedures confirmed that ultrasound-guided techniques are of value for femoral vein cannulation [63].

Furthermore, it has been found that ultrasound-guided techniques should be preferred for femoral cannulation in pediatric patients [66, 67]. The short-axis view was most frequently employed for femoral vein cannulation.

16.2.4 Peripheral Veins

Peripheral vein cannulation is one of the most frequent clinical procedures. In the ICU, emergency departments, and ward settings, peripheral vein cannulation is complicated by the risk of multiple punctures at the same site, hypovolemia (i.e., flat peripheral veins), invisible veins, and many other circumstances. In these situations, ultrasound can help to localize the vein, measure its diameter (in order to choose the most appropriate catheter gauge and length), and insert the catheter [68–73]. Many meta-analyses have demonstrated that ultrasound guidance increases the likelihood of successful peripheral cannulation in difficult-access patients [68–73]. Furthermore, ultrasound-guided techniques are associated with fewer punctures, a shorter time to intravenous access, and greater patient satisfaction [70]. In a recent meta-analysis of nine studies with 1350 infants and older children, Mitchell et al. [73] concluded that ultrasound improves the first pass and overall success rates for pediatric peripheral intravenous catheterization. In a subgroup analysis of difficult-access patients, success rates were high for a single operator and a dynamic, short-axis ultrasound technique.

16.3 Arteries

16.3.1 The Radial Artery

In the ICU, radial catheters are very useful for invasive arterial pressure monitoring and for blood sampling. Ultrasound-guided radial artery cannulation has been evaluated in a number of prospective, randomized studies [74–76]. The results of Hansen et al.'s crossover study showed that in comparison with conventional palpation, an ultrasound-guided dynamic needle tip positioning technique was associated with fewer skin perforations, catheters (40, vs. 46 for palpation; $p = 0.025$), and targeting attempts. The first-attempt success rate was significantly higher in the group with dynamic needle tip-positioning. Gopalasingam et al. also showed that the use of an ultrasound technique was associated with a higher first-attempt success rate and fewer skin perforations and needle retractions [75]. In a randomized study of 260 patients, Kiberenge et al. found that relative to palpation, the use of a dynamic ultrasound-guided needle tip positioning technique by anesthesia residents and faculty members was associated with higher overall and first-attempt success rates [76]. Similar results were found in two prospective studies of older adults [77–79]. The

authors of a Cochrane Collaboration meta-analysis of radial artery catheterization concluded that relative to palpation, real-time B-mode ultrasound guidance may improve the first-attempt success rate, the overall success rate, and the time to success. Furthermore, the incidence of major hematoma is probably lower for real-time B-mode ultrasound guidance than for palpation [80]. Bevel direction appears to be important during ultrasound-guided cannulation; for example, Min et al. have shown that compared with the bevel-up approach during ultrasound-guided radial artery catheterization, the bevel-down had a higher success rate and a lower complication rate [81]. The wrist angle also appears to influence the success of radial artery cannulation [82–84]. In a meta-analysis, a 45° wrist angle was found to facilitate ultrasound-guided radial artery cannulation and so can be recommended [83].

16.3.1.1 Oblique, Short-Axis, and Long-Axis Views

As with the other vessels, oblique, short-axis, and long-axis views have been used during ultrasound-guided cannulation of the radial artery [85–90]. The three approaches appear to be equivalent, although the level of evidence is very weak. Large, prospective studies are needed for a definitive conclusion.

16.3.1.2 Pediatric Patients

In pediatric patients, ultrasound-guided radial artery cannulation is associated with higher first-attempt and total success rates, a shorter overall procedure, and a lower incidence of hematoma. The current literature evidence suggests that ultrasound guidance should be the standard of clinical care for radial artery cannulation [91].

16.3.2 The Femoral Artery

There are very few published studies of ultrasound-guided cannulation of the femoral artery. Five randomized studies were included in a recent meta-analysis [92], and ultrasound guidance was found to be associated with a lower complication rate—driven primarily by a lower incidence of local hematoma [92]. A more recent analysis of seven studies concluded that relative to a standard approach, ultrasound-guided cannulation of the femoral artery is associated with a lower access-related complication rate and greater effectiveness [93].

16.4 Peripherally Inserted Central Catheters (PICCs)

Peripherally inserted central catheters are often useful in the oncology department (and sometimes in the ICU) but are associated with a high risk of venous thrombosis [94]. In a prospective study, the use of B-mode ultrasound for PICC placement reduced the complication rate, the cost of PICC maintenance, and the incidence of tip malposition and improved the patients' level of comfort [95].

16.5 Catheter Infections and Ultrasound Guidance

Whether ultrasound guidance is associated or not with an increased risk of catheter infection is subject to debate, and robust data are lacking. In a meta-analysis, Buetti et al. did not find a greater risk of infection for ultrasound-guided arterial cannulation [96]. In contrast, Buetti et al.'s analysis of three randomized studies evidenced a higher risk of CVC infection with ultrasound guidance. Our experience indicates that this risk is not abnormally high. In any case, precautions to reduce the risk of infection should always be taken when using ultrasound-guided techniques [97].

16.6 Training

Even though many experienced clinicians are comfortable using the landmark method for vascular cannulations, training and learning in this technique constitute a major challenge—especially for young residents. Learning programs should cover vessel anatomy/physiology, ultrasound devices, catheters, and the respective principles of cannulation using landmark-based and ultrasound-guided techniques. Training should be knowledge-based with video-based learning and hands-on simulation with anatomic models. Supervised clinical training also appears to be a very important component. With appropriate training, adequate skills can be acquired rapidly (e.g., after only eight procedures) even by novice operators [98–100]. This training should be followed by supervised ultrasound cannulations; the trainee is coached during the procedure, in order to achieve the required minimum level of skill with the lowest complication rate. It has been suggested that 6–8 h of knowledge-based education, 4 h of hands-on training on inanimate models, and then 6 h of hands-on training on non-patient volunteers is appropriate for the detection of normal vessels with ultrasound [101, 102].

16.7 Nurses

Nurses should be involved in learning and training programs so that they become able to insert peripheral catheters in difficult-access adults and pediatric patients. Many studies have demonstrated that a nurse can rapidly become effective in the use of ultrasound guidance, with a very high success rate after ten procedures [103, 104]. In the future, radial and femoral arteries might be cannulated by nurses in order to improve the quality of care—particularly when physicians lack time to care for patients (e.g., in the emergency department or the ICU).

Summary

In this chapter, we described ultrasound-guided techniques for artery and vein cannulations and reviewed the corresponding levels of evidence. Ultrasound-guided techniques are widely accepted as the gold standard for artery and vein cannulations, with higher overall and first-attempt success rates, lower complication rates, and higher levels of patient comfort. Regardless of the site, short-axis, long-axis, and oblique-

axis views appear to be equivalent in terms of success and complication rates. These ultrasound-guided techniques are recommended for vein and artery cannulations in adult and pediatric patients, whatever the site. All residents should be trained in these techniques so that they can become experienced operators.

16.8 Conclusion

Ultrasound-guided cannulation of arteries and veins has become the gold standard at the bedside and should be used all the time. Although the out-of-plane view is the best documented and most frequently used at all sites, an in-plane view or oblique view can also be used. For subclavian cannulation, the in-plane view appears to be better than the out-of-plane view.

Take-Home Messages

- Ultrasound-guided cannulation of the internal jugular vein is associated with a higher success rate and a lower complication rate; the level of evidence is high.
- Ultrasound-guided punctures of the femoral and subclavian veins are recommended, although the level of evidence is much lower than for the internal jugular vein.
- In children, the supraclavicular approach for subclavian vein cannulation appears to be safer and perhaps more effective than the subclavicular approach.
- Arteries can be cannulated with ultrasound guidance; this technique appears to be associated with a lower local complication rate and a higher success rate.
- In the emergency department and the ICUs, peripheral venous access is often difficult. It has been should that the use of ultrasound guidance helps nurses and physicians to increase their success rate.
- The first-attempt success rate is higher when ultrasound guidance is used during the cannulation of arteries and veins.
- Oblique, short-axis, and long-axis views can be used to cannulate arteries and veins during ultrasound guidance, and none of the three views stands out as being demonstrably better.
- Patients appear to be more comfortable when ultrasound-guided vessel cannulation is used.
- Learning and teaching programs on ultrasound-guided catheterization should be improved and implemented more widely.
- Nurses should be included in teaching and training programs on ultrasound-guided peripheral vein cannulation.

Questions

1. Should an ultrasound-guided technique always be used for internal jugular vein (IJV) cannulation?
   (a) Yes
   (b) No

2. Ultrasound-guided central vein cannulation
   (a) is known to be associated with a low incidence of mechanical complications
   (b) is known to be associated with a low incidence of catheter infections
   (c) should be performed using a "static" ultrasound method
   (d) should be performed using a "dynamic" ultrasound method
   (e) a quick-view ultrasound check before starting the cannulation is mandatory
   (you may give more than one answer, if you wish)
3. Regarding the technical aspects of ultrasound-guided cannulation:
   (a) a high-frequency probe should be preferred for IJV cannulation
   (b) wrapping the probe in a sterile plastic bag is mandatory
   (c) the out-of-plane view should always be used, regardless of the cannulation site
   (d) the out-of-plane view should be preferred for IJV cannulation
   (e) nurses may use ultrasound-guided techniques for peripheral vein cannulation
   (you may give more than one answer, if you wish)

Answers

1. Yes
2. a, d, e
3. a, b, d, e

References

1. iData Research. U.S. market for vascular access devices and accessories. Vancouver: iData Research; 2008.
2. Millennium Research Group. U.S. markets for vascular access devices. Toronto: Millennium Research Group; 2009.
3. Calvert N, Hind D, McWilliams RG, Thomas SM, Beverley C, Davidson A. The effectiveness and cost-effectiveness of ultrasound locating devices for central venous access: a systematic review and economic evaluation. Health Technol Assess. 2003;7(12):1–84.
4. Food and Drug Administration. Precautions necessary with central venous catheters. FDA Drug Bull. 1989:15–6.
5. Slama M, Novara A, Safavian A, Ossart M, Safar M, Fagon JY. Improvement of internal jugular vein cannulation using an ultrasound-guided technique. Intensive Care Med. 1997;23(8):916–9.
6. Denys BG, Uretsky BF, Reddy PS. Ultrasound-assisted cannulation of the internal jugular vein. A prospective comparison to the external landmark-guided technique. Circulation. 1993;87(5):1557–62.
7. Stern W, Sauer W, Dauber W. Complications of central venous catheterization from an anatomical point of view. Acta Anat (Basel). 1990;138(2):137–43.
8. Lamkinsi T, Kettani A, Belkhadir Z, Tadili J, Benjelloun MY, Mosadik A, et al. Internal jugular venous cannulation: what is the best approach? Ann Fr Anesth Reanim. 2012;31:512–6.
9. Chudhari LS, Karmarkar US, Dixit RT, Sonia K. Comparison of two different approaches for internal jugular vein cannulation in surgical patients. J Postgrad Med. 1998;44:57–62.
10. Apiliogullari B, Kara I, Apiliogullari S, Arun O, Saltali A, Celik JB. Is a neutral head position as effective as head rotation during landmark-guided internal jugular vein cannulation? Results of a randomized controlled clinical trial. J Cardiothorac Vasc Anesth. 2012;26(6):985–8.
11. Lamperti M, Subert M, Cortellazzi P, Vailati D, Borrelli P, Montomoli C, D'Onofrio G, Caldiroli D. Is a neutral head position safer than 45-degree neck rotation during ultrasound-guided internal jugular vein cannulation? Results of a randomized controlled clinical trial. Anesth Analg. 2012;114(4):777–84.
12. Maecken T, Marcon C, Bomas S, Zenz M, Grau T. Relationship of the internal jugular vein to the common carotid artery: implications for ultrasound-guided vascular access. Eur J Anaesthesiol. 2011;28(5):351–5.

13. Samy Modeliar S, Sevestre MA, de Cagny B, Slama M. Ultrasound evaluation of central veins in the intensive care unit: effects of dynamic manoeuvres. Intensive Care Med. 2008;34(2):333–8.
14. Garcia-Leal M, Guzman-Lopez S, Verdines-Perez AM, de Leon-Gutierrez H, Fernandez-Rodarte BA, Alvarez-Villalobos NA, Martinez-Garza JH, Quiroga-Garza A, Elizondo-Omaña RE. Trendelenburg position for internal jugular vein catheterization: a systematic review and meta-analysis. J Vasc Access. 2021;24:11297298211031339.
15. Jeon JC, Choi WI, Lee JH, Lee SH. Anatomical morphology analysis of internal jugular veins and factors affecting internal jugular vein size. Medicina (Kaunas). 2020;56(3):135.
16. Piton G, Capellier G, Winiszewski H. Ultrasound-guided vessel puncture: calling for Pythagoras' help. Crit Care. 2018;22:292.
17. Brass P, Hellmich M, Kolodziej L, Schick G, Smith AF. Ultrasound guidance versus anatomical landmarks for internal jugular vein catheterization. Cochrane Database Syst Rev. 2015;1(1):CD006962.
18. Franco-Sadud R, Schnobrich D, Mathews BK, Candotti C, Abdel-Ghani S, Perez MG, Rodgers SC, Mader MJ, Haro EK, Dancel R, Cho J, Grikis L, Lucas BP, SHM point-of-care ultrasound task force, Soni NJ. Recommendations on the use of ultrasound guidance for central and peripheral vascular access in adults: a position statement of the Society of Hospital Medicine. J Hosp Med. 2019;14:E1–E22.
19. Saugel B, Scheeren TWL, Teboul JL. Ultrasound-guided central venous catheter placement: a structured review and recommendations for clinical practice. Crit Care. 2017;21(1):225.
20. Timsit JF, Baleine J, Bernard L, Calvino-Gunther S, Darmon M, Dellamonica J, Desruennes E, Leone M, Lepape A, Leroy O, Lucet JC, Merchaoui Z, Mimoz O, Misset B, Parienti JJ, Quenot JP, Roch A, Schmidt M, Slama M, Souweine B, Zahar JR, Zingg W, Bodet-Contentin L, Maxime V. Expert consensus-based clinical practice guidelines management of intravascular catheters in the intensive care unit. Ann Intensive Care. 2020;10(1):118.
21. Leibowitz A, Oren-Grinberg A, Matyal R. Ultrasound guidance for central venous access: current evidence and clinical recommendations. J Intensive Care Med. 2020;35(3):303–21.
22. Schmidt GA, Blaivas M, Conrad SA, Corradi F, Koenig S, Lamperti M, Saugel B, Schummer W, Slama M. Ultrasound-guided vascular access in critical illness. Intensive Care Med. 2019;45(4):434–46.
23. Lamperti M, Bodenham AR, Pittiruti M, Blaivas M, Augoustides JG, Elbarbary M, Pirotte T, Karakitsos D, Ledonne J, Doniger S, Scoppettuolo G, Feller-Kopman D, Schummer W, Biffi R, Desruennes E, Melniker LA, Verghese ST. International evidence-based recommendations on ultrasound-guided vascular access. Intensive Care Med. 2012;38(7):1105–17.
24. Javeri Y, Jagathkar G, Dixit S, Chaudhary D, Zirpe KG, Mehta Y, Govil D, Mishra RC, Samavedam S, Pandit RA, Savio RD, Clerk AM, Srinivasan S, Juneja D, Ray S, Sahoo TK, Jakkinaboina S, Jampala N, Jain R. Indian Society of Critical Care Medicine position statement for central venous catheterization and management 2020. Indian J Crit Care Med. 2020;24(Suppl 1):S6–S30.
25. Robba C, Wong A, Poole D, Al Tayar A, Arntfield RT, Chew MS, Corradi F, Douflé G, Goffi A, Lamperti M, Mayo P, Messina A, Mongodi S, Narasimhan M, Puppo C, Sarwal A, Slama M, Taccone FS, Vignon P, Vieillard-Baron A, European Society of Intensive Care Medicine task force for critical care ultrasonography. Basic ultrasound head-to-toe skills for intensivists in the general and neuro intensive care unit population: consensus and expert recommendations of the European Society of Intensive Care Medicine. Intensive Care Med. 2021;47(12):1347–67.
26. Maizel J, Ammirati C, Slama M. Posterior vessel wall penetration by needles during internal jugular vein central catheter placement using ultrasound guidance: is that a real danger? Crit Care Med. 2010;38(2):735–6; author reply 736–7.
27. Maitra S, Bhattacharjee S, Baidya DK. Comparison of long-, short-, and oblique-axis approaches for ultrasound-guided internal jugular vein cannulation: a network meta-analysis. J Vasc Access. 2020;21(2):204–9.
28. Miao S, Wang X, Zou L, Zhao Y, Wang G, Liu Y, Liu S. Safety and efficacy of the oblique-axis plane in ultrasound-guided internal jugular vein puncture: a meta-analysis. J Int Med Res. 2018;46(7):2587–94.
29. Baidya DK, Chandralekha DV, Pandey R, Goswami D, Maitra S. Comparative sonoanatomy of classic "short axis" probe position with a novel "medial-oblique" probe position for ultrasound-

guided internal jugular vein cannulation: a crossover study. J Emerg Med. 2015;48(5):590–6. https://doi.org/10.1016/j.jemermed.2014.07.062. Epub 2015 Jan 24
30. Vogel JA, Haukoos JS, Erickson CL, Liao MM, Theoret J, Sanz GE, Kendall J. Is long-axis view superior to short-axis view in ultrasound-guided central venous catheterization? Crit Care Med. 2015;43(4):832–9.
31. Dilisio R, Mittnacht AJ. The "medial-oblique" approach to ultrasound-guided central venous cannulation—maximize the view, minimize the risk. J Cardiothorac Vasc Anesth. 2012;26(6):982–4.
32. Chen JY, Wang LK, Lin YT, Lan KM, Loh EW, Chen CH, Tam KW. Comparing short-, long-, and oblique-axis approaches to ultrasound-guided internal jugular venous catheterization: a meta-analysis of randomized controlled trials. J Trauma Acute Care Surg. 2019;86(3):516–23.
33. Airapetian N, Maizel J, Langelle F, Modeliar SS, Karakitsos D, Dupont H, Slama M. Ultrasound-guided central venous cannulation is superior to quick-look ultrasound and landmark methods among inexperienced operators: a prospective randomized study. Intensive Care Med. 2013;39(11):1938–44.
34. Lau CS, Chamberlain RS. Ultrasound-guided central venous catheter placement increases success rates in pediatric patients: a meta-analysis. Pediatr Res. 2016;80(2):178–84.
35. Chui J, Saeed R, Jakobowski L, Wang W, Eldeyasty B, Zhu F, Fochesato L, Lavi R, Bainbridge D. Is routine chest X-ray after ultrasound-guided central venous catheter insertion choosing wisely?: A population-based retrospective study of 6,875 patients. Chest. 2018;154(1):148–56.
36. Smit JM, Haaksma ME, Lim EHT, Steenvoorden TS, Blans MJ, Bosch FH, Petjak M, Vermin B, Touw HRW, Girbes ARJ, Heunks LMA, Tuinman PR. Ultrasound to detect central venous catheter placement associated complications: a multicenter diagnostic accuracy study. Anesthesiology. 2020;132(4):781–94.
37. Smit JM, Raadsen R, Blans MJ, Petjak M, Van de Ven PM, Tuinman PR. Bedside ultrasound to detect central venous catheter misplacement and associated iatrogenic complications: a systematic review and meta-analysis. Crit Care. 2018;22(1):65.
38. Korsten P, Mavropoulou E, Wienbeck S, Ellenberger D, Patschan D, Zeisberg M, Vasko R, Tampe B, Müller GA. The "rapid atrial swirl sign" for assessing central venous catheters: performance by medical residents after limited training. PLoS One. 2018;13(7):e0199345.
39. Ablordeppey EA, Drewry AM, Beyer AB, Theodoro DL, Fowler SA, Fuller BM, Carpenter CR. Diagnostic accuracy of central venous catheter confirmation by bedside ultrasound versus chest radiography in critically ill patients: a systematic review and meta-analysis. Crit Care Med. 2017;45(4):715–24.
40. Weekes AJ, Keller SM, Efune B, Ghali S, Runyon M. Prospective comparison of ultrasound and CXR for confirmation of central vascular catheter placement. Emerg Med J. 2016;33(3):176–80.
41. Fragou M, Gravvanis A, Dimitriou V, Papalois A, Kouraklis G, Karabinis A, Saranteas T, Poularas J, Papanikolaou J, Davlouros P, Labropoulos N, Karakitsos D. Real-time ultrasound-guided subclavian vein cannulation versus the landmark method in critical care patients: a prospective randomized study. Crit Care Med. 2011;39(7):1607–12.
42. Subramony R, Spann R, Medak A, Campbell C. Ultrasound-guided vs. landmark method for subclavian vein catheterization in an academic emergency department. J Emerg Med. 2022;62(6):760–8.
43. Vezzani A, Manca T, Brusasco C, Santori G, Cantadori L, Ramelli A, Gonzi G, Nicolini F, Gherli T, Corradi F. A randomized clinical trial of ultrasound-guided infra-clavicular cannulation of the subclavian vein in cardiac surgical patients: short-axis versus long-axis approach. Intensive Care Med. 2017;43(11):1594–601.
44. Brass P, Hellmich M, Kolodziej L, Schick G, Smith AF. Ultrasound guidance versus anatomical landmarks for subclavian or femoral vein catheterization. Cochrane Database Syst Rev. 2015;1(1):CD011447.
45. Farina A, Coppola G, Bassanelli G, Bianchi A, Lenatti L, Ferri LA, Liccardo B, Spinelli E, Savonitto S, Mauri T. Ultrasound-guided central venous catheter placement through the axillary vein in cardiac critical care patients: safety and feasibility of a novel technique in a prospective observational study. Minerva Anestesiol. 2020;86(2):157–64.
46. Buzançais G, Roger C, Bastide S, Jeannes P, Lefrant JY, Muller L. Comparison of two ultrasound guided approaches for axillary vein catheterization: a randomized controlled non-inferiority trial. Br J Anaesth. 2016;116(2):215–22.

47. Wang HY, Sheng RM, Gao YD, Wang XM, Zhao WB. Ultrasound-guided proximal versus distal axillary vein puncture in elderly patients: a randomized controlled trial. J Vasc Access. 2020;21(6):854–60.
48. De Cassai A, Galligioni H. Subclavian oblique-axis catheterization technique. Crit Care. 2017;21(1):323.
49. Kim H, Chang JE, Won D, Lee JM, Kim TK, Min SW, Kim C, Hwang JY. Effect of head and shoulder positioning on the cross-sectional area of the subclavian vein in obese subjects. Am J Emerg Med. 2021;50:561–5.
50. Mageshwaran T, Singla D, Agarwal A, Kumar A, Tripathy DK, Agrawal S. Comparative efficacy of supraclavicular versus infraclavicular approach of subclavian vein cannulation under ultrasound guidance: a randomised clinical trial. Indian J Anaesth. 2021;65(Suppl 2):S69–73.
51. Nazir A, Niazi K, Zaidi SMJ, Ali M, Maqsood S, Malik J, Kaneez M, Mehmoodi A. Success rate and complications of the supraclavicular approach for central venous access: a systematic review. Cureus. 2022;14(4):e23781.
52. Chen Q, Long Q, Liang JQ, Tang TX, Yang B. Comparative evaluation of the clinical safety and efficiency of supraclavicular and infraclavicular approaches for subclavian venous catheterization in adults: a meta-analysis. Am J Emerg Med. 2020;38(7):1475–80.
53. Kim YJ, Ma S, Yoon HK, Lee HC, Park HP, Oh H. Supraclavicular versus infraclavicular approach for ultrasound-guided right subclavian venous catheterisation: a randomised controlled non-inferiority trial. Anaesthesia. 2022;77(1):59–65.
54. Adrian M, Kander T, Lundén R, Borgquist O. The right supraclavicular fossa ultrasound view for correct catheter tip positioning in right subclavian vein catheterisation: a prospective observational study. Anaesthesia. 2022;77(1):66–72.
55. Tarbiat M, Manafi B, Davoudi M, Totonchi Z. Comparison of the complications between left side and right side subclavian vein catheter placement in patients undergoing coronary artery bypass graft surgery. J Cardiovasc Thorac Res. 2014;6:147–51.
56. Nardi N, Wodey E, Laviolle B, De La Brière F, Delahaye S, Engrand C, Gauvrit C, Dessard S, Defontaine A, Ecoffey C. Effectiveness and complications of ultrasound-guided subclavian vein cannulation in children and neonates. Anaesth Crit Care Pain Med. 2016;35(3):209–13.
57. Byon HJ, Lee GW, Lee JH, Park YH, Kim HS, Kim CS, Kim JT. Comparison between ultrasound-guided supraclavicular and infraclavicular approaches for subclavian venous catheterization in children—a randomized trial. Br J Anaesth. 2013;111(5):788–92.
58. Rhondali O, Attof R, Combet S, Chassard D, de Queiroz Siqueira M. Ultrasound-guided subclavian vein cannulation in infants: supraclavicular approach. Paediatr Anaesth. 2011;21(11):1136–41.
59. Pirotte T, Veyckemans F. Ultrasound-guided subclavian vein cannulation in infants and children: a novel approach. Br J Anaesth. 2007;98(4):509–14.
60. Hilty WM, Hudson PA, Levitt MA, Hall JB. Real-time ultrasound-guided femoral vein catheterization during cardiopulmonary resuscitation. Ann Emerg Med. 1997;29(3):331–6.
61. Sobolev M, Shiloh AL, Di Biase L, Slovut DP. Ultrasound-guided cannulation of the femoral vein in electrophysiological procedures: a systematic review and meta-analysis. Europace. 2017;19(5):850–5.
62. Yamagata K, Wichterle D, Roubícek T, Jarkovský P, Sato Y, Kogure T, Peichl P, Konecný P, Jansová H, Kucera P, Aldhoon B, Cihák R, Sugimura Y, Kautzner J. Ultrasound-guided versus conventional femoral venipuncture for catheter ablation of atrial fibrillation: a multicentre randomized efficacy and safety trial (ULTRA-FAST trial). Europace. 2018;20(7):1107–14.
63. Triantafyllou K, Karkos CD, Fragakis N, Antoniadis AP, Meletidou M, Vassilikos V. Ultrasound-guided versus anatomic landmark-guided vascular access in cardiac electrophysiology procedures: a systematic review and meta-analysis. Indian Pacing Electrophysiol J. 2022;22(3):145–53.
64. Lazaar S, Mazaud A, Delsuc C, Durand M, Delwarde B, Debord S, Hengy B, Marcotte G, Floccard B, Dailler F, Chirossel P, Bureau-Du-Colombier P, Berthiller J, Rimmelé T. Ultrasound guidance for urgent arterial and venous catheterisation: randomised controlled study. Br J Anaesth. 2021;127(6):871–8.
65. Sazdov D, Srceva MJ, Todorova ZN. Comparative analysis of ultrasound guided central venous catheterization compared to blind catheterization. Pril (Makedon Akad Nauk Umet Odd Med Nauki). 2017;38(2):107–14.

66. Tan Y, Liu L, Tu Z, Xu Y, Xie J, Ye P. Distal superficial femoral vein versus axillary vein central catheter placement under ultrasound guidance for neonates with difficult access: a randomized clinical trial. J Vasc Access. 2021;22(4):642–9.
67. Pietroboni PF, Carvajal CM, Zuleta YI, Ortiz PL, Lucero YC, Drago M, vonDessauer B. Landmark versus ultrasound-guided insertion of femoral venous catheters in the pediatric intensive care unit: an efficacy and safety comparison study. Med Intensiva (Engl Ed). 2020;44(2):96–100.
68. Stolz LA, Stolz U, Howe C, Farrell IJ, Adhikari S. Ultrasound-guided peripheral venous access: a meta-analysis and systematic review. J Vasc Access. 2015;16(4):321–6.
69. Egan G, Healy D, O'Neill H, Clarke-Moloney M, Grace PA, Walsh SR. Ultrasound guidance for difficult peripheral venous access: systematic review and meta-analysis. Emerg Med J. 2013;30(7):521–6.
70. van Loon FHJ, Buise MP, Claassen JJF, Dierick-van Daele ATM, Bouwman ARA. Comparison of ultrasound guidance with palpation and direct visualisation for peripheral vein cannulation in adult patients: a systematic review and meta-analysis. Br J Anaesth. 2018;121(2):358–66.
71. Gottlieb M, Sundaram T, Holladay D, Nakitende D. Ultrasound-guided peripheral intravenous line placement: a narrative review of evidence-based best practices. West J Emerg Med. 2017;18(6):1047–54.
72. Kleidon TM, Schults J, Paterson R, Rickard CM, Ullman AJ. Comparison of ultrasound-guided peripheral intravenous catheter insertion with landmark technique in paediatric patients: a systematic review and meta-analysis. J Paediatr Child Health. 2022;58(6):953–61.
73. Mitchell EO, Jones P, Snelling PJ. Ultrasound for pediatric peripheral intravenous catheter insertion: a systematic review. Pediatrics. 2022;149(5):e2021055523.
74. Hansen MA, Juhl-Olsen P, Thorn S, Frederiksen CA, Sloth E. Ultrasonography-guided radial artery catheterization is superior compared with the traditional palpation technique: a prospective, randomized, blinded, crossover study. Acta Anaesthesiol Scand. 2014;58(4):446–52.
75. Gopalasingam N, Hansen MA, Thorn S, Sloth E, Juhl-Olsen P. Ultrasound-guided radial artery catheterisation increases the success rate among anaesthesiology residents: a randomised study. J Vasc Access. 2017;18(6):546–51.
76. Kiberenge RK, Ueda K, Rosauer B. Ultrasound-guided dynamic needle tip positioning technique versus palpation technique for radial arterial cannulation in adult surgical patients: a randomized controlled trial. Anesth Analg. 2018;126(1):120–6.
77. Shim JG, Cho EA, Gahng TR, Park J, Lee EK, Oh EJ, Ahn JH. Application of the dynamic needle tip positioning method for ultrasound-guided arterial catheterization in elderly patients: a randomized controlled trial. PLoS One. 2022;17(8):e0273563.
78. Kim SY, Kim KN, Jeong MA, Lee BS, Lim HJ. Ultrasound-guided dynamic needle tip positioning technique for radial artery cannulation in elderly patients: a prospective randomized controlled study. PLoS One. 2021;16(5):e0251712.
79. Araj FG, Pena J, Cox J. Aim for the bubbles: agitated saline injection as an adjunct technique to ultrasound-guided subclavian vein cannulation. J Invasive Cardiol. 2019;31(7):E232.
80. Flumignan RL, Trevisani VF, Lopes RD, Baptista-Silva JC, Flumignan CD, Nakano LC. Ultrasound guidance for arterial (other than femoral) catheterisation in adults. Cochrane Database Syst Rev. 2021;10(10):CD013585. https://doi.org/10.1002/14651858.CD013585.pub2.
81. Min SW, Cho HR, Jeon YT, Oh AY, Park HP, Yang CW, Choi WH, Kim BG. Effect of bevel direction on the success rate of ultrasound-guided radial arterial catheterization. BMC Anesthesiol. 2016;16(1):34.
82. Kucuk A, Yuce HH, Yalcin F, Boyacı FN, Yıldız S, Yalcin S. Forty-five degree wrist angulation is optimal for ultrasound guided long axis radial artery cannulation in patients over 60 years old: a randomized study. J Clin Monit Comput. 2014;28(6):567–72.
83. Melhuish TM, White LD. Optimal wrist positioning for radial arterial cannulation in adults: a systematic review and meta-analysis. Am J Emerg Med. 2016;34(12):2372–8.
84. Aydoğan H, Kucuk A, Boyacı FN, Yuce HH, Yalcin F, Altay N, Aydın MS, Buyukfırat E, Yalcin S. Optimal wrist position for long and short axis ultrasound guided radial artery cannulation. Clin Ter. 2013;164(4):e253–7.
85. Abdalla UEM, Elmaadawey A, Kandeel A. Oblique approach for ultrasound-guided radial artery catheterization vs transverse and longitudinal approaches, a randomized trial. J Clin Anesth. 2017;36:98–101.

86. Sethi S, Maitra S, Saini V, Samra T, Malhotra SK. Comparison of short-axis out-of-plane versus long-axis in-plane ultrasound-guided radial arterial cannulation in adult patients: a randomized controlled trial. J Anesth. 2017;31(1):89–94.
87. Berk D, Gurkan Y, Kus A, Ulugol H, Solak M, Toker K. Ultrasound-guided radial arterial cannulation: long axis/in-plane versus short axis/out-of-plane approaches? J Clin Monit Comput. 2013;27(3):319–24.
88. Quan Z, Tian M, Chi P, Cao Y, Li X, Peng K. Modified short-axis out-of-plane ultrasound versus conventional long-axis in-plane ultrasound to guide radial artery cannulation: a randomized controlled trial. Anesth Analg. 2014;119(1):163–9.
89. Wang HH, Wang JJ, Chen WT. Ultrasound-guided short-axis out-of-plane vs. long-axis in-plane technique for radial artery catheterization: an updated meta-analysis of randomized controlled trials. Eur Rev Med Pharmacol Sci. 2022;26(6):1914–22.
90. Breschan C, Graf G, Jost R, Stettner H, Feigl G, Goessler A, Neuwersch S, Koestenberger M, Likar R. Ultrasound-guided supraclavicular cannulation of the right brachiocephalic vein in small infants: a consecutive, prospective case series. Paediatr Anaesth. 2015;25(9):943–9.
91. Huang HP, Zhao WJ, Wen F, Li XY. Application of ultrasound-guided radial artery cannulation in paediatric patients: a systematic review and meta-analysis. Aust Crit Care. 2021;34(4):388–94.
92. Rashid MK, Sahami N, Singh K, Winter J, Sheth T, Jolly SS. Ultrasound guidance in femoral artery catheterization: a systematic review and a meta-analysis of randomized controlled trials. J Invasive Cardiol. 2019;31(7):E192–8.
93. Sorrentino S, Nguyen P, Salerno N, Polimeni A, Sabatino J, Makris A, Hennessy A, Giustino G, Spaccarotella C, Mongiardo A, De Rosa S, Juergens C, Indolfi C. Standard versus ultrasound-guided cannulation of the femoral artery in patients undergoing invasive procedures: a meta-analysis of randomized controlled trials. J Clin Med. 2020;9(3):677.
94. Li J, Fan YY, Xin MZ, Yan J, Hu W, Huang WH, Lin XL, Qin HY. A randomised, controlled trial comparing the long-term effects of peripherally inserted central catheter placement in chemotherapy patients using B-mode ultrasound with modified Seldinger technique versus blind puncture. Eur J Oncol Nurs. 2014;18(1):94–103.
95. Oleti T, Jeeva Sankar M, Thukral A, Sreenivas V, Gupta AK, Agarwal R, Deorari AK, Paul VK. Does ultrasound guidance for peripherally inserted central catheter (PICC) insertion reduce the incidence of tip malposition? - a randomized trial. J Perinatol. 2019;39(1):95–101.
96. Buetti N, Ruckly S, Lucet JC, Bouadma L, Schwebel C, Mimoz O, Timsit JF. Ultrasound guidance and risk for intravascular catheter-related infections among peripheral arterial catheters: a post-hoc analysis of two large randomized-controlled trials. Ann Intensive Care. 2020;10(1):89.
97. Buetti N, Mimoz O, Mermel L, Ruckly S, Mongardon N, Dupuis C, Mira JP, Lucet JC, Mégarbane B, Bailly S, Parienti JJ, Timsit JF. Ultrasound guidance and risk for central venous catheter-related infections in the intensive care unit: a post hoc analysis of individual data of 3 multicenter randomized trials. Clin Infect Dis. 2021;73(5):e1054–61.
98. Tokumine J, Matsushima H, Lefor AK, Igarashi H, Ono K. Ultrasound-guided subclavian venipuncture is more rapidly learned than the anatomic landmark technique in simulation training. J Vasc Access. 2015;16(2):144–7.
99. Maizel J, Guyomarc'h L, Henon P, Modeliar SS, de Cagny B, Choukroun G, Slama M. Residents learning ultrasound-guided catheterization are not sufficiently skilled to use landmarks. Crit Care. 2014;18(1):R36.
100. Moureau N, Lamperti M, Kelly LJ, Dawson R, Elbarbary M, van Boxtel AJ, Pittiruti M. Evidence-based consensus on the insertion of central venous access devices: definition of minimal requirements for training. Br J Anaesth. 2013;110:347–56.
101. Feller-Kopman D. Ultrasound guided internal jugular access: a proposed standardized approach and implications for training and practice. Chest. 2007;132:302–9.
102. Royal College of Radiologists RCR Board of the Faculty of Clinical Radiology. Ultrasound training recommendations for medical and surgical specialties. RCR. 2004. p 1–56. http://www.rcr.ac.uk/docs/radiology/pdf/ultrasound.pdf.
103. Blick C, Vinograd A, Chung J, Nguyen E, Abbadessa MKF, Gaines S, Chen A. Procedural competency for ultrasound-guided peripheral intravenous catheter insertion for nurses in a pediatric emergency department. J Vasc Access. 2021;22(2):232–7.
104. Edwards C, Jones J. Development and implementation of an ultrasound-guided peripheral intravenous catheter program for emergency nurses. J Emerg Nurs. 2018;44(1):33–6.

Deep Venous Thrombosis

Massimo Lamperti, Boris Tufegdzic, and Amit Jain

Contents

17.1 Introduction – 253

17.2 Pathophysiology of Thrombosis – 254

17.3 Risk Factors – 255

17.4 Clinical Manifestations of DVT – 257

17.5 Diagnosis of Deep Venous Thrombosis – 257

17.6 Venous Ultrasonography/Doppler Ultrasound – 258
17.6.1 Point-of-Care Ultrasound – 259

17.7 Probe Selection and Technical Considerations – 260
17.7.1 Linear Probe with a Frequency of 5.0–10.0 MHz – 260
17.7.2 Imaging Tips and Protocol – 260

17.8 Probe Orientation – 262

17.9 Imaging Protocol – 263
17.9.1 Common Femoral Vein – 265
17.9.2 Popliteal Vein – 265
17.9.3 Superficial Femoral Vein – 265
17.9.4 Important Junctions – 265

17.10 Pathologic Ultrasound Findings – 266
17.10.1 Acute DVT – 266
17.10.2 Chronic DVT – 266
17.10.3 Superficial Thrombi – 266

© The Author(s), under exclusive license to Springer Nature Switzerland AG 2023
C. Robba et al. (eds.), *Basic Ultrasound Skills "Head to Toe" for General Intensivists*, Lessons from the ICU,
https://doi.org/10.1007/978-3-031-32462-8_17

17.11 Technical Considerations – 266
17.11.1 Patient Body Habitus – 266
17.11.2 Acute Versus Chronic Thrombi – 267
17.11.3 Internal Echoes – 267
17.11.4 Mistaking Other Structures for Vessels or Clot – 267
17.11.5 Duplicated Venous System – 267
17.11.6 The Adductor Hiatus – 268
17.11.7 Performing a Limited Exam – 268
17.11.8 Other Obstacles to the Exam – 268
17.11.9 Integration of Bedside Diagnostic Venous Ultrasound into Clinical Care – 268

17.12 "Head-to-Toe" Point-of-Care Ultrasonography (POCUS) in the Diagnosis of DVT/CR-DVT – 269

References – 270

Learning Objectives

- Deep vein thrombosis (DVT) is more common in critically ill patients than in the general hospital patient population.
- There are many factors that can lead to DVT and we will describe the pathophysiology of thrombosis that can lead to life-threatening conditions if not recognized on time.
- We will also describe catheter-related thrombosis as this is a unique condition that is related to the presence of central venous catheters that should be considered when a patient is carrying these vascular devices for a long time and whenever signs and symptoms of DVT are present.
- We will present the different diagnostic tools for DVT and in particular the use of compressive ultrasound that should be included in the head-to-toes whenever a patient is examined by point-of-care ultrasound at the ICU bedside.

17.1 Introduction

Deep venous thrombosis (DVT) as a part of the venous thromboembolic spectrum is occult, often underdiagnosed in about 30% of critically ill patients [1], and one of the possible serious complications that can cause disability and, in some cases, death. However, it can be considered a preventable event and not cause severe complications when diagnosed and treated at an early stage. The majority of intensive care unit (ICU) patients could have one or more risk factors for DVT. These patients are characterized by dynamic day-to-day changes due to pre-existing factors, hemodynamic changes, invasive procedures required for their treatment, and pharmacological requirements.

Although DVT most commonly occurs in the deep veins of the lower leg and thigh, it may also occur within the upper limb deep veins, visceral veins, and even the superior/inferior cava vein [2]. The majority of lower limb DVT forms in the deep veins below the popliteal trifurcation (distal DVT) from where it may extend to the proximal veins and subsequently break free to cause pulmonary embolism (PE) [3]. Isolated calf DVT rarely causes leg symptoms and rarely causes clinically significant PE [4]. While, much clinical work has been done to identify and calculate the risks of DVT, a large number (up to 20%) of DVT cases are considered idiopathic, with no clear risk factors identified [5]. As such, DVT can be particularly difficult to predict and prevent.

Upper limb DVT represents less than 10% of all DVTs [6] and can be characterized as primary or secondary DVT. Primary upper limb DVT, also known as Paget–Schroetter syndrome, is defined as a thrombus in the axillary and subclavian veins occurring as a consequence of strenuous upper-extremity activity, a complication of thoracic outlet syndrome, or a spontaneous thrombosis in the absence of identifiable thrombosis risk factors. Secondary upper limb DVT, accounting for 80% of upper limb DVTs, is defined as DVT related to a predisposing factor, such as the presence of central venous catheters, malignancy, or insertion of wires or other devices [7].

The placement of a central venous catheter (CVC) has become an integral part of the care for critically ill patients, providing adequate venous access which is essential for these patients. Unfortunately, although they are extremely important for monitoring and delivering the appropriate therapy, their use is frequently associated with minor and major complications leading to prolonged hospital admission and, less frequently, resulting in life-threatening complications and even the death of the patient. Catheter-related deep venous thrombosis (CR-DVT) is the second most common major long-term complication related to central venous lines after catheter-linked blood-stream infections (CLABSI), and it is the most common major post-insertion mechanical complication. It can lead to distressing patient symptoms, catheter dysfunction, increased risk of infection, long-term central venous stenosis, and increased costs of care [8]. The reported rates of CR-DVT show significant variations, reporting a variable incidence from 2% to 67%. These differences may be related to the use of different modalities of detection, nonuniform definitions of thrombosis, and different timing of examination. Most catheter-related thromboses occur in the upper part of the body, where central venous catheters are most commonly placed. An asymptomatic upper extremity venous thrombosis has been reported to occur in 20–60% of patients with a central venous catheter. Symptomatic deep venous thrombosis has been reported to occur in up to 30% of patients with a central venous catheter. The incidence of CVC-related upper limb DVT screened by venography reportedly varies between 27% and 66% [9, 10].

17.2 Pathophysiology of Thrombosis

Virchow's triad of alterations in the blood flow, endothelial vascular injury, and derangements in the coagulation cascade remain clinically relevant to date in understanding the formation and propagation of thrombus inside vessels [11, 12].

DVT tends to occur in areas with decreased or mechanically altered blood flow such as the pockets adjacent to valves in the deep veins of the leg. While valves help to promote blood flow through the venous circulation, they are also potential locations for venous stasis. Venous stasis has also been associated with hypoxia and increased hematocrit, constituting a potentially hypercoagulable microenvironment [13]. There is general agreement that venous thrombosis involves tissue factor as the initiator of the coagulation response but it also appears to involve P-selectin, an adhesion molecule that can contribute to cell–cell interactions [14, 15].

In the case of CR-DVT, in addition to vessel trauma and venous stasis, the catheter itself becomes a thrombogenic surface when exposed to blood. All catheters, when introduced into the body, are progressively covered with plasma proteins and fibrin. Fibrin formation is a natural process that may occur soon after the insertion

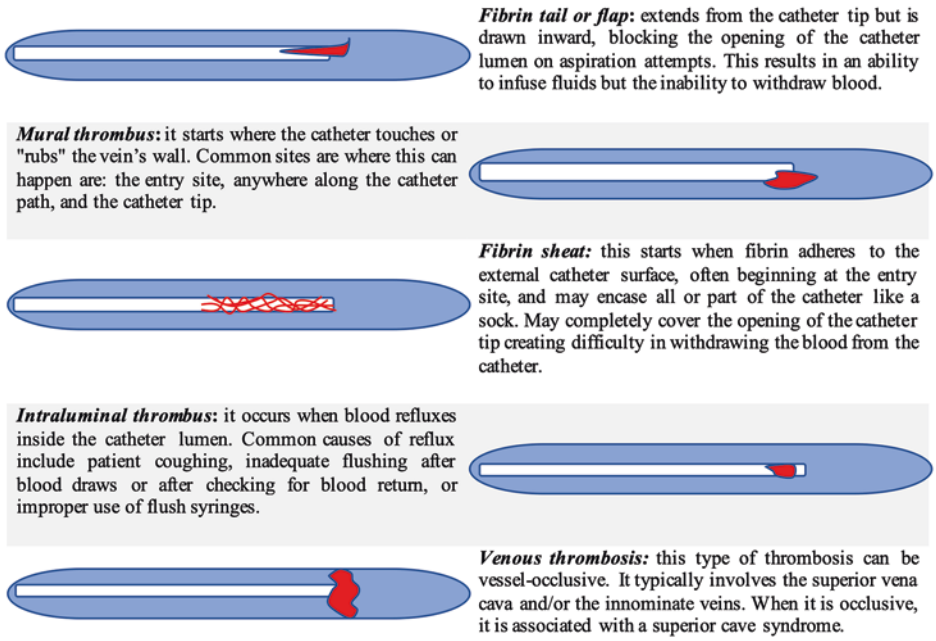
Fibrin tail or flap: extends from the catheter tip but is drawn inward, blocking the opening of the catheter lumen on aspiration attempts. This results in an ability to infuse fluids but the inability to withdraw blood.
Mural thrombus: it starts where the catheter touches or "rubs" the vein's wall. Common sites are where this can happen are: the entry site, anywhere along the catheter path, and the catheter tip.
Fibrin sheat: this starts when fibrin adheres to the external catheter surface, often beginning at the entry site, and may encase all or part of the catheter like a sock. May completely cover the opening of the catheter tip creating difficulty in withdrawing the blood from the catheter.
Intraluminal thrombus: it occurs when blood refluxes inside the catheter lumen. Common causes of reflux include patient coughing, inadequate flushing after blood draws or after checking for blood return, or improper use of flush syringes.
Venous thrombosis: this type of thrombosis can be vessel-occlusive. It typically involves the superior vena cava and/or the innominate veins. When it is occlusive, it is associated with a superior cave syndrome.

Fig. 17.1 Main types of thrombotic catheter occlusions

of a device or develop at any time during intravenous therapy. The fibrin starts to create a layer around the external surface of the catheter within minutes of insertion, starting at either the line entry site or where the tip of the catheter contacts the vein's walls [16]. The blood flow can be reduced up to 60% around the catheter, this phenomenon leads to further cellular adhesion to the catheter and the vein's walls [17]. A partial or total venous occlusion may be the result of a catheter thrombus developing over the fibrin sheath within the next few days (Fig. 17.1).

17.3 Risk Factors

An understanding of the risk factors for DVT is necessary in order to maximize the prevention in high-risk patients.

The risk factors related to patient, catheter, or insertion are summarized in Tables 17.1 and 17.2.

Table 17.1 Risk factors for DVT related to the patient

Related to the patient	
Hereditary factors	**Acquired factors**
Antithrombin deficiency [18]	Age >65 years [19]
Protein S deficiency [18, 20]	Malignancy [21]
Dysfibrinogenemia [18, 20]	Chemotherapy
Factor V Leiden [18, 20]	Systemic or catheter-related infection
Activated protein C resistance without factor V Leiden [18, 20]	Previous venous thromboembolism [22]
Protein C deficiency [18, 20]	Diabetes
Prothrombin gene mutation [18, 20]	Obesity
Plasminogen deficiency [18, 20]	Pregnancy
	Immobilization
	Type of surgery (orthopedic patients at highest risk)
	Parenteral nutrition [23]
	Estrogen replacement
	Trauma

Table 17.2 Risk factors for CR-DVT

Related to the catheter	Related to the insertion
Catheter diameter	Femoral > subclavian > jugular [24]
Multi-lumen > single lumen	Left side > right side [25]
Catheter material [26]	
Catheter/vein ratio 1:3 [27, 28]	
Catheter tip location: proximal to SVC > lower third of SVC	
Time after insertion	
PICC [29–34]	

17.4 Clinical Manifestations of DVT

The clinical manifestations of DVT are variable. The majority of DVTs are asymptomatic which can make their identification quite difficult. Symptomatic DVT/CR-DVT may lead to arm, leg, or neck symptoms (swelling, pain, tenderness, erythema) and possible extension of the thrombosis proximally or distally with septic thrombophlebitis, bacteremia, and sepsis. Very often, in the case of CR-DVT the first clinical sign is the catheter malfunction, which is due to an obstruction within the central venous catheter lumen or occlusion due to an enveloping sheath obstructing the catheter luminal tip [35].

17.5 Diagnosis of Deep Venous Thrombosis

An accurate diagnosis of DVT is extremely important to prevent potentially fatal acute complications such as pulmonary embolism (PE) and long-term complications such as post-thrombotic syndrome.

Clinical probability scores and D-dimer test are commonly used as safe diagnostic tests in the diagnostic workup for thrombosis of the lower limbs. Only limited data are available on the applicability of these diagnostic tools for upper-extremity thrombosis. The Wells' score with its modification is the most widely used and accepted scoring system able to predict DVT. Based on Wells' score, patients can be divided into "DVT unlikely" and "DVT likely" groups [36]. Unfortunately, the Wells' Score is less useful in hospitalized patients [37] (◘ Table 17.3).

◘ **Table 17.3** Wells' score: clinical probability of deep venous thrombosis and pulmonary embolism

Criteria	Points
Active cancer	+1
Paralysis, paresis, or recent plaster immobilization	+1
Recently bedridden (>3 days) or major surgery past 4 weeks	+1
Localized tenderness along the deep venous system	+1
Entire limb swollen	+1
Calf swelling by more than 3 cm compared to asymptomatic leg	+1
Previously documented DVT	+1
Pitting edema—greater in the symptomatic leg	+1
Dilated collateral superficial veins (non-varicose)	+1
Alternative diagnosis likely or more possible that DVT	−2
DVT likely: 2 points or more; DVT unlikely: 1 point or less	

Because clinical probability scores alone do not exclude the presence of DVT, they should be used with D-dimer testing and, when appropriate, imaging. The updated NICE guideline (NG158) recommends that in people with a "likely" score an ultrasound scan should be carried out if the result can be obtained within 4 h. If the ultrasound scan cannot be carried out within 4 h, a D-dimer test and interim 24-h dose of a parenteral anticoagulant should be given and a leg ultrasound performed within 24 h of request. Any patient who has a negative ultrasound scan, but a positive D-dimer test should have the scan repeated 6–8 days later [38].

D-dimer testing has a high sensitivity, so a negative result essentially rules out thrombosis. However, it has low specificity, so a positive result can indicate thrombosis but does not rule out other potential causes. A result of 0.5 μg/mL or more is considered positive and requires confirmation by venous ultrasound. Deep venous thrombosis can be ruled out in a patient who is judged clinically unlikely to have deep venous thrombosis and who has a negative D-dimer test [39].

Signs and symptoms of DVT in general are not sufficiently sensitive or specific to make a diagnosis. Objective testing for DVT is crucial because clinical assessment alone is unreliable, and the consequences of misdiagnosis are serious. Venous ultrasonography is the first-line imaging test; however, alternative imaging modalities are used when venous ultrasonography evaluation is technically inadequate or equivocal. These imaging techniques include contrast venography and MRI venogram.

17.6 Venous Ultrasonography/Doppler Ultrasound

Venous ultrasound is recommended as the standard imaging test for patients suspected of having acute DVT. Various ultrasound protocols have been recommended by different authoritative groups [40]. However, there exist great variabilities and disagreements among these protocols; while some protocols include scanning the entire lower extremity, others recommend scans limited to the thigh and knee supplemented with serial testing. Some protocols use grayscale ultrasound alone, whereas others include Doppler interrogation. The commonly used ultrasound-based protocols for patients suspected of lower extremity DVT are [40] (◘ Fig. 17.2):

- **Two-region compression ultrasound (2-CUS)** indicates compression ultrasound including the femoral veins 1–2 cm above and below the saphenofemoral junction and the popliteal veins up to the calf veins confluence.
- **Extended compression ultrasound (ECUS)**: compression ultrasound from the common femoral vein through the popliteal vein up to the calf vein confluence.
- **Complete compression ultrasound (CCUS)**: compression ultrasound from the common femoral vein to the ankle.
- **Complete duplex ultrasound (CDUS)**: compression ultrasound from the common femoral vein to the ankle (evaluating the posterior tibial and peroneal veins in the calf), color and spectral Doppler of the common femoral (or iliac veins) on both sides and of the popliteal vein on the symptomatic side.

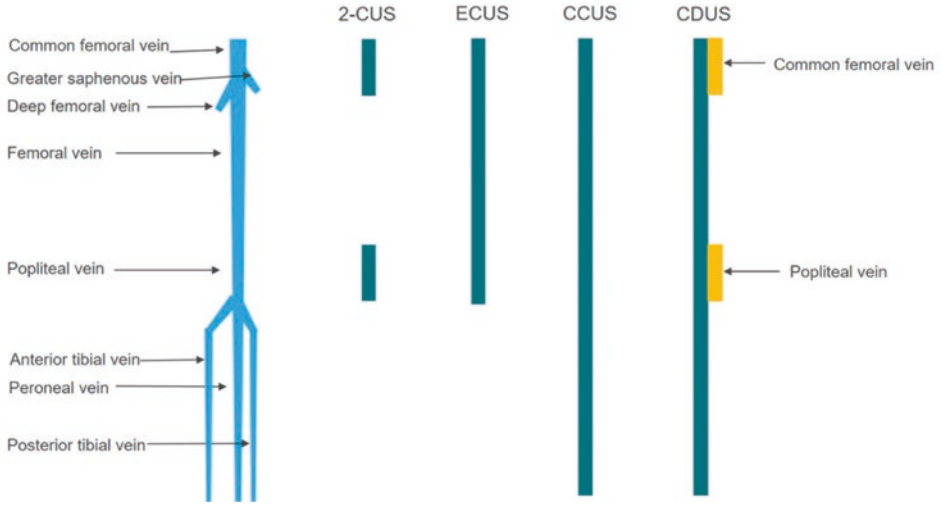

Fig. 17.2 Schematic diagram depicting lower extremity venous system and extent of ultrasound tests. Green rectangles represent the extent of the compression ultrasound. Orange rectangles are sites of duplex Doppler

The expert panel from the Society of Radiologists in Ultrasound recommends the adoption of CDUS protocol rather than a limited or complete compression-only examination as the preferred diagnostic technique. Complete protocols are usually performed by a sonographer or vascular technologist and read by a radiologist. However, in circumstances such as emergency departments or off hours, when CDUS cannot be performed in a clinically relevant time frame, the panel recommends point-of-care ultrasound consisting of ECUS instead of 2-CUS to be performed by a competent practitioner.

17.6.1 Point-of-Care Ultrasound

Bedside ultrasonography can play a pivotal role in the diagnostic algorithms of venous thromboembolic disease. With the greater availability of portable ultrasound units in many EDs and ICUs, there are an increasing number of clinicians performing bedside diagnostic venous sonograms. For the purpose of point-of-care ultrasound, we recommend performing ECUS instead of 2-CUS by a competent practitioner.

Although the accuracy studies determining the ability of individuals besides well-trained ultrasound technicians to diagnose upper extremity DVT has not been thoroughly studied, a few studies have demonstrated that well-trained ED and critical-care physicians can perform a point-of-care ultrasound for lower extremity DVT with sensitivity and specificity of 95% and 96%, respectively. ECUS should be preferred over 2-CUS because ECUS can detect isolated femoral vein thrombosis that accounts for 5–7% of lower extremity DVT.

Bedside ultrasound evaluation for lower extremity DVT should be performed in the following patients:

- The patient with signs and symptoms of lower extremity DVT
- The patient with undifferentiated hypoxemia or shock

17.7 Probe Selection and Technical Considerations

17.7.1 Linear Probe with a Frequency of 5.0–10.0 MHz

A linear probe with a frequency of 7.5 MHz is usually sufficient for most lower extremity vessels. To image deeper vessels, curvilinear probes utilizing lower frequencies (1–5 MHz) should be considered.

17.7.2 Imaging Tips and Protocol

17.7.2.1 Basic Ultrasound Settings to Improve Image Quality

Focal Zone

The focal zone should be adjusted and placed at the depth of the vessel being imaged. This improves the lateral resolution of the image.

Color Flow Doppler

Color flow Doppler (CFD) detects blood flow and therefore is helpful in identifying a blood vessel and distinguishing it from other structures present in the lower extremity. CFD can be especially helpful in obese patients where imaging is more difficult and with smaller vessels, such as the popliteal.

Time Gain Compensation

Time gain compensation (TGC) can be adjusted in order to increase the far gain of the image. Gain should be adjusted so that the image results in uniform brightness and resolution in both the near and far fields. Adjustment of this control may be useful in obese patients with difficult anatomy.

Depth

The depth should be adjusted once the appropriate vessels have been identified. The structures of interest should make up approximately three-fourths of the screen. Inadequate depth, either too shallow or deep, can result in a misidentification of the proper blood vessels.

17.7.2.2 Normal Lower Extremity Venous Anatomy

The lower extremity venous system is divided into deep and superficial vessels. The deep veins are paired with and accompany the arteries. The external iliac vein originates from the inferior vena cava (IVC) and extends distally to the inguinal ligament to become the common femoral vein (cFV). The CFV is then joined medially by the

great saphenous vein (GSV). Approximately 1–2 cm distal to this point, the CFV gives off the deep femoral vein (DFV) laterally. CFV further continues distally as the superficial femoral vein (SFV) which forms the main deep vein of the lower leg. So, it is important to note that the "superficial" femoral vein is part of the deep venous system, and is just more superficial than the DFV. To avoid confusion, many have begun calling the SFV simply the "femoral vein." The DFV can usually be tracked for a short distance before it dives deeper and away from the major venous system. The SFV runs anteromedially down the leg and courses through the adductor canal posteriorly into the popliteal fossa to become the popliteal vein (pV). In the proximal calf, the pV trifurcates into the anterior tibial, peroneal, and posterior tibial veins of the lower leg (◘ Fig. 17.2).

17.7.2.3 Normal Upper Extremity Venous Anatomy

The brachiocephalic vein divides into the jugular vein and subclavian vein. The subclavian vein bifurcates into the axillary vein, deep vein, and cephalic vein, which is a large but superficial vein in the arm and forearm. The axillary vein gives off two branches of the brachial veins, which course alongside the brachial artery, before becoming the basilic vein, another large but superficial vein that continues for the length of the arm and forearm. When the brachial veins reach the antecubital fossa, it branches into radial and ulnar veins which travel in pairs around their corresponding arteries through the anterior compartment of the forearm.

17.7.2.4 Patient Position for Lower Extremity DVT Assessment

In evaluating the femoral vessels, the patient should be placed in the supine position with the lower leg in the frog-leg position slightly extra rotated at 20°. The reverse Trendelenburg positioning can better fill the veins and improve ultrasound visualization (◘ Fig. 17.3a).

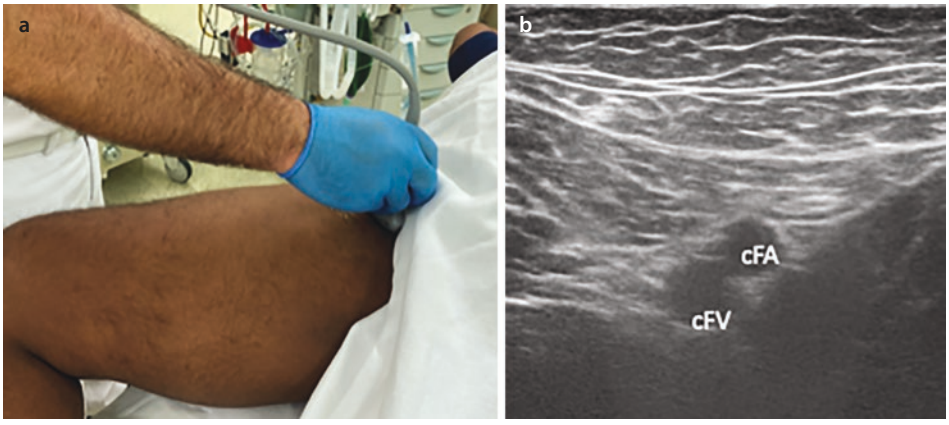

◘ **Fig. 17.3** **a** Demonstration of sonographer and patient positioning during compression of the common femoral vein. The leg is externally rotated with the probe held transverse to the vein; **b** B-mode imaging of the lower extremity vein and artery showing normal common femoral vein (cFV) and common femoral artery (cFA)

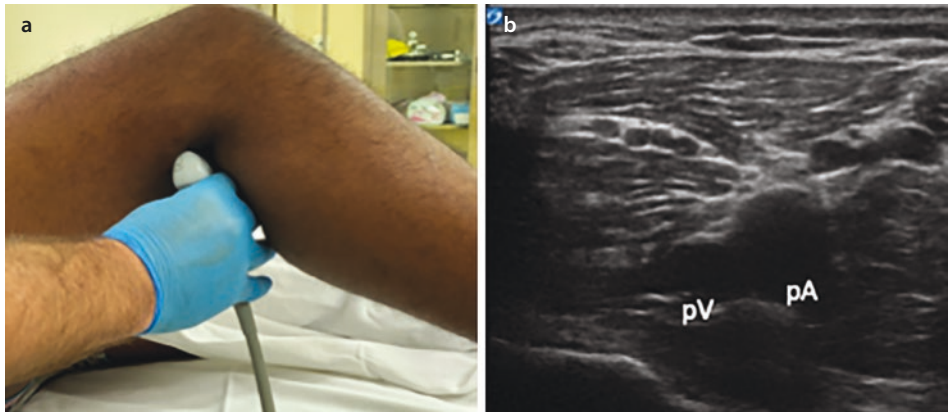

Fig. 17.4 **a** Demonstration of the sonographer and patient positioning during imaging of the popliteal vein in a supine patient. Note that the leg is elevated and slightly flexed while the probe is held posterior and transverse to the vein in the popliteal fossa with upward pressure applied. **b** B-mode imaging showing a normal popliteal vein (pV) and popliteal artery (pA). Notice the positioning of the vein in comparison to the artery

For evaluating the popliteal vessels, the patient can be in the supine position with the knee held in a flexion state, or the patient may be asked to lie in a prone position. The probe should be placed in a transverse position at the back of the knee in the popliteal fossa (Fig. 17.4a).

17.8 Probe Orientation

Lower extremity ultrasound is performed in the transverse position with the probe indicator pointing toward the patient's right side. The vessels are imaged in a transverse position, starting just below the level of the inguinal ligament. At this level, the cFV should be visualized medial and adjacent to the common femoral artery (cFA) (Fig. 17.3b). The GSV will be seen joining the cFV from the medial side, high in the leg. When the probe is slid down about 1–2 cm distally, the cFA can be seen dividing into the superficial femoral artery (SFA) and the deep femoral artery (DFA). As the probe is moved distally and medially down the leg, the SFV should be visualized until it enters the adductor canal.

The popliteal region should also be examined with the probe in a transverse orientation behind the patient's knee. In this view, the PV will be seen on top of the popliteal artery on the screen. Keep in mind that the pV is still deep to the artery (i.e., closer to the bed in a supine patient). Classically, the popliteal vein and artery (pA) will form a "figure eight," with the vein being the upper part of the eight (Fig. 17.4b).

17.9 Imaging Protocol

Ultrasound-based protocols commonly employed for the diagnosis of DVT (as described in the above section) are based on two principal methods: one utilizing B-mode (also known as 2D) imaging to directly visualize the venous segment of interest. This technique allows real-time visualization of the pressure-induced collapse of the vein of interest by a direct compression force applied by an ultrasound probe on the imaging vessels usually referred to as CUS, while other involves using duplex ultrasound that adds Doppler (color or spectral) to the 2D analysis modality, allowing for the visualization of blood flow within the vein. As there exist considerable variations in defining these techniques, in this chapter we followed the nomenclatures recommended by the experts' panel from the European Society of Cardiology working groups of aorta and peripheral vascular diseases and pulmonary circulation and right ventricular function [40].

- CUS uses B-mode (also known as 2D) imaging to allow real-time visualization of the pressure-induced collapse of the vein of interest (Fig. 17.5).
- Duplex ultrasound: adds Doppler (color or spectral) to the 2D analysis modality, allowing for the visualization of blood flow within the vein. Color-gain settings must be set appropriately in order to avoid oversaturation and not obscure small intraluminal clots or areas of incomplete thrombosis. Although duplex is now typically a secondary method to CUS, the term duplex ultrasound is often used to describe a DVT ultrasound, as it was historically a primary method.
- Triplex ultrasound: includes 2D ultrasound, color-flow Doppler, and spectral Doppler. Color-flow Doppler allows for the identification of flow within blood vessels. Flow toward the probe is represented in red and flow away from the probe is represented in blue.

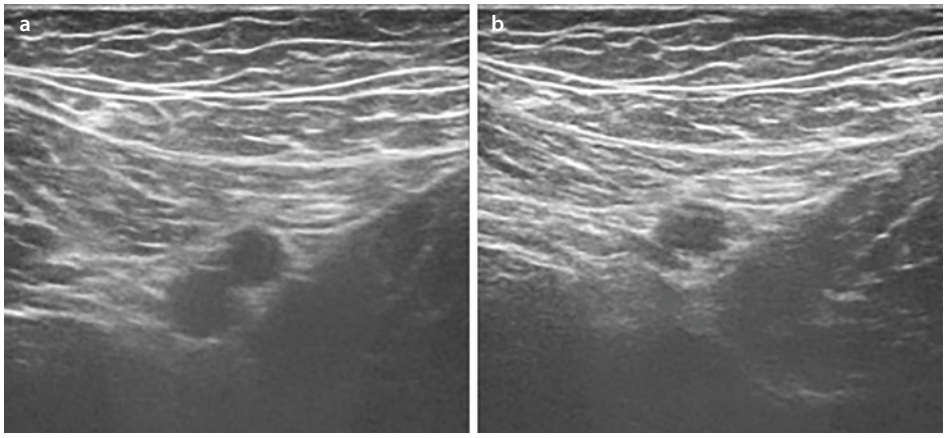

Fig. 17.5 The full compression technique needed to demonstrate the absence of lower extremity deep venous thrombosis. **a** Shows the uncompressed common femoral vein (cFV) next to the common femoral artery (cFA). **b** Shows the compressed cFV vein with obliteration of the previously visualized anechoic lumen next to the cFA

Prior to each compression, an assessment for intraluminal echoes should be performed, although their presence lacks specificity for thrombus. Clots may also be seen directly as more hyperechoic (bright) than the rest of the vessel. Longstanding (chronic) clots are typically more hyperechoic than acute clots. While acute clots may also appear hyperechoic, most acute thrombi are hypoechoic and may not be directly visualized. Nonetheless, the sonographer may encounter situations where an echogenic and well-circumscribed thrombus is found without compression.

Gentle but firm pressure is then applied with the transducer on the transverse axis. The pressure must be sufficient enough to completely collapse the vessel. Patent veins are fully compressible and the visible anechoic lumen should completely disappear, signifying that opposing venous walls have come into full contact (Fig. 17.5b). With this technique, the inability to completely compress the venous lumen is the main criterion for the diagnosis of DVT (Figs. 17.6 and 17.7). The amount of pressure applied needs to be lower than the pressure required to collapse the artery; therefore, only slight tenting of the adjacent artery should be seen. If the vein is not collapsible at this pressure, a venous thrombus is present. Adequate pressure is important since acute thrombi have jellylike consistency and may be frequently partially compressible. Excessive pressure can sometimes collapse the artery, especially in volume-depleted patients, while inadequate pressure can lead to the erroneous conclusion that a vein is noncompressible. A vein may be distinguished from an artery by partially compressing it and watching for pulsations, or using color-flow Doppler. The sonographer must ensure that the probe is transverse to the vessel and that downward pressure is applied directly over the vein. If the transducer is angled

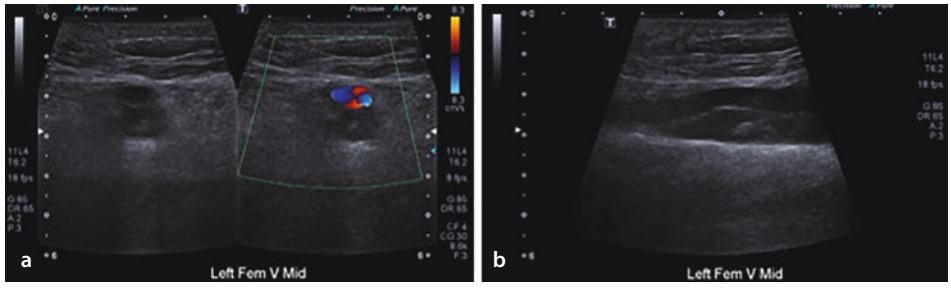

Fig. 17.6 Short **a** and long **b** axial view of the deep vein thrombosis in the left mid-femoral vein

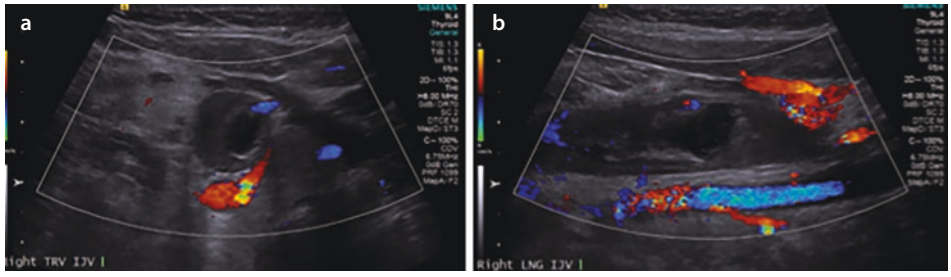

Fig. 17.7 Short **a** and long **b** axial view of the deep vein thrombosis in the right internal jugular vein

or positioned incorrectly, pressure is sometimes directed adjacent to the vein, or the vein inadvertently slides away from the interrogation window, resulting in a false positive finding.

An ECUS exam consists of performing sequential compressions every 1–2 cm over the entire proximal venous system from the iliac vein at the groin to the distal popliteal fossa. A limited or "2-CUS" exam consists of performing compressions at the two main venous confluences alone (see Fig. 17.1). While the majority of clots will be identified either in the cFV, proximal SFV, or pV, some studies have shown the limited exam to have slightly lower sensitivity.

17.9.1 Common Femoral Vein

The exam should begin with the transducer in the transverse axis at the origin of the cFV, just below the inguinal ligament and medial to the femoral artery. Sequential compressions should be performed, advancing 2 cm distally and medially along the vein before the next compression. At a short distance below the inguinal ligament, the GSV should be seen joining the cFV medially. The proximal portion of the GSV must be interrogated, as the thrombus present at this level has a high risk for extension into the cFV and should be treated. Following the cFV distally, it will bifurcate into the deep and superficial femoral vein, also known as simply the femoral vein (being a deep and not a superficial vein). The examiner should continue to follow the cFV distally, compressing along the way, down to the popliteal fossa.

17.9.2 Popliteal Vein

Ideally, the patient should be in a prone position, which is not always possible in most critically ill individuals. In such patients, the knee is flexed approximately 45°, or the patient is positioned in the lateral decubitus position. The paired popliteal artery and vein are located in a central position (see Fig. 17.5) (visualization of associated smaller vessels usually indicates that the transducer is positioned too low in the popliteal fossa). Compressions should be performed sequentially up to a point just distal to the trifurcation of the pV into the three calf veins.

17.9.3 Superficial Femoral Vein

As previously mentioned, if the above two-site technique is negative, the length of the SFV is then interrogated until it is lost medially in the adductor canal.

17.9.4 Important Junctions

Images should be recorded or printed at the following junctions:

- cFV proximal to GSV
- cFV-GSV junction
- cFV-DFV junction

- Mid pV
- pV calf veins junction (trifurcation)
- Proximal SFV
- Mid SFV
- Distal SFV

17.10 Pathologic Ultrasound Findings

17.10.1 Acute DVT

The inability to completely collapse the venous lumen signifies a clot. An acute DVT can sometimes appear as an echogenic structure within the lumen and be identified even before compression. More commonly, acute clots are hypoechoic and are sometimes only partially compressible, and therefore may not be as easy to identify.

17.10.2 Chronic DVT

Chronic clots are usually more easily identifiable before compressions due to their echogenicity. Chronic clots can sometimes recanalize and have a flow of blood through the center of them. In addition, the vessel walls surrounding a chronic DVT may appear thickened with scar tissue, which can also help the sonographer distinguish them from acute clots. Prior ultrasounds, if available, can be helpful in this situation for comparison.

17.10.3 Superficial Thrombi

Clots present in superficial vessels are sometimes encountered when interrogating the lower extremity. These superficial vessels are not accompanied by an artery. It is important to distinguish a superficial clot from a DVT because the treatment, for the most part, differs.

17.11 Technical Considerations

17.11.1 Patient Body Habitus

Obesity often makes ultrasound studies challenging. Applying firm pressure with the transducer can improve the visualization of deeper vessels. Additionally, in order to enhance the signal returning from deeper structures the far gain may need to be increased by using the TGC controls. In the obese patient, positioning should be optimized. Often, the reverse Trendelenburg position is not only better tolerated by

obese patients but can also increase flow to the venous vessels. When interrogating the popliteal fossa attempt to have the patient in the prone position.

17.11.2 Acute Versus Chronic Thrombi

The differentiation between acute and chronic DVT may be difficult. The ultrasound appearance of DVT changes over time and a comparison with prior ultrasound studies may often be helpful. Notably, thrombi become progressively more echogenic as they organize, and the underlying venous wall in the area of thrombosis gets thicker, more echogenic, and resistant to compression.

17.11.3 Internal Echoes

In low-flow states such as hypotensive and or hypovolemic ICU patients, internal echoes ("smoke") may be frequently encountered. Smoke is more easily visualized in large veins (i.e., internal jugular and subclavian in the upper extremities, and common, profound, proximal superficial, and greater saphenous in the lower extremities) and should not be confused with true thrombi.

17.11.4 Mistaking Other Structures for Vessels or Clot

Semisolid structures such as a lymph node or muscle band can be easily confused for a thrombosed vein. Sonographers should be extra careful not to mistake these structures for blood vessels. Lymph nodes usually have a hyperechoic center with a hypoechoic rim. Muscle bands are rounded, well-circumscribed with linear internal echoes. Close attention to the vascular anatomy, such as identifying the paired artery, can help in differentiation. Scanning the structure of interest distally will help as blood vessels will continue while a lymph node will disappear.

Other fluid-filled structures such as an abscess, a simple soft tissue cyst, or Baker's cyst behind the knee can all resemble blood-filled vessels. The use of color-flow Doppler in these situations is often useful: the blood vessels will pick up color flow but the other fluid-filled objects will not. These structures will also not be as easily compressible as a venous vessel wall, so pressure over the suspected object of interest can help in differentiating the two.

17.11.5 Duplicated Venous System

The presence of a duplicated venous system can cause the unsuspecting sonographer to miss the thrombosed segment. Conversely, a large collateral system could be mistaken for a patent venous segment while thrombosis is present in an underlying vein. This can be avoided by scanning the opposite extremity for comparison and also by referencing prior studies, if available.

17.11.6 The Adductor Hiatus

As the (superficial) femoral vein passes through the adductor hiatus, it is surrounded by fibrous tissue that can make it difficult to compress directly and may result in a false-positive interpretation of the clot. This can be addressed by keeping the probe anterior and medial on the leg while compressing the vein and pressing with the other hand in the popliteal fossa.

17.11.7 Performing a Limited Exam

Because bedside ultrasound may be more limited and does not typically include the calf veins, ultrasound should be repeated in 3–7 days in a patient with continued symptoms or a high pretest probability to avoid missing calf vein clots that may propagate proximally.

17.11.8 Other Obstacles to the Exam

The presence of local tenderness, obscuring dressings, edema, burn areas, and local recent surgery may render the study difficult to perform or altogether unobtainable.

17.11.9 Integration of Bedside Diagnostic Venous Ultrasound into Clinical Care

Based on extensive evidence in symptomatic outpatients, ultrasonography is currently the primary means of diagnosing DVT in the lower extremities.

Although studies have suggested that the sensitivity of ultrasonography in asymptomatic, high-risk, inpatient populations is considerably lower, it remains the test of choice in acutely ill patients due to its accuracy, noninvasiveness, ease of performance, availability, low cost, and ability to be repeated without restrictions. DVT can be confidently diagnosed when an absence of venous collapse under sufficient pressure is present. Assessment of venous flow patterns can assist in confirming the diagnosis, but the significance of isolated abnormalities of spectral or color Doppler signal analysis should be questioned and alternative diagnostic tests should be considered (venography, CT venogram, MR venography). Color interrogation and maneuvers to augment flow help identify venous segments that are difficult to visualize with real-time sonography, but do not increase diagnostic accuracy.

Appropriately trained clinicians can perform bedside ultrasound to diagnose LEDVT, using the CUS technique, with similar sensitivities and specificities as radiological exams. The benefit of this "point-of-care" exam is that it obviates the need for patient transport, venous access, and radiation exposure inherent in other diagnostic modalities. Further studies are required to better define the accuracy of ultrasound in the ICU population as well as the accuracy of bedside clinician exams in this challenging population of patients.

17.12 "Head-to-Toe" Point-of-Care Ultrasonography (POCUS) in the Diagnosis of DVT/CR-DVT

Case scenario a 76-year-old patient is admitted to ICU for urosepsis and acute respiratory failure. In her past medical history: hypertension, diabetes, chronic renal failure (no dialysis), and a recent diagnosis of cholangiocarcinoma. While admitted to ICU, she required a central venous catheter placement and broad-spectrum antibiotic therapy. After 14 days after admission, the nurse taking care of her called for help during the morning nursing care after turning her on her side; the patient started deteriorating in her oxygenation with SpO2 dropping to 80% with face mask oxygen at 50% and was tachycardic and tachypneic and obtunded.

This could be a typical scenario for a patient who has multiple risk factors for developing DVT and the presence of a central line could be a possible risk for CR-DVT.

There should be a systematic approach in our POCUS that could allow us to diagnose quickly the presence of a thrombus in one of the most probable sites for DVT.

We suggest a stepwise approach as the following:

1. Consider the patient's past medical history and risk factors.
2. If Wells' score is 2 or higher, prepare for venous POCUS.
3. Use linear ultrasound probes with lower frequency (2–10 MHz), so you can explore deeper vessels, in case you need to explore vessels deeper than 8 cm, use a convex probe (2–5 MHz).
4. Start from a toes-to-head approach: first CDUS. If no sign of thrombus is detected in the lower limbs, explore the upper limbs starting from one of the two arms, starting from the deep peripheral veins (brachial and basilic) and the cephalic vein going up to the axillary area; continue the exploration into the axillary vein in all its infraclavicular tract up to the subclavian vein, and then explore the internal and external jugular veins.
5. In case a thrombus is detected inside a vein, perform CUS to evaluate the full collapsibility of the vein, and in case the vein is obstructed, apply the color Doppler function and the Doppler sonography to evaluate the rate of obstruction of the venous velocity.
6. In case the thrombosis is related to the presence of a vascular catheter (peripheral or central venous), scan the vessel to evaluate to what extent the catheter-related thrombosis has obstructed the vein and consider not to remove the catheter to avoid venous emboli during the removal. In case the central venous catheter was in place of long period (more than 1 month), consider an echocardiography to rule out the possible presence of a thrombus on the catheter tip.

Take-Home Messages

- DVT is not rare but undiagnosed in critically ill patients. Many risk factors for increased thrombosis can be present when patients are admitted to ICU.
- Catheter-related thrombosis is related not only to the patient's related risk factors but also to the fluid dynamics of the venous flow around the venous catheter that can be impaired.
- Compressive ultrasound (CUS) of the upper and lower extremities' deep vessels should be performed anytime there are clinical signs of DVT to rule out an immediate strategy for treatment to avoid life-threatening complications.

Summary

Clinical and subclinical DVT is not uncommon in critically ill patients. CUS is an easy, quick, and sensitive exam that can start to rule out a suspected DVT especially when other clinical or laboratory signs are already present to start treating it before it could lead to life-threatening conditions.

References

1. Attia J, Ray JG, Cook DJ, Douketis J, Ginsberg JS, Geerts WH. Deep vein thrombosis and its prevention in critically ill adults. Arch Intern Med. 2001;161(10):1268–79. https://doi.org/10.1001/archinte.161.10.1268.
2. Bevis PM, Smith FCT. Deep vein thrombosis. Surgery. 2016;34(4):159–64. https://doi.org/10.1016/j.mpsur.2016.02.001.
3. Kearon C. Natural history of venous thromboembolism. Circulation. 2003;107(23 Suppl 1):I22–30. https://doi.org/10.1161/01.CIR.0000078464.82671.78. PMID: 12814982
4. Wu AR, Garry J, Labropoulos N. Incidence of pulmonary embolism in patients with isolated calf deep vein thrombosis. J Vasc Surg Venous Lymphat Disord. 2017;5(2):274–9. https://doi.org/10.1016/j.jvsv.2016.09.005. Epub 2016 Dec 14. PMID: 28214497
5. Fleck D, Albadawi H, Shamoun F, Knuttinen G, Naidu S, Oklu R. Catheter-directed thrombolysis of deep vein thrombosis: literature review and practice considerations. Cardiovasc Diagn Ther. 2017;7(Suppl 3):S228–37. https://doi.org/10.21037/cdt.2017.09.15. PMID: 29399526; PMCID: PMC5778526
6. Heil J, Miesbach W, Vogl T, Bechstein WO, Reinisch A. Deep vein thrombosis of the upper extremity. Dtsch Arztebl Int. 2017;114(14):244–9. https://doi.org/10.3238/arztebl.2017.0244.
7. Mai C, Hunt D. Upper-extremity deep venous thrombosis: a review. Am J Med. 2011;124(5):402–7. https://doi.org/10.1016/j.amjmed.2010.11.022. PMID: 21531227
8. Geerts W. Central venous catheter-related thrombosis. Am Soc Hematol Hematol. 2014;1:306–11.
9. Bates SM, Ginsberg JS. Clinical practice. Treatment of deep-vein thrombosis. N Engl J Med. 2004;351(3):268–77. https://doi.org/10.1056/NEJMcp031676. PMID: 15254285
10. Olaf M, Cooney R. Deep venous thrombosis. Emerg Med Clin North Am. 2017;35(4):743–70. https://doi.org/10.1016/j.emc.2017.06.003. Epub 2017 Aug 23. PMID: 28987427
11. Hamer JD, Malone PC, Silver IA. The PO2 in venous valve pockets: its possible bearing on thrombogenesis. Br J Surg. 1981;68(3):166–70. https://doi.org/10.1002/bjs.1800680308. PMID: 7470818
12. Esmon CT. Basic mechanisms and pathogenesis of venous thrombosis. Blood Rev. 2009;23(5):225–9. https://doi.org/10.1016/j.blre.2009.07.002. PMID: 19683659; PMCID: PMC2762278
13. Stone J, Hangge P, Albadawi H, et al. Deep vein thrombosis: pathogenesis, diagnosis, and medical management. Cardiovasc Diagn Ther. 2017;7(Suppl 3):S276–84. https://doi.org/10.21037/cdt.2017.09.01.
14. Ryder M. The role of biofilm in vascular catheter-related infections. N Dev Vasc Dis. 2001;2:15–25.

15. Nifong TP, McDevitt TJ. The effect of catheter to vein ratio on blood flow rates in a simulated model of peripherally inserted central venous catheters. Chest. 2011;140:48–53. www.cathmatters.com
16. Centers of Disease Control and Prevention (CDC). Data and statistics on venous thromboembolism. https://www.cdc.gov/ncbddd/dvt/data.html.
17. Verso M, Agnelli G. Venous thromboembolism associated with long-term use of central venous catheters in cancer patients. J Clin Oncol. 2003;21:3665–75.
18. De Cicco M, Matovic M, Balestreri L, De AV, Fracasso A, Morassut S, Coran F, Babare R, Buonadonna A, Testa V. Antithrombin III deficiency as a risk factor for catheter-related central vein thrombosis in cancer patients. Thromb Res. 1995;78:127–37.
19. Biffi R, Orsi F, Pozzi S, Pace U, Bonomo G, Monfardini L, Della Vigna P, Rotmensz N, Radice D, Zampino MG, Fazio N, de Braud F, Andreoni B, Goldhirsch A. Best choice of central venous insertion site for the prevention of catheter-related complications in adult patients who need cancer therapy: a randomized trial. Ann Oncol. 2009;20:935–40.
20. Beck C, Dubois J, Grignon A, Lacroix J, David M. Incidence and risk factors of catheter-related deep vein thrombosis in a pediatric intensive care unit: a prospective study. J Pediatr. 1998;133:237–41.
21. Timsit JF, Farkas JF, Boyer JM, Martin JB, Misset B, Renaud B, Carlet J. Central vein catheter-related thrombosis in intensive care. Chest. 1998;114:207–13.
22. Waheed SM, Kudaravalli P, Hotwagner DT. Deep vein thrombosis. In: StatPearls [Internet]. Treasure Island, FL: StatPearls Publishing; 2022. https://www.ncbi.nlm.nih.gov/books/NBK507708/.
23. Saber W, Moua T, Williams EC. Risk factors for catheter-related thrombosis (CRT) in cancer patients: a patient level data (IPD) meta-analysis of clinical trials and prospective studies. J Thromb Haemost. 2011;9:312–9.
24. Eastridge BJ, Lefor AT. Complications of indwelling venous access devices in cancer patients. J Clin Oncol. 1995;13:233–8.
25. Merrer J, De Jonghe B, Golliot F, Lefrant JY, Raffy B, Barre E, Rigaud JP, Casciani D, Misset B, Bosquet C, Outin H, Brun-Buisson C, Nitenberg G, for the French Catheter Study Group in Intensive Care. Complications of femoral and subclavian venous catheterization in critically ill patients. A randomized controlled trial. JAMA. 2001;286:700–7.
26. Dollery CM, Sullivan ID, Bauraind O, Bull C, Milla PJ. Thrombosis and embolism in long-term central venous access for parenteral nutrition. Lancet. 1994;344:1043–5.
27. Pottecher T, Forrler M, Picardat P, Krause D, Bellocq JP, Otteni JC. Thrombogenicity of central venous catheters: prospective study of polyethylene, silicone and polyurethane catheters with phlebography or post-mortem examination. Eur J Anaesthesiol. 1984;1:361–5.
28. Gorski LA, Hadaway L, Hagle ME, McGoldrick M, Orr M, Doellman D. Infusion nursing standards of practice. J Infus Nurs. 2016;39(1S):S1–S159.
29. Fletcher SJ, Bodenham AR. Safe placement of central venous catheters: where should the tip of the catheter lie? Br J Anaesth. 2000;85:188–91.
30. Chopra V, Anand S, Hickner A, Buist M, Rogers M, Saint S, Flanders S. Risk of venous thromboembolism associated with peripherally inserted central catheters: a systematic review and meta-analysis. JAMA. 2013;382:311–25.
31. Hoshal VL Jr. Total intravenous nutrition with peripherally inserted silicone elastomer central venous catheters. Arch Surg. 1975;110:644–6.
32. Chemaly RF, de Parres JB, Rehm SJ, et al. Venous thrombosis associated with peripherally inserted central catheters: a retrospective analysis of the Cleveland Clinic experience. Clin Infect Dis. 2002;34:1179–83.
33. Paauw JD, Borders H, Ingalls N. The incidence of PICC line-associated thrombosis with and without the use of prophylactic anticoagulants. J Parenter Enteral Nutr. 2008;32:443–7.
34. Liu Y, Gao Y, Wei L, Chen W, Ma X, Song L. Peripherally inserted central catheter thrombosis incidence and risk factors in cancer patients: a double-center prospective investigation. Ther Clin Risk Manag. 2015;11:153–60.
35. Van Rooden CJ, Tesselaar ME, Osanto S, et al. Deep vein thrombosis associated with central venous catheters–a review. J Thromb Haemost. 2005;3:2409–19.
36. Tapson VF. Acute pulmonary embolism. N Engl J Med. 2008;358(10):1037–52. https://doi.org/10.1056/NEJMra072753. PMID: 18322285

37. Stein PD, Terrin ML, Hales CA, Palevsky HI, Saltzman HA, Thompson BT, Weg JG. Clinical, laboratory, roentgenographic, and electrocardiographic findings in patients with acute pulmonary embolism and no pre-existing cardiac or pulmonary disease. Chest. 1991;100(3):598–603. https://doi.org/10.1378/chest.100.3.598. PMID: 1909617
38. Owens CA, et al. Pulmonary embolism from upper extremity deep vein thrombosis and the role of superior vena cava filters: a review of the literature. JVIR. 2010;21:779–87.
39. National Institute for Health and Care Excellence, Venous thromboembolic diseases: diagnosis, management and thrombophilia testing, NICE guideline [NG158]. 2020. https://www.nice.org.uk/guidance/NG158.
40. Mazzolai L, Aboyans V, Ageno W, Agnelli G, Alatri A, Bauersachs R, Brekelmans MPA, Büller HR, Elias A, Farge D, Konstantinides S, Palareti G, Prandoni P, Righini M, Torbicki A, Vlachopoulos C, Brodmann M. Diagnosis and management of acute deep vein thrombosis: a joint consensus document from the European Society of Cardiology working groups of aorta and peripheral vascular diseases and pulmonary circulation and right ventricular function. Eur Heart J. 2018;39(47):4208–18. https://doi.org/10.1093/eurheartj/ehx003.

Brain

Contents

Chapter 18 **Cranial Ultrasound for Intracerebral Pathology – 000**
Aarti Sarwal

Chapter 19 **Role of Brain Ultrasound for the Assessment of Intracranial Hypertension – 000**
Corina Puppo

Chapter 20 **Transcranial Doppler (TCD): Clinical Applications in Acute Brain Injury – 000**
Carla Bittencourt Rynkowski, Juliana Caldas, and Fabio Silvio Taccone

Chapter 21 **Regional Anaesthesia for the Intensivist – 000**
Edmund Chan, Cosmin Balan, and Amit Pawa

Cranial Ultrasound for Intracerebral Pathology

Aarti Sarwal

Contents

18.1 Introduction – 276

18.2 Evaluation of Parenchymal Pathology – 281

References – 286

© The Author(s), under exclusive license to Springer Nature Switzerland AG 2023
C. Robba et al. (eds.), *Basic Ultrasound Skills "Head to Toe" for General Intensivists*, Lessons from the ICU,
https://doi.org/10.1007/978-3-031-32462-8_18

Learning Objectives

- Critical appraisal of available literature on feasibility and diagnostic accuracy of the use of cranial ultrasound to diagnose intracerebral pathology relevant to critical care.
- Described image acquisition techniques with pearls and pitfalls of cranial B-mode ultrasonography.
- Outline the clinical indications in critically ill patients where cranial B-mode ultrasonography can be useful for the diagnosis and monitoring of patients with otherwise limited access to conventional neuroimaging modalities.

18.1 Introduction

Transcranial ultrasound, which includes transcranial Doppler (TCD), transcranial color-coded sonography (TCCS), and brain echography or cranial ultrasound, allows two-dimensional imaging of the brain parenchyma and intracranial vessels [1–3]. Acquisition of B-mode images to identify the midbrain is the first step before vessel insonation for all transcranial ultrasound studies [4]. Since TCD or TCCS inherently includes vessel Doppler insonation, and brain parenchyma assessment only requires B-mode images on ultrasound, the term "brain echography" or "cranial ultrasound" was introduced to distinguish between the two studies. When performed by a point-of-care clinical provider rather than a trained sonographer, the term cranial point-of-care ultrasound is used (cPOCUS) or neuroPOCUS [5]. While B-mode cranial ultrasound has been performed in children for the last 40 years and neonates through the transfontanelle approach, clinical applications in older children or adults with intact skulls have developed only subsequently, since the thickening of temporal bones with increasing age makes insonation much more difficult in adults [3, 6]. Increasing developments in advanced hemodynamic support in emergency and critical care settings have necessitated the use of point-of-care tools in patients that are difficult to transport for traditional diagnostic imaging modalities [7, 8]. Interestingly, point-of-care applications of cranial ultrasound are being revisited for clinical application in austere and resource-limited environments [5].

Recent consensus statement on skill recommendations and competence [9], as well as the report of the Neuro-POCUS working group commissioned by the European Society of Neurosonology and Cerebral Hemodynamics, has designated cranial ultrasound as intermediate to high-level skill requiring >100 measurements with >20 comparisons with CT scans for parenchymal diagnostics. With the increasing use of systemic POCUS and increasing recognition of the utility of Neuro-POCUS in acute care settings, this gap is expected to narrow over time. This chapter discusses the emerging clinical applications of cranial ultrasound in patients with intact skulls as well as surgical skull defects.

Image acquisition About 80–90% of the population has sufficiently thin temporal bones (acoustic windows) that permit high-resolution B-mode imaging of brain parenchymal structures through the temporal bone (Fig. 18.1). Insufficient insonation due to a thick skull impedes diagnosis in 10–20% of patients [10, 11].

Fig. 18.1 Skull held against light to show the presence of temporal windows that allow insonation of the brain through an intact cranium

B-mode cranial ultrasonography is facilitated in patients with skull defects related to prior craniotomy or craniectomy, and clinical applications in this specific subset are described separately in the end to distinguish sonography applications in patients with intact skulls.

A cranial ultrasound can be performed using a 1–2 MHz probe (echo probe, phased-array probe) placed on the temporal bone to obtain B-mode or grayscale images of the brain. The probe is positioned with the index marker pointed anteriorly toward the eyes to provide axial images of the brain at the midbrain level (Fig. 18.1). The temporal windows typically extend from the tragus of the ear to the lateral canthus of the eye with most frequent successful insonation superior and anterior to the tragus. Depth is adjusted to allow visualization of the opposite skull which signifies probe placement on the temporal window. The probe direction is adjusted to align the line of consolidation along the midbrain which is visible as a butterfly-shaped structure with cerebral peduncles pointed to the left of the screen and superior colliculi pointed to the right of the screen (Figs. 18.2 and 18.3). A convex hyperechoic signal closest to the probe signifies the petrous part of the temporal bone and the lesser wing of the sphenoid outlining the middle cranial fossa. Further movements of the probe can visualize structures anteriorly, posteriorly, and superiorly. The thickness of the base of the skull classically impedes any meaningful insonation below the level of the midbrain.

Insonation of the brain through an intact skull is typically done on a transcranial Doppler preset with a high mechanical index and thermal index to allow penetration of sound waves to the skull. In patients insonated through a craniotomy or craniectomy defects, an abdominal preset is typically recommended to outline parenchymal details with lesser MI and TI. While B-mode imaging on abdominal preset is enhanced by tissue harmonic imaging, this artifact-reducing option can be switched off for Doppler indications.

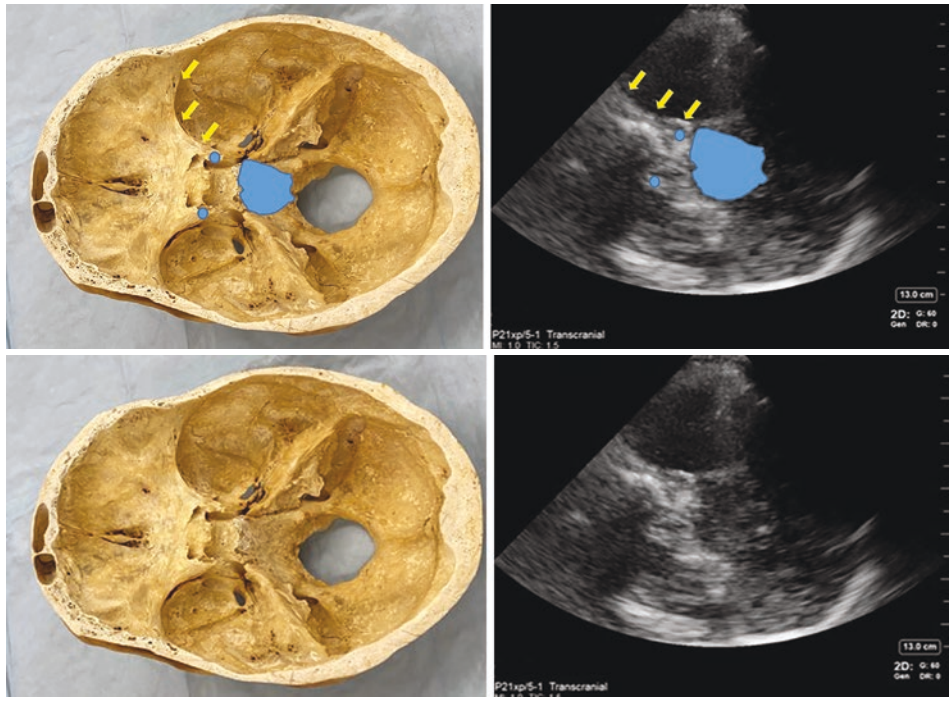

Fig. 18.2 Axial section of the skull with the corresponding B-mode image of the cranial ultrasound showing key landmarks. The lesser wing of the sphenoid (yellow arrows), clinoid processes (blue dots), and midbrain (blue outline) are visible at the level of the basal cisterns

Cranial topography on B-mode ultrasound A typical B-mode cranial ultrasound image spanning the axial section of the brain is shown in Figs. 18.3 and 18.4 showing the opposite skull, midbrain, and ipsilateral convexity showing the bony landmarks outlined in the middle cranial fossa. Significant artifacts produced by the petrous part of the temporal bone and the lesser wing of the sphenoid impair meaningful evaluation of the ipsilateral parenchyma. The contralateral parenchyma is less affected by such artifacts and can be more consistently evaluated on B-mode images. The bony landmarks clearly visible on the B-mode cranial ultrasound include as follows [12]:

- Opposite skull which appears as a relatively sharply demarcated hyperechoic signal
- Ipsilateral convexity formed by the petrous part of the temporal bone and the lesser wing of the sphenoid
- Anterior part of the skull/frontal bone
- Outline of the orbital fossa
- Posterior part of the skull/occipital bone
- Convex wedge in the occipital bone denoting the site of the transverse sinus
- Crista galli
- Clivus and anterior clinoid processes outlining the pituitary fossa

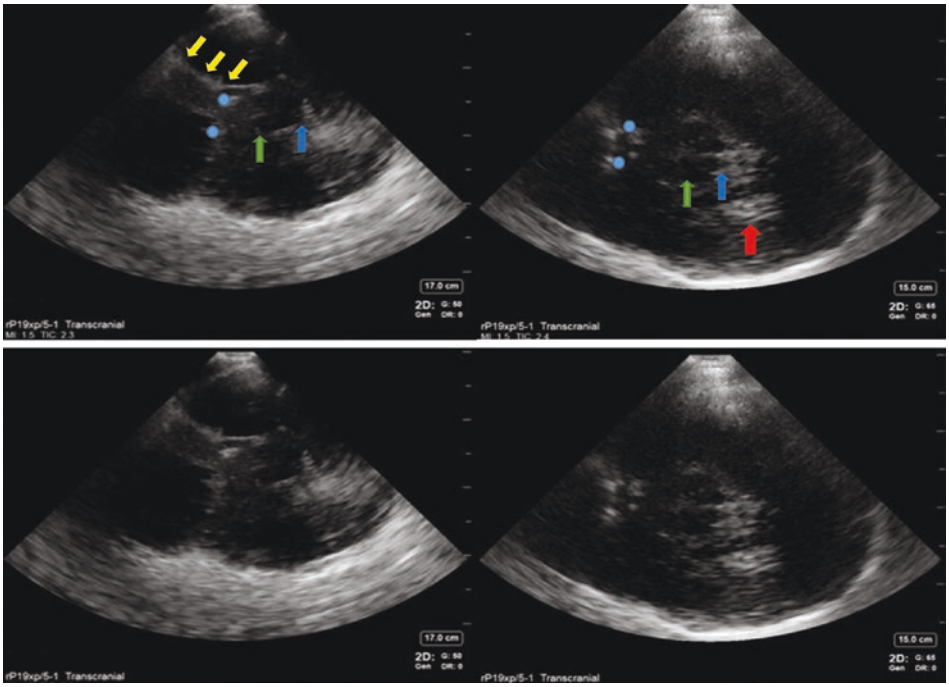

Fig. 18.3 Cranial ultrasound showing the clinoid processes blue dots, sphenoid wing (yellow arrows), midbrain green arrow, and basal cisterns (blue arrow). The Choroid plexus in the temporal horn is visible as a hyperechoic signal (red arrow)

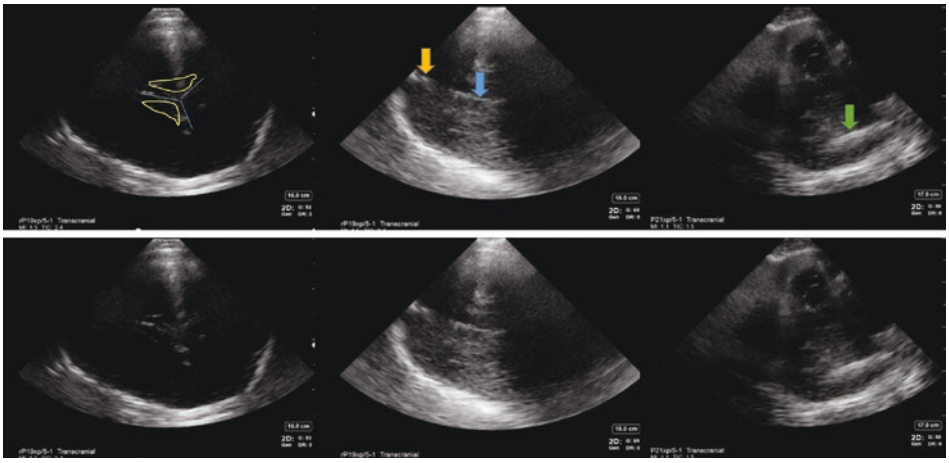

Fig. 18.4 Left images show the appearance of lateral ventricles with the anechoic appearance of cerebrospinal fluid and hyperechoic signals produced by the ependymal (yellow line) and choroid plexus (blue line). The middle image shows the crista galli (yellow arrow) and falx cerebri (blue arrow) with acoustic enhancement artifacts created by the falx. The right image shows the occipital bone with a ridge (green arrow) outlining the transverse venous sinus

Other reproducible structures produced on B-mode cranial ultrasound include:

- The arachnoid in the basal cisterns outlining the hypoechoic appearance of the midbrain.
- Thalami can be visible on either side of the midline at the level above the midbrain.
- Lateral ventricles that appear hypoechoic with Y-shaped outline created by the hyperechoic choroid plexus. Cerebrospinal fluid is typically hypoechoic or anechoic with ependyma or choroid plexus forming brighter margins. Calcified choroid plexus in the temporal horns can also be visible at the level of the midbrain.
- The cerebral aqueduct visible as a hyperechoic signal within the midbrain
- The third ventricle visible as two hyperechoic parallel lines anterior to the hypoechoic midbrain or the surrounding hypoechoic thalamus.
- The falx cerebri visible as hyperechoic linear density outlining the middle part of the brain.
- The pineal gland can be seen as a hyperechoic structure posterior to the midbrain.

There are several artifacts produced by the posterior through-transmission in cranial ultrasound (◘ Fig. 18.5). Most of these artifacts appear geometric and conform to the boundaries of the hypoechoic signal marking the proximal origin and disappearing when the brain is scanned from a different angle.

These include:

- Acoustic shadows created by the petrous part of the temporal bone.
- Acoustic enhancement creating shadows related to the midbrain as well as tentorium cerebelli
- Ring-down artifact visualized especially in relation to the clinoid processes

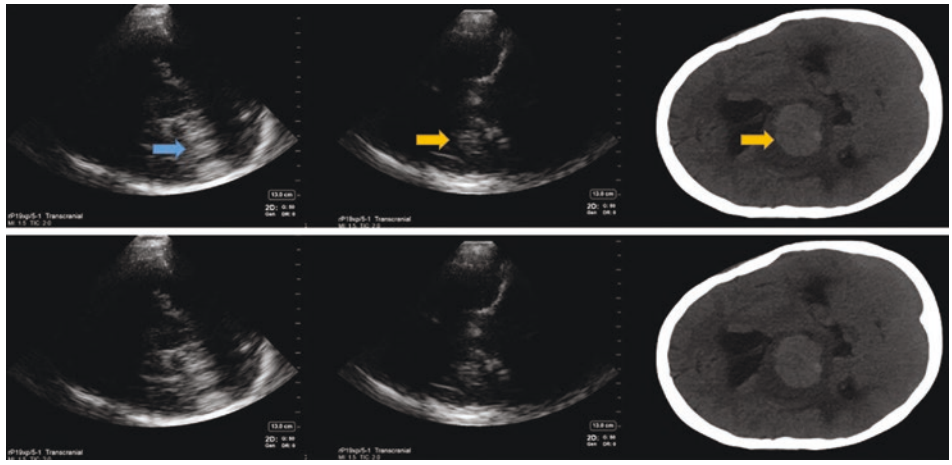

◘ **Fig. 18.5** The left image shows the axial section of the brain with acoustic enhancement (blue arrow) in line with the midbrain caused by posterior through transmission. The middle image shows the distinct appearance of a basal ganglia tumor (yellow arrow) next to the midbrain shadow and the corresponding images on computed tomography (right image)

A distinction of the brain structures in the basal ganglia or distinction between the white and gray matter in the brain parenchyma is typically not possible with conventional B-mode cranial ultrasound in a patient with an intact skull. Patients with skull defects or hemicraniectomy often have significant high-resolution images on cranial ultrasound [13].

18.2 Evaluation of Parenchymal Pathology

The use of cranial ultrasound for the distinction of parenchymal pathology has been investigated in the past but was foregone due to easy accessibility to computed tomography scan which has much better resolution and higher accuracy. The increasing acuity of patients in critical care and acute care setting has since brought forth the emergence of interest in exploring cranial ultrasound applications. Most current studies informing the accuracy of ultrasound-based detection of intracranial pathology are limited by case-control studies in small populations, and there is a dire need for widespread population-based blinded studies to assess the true feasibility of using cranial ultrasound for the detection of brain abnormalities in the community settings.

Ischemic stroke evaluation While evaluation of ischemic stroke using transcranial Doppler to assess for large vessel occlusions has been explored, studies have not shown any distinguishing features of ischemic stroke or cytotoxic edema that can help in point-of-care detection of brain infarcts on B-mode cranial ultrasound [12, 14, 15]. Extensive white matter disease, or leukoaraiosis, and vasogenic cerebral edema can both produce hyperechoic signals [16]. Encephalomalacia typically does not reveal distinct signals on ultrasound.

Intracranial hemorrhage Intracerebral hemorrhage in the brain parenchyma can produce distinct hyperechoic signals to allow ultrasound-based detection of ICH (Fig. 18.6). Detection of ICH is most facilitated by imaging the contralateral half of the brain and adjusting the probe direction to visualize the maximum dimension of the hematoma. The current repertoire of studies favors the feasibility of ultrasound-based detection of ICH in supratentorial bleeds more than 1 cm in size, restricted to basal ganglia and lobar locations below high vertex. The hyperechoic signal of ICH fades away after 5–7 days and becomes indistinguishable from normal brain parenchyma in 2–4 weeks [14, 16–32]. Some studies have explored sonographic volumetry in supratentorial intracerebral hemorrhage and shown significant correlations between cranial ultrasound-derived hemorrhage volume with ICH volume measured on CT scan [22, 33]. Efforts have also been made to improve the detection of hemorrhage and its volumes by ultrasound perfusion imaging though widespread validation has not been investigated [26].

The characteristic appearance of hemorrhage-producing hyperechoic signals has been utilized to assess for hemorrhagic conversion in ischemic strokes after reperfusion but studies validating the degree of hemorrhagic conversion against known quantitative classification for hemorrhagic conversion have not been performed [21, 34–36].

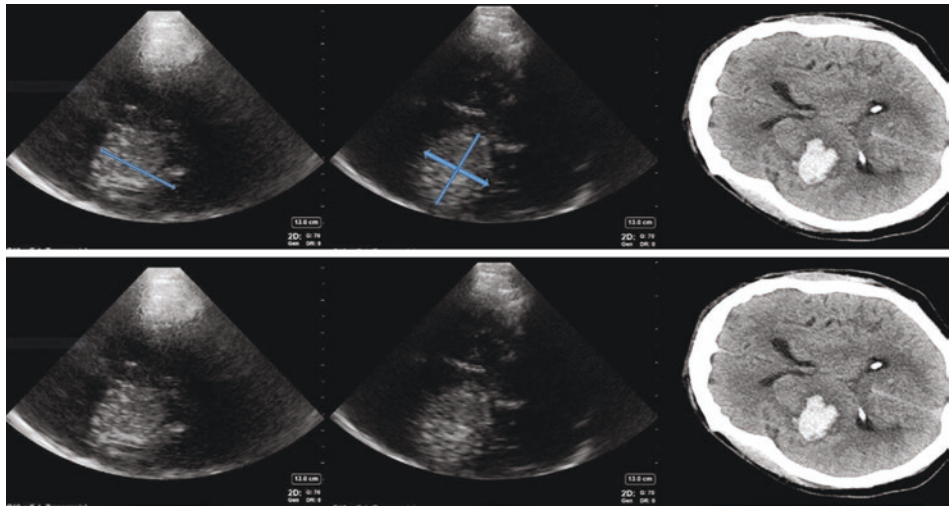

Fig. 18.6 Appearance of intracranial hemorrhage in the coronal plane (left image) and the axial plane (middle image) through the temporal windows on cranial ultrasound to get volume measurements of the hemorrhage. Corresponding images of the computer tomography are shown in the right image

Subarachnoid hemorrhage typically produces a hyperechoic signal that looks similar to the hyperechoic signal seen in basal cisterns and hence cannot be distinctly diagnosed using ultrasound (Fig. 18.3). Only one study showed a visualization of subarachnoid hemorrhage with ultrasound [37]. Intraventricular hemorrhage is more distinctly visible with a significantly hyperechoic signal in the expected anechoic ventricular location with the density of the signals more in line with the skull density than that is seen by the lesser density abnormal choroid plexus [37].

The distinct appearance of the opposite skull and inner table has been used to investigate the possibility of diagnosing epidural and subdural hematomas using cranial ultrasound on the side opposite to probe placement. Hyperacute extra-axial intracranial bleeds can be visible as hyperechoic signals increasing the width of the opposite skull and obscuring the crisp-clear inner table otherwise visible in normal skulls [19, 38, 39]. Subdural hemorrhage of different ages or septations may be difficult to diagnose with ultrasound.

Tumors A series of studies have investigated diagnoses and follow-up for intracranial tumors using B-mode cranial ultrasound [40–43] (Fig. 18.5). Most of the studies have been restricted to the diagnosis of gliomas and pineal gland cysts [44, 45]. There has been an exploration of the intraoperative use of ultrasound in detecting residual brain tumors after resection. The reliability of intraoperative ultrasound in detecting tumor residuals after brain diffuse glioma surgery has been explored but diagnostic accuracy is compromised by previous radiation and surgical treatments, surgical artifacts, and small tumor residue volumes [46].

Neurodegenerative diseases Myriad studies have assessed the use of ultrasound for the diagnosis of Wilson's disease, Parkinson's disease, Huntington's disease, and progressive supranuclear palsy patients [47–61]. Although high-resolution cranial ultrasound can detect classical basal ganglia findings in the disease processes, the low sensitivity, specificity, and accuracy of cranial ultrasound and lack of acute care-/critical care-related presentations impacted by ultrasound precludes point-of-care application of ultrasound in these disease processes.

Cerebral edema assessment with midline shift Assessment of cerebral edema progression in a patient with acute brain injury is one of the most exacting clinical applications of point-of-care ultrasound especially in patients with high intracranial pressure that cannot be lying flat for neuroimaging. Direct representation of cisternal or ventricular effacement or gray-white de-differentiation has been attempted but not found to have a distinct appearance on B-mode cranial ultrasound [37]. Midline shift assessment has been a reproducible surrogate for cerebral edema assessment and the midline structure most commonly used for assessing the shift on ultrasound has been the third ventricle [33, 62–65] (◘ Fig. 18.7). An axial image of the brain using B-mode cranial ultrasound is used with the third ventricle visualized in the middle. Typically, the same image acquired from one side is used to calculate the distance between the ipsilateral skull and the third ventricle and then the distance between the third ventricle and the contralateral skull. Some people prefer measuring midline shift from each side if both temporal windows are present. Such assessment of midline shift using ultrasound has been correlated to CT measures of midline shift with high correlation coefficients when the same midline structure was used [64, 66–68]. The pineal gland and septum pellucidum can also be used for midline shift but have not been explored in cranial ultrasound literature.

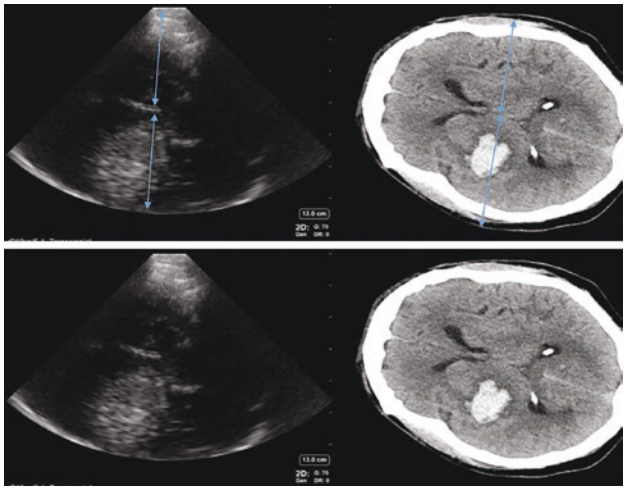

◘ **Fig. 18.7** Measurement of the midline shift in the axial plane (left image) through the temporal windows on cranial ultrasound with ipsilateral and contralateral measurements in the same plane. Corresponding images of the computer tomography are shown in the right image

Evaluation of hydrocephalus Multiple studies have explored the detection of hydrocephalus using cranial ultrasound by using the axial dimensions of the third ventricle and lateral ventricle as surrogates [3, 69, 70] (Fig. 18.8). While studies correlating the size of individual ventricles with CT scans showed early promising results, a widespread application has not materialized due to challenges in exact identification of ventricular structures and lack of availability of age validated normal cutoffs for size adjusting for an increase in ventricular size due to cerebral atrophy [37, 71, 72]. In addition, comprehensive ventricular assessment using ultrasound for accurate detection of hydrocephalus has been lacking. Investigations in posthemorrhagic hydrocephalus undergoing an external ventricular drainage clamp trial have shown correlations between ventricular size and success of the EVD clamp trial [69]. This may provide signals for the use of ventricular size on ultrasound for serial assessments rather than absolute values. Pneumocephalus is typically not visible with ultrasound.

External ventricular drainage placement EVD catheters with stylet can be visualized as distinct geometric structures that appear as hyperechoic lines (Fig. 18.9). Anecdotal reports have shown the use of ultrasound to guide and confirm the placement of external ventricular drainage catheter in-patient with hemicraniectomy [73, 74]. Cranial ultrasound examination during catheter insertion is made feasible by visualization of the metal stylet from the temporal window opposite to the site of insertion. EVD catheters themselves may not be clearly visible after the stylet is withdrawn.

Clinical application in hemicraniectomy patients Multiple series have described the use of cranial ultrasound in axial and coronal planes in patients with hemicraniectomy beyond the cerebral hemodynamic monitoring using transcranial Doppler [13, 75, 76] (Fig. 18.10). Transcranial preset has high mechanical and thermal index and has potential of heating the brain tissue hence imaging in patients with skull defects is recommended in abdominal preset that has considerably lower mechanical and thermal

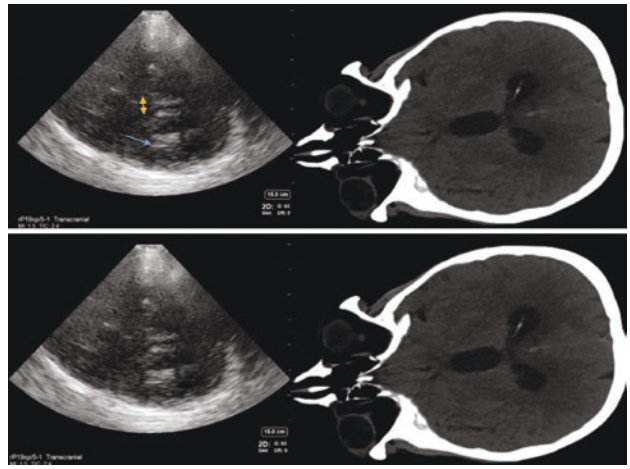

Fig. 18.8 The left image shows an enlargement of the third ventricle (double-headed yellow arrow) seen on the axial section on cranial ultrasound. The choroid plexus in the temporal horn of the lateral ventricle is also visible as a hyperechoic signal (blue arrow). Corresponding computed tomography images on the right side

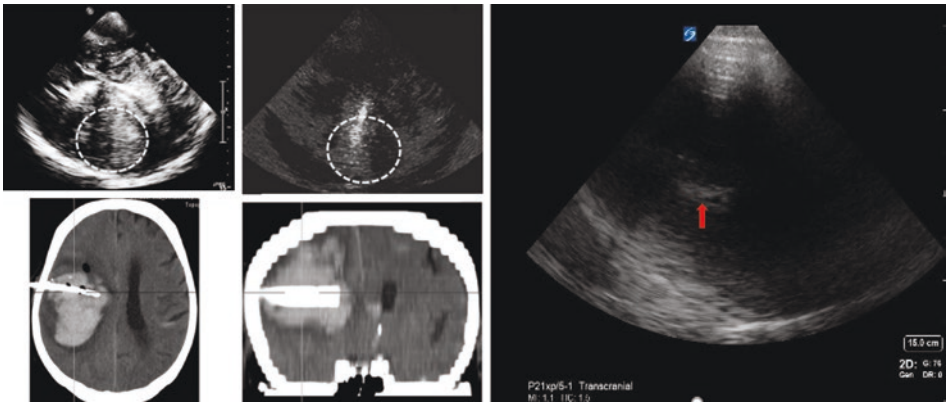

Fig. 18.9 The right panel shows B-mode cranial ultrasound showing intracranial hematoma and positioning of an external ventricular drainage catheter in the right frontal ventricle (image from Neisen et al. Front Neurol 2018;9;651 Open access distributed under the terms of Creative Commons Attribution License). The left image shows the cranial ultrasound appearance of the external ventricular drain in the right frontal area

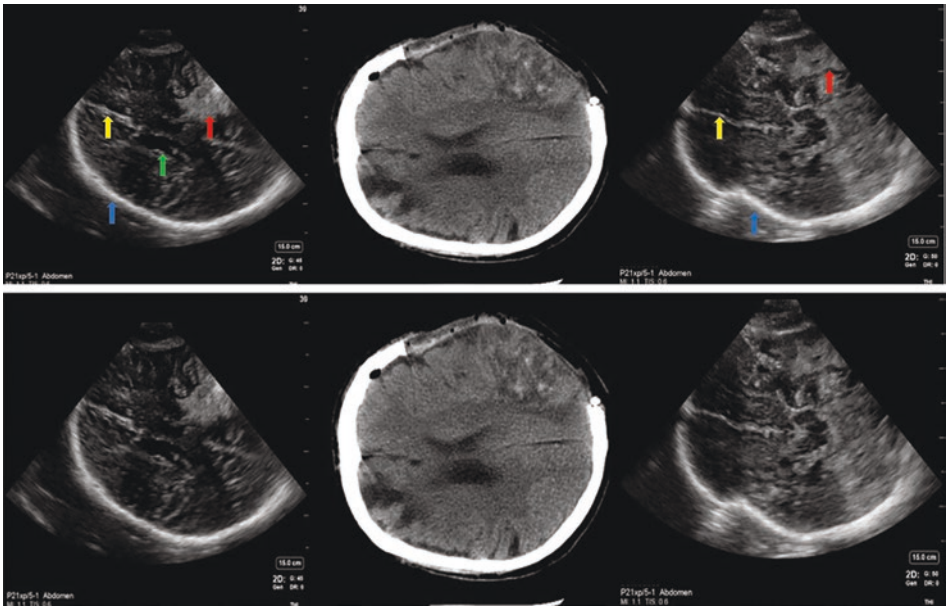

Fig. 18.10 B-mode cranial ultrasound in the abdominal present in a patient with hemicraniectomy. In addition to the opposite skull, the falx cerebri, lateral ventricles, midbrain, and vasogenic edema related to hemorrhage after evacuation are clearly visible. The middle image shows the computed tomography image

index (Fig. 18.10). The studies have described serial monitoring for frontal horn size, third ventricular size, midline shift assessment, evaluation of interhemispheric hygromas, and evaluation for uncal herniation marked by effacement of the basal cistern hyperechoic signal [77]. Other studies involving ultrasound in hemicraniectomy patients and intraoperative ultrasound have described its use in diagnosing cytotoxic edema and

have defined cerebral edema as moderately hyperechoic that becomes isoechoic to the surrounding brain parenchyma with time [78]. Without the restrictions of the skull, ventricular size measurements have been hypothesized to be more accurate in the coronal rather than the axial plane.

Take-Home Messages

- B-mode cranial ultrasound is a low-risk bedside diagnostic tool that can be used in the evaluation of patients in critical care or austere environments where conventional neuroimaging may not be accessible.
- Further investigations into the topography of normal and abnormal brain on B-mode cranial ultrasound will help streamline future clinical trials testing the utility of field applications of B-mode cranial ultrasound.

Summary

Cranial ultrasound has the potential of being a diagnostic tool in patients with temporal windows or skull defects to assess for intracranial pathology as well as surrogates of cerebral edema in the critical care setting where conventional neuroimaging is not feasible. Widespread clinical applications will require enhancing awareness and knowledge of cranial topography on B-mode ultrasound.

References

1. Walter U. Transcranial sonography of the cerebral parenchyma: update on clinically relevant applications. Pers Med. 2012;1(1):334–43.
2. Caricato A, Pitoni S, Montini L, Bocci MG, Annetta P, Antonelli M. Echography in brain imaging in intensive care unit: state of the art. World J Radiol. 2014;6(9):636–42.
3. Robba C, Goffi A, Geeraerts T, Cardim D, Via G, Czosnyka M, et al. Brain ultrasonography: methodology, basic and advanced principles and clinical applications. A narrative review. Intensive Care Med. 2019;45(7):913–27.
4. Kaps MN, Erwin S, Tibo G, Ralf WB, Giovanni M, Guenter S, et al. Consensus recommendations for transcranial color-coded duplex sonography for the assessment of intracranial arteries in clinical trials on acute stroke. 2009.
5. Valaikiene J, Schlachetzki F, Azevedo E, Kaps M, Lochner P, Katsanos AH, et al. Point-of-care ultrasound in neurology - report of the EAN SPN/ESNCH/ERcNsono Neuro-POCUS Working Group. Ultraschall Med. 2022;43(4):354–66.
6. Millet A, Evain JN, Desrumaux A, Francony G, Bouzat P, Mortamet G. Clinical applications of transcranial Doppler in non-trauma critically ill children: a scoping review. Childs Nerv Syst. 2021;37(9):2759–68.
7. Lau VI, Arntfield RT. Point-of-care transcranial Doppler by intensivists. Crit Ultrasound J. 2017;9(1):21.
8. Robba C, Wong A, Poole D, Al Tayar A, Arntfield RT, Chew MS, et al. Basic ultrasound head-to-toe skills for intensivists in the general and neuro intensive care unit population: consensus and expert recommendations of the European Society of Intensive Care Medicine. Intensive Care Med. 2021;47(12):1347–67.
9. Robba C, Poole D, Citerio G, Taccone FS, Rasulo FA. Brain ultrasonography consensus on skill recommendations and competence levels within the critical care setting. Neurocrit Care. 2020;32(2):502–11.
10. Marinoni M, Ginanneschi A, Forleo P, Amaducci L. Technical limits in transcranial Doppler recording: inadequate acoustic windows. Ultrasound Med Biol. 1997;23(8):1275–7.

11. Lin Y-P, Fu M-H, Tan T-Y. Factors associated with no or insufficient temporal bone window using transcranial color-coded sonography. J Med Ultrasound. 2015;23(3):129–32.
12. Kapoor S, Offnick A, Allen B, Brown PA, Sachs JR, Gurcan MN, et al. Brain topography on adult ultrasound images: techniques, interpretation, and image library. J Neuroimaging. 2022;32:1013.
13. Sarwal A, Elder NM. Point-of-care cranial ultrasound in a hemicraniectomy patient. Clin Pract Cases Emerg Med. 2018;2(4):375–7.
14. Becker G, Winkler J, Hofmann E, Bogdahn U. Differentiation between ischemic and hemorrhagic stroke by transcranial color-coded real-time sonography. J Neuroimaging. 1993;3(1):41–7.
15. Antipova D, Eadie L, Macaden AS, Wilson P. Diagnostic value of transcranial ultrasonography for selecting subjects with large vessel occlusion: a systematic review. Ultrasound J. 2019;11(1):29.
16. Mäurer M, Shambal S, Berg D, Woydt M, Hofmann E, Georgiadis D, et al. Differentiation between intracerebral hemorrhage and ischemic stroke by transcranial color-coded duplex-sonography. Stroke. 1998;29(12):2563–7.
17. Camps-Renom P, Méndez J, Granell E, Casoni F, Prats-Sánchez L, Martínez-Domeño A, et al. Transcranial duplex sonography predicts outcome following an intracerebral hemorrhage. AJNR Am J Neuroradiol. 2017;38(8):1543–9.
18. Lindner A, Gahn G, Becker G. Transcranial duplex sonography of hyperacute intracerebral hemorrhages. J Neuroimaging. 1997;7(3):199–202.
19. Masaeli M, Chahardoli M, Azizi S, Shekarchi B, Sabzghabaei F, Shekar Riz Fomani N, et al. Point of care ultrasound in detection of brain hemorrhage and skull fracture following pediatric head trauma; a diagnostic accuracy study. Arch Acad Emerg Med. 2019;7(1):e53.
20. Matsumoto N, Kimura K, Iguchi Y, Aoki J. Evaluation of cerebral hemorrhage volume using transcranial color-coded duplex sonography. J Neuroimaging. 2011;21(4):355–8.
21. Niesen WD, Schläger A, Reinhard M, Fuhrer H. Transcranial sonography to differentiate primary intracerebral hemorrhage from cerebral infarction with hemorrhagic transformation. J Neuroimaging. 2018;28(4):370–3.
22. Niesen WD, Schlaeger A, Bardutzky J, Fuhrer H. Correct outcome prognostication via sonographic volumetry in supratentorial intracerebral hemorrhage. Front Neurol. 2019;10:492.
23. Ovesen C, Christensen AF, Krieger DW, Rosenbaum S, Havsteen I, Christensen H. Time course of early postadmission hematoma expansion in spontaneous intracerebral hemorrhage. Stroke. 2014;45(4):994–9.
24. Wang HS, Kuo MF, Huang SC, Chou ML, Hung PC, Lin KL. Transcranial ultrasound diagnosis of intracranial lesions in children with headaches. Pediatr Neurol. 2002;26(1):43–6.
25. Woydt M, Greiner K, Perez J, Becker G, Krone A, Roosen K. Transcranial duplex-sonography in intracranial hemorrhage. Evaluation of transcranial duplex-sonography in the diagnosis of spontaneous and traumatic intracranial hemorrhage. Zentralbl Neurochir. 1996;57(3):129–35.
26. Kern R, Kablau M, Sallustio F, Fatar M, Stroick M, Hennerici MG, et al. Improved detection of intracerebral hemorrhage with transcranial ultrasound perfusion imaging. Cerebrovasc Dis (Basel, Switzerland). 2008;26(3):277–83.
27. Kukulska-Pawluczuk B, Książkiewicz B, Nowaczewska M. Imaging of spontaneous intracerebral hemorrhages by means of transcranial color-coded sonography. Eur J Radiol. 2012;81(6):1253–8.
28. Seidel G, Kaps M, Dorndorf W. Transcranial color-coded duplex sonography of intracerebral hematomas in adults. Stroke. 1993;24(10):1519–27.
29. Seidel G, Cangur H, Albers T, Meyer-Wiethe K. Transcranial sonographic monitoring of hemorrhagic transformation in patients with acute middle cerebral artery infarction. J Neuroimaging. 2005;15(4):326–30.
30. Seidel G, Cangür H, Albers T, Burgemeister A, Meyer-Wiethe K. Sonographic evaluation of hemorrhagic transformation and arterial recanalization in acute hemispheric ischemic stroke. Stroke. 2009;40(1):119–23.
31. Meyer-Wiethe K, Sallustio F, Kern R. Diagnosis of intracerebral hemorrhage with transcranial ultrasound. Cerebrovasc Dis (Basel, Switzerland). 2009;27(Suppl 2):40–7.
32. Seidel G, Kaps M, Gerriets T. Potential and limitations of transcranial color-coded sonography in stroke patients. Stroke. 1995;26(11):2061–6.
33. Tang SC, Huang SJ, Jeng JS, Yip PK. Third ventricle midline shift due to spontaneous supratentorial intracerebral hemorrhage evaluated by transcranial color-coded sonography. J Ultrasound Med. 2006;25(2):203–9.

34. Seidel G, Cangür H, Albers T, Burgemeister A, Meyer W. Sonographic evaluation of hemorrhagic transformation and arterial recanalization in acute hemispheric ischemic stroke. Stroke. 2009;40(1):119.
35. Seidel G, Cangür H, Albers T, Meyer W. Transcranial sonographic monitoring of hemorrhagic transformation in patients with acute middle cerebral artery infarction. J Neuroimaging. 2005;15(4):326.
36. Kummer RV, Broderick JP, Campbell BCV, Demchuk A, Goyal M, Hill MD, et al. The Heidelberg bleeding classification. Stroke. 2015;46(10):2981–6.
37. Becker G, Greiner K, Kaune B, Winkler J, Brawanski A, Warmuth-Metz M, et al. Diagnosis and monitoring of subarachnoid hemorrhage by transcranial color-coded real-time sonography. Neurosurgery. 1991;28(6):814–20.
38. Niesen WD, Rosenkranz M, Weiller C. Bedsided transcranial sonographic monitoring for expansion and progression of subdural hematoma compared to computed tomography. Front Neurol. 2018;9:374.
39. Niesen WD, Burkhardt D, Hoeltje J, Rosenkranz M, Weiller C, Sliwka U. Transcranial grey-scale sonography of subdural haematoma in adults. Ultraschall Med. 2006;27(3):251–5.
40. Becker G, Hofmann E, Woydt M, Hülsmann U, Maurer M, Lindner A, et al. Postoperative neuroimaging of high-grade gliomas: comparison of transcranial sonography, magnetic resonance imaging, and computed tomography. Neurosurgery. 1999;44(3):469–78.
41. Becker G, Krone A, Koulis D, Lindner A, Hofmann E, Roggendorf W, et al. Reliability of transcranial colour-coded real-time sonography in assessment of brain tumours: correlation of ultrasound, computed tomography and biopsy findings. Neuroradiology. 1994;36(8):585–90.
42. Becker G, Krone A, Schmitt K, Woydt M, Hofmann E, Lindner A, et al. Preoperative and postoperative follow-up in high-grade gliomas: comparison of transcranial color-coded real-time sonography and computed tomography findings. Ultrasound Med Biol. 1995;21(9):1123–35.
43. Meyer K, Seidel G, Knopp U. Transcranial sonography of brain tumors in the adult: an in vitro and in vivo study. J Neuroimaging. 2001;11(3):287–92.
44. Budisic M, Bosnjak J, Lovrencic-Huzjan A, Mikula I, Bedek D, Demarin V. Pineal gland cyst evaluated by transcranial sonography. Eur J Neurol. 2008;15(3):229–33.
45. Budisić M, Bosnjak J, Lovrencić-Huzjan A, Strineka M, Bene R, Azman D, et al. Transcranial sonography in the evaluation of pineal lesions: two-year follow up study. Acta Clin Croat. 2008;47(4):205–10.
46. Trevisi G, Barbone P, Treglia G, Mattoli MV, Mangiola A. Reliability of intraoperative ultrasound in detecting tumor residual after brain diffuse glioma surgery: a systematic review and meta-analysis. Neurosurg Rev. 2020;43(5):1221–33.
47. Alonso-Canovas A, Lopez-Sendon Moreno JL, Buisan J, Sainz de la Maza S, Costa-Frossard L, Garcia-Ribas G, et al. Does normal substantia nigra echogenicity make a difference in Parkinson's disease diagnosis? A real clinical practice follow-up study. J Neurol. 2018;265(10):2363–9.
48. Bártová P, Kraft O, Bernátek J, Havel M, Ressner P, Langová K, et al. Transcranial sonography and (123)I-FP-CIT single photon emission computed tomography in movement disorders. Ultrasound Med Biol. 2014;40(10):2365–71.
49. Bor-Seng-Shu E, Pedroso JL, Felicio AC, Ciampi de Andrade D, Teixeira MJ, Braga-Neto P, et al. Substantia nigra echogenicity and imaging of striatal dopamine transporters in Parkinson's disease: a cross-sectional study. Parkinsonism Relat Disord. 2014;20(5):477–81.
50. Doepp F, Plotkin M, Siegel L, Kivi A, Gruber D, Lobsien E, et al. Brain parenchyma sonography and 123I-FP-CIT SPECT in Parkinson's disease and essential tremor. Mov Disord. 2008;23(3):405–10.
51. Gaenslen A, Unmuth B, Godau J, Liepelt I, Di Santo A, Schweitzer KJ, et al. The specificity and sensitivity of transcranial ultrasound in the differential diagnosis of Parkinson's disease: a prospective blinded study. Lancet Neurol. 2008;7(5):417–24.
52. Hagenah JM, König IR, Becker B, Hilker R, Kasten M, Hedrich K, et al. Substantia nigra hyperechogenicity correlates with clinical status and number of Parkin mutated alleles. J Neurol. 2007;254(10):1407–13.
53. Hellwig S, Reinhard M, Amtage F, Guschlbauer B, Buchert R, Tüscher O, et al. Transcranial sonography and [18F]fluorodeoxyglucose positron emission tomography for the differential diagnosis of parkinsonism: a head-to-head comparison. Eur J Neurol. 2014;21(6):860–6.

54. Li DH, Zhang LY, Hu YY, Jiang XF, Zhou HY, Yang Q, et al. Transcranial sonography of the substantia nigra and its correlation with DAT-SPECT in the diagnosis of Parkinson's disease. Parkinsonism Relat Disord. 2015;21(8):923–8.
55. Lobsien E, Schreiner S, Plotkin M, Kupsch A, Schreiber SJ, Doepp F. No correlation of substantia nigra echogenicity and nigrostriatal degradation in Parkinson's disease. Mov Disord. 2012;27(3):450–3.
56. Mašková J, Školoudík D, Burgetová A, Fiala O, Brůha R, Záhoráková D, et al. Comparison of transcranial sonography-magnetic resonance fusion imaging in Wilson's and early-onset Parkinson's diseases. Parkinsonism Relat Disord. 2016;28:87–93.
57. Schweitzer KJ, Hilker R, Walter U, Berg D. Substantia nigra hyperechogenicity as a marker of predisposition and slower progression in Parkinson's disease. Mov Disord. 2006;21(1):94–8.
58. Spiegel J, Hellwig D, Möllers MO, Behnke S, Jost W, Fassbender K, et al. Transcranial sonography and [123I]FP-CIT SPECT disclose complementary aspects of Parkinson's disease. Brain. 2006;129(Pt 5):1188–93.
59. Sprenger FS, Wurster I, Seppi K, Stockner H, Scherfler C, Sojer M, et al. Substantia nigra hyperechogenicity and Parkinson's disease risk in patients with essential tremor. Mov Disord. 2016;31(4):579–83.
60. Vlaar AM, de Nijs T, van Kroonenburgh MJ, Mess WH, Winogrodzka A, Tromp SC, et al. The predictive value of transcranial duplex sonography for the clinical diagnosis in undiagnosed parkinsonian syndromes: comparison with SPECT scans. BMC Neurol. 2008;8:42.
61. Weise D, Lorenz R, Schliesser M, Schirbel A, Reiners K, Classen J. Substantia nigra echogenicity: a structural correlate of functional impairment of the dopaminergic striatal projection in Parkinson's disease. Mov Disord. 2009;24(11):1669–75.
62. Seidel G, Gerriets T, Kaps M, Missler U. Dislocation of the third ventricle due to space-occupying stroke evaluated by transcranial duplex sonography. J Neuroimaging. 1996;6(4):227–30.
63. Gerriets T, Stolz E, König S, Babacan S, Fiss I, Jauss M, et al. Sonographic monitoring of midline shift in space-occupying stroke. Stroke. 2001;32(2):442–7.
64. Motuel J, Biette I, Srairi M, Mrozek S, Kurrek MM, Chaynes P, et al. Assessment of brain midline shift using sonography in neurosurgical ICU patients. Crit Care. 2014;18(6):676.
65. Siepen BM, Grubwinkler S, Wagner A, Gruber C, Dickopf A, Linker RA, et al. Neuromonitoring using neurosonography and pupillometry in a weaning and early neurorehabilitation unit. J Neuroimaging. 2020;30(5):631–9.
66. Stolz E, Gerriets T, Fiss I, Babacan SS, Seidel G, Kaps M. Comparison of transcranial color-coded duplex sonography and cranial CT measurements for determining third ventricle midline shift in space-occupying stroke. AJNR Am J Neuroradiol. 1999;20(8):1567–71.
67. Llompart Pou JA, Abadal Centellas JM, Palmer Sans M, Pérez Bárcena J, Casares Vivas M, Homar Ramírez J, et al. Monitoring midline shift by transcranial color-coded sonography in traumatic brain injury. A comparison with cranial computerized tomography. Intensive Care Med. 2004;30(8):1672–5.
68. Bertram M, Khoja W, Ringleb P, Schwab S. Transcranial colour-coded sonography for the bedside evaluation of mass effect after stroke. Eur J Neurol. 2000;7(6):639–46.
69. Kiphuth IC, Huttner HB, Struffert T, Schwab S, Köhrmann M. Sonographic monitoring of ventricle enlargement in posthemorrhagic hydrocephalus. Neurology. 2011;76(10):858–62.
70. Harrer JU, Tsivgoulis G. Transcranial sonography for monitoring hydrocephalus: an underestimated imaging modality. Neurology. 2011;76(10):852–3.
71. Müller M, Esser R, Kötter K, Voss J, Müller A, Stellmes P. Width of 3. Ventricle: reference values and clinical relevance in a cohort of patients with relapsing remitting multiple sclerosis. Open Neurol J. 2013;7:11–6.
72. Caricato A, Ioannoni E, Gelormini C. Is it really third ventricle? A pitfall in the diagnosis of hydrocephalus by brain ultrasound. Neurocrit Care. 2020;33(3):844–6.
73. Robba C, Simonassi F, Ball L, Pelosi P. Transcranial color-coded duplex sonography for bedside monitoring of central nervous system infection as a consequence of decompressive craniectomy after traumatic brain injury. Intensive Care Med. 2019;45(8):1143–4.
74. Niesen WD, Reinhard M, Gierthmuehlen M, Fuhrer H. Sonographic-assisted catheter-positioning in intracerebral hemorrhage. Front Neurol. 2018;9:651.
75. Srinivasan V, Smith M, Bonomo J. Bedside cranial ultrasonography in patients with hemicraniectomies: a novel window into pathology. Neurocrit Care. 2019;31(2):432–3.

76. Caricato A, Mignani V, Bocci MG, Pennisi MA, Sandroni C, Tersali A, et al. Usefulness of transcranial echography in patients with decompressive craniectomy: a comparison with computed tomography scan. Crit Care Med. 2012;40(6):1745–52.
77. Bendella H, Maegele M, Hartmann A, Spreer J, Rommel N, Lefering R, et al. Cerebral ventricular dimensions after decompressive craniectomy: a comparison between bedside sonographic duplex technique and cranial computed tomography. Neurocrit Care. 2017;26(3):321–9.
78. Ivanov M, Wilkins S, Poeata I, Brodbelt A. Intraoperative ultrasound in neurosurgery - a practical guide. Br J Neurosurg. 2010;24(5):510–7.

Role of Brain Ultrasound for the Assessment of Intracranial Hypertension

Corina Puppo

Contents

19.1 Introduction – 292

19.2 Transcranial Doppler-Based Models Grounded in the Changes of Flow Velocities and Pulsatility Index – 293

19.2.1 TCD Models to Estimate ICP – 295

19.3 Other methods to evaluate ICP with ultrasound – 298

19.3.1 Duplex-Based Methods – 298

19.3.2 Method Based on Ophthalmic Artery (OA) Blood Flow Velocity – 300

19.3.3 Optic Nerve Sheath Diameter (ONSD) – 300

19.3.4 Ultrasonographic Pupillary Assessment – 301

19.4 Big data and Future Research – 303

References – 307

© The Author(s), under exclusive license to Springer Nature Switzerland AG 2023
C. Robba et al. (eds.), *Basic Ultrasound Skills "Head to Toe" for General Intensivists*, Lessons from the ICU,
https://doi.org/10.1007/978-3-031-32462-8_19

Learning Objectives

After reading this chapter, readers should be able to:

- Explain the pathophysiology of intracranial hypertension (ICH).
- List which changes in the TCD sonogram appear when ICH is present.
- Describe when the patient's clinical picture should alert the treating physician about the possibility of existing ICH.
- List different ultrasound methods that can be used in these patients to discard o suspect ICH.
- Discuss which circumstances can mimic intracranial hypertension with ultrasound-based methods.

19.1 Introduction

Mortality and morbidity resulting from severe head trauma are strongly related to increased intracranial pressure (ICP) which is a life-threatening complication of primary brain injury [1]. Intracranial hypertension (ICH) has been shown to be one of the most important predictors of neurological worsening and poor outcome after traumatic brain injury (TBI) [2]. Raised ICP can also occur with different etiologies of brain injuries: hemorrhagic or ischemic strokes, infections, tumors, and hydrocephalus. The direct result of elevated ICP is reduced cerebral perfusion pressure (CPP), which can result in cerebral ischemia or herniation, potentially leading to disability and increased mortality rate [3]. Clinical examination at the bedside can raise the suspicion of elevated ICP, but its ability to predict/quantify ICP is poor [4]. Limitations of clinical examination in the assessment of ICP increase significantly when the patient is unconscious, sedated, or paralyzed and intubated [5]. At present, external ventricular drainage (EVD) is considered the gold standard for ICP monitoring, and it also offers the possibility of draining cerebral spinal fluid (CSF) [6]. Intraparenchymal microtransducers also provide accurate ICP values and are currently considered standard of care. However, both techniques are positioned through an invasive technique that requires at least a drill hole through the skull, so they are not exempt from complications, such as malposition, bleeding, puncture site hematomas, seizures, and infections [7]. Moreover, in some patients it is difficult or even impossible to perform invasive ICP monitoring, because of bleeding diathesis, platelet aggregation, or coagulation disorders. In addition, there might be difficulties in finding an expert clinician able to place the transducer, the material to be used might not be always available, or the medical indication is not clear. In this context, an easy, accurate, and noninvasive ICP monitoring has been described as one of the "holy grails" of neurocritical care [3]. Ultrasonography has been extensively studied to detect intracranial hypertension at bedside. Ultrasonic methods provide the physician with a noninvasive method, widely available, and easy to be performed at bedside in severely injured patients.

Ultrasonographic methods can explore two different intracerebral effects of ICP rise: physiological and anatomical alterations. Physiologically, the hemodynamic repercussion of increased ICP consists in the reduction of the flow inside the vessels, in particular the diastolic component (this is shown by the Doppler flow velocity

measurement), whereas anatomical repercussions can be diagnosed in different ways, such as the presence of midline shift assessed through TCCD; the assessment of hematomas or hydrocephalus; the increase of the optic nerve sheath diameter (ONSD); and the concomitant use of ultrasonic pupillometry, which can evaluate the clinical changes in pupils secondary to global ischemia or to tissue distortion.

In this chapter, we provide a review of the different ultrasonic methods used for noninvasive ICH estimation.

19.2 Transcranial Doppler-Based Models Grounded in the Changes of Flow Velocities and Pulsatility Index

The most studied artery when evaluating noninvasive intracranial pressure (nICP) is the middle cerebral artery (MCA). MCA is generally found between 45 and 60 mm from the transducer through the transtemporal window. The posterior cerebral artery (PCA), anterior cerebral artery (ACA), basilar artery (BA), and ophthalmic artery (OA) can also be studied.

In a TCD sonogram, a spectrum of velocities (each point of the spectrum represents the velocity of the different blood particles) is plotted over time. These values are obtained using the Doppler principle. From this spectrum, only the instantaneous maximum velocities are extracted. The line following the instantaneous maximum velocities is called the envelope. From this envelope, three main values are defined for each pulse: peak systolic velocity (PSV), end-diastolic velocity (EDV), and mean velocity (MFV) [8]. The other important value, obtained through the relations betrween these velocities, is the pulsatility index (PI):

$$\mathrm{PI} = \left(\mathrm{PSV} - \mathrm{EDV}\right) / \mathrm{MFV}.$$

A normal PI is lower than 1, 0 (1.20 in older patients) [8]. Figure 19.1 shows a normal adult MCA Doppler sonogram. The effect of the increase in ICP results in a reduction in EDV, which occurs earlier than changes in PSV, with a consequent increase in PI. However, the use of this parameter is controversial, as the value depends not only on the change in resistance (increase in ICP), but also on CPP, arte-

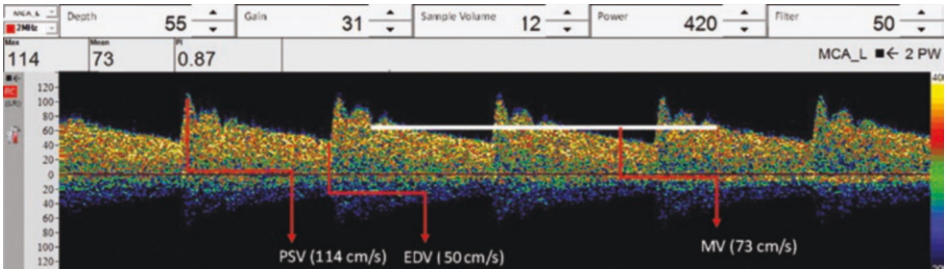

Fig. 19.1 Normal TCD sonogram of the middle cerebral artery. *PSV* peak systolic velocity, *EDV* end-diastolic velocity, *MV* mean velocity, *PI* pulsatility index. PSV: 114 cm/s, MFV: 73 cm/s, EDV: 50 cm/s, PI: 0.87

rial blood pressure, and changes in partial pressure of carbon dioxide ($PaCO_2$). A value of PI of 2.13 should be the cutoff for intracranial hypertension, as it yields an ICP value of 22 mmHg or more using Bellner's formula (see below).

More specifically, intracranial hypertension makes it difficult for the blood to go through the vascular circuit. In this situation, the cardiac reaction is to generate a more energetic systole with increased arterial pressure, and frequently bradycardia, to counteract that high ICP. As a result, the TCD waveform will initially show an increased PSV and a decreased EDV. With a further increase in ICP, all velocities will decrease. At that point, the most affected component of flow velocity will be the EDV, in second place the MFV and lastly the PSV (Fig. 19.2). If this situation worsens and the ICP continues to increase, CPP continues to decrease and the flow in diastole disappears (EDV = 0); afterwards, the flow in diastole is reversed, and later on only small images of antegrade flow are seen, at the beginning of diastole (systolic spikes). Reverberant flow, systolic spikes, and absence of flow are the three patterns included in what has been called "cerebral circulatory arrest." When this pattern is found simultaneously in the whole Willis circle, and is maintained, with a consistent clinical scenario, it supports the diagnosis of brain death (Fig. 19.3) [9].

Since PI is the wave amplitude divided by its mean velocity, as intracranial pressure increases, PI will increase, because of the higher difference between PSV and EDV and the decrease of MFV. PI correlates positively with ICP: if ICP increases, PI increases. However, increased PI is not specific to an increased ICP. There are other situations or drugs that increase pulsatility index regardless of ICP: for example, hypocapnia (which generates vasoconstriction of small resistance vessels) slows cir-

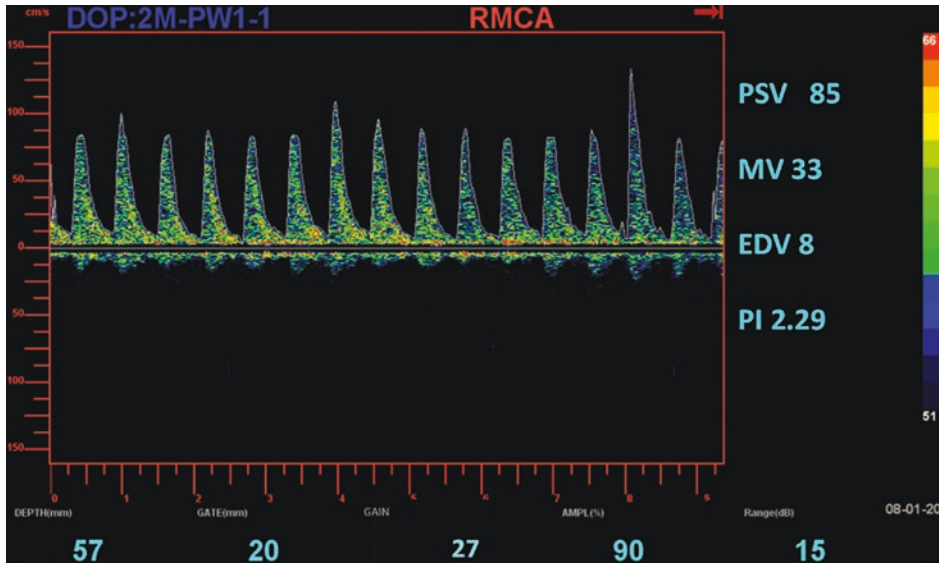

Fig. 19.2 Sonogram consistent with intracranial hypertension (ICH) in a 40-year-old patient who suffered a severe TBI during a motorcycle crash. The patient is at the ICU, sedated, and ventilated, with a GCS of 3. Symmetric pupils, hemodynamic stability. Note the increased pulsatility index (PI) and decreased mean and diastolic velocities, and the different shape of the normal sonogram, which becomes "spiky." If other circumstances which can mimic ICH are absent (severe hyperventilation, hypotension), there is a high probability that this patient has a rise in ICP

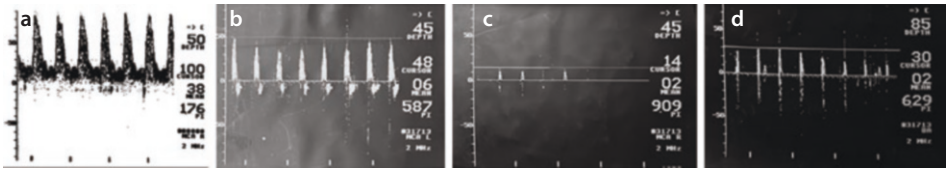

Fig. 19.3 TCD sonograms in a severe TBI 25-year-old patient. In the first sonogram (panel **a**), a high resistance pattern is seen; the mean flow velocity is 38 cm/s, and the end-diastolic velocity is 20 cm/s, with an IP of 1.76. The three images on the right were registered 24 h later. They show a cerebral circulatory arrest pattern, with a reverberant flow in panel **b** and systolic spikes in **c** and **d**. Refractory intracranial hypertension leads to cerebral circulatory arrest and brain death

culation and reduces FV velocities, diastolic above all. Indomethacin also has a similar effect. Hypotension (lower than the lower limit of cerebral autoregulation) also increases PI. PI is inversely proportional to CPP, directly proportional to ABP pulse amplitude, and nonlinearly proportional to cerebral arterial bed compliance, cerebrovascular resistance, and heart rate decrease. It must be underlined, however, that there are situations in which cerebral vascular resistance (CVR) decreases and PI increases, for example, in plateau waves of intracranial hypertension [10, 11].

19.2.1 TCD Models to Estimate ICP

These models can be schematically classified into:

(a) Models using just TCD data obtained from the FV waveform
(b) Values calculated from simultaneous FV and ABP waveform data
(c) Models of increasing complexity based on prolonged neuromonitoring registers (TCD as the unique parameter in prolonged monitoring or TCD integrating multimodal simultaneous prolonged monitoring)

(a) **Values Defined Using Only Data Obtained from the FV Wave**

- **TCD-based models** (no need for multiple neuromonitoring, just a TCD device—duplex or Doppler—with a good quality sonogram): These models can be used without a sophisticated methodology, with just a TCD at the patient's bedside. They use the PI and have variable precision. It must be remembered that PI can change due to other factors (severe arterial hypotension, indomethacin, deep sedation, $PaCO_2$, etc.). If a single sonogram is studied, a single nICP value will be obtained, not a continuous curve. nICP can also be calculated from a continuous curve of values obtained from continuous neuromonitoring of FV with TCD. In Cardim's review, data from 22 publications that used the PI were examined [11]. Among these, the one that showed better precision was Bellner's [12]. The results of this study show that the distribution of the differences (Bland-Altman plot) between invasive and noninvasive ICP has an approximate mean of zero, and 95% of the differences are between ±4.2 mmHg. However, there have been no publications replicating these results.

Bellner's formula: nICP = (11.1 × PI) − 1.43 (nICP: noninvasive ICP)

- **TCD continuous monitoring (as a unique method)**: Velocity wave analysis over time can be performed by continuous neuromonitoring of FV with TCD. It should be emphasized that only TCD, and not TCCD-based TCD, can be used for continuous FV monitoring. The TCD monitoring transducer is significantly lighter and smaller than the duplex transducer (Fig. 19.4). It can be fixed by a circumferential band or a helmet, therefore having a reduced risk of movement and change in direction after being fixed. If the transducer moves, the insonation angle changes, and therefore the measured velocity also changes, leading to erroneous interpretation. A continuous TCD monitoring can show changes over time of an ICH wave (e.g., plateau wave), in which the diastolic and mean velocities decrease and PI increases. If TCD FV monitoring is part of a multiple neuromonitoring tool, including ABP and ICP changes, the ICP wave can be seen, and the simultaneous changes in FV and ABP can be also observed (Fig. 19.5).

(b) **Values Calculated from Simultaneous FV and ABP Waveform Data**

In this model there is no need for continuous neuromonitoring, but only:

- A TCD device—duplex or Doppler—with a good-quality sonogram
- An ABP monitor—invasive or noninvasive—showing a continuous ABP wave
- These methods have initially focused on noninvasive CPP calculation. They (1) estimate the noninvasive CPP (nCPP) and then (2) calculate the noninvasive ICP (ICP = ABP − CPP). Different researchers have approached the problem in this way:
- Czosnyka's model is based on the concept that EDV is the most altered when ICP rises. In their work, in 68% of the measurements, the error in the nICP estimate was less than 10 mmHg, and in 39% of the measurements, it was less than 5 mmHg. The formula introduced by these researchers is:
- nCPP: ABPm × EDV/MFV + 14 mmHg [13]. A recent trial using this formula in a prospective, international, multicenter study to evaluate the discriminant accuracy of TCD showed that it had a negative predictive value of 91%, 97%, and 99% for an ICP of 20, 22, and 25 mmHg, respectively [14].

Fig. 19.4 Different sizes of TCD and TCCD transducers

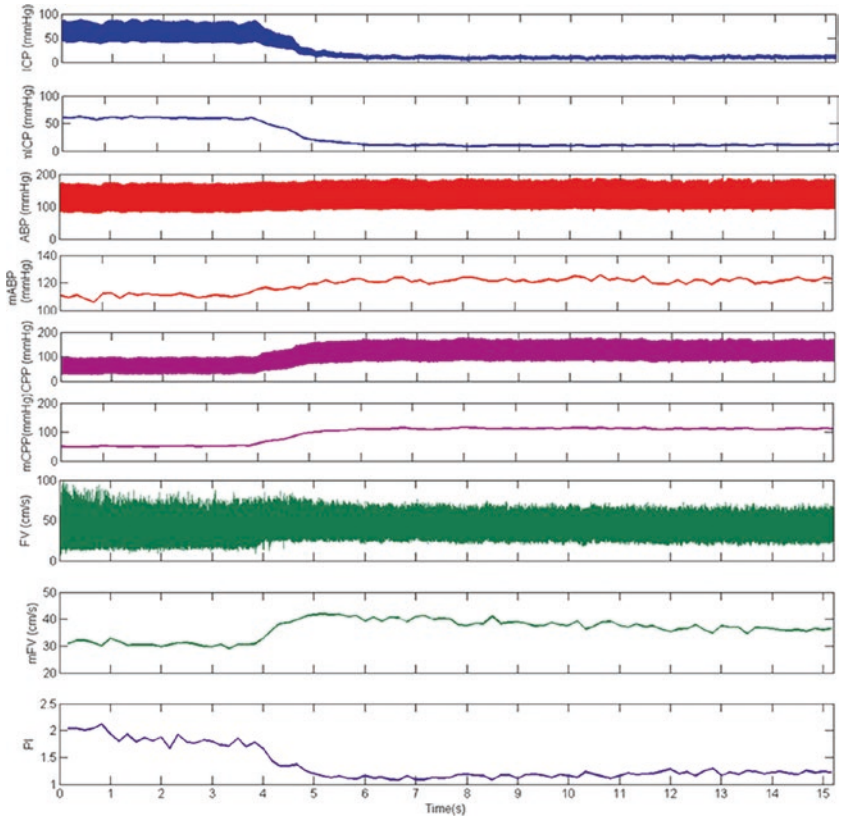

Fig. 19.5 Fifteen first minutes of a one-hour multiple neuromonitoring, in a young severe head injured patient. The following signals were monitored: intracranial pressure (ICP), arterial pressure (ABP), and cerebral blood flow velocity (FV) with transcranial Doppler (TCD). Cerebral perfusion pressure (CPP) was calculated as the difference between ABP and ICP. PI was calculated from the FV values [PI= (systolic FV - diastolic FV)/ mFV}. In the first six rows the pressure signals are shown. In descending order, the raw (showing systo-diastolic values) and mean values of each parameter (ICP, mICP, ABP, mABP, CPP, mCPP) can be seen. ICP shows a wave of intracranial hypertension (ICH) at the beginning (four initial minutes) with very high values, reaching 90 mm Hg of systolic ICP and 50 mm Hg of diastolic ICP. Mean ICP reaches 60 mm Hg. This pressure increase leads to a CPP decrease. In the three last rows the simultaneous TDC derived parameters can be observed. Systo-diastolic FV (FV), mean FV (mFV) and PI. During the plateau wave, systolic FV increases slightly, and diastolic FV decreases, increasing the FV systo-diastolic difference, (increased pulsatility). FVm during the plateau wave is decreased (30 cm/s), also contributing to the increased PI during the ICH wave shown below (violet). When ICP normalizes, which takes around one minute, PI and VF also normalize

- Edouard's model also combines the phasic values of flow velocities and arterial blood pressure. In this case, the formula is:

$$\mathrm{nCPP}: \mathrm{MFV} / \left(\mathrm{MFV} - \mathrm{EDV}\right)] \times \left(\mathrm{ABPm} - \mathrm{ABPd}\right).$$

- This model calculated the CPP as the "effective CPP" which is based on the concept of critical closing pressure [15].
- Other researchers, based on the same concept of critical closing pressure, used a more sophisticated formula to calculate nCPP in 280 patients with

traumatic injury from a big multiple neuromonitoring database. Their results showed a bias ±SD of 4.02 ± 6.01 mmHg [16].

- More models are available in Cardim's review [11].

(c) **Values Obtained from Models of Increasing Complexity Based on Data from Continuously Integrated Neuromonitoring**

Simultaneous integrated neuromonitoring includes continuous ABP and TCD. These methods need special hardware and software to capture and evaluate registered data. This allows us to obtain data of the FV and ABP waves, and frequently other monitoring devices, at a frequency of 50 Hz each. Very large files ("big data") are frequently generated that need to be studied with special computing methods, which are increasingly used in parallel with the increase in the sophistication of computing. This kind of monitoring is gradually achieving better accuracy and precision.

(d) **Limitations of TCD Continuous Monitoring**

Despite the capability to provide continuous information, TCD monitoring is laborious especially regarding the ability to fix the transducer, principally in neurocritical patients. It is even more laborious to maintain fixation: critical patients have surgical or traumatic wounds, or other monitoring tools, that hinder helmet placement. Different maneuvers or patient transfers can displace the transducer. Therefore, the helmets or bands to fix the transducers have become progressively more sophisticated. Czosnyka's group has recently evaluated a new "robotic" transducer, which uses multiple ultrasound beams and is automatically mobilized in search of the optimal signal, thereby returning to find the best place and angle if the signal is lost or if it begins to diminish, allowing longer monitoring. Using this new transducer, they showed that monitoring can last a 4-h time span [17].

19.3 Other methods to evaluate ICP with ultrasound

19.3.1 Duplex-Based Methods

Transcranial color-coded duplex ultrasonography (TCCD) can also be used to estimate nICP. It adds two modalities to TCD: a) echography and b) color-coded visualization of brain vessels. Once these are visualized, the Doppler mode is added at the identified vessels, to analyze their spectra and waveforms.

(a) **Transcranial Echography**

It shows a two-dimensional image of the brain parenchyma that can be studied in different planes. Some brain structures act as pivotal reference landmarks, like the mesencephalon, the thalamus, and the third ventricle.

Mesencephalic and diencephalic planes are obtained through axial planes. They are the most used for a noninvasive indirect ICP estimation:

- The mesencephalic plane is found by positioning the probe perpendicular to the temporal bone, cephalad to the zygomatic arch; the midbrain is seen as a hypoechogenic structure, with a butterfly shape (Fig. 19.6).

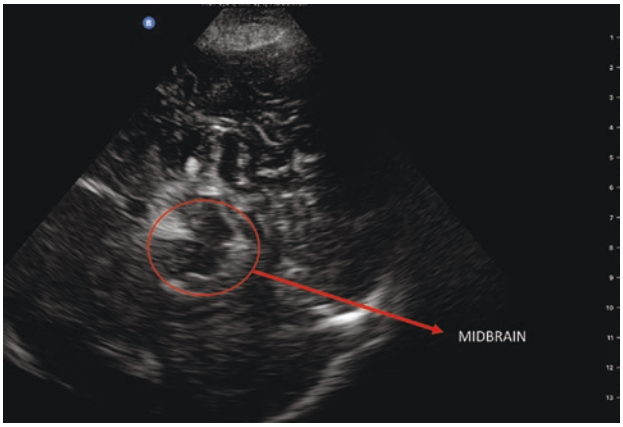

Fig. 19.6 Mesencephalic plane with TCCD. The midbrain can be seen, with its characteristic hypoechogenic "butterfly wings" shape. At this plane Willis circle will appear, with its arteries coded in red or blue depending on the blood direction, after activating the color-coded Doppler modality

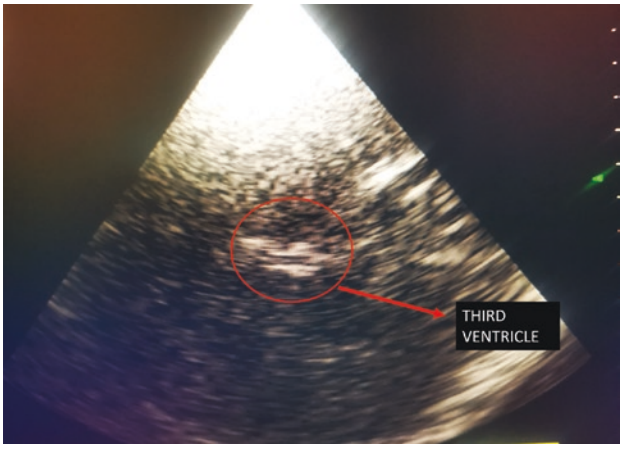

Fig. 19.7 Third ventricle plane with TCCD. The third ventricle is seen as a double hyperechogenic line. At this plane the midline shift can be measured

- The diencephalic plane, obtained by slightly tilting the transducer 10° upwards, shows the third ventricle as a bi-lineal hyperechogenic structure (Fig. 19.7). Third ventricle identification allows the measurement of midline shift (MLS), by registering the distance in mm (*A* and *B*) from the skull to the third ventricle on both sides. The formula $[(A - B)/2]$ corresponds to the midline shift. In a trial comparing CT and TCCD, the coefficient of correlation, bias, precision, and limits of agreement between MLS measured by CT and TCCDS were 0.88 mm, 0.12 mm, 1.08 mm, and +2.33 to −2.07 mm, respectively [18]. An MLS ≥ 5 mm should prompt further ICH investigation. In this plane, the hyperechogenic pineal gland can be also identified behind the third ventricle, while the thalamus and internal capsule are located anteriorly to it. The lateral ventricles can also be observed.

(b) **Color-Coded Doppler Visualization of the Brain Vessels**

Color-coded Doppler displays all the vessels found by the different echos in a selected area, colored in red if the flow direction is towards the transducer and in blue if it circulates away from the transducer. The Willis circle, MCA, and ACA can be observed at the mesencephalic plane when adding color-coded Doppler. Any segment of these blue or red displayed vessels can be selected to obtain the complete Doppler sonogram, with its full characteristics: spectrum, envelope, EDV, PFV, MFV, and PI. The changes in these characteristics when ICP increases have been referred to above, at the TCD section (19.2.2.a).

TCCD is easier in the pediatric population, due to thinner skulls and, at earlier ages, fontanelle permeability. In patients with decompressive craniectomy, the image resolution is better. In 99 adults with intact skulls, a bilateral absence of temporal acoustic window was reported in six patients when studied with both conventional TCD and TCCD, without significant differences [19]. However, there are discrepancies between authors about permeability differences. In our experience, the absence of a temporal acoustic window is more frequent when using TCCD than TCD.

19.3.2 Method Based on Ophthalmic Artery (OA) Blood Flow Velocity

Researchers from the "Health Telematics Science Institute," Kaunas University of Technology, Lithuania, have introduced a noninvasive ICP measurement method based on ophthalmic artery (OA) blood flow velocity. One of the differences between the OA and the other arteries studied with TCD is that in this artery blood flow is directed outwards: from its origin at the carotid siphon, to the orbit. It has a first deeper intracranial segment, subjected to ICP, and a more superficial extracranial segment subjected to extracranial (intraorbital) pressure. If ICP is elevated, the intracranial segment is compressed, thereby increasing its velocity to maintain flow. When it comes out, it dilates because the artery is no longer compressed. As a result, blood flow velocity decreases in the extracranial segment. The equipment developed by this group, called the "Vittamed ICP monitor," simultaneously examines the OA at both depths, using Doppler ultrasound, and then performs a progressive superficial compression of the orbital region, increasing the intraorbital pressure, until the sonograms match. The resultant nICP is the pressure needed to make both sonograms equal [20]. This method allows ICP to be measured once or intermittently; continuous monitoring cannot be performed. This system has been evaluated at NASA, because astronauts who spend a long time in space frequently have papilledema and vision loss, a condition that has been linked, among other possible causes, to ICH [21].

19.3.3 Optic Nerve Sheath Diameter (ONSD)

The ONSD measurement is based on echography. It does not evaluate the Doppler signal. It is performed at the intraorbital segment of the optic nerve (ON). This segment is elongated, has an italic S-shape, is 25–30 mm long, and is up to 3 mm in diameter. It extends from the ocular bulb to the optic canal, surrounded by CSF and

dura. The subarachnoid space surrounding the ON is connected with the intracranial subarachnoid space, specifically with the chiasmatic cistern. The ON sheath is distensible; therefore, variations in intracranial CSF pressure affect the pressure of CSF in the ON sheath, especially in its anterior compartment, conditioning an increase in its diameter. This is the basis for measuring ONSD as a noninvasive strategy for the indirect assessment of ICP. The technique uses an ultrasound machine and a linear probe, 7–15 MHz. The mode is set at "small parts" or "ophthalmic examination." The ON sheath is measured 3 mm behind the retina. At this depth, a transverse line is drawn from the inner edges of both vertical hypoechoic lines (inner borders of the dura sheath). The distance between these two points is the ONSD. In general, observational studies and meta-analyses suggest promising results regarding the correlation between ONSD and nICP, showing moderate to high sensitivity for the detection of elevated ICP (86–97%) [22]. However, there is not yet a consensus on the methodology: transducers, selected frequencies, planes, number of measures, one or both eyes, and quality of the images vary in different studies. One major question, not yet answered, is the dynamics of the ONSD changes following changes in ICP. After subarachnoid hemorrhage, a steep rise in ICP following an aneurysm rupture can cause a loss of the elastic properties of the sheath.

There is a large variation in the ONSD cutoff accepted to be related to an ICP > 20 mmHg, ranging from 4.2 to 6.5 mm with wide confidence intervals. Since a single cutoff is insufficient for the diagnosis of intracranial hypertension, some authors have incorporated a logistic regression model from which the probability of finding elevated ICP from the ONSD measurement can be determined [23]. It was observed that with ONSD values less than 5.7 mm, the probability of being in the presence of ICP above 20 mmHg is very low, while for ONSD values greater than 5.7 mm, said probability clearly increases [23]. If doubts persist, it is safer to complement the screening with other noninvasive techniques such as TCD and/or quantitative pupillometry, or even invasive ICP monitoring may be required. Further research and training projects should tend to standardize ONSD measurement techniques to implement this method at bedside in the context of a "head to toes" ultrasound patient assessment [22].

19.3.4 Ultrasonographic Pupillary Assessment

Ultrasound pupillometry (UP) is emerging as a potential surrogate of infrared pupillometry, especially when orbital trauma makes clinical and infrared examination impossible [24]. The most important application of UP would be to provide accurate pupillary assessment in patients in whom eye-opening is not possible (e.g., periorbital soft tissue posttraumatic edema) as well as in patients with significant eyelid edema that frequently appears after extensive burn injuries. This method has the advantage of allowing the use of the same instrument. The transducer (7.5–15 MHz) is placed tangentially over the inferior orbital margin, thus allowing the trans-palpebral illumination stimulus. Ultrasonographic pupillary assessment strongly correlates with infrared pupillary assessment in critically ill patients. Further studies with a larger patient population are needed.

In ◘ Table 19.1 the main characteristics of the different ultrasound methods available for noninvasive assessment of ICH are shown.

Table 19.1 Main characteristics of the different ultrasound methods available for noninvasive assessment of ICH

Device	Equipment/transducer	Pathophysiological events	Anatomical findings	Mon.	Pros	Cons
TCD	TCD device 2 MHz Pulsed Doppler transducer ± M mode	MFV ↓ EDV ↓ PI ↑	Can indirectly estimate midline shift	Yes	Can be used for continuous monitoring	– Temporal window permeability
TCCD	Ultrasound machine duplex + color Doppler Low-frequency (1.75–3.5 MHz) phased array probe	MFV ↓ EDV ↓ PI ↑	Midline shift Hydrocephalus Space occupying lesion	No	Easier if there is no experience with identifying the vessels	– Temporal window permeability
Vittamed	"Vittamed": 2 depths pulsed Doppler probe + extraocular pressure chamber	Pressure needed to equalize sonograms from both depths = ICP	No	No		– Eye/orbital trauma – Cataracts
ONSD	Ultrasound machine probe: linear 7.5–15 MHz Setting: small parts	Diameter ↑	ONSD ↑	No		– Lack of uniform methodology
Ultrasonic pupillometry	Ultrasound machine probe: linear 7.5–15 MHz Setting: small parts	Changes in pupillary light reflex (herniation, ischemia)	Pupillary diameter changes with the light	No	Useful in orbital trauma or burns	– More research is still needed

Mon Ability of the method to perform continuous neuromonitoring, *TCD* transcranial Doppler, *TCCD* transcranial color-coded duplex, *ONSD* optic nerve sheath diameter, *MFV* mean flow velocity, *EDV* end-diastolic velocity, *PI* pulsatility index

19.4 Big data and Future Research

nICP estimation Based on Big Data and Future Research Big Data is the name given to massive amounts of digital data whose processing is impossible for conventional computer systems. Therefore, such processing can only be done using special techniques and systems.

Integrated continuous monitoring generates Big Data. It registers simultaneous data from FV, ABP, expired CO_2, electrocardiographic signals, near-infrared spectroscopy, etc. It can acquire the shape of the different waves over time.

The special techniques and systems that analyze Big Data are called "machine learning." It is a branch of artificial intelligence whose goal is to develop techniques that allow computers to learn. They require large amounts of data and tend to reveal patterns, trends, and associations. In this section, a brief reference will be made to some of the methods based on computer systems. They start by generating algorithms based on the data previously registered. Initially, the algorithms are generated and used in the same patient, but the main objective is to be able to apply them to any new patient.

(a) A "black box" refers to a system whose behavior must be observed entirely by inputs and outputs, without knowing how it is processed inside the box. The box is the skull, the "input" data is represented by ABP and FV. A model is generated inside the box giving a result "as similar as possible" to the output data that is already known (ICP). Different levels of algorithms are generated, which tend to reproduce the already-known results (ICP). These algorithms are then used without having invasive ICP data. Schmidt et al. have worked for years on the calculation of noninvasive ICP based on continuous neuromonitoring including TCD [25]. Their model uses BP curves as input, estimating its relationship with FV, and considers invasive ICP as output. They use the coefficients *f* and *w*, which study the linear relationship between ABP and ICP (coefficient *f*), and between ABP and FV (coefficient *w*). A third step is to study the relationship between the coefficients *f* and *w*. In a 2003 publication, the same group compared their "fixed matrix" method, based on the coefficients *f* and *w*, with a new one based on "autoregulatory feedback" control. The monitoring of the dynamics of the invasive ICP curve with the fixed matrix method was "flatter" compared to the one controlled by autoregulatory feedback, both during B waves and in plateau waves. The feedback method slightly overestimated changes in ICP and peak values [26].

(b) The "modified black box model" [27] is similar to the abovementioned one, but it is based on the premise that the correlations between the various parameters that enter the "box" and those that leave it are not linear. They worked with support vector machines and kernel spectral regression, which have shown better prediction than linear ones. They use the same coefficients *f* and *w* that the Schmidt model (using a nonlinear correlation), and then they study the relationship between *f* and *w*.

(c) ICP estimation model based on cerebrovascular dynamics. Heldt's group, from the Massachusetts Institute of Technology, has obtained a good correlation and concordance [28]. Their model is based on a dynamic model of cerebral circulation. ICP estimates are produced in each patient by an automatic algorithm, without the need for a calibration process or training in specific populations.

(d) Data mining. This is a type of study based on big data that uses a large amount of information recorded without a mathematical model, in a complex system of neural networks that will generate an ICP value [11].

(e) An artificial intelligence method called "support vector machine" was used by the group led by engineer Max Chacon from the University of Santiago de Chile, working in collaboration with our group from the Hospital de Clinicas, Montevideo [29]. They generated a model from the neuromonitoring data of eight patients in 2010. Figure 19.8 shows a 5-min portion extracted from a 45-min monitoring of a patient with severe TBI included in the cited work. Multiple neuromonitoring with ABP, ICP, and FV with TCD was performed, for 45 min in each patient. An nICP model was generated from parameters extracted from ABP and FV waveforms, their relationships, and heart rate (Table 19.2). They were entered into

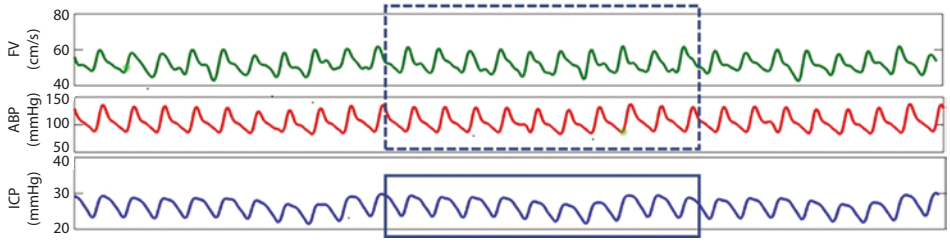

Fig. 19.8 For each time window (5 s), features are extracted from FV and ABP waveforms (dashed line box), and mean ICP is calculated (continuous line box)

Table 19.2 Twenty-three relevant signal characteristics of arterial blood pressure (ABP), cerebral blood flow velocity (VF), and the relationship between both (ABP-VF). Of these 23 features, 10 (marked with an asterisk) were chosen to build the model [29]

Signals characteristics (Ref. 29)					
	ABP		**FV**		**ABP_FV**
*	Mean diastolic-systolic time	*	Mean area under the curve	*	nMx [29]
*	Mean systolic-diastolic time	*	Mean diastolic velocity	*	Combined index
*	Mean systolic pressure	*	Mean velocity		Critical closing pressure
*	Mean area under the curve	*	Pulsatility index		Resistance area product
	Mean diastolic pressure		Mean systolic velocity		Cerebrovascular resistance
	Mean upstroke		Mean diastolic-systolic time		
	Tendency		Mean systolic-diastolic time		
	Mean pulse pressure		Mean amplitude		
	Mean arterial pressure		Pourcelot index		

nMx noninvasive Mx
*Features selected for building the model

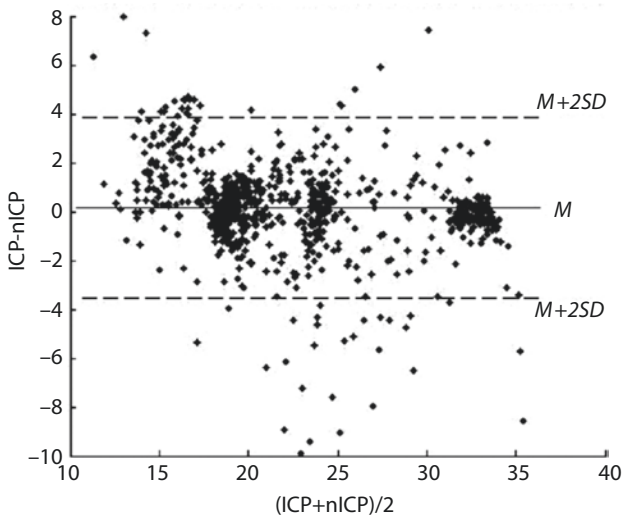

Fig. 19.9 Bland-Altman plot for the nonlinear model using 5 s window. The mean (M) is 0.14, upper limit of agreement (M + 2SD) is 3.8, and lower limit of agreement (M − 2SD) is −3.5

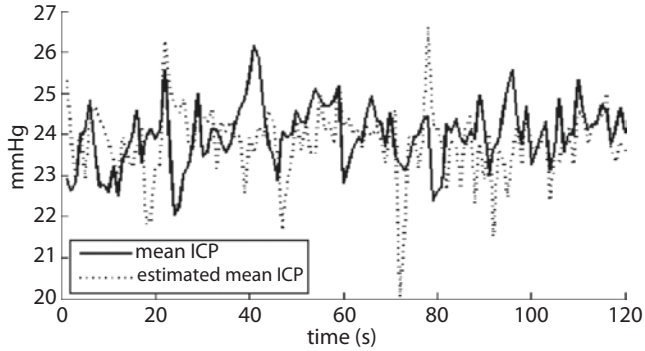

Fig. 19.10 Average nonlinear ICP estimation for a representative patient, using 5 s time window

an "intelligent" system which originated different algorithms to calculate ICP. The chosen algorithm was the one whose results showed the best coincidence with the patient's real ICP. Figures 19.9 and 19.10 show the Bland-Altman plot and the dynamic changes with the invasive and the estimated ICP. The lack of agreement in absolute values is a drawback of all these models. However, the agreement has gradually improved. Published studies have different precisions, with a predictive capacity (area under the curve) between 0.62 and 0.92, to detect an ICP > 20 mmHg [11]. Furthermore, continuous neuromonitoring with noninvasive methods can reproduce the dynamic changes of the prolonged ICP neuromonitoring curve: slow waves, faster waves, and plateau waves of ICH.

Summary

Intracranial hypertension is a marker of unfavorable results in neurocritical patients. ICH is difficult to be clinically diagnosed in ventilated and sedated patients, without an invasive method. Invasive ICP monitoring is the gold standard technique, but it is expensive, requires technical skills, and is frequently contraindicated or not always available. Ultrasound methods can help to increase the suspicion, or exclude, ICH in these patients. These methods are noninvasive and can be performed at bedside. If suspicion increases, a brain image (CT scan or MR), or invasive ICH, depending on the clinical scenario, should be performed.

TCD can be used to estimate ICH by itself, or as part of multiple neuromonitoring modalities. Transcranial Doppler basic changes are a decrease in blood flow velocity and an increase in the pulsatility index. A normal waveform and values most likely exclude intracranial hypertension. On the other hand, a pathological waveform can be caused by other alterations that have to be ruled out. A change in the sonogram waveform, with EDV values lower than 20–25 cm/s in the MCA, and a PI greater than 1.25 are suspicious of high ICP. It must be remembered that vasospasm and intracranial hypertension can coexist, leading to pseudonormal patterns. Big Data analysis is improving its sensibility and specificity for ICH diagnosis and can show the ICP trend and the different existing waves. Currently, continuous TCD monitoring alone or as part of multiple neuromonitoring can be performed for a maximum of around 1 h; in the future this lapse will surely increase. TCCD can show anatomical changes, color-coded vessels in the selected plane, and flow direction. This technique lacks the possibility of continuous monitoring. Anatomic changes are not directly related to the rise in ICP, and they can also appear with normal ICP, but a midline shift greater than 5 mm should trigger a rapid response, like performing a brain image and/or ICP monitoring. Vittamed is an interesting method based on the pressure needed to equalize TCD-measured velocities at two depths of the ophthalmic artery. ONSD increases when ICP rises. It was observed that with ONSD values less than 5.7 mm, the probability of being in the presence of ICP above 20 mmHg is very low, while for ONSD values greater than 5.7 mm, said probability clearly increases. Finally, ultrasonic pupillometry can be also used, giving helpful information to patients with orbital trauma, hematomas, or edema. Although brain ultrasonography is not able to replace neuroimaging or invasive neurological monitoring, it still finds its place in ICU, in the follow-up of patients with either traumatic brain injury or other acute neurological injuries especially in situations where invasive monitoring is not available or not fully indicated.

Take-Home Messages

- Severe head injured patients, traumatic or from other etiologies, can present with ICH, which is a marker of unfavorable outcomes. When patients are sedated and paralyzed, neurological clinical evaluation becomes impossible, and in particular, pupillary clinical changes are late. Therefore, in these severely injured patients, the clinician should benefit from tools which can help in raising the suspicion of ICH. Ultrasonographic methods are becoming increasingly available at patients' bedside. When using TCD, the main changes are a decrease in cerebral blood flow velocity increase in pulsatility index. Ultrasound educational projects and research should focus on the standardization of the different methods to estimate intracranial hypertension or the mass effect of different lesions which put the patients' lives at risk. Training in the implementation of these methods at bedside in the context of a "head to toes" ultrasound patient evaluation is extremely necessary.

References

1. Brain Injury Foundation, American Association of Neurological Surgeons, Joint Section on Neurotrauma and Critical Care. Initial management. J Neurotrauma. 2000;17:463–9.
2. Badri S, Chen J, Barber J, Temkin NR, Dikmen SS, Chesnut RM, Deem S, Yanez ND, Treggiari MM. Mortality and long-term functional outcome associated with intracranial pressure after traumatic brain injury. Intensive Care Med. 2020;8:1800–9.
3. Canac N, Jalaleddini K, Thorpe SG, Thibeault CM, Hamilton RB. Review: Pathophysiology of intracranial hypertension and noninvasive intracranial pressure monitoring. Fluids Barriers CNS. 2020;17:40.
4. Fernando SM, Tran A, Cheng W, Rochwerg B, Taljaard M, Kyeremanteng K, English SW, Sekhon MS, Griesdale DEG, Dowlatshahi D, McCredie VA, Wijdicks EFM, Almenawer SA, Inaba K, Rajajee V, Perry JJ. Diagnosis of elevated intracranial pressure in critically ill adults: systematic review and meta-analysis. BMJ. 2019;24:l4225.
5. Musick S, Alberico A. Neurologic assessment of the neurocritical care patient. Front Neurol. 2021;12:588989.
6. Hawryluk GWJ, Aguilera S, Buki A, et al. A management algorithm for patients with intracranial pressure monitoring: the Seattle International Severe Traumatic Brain Injury Consensus Conference (SIBICC). Intensive Care Med. 2019;45:1783–94.
7. Rangel-Castilla L, Gopinath S, Robertson CS. Management of intracranial hypertension. Neurol Clin. 2008;26:521–41. Erratum in: Neurol Clin. 2008; 26: xvii. Rangel-Castillo, Leonardo [corrected to Rangel-Castilla, Leonardo]
8. Aaslid R, Markwalder TM, Nornes H. Noninvasive transcranial Doppler ultrasound recording of flow velocity in basal cerebral arteries. J Neurosurg. 1982;57:769–74.
9. Consensus Group on Transcranial Doppler in Diagnosis of Brain Death. Latin American consensus on the use of transcranial Doppler in the diagnosis of brain death. Rev Bras Ter Intensiva. 2014;26:240–52.
10. Cardim D, Schmidt B, Robba C, Donnelly J, Puppo C, Czosnyka M, Smielewski P. Transcranial Doppler monitoring of intracranial pressure plateau waves. Neurocrit Care. 2017;26:330–8.
11. Cardim D, Robba C, Bohdanowicz M, Donnelly J, Cabella B, Liu X, Cabeleira M, Smielewski P, Schmidt B, Czosnyka M. Non-invasive monitoring of intracranial pressure using transcranial Doppler ultrasonography: is it possible? Neurocrit Care. 2016;25:473–91.
12. Bellner J, Romner B, Reinstrup P, Kristiansson KA, Ryding E, Brandt L. Transcranial Doppler sonography pulsatility index (PI) reflects intracranial pressure (ICP). Surg Neurol. 2004;62:45–51.
13. Czosnyka M, Matta BF, Smielewski P, Kirkpatrick PJ, Pickard JD. Cerebral perfusion pressure in head-injured patients: a noninvasive assessment using transcranial Doppler ultrasonography. J Neurosurg. 1998;88:802–8.

14. Rasulo FA, Calza S, Robba C, Taccone FS, Biasucci DG, Badenes R, Piva S, Savo D, Citerio G, Dibu JR, Curto F, Merciadri M, Gritti P, Fassini P, Park S, Lamperti M, Bouzat P, Malacarne P, Chieregato A, Bertuetti R, Aspide R, Cantoni A, McCredie V, Guadrini L, Latronico N. Transcranial Doppler as a screening test to exclude intracranial hypertension in brain-injured patients: the IMPRESSIT-2 prospective multicenter international study. Crit Care. 2022;26:110.
15. Edouard AR, Vanhille E, Le Moigno S, Benhamou D, Mazoit JX. Non-invasive assessment of cerebral perfusion pressure in brain injured patients with moderate intracranial hypertension. Br J Anaesth. 2005;94:216–21.
16. Varsos GV, Kolias AG, Smielewski P, Brady KM, Varsos VG, Hutchinson PJ, Pickard JD, Czosnyka M. A noninvasive estimation of cerebral perfusion pressure using critical closing pressure. J Neurosurg. 2015;123:638–48.
17. Zeiler FA, Czosnyka M, Smielewski P. Optimal cerebral perfusion pressure via transcranial Doppler in TBI: application of robotic technology. Acta Neurochir (Wien). 2018;160:2149–57.
18. Llompart Pou JA, Abadal Centellas JM, Palmer Sans M, Pérez Bárcena J, Casares Vivas M, Homar Ramírez J, Ibáñez Juvé J. Monitoring midline shift by transcranial color-coded sonography in traumatic brain injury. A comparison with cranial computerized tomography. Intensive Care Med. 2004;30:1672–5.
19. Krejza J, Swiat M, Pawlak MA, Oszkinis G, Weigele J, Hurst RW, Kasner S. Suitability of temporal bone acoustic window: conventional TCD versus transcranial color-coded duplex sonography. J Neuroimaging. 2007;17:311–4.
20. Ragauskas A, Matijosaitis V, Zakelis R, Petrikonis K, Rastenyte D, Piper I, Daubaris G. Clinical assessment of noninvasive intracranial pressure absolute value measurement method. Neurology. 2012;78:1684–91.
21. https://humanresearchroadmap.nasa.gov/tasks/task.aspx?i=1415.
22. Robba C. Measuring optic nerve sheath diameter using ultrasonography for the detection of non invasive intracranial pressure: what it is and what it is not. Arq Neuropsiquiatr. 2022;80:547–9.
23. Yic CD, Pontet J, Mercado M, Muñoz M, Biestro A. Ultrasonographic measurement of the optic nerve sheath diameter to detect intracranial hypertension: an observational study. Ultrasound J. 2023;15:4.
24. Yic CD, Prada G, Paz SI, Moraes L, Pontet JC, Lasso ME, Biestro A. Comparison of ultrasonographic versus infrared pupillary assessment. Ultrasound J. 2020;12:38.
25. Schmidt B, Klingelhöfer J, Schwarze JJ, Sander D, Wittich I. Noninvasive prediction of intracranial pressure curves using transcranial Doppler ultrasonography and blood pressure curves. Stroke. 1997;28:2465–72.
26. Schmidt B, Czosnyka M, Raabe A, Yahya H, Schwarze JJ, Sackerer D, Sander D, Klingelhöfer J. Adaptive noninvasive assessment of intracranial pressure and cerebral autoregulation. Stroke. 2003;34:84–9.
27. Xu P, Kasprowicz M, Bergsneider M, Hu X. Improved noninvasive intracranial pressure assessment with nonlinear kernel regression. IEEE Trans Inf Technol Biomed. 2010;14:971–8.
28. Kashif FM, Verghese GC, Novak V, Czosnyka M, Heldt T. Model-based noninvasive estimation of intracranial pressure from cerebral blood flow velocity and arterial pressure. Sci Transl Med. 2012;4:129ra44.
29. Chacón M, Pardo C, Puppo C, Curilem M, Landerretche J. Non-invasive intracranial pressure estimation using support vector machine. Annu Int Conf IEEE Eng Med Biol Soc. 2010;2010:996–9.

Transcranial Doppler (TCD): Clinical Applications in Acute Brain Injury

Carla Bittencourt Rynkowski, Juliana Caldas, and Fabio Silvio Taccone

Contents

20.1 Introduction – 310

20.2 Vasospasm – 310
20.2.1 Diagnosis – 311
20.2.2 The Importance of the MCA – 311
20.2.3 Vasospasm Grading – 312
20.2.4 Differential Diagnosis – 313
20.2.5 Vasospasm of the Posterior Circulation – 314
20.2.6 Use to Follow Response to Treatment – 314
20.2.7 Important Additional Considerations – 314

20.3 Cerebral Circulatory Arrest (in the Diagnosis of Brain Death) – 315

20.4 TCD in Stroke Patients – 317
20.4.1 Search for Etiology – 317
20.4.2 Acute Phase – 317
20.4.3 Cerebral Autoregulation in Stroke – 319
20.4.4 Evaluation of ICP in Stroke – 320

References – 321

© The Author(s), under exclusive license to Springer Nature Switzerland AG 2023
C. Robba et al. (eds.), *Basic Ultrasound Skills "Head to Toe" for General Intensivists*, Lessons from the ICU,
https://doi.org/10.1007/978-3-031-32462-8_20

Learning Objectives

- Understand why TCD is a useful tool in the management of neurocritical patients.
- Identify the main uses of TCD for neurocritical patients.
- Appreciate the advantages of TCD over other methods used in similar situations in neurocritical patients.
- Recognize the limitations of TCD depending on its specific application.
- Identify TCD waves that can be pathological and correspond to vasospasm, CBF alteration in stroke patients, and situations evolving to cerebral circulatory arrest.

20.1 Introduction

Transcranial Doppler (TCD) is a noninvasive method that can be used to indirectly assess cerebral blood flow (CBF) velocity through the insonation of the main intracerebral arteries [1]. TCD can be performed at the bedside, repeated if necessary, is radiation-free, and provides information in real-time that enables evaluation of trends in CBF velocities over time [2].

TCD was originally developed to detect cerebral vasospasm after subarachnoid hemorrhage (SAH) [1]; however, its range of applications has increased over the years. In addition to vasospasm detection, the leading uses of TCD include diagnosis of stenosis or occlusion of the main intracranial arteries (chronic or acute) during stroke, detection of microemboli and cerebrovascular reserve capacity, assessment of autoregulation and neurovascular coupling status, estimation of increased intracranial pressure (ICP), and detection of cerebral circulatory arrest [3].

Here, we focused on some of the most common and current applications of TCD, notably the detection of vasospasm; recognition, investigation, and follow-up of the CBF compromise in stroke; and diagnosis of cerebral circulatory arrest.

20.2 Vasospasm

Cerebral vasospasm is the narrowing of cerebral arteries as evidenced by brain imaging. Using TCD, the reduction in vessel diameter is demonstrated by an increase in CBF velocities, because of the inverse relationship between cerebral blood vessel diameter and TCD velocity [4]. In a recent consensus on grades of competency for brain ultrasonography, recognition of sonographic vasospasm was considered a basic plus skill for sonographers and clinicians who are learning the skills of brain ultrasonography [5].

Although TCD is commonly performed in most centers treating SAH patients [6], there is no precise recommendation about when and how often TCD should be performed in this setting [7]. Vasospasm can occur in patients who develop delayed cerebral ischemia (DCI), one of the most feared complications in SAH, but the two conditions are not synonymous [2]. It is essential to remember that vasospasm is a diagnosis of imaging, which does not always correspond to the neurological deficit of DCI [8]. In the TACTICS study [9], vasospasm was present on 95% of angiographs, but only on 45% of TCD scans; 30% of these patients had confirmed DCI, and 20% had an unfavorable outcome. Importantly, DCI can be present even when

CBF is normal, without vasospasm [7, 10], and reversal of vasospasm, when present, does not guarantee clinical improvement [11]. Information provided by TCD at the bedside can therefore be of use when assessing vasospasm but must be interpreted within the clinical context of the patient.

TCD can also be of use to identify vasospasm in conditions other than SAH. Vasospasm can be detected in around 7–17% of patients with ruptured arteriovenous malformations [12]. In traumatic brain injury, vasospasm can be present even in patients without traumatic SAH, and its occurrence is related to unfavorable outcomes [13]. Finally, TCD is a helpful tool for the diagnosis and monitoring of vasospasm in reversible cerebral vasoconstriction syndrome [14, 15].

20.2.1 Diagnosis

Vasospasm is detected by TCD by an increase in the CBF mean flow velocity (MFV), due to vessel narrowing. Each vessel has a reference threshold value, defined according to the degree of vessel narrowing identified on angiography, to be considered vasospasm [16, 17] (Table 20.1). The evidence for the threshold values for the middle cerebral artery (MCA) and basilar artery (BA) is more reliable than that for other vessels [16].

20.2.2 The Importance of the MCA

The MCA is frequently affected by the occurrence of cerebral vasospasm, because 70–80% of CBF is provided by the carotid arteries and 70% by the MCA to the ipsilateral hemisphere, as shown by the Willis polygon analysis. The assessment of MCA using TCD techniques is considered a basic skill for point-of-care ultrasound [5]. Analyzing specifically MCA vasospasm detected by TCD, Mastantuono et al. [18] showed in a meta-analysis a prevalence of 70%, with a sensitivity of 66.7% (95% CI, 55.9–75.9) and specificity of 89.5% (80.3–94.7) for TCD to detect vasospasm; there

Table 20.1 Transcranial Doppler criteria of vasospasm based on the mean flow velocity (MFV) of intracranial arteries

Vessel	Normal (MFV cm/s)	Vasospasm (MFV cm/s)
ACA	<90	>120
PCA	<60	>90
VA	<60	>90
ICA	<80	>110

Values of MFV in between normal and vasospasm reference values must be carefully evaluated according to the subsequent measurements because abnormal values can represent the beginning of vasospasm. *ACA* anterior cerebral artery, *PCA* posterior cerebral artery, *VA* vertebral artery, *ICA* internal carotid artery [16]

was no difference in detection between the methods of "blind" TCD and transcranial color-coded duplex Doppler. These results reinforce the concept that TCD can detect vasospasm but is not a good method to exclude it. To be considered vasospasm, the most common cutoff for the MCA is a minimum MFV of 120 cm/s [16], which would correspond to a vessel narrowing on angiography of around 25%. However, a recent study demonstrated a higher threshold value of 160 cm/s to detect those patients who would benefit from vasospasm treatment [17]. The diagnosis of MCA vasospasm can also be made based on a rapid increase of 50% in CBF compared to a previous measurement 24 h earlier and also by an MFV 50% greater than that of the opposite MCA [18].

20.2.3 Vasospasm Grading

Vasospasm can be classified according to the degree of reduction in the vessel diameter, as reflected by the MFV. One system considers the range of MFV values in the MCA [19]:

- Hyperemia: MFV >80 and <120 cm/s;
- Mild vasospasm: MFV of 120–159 cm/s (Fig. 20.1);
- Moderate vasospasm: MFV of 160–199 cm/s (Fig. 20.2);
- Severe vasospasm: MFV >200 cm/s (Fig. 20.3). In some cases, extreme vessel narrowing can indicate distal cerebral infarction leading to intracranial hypertension, which can also be detected by TCD.

Another classification system for vasospasm in the anterior circulation is the Lindegaard index (LI), the ratio between MFV in the MCA or anterior cerebral artery and the internal carotid artery, measured using the submandibular window [20]; LI = MFV of MCA/MFV of extracranial ICA. In hyperemia, the LI is <3, in mild vasospasm it is 3–4, in moderate vasospasm 4–5, and in severe vasospasm, the LI is 5–6.

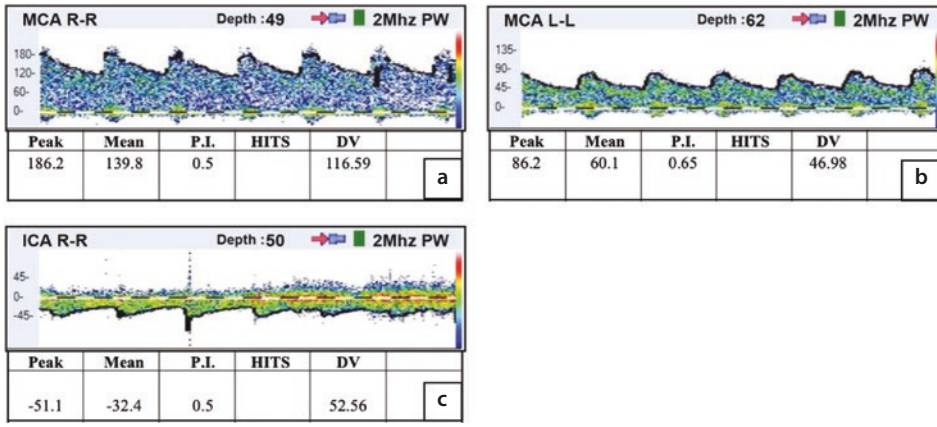

Fig. 20.1 Mild vasospasm in the right middle cerebral artery (MCA R-R) shown by transcranial Doppler. Diagnosis of mild vasospasm is based on the mean flow velocity (MFV) value of 139.8 cm/s **a**, with a Lindegaard index (LI) of 4 (MFV of MCA 139.8/MFV of extracranial ICA 32.4) **c** and more than 50% the value of contralateral side (left MCA—MCA L-L—of 60.1 cm/s) **b**

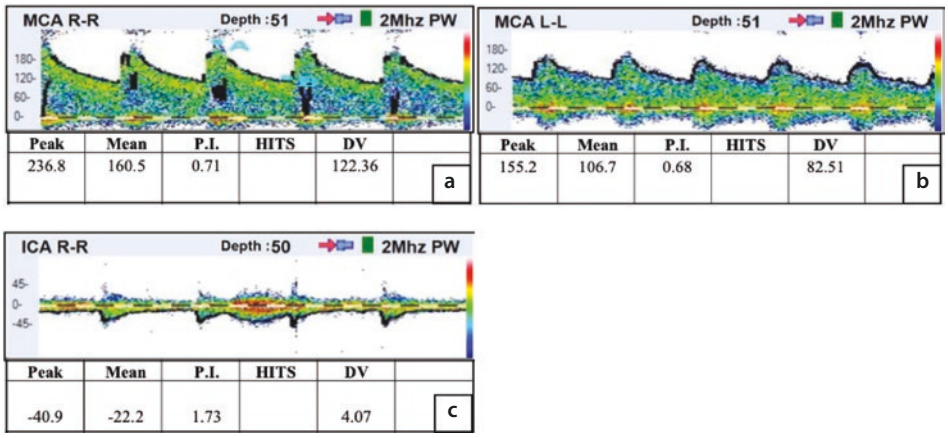

Fig. 20.2 Image of moderate-severe vasospasm in the right middle cerebral artery (MCA R-R) shown by transcranial Doppler. The diagnosis of moderate vasospasm in the right MCA (MCA R-R) is based on the mean flow velocity (MFV) value of 160.5 cm/s **a**; however, with a Lindegaard index (LI) of 7 (MFV of MCA 160.5/MFV of extracranial ICA 22.2) **c**, this is considered severe vasospasm and 40% higher than the value of contralateral side (left MCA—MCA L-L—of 106.7 cm/s) **b**

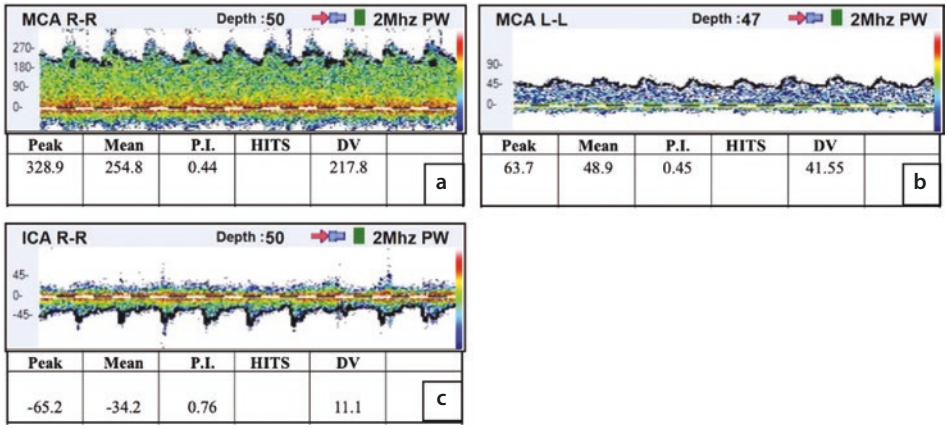

Fig. 20.3 Image of severe vasospasm in the right middle cerebral artery (MCA R-R) shown by transcranial Doppler. The diagnosis of severe vasospasm in the right MCA (MCA R-R) based on the mean flow velocity (MFV) value of 254.8 cm/s **a**, with a Lindegaard index (LI) of 7 (MFV of MCA 254.8/MFV of extracranial ICA 34.2) **c**, and the MFV of the right MCA is five times the value of contralateral side (left MCA—MCA L-L—of 48.9 cm/s) **b**

20.2.4 Differential Diagnosis

Vasospasm must be distinguished from hyperemia, in which CBF MFV is also high. To distinguish these conditions, the LI at the level of the anterior circulation can be considered: a LI >3 is considered vasospasm and <3 hyperemia.

20.2.5 Vasospasm of the Posterior Circulation

There is also an index of adjustment that needs to be made to meet the vasospasm criteria in the BA. To be considered as vasospasm, the Sloan index (SI) [21], the ratio between the MFV in the BA and the MFV of the extracranial vertebral artery, must be >2; SI = MFV of BA/MFV of extracranial VA, measured using the posterior suboccipital window. The extracranial proximal VA can be analyzed at a depth of 60 mm. An SI of 2.5–3 represents moderate vasospasm and >3 indicates severe vasospasm.

20.2.6 Use to Follow Response to Treatment

TCD can be used at the bedside to follow the response to the treatment of vasospasm in patients with DCI [22]. However, TCD measures must always be considered together with clinical findings [23], because reversal of vasospasm on TCD or imaging is not a guarantee of clinical recovery [8].

20.2.7 Important Additional Considerations

- There is as yet no solid evidence about the best time interval to perform TCD after SAH [24]. Vasospasm is expected to occur between 4 and 14 days after SAH. The previous recommendation to perform TCD every day or every other day could be adjusted to individual patient needs and clinical status [2, 6, 25–27]. We must consider SAH as a complex disease, and TCD findings must be interpreted taking into consideration the clinical condition of the patient, because the neurological examination remains the optimal tool to detect DCI [7, 28]. It would be unusual to prescribe vasospasm treatment based on imaging findings in a patient who is completely asymptomatic, although such patients need careful monitoring [29–34]. As such, clinical examination, previous TCD findings (at least one TCD assessment is recommended in all patients with SAH to form a baseline for future comparisons) and evaluation of the contralateral side should be carefully considered in the diagnostic process. Unconscious patients or those on profound sedation may benefit from TCD evaluation more than once a day.
- TCD can also be used in patients with SAH to detect information other than that related to vasospasm detection. Cerebral autoregulation status, which is associated with SAH course and outcome, can be assessed and monitored continuously, with advanced software or even simple maneuvers, such as transient carotid compression [35, 36]. Moreover, TCD can be used to assess cerebral perfusion pressure [37], thus excluding, for example, a situation of intracranial hypertension [37, 38], which can complicate some cases of DCI involving large cerebral infarcts. In this setting, TCD can even detect the evolution toward cerebral circulatory arrest [38].

20.3 Cerebral Circulatory Arrest (in the Diagnosis of Brain Death)

Each country has specific legal requirements for a diagnosis of brain death. Although the most recent guidelines report insufficient evidence to determine brain death with ancillary tests, such as electroencephalogram (EEG), evoked potentials, and brain imaging, in some countries adding ancillary testing to clinical tests is required. Furthermore, in certain circumstances an apnea test cannot be used for brain death diagnosis, for example, in clinically unstable patients, patients with chronic obstructive pulmonary disease, and those receiving barbiturate therapy or with hypothermia. Ancillary testing can be used to complement the standard clinical examination and confirm brain death in such cases.

Within the spectrum of ancillary brain death tests, TCD plays an important role. A recent meta-analysis that included 22 articles with a total of 1671 patients suggested that TCD is a highly accurate ancillary test for brain death confirmation [39]. The sensitivity and specificity were 90% and 98%, respectively, with an area under the receiver operating characteristic (ROC) curve estimated at 0.964. Sensitivity cannot be higher because of some inherent limitations of the TCD assessment, including structural abnormalities related to the bone windows (insufficient insonation in around 9% of patients) or to the cranium that provide relief of ICP (decompressive hemicraniectomy, external ventricular device, even malleable cranium of young children). The results of this systematic review, combined with a study by Monteiro et al. [40], support the use of TCD as a standard ancillary test for brain death diagnosis.

To detect cerebral circulatory arrest (CCA) using TCD, the absence of blood flow must be shown in four vessels: left and right MCA and intracranial vertebral arteries (VA) [41]. The absence of blood flow is detected by the lack of end-diastolic velocity. A minimal peak systolic velocity may be present but diastolic velocity is generally non-detectable or has a "negative" value (i.e. "diastolic backflow"). At least one of these findings must therefore be detected in each of the four vessels (not necessarily the same finding in all vessels): reverberating flow, systolic spikes, and disappearance of previously registered Doppler flow signals (Fig. 20.4).

At the time of the TCD examination, the patient must have a minimum systolic blood pressure (SBP) of 90–100 mmHg. In situations of extremely high ICP or extremely low arterial pressure, the end-diastolic velocity can be very low and almost disappear. At this sudden moment of instability, a low CBF can still be present, and an irreversible CCA status [3] cannot be considered. Physiological parameters to be respected before starting the TCD exam in this setting are therefore: SBP >90–100 mmHg, temperature >35 °C, and oxygen saturation >94% (Fig. 20.5). Another important observation is that the TCD exam to detect CCA must be performed over a 30-min period, to avoid transient episodes of extremely high ICP.

In situations when MCA and VA flows cannot be detected, insonation of the internal carotid artery (Siphon) is allowed through the transorbital window and evaluation of the extracranial vertebral arteries. The same CCA patterns are expected in those vessels. Although the blood flow in those arteries is compromised later than in the MCA or VA, an early false-negative "CCA" can be observed in situations of loss of skull hermiticity. This situation may occur in decompressive craniectomy, with a large skull fracture, or in the presence of a ventriculostomy [39]. In these cases, a

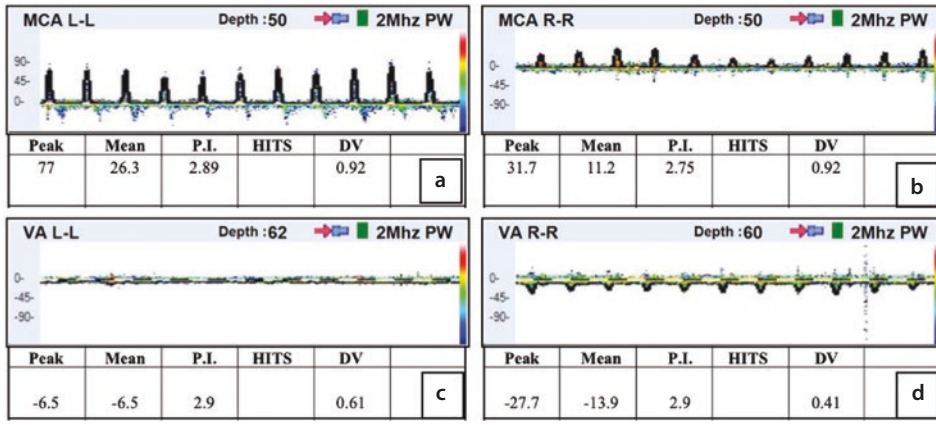

Fig. 20.4 These images illustrate different findings in cerebral circulatory arrest (CCA) using transcranial Doppler. The cerebral blood flow (CBF) velocities of the middle cerebral artery (MCA) and intracranial vertebral arteries (VA) are shown with systolic spikes and reverse waves in the left MCA (MCA L-L) **a**, systolic spikes in the right MCA (MCA L-L) **b**, a disappearance of previously registered Doppler flow signals in the left VA (VA L-L) **c**, and systolic spikes in the right VA (VA R-R) **d**

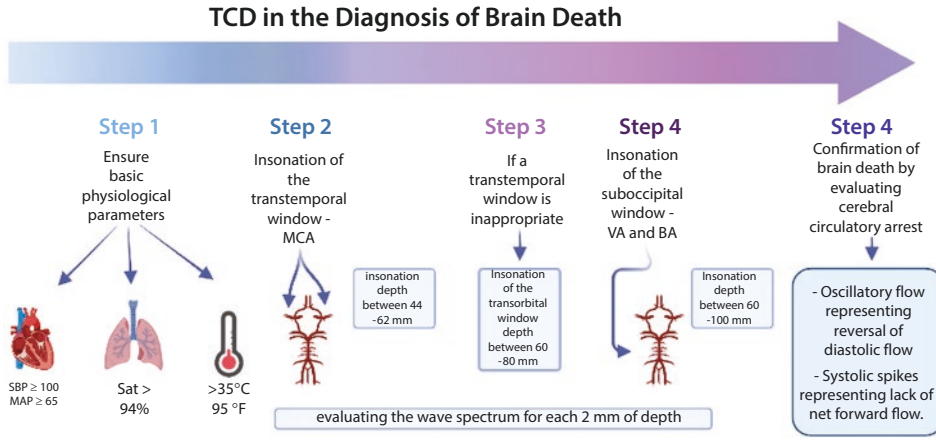
TCD in the Diagnosis of Brain Death
Step 1
Ensure basic physiological parameters
SBP ≥ 100
MAP ≥ 65
Sat > 94%
>35°C
95 °F
Step 2
Insonation of the transtemporal window - MCA
insonation depth between 44 -62 mm
Step 3
If a transtemporal window is inappropriate
Insonation of the transorbital window depth between 60 -80 mm
Step 4
Insonation of the suboccipital window - VA and BA
Insonation depth between 60 -100 mm
Step 4
Confirmation of brain death by evaluating cerebral circulatory arrest
- Oscillatory flow representing reversal of diastolic flow
- Systolic spikes representing lack of net forward flow.
evaluating the wave spectrum for each 2 mm of depth

Fig. 20.5 A step-by-step algorithm for transcranial Doppler (TCD) use in the diagnosis of brain death. *SBP* systolic blood pressure, *MAP* mean arterial pressure, *Sat* saturation of oxygen, *MCA* middle cerebral artery, *VA* vertebral artery, *BA* basilar artery. (Figure reproduced from Caldas et al., 2022 [53] under a Creative Commons Attribution 4.0 International License)

delay in CCA diagnosis is observed and can lead to a delay in brain death diagnosis and organ donation processes. In such cases, a reasonable alternative to conclude the brain death diagnosis is the use of an ancillary method that does not depend on the blood flow, such as electroencephalogram or brain scintigraphy.

The TCD evaluates cortical cerebral perfusion rather than brain stem function, and this limitation needs to be taken into account. However, in countries where an ancillary test is required or when clinical conditions or medications make the clinical examination unsuitable, TCD is still the most reliable ancillary test for brain death confirmation.

20.4 TCD in Stroke Patients

20.4.1 Search for Etiology

In the course of a cryptogenic stroke, TCD is considered a class II screening tool to investigate the presence of right-left cardiopulmonary shunts along with transesophageal echocardiography (TEE). A patent foramen ovale (PFO) is a common cause of intracardiac shunt between the right and left atria. Although most people with a PFO have no symptoms, right-left shunt through a PFO has been linked with strokes, especially in patients who are younger, have healthy weight, have no diabetes, and are nonsmokers. Such cases may require aggressive screening for PFO [42, 43] and TCD can play an important role in this purpose.

TCD can detect both intra-cardiac and extra-cardiac shunts (in cases of pulmonary arteriovenous malformation). This method can even grade the shunt using the "microembolic signals grading score" and is less invasive than TEE as a first investigation. It involves insonation of the major cerebral arteries, typically the MCA, with a standalone Doppler transducer to assess the blood velocity profile of each MCA. After insonation of the MCA by TCD, agitated saline should be injected during the rest period and a Valsalva maneuver. If a right-left shunt is present, the sonographer will visualize the microbubble contrast and hear audible blips (high-intensity transient signals, HITS) in the arterial circulation (Fig. 20.6).

20.4.2 Acute Phase

In stroke patients, TCD can contribute to the early detection of proximal vascular obstruction or stenosis, provide continuous monitoring during thrombolysis to detect the exact moment of recanalization or no response to therapy, and even detect early reocclusion [44, 45]. There is a TCD grading [45] system to classify CBF in acute stroke, the TIBI score (thrombolysis in brain ischemia—transcranial doppler flow grades), that goes from no flow (grade 0) to normal flow (grade 5) (Table 20.2). It was originally described to quantify the residual intracranial cerebral flow after thrombolysis, but its use can be extended to quantify the flow after thrombectomy, even in suspicion of vessel re-occlusion (Fig. 20.7).

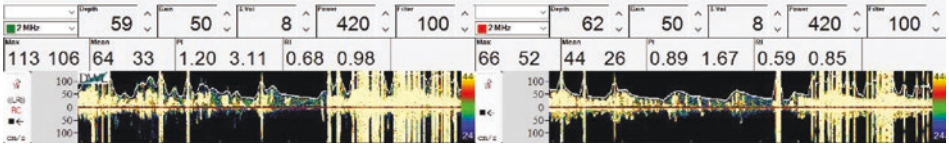

Fig. 20.6 This image represents bilateral monitoring of middle cerebral arteries during a microbubble test. The presence of high-intensity transient signals (HITS) in the arterial circulation can be seen, representing the presence of a right-left shunt

Table 20.2 Thrombolysis in brain ischemia (TIBI) classification using transcranial Doppler (TCD) flow in stroke [45]

TIBI grade	TCD flow	Waveform shape
0	Absent	Absent signal
1	Minimal	Systolic spikes or reverberation flow; no diastolic flow
2	Blunted	Flattened systolic flow; positive end-diastolic flow
3	Dampened	Normal systolic and positive end-diastolic velocity + low MFV (>30% reduction of MFV compared to contralateral side)
4	Stenotic	MFV >80 cm/s + >30% of the difference to the contralateral side
5	Normal	Normal wave pattern; <30% MFV difference compared to the contralateral side

MFV mean flow velocity

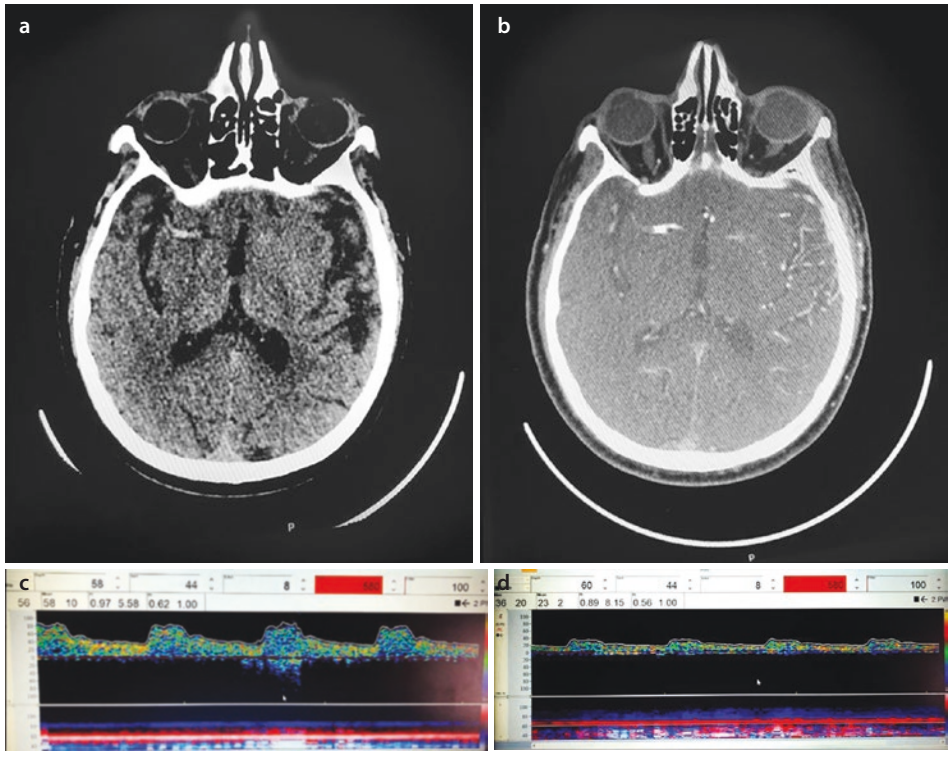

Fig. 20.7 Computed tomography (CT) scan and transcranial Doppler (TCD) of an 80-year-old man with 2-h onset stroke. **a** CT scan with a hyperdense right middle cerebral artery (MCA) signal. **b** Absence of collateral circulation and vascular stop in the right MCA. **c** The TCD image with the blood flow velocity in the left MCA (unaffected side). **d** The TCD image shows oligemia, specifically thrombolysis in brain ischemia (TIBI) grade 2 (blunted waveform) in the right MCA, with no reperfusion after the thrombolysis and thrombectomy

Case Report

An 80-year-old man with 2-h onset of stroke and a National Institutes of Health Stroke Scale (NIHSS) score of 20 was admitted to the Emergency room. He was immediately referred for thrombolysis and thrombectomy procedures. Two hours after the procedure he was admitted to the neuro-ICU with the same NIHSS. TCD was performed and low right MCA MFV, suggesting residual oligemia with no reperfusion (Fig. 20.7); as such, mean arterial pressure was increased from 85 mmHg (baseline values) to 105 mmHg and individualized on the clinical improvement of the patient, along with an increase of MCA MFV. TCD may be a helpful tool to evaluate reperfusion therapy and guide blood pressure targets after these procedures.

In the evaluation of stroke patients, TCD can also contribute to prognostication. A normal CBF on TCD around 6 h after ischemic stroke is an independent predictor of early improvement [46]. On the other hand, if the MCA remains occluded 6 h after stroke onset, this carries a predictive value of 72% for spontaneous hemorrhagic transformation [46]. An MFV less than 30 cm/s around 12 h after stroke is associated with poor recovery. Furthermore, the early presence of microemboli is a predictor of early ischemic recurrence [46]. Because TCD is available for use at the bedside, without contrast, it can be especially useful in acute stroke patients.

In addition to use during the acute phase, TCD can also contribute to evaluate intracranial steno-occlusive disease through signs like a focal increase in MFV at the site of luminal narrowing, decreased MFV, and increased pulsatility upstream from the lesion and abnormal MFV immediately downstream from the lesion. TCD can also detect some extracranial abnormalities in the carotid system, such as a decrease in MFV, with diminished pulsatility in the ipsilateral MCA together with the normal flow in the contralateral MCA and diminished flow acceleration in the ipsilateral MCA among other signs [46].

20.4.3 Cerebral Autoregulation in Stroke

Cerebral autoregulation is the mechanism responsible for maintaining an adequate CBF according to cerebral metabolic needs and for rapidly reacting to external stimuli, such as variations in arterial blood pressure, and has an important role during stroke. Some stroke patients have impaired cerebral autoregulation, and this may be associated with poor functional outcome, as a result of an increased likelihood of hemorrhagic transformation and cerebral edema [47–49].

Studies have reported that, in the acute stroke phase, cerebral autoregulation is significantly impaired in the affected hemisphere and is further compromised with increasing stroke severity [48]. Close monitoring of cerebral autoregulation status may be particularly important during the early stages of clinically severe stroke and/or in the reperfusion phase in large-vessel occlusion strokes [50, 51]. Blood pressure fluctuations generally occur in this acute stage [52] and, in combination with changes in cerebral autoregulation, may provide a target for therapeutic interventions to salvage the ischemic penumbra. TCD enables static and dynamic cerebral autoregulation evaluation with various indexes that have been published in the literature [53].

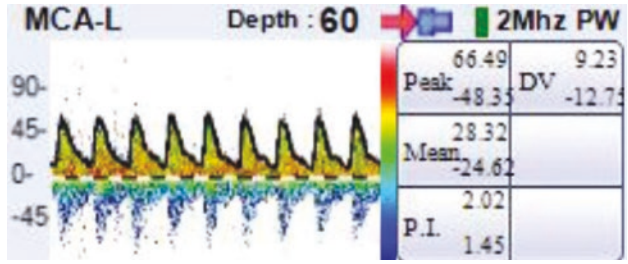

Fig. 20.8 A cerebral blood flow (CBF) velocity of the left middle cerebral artery (MCA-L) with a high pulsatility index (2.02) and oligemia (MFV 28.23 cm/s). These parameters suggest a high intracranial pressure before the craniectomy

20.4.4 Evaluation of ICP in Stroke

Patients with a large hemispheric infarction may have increased ICP resulting in cerebral herniation and subsequent mechanical and ischemic damage to healthy cerebral territories. With decompressive craniectomy, a proportion of the skull is surgically removed to allow the edematous brain tissue to herniate to the outside and thus prevent neuronal damage in other regions of the brain.

TCD is a good method to detect intracranial hypertension development early, thus helping to determine the best moment for a decompressive craniectomy. The TCD waveform shows a sharp decrease in diastolic flow velocity and an elevated PI (more than 1.4) in a scenario of intracranial hypertension (Fig. 20.8). TCD parameters also enable noninvasive estimation of the value of ICP (ICPtcd) using the formula:

$$\text{ICPtcd} = \text{MAP} - \text{CPPe}$$

$$\text{CPPe} = \text{MAP} * \text{EDV} / \text{MFV} + 14$$

where MAP is mean arterial pressure, CPPe cerebral pressure perfusion estimation, EDV end-diastolic velocity, and MFV mean flow velocity. TCD measurement can be associated with the assessment of optic nerve sheath diameter (ONSD), as both elevated ICPtcd and enlarged ONSD (i.e., >6 mm) have a higher accuracy to predict intracranial hypertension [54]. However, most of the studies investigating ICPtcd and ONSD did not include stroke patients. Whether elevated ICPtcd and enlarged ONSD might help to identify patients at risk of further clinical deterioration and requiring decompressive craniectomy remains unknown.

Take-Home Messages

- TCD is a versatile tool that can be applied at the bedside, repeated many times if necessary, and advantageous as a noninvasive multimodality monitoring.
- TCD has good specificity to identify vasospasm, but this finding must be considered within the clinical context of the patient.
- In acute brain injury, the TCD has a wide spectrum of applications, enabling the recognition of intracranial hypertension, critical CBF evolving into CCA, cerebral autoregulation status, as well as characteristic blunted, dampened, or vasospasm waveforms.

- In countries where an ancillary test is necessary or when clinical conditions make clinical examination unreliable, TCD represents the optimal tool for an ancillary test to be performed for brain death confirmation.
- Before starting any TCD examination, it is important to check the hemodynamic status of the patient is adequate in order to avoid wrong interpretation of the TCD wave.
- The search for the etiology of stroke should start in the early phase, and TCD is a useful tool for this purpose.
- TCD can be used to detect CBF velocity after reperfusion therapies in stroke patients and is a helpful tool to guide blood pressure targets after these procedures.

Summary

TCD is a practical, noninvasive, bedside examination that has some advantages in the assessment of critically ill patients with acute brain injury. Despite some limitations related to insonation windows and the need for sonographer expertise, recommendations for training in the use of this technique are growing, especially in neurocritical units. TCD might be useful to confirm the presence of cerebral vasospasm in SAH patients with clinical deterioration. Also, TCD is an effective ancillary test to confirm the diagnosis of brain death. Finally, TCD should be implemented in the follow-up of patients treated for acute ischemic stroke, to assess vascular perfusion, individualize blood pressure targets, and potentially identify the occurrence of intracranial hypertension.

References

1. Aaslid R, Markwalder TM, Nornes H. Noninvasive transcranial Doppler ultrasound recording of flow velocity in basal cerebral arteries. J Neurosurg. 1982;57(6):769–74.
2. Neifert SN, Chapman EK, Martini ML, Shuman WH, Schupper AJ, Oermann EK, Mocco J, Macdonald RL. Aneurysmal subarachnoid hemorrhage: the last decade. Transl Stroke Res. 2021;12(3):428–46.
3. Blanco P, Abdo-Cuza A. Transcranial Doppler ultrasound in neurocritical care. J Ultrasound. 2018;21(1):1–16. https://doi.org/10.1007/s40477-018-0282-9. Epub 2018 Feb 10.
4. Lau VI, Arntfield RT. Point-of-care transcranial Doppler by intensivists. Crit Ultrasound J. 2017;9(1):21. https://doi.org/10.1186/s13089-017-0077-9.
5. Robba C, Poole D, Citerio G, Taccone FS, Rasulo FA, Consensus on Brain Ultrasonography in Critical Care Group. Brain ultrasonography consensus on skill recommendations and competence levels within the critical care setting. Neurocrit Care. 2020;32(2):502–11. https://doi.org/10.1007/s12028-019-00766-9.
6. Sloan MA, Alexandrov AV, Tegeler CH, Spencer MP, Caplan LR, Feldmann E, Wechsler LR, Newell DW, Gomez CR, Babikian VL, Lefkowitz D, Goldman RS, Armon C, Hsu CY, Goodin DS, Therapeutics and Technology Assessment Subcommittee of the American Academy of Neurology. Assessment: transcranial Doppler ultrasonography: report of the Therapeutics and Technology Assessment Subcommittee of the American Academy of Neurology. Neurology. 2004;62(9):1468–81. https://doi.org/10.1212/wnl.62.9.1468.
7. Rabinstein AA, Lanzino G. Aneurysmal subarachnoid hemorrhage: unanswered questions. Neurosurg Clin N Am. 2018;29(2):255–62. https://doi.org/10.1016/j.nec.2018.01.001.

8. Vergouwen MD, Vermeulen M, van Gijn J, et al. Definition of delayed cerebral ischemia after aneurysmal subarachnoid hemorrhage as an outcome event in clinical trials and observational studies: proposal of a multidisciplinary research group. Stroke. 2010;41(10):2391–5. https://doi.org/10.1161/STROKEAHA.110.589275. Epub 2010 Aug 26.
9. van der Harst JJ, Luijckx GR, Elting JWJ, Bokkers RPH, van den Bergh WM, Eshghi OS, Metzemaekers JDM, Groen RJM, Mazuri A, van Dijk JMC, Uyttenboogaart M. Transcranial Doppler versus CT-angiography for detection of cerebral vasospasm in relation to delayed cerebral ischemia after aneurysmal subarachnoid hemorrhage: a prospective single-center cohort study: the transcranial Doppler and CT-angiography for investigating cerebral vasospasm in subarachnoid hemorrhage (TACTICS) study. Crit Care Explor. 2019;1(1):e0001. https://doi.org/10.1097/CCE.0000000000000001.
10. Dorsch NW, King MT. A review of cerebral vasospasm in aneurysmal subarachnoid haemorrhage part I: incidence and effects. J Clin Neurosci. 1994;1(1):19–26.
11. Macdonald RL, Kassell NF, Mayer S, Ruefenacht D, Schmiedek P, Weidauer S, Frey A, Roux S, Pasqualin A, CONSCIOUS-1 Investigators. Clazosentan to overcome neurological ischemia and infarction occurring after subarachnoid hemorrhage (CONSCIOUS-1): randomized, double-blind, placebo-controlled phase 2 dose-finding trial. Stroke. 2008;39(11):3015–21. https://doi.org/10.1161/STROKEAHA.108.519942. Epub 2008 Aug 7.
12. Dicpinigaitis AJ, Feldstein E, Shapiro SD, Kamal H, Bauerschmidt A, Rosenberg J, Amuluru K, Pisapia J, Dangayach NS, Liang JW, Bowers CA, Mayer SA, Gandhi CD, Al-Mufti F. Cerebral vasospasm following arteriovenous malformation rupture: a population-based cross-sectional study. Neurosurg Focus. 2022;53(1):E15. https://doi.org/10.3171/2022.4.FOCUS2277.
13. Fatima N, Shuaib A, Chughtai TS, Ayyad A, Saqqur M. The role of transcranial Doppler in traumatic brain injury: a systemic review and meta-analysis. Asian J Neurosurg. 2019;14(3):626–33. https://doi.org/10.4103/ajns.AJNS_42_19.
14. Oliveira R, Inácio N, Baptista P, Gil-Gouveia R. Transcranial Doppler findings in a population with clinical probable reversible cerebral vasoconstriction syndrome. Rev Neurol (Paris). 2022;178(4):385–90. https://doi.org/10.1016/j.neurol.2021.06.015. Epub 2021 Oct 21.
15. Hathidara M, Patel NH, Flores A, Cabrera Y, Cabrera F, Koch S. Transcranial Doppler findings in reversible cerebral vasoconstriction syndrome. J Neuroimaging. 2022;32(2):345–51. https://doi.org/10.1111/jon.12946. Epub 2021 Nov 16.
16. Kumar G, Alexandrov AV. Vasospasm surveillance with transcranial Doppler sonography in subarachnoid hemorrhage. J Ultrasound Med. 2015;34(8):1345–50. https://doi.org/10.7863/ultra.34.8.1345.
17. Darsaut TE, Keough MB, Chan AM, Farzin B, Findlay JM, Chow MM, Chagnon M, Zehr J, Gevry G, Raymond J. Transcranial Doppler velocities and angiographic vasospasm after SAH: a diagnostic accuracy study. AJNR Am J Neuroradiol. 2022;43(1):80–6. https://doi.org/10.3174/ajnr.A7347. Epub 2021 Nov 18.
18. Mastantuono JM, Combescure C, Elia N, Tramèr MR, Lysakowski C. Transcranial Doppler in the diagnosis of cerebral vasospasm: an updated meta-analysis. Crit Care Med. 2018;46(10):1665–72. https://doi.org/10.1097/CCM.0000000000003297.
19. Vora YY, Suarez-Almazor M, Steinke DE, Martin ML, Findlay JM. Role of transcranial Doppler monitoring in the diagnosis of cerebral vasospasm after subarachnoid hemorrhage. Neurosurgery. 1999;44(6):1237–47; discussion 1247–8.
20. Lindegaard KF, Nornes H, Bakke SJ, Sorteberg W, Nakstad P. Cerebral vasospasm after subarachnoid haemorrhage investigated by means of transcranial Doppler ultrasound. Acta Neurochir Suppl (Wien). 1988;42:81–4. https://doi.org/10.1007/978-3-7091-8975-7_16.
21. Soustiel JF, Shik V, Feinsod M. Basilar vasospasm following spontaneous and traumatic subarachnoid haemorrhage: clinical implications. Acta Neurochir. 2002;144(2):137–44; discussion 144. https://doi.org/10.1007/s007010200016.
22. Rouanet C, Chaddad F, Freitas F, Miranda M, Vasconcellos N, Valiente R, Muehlschlegel S, Silva GS. Kinetics of cerebral blood flow velocities during treatment for delayed cerebral ischemia in aneurysmal subarachnoid hemorrhage. Neurocrit Care. 2022;36(1):226–39. https://doi.org/10.1007/s12028-021-01288-z. Epub 2021 Jul 20.
23. Robba C, Taccone FS. How I use transcranial Doppler. Crit Care. 2019;23(1):420. https://doi.org/10.1186/s13054-019-2700-6.

24. Majewska P, Hara S, Gulati S, Solheim O. Association between transcranial Doppler vasospasm and functional outcome after subarachnoid hemorrhage. Brain Circ. 2021;7(4):271–6. https://doi.org/10.4103/bc.bc_63_21.
25. Alexandrov AV, Sloan MA, Tegeler CH, Newell DN, Lumsden A, Garami Z, Levy CR, Wong LK, Douville C, Kaps M, Tsivgoulis G, American Society of Neuroimaging Practice Guidelines Committee. Practice standards for transcranial Doppler (TCD) ultrasound. Part II. Clinical indications and expected outcomes. J Neuroimaging. 2012;22(3):215–24. https://doi.org/10.1111/j.1552-6569.2010.00523.x. Epub 2010 Oct 26.
26. Aaslid R, Huber P, Nornes H. Evaluation of cerebrovascular spasm with transcranial Doppler ultrasound. J Neurosurg. 1984;60(1):37–41. https://doi.org/10.3171/jns.1984.60.1.0037.
27. Hakimi R, Alexandrov AV, Garami Z. Neuro-ultrasonography. Neurol Clin. 2020;38(1):215–29. https://doi.org/10.1016/j.ncl.2019.09.006.
28. Ditz C, Leppert J, Neumann A, Krajewski KL, Gliemroth J, Tronnier VM, Küchler J. Cerebral vasospasm after spontaneous subarachnoid hemorrhage: angiographic pattern and its impact on the clinical course. World Neurosurg. 2020;138:e913–21. https://doi.org/10.1016/j.wneu.2020.03.146. Epub 2020 Apr 2.
29. Weiss M, Albanna W, Conzen C, Megjhani M, Tas J, Seyfried K, Kastenholz N, Veldeman M, Schmidt TP, Schulze-Steinen H, Wiesmann M, Clusmann H, Park S, Aries M, Schubert GA. Optimal cerebral perfusion pressure during delayed cerebral ischemia after aneurysmal subarachnoid hemorrhage. Crit Care Med. 2022;50(2):183–91. https://doi.org/10.1097/CCM.0000000000005396.
30. Megjhani M, Weiss M, Ford J, Terilli K, Kastenholz N, Nametz D, Kwon SB, Velazquez A, Agarwal S, Roh DJ, Conzen-Dilger C, Albanna W, Veldeman M, Connolly ES Jr, Claassen J, Aries M, Schubert GA, Park S. Optimal cerebral perfusion pressure and brain tissue oxygen in aneurysmal subarachnoid hemorrhage. Stroke. 2022;54:189. https://doi.org/10.1161/STROKEAHA.122.040339. Epub ahead of print.
31. Raymond J, Létourneau-Guillon L, Darsaut TE. Angiographic vasospasm and delayed cerebral ischemia after subarachnoid hemorrhage: moving from theoretical to practical research pertinent to neurosurgical care. Neurochirurgie. 2022;68(4):363–6. https://doi.org/10.1016/j.neuchi.2021.10.001. Epub 2021 Nov 26.
32. Rebeiz T, Sabirov T, Wanchoo S, White TG, Da Silva I, Stefanov DG, Temes RE. Angiographic treatment of asymptomatic cerebral vasospasm following aneurysmal subarachnoid hemorrhage for the prevention of delayed cerebral ischemia. World Neurosurg. 2022;166:e135–9. https://doi.org/10.1016/j.wneu.2022.06.129. Epub 2022 Jul 3.
33. Shamshad A, Persad-Paisley EM, Wendell LC, Thompson BB, Reznik ME, Furie KL, Mahta A. Association of asymptomatic cerebral vasospasm with outcomes in survivors of aneurysmal subarachnoid hemorrhage. J Stroke Cerebrovasc Dis. 2022;31(12):106821. https://doi.org/10.1016/j.jstrokecerebrovasdis.2022.106821. Epub 2022 Oct 12.
34. Hollingworth M, Jamjoom AAB, Bulters D, Patel HC. How is vasospasm screening using transcranial Doppler associated with delayed cerebral ischemia and outcomes in aneurysmal subarachnoid hemorrhage? Acta Neurochir. 2019;161(2):385–92. https://doi.org/10.1007/s00701-018-3765-8. Epub 2019 Jan 12.
35. Lidington D, Wan H, Bolz SS. Cerebral autoregulation in subarachnoid hemorrhage. Front Neurol. 2021;12:688362. https://doi.org/10.3389/fneur.2021.688362.
36. Rynkowski CB, de Oliveira Manoel AL, Dos Reis MM, Puppo C, Worm PV, Zambonin D, Bianchin MM. Early transcranial Doppler evaluation of cerebral autoregulation independently predicts functional outcome after aneurysmal subarachnoid hemorrhage. Neurocrit Care. 2019;31(2):253–62. https://doi.org/10.1007/s12028-019-00732-5.
37. Robba C, Pozzebon S, Moro B, Vincent JL, Creteur J, Taccone FS. Multimodal non-invasive assessment of intracranial hypertension: an observational study. Crit Care. 2020;24(1):379. https://doi.org/10.1186/s13054-020-03105-z.
38. Rasulo FA, Bertuetti R, Robba C, Lusenti F, Cantoni A, Bernini M, Girardini A, Calza S, Piva S, Fagoni N, Latronico N. The accuracy of transcranial Doppler in excluding intracranial hypertension following acute brain injury: a multicenter prospective pilot study. Crit Care. 2017;21(1):44. https://doi.org/10.1186/s13054-017-1632-2.

39. Chang JJ, Tsivgoulis G, Katsanos AH, Malkoff MD, Alexandrov AV. Diagnostic accuracy of transcranial Doppler for brain death confirmation: systematic review and meta-analysis. AJNR Am J Neuroradiol. 2016;37(3):408–14. https://doi.org/10.3174/ajnr.A4548. Epub 2015 Oct 29.
40. Monteiro LM, Bollen CW, van Huffelen AC, et al. Transcranial Doppler ultrasonography to confirm brain death: a meta-analysis. Intensive Care Med. 2006;32:1937–44.
41. Consensus Group on Transcranial Doppler in Diagnosis of Brain Death. Latin American consensus on the use of transcranial Doppler in the diagnosis of brain death. Rev Bras Ter Intens. 2014;26(3):240–52. https://doi.org/10.5935/0103-507x.20140035.
42. Homma S, Messé SR, Rundek T, Sun YP, Franke J, Davidson K, Sievert H, Sacco RL, Di Tullio MR. Patent foramen ovale. Nat Rev Dis Primers. 2016;2:15086. https://doi.org/10.1038/nrdp.2015.86.
43. Komar M, Olszowska M, Przewłocki T, Podolec J, Stępniewski J, Sobień B, Badacz R, Kabłak-Ziembicka A, Tomkiewicz-Pająk L, Podolec P. Transcranial Doppler ultrasonography should it be the first choice for persistent foramen ovale screening? Cardiovasc Ultrasound. 2014;12:16. https://doi.org/10.1186/1476-7120-12-16.
44. Viski S, Olah L. Use of transcranial Doppler in intensive care unit. J Crit Care Med (Targu Mures). 2017;3(3):99–104. https://doi.org/10.1515/jccm-2017-0021.
45. Demchuk AM, Burgin WS, Christou I, Felberg RA, Barber PA, Hill MD, Alexandrov AV. Thrombolysis in brain ischemia (TIBI) transcranial Doppler flow grades predict clinical severity, early recovery, and mortality in patients treated with intravenous tissue plasminogen activator. Stroke. 2001;32(1):89–93. https://doi.org/10.1161/01.str.32.1.89.
46. Sarkar S, Ghosh S, Ghosh SK, Collier A. Role of transcranial Doppler ultrasonography in stroke. Postgrad Med J. 2007;83(985):683–9. https://doi.org/10.1136/pgmj.2007.058602.
47. Salinet AS, Panerai RB, Robinson TG. The longitudinal evolution of cerebral blood flow regulation after acute ischaemic stroke. Cerebrovasc Dis Extra. 2014;4(2):186–97. https://doi.org/10.1159/000366017.
48. Salinet AS, Silva NC, Caldas J, de Azevedo DS, de-Lima-Oliveira M, Nogueira RC, Conforto AB, Texeira MJ, Robinson TG, Panerai RB, Bor-Seng-Shu E. Impaired cerebral autoregulation and neurovascular coupling in middle cerebral artery stroke: influence of severity? J Cereb Blood Flow Metab. 2019;39(11):2277–85. https://doi.org/10.1177/0271678X18794835. Epub 2018 Aug 17.
49. Nogueira RC, Aries M, Minhas JS, Petersen N, Xiong L, Kainerstorfer JM, Castro P. Review of studies on dynamic cerebral autoregulation in the acute phase of stroke and the relationship with clinical outcome. J Cereb Blood Flow Metab. 2022;42(3):430–53. https://doi.org/10.1177/0271678X211045222. Epub 2021 Sep 13.
50. Meyer M, Juenemann M, Braun T, Schirotzek I, Tanislav C, Engelhard K, Schramm P. Impaired cerebrovascular autoregulation in large vessel occlusive stroke after successful mechanical thrombectomy: a prospective cohort study. J Stroke Cerebrovasc Dis. 2020;29(3):104596. https://doi.org/10.1016/j.jstrokecerebrovasdis.2019.104596. Epub 2020 Jan 3.
51. Tian G, Ji Z, Huang K, Lin Z, Pan S, Wu Y. Dynamic cerebral autoregulation is an independent outcome predictor of acute ischemic stroke after endovascular therapy. BMC Neurol. 2020;20(1):189. https://doi.org/10.1186/s12883-020-01737-w.
52. Rasmussen M, Schönenberger S, Hendèn PL, Valentin JB, Espelund US, Sørensen LH, Juul N, Uhlmann L, Johnsen SP, Rentzos A, Bösel J, Simonsen CZ, SAGA Collaborators. Blood pressure thresholds and neurologic outcomes after endovascular therapy for acute ischemic stroke: an analysis of individual patient data from 3 randomized clinical trials. JAMA Neurol. 2020;77(5):622–31. https://doi.org/10.1001/jamaneurol.2019.4838.
53. Caldas J, Rynkowski CB, Robba C. POCUS, how can we include the brain? An overview. J Anesth Analg Crit Care. 2022;2:55. https://doi.org/10.1186/s44158-022-00082-3.
54. Meyfroidt G, Bouzat P, Casaer MP, Chesnut R, Hamada SR, Helbok R, Hutchinson P, Maas AIR, Manley G, Menon DK, Newcombe VFJ, Oddo M, Robba C, Shutter L, Smith M, Steyerberg EW, Stocchetti N, Taccone FS, Wilson L, Zanier ER, Citerio G. Management of moderate to severe traumatic brain injury: an update for the intensivist. Intensive Care Med. 2022;48(6):649–66. https://doi.org/10.1007/s00134-022-06702-4. Epub 2022 May 20. Erratum in: Intensive Care Med. 2022 Jul;48(7):989–991.

Regional Anaesthesia for the Intensivist

Edmund Chan, Cosmin Balan, and Amit Pawa

Contents

21.1 Introduction – 326
21.1.1 The Case for Regional Analgesia in the Intensive Care Unit – 326
21.1.2 The Common Indications for Regional Analgesia in the ICU – 327

21.2 The Thoracic Wall – 328
21.2.1 Thoracic Trauma Analgesia – 328
21.2.2 Analgesia Post-Thoracic Surgery – 332
21.2.3 Developments in Cardiac Surgery – 335

21.3 The Abdomen – 338
21.3.1 The Emergency Laparotomy – 340
21.3.2 Other Abdominal Wall Blocks – 342

21.4 The Extremities – 344
21.4.1 Acute Compartment Syndrome (ACS) – 346
21.4.2 Changes to Nomenclature in Regional Anaesthesia – 347

References – 348

© The Author(s), under exclusive license to Springer Nature Switzerland AG 2023
C. Robba et al. (eds.), *Basic Ultrasound Skills "Head to Toe" for General Intensivists*, Lessons from the ICU,
https://doi.org/10.1007/978-3-031-32462-8_21

21

Learning Objectives

- Recognise the patient groups who may benefit from regional anaesthetic techniques.
- Describe the various techniques available to treat pain in the various body compartments.

21.1 Introduction

21.1.1 The Case for Regional Analgesia in the Intensive Care Unit

Delivering optimum analgesia without side effects continues to represent an unmet goal of critically ill therapeutics. Two distinct factors often contribute to enhance this liability: (1) quantitative and objective assessment of pain and/or nociception is still unattainable in the intensive care unit (ICU), resulting in poor awareness of actual patient pain intensity [1], and (2) opioids constitute the mainstay of most multimodal analgesia regimens, resulting in inadequate patient cooperation secondary to several complications such as delirium and decreased level of consciousness.

Regional analgesia has recently emerged as a versatile tool promising to resolve the dilemma of adequate pain relief in the ICU environment [2, 3]. By minimising or avoiding opioids, regional analgesia emulates opioid-free anaesthesia (OFA) pathways in a quest to rationalise opioid use [4].

Within the critically ill population, attributes of regional analgesia relate to and extend beyond those commended by the enhanced recovery after surgery (ERAS) algorithms [5]. Putative benefits specific to the critically ill, which could result from early and individualised institution of regional blockade, include improved pulmonary mechanics and patient–ventilator synchrony [6]; increased alertness and prevention of delirium, augmented gut motility and splanchnic microperfusion [7]; mitigation of post-traumatic stress disorder and chronic neuropathic pain, attenuation of surgery and trauma—stress and shock-driven sympatho-adrenal hyperactivation and ensuing endotheliopathy (SHINE) [8, 9] and overall accelerated rehabilitation.

When adequately performed, regional analgesia techniques are virtually devoid of systemic effects owing to their site-specific characteristics although, depending on choice (neuraxial vs peripheral nerve blocks) and underlying pathology, challenges may still arise and usually pertain to drug, patient, environmental and nursing-staff factors. Amongst these, patient-related problems are the commonest to deal with and are represented by sepsis, coagulopathy and dependence on vasoactive drugs. Risk versus benefit also needs to be considered carefully, as these procedures may be performed in sedated patients [9–12]. The risk of local anaesthetic toxicity (LAST) must also be borne in mind, especially in the context of continuous regional anaesthetic modalities.

With the advent of point-of-care ultrasonography and portable ultrasound machines, use of regional analgesia in ICU is poised to grow and evolve as risks and complications become more amenable to quantification and preventive care.

The scope of this chapter is to explore practicable regional analgesia options in specific clinical ICU circumstances, including analgesic techniques for the thoracic wall, abdomen and peripheries, with a special emphasis on ultrasound-guided regional techniques.

21.1.2 The Common Indications for Regional Analgesia in the ICU

The common indications for regional anaesthesia in intensive care are summarised in Table 21.1 [10].

Table 21.1 Common indications and potential options for regional anaesthesia in intensive care. Table was adapted from and published in BJA Education, Vol 16, Venkataraju A & Narayanan M, "Analgesia in intensive care: part 2", pages 397–404. Copyright Elsevier 2016

Indications	Regional analgesia options
Surgical indications	
Thoracotomy	Thoracic epidural Paravertebral blocks Serratus anterior plane block Erector spinae plane block
Laparotomy	Neuraxial blockade Transversus abdominis plane blocks Rectus sheath blocks Local infiltration
Rib fractures	Thoracic epidural Paravertebral blocks Interpleural block Intercostal blocks Serratus anterior plane block Erector spinae plane block
Limb fractures	Lower limb: Neuraxial blockade, fascia iliaca plane block, femoral and sciatic peripheral nerve blocks Upper limb: Brachial plexus blocks, peripheral nerve blocks
Non-surgical indications and ICU procedures	
Acute pancreatitis	Thoracic epidural
Chest drains	Intercostal blocks, serratus anterior plane block
Tracheostomy	Superficial cervical plexus block
Debridement/dressing changes	Upper/lower limb blocks as appropriate

21.2 The Thoracic Wall

In recent years, numerous techniques have developed for thoracic wall analgesia [13]. In addition to the more established paravertebral (PVB) and thoracic epidural blocks [12, 14], examples of these include:

1. Those covering the anterolateral aspect of the chest: serratus anterior plane (SAP) blocks, pectoralis 1 and 2 (PECS) blocks; those covering the anteromedial aspect: the parasternal intercostal fascial plane blocks. These include the pecto-intercostal fascial plane block (PIFB) and the transversus thoracis muscle plane blocks (TTMPB), covering superficial and deep planes, respectively.
2. Those included under the umbrella of "paravertebral by proxy" where access to the paravertebral space may be made indirectly by more distant needle-tip positions: erector spinae plane (ESP), retrolaminar and the midpoint transverse process to pleura (MTP) blocks. Other novel blocks include the paraspinal intercostal plane blocks, which include the paraspinal intercostal block [15], and the rhomboid intercostal with subserratus plane block [16].

In an ICU setting, two main indications for thoracic wall regional techniques predominate: analgesia post-thoracotomy and rib fracture analgesia. There has also been ongoing work regarding use of regional anaesthesia in cardiac surgery.

21.2.1 Thoracic Trauma Analgesia

Clinical Vignette 21.1

A 48-year-old man, who was previously fit-and-well with no other comorbidities, has fallen from a ladder. He sustained multiple undisplaced posterolateral rib fractures on the right-hand side at T6 to T10 levels without a flail segment. He has been admitted to critical care for low saturations and inadequate analgesia.

Rib fractures are common and have a prevalence of 4–10% in trauma patients [10]. Morbidity rises after the age of 45 [17], and mortality in the elderly has been quoted to be as high as 22% [18]. Rib fractures generally result from blunt chest wall trauma, with younger adults tending to sustain higher impact injuries, whilst the elderly usually sustain fragility fractures. Other causes may include stress and pathological fractures [19].

Rib fractures may be associated with other complications, which impair ventilation. Immediate impairment of ventilation may arise from direct damage to pleural and blood vessels, leading to pneumo- and haemothoraces. Flail segments may lead to inefficient paradoxical movement and lead to an increased mortality. Further ventilatory impairment may occur in the next hours to days as contusions develop, whilst pain may impair the patient's inability to generate adequate tidal volumes and to cough, leading to atelectasis, sputum retention and pneumonia [19].

Adequate analgesia, therefore, forms a cornerstone of rib fracture management, and usually, a stepwise approach is implemented [19]. Traditional management has been largely based on systemic analgesia, with only small numbers receiving thoracic epidural or paravertebral blockade [20].

A recent meta-analysis [21] showed that whilst epidural anaesthesia improved pain relief when compared with systemic analgesia, there were no statistically significant differences in ICU lengths of stay, duration of mechanical ventilation or hospital length of stay. When epidural analgesia was compared with paravertebral blockade, no differences were found in analgesia effectiveness, hospital length of stay or ICU length of stay.

Only one randomised controlled trial comparing paravertebral block against systemic analgesia was included in this meta-analysis. This single-centre study, with small patient numbers, favoured paravertebral blockade against intravenous analgesia in analgesia effectiveness [21, 22]. Others have suggested paravertebral blockade may be associated with improved mortality when compared with systemic analgesia using retrospective data [20, 23]. Overall, data for paravertebral blockade in rib fractures remain scant [24].

Further, all have these techniques have their drawbacks. Systemic analgesia may lead to adverse effects, especially in the elderly with comorbidities. Central neuraxial blockade may be inappropriate in polytrauma patients with coagulopathy and may lead to other adverse effects such as hypotension, leading to a need for vasopressor support. Both epidurals and paravertebral blocks are techniques, which require specific training, and are not necessarily simple to perform practically, especially if the patient is supine, sedated and ventilated.

What alternatives may be available to the ICU clinician, especially in the context of a critically unwell patient?

Intercostal nerve blocks are relatively simple to perform but usually require multiple injections, with potentially limited use for catheters. In three previous studies [25–27], looking at continuous intercostal nerve blocks for rib fracture analgesia each describe different catheter insertion techniques, making it difficult to reproduce and standardise.

Two fascial plane blocks have emerged recently for rib fracture analgesia: the SAP block (◘ Fig. 21.1) and the ESP block (◘ Fig. 21.2) [13]. As pointed out by El-Boghdadly and Wiles [24], most of the evidence supporting these blocks are from case reports, case series and retrospective data, with little prospective data. A recent retrospective study showed that the ESP block was associated with reduced pain scores and improved incentive spirometry volumes [28]. Another retrospective observational study compared SAP catheters with epidural and paravertebral catheters and showed that whilst all three were associated with reduced pain scores and increased inspiratory volumes post-block, there were no significant differences between the techniques [29]. Considering the perceived technical challenges of siting epidural and paravertebral catheters, this may be an advantage of the SAP catheter.

The decision of which block to perform may be determined by the location of the fracture. There have been suggestions that SAP blocks are mostly suited for anterolateral rib fractures, whilst the ESP block also covers posterior rib fractures [19, 24, 30]. It should be noted, however, that one group has suggested that SAP catheters may be helpful with posterior rib fractures, although the evidence presented is only in a case report and a case series [31, 32].

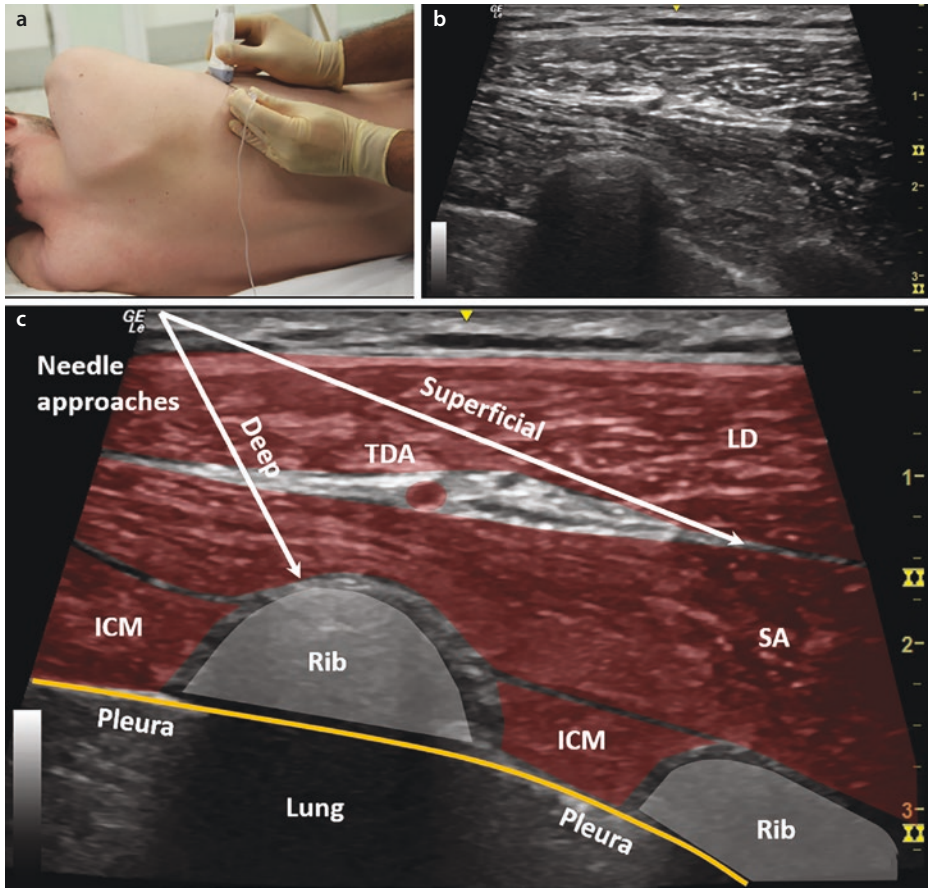

Fig. 21.1 SAP block performed in a lateral position with the probe placed transverse in the mid-axillary line at the level of rib 5 **a** with an unlabelled **b** and a labelled **c** ultrasound image. It may also be performed with the patient supine, with the arm brought forward or elevated to allow access to the axilla. Typically, a linear probe is used with an echogenic needle 80 mm in length, injecting 0.4 mL/kg of LA. The SAP block may be performed with the superficial approach, with LA deposited in the plane between the latissimus dorsi (LD) and the serratus anterior (SA) muscles or with the deep approach, with LA deposited in the plane between the SA muscle and the rib and intercostal muscles (ICM). Only one end point is required: there is no evidence clinically which end point is preferable. Note the thoracodorsal artery (TDA) running between LD and SA can be seen at this level and should be avoided [123, 124]

Although there is little prospective data for either block, several aspects of each mean that they should be a serious consideration for the ICU clinician [13]. First, as fascial plane blocks, they may be technically simpler to learn and implement than epidural or paravertebral catheters. Both techniques are undertaken with ultrasound guidance, with the needle end point relatively distant from critical anatomical structures. Second, they may be practically simpler in an ICU setting when compared with epidural or paravertebral analgesia: SAP blocks may be performed in a supine patient, whereas ESP blocks can be performed on a sitting, prone or laterally positioned patient. Third, although there may be a small risk for local anaesthetic to

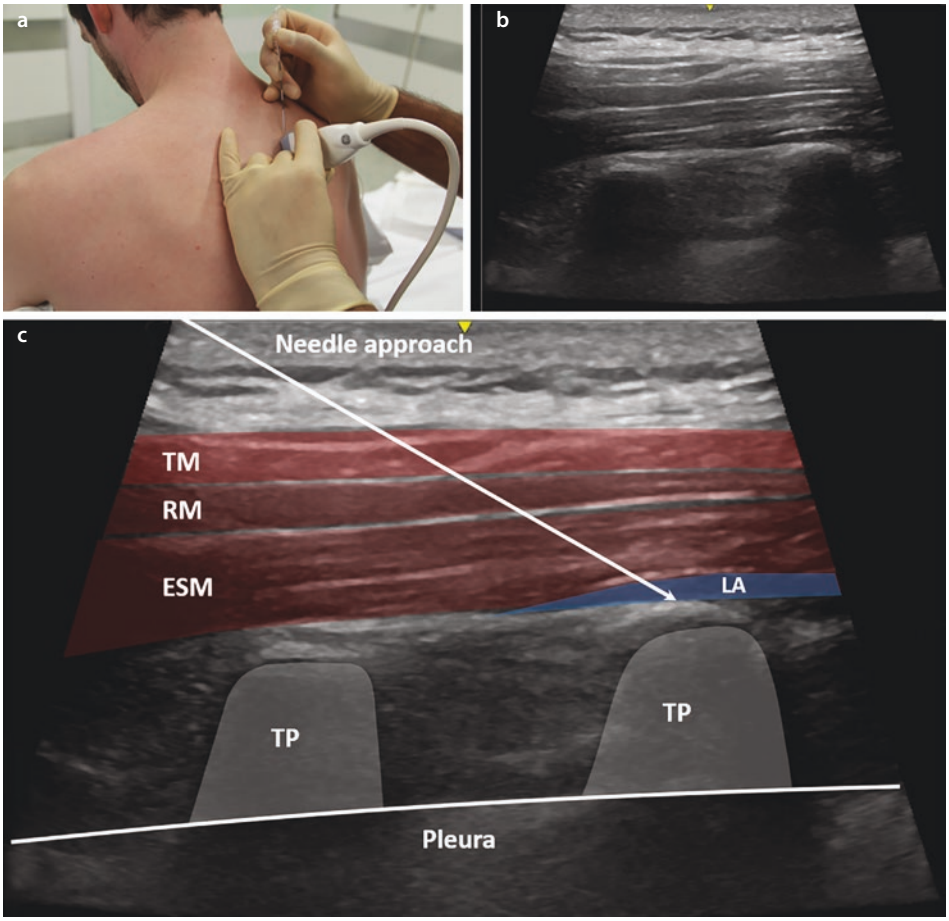

Fig. 21.2 Erector spinae plane (ESP) block performed in a sitting position **a**, with an unlabelled **b** and a labelled **c** ultrasound image: it can also be performed with the patient lying lateral or prone. The transverse process (TP) is identified by scanning sagittally initially in the midline, identifying the spinous processes, moving laterally approximately 3 cm until the typical squared-off, oblong-shaped hyperechoic acoustic shadows of the TPs are seen. Moving too laterally will show the ribs, which have much more rounded shadows (not shown here). Typically performed using an 80 mm echogenic needle, advancing through the muscle layers towards the TP. 20 mL of LA is deposited in the fascial plane between the erector spinae muscle (ESM) and TP [124, 125]. In the authors' experience, a Tuohy needle may provide better needle visibility. *TM* trapezius muscle, *RM* rhomboid muscle, *LA* local anaesthetic

reach the epidural space with ESP blocks, leading to hypotension, the mass of local anaesthetic is likely to be too small. Fourth, although careful risk–benefit analyses must be undertaken by the clinician when undertaking regional anaesthesia in a patient with potential coagulopathy, neither ESP nor SAP blocks have major vessels at their expected needle end points, and both are relatively superficial, allowing for compression.

Important considerations beyond coagulopathy and hypotension of these blocks include LAST, especially in those requiring bilateral blockade, as larger volumes of local anaesthetics are generally required in fascial plane blocks. Methods of mitiga-

tion include using dilute concentrations of local anaesthetic, using less cardiotoxic agents such as levobupivacaine and ropivacaine and using adrenaline-containing solutions. There may be variation in individual response, as these blocks rely on passive spread of local anaesthetic through fascial planes. Although it is considered unlikely that SAP block performance under ultrasound guidance would be complicated by pneumothoraces, there has been a reported case [33].

Despite the lack of high-quality, prospective evidence, the uptake of these blocks by those managing rib fractures has been rapid, driven by a combination of technical simplicity, widespread use of ultrasound and good theoretical safety profile. Other techniques, such as surgical fixation, should also be considered in the management of rib fractures [19]. Ultimately, further studies will be required to elucidate the optimal regional anaesthetic technique in the management of rib fractures, and it remains to be seen whether the promising data we have seen so far would be borne out in larger, higher-quality randomised controlled trials. Nevertheless, their role in rib fracture management appears to be becoming more established.

Clinical Vignette 21.2

A 72-year-old female has had video-assisted thoracoscopic (VATS) lobectomy for lung cancer. Her comorbidities include chronic obstructive pulmonary disease, ischaemic heart disease and mild renal impairment. She has been transferred, extubated, to the high dependency unit post-operatively for monitoring.

21.2.2 Analgesia Post-Thoracic Surgery

Multiple post-operative analgesia strategies exist for thoracic surgery, although there has been recent focus on comparing paravertebral blocks (PVB) with other techniques, including thoracic epidurals. Minimally invasive VATS procedures have become increasingly popular and are recommended for early stage lung cancer resection surgery [34].

A Cochrane meta-analysis in 2016 [35] found comparable analgesic efficacy at rest and after coughing at all time-points when PVB is compared with thoracic epidurals. They found no differences in 30-day mortality, major complications (e.g. hypotension requiring inotropic support, arrhythmias, myocardial infarctions, requirement for ventilation, acute CO_2 retention and pneumonia), unexpected intensive care admissions or length of hospital stay. PVB was found to have a better minor complication profile (e.g. hypotension not requiring inotropic support, nausea and vomiting, pruritus and urinary retention). However, the authors noted the results of this Cochrane meta-analysis be interpreted with caution due to data heterogeneity, echoing the findings from an earlier meta-analysis [36].

Other regional techniques, such as intercostal blocks and interpleural blocks, were compared in a systematic review [37]. Both thoracic epidural and PVB were superior to systemic analgesia. Intercostal blocks also showed benefit when compared with systemic analgesia. Like the previous studies, PVB was comparable with

thoracic epidurals for efficacy but had reduced hypotension. The authors found that interpleural analgesia was inconsistent in providing analgesia. Only one small study included in this review compared PVB with intercostal blocks, showing no significant differences in pain scores or supplementary morphine use [38].

The increasing popularity of SAP and ESP blocks have meant they are beginning to be used for post-thoracic surgery analgesia, especially with VATS procedures. A possible role has been suggested for the SAP block in recent "*Guidelines for enhanced recovery after lung surgery*" from the Enhanced Recovery After Surgery Society and the European Society of Thoracic Surgeons [34], as analgesia for uniported VATS, or where PVB is inappropriate, such as in pleurectomy. Both SAP and ESP blocks are theoretically well-suited anatomically and practically, and their side effect profile may be better than thoracic epidurals with reduced hypotension and potential of nerve damage. The lateral decubitus positioning of the patient facilitates the performance of these blocks after induction if desired.

Considering their relatively novelty, there is limited high-quality evidence for their use in this context, especially for catheter-based techniques. There are numerous case reports and case series [39–44], and some promising prospective data is starting to emerge. Both have been studied in randomised controlled trials, although most of these are single centred, with relatively small numbers.

Park et al. [45] compared the effects of preoperative single-injection SAP block on post-operative pain and opioid consumption after VATS with controls, where all patients received intravenous patient-controlled analgesia (PCA) and adjuvant analgesia. Small reductions in intraoperative remifentanil and post-operative fentanyl consumption were found. Pain severity, measured using the numeric rating scale (NRS), was modestly reduced with SAP blockade and improved patient satisfaction reported. However, this study is limited by the lack of placebo procedures, which increased the inherent risk of bias. These findings are echoed in another trial by Semyonov et al. [46]. Kim et al. [47] found improved Quality of Recovery-40 (QoR-40) scores, pain scores at rest and opioid consumption in the early post-operative period in a similarly sized RCT between SAP blockade and normal saline controls.

It should be noted that all three trials are small, single-centre studies, using single-shot techniques, on the background of multimodal analgesia. More high-quality data is required to further elucidate the role of SAP blocks in this setting and compare it against other methods of regional analgesia.

Saad et al. [48] compared single-injection SAP blockade against PVB and controls in the context of thoracotomy and may provide better evidence of the analgesia efficacy of SAP blockade for thoracic procedures. Further, they compared it against PVB. They reported that whilst the visual analogue score (VAS) in the early post-operative period (9 h) for both SAP and PVB were significantly lower than control, the PVB group had lower VAS compared to SAP and control groups at 12 and 24 h. Only 23% of the PVB group required supplemental morphine compared with 97% in the SAP group. On the other hand, the PVB group seem to experience more hypotension: 13% of the PVB group compared with none in the SAP group.

In a critical care setting, catheter techniques may be preferred. Khalil et al. [49] compared a SAP block and catheter technique with thoracic epidural in patients undergoing thoracotomy, and found that whilst VAS and postoperative morphine consumption were comparable between the two groups, the thoracic epidural group recorded lower mean arterial pressures. Although this study was small, with only 20

patients in each arm, the comparable analgesic effect of SAP continuous blockade, without the hypotension, shows promise.

Like the SAP block, there is a relative paucity of prospective data regarding the ESP block. Nevertheless, data has begun to emerge.

With regards to thoracotomy, Wang et al. [50] found that a single-shot ESP block compared favourably against wound infiltration in patients undergoing open oesophagectomy. They found lower intraoperative and post-operative opioid use, reduced nausea and vomiting and lower pain scores immediately on days 1 and 2. Fang et al. [51] compared single-injection ESP block with PVB block in patients undergoing posterolateral thoracotomy. They looked at VAS pain scores at rest and on coughing at various time points post-operatively, together with PCA use, adverse effects, puncture time and success rate of one puncture and found that there were no significant differences in pain scores, opioid consumption and post-operative nausea and vomiting (PONV), but reduced hypotension, haematoma, and a higher success rate of one puncture in the ESP group.

Both studies show promising results in favour of ESP blocks, but it must be noted that both are single-centred studies with small numbers, and both used single-injection techniques. In particular, the former did not use a sham procedure, increasing the risk of bias. Further studies comparing ESP catheters with other techniques would be useful in truly determining analgesic efficacy in this population, especially in a critical care setting.

With regards to minimally invasive thoracic surgery, Ciftci et al. [52] compared single-injection ESP blockade against controls in patients undergoing VATS and found that passive and active VAS scores and opioid consumption was reduced at all time-points up to 24 h post-operatively in the ESP group, with greater nausea and pruritus rates in the control group, suggesting that ESP block may be of benefit in the VATS population.

How does ESP blockade compare with other types of regional anaesthesia in this setting?

Finnerty et al. [53] compared single-injection ESP blockade with SAP blockade. They found that ESP blockade compared favourably against SAP blockade with regards to post-operative Quality of Recovery-15 (QoR-15) score and time to first analgesia in recovery. There was no difference in opioid consumption, and this study was not appropriately powered to detect differences in length of stay. Interestingly, they attempted to detect differences in complications using the Comprehensive Complication Index between the groups and showed that the ESP block group achieved better scores.

Perhaps of greatest interest is from a recent trial by Taketa et al. [54] where they compared continuous ESP blockade with PVB, with the authors concluding that the continuous ESP block was non-inferior to PVB at rest, 24 h post-operatively. They found that the ESP block group had statistically significantly higher pain scores at 1, 2 and 24 h at rest, though with the latter the confidence interval was under 1, which allowed the authors to conclude non-inferiority. They found no differences in pain score on movement or opioid consumption (per body weight).

Although the authors have suggested that an ESP catheter technique may be comparable to continuous PVB in the VATS setting, it is difficult to ignore the significant pain score differences at the earlier post-operative time points. A further study powered to study differences at these time points may be required to prove

non-inferiority of the ESP catheter technique more comprehensively. Nevertheless, these results are promising in view of the potentially simpler ESP technique.

21.2.3 Developments in Cardiac Surgery

The use of regional anaesthesia in cardiac surgery has traditionally been limited, primarily due to concerns regarding anticoagulation. With the development of ERAS protocols in cardiac surgery, however, there has been a renewed interest in regional anaesthesia and other opioid-sparing techniques, looking to reduce length of stay, and improving efficiency in resource utilisation [55].

With regards to thoracic epidurals, the most recent Cochrane review and meta-analysis in 2019 demonstrated no mortality benefit at 0–30 days in those receiving thoracic epidural blockade when compared with comparators (systemic analgesia, peripheral nerve block, wound infiltration, intrapleural analgesia) [56]. None of the studies included reported epidural haematomas. A separate review in 2015 identified 25 haematomas from an estimated 88,820 epidurals, leading to an estimated risk of 1:3552 [57].

With regards to PVB, bilateral catheters are required if it is to cover a midline sternotomy, and like thoracic epidurals, catheter misplacement, LAST and anticoagulation remain a concern in this deep space. One RCT compared bilateral paravertebral catheters with subcutaneous lidocaine infusions, where the subcutaneous catheters were inserted in the same locations as the paravertebral catheters, in patients undergoing coronary artery bypass surgery. No difference in morphine consumption between groups was found [58].

Understandably, with uncertain evidence and the potentially devastating risk of epidural haematomas with thoracic epidurals, and a lack of evidence of benefit in bilateral paravertebral blockade, other blocks have been explored for cardiac surgery. As with previous clinical applications, these newer blocks have a limited evidence base, but the relative technical simplicity and lower risk in the context of anticoagulation make a compelling case for their consideration.

The ESP block stands out as a potential candidate amongst the new thoracic myofascial plane blocks. One RCT compared bilateral single-shot ESP blockade with control in 106 patients undergoing elective cardiac surgery with cardiopulmonary bypass and found reduced pain scores up to 12 h post-extubation and greater duration of analgesia [59]. They also found that the ESP group was extubated significantly earlier than controls, with earlier time to ambulation and reduced total length of ICU stay. Another study compared bilateral continuous ESP blockade with thoracic epidurals [60]. They found that pain scores, incentive spirometry, ventilator and ICU stay durations were all comparable, suggesting that bilateral ESP blockade may be a viable alternative to thoracic epidurals in cardiac surgery. It should be noted that both these studies used relatively young surgical populations with means ages between 40 and 50, had relatively small numbers, and the patients were unblinded due to the methodology, leading to potential issues with generalisability and bias.

Finally, a before-and-after study, comparing 47 prospective consecutive open cardiac surgery patients that had bilateral ESP catheters with 20 historical patient-matched controls, found that continuous ESP block was associated with reduced opioid consumption post-operatively; improved times to chest drain removal, time to first mobilisation; pain scores both at 2 h after chest drain removal and at rest 1

month after surgery, though no differences were found in time to extubation; pain at rest and during first mobilisation and pain during mobilisation at 1 month after surgery. The authors also noted reduced post-operative adverse events (hypotension, PONV, hyperglycaemia) [61].

Whilst all three of these studies show promising results, especially in the context of ERAS programmes, small numbers and problems with methodology mean that firm conclusions and recommendations cannot be made. Further, ESP block complications and their occurrence rates remain relatively unknown. Although no complications related to the regional technique were reported in any of these studies, they were probably not sufficiently powered to detect them and, therefore, require further investigation. Nevertheless, these results are compelling enough for further study.

The pectoralis (PECS I and II), SAP, sternal bed, TTMPB and PIFB have all been reported to have been used in cardiac surgery. The PECS block, TTMPB, and PIFB have each undergone at least one RCT [62–65]. The SAP block has been studied in the context of minimally-invasive cardiac surgery, undertaken through a thoracotomy incision, and in thoracotomy-based paediatric cardiac surgery [66, 67].

The PECS I block targets the pectoral nerve between the pectoralis major and minor muscles, and the PECS II block targets the lateral cutaneous intercostal branches of T2-T6 between the pectoralis minor and serratus anterior muscles, in addition to the PECS I target. The PECS blocks are performed optimally with the patient supine under ultrasound guidance, which is particularly applicable in an ICU setting.

The PECS II block has been studied in a small RCT in the context of cardiac surgery, where post-operative placement of bilateral PECS II block with drain site infiltration is compared with no block in patients undergoing midline sternotomy [65]. The authors reported that patients receiving the block required lower duration of ventilator support, with lower pain scores at rest and during coughing early in the post-extubation period, and reduced need for rescue analgesia. Pain scores became comparable at 24 h post-extubation between the PECS group and the control. Although further studies with larger numbers are needed, the PECS II with mediastinal drain site infiltration combination described in this study represents a potentially viable method of longer-lasting non-opioid based rescue analgesia once a patient arrives in cardiac intensive care, where its placement is facilitated by the supine positioning of the patient.

The PIFB (Fig. 21.3) aims to target the anterior branches of the intercostal nerves as they run in the plane between the pectoral and the intercostal muscles and emerge on either side of the sternum. It was studied in 80 patients undergoing median sternotomy, randomised to bilateral PIFB or sham injection [62]. Although there was a trend in the primary outcome towards reduced cumulative opioid use, this did not reach significance. Pain scores, a secondary outcome, were reportedly reduced.

The TTMPB (Fig. 21.3), described by Ueshima et al. [68], is where local anaesthetic is injected in a deeper plane than PIFB, between the transversus thoracic muscle and the internal intercostal muscle, and covers the T2–T6 intercostal nerves and their anterior cutaneous branches. Aydin et al. [63] studied 48 patients undergoing cardiac surgery via midline sternotomy, where half received bilateral TTMPB and the other saline sham injections. They found the TTMPB block reduced post-operative 24-h opioid consumption and pain scores at rest and on movement for up to 12 h. The block group also had reduced PONV and pruritus than controls. A second study in children undergoing elective cardiac surgery also showed reduced post-operative opioid consumption and pain scores. They showed reduced time to

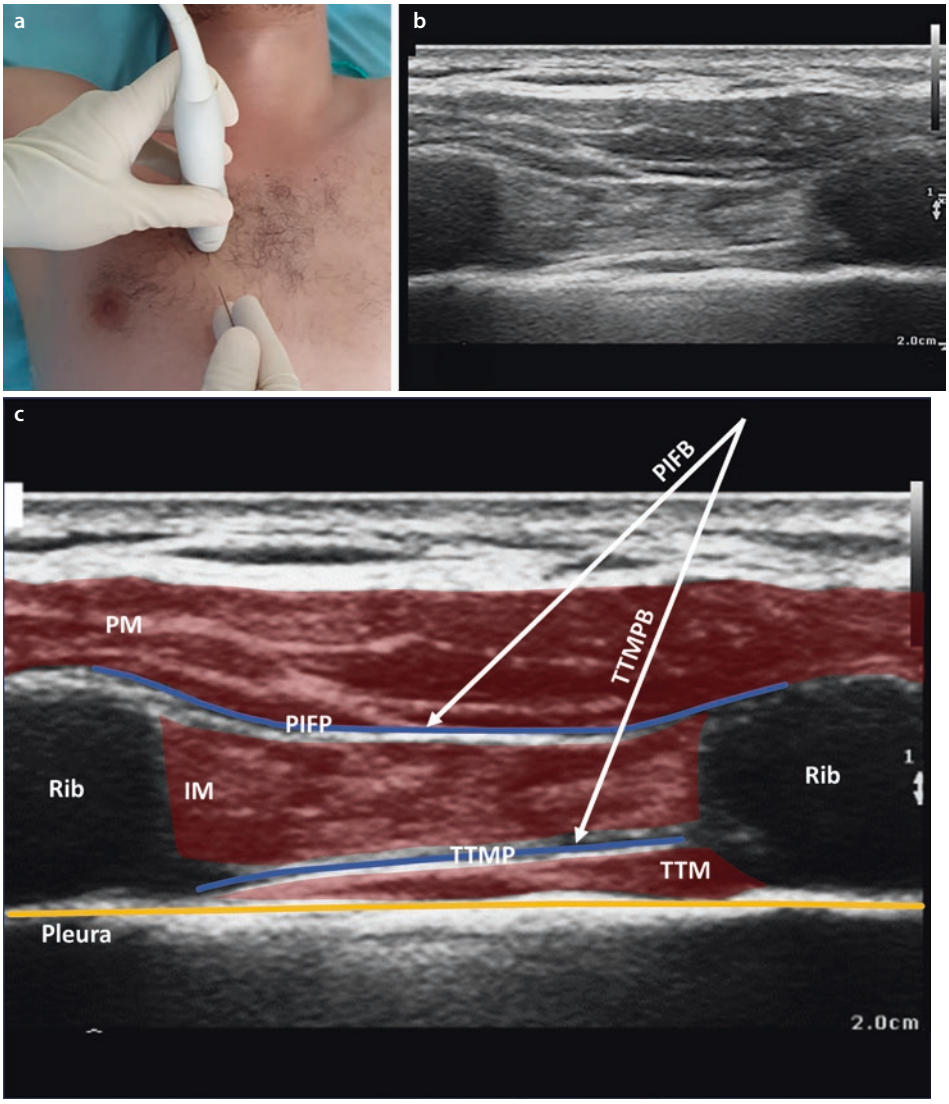

Fig. 21.3 Image demonstrating the surface anatomy **a** and an unlabelled **b** and labelled **c** ultrasound image in the paramedian sagittal plane of the PIFB and TTMPB. The TTMPB may be preferentially performed imaged in the transverse plane as it allows for better visualisation and avoidance of the internal mammary vessels, but has been demonstrated here in combination with the PIFB for convenience. *PM* pectoralis major, *IM* intercostal muscle, *IIM* internal intercostal muscle, *InnIM* innermost intercostal muscle, *TTM* thoracic transversus muscle, *PIFP* pecto-intercostal fascial plane, target for PIFB, *TTMP* thoracic transversus muscle plane, target for TTMPB

extubation and ICU length of stay as secondary outcomes [64]. Like the PIFB and PECS blocks, this block can be placed under ultrasound guidance with the patient in supine position. However, as the transversus thoracic muscle thins, it can be difficult to appreciate even with ultrasound [69].

The SAP block has been trialled in paediatric cardiac surgery through a thoracotomy incision [67], where intercostal nerve blocks, PECS II and SAP blocks were compared. They found that SAP and PECS blocks were comparable to each other and provided longer-lasting pain relief in comparison to intercostal nerve blocks. SAP blocks may also be considered in minimally invasive heart surgery, which is undertaken through thoracotomy. A retrospective study found that a single-shot SAP block was associated with lower morphine consumption and pain scores when compared with continuous wound infiltration through a catheter. Interestingly, ICU length of stay and in hospital were also lower in the SAP group. Both studies show that fascial plane blocks may be useful in thoracotomy-based minimally invasive surgery, warranting larger-scale studies.

With renewed interest in ICU resource management and ERAS programmes in cardiac surgery, the fascial plane blocks described here may become increasingly useful in the anaesthetists and intensivists armamentarium to combat pain post-cardiac surgery, especially considering their theoretical safety profile. Clearly, greater numbers of high-quality studies are required to demonstrating conclusively their safety profile and efficacy. Nevertheless, the currently presented data seem promising and warrant further investigation.

21.3 The Abdomen

Epidural anaesthesia is commonly used within critical care, and its benefits may stretch beyond analgesia alone [12]. A Cochrane review [70] compared epidural analgesia with local anaesthetics with systemic or epidural opioids in a broad range of abdominal surgeries and found that epidurals with local anaesthetic-based regimes reduced pain on movement and gastrointestinal transit time by approximately 17 h. Specifically, for open abdominal surgery, epidurals also reduced length of hospital stay.

"A systematic review by Smith et al. compared neuraxial, combined neuraxial/general anaesthesia with general anaesthesia alone in major truncal and lower limb surgery and found that the combined approach was associated with reduced odds of pulmonary complications and need for mechanical ventilation, surgical site infection, thromboembolic events, length of stay and ICU admissions when compared with general anaesthesia alone [71]. It did not find a reduction in 30-day mortality, which contrasted with an earlier meta-analysis [72]. Interestingly, Smith et al. found that combined neuraxial/general anaesthesia was associated with increased odds for myocardial infarction when compared with general anaesthesia alone. No cause for this association was identified. They did not find any increased odds for other cardiac complications, however, which matched the findings of the earlier analysis.

The finding that neuraxial anaesthesia led to benefits in reducing pulmonary complications is further reinforced by an earlier propensity-matched cohort study comparing regional anaesthesia with general anaesthesia in patient with chronic obstructive pulmonary disease, in which patients underwent a variety of truncal, lower limb and vascular procedures (including carotid endarterectomy) [73]. The authors found that regional anaesthesia was associated with reduced incidence of

post-operative pneumonia, length of ventilator dependence and unplanned post-operative intubation.

Epidural anaesthesia is also widely used in other surgical sub-specialties, such as in oesophagectomy. In this context, epidural anaesthesia has been shown to reduce pulmonary complications, mitigate the inflammatory response, and is associated with reduced ICU length of stay in a retrospective study [74, 75]. These benefits are often at the expense of hypotension, which needs to be carefully managed to avoid anastomotic hypoperfusion, and potentially leaks [75, 76]. In vascular surgery, a Cochrane review found that for elective abdominal aortic aneurysm repair, the addition of epidural anaesthesia to general anaesthesia reduced myocardial infarction and post-operative respiratory failure risk, pain scores up to 3 days, time to extubation and time spent in intensive care, and risk of gastrointestinal bleeding. However no mortality benefit was found [77]. In liver transplantation, one retrospective study found that the use of epidural anaesthesia was an independent predictor for early extubation [78].

Epidural anaesthesia is also well-studied in the context of acute pancreatitis, where a large multicentre retrospective observational study found that critically ill patients who received epidural analgesia had lower 30-day mortality rates [79]. A review summarised the potential mechanisms through which acute pancreatitis patients may benefit, including the induction of a targeted, localised sympathectomy, which may lead to splanchnic vasodilatation and improved pancreatic perfusion through its microcirculation, in addition to analgesia [80].

Epidural anaesthesia, therefore, has a role in selected patients undergoing major abdominal surgery or in those with acute pancreatitis, potentially with implications on ICU resources, beyond effective analgesia. However, they are not without their risk of complications, they have a potentially high failure rate of about 30% [81], and in some cases, data for efficacy remains inconclusive. For example, despite widespread use in oesophagectomy, recent meta-analyses [82, 83] have not demonstrated clear differences in analgesia efficacy in favour of epidurals when compared with systemic analgesia, with both sets of authors noting that further data is needed to determine the optimal analgesic modality. In liver surgery, coagulopathy remains a concern, and a recent meta-analysis comparing epidural analgesia against local anaesthetic infiltration via a wound catheter found that whilst pain scores were lower in those with an epidural on post-operative day 1, this difference diminished to insignificance on days 2 and 3, with possibly an increase in complications [84]. Further, the ERAS Society failed to recommend routine use of epidural analgesia in their guideline for liver surgery [85].

Clinical Vignette 21.3

A 56-year-old male has undergone emergency laparotomy for bowel perforation with peritonitis. His comorbidities include chronic obstructive pulmonary disease and hypertension. He has been transferred, whilst intubated and ventilated, to intensive care post-operatively.

21.3.1 The Emergency Laparotomy

The use epidural anaesthesia in the emergency laparotomy patient is contentious, as epidural anaesthesia may lead to hypotension in a potentially septic patient, who may also be coagulopathic. Further, some anaesthetists will be reluctant to site epidural catheters in the presence of possible bacteraemia [86]. There is no firm international consensus, with varying international guidelines differing in their recommendations for the use of epidural catheters in this cohort of patients [87–89]. The Practice Advisory from the American Society of Anesthesiologists and the

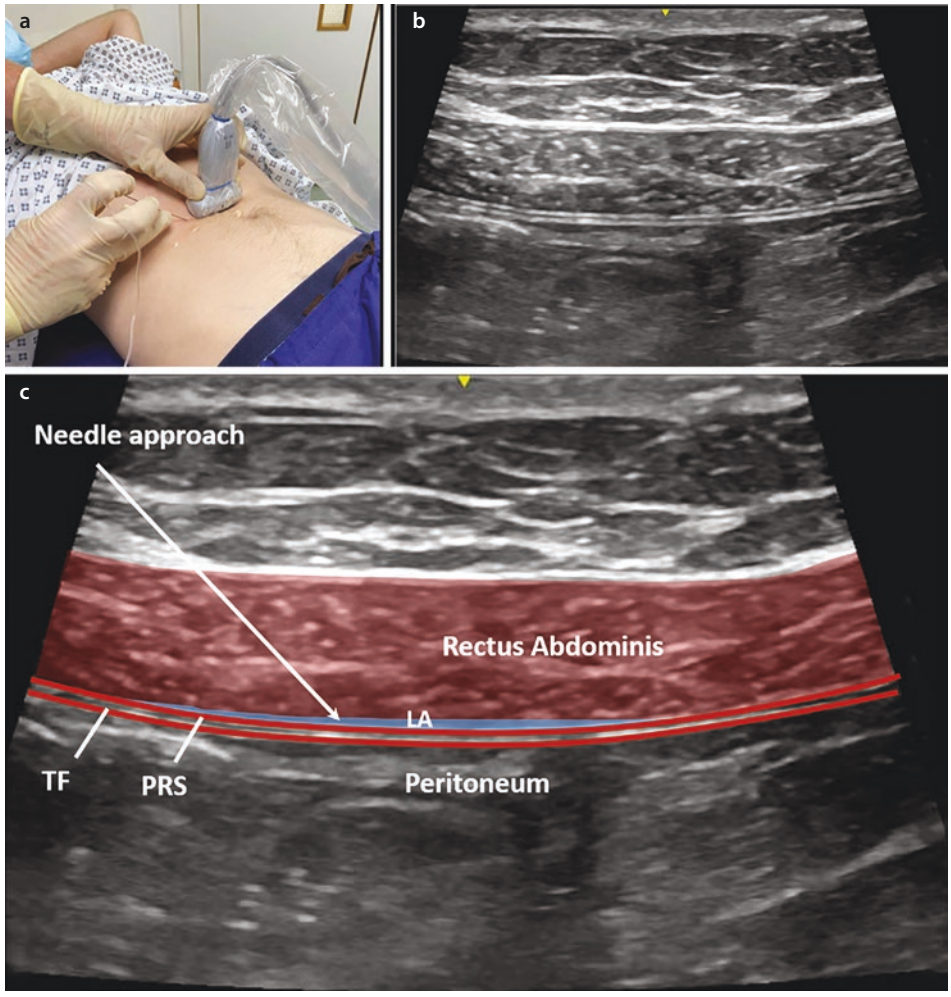

Fig. 21.4 Rectus sheath block performed using a linear probe, although a curvilinear may be preferable dependent on body habitus **a**, with an unlabelled **b** and labelled **c** ultrasound image. The transducer is placed just lateral to the umbilicus in the transverse plane, and the needle advanced through the rectus muscle to deposit 20 mL of LA between the rectus and the posterior rectus sheath (PRS) [126]. *TF* transversalis fascia, *LA* local anaesthetic

American Society of Regional Anesthesia and Pain Medicine advises that decision on their use be made on a case-by-case basis in this context, and to '*consider alternatives to neuraxial techniques in patients with high risk*'.

The rectus sheath block or catheter, where local anaesthetic is placed between the rectus abdominus and the posterior rectus sheath, may provide a suitable alternative (◘ Fig. 21.4). It targets the terminal muscular branches and anterior cutaneous branches of the thoracoabdominal nerves [90]. These can be placed under ultrasound guidance in the supine position or surgically under direct vision at the end of laparotomy. Their placement in a supine patient may be more pragmatic in an intubated, ventilated patient. When bilaterally placed, they are effective for midline incisions, laparoscopies and umbilical hernia repairs at locations above and below the umbilicus [12]. In terms of safety, the main complications are local anaesthetic toxicity, infection, vascular injury and puncture of the posterior rectus sheath and peritoneum, leading to possible bowel injury. Use of ultrasound guidance reduces this risk, however [91]. At normal local anaesthetic doses, there is little to no risk of hypotension.

In terms of efficacy, various small randomised controlled trials have shown bilateral blocks or catheters to be helpful in midline laparotomy, usually in the elective setting. Bakshi et al. [92] showed reduced morphine consumption and pain scores at rest and with movement with 6-hourly boluses of bupivacaine through surgically placed rectus sheath catheters, when compared with normal saline boluses, in 74 patients undergoing midline laparotomy for gynaecological cancer surgery. Hong et al. [93] showed that preoperative bilateral rectus sheath blocks reduced opioid use in open gastrectomy intraoperatively and immediately post-operatively when compared to sham injections, but only for up to 2 h, demonstrating the drawbacks of a single-shot technique in this context.

When epidural analgesia is compared against continuous local anaesthetic infusions through bilateral rectus sheath catheters, Gupta et al. [94] demonstrated similar opioid consumption between the two groups and showed reduced VAS pain scores in the rectus sheath group in the immediate post-operative period when compared with the epidural group. In contrast, when continuous epidural infusions were compared with intermittent boluses of local anaesthetic through bilateral rectus sheath catheters in a separate study [95], the epidural group required less rescue analgesia, with reduced sedation scores. However, the rectus sheath catheter group mobilised earlier. This latter finding echoes an observational study [96] where the mean time to mobilisation was shorter in the intermittent-bolus rectus sheath group when compared with epidurals. This study, however, found no differences in pain scores between the two groups.

The usefulness of rectus sheath catheters in the intensive care unit is illustrated in an intensive care case series, where seven patients underwent bilateral rectus sheath catheter insertion post-laparotomy, all with contraindications to epidural anaesthesia. The authors found low pain scores, low opioid consumption and good cardiovascular stability [97].

Clearly, data so far have been from small RCTs with significant heterogeneity. Further, higher-quality, larger studies comparing epidurals with rectus sheath catheters are required, as well as more concrete data on failure rates, but these show their potential as an alternative technique in multimodal analgesia.

21.3.2 Other Abdominal Wall Blocks

Beyond the rectus sheath block, other abdominal wall blocks may also be considered in specific circumstances. The transversus abdominus plane (TAP) block targets the anterior rami of the lower six thoracic and the first lumbar nerve, providing unilateral somatic analgesia, though in clinical practice the spread is variable. It is generally suitable for incisions below the T10 dermatome, with a subcostal variant suitable for incisions above the T10 dermatome [12]. Like rectus sheath blockade, TAP blocks can be performed in the supine patient under ultrasound guidance, with none of the implications of accessing the central nervous system.

TAP blocks have been studied in various surgical subspecialties: a review by Abdallah et al. [98] concluded that whilst there is data to suggest benefit in colorectal surgery, open and laparoscopic appendectomy and laparoscopic cholecystectomy, there is less clear evidence for hepatobiliary, renal, caesarean delivery, gynaecological surgery and open inguinal repair. This may be due to the visceral components not being adequately covered by the TAP block.

In terms of efficacy, a meta-analysis in 2015 found that TAP blocks reduced intravenous morphine consumption 6 h post-operatively by 6 mg on average. Pain scores were also reduced in the same time period [99]. A more recent meta-analysis by Desai et al. [100] compared TAP blocks (both single-shot and continuous catheter techniques) against epidural blockade. Whilst epidural analgesia was statistically superior, in terms of pain scores at 12 h (by 0.69 units) and reduced need for opioids in the first 24 h (by 5.91 mg intravenous morphine equivalents), the authors questioned whether these findings were clinically significant, especially in the face of loss of significance in the leave-one-out sensitivity analysis, a relatively high epidural failure rate [81] and the potential for the rare but serious complications of epidural anaesthesia.

Finally, in a review specifically referring to TAP catheters, Sanderson and Doane posit that whilst the studies performed thus far are limited and the data heterogeneous, the general picture painted shows that TAP catheters present another option for extended analgesia [101].

Taken together, TAP blocks and catheters may present a useful adjunct in multimodal analgesia for the intensive care physician in post-operative patients. Several factors must be considered for TAP catheters, however: the timing of catheter insertion, the region that needs to be covered and, therefore, the number of catheters required and the dosing regimen. Inserting the catheters post-operatively may be difficult with disrupted sonoanatomy. Incision crossing the midline will need two catheters, and if both supra-umbilical and infra-umbilical coverage are needed, then four catheters will be required, with all the inherent logistical challenges. Finally, there is no data in terms of whether intermittent or continuous dosing is optimal [90].

A more recent development is the quadratus lumborum block (QLB). Using the quadratus lumborum muscle as the principle sonoanatomical landmark, it is usually performed with the curvilinear ultrasound probe placed in a transverse orientation, parallel and superior to the iliac crest in the posterior axillary line with multiple points of local anaesthetic injection described. Its basis is more extensive abdominal analgesia when compared with the TAP block, though it has been noted that local

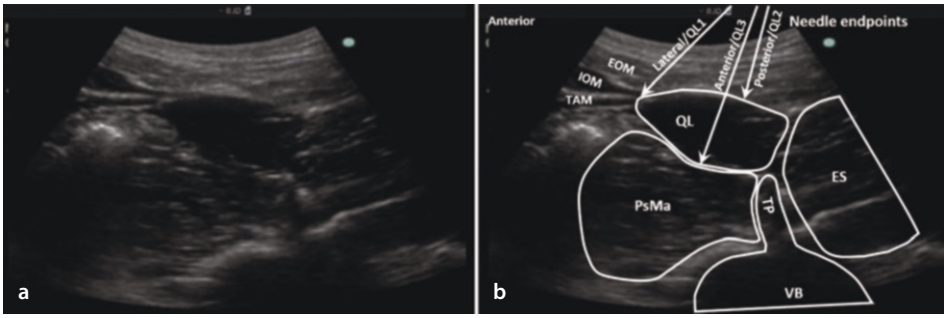

Fig. 21.5 Ultrasound image of QLB **a**, with a labelled schematic showing potential needle end points for each of lateral (QL1), posterior (QL2) and anterior (QL3) **b**. The ultrasound probe is placed in the transverse plane in between the iliac crest and the costal margin. The patient is ideally positioned laterally, although this can also be performed supine. *EOM* external oblique muscle, *IOM* internal oblique muscle, *TAM* transversus abdominis muscle, *QL* quadratus lumborum muscle, *ES* erector spinae muscle, *PsMa* psoas major, *TP* transverse process, *VB* vertebral body

anaesthetic may also spread to the lumbar plexus, potentially highlighting a use in hip surgery [90].

There have been various needle end points described for the QLB (Fig. 21.5). The lateral QLB (previously known as QL1) is defined as an injection to the anterolateral aspect of the quadratus lumborum muscle, lateral to the tapered end of the transversus abdominus muscle, in the plane between the aponeurosis of the internal oblique and transversus abdominus muscles and the transversalis fascia. Posterior QLB (previously known as QL2) is described as an injection to the posterior aspect of the quadratus lumborum muscle, in the plane between it and the overlying layer of thoracolumbar fascia separating it from the overlying latissimus dorsi. The anterior QLB (previously known as QL3) has been described as an injection in the plane between the anterior aspect of the quadratus lumborum muscle and the psoas major, reached through a trans-quadratus lumborum approach [90, 102].

With mounting interest, several meta-analyses have been published recently, describing the use of QLBs in caesarean delivery, gynaecological surgery, abdominal general surgery, orthopaedic surgery and urological procedures, although much of the work focuses on caesarean delivery [102–106]. In caesarean delivery, the consensus seems to be that QLB reduced post-operative morphine consumption and is superior to no block or placebo when no intrathecal morphine is used, but no differences are found in the presence of intrathecal morphine. In addition, a network meta-analysis comparing QLB with TAP in caesarean section showed comparable results for the TAP block [106]. Of these reviews, only one analysed non-obstetric data separately, where the authors found anterior QLB to reduce opioid use post-operatively, enabled early mobilisation when compared with placebo in abdominal surgery, and that in general, QLBs were associated with longer time to first analgesic request when compared with TAP blocks, and marginal reduction in opioid consumption. Similar results were obtained for hip surgery, with modest reductions in opioid use after anterior or lateral QLB compared with no block [103]. Amongst review data, one trial compared epidural with QLB, in the context of analgesia post-caeserean section, where it showed clear superiority of epidural analgesia in terms of morphine consumption [107].

Beyond case reports and case series, there is limited trial data regarding continuous QLB via catheters. One trial compared continuous anterior QL blocks with surgically placed pre-peritoneal catheters in patients undergoing midline laparotomies and found no differences in pain scores on coughing and fentanyl use; the QLB group had a small reduction in pain score at rest, but the pre-peritoneal catheters were cheaper to utilise [108]. Another trial compared epidural analgesia with continuous bilateral anterior QL blocks in patients undergoing laparoscopic nephrectomy, with the incisions limited to the ports and a Pfannenstiel incision. The authors found comparable pain scores and 24 h cumulative morphine requirements, and the extent of sensory blockade was similar. Unsurprisingly, they found that the epidural group had lower mean arterial pressures, and the QLB group had reduced urinary catheterisation times [109].

As a novel technique, the role of QLB has not yet been firmly established, not least in the ICU setting. A recent case report discussed the use of posterior QLB block in a polytrauma patient undergoing surgical correction of pelvic fractures as part of multimodal analgesia [110]. Further trial data, especially involving the use of QLB catheters, and unification and clarification of nomenclature would be helpful in determining its role on the ICU.

Clinical Vignette 21.4

A 44-year-old cyclist has been admitted for polytrauma after a car-versus-bike road traffic accident. His injuries include right T6–T10 rib fractures unilaterally, splenic lacerations (managed conservatively), right distal humeral fracture and a right femoral fracture. He has no other comorbidities.

Taken together, QLB and TAP blocks may have their role in specific scenarios. The rectus sheath block and catheters may present the most viable alternative to central neuraxial blockade in the context of midline laparotomy, especially in the emergent context.

21.4 The Extremities

Regional anaesthesia for upper and lower extremity limb perioperative anaesthesia and analgesia is well-established in the elective setting. For example, a recent retrospective study found the use of regional techniques to be associated with reduced odds for adverse outcomes in patient undergoing hip and knee arthroplasties. Specifically, peripheral nerve block use was associated with reduced odds ratios for wound complications in hip arthroplasties and pulmonary complications in those undergoing knee arthroplasties. Moreover, the authors found reduced opioid consumption, resource utilisation (including intensive-care admission and transfusion) and length of stay in both groups [111].

Regional anaesthesia may also be useful in the setting of extremity trauma or in emergency surgery where the patient may be too frail to undergo general anaesthesia, such as in vascular surgery. In traumatic hip fracture, the fascia iliac compartment

Table 21.2 Suggested regional anaesthesia techniques for various fracture sites

Fracture site	Suggested block
Clavicle	Cervical plexus block with interscalene brachial plexus block[a]
Scapula	Cervical plexus block with interscalene brachial plexus block[a]
Shoulder and proximal humerus	Interscalene brachial plexus block
Mid-humerus	Supraclavicular or infraclavicular (Fig. 21.6) brachial plexus block
Elbow and forearm	Supraclavicular, infraclavicular or axillary brachial plexus block
Hip and proximal femur	Fascia iliaca block
Knee	Femoral with adductor canal blocks ± sciatic nerve block or iPACK (**i**nfiltration between **p**opliteal **a**rtery and **c**apsule of the **k**nee) block
Tibia/fibula and ankle	Popliteal sciatic nerve block with saphenous/adductor canal block
Foot	Selective blocks of tibial, sural, saphenous, superficial and/or deep peroneal nerves

[a] Can lead to diaphragmatic paralysis

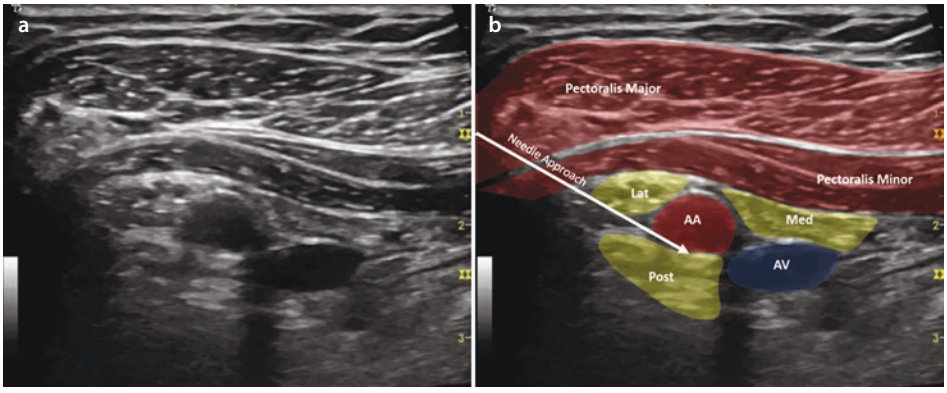

Fig. 21.6 Infraclavicular block ultrasound image **a**, with a labelled overlay **b**. The patient is positioned supine, with head up and the arm to be blocked abducted. A linear probe is usually used. The probe is positioned parasagittally just below the clavicle, scanning laterally until the structures above are seen. The needle is inserted in-plane, to approximately the 6 o'clock position to the AA, where up to 30 mL of LA is injected, spreading peri-arterially, though minor readjustments to needle positioning may be required to ensure all cords are covered [127]. *Lat* lateral cord, *Med* medial cord, *post* posterior cord, *AA* axillary artery, *AV* axillary vein

block (FICB) was found in a meta-analysis to significantly reduce pain intensity, opioid consumption and nausea when compared to control, although this effect on pain is limited to 1–8 h post-block [112]. A randomised controlled trial comparing general anaesthesia against ultrasound-guided infraclavicular blockade in distal

radial fracture fixation found better pain scores up to 48 h post-operatively, reduced morphine consumption in recovery and better patient satisfaction [113].

A recent review by Saranteas et al. [114] discusses in detail which block or blocks to use when dealing with upper limb and lower limb trauma in a rational, anatomical manner. A complete neurological examination should be performed prior to blockade and documented, noting any sensory and/or motor impairments. ◘ Table 21.2 below summarises their suggestions.

Although single-shot blocks would be effective in pain control in the short term, continuous nerve blockade with the use of catheters would likely be more practical in an ICU setting. These would allow better pain control than patient-controlled opioid-based analgesia, reduce opioid consumption, allow for earlier mobilisation and functional recovery, shorten hospital stay and improve sleep [115].

Practical considerations must be made in the context of catheters, such as expected duration of infusion, concurrent use of anticoagulants and location of injury. This is in addition to block-related factors, such as patient positioning and anatomical disruption secondary to trauma. In a patient with potential respiratory embarrassment, further respiratory impairment secondary to the side effects, or complications, of a block should also be borne in mind, such as the blockade of the phrenic nerve or pneumothorax.

Infection and prolonged catheter use must also be considered. A recent retrospective registry analysis found that the probability of infection-free catheter use decreases with each day, with a probability of 99% on day 4, 96% on day 7 and 73% on day 15 in peripheral catheters and similar probabilities in epidural catheters. The study also noted that infected catheters should be removed as soon as practical [116].

Other issues include LAST, local anaesthetic dosing and delivery regimen, especially in the context of multiple injury sites and the potential use of multiple catheters. Interestingly, a network meta-analysis comparing different local anaesthetic delivery regimens, including continuous infusion, patient-controlled boluses and programmed intermittent boluses, found that programmed intermittent boluses modestly improved pain scores, reduced opioid use and improved patient satisfaction levels, mostly in lower limb and truncal catheter studies [117]. The authors did note that when studies flagged as being at high risk of bias were excluded, this difference in pain score became insignificant, although the differences in patient satisfaction remained. Their suggested mechanism is that bolus techniques allow for greater spread of local anaesthetic than continuous infusions and that programmed intermittent boluses may be more effective than patient-controlled boluses due to the regularity of delivery.

21.4.1 Acute Compartment Syndrome (ACS)

A controversial issue in the use of regional anaesthesia in the context of trauma is the ability to detect acute compartment syndrome. This refers to an acute rise in interstitial pressure within a closed muscular compartment, exceeding the capillary perfusion pressure, leading to inadequate tissue perfusion and ischaemia, which can in turn lead to irreversible tissue damage. General risk factors for ACS include young age, high energy injuries of the forearm and femoral shaft, tibial fractures,

polytrauma, coagulopathy, transfusion and an increase in lactate or base deficit [118, 119].

Traditionally, ACS is diagnosed by clinical examination: pain out of proportion to the injury and pain on passive stretch of the compartment. It should be noted, however, that pain has a high specificity (97%) but low sensitivity (19%) [118]. Intracompartment pressures can also be measured to guide diagnosis.

The argument posed is that peripheral nerve blocks limit the perception of pain, therefore, potentially leading to a delayed diagnosis. Multiple reviews have been conducted on this topic, although all found difficulties drawing conclusions based on very limited, low-quality clinical data [119–122]. One review noted that dense bilateral blockade from epidural analgesia may have contributed to a delay in diagnosis and suggested using dilute local anaesthetic solutions instead to avoid dense sensory and motor blockade [120]. None of the four reviews were able to identify a link between regional anaesthesia use and ACS. All suggested ongoing assessment, a high index of suspicion and compartment pressure measurements to help with early diagnosis and treatment of ACS.

Two of the reviews argued that as using PCAs do not remove the risk of delayed diagnosis of compartment syndrome, regional anaesthesia should not be withheld as an effective analgesic modality [121, 122]. Only one review suggested that regional anaesthesia should be performed in 'strictly controlled research environments' in long-bone fractures, with the authors stating that it is in their practice to not offer peripheral nerve blocks in patients with particularly high risk for ACS. These risk factors include tibial fractures, mid-shaft radius and ulnar fractures, high energy mechanism with supporting findings (i.e. segmental fracture), significant soft tissue injuries (i.e. high-grade open fracture, or mangled extremity), crush injuries and vascular injuries (at risk of compartment syndrome from ischaemia-reperfusion injury) [119].

Ultimately, close liaison between trauma, anaesthetics and intensive care teams will be needed to weigh up the risk and benefit on a case-by-case basis. In our clinical vignette, infraclavicular and fascia iliaca catheters may be considered for analgesia, using low-concentration local anaesthetic solutions, with hypervigilance for the development of ACS.

21.4.2 Changes to Nomenclature in Regional Anaesthesia

Since the original generation of this manuscript, wide-ranging efforts have been made to standardise the nomenclature used within regional anaesthesia. Reducing heterogeneous nomenclature reduces confusion in teaching, training, and research, and was undertaken through a Delphi process by [128].

Of relevance are the changes to the nomenclature of the chest wall blocks. The PECS I block, where local anaesthetic is injected into the fascial plane between pectoralis major and minor muscles, may now be referred to as the interpectoral plane (IPP) block. PECS II, where injection is made between pectoralis minor and serratus anterior muscles, may now be referred to as the pectoserratus plane (PSP) block. Changes to the naming of the PIFB and TTMPB have also been suggested with strong consensus. The PIFB, where injection is made between the pectoralis major and intercostal muscles, may now be referred to as the superficial parasternal

intercostal plane (PIP) block, whilst the TTMPB, where injection is made between internal intercostal and transversus thoracis muscles, may be referred to as the deep PIP block.

Regarding the paraspinal blocks, PVB and ESP blocks remain as names previously. However, the MTP and other injections made between two transverse processes, posterior to the superior costotransverse ligament, or midway between the posterior aspect of the transverse process and pleura, may now be known as intertransverse process (ITP) blocks.

The authors have included it to ensure that the reader has been introduced to the new, standardised nomenclature as the field of regional anaesthesia continues to advance. The changes in nomenclature should not alter the general principles described in this chapter.

Summary

In this chapter, we have discussed advances in ultrasound-guided regional anaesthesia in the context of their use in intensive care. We have considered developments in thoracic and abdominal wall anaesthesia, discussed the utility of central neuraxial blockade and summarised recent advances in regional anaesthesia for the extremities in this context.

Intensive care patients are a complex, heterogenous cohort for which regional anaesthesia may offer numerous clinical benefits, such as in terms of pain, pulmonary complications, ileus, surgical site infections and thromboembolic events. These benefits have implications on resource utilisation that should not be overlooked.

Many of the techniques discussed have shown promise in small studies but otherwise a limited evidence base, except for epidural anaesthesia. The implementation of regional anaesthesia must, therefore, be in the context of a multimodal, multidisciplinary strategy, considering the indications, contraindications and potential side effects and complications of each patient and used on a case-by-case basis.

The advances in ultrasound availability and the development of more superficial, fascial plane blocks, with theoretically fewer side effects and complications, should hopefully encourage use of regional anaesthesia in this cohort of complex patients.

References

1. Whipple JK, Lewis KS, Quebbeman EJ, et al. Analysis of pain management in critically ill patients. Pharmacotherapy. 1995;15:592–9.
2. Schulz-Stübner S, Boezaart A, Hata JS. Regional analgesia in the critically ill. Crit Care Med. 2005;33:1400–7.
3. Schulz-Stübner S. The critically ill patient and regional anesthesia. Curr Opin Anaesthesiol. 2006;19:538–44.
4. Lavand'homme P, Estebe JP. Opioid-free anesthesia: a different regard to anesthesia practice. Curr Opin Anaesthesiol. 2018;31:556–61.
5. Ljungqvist O, Scott M, Fearon KC. Enhanced recovery after surgery a review. JAMA Surg. 2017;152:292–8.
6. Ho AMH, Karmakar MK, Critchley LAH. Acute pain management of patients with multiple fractured ribs: a focus on regional techniques. Curr Opin Crit Care. 2011;17:323–7.

7. Bachmann KA, Trepte CJC, Tomkötter L, et al. Effects of thoracic epidural anesthesia on survival and microcirculation in severe acute pancreatitis: a randomized experimental trial. Crit Care. 2013;17:R281.
8. Johansson PI, Stensballe J, Ostrowski SR. Shock induced endotheliopathy (SHINE) in acute critical illness—a unifying pathophysiologic mechanism. Crit Care. 2017;21:25.
9. Capdevila M, Ramin S, Capdevila X. Regional anesthesia and analgesia after surgery in ICU. Curr Opin Crit Care. 2017;23:430–9.
10. Venkataraju A, Narayanan M. Analgesia in intensive care: part 2. BJA Educ. 2016;16:397–404.
11. Stundner O, Memtsoudis SG. Regional anesthesia and analgesia in critically ill patients: a systematic review. Reg Anesth Pain Med. 2012;37:537–44.
12. Rubio-Haro R, Morales-Sarabia J, Ferrer-Gomez C, de Andres J. Regional analgesia techniques for pain management in patients admitted to the intensive care unit. Minerva Anestesiol. 2019;85:1118–28.
13. Chin KJ. Thoracic wall blocks: from paravertebral to retrolaminar to serratus to erector spinae and back again—a review of evidence. Best Pract Res Clin Anaesthesiol. 2019;33:67.
14. Albrecht E, Chin KJ. Advances in regional anaesthesia and acute pain management: a narrative review. Anaesthesia. 2020;75:e101–10.
15. Elsharkawy H, Saifullah T, Kolli S, Drake R. Rhomboid intercostal block. Anaesthesia. 2016;71:856–7.
16. Elsharkawy H, Maniker R, Bolash R, Kalasbail P, Drake RL, Elkassabany N. Rhomboid intercostal and subserratus plane block: a cadaveric and clinical evaluation. Reg Anesth Pain Med. 2018;43:745–51.
17. Holcomb JB, McMullin NR, Kozar RA, Lygas MH, Moore FA. Morbidity from rib fractures increases after age 45. J Am Coll Surg. 2003;196:549–55.
18. Bulger E, Arneson M, Mock C, Jurkovich G. Rib fractures in the elderly. J Trauma. 2000;48:1040–7.
19. Williams A, Bigham C, Marchbank A. Anaesthetic and surgical management of rib fractures. BJA Educ. 2020;20:332–40.
20. Malekpour M, Hashmi A, Dove J, Torres D, Wild J. Analgesic choice in management of rib fractures: paravertebral block or epidural analgesia? Anesth Analg. 2017;124:1906–11.
21. Peek J, Smeeing DPJ, Hietbrink F, Houwert RM, Marsman M, de Jong MB. Comparison of analgesic interventions for traumatic rib fractures: a systematic review and meta-analysis. Eur J Trauma Emerg Surg. 2019;45:597–622.
22. Yeying G, Liyong Y, Yuebo C, et al. Thoracic paravertebral block versus intravenous patient-controlled analgesia for pain treatment in patients with multiple rib fractures. J Int Med Res. 2017;45:2085–91.
23. Womack J, Pearson JD, Walker IA, Stephens NM, Goodman BA. Safety, complications and clinical outcome after ultrasound-guided paravertebral catheter insertion for rib fracture analgesia: a single-centre retrospective observational study. Anaesthesia. 2019;74:594–601.
24. El-Boghdadly K, Wiles MD. Regional anaesthesia for rib fractures: too many choices, too little evidence. Anaesthesia. 2019;74:564–8.
25. Truitt MS, Murry J, Amos J, et al. Continuous intercostal nerve blockade for rib fractures: ready for primetime? J Trauma. 2011;71:1548–52.
26. Shelley CL, Berry S, Howard J, et al. Posterior paramedian subrhomboidal analgesia versus thoracic epidural analgesia for pain control in patients with multiple rib fractures. J Trauma Acute Care Surg. 2016;81:463–7.
27. Britt T, Sturm R, Ricardi R, Labond V. Comparative evaluation of continuous intercostal nerve block or epidural analgesia on the rate of respiratory complications, intensive care unit, and hospital stay following traumatic rib fractures: a retrospective review. Local Reg Anesth. 2015;8:79–84.
28. Adhikary SD, Liu WM, Fuller E, Cruz-Eng H, Chin KJ. The effect of erector spinae plane block on respiratory and analgesic outcomes in multiple rib fractures: a retrospective cohort study. Anaesthesia. 2019;74:585–93.
29. Beard L, Hillermann C, Beard E, et al. Multicenter longitudinal cross-sectional study comparing effectiveness of serratus anterior plane, paravertebral and thoracic epidural for the analgesia of multiple rib fractures. Reg Anesth Pain Med. 2020;45:351–6.

30. Thiruvenkatarajan V, Cruz Eng H, Adhikary SD. An update on regional analgesia for rib fractures. Curr Opin Anaesthesiol. 2018;31:601–7.
31. Rose P, Ramlogan R, Madden S, Lui A. Serratus anterior plane block home catheter for posterior rib fractures and flail chest. Can J Anesth. 2019;66:997–8.
32. Rose P, Ramlogan R, Sullivan T, Lui A. Serratus anterior plane blocks provide opioid-sparing analgesia in patients with isolated posterior rib fractures: a case series. Can J Anesth. 2019;66:1263–4.
33. Desai M, Narayanan MK, Venkataraju A. Pneumothorax following serratus anterior plane block. Anaesth Rep. 2020;8:14–6.
34. Batchelor TJP, Rasburn NJ, Abdelnour-Berchtold E, et al. Guidelines for enhanced recovery after lung surgery: recommendations of the Enhanced Recovery after Surgery (ERAS®) Society and the European Society of Thoracic Surgeons (ESTS). Eur J Cardiothorac Surg. 2019;55:91–115.
35. Yeung JH, Gates S, Naidu BV, Wilson MJ, Gao SF. Paravertebral block versus thoracic epidural for patients undergoing thoracotomy. Cochrane Database Syst Rev. 2016;2016 https://doi.org/10.1002/14651858.CD009121.pub2.
36. Ding X, Jin S, Niu X, Ren H, Fu S, Li Q. A comparison of the analgesia efficacy and side effects of paravertebral compared with epidural blockade for thoracotomy: an updated meta-analysis. PLoS One. 2014;9:e96233.
37. Joshi GP, Bonnet F, Shah R, et al. A systematic review of randomized trials evaluating regional techniques for postthoracotomy analgesia. Anesth Analg. 2008;107:1026–40.
38. Perttunen K, Nilsson E, Heinonen J, Hirvisalo EL, Salo JA, Kalso E. Extradural, paravertebral and intercostal nerve blocks for post-thoracotomy pain. Br J Anaesth. 1995;75:541–7.
39. Bang S, Chung K, Chung J, Yoo S, Baek S, Lee SM. The erector spinae plane block for effective analgesia after lung lobectomy: three cases report. Medicine. 2019;98:e16262.
40. Rao Kadam V, Currie J. Ultrasound-guided continuous erector spinae plane block for postoperative analgesia in video-assisted thoracotomy. Anaesth Intensive Care. 2018;46:243–5.
41. Forero M, Rajarathinam M, Adhikary S, Chin KJ. Continuous erector spinae plane block for rescue analgesia in thoracotomy after epidural failure: a case report. A&A Case Rep. 2017;8:254–6.
42. Vig S, Bhan S, Ahuja D, et al. Serratus anterior plane block for post-thoracotomy analgesia: a novel technique for the surgeon and anaesthetist. Indian J Surg Oncol. 2019;10:535–9.
43. Adhikary SD, Pruett A, Forero M, Thiruvenkatarajan V. Erector spinae plane block as an alternative to epidural analgesia for post-operative analgesia following video-assisted thoracoscopic surgery: a case study and a literature review on the spread of local anaesthetic in the erector spinae plane. Indian J Anaesth. 2018;62:75–8.
44. Scimia P, Ricci EB, Droghetti A, Fusco P. The ultrasound-guided continuous erector spinae plane block for postoperative analgesia in video-assisted thoracoscopic lobectomy. Reg Anesth Pain Med. 2017;42:2017.
45. Park MH, Kim JA, Ahn HJ, Yang MK, Son HJ, Seong BG. A randomised trial of serratus anterior plane block for analgesia after thoracoscopic surgery. Anaesthesia. 2018;73:1260–4.
46. Semyonov M, Fedorina E, Grinshpun J, et al. Ultrasound-guided serratus anterior plane block for analgesia after thoracic surgery. J Pain Res. 2019;12:953–60.
47. Kim DH, Oh YJ, Lee JG, Ha D, Chang YJ, Kwak HJ. Efficacy of ultrasound-guided serratus plane block on postoperative quality of recovery and analgesia after video-assisted thoracic surgery: a randomized, triple-blind, placebo-controlled study. Anesth Analg. 2018;126:1353–61.
48. Saad FS, El Baradie SY, Abdel Aliem MAW, Ali MM, Kotb TAM. Ultrasound-guided serratus anterior plane block versus thoracic paravertebral block for perioperative analgesia in thoracotomy. Saudi J Anaesth. 2018;12:565–70.
49. Khalil AE, Abdallah NM, Bashandy GM, Kaddah TA-H. Ultrasound-guided serratus anterior plane block versus thoracic epidural analgesia for thoracotomy pain. J Cardiothorac Vasc Anesth. 2017;31:152–8.
50. Wang Q, Zhang G, Wei S, He Z, Sun L, Zheng H. Comparison of the effects of ultrasound-guided erector spinae plane block and wound infiltration on perioperative opioid consumption and postoperative pain in thoracotomy. J Coll Physicians Surg Pak. 2019;29:1138–43.

51. Fang B, Wang Z, Huang X. Ultrasound-guided preoperative single-dose erector spinae plane block provides comparable analgesia to thoracic paravertebral block following thoracotomy: a single center randomized controlled double-blind study. Ann Transl Med. 2019;7:174.
52. Ciftci B, Ekinci M, Celik EC, Tukac IC, Bayrak Y, Atalay YO. Efficacy of an ultrasound-guided erector spinae plane block for postoperative analgesia management after video-assisted thoracic surgery: a prospective randomized study. J Cardiothorac Vasc Anesth. 2020;34:444–9.
53. Finnerty DT, McMahon A, McNamara JR, Hartigan SD, Griffin M, Buggy DJ. Comparing erector spinae plane block with serratus anterior plane block for minimally invasive thoracic surgery: a randomised clinical trial. Br J Anaesth. 2020;125:802–10.
54. Taketa Y, Irisawa Y, Fujitani T. Comparison of ultrasound-guided erector spinae plane block and thoracic paravertebral block for postoperative analgesia after video-assisted thoracic surgery: a randomized controlled non-inferiority clinical trial. Reg Anesth Pain Med. 2020;45:10–5.
55. Smith LM, Barrington MJ. Ultrasound-guided blocks for cardiovascular surgery: which block for which patient? Curr Opin Anaesthesiol. 2020;33:64–70.
56. Guay J, Kopp S. Epidural analgesia for adults undergoing cardiac surgery with or without cardiopulmonary bypass. Cochrane Database Syst Rev. 2019;2019:CD006715. https://doi.org/10.1002/14651858.CD006715.pub3.
57. Landoni G, Isella F, Greco M, Zangrillo A, Royse CF. Benefits and risks of epidural analgesia in cardiac surgery. Br J Anaesth. 2015;115:25–32.
58. Lockwood GG, Cabreros L, Banach D, Punjabi PP. Continuous bilateral thoracic paravertebral blockade for analgesia after cardiac surgery: a randomised, controlled trial. Perfusion (United Kingdom). 2017;32:591–7.
59. Krishna SN, Chauhan S, Bhoi D, et al. Bilateral erector spinae plane block for acute post-surgical pain in adult cardiac surgical patients: a randomized controlled trial. J Cardiothorac Vasc Anesth. 2019;33:368–75.
60. Nagaraja P, Ragavendran S, Singh N, et al. Comparison of continuous thoracic epidural analgesia with bilateral erector spinae plane block for perioperative pain management in cardiac surgery. Ann Card Anaesth. 2018;21:323.
61. Macaire P, Ho N, Nguyen T, et al. Ultrasound-guided continuous thoracic erector spinae plane block within an enhanced recovery program is associated with decreased opioid consumption and improved patient postoperative rehabilitation after open cardiac surgery—a patient-matched, controlled. J Cardiothorac Vasc Anesth. 2019;33:1659–67.
62. Khera T, Murugappan KR, Leibowitz A, et al. Ultrasound-guided pecto-intercostal fascial block for postoperative pain management in cardiac surgery: a prospective, randomized, placebo-controlled trial. J Cardiothorac Vasc Anesth. 2021;35:896–903.
63. Aydin ME, Ahiskalioglu A, Ates I, et al. Efficacy of ultrasound-guided transversus thoracic muscle plane block on postoperative opioid consumption after cardiac surgery: a prospective, randomized, double-blind study. J Cardiothorac Vasc Anesth. 2020;34:2996–3003.
64. Abdelbaser II, Mageed NA. Analgesic efficacy of ultrasound guided bilateral transversus thoracis muscle plane block in pediatric cardiac surgery: a randomized, double-blind, controlled study. J Clin Anesth. 2020;67:110002.
65. Kumar K, Kalyane R, Singh N, et al. Efficacy of bilateral pectoralis nerve block for ultrafast tracking and postoperative pain management in cardiac surgery. Ann Card Anaesth. 2018;21:333.
66. Berthoud V, Ellouze O, Nguyen M, et al. Serratus anterior plane block for minimal invasive heart surgery. BMC Anesthesiol. 2018;18:1–6.
67. Kaushal B, Chauhan S, Saini K, et al. Comparison of the efficacy of ultrasound-guided serratus anterior plane block, pectoral nerves II block, and intercostal nerve block for the management of postoperative thoracotomy pain after pediatric cardiac surgery. J Cardiothorac Vasc Anesth. 2019;33:418–25.
68. Ueshima H, Kitamura A. Blocking of multiple anterior branches of intercostal nerves (Th2-6) using a transversus thoracic muscle plane block. Reg Anesth Pain Med. 2015;40:388–9.
69. Kelava M, Alfirevic A, Bustamante S, Hargrave J, Marciniak D. Regional anesthesia in cardiac surgery: an overview of fascial plane Chest Wall blocks. Anesth Analg. 2020;131:127–35.
70. Guay J, Nishimori M, Kopp S. Epidural local anaesthetics versus opioid-based analgesic regimens for postoperative gastrointestinal paralysis, vomiting and pain after abdominal surgery. Cochrane Database Syst Rev. 2016;2017:CD001893. https://doi.org/10.1002/14651858.CD001893.pub2.

71. Smith LM, Cozowicz C, Uda Y, Memtsoudis SG, Barrington MJ. Neuraxial and combined neuraxial/general anesthesia compared to general anesthesia for major truncal and lower limb surgery: a systematic review and meta-analysis. Anesth Analg. 2017;125:1931–45.
72. Pöpping DM, Elia N, Van Aken HK, et al. Impact of epidural analgesia on mortality and morbidity after surgery: systematic review and meta-analysis of randomized controlled trials. Ann Surg. 2014;259:1056–67.
73. Hausman MS, Jewell ES, Engoren M. Regional versus general anesthesia in surgical patients with chronic obstructive pulmonary disease: does avoiding general anesthesia reduce the risk of postoperative complications? Anesth Analg. 2015;120:1405–12.
74. Heinrich S, Janitz K, Merkel S, Klein P, Schmidt J. Short- and long term effects of epidural analgesia on morbidity and mortality of esophageal cancer surgery. Langenbeck's Arch Surg. 2015;400:19–26.
75. Durkin C, Schisler T, Lohser J. Current trends in anesthesia for esophagectomy. Curr Opin Anaesthesiol. 2017;30:30–5.
76. Feltracco P, Bortolato A, Barbieri S, et al. Perioperative benefit and outcome of thoracic epidural in esophageal surgery: a clinical review. Dis Esophagus. 2018;31:1–14.
77. Guay J, Kopp S. Epidural pain relief versus systemic opioid-based pain relief for abdominal aortic surgery. Cochrane Database Syst Rev. 2016;2017:CD005059. https://doi.org/10.1002/14651858.CD005059.PUB4.
78. Błaszczyk B, Wrońska B, Klukowski M, et al. Factors affecting breathing capacity and early tracheal extubation after liver transplantation: analysis of 506 cases. Transplant Proc. 2016;48:1692–6.
79. Jabaudon M, Belhadj-Tahar N, Rimmelé T, et al. Thoracic epidural analgesia and mortality in acute pancreatitis: a multicenter propensity analysis. Crit Care Med. 2018;46:e198–205.
80. Windisch O, Heidegger CP, Giraud R, Morel P, Bühler L. Thoracic epidural analgesia: a new approach for the treatment of acute pancreatitis? Crit Care. 2016;20:116.
81. Hermanides J, Hollmann MW, Stevens MF, Lirk P. Failed epidural: causes and management. Br J Anaesth. 2012;109:144–54.
82. Visser E, Marsman M, van Rossum PSN, et al. Postoperative pain management after esophagectomy: a systematic review and meta-analysis. Dis Esophagus. 2017;30:1–11.
83. Hughes M, Yim I, Deans DAC, Couper GW, Lamb PJ, Skipworth RJE. Systematic review and meta-analysis of epidural analgesia versus different analgesic regimes following oesophagogastric resection. World J Surg. 2018;42:204–10.
84. Bell R, Pandanaboyana S, Prasad KR. Epidural versus local anaesthetic infiltration via wound catheters in open liver resection: a meta-analysis. ANZ J Surg. 2015;85:16–21.
85. Melloul E, Hübner M, Scott M, et al. Guidelines for perioperative care for liver surgery: enhanced recovery after surgery (ERAS) society recommendations. World J Surg. 2016;40:2425–40.
86. American Society of Anesthesiologists Task Force on Infectious Complications Associated with Neuraxial Techniques and the American Society of Regional Anesthesia and Pain Medicine. Practice advisory for the prevention, diagnosis, and management of infectious complications associated with neuraxial techniques: an updated report by the American Society of Anesthesiologists Task Force on Infectious Complications Associated with Neuraxi. Anesthesiology. 2017;126:585–601.
87. Burcharth J, Abdulhady L, Danker J, et al. Implementation of a multidisciplinary perioperative protocol in major emergency abdominal surgery. Eur J Trauma Emergency Surg. 2019;47:467. https://doi.org/10.1007/s00068-019-01238-7.
88. Huddart S, Peden CJ, Swart M, et al. Use of a pathway quality improvement care bundle to reduce mortality after emergency laparotomy. Br J Surg. 2015;102:57–66.
89. Tengberg LT, Bay-Nielsen M, Bisgaard T, et al. Multidisciplinary perioperative protocol in patients undergoing acute high-risk abdominal surgery. Br J Surg. 2017;104:463–71.
90. Chin KJ, McDonnell JG, Carvalho B, Sharkey A, Pawa A, Gadsden J. Essentials of our current understanding: abdominal wall blocks. Reg Anesth Pain Med. 2017;42:133–83.
91. Webster K. Ultrasound guided rectus sheath block—analgesia for abdominal surgery. Update in Anaesthesia. 2007;26:12–7.
92. Bakshi SG, Mapari A, Shylasree TS. Bloc de la gaine des grands droits pour une analgésie postopératoire en chirurgie gynéco-oncologique: RESONS, une étude randomisée contrôlée. Can J Anesth. 2016;63:1335–44.

93. Hong S, Kim H, Park J. Analgesic effectiveness of rectus sheath block during open gastrectomy: a prospective double-blinded randomized controlled clinical trial. Medicine. 2019;98:e15159.
94. Gupta N, Kumar A, Harish RK, Jain D, Swami AC. Comparison of postoperative analgesia and opioid requirement with thoracic epidural vs. continuous rectus sheath infusion in midline incision laparotomies under general anaesthesia—a prospective randomised controlled study. Indian J Anaesth. 2020;64:750–5.
95. Yassin HM, Abd Elmoneim AT, El Moutaz H. The analgesic efficiency of ultrasound-guided rectus sheath analgesia compared with low thoracic epidural analgesia after elective abdominal surgery with a midline incision: a prospective randomized controlled trial. Anesthesiol Pain Med. 2017;7:e14244.
96. Tudor ECG, Yang W, Brown R, Mackey PM. Rectus sheath catheters provide equivalent analgesia to epidurals following laparotomy for colorectal surgery. Ann R Coll Surg Engl. 2015;97:530–3.
97. Webster K, Hubble S. Rectus sheath analgesia in intensive care patients: technique description and case series. Anaesth Intensive Care. 2009;37:855.
98. Abdallah FW, Chan VW, Brull R. Transversus abdominis plane block: a systematic review. Reg Anesth Pain Med. 2012;37:193–209.
99. Baeriswyl M, Kirkham KR, Kern C, Albrecht E. The analgesic efficacy of ultrasound-guided transversus abdominis plane block in adult patients: a meta-analysis. Anesth Analg. 2015;121:1640–54.
100. Desai N, El-Boghdadly K, Albrecht E. Epidural vs. transversus abdominis plane block for abdominal surgery—a systematic review, meta-analysis and trial sequential analysis. Anaesthesia. 2020;76:1–17.
101. Sanderson BJ, Doane MA. Transversus abdominis plane catheters for analgesia following abdominal surgery in adults. Reg Anesth Pain Med. 2018;43:5–13.
102. Korgvee A, Junttila E, Koskinen H, Huhtala H, Kalliomaki M-L. Ultrasound-guided quadratus lumborum block for postoperative analgesia. Eur J Anaesthesiol. 2020;38:115–29.
103. Uppal V, Retter S, Kehoe E, McKeen DM. Quadratus lumborum block for postoperative analgesia: a systematic review and meta-analysis. Can J Anesth. 2020;67:1557–75.
104. Sen TH, Taylor C, Weikel D, Barton K, Habib AS. Quadratus lumborum block for postoperative analgesia after cesarean delivery: a systematic review with meta-analysis and trial-sequential analysis. J Clin Anesth. 2020;67:110003.
105. Xu M, Tang Y, Wang J, Yang J. Quadratus lumborum block for postoperative analgesia after cesarean delivery: a systematic review and meta-analysis. Int J Obstet Anesth. 2020;42:87–98.
106. El-Boghdadly K, Desai N, Halpern S, et al. Quadratus lumborum block vs. transversus abdominis plane block for caesarean delivery: a systematic review and network meta-analysis. Anaesthesia. 2020;76:1–11.
107. Kang W, Lu D, Yang X, et al. Postoperative analgesic effects of various quadratus lumborum block approaches following cesarean section: a randomized controlled trial. J Pain Res. 2019;12:2305–12.
108. Rao Kadam V, Ludbrook G, van Wijk RM, et al. Comparison of ultrasound-guided transmuscular quadratus lumborum block catheter technique with surgical pre-peritoneal catheter for postoperative analgesia in abdominal surgery: a randomised controlled trial. Anaesthesia. 2019;74:1381–8.
109. Aditianingsih D, Pryambodho AN, Tantri AR, Mochtar CA. A randomized controlled trial on analgesic effect of repeated Quadratus Lumborum block versus continuous epidural analgesia following laparoscopic nephrectomy. BMC Anesthesiol. 2019;19:1–11.
110. Segura-Grau E, Afonso A. Quadratus lumborum type 2 block as a complementary regional anesthesia for polytrauma intensive care patient. J Clin Anesth. 2019;54:141.
111. Memtsoudis SG, Poeran J, Cozowicz C, Zubizarreta N, Ozbek U, Mazumdar M. The impact of peripheral nerve blocks on perioperative outcome in hip and knee arthroplasty—a population-based study. Pain. 2016;157:2341–9.
112. Hong HK, Ma Y. The efficacy of fascia iliaca compartment block for pain control after hip fracture: a meta-analysis. Medicine (United States). 2019;98:1–11.
113. Wong SS, Chan WS, Fang C, et al. Infraclavicular nerve block reduces postoperative pain after distal radial fracture fixation: a randomized controlled trial. BMC Anesthesiol. 2020;20:1–11.

114. Saranteas T, Koliantzaki I, Savvidou O, et al. Acute pain management in trauma: anatomy, ultrasound-guided peripheral nerve blocks and special considerations. Minerva Anestesiol. 2019;85:763–73.
115. Chelly JE, Ghisi D, Fanelli A. Continuous peripheral nerve blocks in acute pain management. Br J Anaesth. 2010;105:i86–96.
116. Bomberg H, Bayer I, Wagenpfeil S, et al. Prolonged catheter use and infection in regional anesthesia: a retrospective registry analysis. Anesthesiology. 2018;128:764–73.
117. Law WZW, Sara RA, Cameron AJD, Lightfoot NJ. Local anaesthetic delivery regimens for peripheral nerve catheters: a systematic review and network meta-analysis. Anaesthesia. 2020;75:395–405.
118. Duckworth AD, McQueen MM. The diagnosis of acute compartment syndrome: a critical analysis review. JBJS Rev. 2017;5:e1.
119. Tran AA, Lee D, Fassihi SC, Smith E, Lee R, Siram G. A systematic review of the effect of regional anesthesia on diagnosis and management of acute compartment syndrome in long bone fractures. Eur J Trauma Emerg Surg. 2020;46:1281–90.
120. Mar GJ, Barrington MJ, Mcguirk BR. Acute compartment syndrome of the lower limb and the effect of postoperative analgesia on diagnosis. Br J Anaesth. 2009;102:3–11.
121. Walker BJ, Noonan KJ, Bosenberg AT. Evolving compartment syndrome not masked by a continuous peripheral nerve block: evidence-based case management. Reg Anesth Pain Med. 2012;37:393–7.
122. Klucka J, Stourac P, Stouracova A, Masek M, Repko M. Compartment syndrome and regional anaesthesia: critical review. Biomed Papers. 2017;161:242–51.
123. Ramlogan R, Tierney S. How I do it: serratus anterior plane block for rib fractures. ASRA News. 2020. https://www.asra.com/guidelines-articles/how-i-do-it/asra-news/2020/05/02/how-i-do-it-serratus-anterior-plane-block-for-rib-fractures. Accessed 19 Mar 2021.
124. FitzGerald S, Odor PM, Barron A, Pawa A. Breast surgery and regional anaesthesia. Best Pract Res Clin Anaesthesiol. 2019;33:95–110.
125. Eng HC, Chin KJ, Adhikary S. How I do it: erector spinae block for rib fractures: the Penn State health experience. ASRA News. 2020. https://www.asra.com/guidelines-articles/how-i-do-it/asra-news/2020/05/01/how-i-do-it-erector-spinae-block-for-rib-fractures-the-penn-state-health-experience. Accessed 19 Mar 2021.
126. Salinas F. How I do it: ultrasound-guided bilateral rectus sheath blocks. ASRA News. 2019. https://www.asra.com/guidelines-articles/how-i-do-it/legacy-b-blog-posts/2019/08/07/how-i-do-it-ultrasound-guided-bilateral-rectus-sheath-blocks. Accessed 19 Mar 2021.
127. Gürkan Y. How I do it: infraclavicular block. ASRA News. 2019. https://www.asra.com/guidelines-articles/original-articles/article-item/legacy-b-blog-posts/2019/08/07/how-i-do-it-infraclavicular-block. Accessed 19 Mar 2021.
128. El-Boghdadly K, Wolmarans M, Stengel AD, Albrecht E, Chin KJ, Elsharkawy H, et al. Standardizing nomenclature in regional anesthesia: An ASRA-ESRA Delphi consensus study of abdominal wall, paraspinal, and chest wall blocks. Reg Anesth Pain Med. 2021;46(7):571–80.

Ultrasound Training

Contents

Chapter 22 Training in Ultrasound for Intensivists – 000
Laura Galarza

Training in Ultrasound for Intensivists

Laura Galarza

Contents

22.1 Introduction – 358

22.2 Competencies – 358

22.3 Training to Achieve Competence – 361
22.3.1 Introductory Courses – 361
22.3.2 Longitudinal Competence Program – 361
22.3.3 Final Assessment – 363

22.4 Barriers to Ultrasound Training – 363

22.5 Ultrasound Educational Tools – 363
22.5.1 E-Learning – 364
22.5.2 Simulation – 364
22.5.3 Peer Teaching – 364
22.5.4 Remote Supervision and Tele-Ultrasound – 365

22.6 Conclusions – 365

References – 366

© The Author(s), under exclusive license to Springer Nature Switzerland AG 2023
C. Robba et al. (eds.), *Basic Ultrasound Skills "Head to Toe" for General Intensivists*, Lessons from the ICU,
https://doi.org/10.1007/978-3-031-32462-8_22

22

Learning Objectives

- Understand the importance of ultrasound training programs.
- List the most important ultrasound competencies in critical care.
- Describe the different learning techniques to achieve competence.

22.1 Introduction

In the past three decades, ultrasound has gone out of the Radiology and Cardiology departments and has become increasingly available at bedside. The role that ultrasound plays in the diagnosis and management of patients and the safety that it provides while performing an invasive procedure has led clinicians to incorporate it as an invaluable tool in their daily practice. However, this widespread and still expanding use of ultrasound in healthcare has created the need for training: the use of ultrasound by individuals without proper training and experience adds to the likelihood of unnecessary examinations and misdiagnosis. As the American Medical Association stated "Ultrasound imaging is within the scope of practice of appropriately trained physicians. Ultrasound has broad and diverse use and applications in medical practice" [1].

Historically, ultrasound training programs began with machine acquisition and basic training, but, as clinicians started to use ultrasound, there were unique characteristics to their use compared to traditional imaging. Clinicians started to use ultrasound in a focused manner to answer clinical questions at bedside and not as a comprehensive imaging examination in a dedicated room; therefore, physician should not just only learn how to perform and interpret the findings but also how to integrate them into patient care.

In the early 1990s, point-of-care ultrasound (POCUS) was integrated into diverse areas of clinical practice, including critical care. Prof. Daniel Lichtenstein described the ultrasound artefacts of the lung and pleura and also published one of the first studies that demonstrated the utility of ultrasound in the intensive care units (ICUs) [2–4]. This led to an international movement to define critical care ultrasound (CCUS) as a basic competence for intensive care physicians that culminated in the publication of the American College of Chest Physicians (ACCP)/Société de Réanimation de Langue Française (SRLF) consensus document [5]. Up to this point, CCUS training was only pursued by a few with self-learning or establishing informal teaching relationships with colleagues of outside of the ICU, but from that moment on, we had a guide to build our own curriculum and training program at a national level and have intensivists teach their peers.

22.2 Competencies

In order to start a training program in critical care ultrasound, it is crucial to agree on the competencies that should be achieved. In the last 20 years, many consensus statements and guidelines have been published to address the issue of ultrasound training in critical care, and many national societies and other entities have proposed their own programs [5–9]. These consensuses overlap in most of the competencies required,

although there are some differences [10]. For instance, in echocardiography, there is a lack of agreement on the qualitative or quantitative assessment of some measures like left ventricular systolic function, the need of valvular assessment or the use of Colour Doppler. There are also differences in the abdominal module: while all agree on the need of free fluid detection, some also require identifying hepatobiliary pathology.

The basis for the scope of CCUS practice around the world was the ACCP/SRLF consensus document, which defined CCUS itself and determined what specific applications fall within its purview [5]. This document divided CCUS competencies into general (thoracic, abdominal and vascular) and echocardiography (■ Table 22.1). It took more than a decade to produce new consensuses on core competencies, until the European Society of Intensive Care Medicine (ESICM) endorsed two new documents, in 2020 and 2021, aiming to give an updated version of the competencies [11, 12]. The main differences between these consensuses are the incorporation of diaphragm and brain ultrasound in the last one (■ Table 22.1).

Echocardiography was the first ultrasound modality incorporated in the ICUs, so consequently, it is the most developed CCUS modality. Among guidelines, there is an agreement that we should distinguish between basic and advanced competencies [5, 13].

■ **Table 22.1** Comparison of CCUS core competencies in various consensuses [5, 11, 12]

		2009	2020	2021
Echocardiography	Syndromes	Severe hypovolemia LV failure RV failure Tamponade Acute massive left-sided valvular regurgitation Circulatory arrest: during and after resuscitation	Severe hypovolemia LV failure RV failure Tamponade Acute cor pulmonale Severe valvular abnormalities	LV failure RV failure Pulmonary embolism[a] Pericardial effusion and tamponade Severe hypovolemia Acute severe left-sided valvulopathy
	Cognitive skills	Echocardiographic patterns LV size and systolic function LV contraction pattern RV size and systolic function Pericardial fluid/tamponade IVC size and respiratory variation Basic colour Doppler for severe valvular regurgitation	LV size and systolic function (qualitative) LV contraction pattern (qualitative) RV size (qualitative) and systolic function (quantitative: TAPSE, RV/LV ratio) Valvular disease (qualitative: colour Doppler) IVC size and respiratory variation (quantitative)	LV systolic function (qualitative) LV contraction pattern LV outflow tract VTI for SV estimation RV size and wall thickness IVC size and respiratory variation Valvular disease (qualitative: anatomical abnormalities)

(continued)

Table 22.1 (continued)

		2009	2020	2021
Thoracic ultrasound	Syndromes	Pneumothorax Consolidation Alveolar-interstitial pattern Pleural effusion Pleural-based masses or thickening	Consolidation Pleural effusion Interstitial syndrome Pneumothorax	Pneumothorax Pleural effusion Respiratory failure Interstitial syndrome Consolidation Pulmonary embolism[a] Diaphragmatic dysfunction (quantitative: excursion)
	Procedures	Thoracentesis Intrapleural device placement	Pleural effusion drainage	Pleural effusion drainage
Abdominal ultrasound	Syndromes	Free fluid Bladder content and volume Intravesicular volume and overdistention Hydronephrosis Aortic aneurysm	Free fluid Bladder volume Hydronephrosis	Aortic aneurysm Bladder volume Hydronephrosis Free fluid
	Procedures	Paracentesis	Paracentesis	Paracentesis
Vascular ultrasound	Syndromes	Venous thrombosis	DVT	Pulmonary embolism[a] DVT
	Procedures	Vascular access	Vascular access	Vascular access
Brain ultrasound	Syndromes			Intracranial hypertension (TCCD of MCA: qualitative waveform analysis and PI)

LV left ventricle, *RV* right ventricle, *IVC* inferior vena cava, *VTI* velocity time integral, *SV* stroke volume, *TAPSE* tricuspid annulus plane systolic excursion, *DVT* deep vein thrombosis, *TCCD* transcranial colour Doppler, *MCA* middle cerebral artery, *PI* pulsatility index

[a] Integrated approach in patients with high probability and contraindication for computer tomography

Advanced critical care echocardiography (CCE) is complex and requires a deeper evaluation of cardiac anatomy and function, including haemodynamic assessment, and a significantly longer training time to achieve competence. It is not a skill for all intensivists, but every ICU will benefit from having various physicians with this ability.

22.3 Training to Achieve Competence

Once we have defined the competencies for the training program, we should focus on how to become competent and maintain this new competence. To achieve competence, several expert guidelines have outlined a similar training program [6, 7, 14]. On one hand, most of them recommend the following structure: an introductory short-term course followed by supervision and regular feedback over a minimum number of scans, to culminate in a final assessment of competence. On the other hand, there is a huge variability among guidelines, especially in the number of scans required to develop a competency, probably because there is little high-quality evidence on ultrasound imaging competence, and many recommendations rely on expert opinion [10, 14, 15]. Recently, a new consensus defined the whole process to attain competence in basic CCE, but it could be easily applied to other ultrasound modalities (Fig. 22.1) [16].

22.3.1 Introductory Courses

Introductory courses are recommended by almost every guideline; they are easy to organize and adequate to get a first taste. Typically, these courses are 1–3 days long and had a mixture of lectures, hands-on sessions and case-interpretation workshops. Lectures are still one of the most common teaching methods and should include ultrasound physics, machine instrumentation, theory and practice of image acquisition and interpretation. Hands-on sessions consist of supervised scanning practices on simulator mannequins, healthy volunteers and subjects with/without pathology or patients. In addition, pre- and post-course tests are suggested as a good way of knowing the level of skill acquisition.

Nevertheless, the long-term retention of ultrasound knowledge and skills decreases over time, and only longitudinal competence programs—which not all participants attend—have been shown to improve skill retention [17, 18]. An observational study showed that practicing physicians can retain ultrasound knowledge and hands-on skills 8 months after participating in an introductory course [19]. Also, a survey found that a small proportion of people who attended these courses attained competence, but most of them performed unsupervised exams afterwards [20].

22.3.2 Longitudinal Competence Program

Longitudinal competence programs are teaching programs that involve a trainee performing ultrasound scans on patients while receiving supervision and periodic formative training from a trainer. The main goal is that the trainee experiences an incremental improvement in image acquisition and interpretation skills until the trainee is ready to take a final summative assessment.

As previously stated, there is a huge variability in the number of scans that should be performed before the final assessment [10]. We can set a minimum number of scans but not a maximum, given that each trainee will learn at a different path and will acquire the skills at different rates, so we should not judge the readiness to

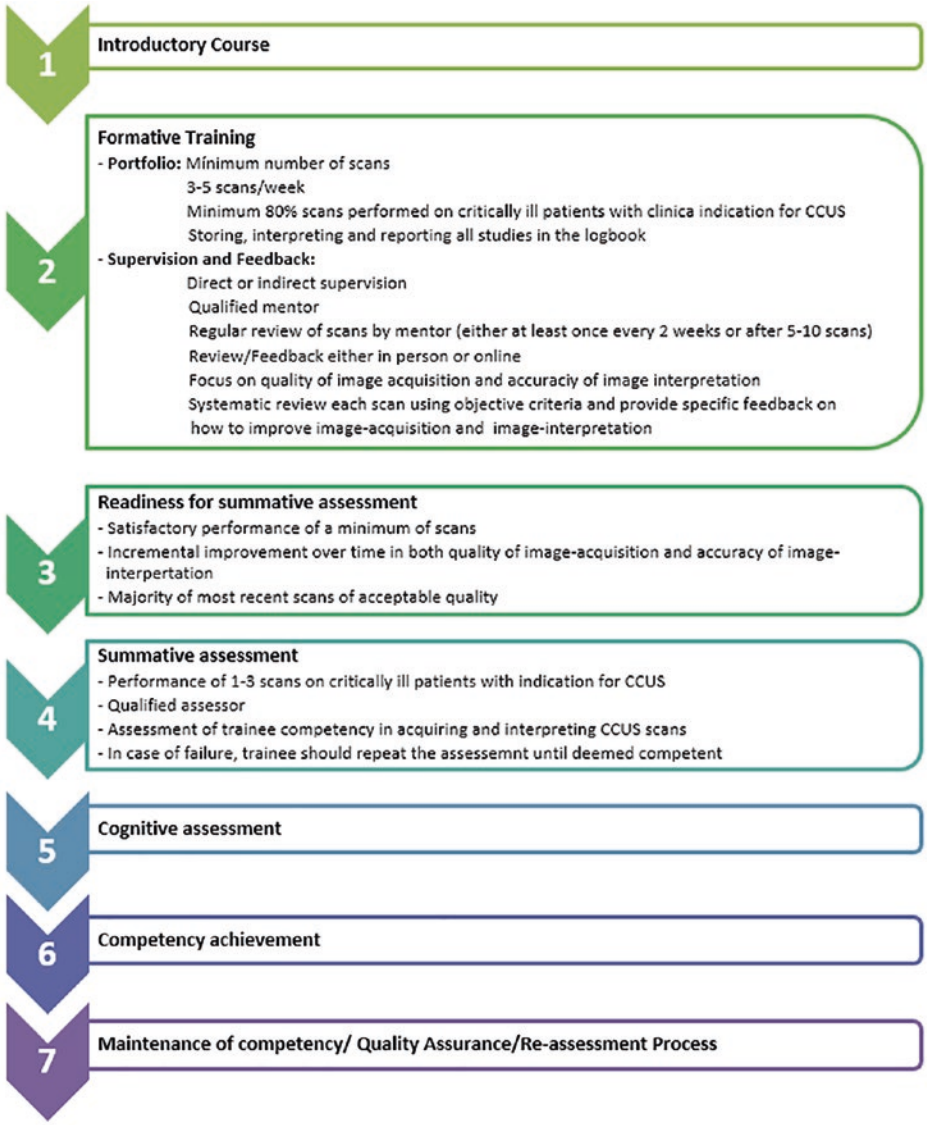
1
Introductory Course
2
Formative Training
- Portfolio: Minimum number of scans
3-5 scans/week
Minimum 80% scans performed on critically ill patients with clinica indication for CCUS
Storing, interpreting and reporting all studies in the logbook
- Supervision and Feedback:
Direct or indirect supervision
Qualified mentor
Regular review of scans by mentor (either at least once every 2 weeks or after 5-10 scans)
Review/Feedback either in person or online
Focus on quality of image acquisition and accuraciy of image interpretation
Systematic review each scan using objective criteria and provide specific feedback on how to improve image-acquisition and image-interpretation
3
Readiness for summative assessment
- Satisfactory performance of a minimum of scans
- Incremental improvement over time in both quality of image-acquisition and accuracy of image-interpertation
- Majority of most recent scans of acceptable quality
4
Summative assessment
- Performance of 1-3 scans on critically ill patients with indication for CCUS
- Qualified assessor
- Assessment of trainee competency in acquiring and interpreting CCUS scans
- In case of failure, trainee should repeat the assessemnt until deemed competent
5
Cognitive assessment
6
Competency achievement
7
Maintenance of competency/ Quality Assurance/Re-assessment Process

Fig. 22.1 Proposed pathway for longitudinal basic Critical Care Ultrasound (CCUS) competence training. (Adapted with permission from Rajamani et al. [16])

undergo summative assessment by a capricious number of scans. The mentor must directly supervise the initial scans although it is not feasible to directly supervise all scans.

During this process, the trainee should store every scan and report the findings of each scan in a logbook. The mentor will review the logbook and provide feedback not only on the image acquisition quality but also on the accuracy of image interpretation [16].

22.3.3 Final Assessment

The trainee will face the final assessment once the mentor is satisfied with his/her progress and consider that he/she has acquired the needed skills. This final assessment will have two parts: a cognitive assessment or a knowledge test based on the curriculum, and a practical assessment that will entail examining various critically ill patients. In this practical test, a qualified assessor will evaluate the quality of the image acquisition, the accuracy of the image interpretation and the reporting ability.

22.4 Barriers to Ultrasound Training

Despite the great number of consensuses published and the perceived demand for CCUS training, implementation of these recommendations at national and local level is not as widespread as expected. Many barriers to deliver a high-quality training program have been identified (► Box 22.1); they were described more than 10 years ago, and we still have not solved them [21–24]. The top two barriers highlighted are the lack of trainers and of formal ultrasound curriculum. To overcome some of these barriers, new guidelines have been published [11, 12, 16], and various new educational techniques have been introduced into ultrasound training. However, the optimal methodology of training has yet to be defined and supported with high-quality evidence, and further research is required to assess the impact of these methods [14].

Box 22.1 Barriers/Challenges to Learning Ultrasound

- Lack of trainers
- Lack of formal ultrasound curriculum
- Time constraints
- Resistance from colleagues outside and inside of ICU
- Lack of equipment
- Lack of interest among trainees
- Perceived lack of utility

22.5 Ultrasound Educational Tools

Performing ultrasound requires an assortment of skills. The didactic portion of the education can be covered by lectures and textbooks, free online education and digital courses. However, these useful tools leave the trainee with no opportunity to fix their knowledge with real-time ultrasound use. Hands-on sessions are needed to enable trainees to develop spatial coordination and to practice obtaining the standard views. This need of hands-on experience means that ultrasound should be taught in small groups. There is no agreement on an optimal tutor/trainee ratio for these sessions, probably four or five per instructor is ideal, granting efficient use of human resources without compromising on quality and close supervision.

22.5.1 E-Learning

E-learning has different tools such as videos, webinars and e-books. It allows the trainee to tailor their learning pace, duration and location and can be a solution for training in areas with limited educational resources. Free Online Access Medical education (FOAMed) is described as an online collection of medical resources that includes podcasts, videos, tweets or blogs. FOAMed has expanded rapidly in recent years with a great amount of resources available online to learn ultrasound. There are many online resources available; a summary of some of them could be found on ► https://spocus.org/resources-programs/foamed/. The use of e-learning before an introductory course can provide an opportunity to create a flipped classroom.

With the outbreak of the COVID-19 pandemic, due to travel restrictions and physical distancing, most in-person POCUS training courses were cancelled, despite their increased demand given the utility of POCUS in COVID-19, so online solutions became even more necessary [25].

22.5.2 Simulation

Simulation is an imitation of a real situation that can be repeated as needed and shows real effects of actions in a controlled environment. Simulation has long been used in fields outside medicine, and, in recent years, it is broadly adopted by many medical specialties. Simulators offer the possibility of exposure to ultrasound cases that are rarely encountered by trainees or happen during situations where teaching is not possible, such as cardiac arrest. The use of low- and high-fidelity ultrasound simulation was found to be a useful tool for ultrasound training, mostly via improvement in trainee competence in post-course-simulated environments and improved skill in post-training assessments [26]. While learning basic CCE, it can accelerate the learning curve by improving practical and technical skills [27, 28]. Simulation can also be used for formative assessment during the longitudinal competence program to assess the competencies that have already been achieved [29].

22.5.3 Peer Teaching

Hands-on exercises are the best to learn practical skills. Nevertheless, they require a high number of trainers to teach trainees in small groups, and it could be problematic due to time and personal constraints. The problem may be solved by choosing teaching formats that have a multiplier effect; senior mentors train peer tutor, such as recent-certified trainees, who, in turn, teach peers practical ultrasound skills. Tutors that are developmentally close to the learner can understand their challenges better and can be seen as less threatening. This has been extensibly used in undergraduate medical education and can be also used in our setting [30–32].

22.5.4 Remote Supervision and Tele-Ultrasound

Remote supervision may be a solution for the shortage of trainers. For the trainee, it is required Internet connection and the possibility of wireless image transmission from ultrasound machines, and for the mentor, it is required having the corresponding software to remotely review the images and Internet connection to deliver the written feedback. A 1-year experience, using a CCUS curriculum that comprised didactic lectures and longitudinal program, showed that remote oversight permitted a single faculty member to train and oversee 29 residents who carried out more than 2000 ultrasound examinations with notable efficiency; 80% of the trainees achieved CCUS competence [33].

Tele-ultrasound is a merge between telemedicine and point-of-care ultrasound. It allows learners to perform bedside ultrasound receiving instructions and feedback asynchronously and synchronously from instructors at different geographical sites. Tele-ultrasound platforms include cell phone applications for videoconferencing and dedicated ultrasound platforms to share images. It has been successfully implemented in various situations to guide ultrasound training, mainly in resource-limited settings [34]. During the COVID-19 pandemic, tele-ultrasound was compared to face-to-face training and showed that both methods significantly improved learners' post-course knowledge to a similar level [35].

22.6 Conclusions

Critical care ultrasound is an essential part of intensive care practice, but it needs a proper training. Despite many published guidelines, its applicability in the field is still low due to some barriers. The lack of an agreed CCUS curriculum may have been solved with the publication in recent years of new consensuses. Shortage of trainers and training in resource-limited settings could be overcome using new educational tools. However, we should bear in mind that as years come by, we will update our training guidelines to include new ultrasound modalities, which will be incorporated into our daily practice, and new educational tools, which newer technology will enable.

Take-Home Messages

- Ultrasound is a fundamental skill in clinics that should be taught during residency training if possible.
- Consensuses should guide the creation and implementation of training programs in CCUS, but we should develop training frameworks that are tailored to meet the needs of our country.
- New educational techniques will help us bridge the gap in CCUS training in the coming years.

Summary

This chapter describes the history of ultrasound penetration into intensive care curricula, the competencies needed and how a training program should be structured to achieve competence. Lastly, it lists the current challenges to deliver a high-quality program and provides a list of educational tools beside lectures and hands-on sessions.

References

1. American Medical Association. American Medical Association policy. H-230.960 Privileging for ultrasound imaging. https://policysearch.ama-assn.org. Accessed 12 Jul 2022.
2. Lichtenstein D, Axler O. Intensive use of general ultrasound in the intensive care unit. Prospective study of 150 consecutive patients. Intensive Care Med. 1993;19(6):353–5.
3. Lichtenstein DA, Menu Y. A bedside ultrasound sign ruling out pneumothorax in the critically ill. Lung sliding. Chest. 1995;108(5):1345–8.
4. Lichtenstein D, Meziere G, Biderman P, Gepner A, Barre O. The comet-tail artefact: an ultrasound sign of alveolar-interstitial syndrome. Am J Respir Crit Care Med. 1997;156:1640–6.
5. Mayo PH, Beaulieu Y, Doelken P, Feller-Kopman D, Harrod C, Kaplan A, et al. American College of Chest Physicians/La Société de Réanimation de Langue Française statement on competence in critical care ultrasonography. Chest. 2009;135(4):1050–60.
6. Expert Round Table on Ultrasound in ICU. International expert statement on training standards for critical care ultrasonography. Intensive Care Med. 2011;37(7):1077–83.
7. Arntfield RT, Millington SJ, Ainsworth CD, Arora RC, Boyd J, Finlayson G, et al. Canadian recommendations for critical care ultrasound training and competency. Can Respir J. 2014;21(6):341–5.
8. Price S, Via G, Sloth E, Guarracino F, Breitkreutz R, Catena E, et al. Echocardiography practice, training and accreditation in the intensive care: document for the World Interactive Network Focused on Critical Ultrasound (WINFOCUS). Cardiovasc Ultrasound. 2008;6(49):1.
9. Pustavoitau A, Blaivas M, Brown SM, Gutierrez C, Kirkpatrick AW, Kohl BA, et al. Recommendations for achieving and maintaining competence and credentialing in critical care ultrasound with focused cardiac ultrasound and advanced critical care echocardiography summary of recommendations. http://journals.lww.com/ccmjournal/Documents/CriticalCareUltrasound.pdf. Accessed 12 Jul 2022.
10. Wong A, Galarza L, Duska F. Critical care ultrasound: a systematic review of international training competencies and programmes. Crit Care Med. 2019;47(3):e256–62.
11. Wong A, Galarza L, Forni L, De Backer D, Slama M, Cholley B, et al. Recommendations for core critical care ultrasound competencies as a part of specialist training in multidisciplinary intensive care: a framework proposed by the European Society of Intensive Care Medicine (ESICM). Crit Care. 2020;24(1):1–6.
12. Robba C, Wong A, Poole D, Al Tayar A, Arntfield RT, Chew MS, et al. Basic ultrasound head-to-toe skills for intensivists in the general and neuro intensive care unit population: consensus and expert recommendations of the European Society of Intensive Care Medicine. Intensive Care Med. 2021;47(12):1347–67.
13. Vieillard-Baron A, Mayo PH, Vignon P, Cholley B, Slama M, Pinsky MR, et al. International consensus statement on training standards for advanced critical care echocardiography. Intensive Care Med. 2014;40(5):654–66.
14. Rajamani A, Shetty K, Parmar J, Huang S, Ng J, Gunawan S, et al. Longitudinal competence programs for basic point-of-care ultrasound in critical care: a systematic review. Chest. 2020;158(3):1079–89.
15. Rajamani A, Smith L, Gunawan S, Gunawan G, Parmar J, Arvind H, et al. Methodologic quality of guidelines for training or competence processes for basic point-of-care echocardiography in critical care: a systematic review of the literature. Chest. 2021;160(2):616–23.
16. Rajamani A, Galarza L, Sanfilippo F, Wong A, Goffi A, Tuinman P, et al. Criteria, processes, and determination of competence in basic critical care echocardiography training: a Delphi process

consensus statement by the learning ultrasound in critical care (LUCC) initiative. Chest. 2022;161(2):492–503.
17. Kelm DJ, Ratelle JT, Azeem N, Bonnes SL, Halvorsen AJ, Oxentenko AS, et al. Longitudinal ultrasound curriculum improves long-term retention among internal medicine residents. J Grad Med Educ. 2015;7(3):454.
18. Rappaport CA, McConomy BC, Arnold NR, Vose AT, Schmidt GA, Nassar B. A prospective analysis of motor and cognitive skill retention in novice learners of point of care ultrasound. Crit Care Med. 2019;47(12):e948.
19. Schott CK, LoPresti CM, Boyd JS, Core M, Haro EK, Mader MJ, et al. Retention of point-of-care ultrasound skills among practicing physicians: findings of the VA national POCUS training program. Am J Med. 2021;134(3):391–9.
20. Rajamani A, Miu M, Huang S, Elbourne-Binns H, Pracher F, Gunawan S, et al. Impact of critical care point-of-care ultrasound short-courses on trainee competence. Crit Care Med. 2019;47(9):e782–4.
21. Eisen LA, Leung S, Gallagher AE, Kvetan V. Barriers to ultrasound training in critical care medicine fellowships: a survey of program directors. Crit Care Med. 2010;38(10):1978–83.
22. Shah S, Bellows BA, Adedipe AA, Totten JE, Backlund BH, Sajed D. Perceived barriers in the use of ultrasound in developing countries. Crit Ultrasound J. 2015;7(1):3–7.
23. Galarza L, Wong A, MLNG M. The state of critical care ultrasound training in Europe: a survey of trainers and a comparison of available accreditation programmes. Anaesthesiol Intensive Ther. 2017;49(5):382–6.
24. Brady AK, Spitzer CR, Kelm D, Brosnahan SB, Latifi M, Burkart KM. Pulmonary critical care fellows' use of and self-reported barriers to learning bedside ultrasound during training: results of a national survey. Chest. 2021;160(1):231–7.
25. Eke OF, Henwood PC, Wanjiku GW, Fasina A, Kharasch SJ, Shokoohi H. Global point-of-care ultrasound education and training in the age of COVID-19. Int J Emerg Med. 2021;14(1):1–4.
26. Lewiss RE, Hoffmann B, Beaulieu Y, Phelan MB. Point-of-care ultrasound education: the increasing role of simulation and multimedia resources. J Ultrasound Med. 2014;33(1):27–32.
27. Vignon P, Pegot B, Dalmay F, Jean-Michel V, Bocher S, L'her E, et al. Acceleration of the learning curve for mastering basic critical care echocardiography using computerized simulation. Intensive Care Med. 2018;44(7):1097–105.
28. Prat G, Charron C, Repesse X, Coriat P, Bailly P, L'her E, et al. The use of computerized echocardiographic simulation improves the learning curve for transesophageal hemodynamic assessment in critically ill patients. Ann Intensive Care. 2016;6(1):27.
29. Sheehan FH, McConnaughey S, Freeman R, Zierler RE. Formative assessment of performance in diagnostic ultrasound using simulation and quantitative and objective metrics. Mil Med. 2019;184(Suppl 1):386–91.
30. Garcia-Casasola G, Sánchez FJG, Luordo D, Zapata DF, Frías MC, Garrido VV, et al. Basic abdominal point-of-care ultrasound training in the undergraduate: students as mentors. J Ultrasound Med. 2016;35(11):2483–9.
31. Arias Felipe A, Doménech García J, Sánchez Los Arcos I, Luordo D, García Sánchez FJ, Villanueva Martínez J, et al. Teaching the basics of echocardiography in the undergraduate: students as mentors. Rev Clin Esp. 2017;217(5):245–451.
32. Ahn JS, French AJ, Thiessen MEW, Kendall JL. Training peer instructors for a combined ultrasound/physical exam curriculum. Teach Learn Med. 2014;26(3):292–5.
33. Arntfield RT. The utility of remote supervision with feedback as a method to deliver high-volume critical care ultrasound training. J Crit Care. 2015;30(2):441.e1–6.
34. Salerno A, Tupchong K, Verceles AC, Mccurdy MT. Point-of-care teleultrasound: a systematic review. Telemed e-Health. 2020;26(11):1314–21.
35. Soni NJ, Boyd JS, Mints G, Proud KC, Jensen TP, Liu G, et al. Comparison of in-person versus tele-ultrasound point-of-care ultrasound training during the COVID-19 pandemic. Ultrasound J. 2021;13(1):1–7.

Integration of Different US Skills in Clinical Scenarios at the Bedside

Contents

Chapter 23 **Combined Echocardiography and Lung Ultrasound in Shocked Patient – 000**
Luigi Vetrugno, Fabrizio Tritapepe, Marco Ventin, Gian Marco Anzellotti, and Salvatore Maurizio Maggiore

Chapter 24 **Role of Lung Ultrasound and Echocardiography in Acute Respiratory Failure, Acute Respiratory Distress Syndrome, and Weaning in Mechanically Ventilated Patients – 000**
Luigi Pisani, Marry R. Smit, and Pieter R. Tuinman

Chapter 25 **Use of Ultrasound for the Assessment of Fluid Responsiveness in Critically Ill Patients – 000**
Filippo Sanfilippo, Stephen Huang, and Alberto Noto

Chapter 26 **Extended-FAST Protocol in Polytrauma Patients – 000**
Francesco Corradi, Federico Dazzi, Erika Taddei, Giada Cucciolini, and Samuele Ferrari

Combined Echocardiography and Lung Ultrasound in Shocked Patient

Luigi Vetrugno, Fabrizio Tritapepe, Marco Ventin, Gian Marco Anzellotti, and Salvatore Maurizio Maggiore

Contents

23.1 Shock Definition and Classification – 372
23.1.1 Shock Vital Parameters and Clinical Signs – 372

23.2 Ultrasound and Shock – 373
23.2.1 Basic and Advanced Critical Care Echocardiography – 373
23.2.2 Basic Skills – 374
23.2.3 Advanced Skills – 374

23.3 Fluid Resuscitation – 376
23.3.1 Fluid Responsiveness – 377
23.3.2 Fluid Tolerance – 377

23.4 Lung Ultrasound – 379

23.5 Transesophageal Cardiac and Lung Ultrasound for Hemodynamic Instability and Shock – 382

References – 383

Supplementary Information The online version contains supplementary material available at https://doi.org/10.1007/978-3-031-32462-8_23.

© The Author(s), under exclusive license to Springer Nature Switzerland AG 2023
C. Robba et al. (eds.), *Basic Ultrasound Skills "Head to Toe" for General Intensivists*, Lessons from the ICU,
https://doi.org/10.1007/978-3-031-32462-8_23

Learning Objectives

- The reader will receive an overview of the skills required for the use of basic and advanced cardiac and lung ultrasound and the main reasons for their use in the clinical evaluation and management of patients with shock.

23

23.1 Shock Definition and Classification

Shock is defined as a clinical condition characterized by an inadequate blood circulation and oxygen delivery sufficient to satisfy the cellular metabolic demands ultimately leading to cellular and tissue hypoxia [1]. Shock can be divided into (1) hypovolemic—secondary to an external or internal fluid loss for a different reason; (2) cardiogenic—from acute myocardial infarction, severe myocarditis/valve disease, or aberrant rhythm conduction; (3) obstructive—due to cardiac tamponade, tension pneumothorax, or pulmonary embolism, and (4) distributive—mainly septic shock and in a small portion of cases anaphylactic or neurogenic shock. The most frequent type of shock encountered in clinical practice is distributive shock in 66% of the cases; hypovolemic and cardiogenic shock occur in 32% (16% each), while obstructive shock in the remaining 2% of the cases [2].

As the type of shock at the first patient's evaluation can only be suspected, and two types of shock can also overlap (e.g., cardiac and septic shock), an alternative approach is to define the clinical state based on the cardiac output (CO), intended as low or normal/high. A low CO syndrome with insufficient peripheral oxygen transport is most commonly due to hypovolemic, cardiogenic, or obstructive shock, whereas a normal or high CO syndrome, usually associated with low peripheral vascular resistance, is seen in septic shock. Patients with septic shock can also develop a low CO state with a reduced left ventricular ejection fraction (EF%) or isolated diastolic dysfunction (DD), which is observed in 39% and 20% of the patients, respectively [3]. In the first case, a low EF% can manifest following afterload restoration with norepinephrine; in the second case, DD can be present when liberal fluid therapy is applied. However, sepsis-induced cardiac dysfunction is a reversible state, and patients surviving the infection usually gradually improve within few weeks.

23.1.1 Shock Vital Parameters and Clinical Signs

Altered hemodynamic parameters such as hypotension, with systolic arterial pressure less than 90 mmHg or mean arterial pressure less than 65 mmHg, with tachycardia on the screen (heart rate >100/min), are often the first clinical sign to be noted in shocked patients. However, hypotension is not an essential condition to diagnose a shock since compensatory mechanisms such as vasoconstriction—which diverts blood from the peripheral circulation to the vital organs—can preserve blood pressure in the short term [4].

Additional shock-related clinical signs are cyanosis, confusion with or without altered mental state, and reduced urine output (diuresis <0.5 mL/kg/h); nonetheless, also the other organ systems can be affected.

A capillary refill time test (CRT) is usually performed to assess the blood flow through peripheral tissues by the application of gentle pressure over the nail bed. Pink color restoration over the nail bed within 2 s is usually an indicator of good blood flow and good CO. On the other hand, a CRT >2 s is a suggestive early sign of shock. Elevated lactates >1.5 mmol/L are usually also present during shock [5, 6].

23.2 Ultrasound and Shock

In the last 20 years, cardiac and lung point-of-care ultrasound (POCUS) in the context of shocked patients demonstrated a major clinical significance since it has been the most compelling new bedside diagnostic tool able to conjugate diagnostics and treatment effects monitoring bedside. In the 1980s, the advent of portable ultrasound machines revolutionized the diagnostic paradigm from "transferring the patient to the cardiology suite" to " moving the machine to the patient's bed," and the POCUS was born [7]. In the same years, the first use of transesophageal echocardiography (TEE) was documented in the attempt to promptly evaluate the surgical proceedings and monitor the hemodynamic state in patients with postcardiotomy shock in the operating room. The first guidelines related to the perioperative TEE practice were then published in 1996, and after that, many training programs in cardiac anesthesia were established by cardiovascular societies worldwide [8]. In 2009, the American College of Chest Physicians (ACCP) and "La Société de Reanimation de Langue Française" (SRLF) published a consensus statement to describe how ultrasound should be used in the intensive care unit (ICU) setting and defined the type of skills to be mastered to reach full proficiency [9]. The consensus dived the use of ultrasound in two main branches: (1) general critical care ultrasound (GCCU) with a focus on the assessment of the thorax, abdominal, and vascular structures and (2) the critical care echocardiography (CCE). The latter consists of two skill categories, basic and advanced (including the use of TEE), considering that the window success of transthoracic echocardiography (TTE) in ventilated patients is reduced approximately to 50% versus 97% with TEE [10].

23.2.1 Basic and Advanced Critical Care Echocardiography

Basic CCE with TTE should be utilized to categorize patients with unmotivated hemodynamic instability. The required skills are the optimal machine setup and the correct positioning of the probe to obtain the canonic windows. M-mode, B-mode, and color Doppler use are indicated to investigate the inferior vena cava (IVC) respiratory variation. On the other hand, advanced critical care echocardiography (CCE) should provide complete echocardiography and Doppler skills to perform a cardiopulmonary evaluation through imaging acquisition, basic Doppler function views, and Doppler to assess the systolic pulmonary pressure, stroke volume, and diastolic function. As stated before, TEE is also considered an advanced skill. Cardiac (as well as lung) ultrasound should be performed following rigorous methodology.

23.2.2 Basic Skills

In the ICU, ventilators are usually located on the patient's left side; therefore, more space is available on the right side of the bed. Modern ultrasound devices are smaller and more manageable than they used to be, so the right side is an optimal space to hold them. The operator can use the left hand to control the screen and the right hand to direct the probe while searching for the patient's cardiac views. The acquisition of the following standard views is required: (1) parasternal long and short axis view; (2) apical four-chamber view; (3) subcostal four-chamber view and IVC view. The exam is purely **qualitative**, essentially aimed to address to the following questions: is left ventricle dimension small, normal, or severely dilated? Is left ventricle contractile function normal, hyperdynamic, moderately, or severely depressed? Is the observed dysfunction homogeneous or heterogeneous? What about the right ventricle? Is its cavity normal or dilated? What about right atrial and right ventricle collapse? Is there evidence of pericardial effusion? What about valve function from the Doppler view? Is there evidence of **severe** valve insufficiency? Is IVC respiratory variation present? Basic CCE was intended to use ultrasound to perform a "**goal-directed examination**" in a simple manner [9].

The focused assessment with sonography (FAST) protocol was the first to describe the use of the cardiac subcostal view to exclude cardiac tamponade, as a cause of **obstructive shock** in trauma patients. Of note, the FAST exam is a part of the advanced trauma life support (ATLS) course since 1997 [11].

This protocol is now extended to incorporated lung ultrasound as Extended Focused Assessment with Sonography in Trauma (E-FAST) in the Advanced Trauma Life Support (ATLS) to rule out pneumothorax and hemothorax, which are other two examples of obstructive and hypovolemic shock state [12].

23.2.3 Advanced Skills

Mastery of image acquisition for Doppler use with TTE and TEE is required, as well as competence in measuring hemodynamic function through the assessment of:

1. Dynamic index of preload sensitivity and detailed flow measurement (see below)
2. Systolic pulmonary arterial pressure (sPAP)
3. Left ventricular ejection fraction (EF)
4. Stroke volume (SV)
5. Alteration in regional wall motion

Additional assessments include:

6. DD grade evaluation.
7. Valve dysfunction evaluation and grading with Doppler.
8. Right ventricular size and function. The latter is expressed as the ratio between the right and left ventricular diastolic area ratio (RVEDA/LVEDA), which can be normal (<0.6), moderately dilated (between 0.6 and 1), or severely dilated (>1).

9. IVC respiratory variation (%) (subcostal view).
10. TEE and SVC respiratory variation with long axis view measurement.

Most importantly, noninvasive CO estimation (as the product of heart rate, HR, and stroke volume, SV) is essential. SV is equal to the product of the velocity time integral (VTI) over the aortic valve obtained with Doppler and the aortic cross-section area (CSA). CSA is equal to $\pi \times$ (aortic diameter in cm/2)^2. The aortic diameter of the left ventricular outflow tract (dLVOT) can be obtained from the parasternal long axis window. However, in this setting minimal errors may become magnified and generate significant discrepancies in CO evaluations. Measuring the VTI obtained with TTE in the apical five-chamber view using pulsed waves (PW) and searching for normal values (VTI 18–22 cm) could overcome this limitation [13]. Doppler-derived hemodynamic TTE systolic parameters have been strongly associated with mortality, particularly VTI <16 cm after ICU admission. Incorporating these simplified Doppler-derived hemodynamic parameters facilitates early risk stratification and strengthens the clinical yield of the ultrasound exam [9].

Diastolic dysfunction (DD) can be defined as the left ventricle (LV) progressively reduced ability to accept the normal preload with a progressive increase in left ventricular end-diastolic pressure (LVEDP) [10].

A simple explanation of DD is described elsewhere [14]. In recent years, DD assessment has gained popularity due to the growing body of evidence indicating its association with negative outcomes in critically ill patients [15].

The study of DD with echocardiography is an advanced skill and relies on four parameters obtained in the apical four-chamber view as described in the latest 2016 guidelines [16]: trans-mitral flow, early and late diastolic tissue waves (e′ and a′, respectively), septal and lateral ventricular wall tissue Doppler (TDI), left atrial volume, and peak velocity of tricuspid regurgitation jet (if present).

The trans-mitral flow is measured with the pulsed wave (PW) Doppler signal obtained at the level of the mitral valve leaflet tips, recording the LV inflow patterns. PW Doppler describes the LV filling process in terms of an early wave (E) followed by the late atrial wave (A). TDI evaluation positioned at the myocardial basal level allows to investigate both septal and lateral ventricular wall regions to obtain the e′ and a′ waves. Left atrial (LA) volume is measured at the end of systole excluding the confluences of pulmonary veins and the LA appendage. In case of tricuspid regurgitation, continuous wave (CW) Doppler through the tricuspid valve allows to measure the peak jet velocity, which is used as a surrogate of postcapillary right ventricular (RV) pressure ($P = 4V^2$). Adding the value of central venous pressure to the calculated RV pressure, it is possible to estimate sPAP.

Following the new guidelines by the American Society of Echocardiography and the European Association of Cardiovascular Imaging [16] to obtain these parameters, DD can be classified in three stages.

Diastolic Dysfunction Classification

- Stage I is called abnormal relaxation: at this stage, the LV relaxation is impaired but without a significant change in LA pressures.
- Stage II results from chronically impaired LV relaxation. The LA pressure increases to restore the LA-to-LV gradient filling pattern. It is also called "pseudo-normal"; LVEDP is now increased.
- Stage III, or restrictive pattern, is characterized by a significant increase in LVEDP. The physiological compensation of increased LA pressure has already reached its ceiling, and atrial contraction can transfer only a minimal amount of blood into the LV with high LVEDP. Stage III is divided into a reversible or irreversible pattern (the latter also known as stage IV); this separation is probably not meaningful in the ICU setting [17].

Studies have showed that the increase of LVEDP is correlated with lung ultrasound B-lines in case of cardiogenic shock. Diffuse B-lines and DD with E/e′ ratio >15 have been shown to strongly correlate with ICU mortality [18].

23.3 Fluid Resuscitation

Fluid resuscitation is the cornerstone of septic shock, and four phases of fluid therapy should be considered: the resuscitation phase (R), the optimization phase (O), the stabilization phase (S), and the evacuation phase (E). All phases are equally important, but the R phase, if correctly and timely performed, can reverse the shock state and the associated multiorgan failure (MOF), significantly reducing patients' mortality [19].

The Surviving Sepsis Campaign, for patients with sepsis-induced hypoperfusion or septic shock, suggests that at least 30 mL/kg of intravenous (IV) crystalloid fluid should be given within the first 3 h [1].

Fluid resuscitation should be guided by fluid challenge (FC) or alternatively with passive leg raising (PLR). Both tests aim to assess if the patient is a fluid responder. The PLR test is thoroughly discussed in the European Society of Intensive Care Medicine (ESICM) consensus on hemodynamic monitoring [20]. PLR displaces a volume of 150–300 mL from periphery to center and, therefore, determines a change in the distribution of intravascular volume. An increase in 8–15% in CO with PLR defines a patient as "fluid responder." However, the PLR test remains an alternative to the FC. FC consists in giving 4 mL/kg of crystalloid in 5–10 min to the patient to test their "fluid responsiveness." An increase in baseline CO measurement greater than 10–15%, regardless of the method used to evaluate it, defines the patient as a "fluid responder" [20]. On the contrary, if there is no CO increase but only an increase in central venous pressure >5 mmHg is observed, the patient should be defined as "fluid nonresponder" and FC abolished. Considering that the last 15 years have been characterized by a decline in the invasive hemodynamic monitoring to measure CO with pulmonary arterial catheter (PAC), advanced cardiac ultrasound can be an easy alternative to measure CO in a semicontinuous manner. However, as stated above, CO with echocardiography should consider the limitations in obtaining the dLVOT [21].

23.3.1 Fluid Responsiveness

Dynamic parameters of fluid responsiveness such as stroke volume (SV), stroke volume variation (SVV), and pulse pressure variation (PPV) are outside the scope of this chapter. They use the concept of functional hemodynamic monitoring due to cardiopulmonary interaction, to assess the response of the patient to the fluid. However, the same concept can be used with ultrasound, understanding their limitations in detect minimal changes of CO/SV variations [22].

The most frequently utilized echocardiographic dynamic parameters of FR are: aortic blood flow (ABF) velocity (*V*), the variation of the maximal Doppler velocity (*V*peak) in the left ventricular outflow tract (*V*maxAo variation) calculated as $(V\text{peak}_{max} - V\text{peak}_{min})/(V\text{peak}_{max} + V\text{peak}_{min}/2) \times 100$; and the variation of aortic VTI, calculated as $(\text{VTI}_{aomax} - \text{VTI}_{aomin})/(\text{VTI}_{aomax} + \text{VTI}_{aomin}/2) \times 100$. Of note, the concept of mini-fluid challenge, in which 100 mL of fluid are given over just 1 min, can be done with VTI to assess the FR in unstable patients reducing the risk of giving more fluids in nonresponders [23]. Furthermore, echocardiography can reveal right ventricular dysfunction responsible for erroneous interpretations of the dynamic indices (false positive) [24, 25].

A separate discussion is deserved for the IVC and superior vena cava (SVC) respiratory variation to assess FR responsiveness in septic shock. It has been reported that IVC (with TTE) and SVC (with TEE) variability of >18% and >38%, respectively, can be predictive of a significant increase in CO in FR patients.

However, a recent study showed that with ultrasound the areas under the receiver operating characteristic (ROC) curves for SVC and IVC variation, after a FC of 300 mL were 0.755 and 0.635, respectively. In addition, SVC always showed an area under the ROC curve (AUC) greater than IVC. In light of these results, the usefulness of IVC to predict FR has been questioned by many authors [26, 27]. However, to measure the SVC, TEE is required. Lastly, but not less importantly, lung ultrasound completes the cardiac evaluation over fluid resuscitation with the new concept of fluid tolerance (see below).

23.3.2 Fluid Tolerance

Fluid tolerance can be defined as the degree to which a patient can tolerate fluid administration without inducing organ dysfunction. Fluid tolerance can involve not only the lung, but all organs can be affected according to different thresholds (lung, gut, liver, kidney, central nervous system). Lung tolerance can be primary or secondary [28]. For example, with lung ultrasound, B-lines are associated with extravascular lung water (EVLW) in the case of elevated pulmonary capillary wedge pressure from heart failure or after capillary leak syndrome from pneumonia and acute respiratory distress syndrome (ARDS). There is sufficient evidence to think that fluid overload and venous congestion can contribute to a poor clinical outcome, notably in septic shock fluid intolerance invites to avoid FR and start vasoactive agents [27].

Case Vignette 23.1

A 63-year-old patient with history of paroxysmal atrial fibrillation and systemic hypertension was admitted to the emergency department (ED). Patient's history of present illness was notable for abdominal pain associated with postprandial vomiting. Abdominal ultrasound showed sub-acute cholecystitis and the patient was admitted to the medical ward. During the night, the patient became oliguric, hypotensive, and tachycardic. The arterial blood gases showed: pH 7.33, pCO_2 23.5 mmHg, pO_2 81 mmHg, HCO_3 12 mmol/L, K 6.22 mmol/L, Glycaemia 50 mg/dL, Lac 9.53 mmol/L. The patient also experienced acute-on-chronic renal failure indicated by serum creatinine >3 mg/dL and elevated blood urea nitrogen 114 mg/dL with also a raise in liver enzymes alanine aminotransferase (ALT) and aspartate aminotransferase (AST) up to >4.000 IU/L.

Cardiac and lung ultrasound were performed: the complete exam of the patient is reported in ◘ Fig. 23.1, ◘ Videos 23.1 and 23.2.

The patient showed diffuse cardiac hypokinesia with a reduced EF 35% and atrial fibrillation. IVC was dilated to a 2.03 cm diameter and lacked respiratory variation. Lung ultrasound revealed a large bilateral pleural effusion >4 cm in the posterior thoracic zone, while confluent B-lines were present in the lateral and anterior lung area. The measure of VTI was 10.5 cm as a mean of 5 cycles for atrial fibrillation, and dLVOT was 2.18 cm. With heart rate of 130 beats/min and a body surface area (BSA) of 1.98, we calculated a SV of 39 mL and a CI of 2.571 mL/min. As a collateral ultrasound measurement of subcostal cardiac view, the Doppler of the right hepatic vein showed a pattern of mild-abnormal liver congestion and liver fluid intolerance (for more explanation see VEXUS score) [28, 29]. After the cardiac and lung ultrasound

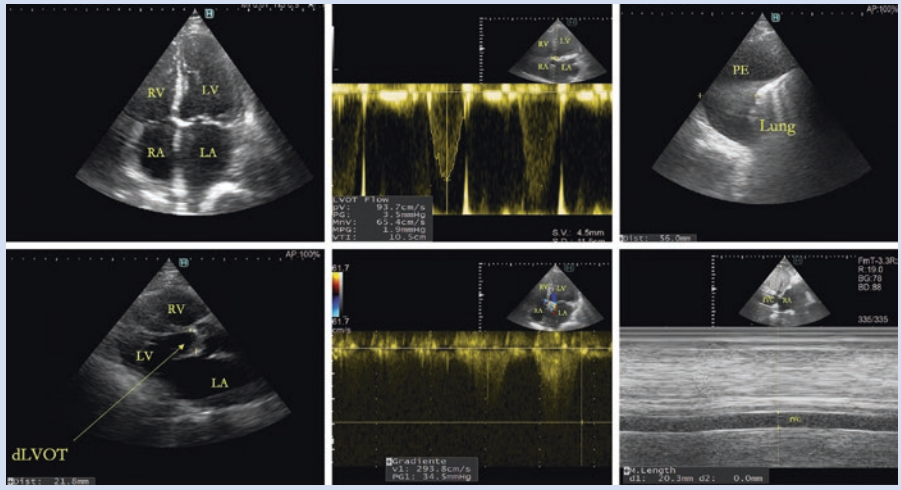

◘ **Fig. 23.1** Top left transthoracic apical four chambers view, down left parasternal long axis view and LVOT diameter measurement; middle top five chambers view, VTI measurement and middle down four chambers view, tricuspid jet and gradient; top right pleural effusion, posterior BLUE point; downright IVC diameter. *dLVOT* left ventricle outflow diameter, *VTI* velocity time integral, IVC% inferior vena cava variation

assessment, no additional fluids were given to the patient, and he was given antibiotic piperacillin/tazobactam, dobutamine, and noradrenaline at a lower dose of 3 and 0.05 mcg/kg/min, respectively. A continuous renal replacement therapy (CRRT) was also initiated to remove 100 mL/h fluid per hour and to overcome renal failure. In the next days the hemodynamic status of the patient improved, liver enzymes gradually decreased, and diuresis reappeared. Finally, the patient returned to sinus rhythm. A recent study has shown that dobutamine improves the clinical status in shocked patients with an increase in EF% and VTI without an increase (or even a decrease) in heart rate. Moreover, a recent network meta-analysis found that dobutamine is significantly associated with reduced mortality in patients with severe sepsis or septic shock [3, 30].

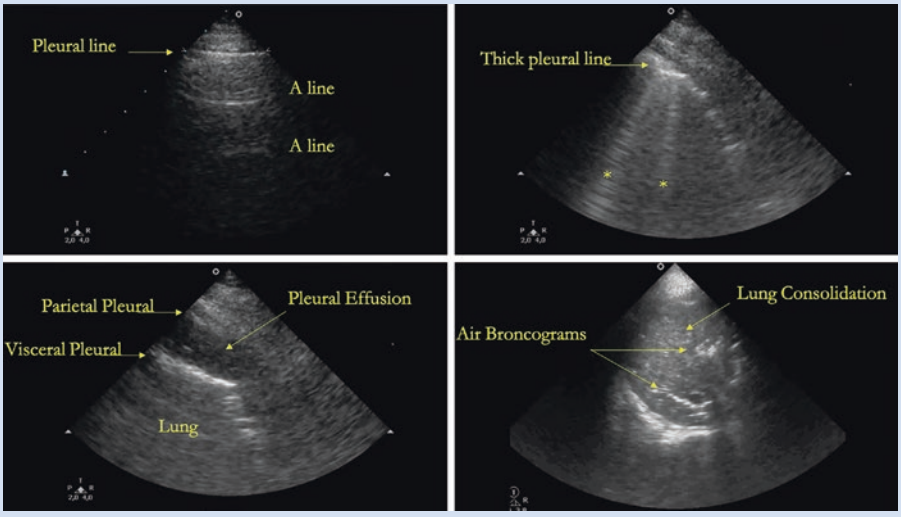

Fig. 23.2 Top left, normal lung with A-lines at regular interval (clip with lung sliding); top right irregular pleural line and two B-lines; down left, pleural effusion (clip with blue arrows); down right lung consolidation C-profile and dynamic air bronchogram (clip with dynamic bronchogram)

23.4 Lung Ultrasound

Lung ultrasound (LUS) is an easy-to-use, repeatable, bedside tool for critically ill patients. After the COVID-19 pandemic, LUS ultrasound in ICU has become the first-line diagnostic modality to rule out potential severe complications such as pneumothorax, large pleural effusions, and VAP, providing better accuracy than chest X-rays [31]. The use of LUS follows the same methodological principles of cardiac ultrasound, with the device placed on the patient right side. The employed probe can differ from operator to operator, with micro-convex, cardiac, and convex probes usually used in adults and linear probes in children. The selection of each probe can also depend on the peculiarities during each examination, for example, the use of the linear probe in the adult to identify the challenging "lung point" sign or the use a

convex probe in the children to look deeply into the lung parenchyma or look for pleural effusion.

The probe should be placed over the BLUE points that are three standardized points described in the BLUE-protocol for ultrasound assessment of the lung in acute respiratory failure [32]. Starting from the upper right BLUE point, the operator will compare the findings with the left BLUE point and-so-forth from the right to the left for the other inferior and posterior BLUE points. Compared with computed tomography (CT) scans, LUS offers a dynamic "real-time" overview of the lung morphology without transferring the patient to the radiology suite.

As air precludes ultrasound from travelling through the lung, a normal A-lung pattern is characterized by the reverberation of pleural lines over the screen at regular intervals associated with lung sliding (◘ Fig. 23.2, top left, ◘ Video 23.3).

The progressive loss of aeration and increased extravascular lung water (EVLW), secondary to pulmonary edema or ARDS, generate different extents of B-lines as a vertical artifact. B-lines allow good prediction of pulmonary congestion [33]. B-lines can be interpreted as a sign of lung fluid intolerance but should be integrated with cardiac ultrasound in the clinical overview of the patient (◘ Fig. 23.2, top right, ◘ Video 23.4). The complete loss of aeration, with dynamic air bronchograms (hyperechoic air travels into the bronchus) and tissue-like pattern, is a hallmark of pneumonia, with a 90% sensitivity and 98% specificity in distinguishing it from resorptive atelectasis in which the bronchogram is absent (◘ Fig. 23.2, down right, ◘ Video 23.5) [34]. Patients in ICU can also be monitored with LUS to discover early ventilation associated pneumonia (VAP) as a source of septic shock. Pneumonia can be also associated with pleural effusion, which can be seen as anechoic space between the two pleural lines (◘ Fig. 23.2, down left, ◘ Video 23.6).

After an initial assessment of the lung following the BLUE points, the thorax can be further scanned in detail using the 12-zone LUS protocol ◘ Fig. 23.3 [35]. The lung ultrasound score (LUS) can be applied to assess the loss of aeration.

Briefly, three areas of the thorax can be evaluated: anterior, lateral, and posterior. To each of the four patterns described above, a number or a color code from 0 = nor-

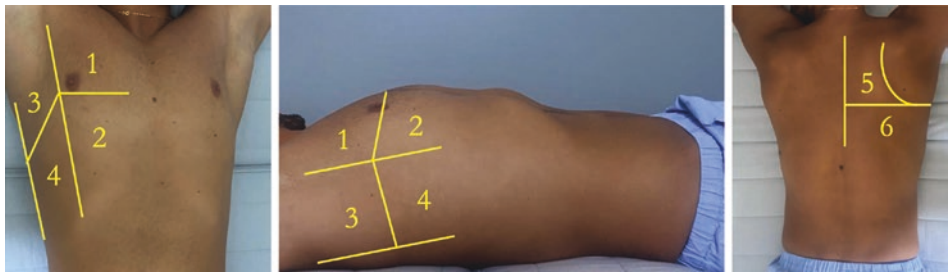

◘ **Fig. 23.3** Lung ultrasound score using the anterior and posterior axillary lines as anatomical landmarks, three areas per hemithorax (anterior, lateral, and posterior) can be identified. Each area is divided in two, superior and inferior. The scapula can determine a blind spot. **Score**: 0 = normal aeration (A-lines and lung sliding or maximum 2 well-spaced B-lines); score 1 = moderate loss of aeration (≥3 well-spaced B-lines with lung sliding, coalescent B-lines/subpleural consolidations occupying <50% of the pleural line); score 2 = severe loss of aeration (≥3 well-spaced B-lines with lung sliding, coalescent B-lines/subpleural consolidations occupying clearly >50% of the pleural line); score 3 = complete loss of aeration: lobar/hemilobar consolidation with predominant tissue like pattern

mal lung (green), 1 = the septal syndrome (blue), 2 = interstitial syndrome (orange), and 3 = consolidation (red) can be assigned to each of the six areas for hemithorax. Following this approach, the global LUS score or a regional-colored image map can be obtained [34].

This score is a continuum ranging from 0, in the case of complete aerated lungs (green lung), to 36, in the case of complete de-aerated lungs (red lung). LUS score is gaining greater importance for its prognostic implications. LUS scores are demonstrated to correlate with ARDS severity and ARDS-related mortality rates; furthermore, the number of B-lines identified at the ultrasound evaluation seems to directly correlate with EVLW, measured by the transpulmonary thermodilution technique. In the case of ARDS, B-lines are jeopardized with some sparing area of A-lines in the presence of lung sliding. On the contrary, acute B-lines over the entire thoracic field are frequently associated with systolic or diastolic cardiogenic shock. After a fluid resuscitation, it has also been shown that B-lines increase by 8% after each fluid challenge [36]. In other words, the hemodynamic benefits of the fluid resuscitation could be sometimes lower and worsen the lung congestion as an expression of lung intolerance.

Case Vignette 23.2

A 72-year-old patient was admitted to Emergency Department for a suspected septic shock with shortness of breath and fever. At ICU admission PaO_2/FiO_2 ratio was 130, pCO_2 35 and PaO_2 71, lactate 3.7 mmol/L, temp 38.6 °C. Blood pressure was 80/60 mmHg, heart rate was 123 beats/min, and respiratory rate was 25 breaths/min. The patient was intubated and ventilated with 8 mL/kg of tidal volume, FiO_2 of 50% and PEEP of 10 cmH_2O. Procalcitonin was 42 ng/mL, white blood cells 37,000/μL. At LUS, the patient showed a tissue-like sign with air bronchogram (C profile) in the lower right lobe (Fig. 23.4, top, Video 23.7). B-lines were present over the entire right hemithorax with a LUS score of 17. Urinary antigen was positive for legionella sp. Transesophageal cardiac ultrasound showed a hyperkinetic and hypovolemic ventricle, in short axis transgastric view (Fig. 23.4, Video 23.8) and a VTI of 14. SVC variation diameter was 45%. As a result, a fluid challenge of 320 mL (4 mg/kg) of crystalloid over 10 min was initiated. After 30 min, the patients were re-evaluated. LUS score showed no difference while VTI increased to 16 (>13%). This was followed by a

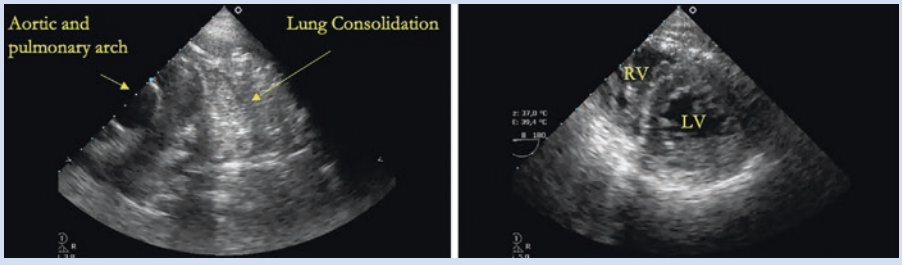

Fig. 23.4 **Left image**, B-lines were present over the entire right hemithorax. C-profile was present on the left hemithorax (**left**). Transesophageal cardiac ultrasound showed a hyperkinetic and hypovolemic ventricle, in short axis trans-gastric view (**right**)

new FC of 320 mL leading to normalized VTI up to 18. After this, patient respiratory gas exchange ameliorated, PaO_2/FiO_2 ratio increased to 170, blood pressure increased to 100/65 mmHg with HR reduction to 100 beats/min, and lactate decreased to 1.8 mmol/L. The patient showed to be fluid responsive and fluid tolerant at the same time. After a third FC, the hemodynamic parameters remained unchanged, but LUS score increased and PaO_2/FiO_2 decreased to 140; therefore, a low dose of noradrenaline was started (0.05 mcg/kg/min).

23.5 Transesophageal Cardiac and Lung Ultrasound for Hemodynamic Instability and Shock

Transient apical ballooning (also known as Takotsubo), dynamic left ventricular outflow tract (LVOT) obstruction, and pulmonary embolism (PE) can present as a **refractory shock**, a condition best defined as a state in which escalation of vasoactive agents in the absence of hypovolemia does not restore adequate tissue perfusion [37, 38].

Briefly, a transient apical ballooning is induced by the mid-ventricular hyperdynamic basal contraction, which enlarges and impairs the ventricular apex, significantly reducing the SV (Fig. 23.5, Video 23.9). The dynamic LVOT obstruction, due to the abnormally increased contractile function, obliterates the upper LV cavity before the end of systole and consequently induces a decreased CO (Fig. 23.5, Video 23.10). LVOT obstruction can be associated with severe mitral regurgita-

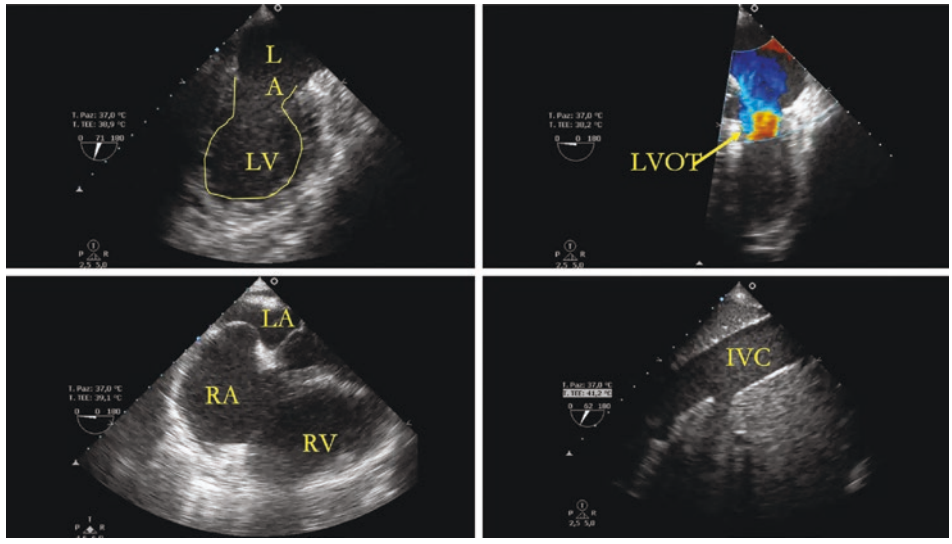

Fig. 23.5 Top left, a transient apical ballooning is induced by the mid-ventricular hyperdynamic basal contraction which enlarges and impairs the ventricular apex; top right dynamic LVOT obstruction, due to the abnormally increased contractile function, obliterates the upper LV cavity before the end of systole with mitral insufficient; down left RV dysfunction supports the suspicion of PE in high-risk patients and dilated IVC down right

tion. In a patient with hemodynamic instability, acute RV dysfunction supports the suspicion of PE in high-risk patients (Fig. 23.5, Video 23.11). If available, computed tomography (CT) scan and pulmonary angiography should be done, otherwise PE treatment should be initiated [39].

Cavayas et al. recently introduced a systematic approach for the study of transesophageal lung ultrasound (TELU) [40]. The authors describe this topography: "with TELU, the craniocaudal axis of each lung is divided into apical, middle, and basal regions; the left subclavian artery is used as a landmark to identify the apical regions; the superior pulmonary veins are used to mark the middle regions; and finally, the inferior vena cava and the right atrial junction are used to identify the basal segments. The lungs are scanned along the longitudinal axis from each of these landmarks by rotating the ultrasound plane at 0° and 90°. The detection of atelectasis and/or lung consolidation is also possible due to the mild acoustic windows provided by the esophagus, from where a larger portion of the dorsal respiratory system can be rapidly examined."

In cases of unexpected **hypoxia and shock**, the main advantage of transesophageal approach lies in its ability to examine both lung and cardiac regions. TELU is an advanced skill.

Take-Home Messages

- Shock is a life-treating condition requiring immediate intervention.
- Cardiac and lung ultrasound can noninvasively recognize the main causes of shock bedside.
- Cardiac and lung ultrasound combine different information to distinguish the different types of shock and should be integrated to assess fluid responsiveness.
- In case of refractory shock of unexplained reason transesophageal echocardiography should be performed looking at cardiac and lung ultrasound views.

References

1. Evans L, Rhodes A, Alhazzani W, Antonelli M, Coopersmith CM, French C, Machado FR, Mcintyre L, Ostermann M, Prescott HC, Schorr C, Simpson S, Wiersinga WJ, Alshamsi F, Angus DC, Arabi Y, Azevedo L, Beale R, Beilman G, Belley-Cote E, Burry L, Cecconi M, Centofanti J, Coz Yataco A, De Waele J, Dellinger RP, Doi K, Du B, Estenssoro E, Ferrer R, Gomersall C, Hodgson C, Møller MH, Iwashyna T, Jacob S, Kleinpell R, Klompas M, Koh Y, Kumar A, Kwizera A, Lobo S, Masur H, McGloughlin S, Mehta S, Mehta Y, Mer M, Nunnally M, Oczkowski S, Osborn T, Papathanassoglou E, Perner A, Puskarich M, Roberts J, Schweickert W, Seckel M, Sevransky J, Sprung CL, Welte T, Zimmerman J, Levy M. Surviving sepsis campaign: international guidelines for management of sepsis and septic shock 2021. Intensive Care Med. 2021;47(11):1181–247. https://doi.org/10.1007/s00134-021-06506-y.
2. Vincent JL, De Backer D. Circulatory shock. N Engl J Med. 2013;369(18):1726–34. https://doi.org/10.1056/NEJMra1208943.
3. Geri G, Vignon P, Aubry A, Fedou AL, Charron C, Silva S, Repessé X, Vieillard-Baron A. Cardiovascular clusters in septic shock combining clinical and echocardiographic parameters: a post hoc analysis. Intensive Care Med. 2019;45(5):657–67. https://doi.org/10.1007/s00134-019-05596-z.
4. van Genderen ME, Paauwe J, de Jonge J, van der Valk RJ, Lima A, Bakker J, van Bommel J. Clinical assessment of peripheral perfusion to predict postoperative complications after major

abdominal surgery early: a prospective observational study in adults. Crit Care. 2014;18(3):R114. https://doi.org/10.1186/cc13905.
5. Beecher HK, Simeone FA, Burnett CH, Shapiro SL, Sullivan ER, Mallory TB. The internal state of the severely wounded man on entry to the most forward hospital. Surgery. 1947;22:672–711.
6. Pickard A, Karlen W, Ansermino JM. Capillary refill time: is it still a useful clinical sign? Anesth Analg. 2011;113(1):120–3. https://doi.org/10.1213/ANE.0b013e31821569f9.
7. Szabo TL. Hewlett Packard—innovations that transformed diagnostic ultrasound imaging. Med Phys Int J Special Issue Hist Med Phys. 2021;6. http://www.mpijournal.org. Accessed 16 May 2022
8. Practice guidelines for perioperative transesophageal echocardiography. A report by the American Society of Anesthesiologists and the Society of Cardiovascular Anesthesiologists Task Force on Transesophageal Echocardiography. Anesthesiology. 1996;84:986–1006.
9. Mayo PH, Beaulieu Y, Doelken P, Feller-Kopman D, Harrod C, Kaplan A, Oropello J, Vieillard-Baron A, Axler O, Lichtenstein D, Maury E, Slama M, Vignon P. American College of Chest Physicians/La Société de Réanimation de Langue Française statement on competence in critical care ultrasonography. Chest. 2009;135:1050–60. https://doi.org/10.1378/chest.08-2305.
10. Heidenreich PA, Stainback RF, Redberg RF, Schiller NB, Cohen NH, Foster E. Transesophageal echocardiography predicts mortality in critically ill patients with unexplained hypotension. J Am Coll Cardiol. 1995;26:152–8. https://doi.org/10.1016/0735-1097(95)00129-n.
11. Scalea TM, Rodriguez A, Chiu WC, Brenneman FD, Fallon WF Jr, Kato K, McKenney MG, Nerlich ML, Ochsner MG, Yoshii H. Focused assessment with sonography for trauma (FAST): results from an international consensus conference. J Trauma. 1999;46(3):466–72. https://doi.org/10.1097/00005373-199903000-00022.
12. Kirkpatrick AW, Sirois M, Laupland KB, Liu D, Rowan K, Ball CG, Hameed SM, Brown R, Simons R, Dulchavsky SA, Hamiilton DR, Nicolaou S. Hand-held thoracic sonography for detecting post-traumatic pneumothoraces: the Extended Focused Assessment with Sonography for Trauma (EFAST). J Trauma. 2004;57(2):288–95. https://doi.org/10.1097/01.ta.0000133565.88871.e4.
13. Blanco P. Rationale for using the velocity-time integral and the minute distance for assessing the stroke volume and cardiac output in point-of-care settings. Ultrasound J. 2020;12(1):21.Published 2020 Apr 21. https://doi.org/10.1186/s13089-020-00170-x.
14. Sanfilippo F, Bignami EG, Astuto M, Messina A, Cammarota G, Maggiore SM, Vetrugno L. Understanding left ventricular diastolic dysfunction in anesthesia and intensive care patients: "a glass with progressive shape change". Minerva Anestesiol. 2022;88:950. https://doi.org/10.23736/S0375-9393.22.16425-4.
15. Ha JW. Assessing diastolic function as an important tool for clinical decision-making in critically ill patients. J Cardiovasc Imaging. 2020;28(3):165–73. https://doi.org/10.4250/jcvi.2020.0042.
16. Nagueh SF, Smiseth OA, Appleton CP, Byrd BF 3rd, Dokainish H, Edvardsen T, et al., Houston, Texas; Oslo, Norway; Phoenix, Arizona; Nashville, Tennessee; Hamilton, Ontario, Canada; Uppsala, Sweden; Ghent and Liège, Belgium; Cleveland, Ohio; Novara, Italy; Rochester, Minnesota; Bucharest, Romania; and St. Louis, Missouri. Recommendations for the evaluation of left ventricular diastolic function by echocardiography: an update from the american society of echocardiography and the European Association of Cardiovascular Imaging. Eur Heart J Cardiovasc Imaging. 2016;17:1321–60.
17. Nagueh SF, Smiseth OA, Appleton CP, Byrd BF 3rd, Dokainish H, Edvardsen T, Flachskampf FA, Gillebert TC, Klein AL, Lancellotti P, Marino P, Oh JK, Popescu BA, Waggoner AD. Recommendations for the evaluation of left ventricular diastolic function by echocardiography: an update from the American Society of Echocardiography and the European Association of Cardiovascular Imaging. J Am Soc Echocardiogr. 2016;29(4):277–314. https://doi.org/10.1016/j.echo.2016.01.011.
18. Jentzer JC, Tabi M, Wiley BM, Lanspa MJ, Anavekar NS, Oh JK. Doppler-derived haemodynamics performed during admission echocardiography predict in-hospital mortality in cardiac intensive care unit patients. Eur Heart J Acute Cardiovasc Care. 2022;11:640. https://doi.org/10.1093/ehjacc/zuac084.
19. Malbrain MLNG, Van Regenmortel N, Saugel B, De Tavernier B, Van Gaal PJ, Joannes-Boyau O, Teboul JL, Rice TW, Mythen M, Monnet X. Principles of fluid management and stewardship in septic shock: it is time to consider the four D's and the four phases of fluid therapy. Ann Intensive Care. 2018;8(1):66. https://doi.org/10.1186/s13613-018-0402-x.

20. Cecconi M, De Backer D, Antonelli M, Beale R, Bakker J, Hofer C, Jaeschke R, Mebazaa A, Pinsky MR, Teboul JL, Vincent JL, Rhodes A. Consensus on circulatory shock and hemodynamic monitoring. Task force of the European Society of Intensive Care Medicine. Intensive Care Med. 2014;40(12):1795–815. https://doi.org/10.1007/s00134-014-3525-z.
21. Zhang Y, Wang Y, Shi J, Hua Z, Xu J. Cardiac output measurements via echocardiography versus thermodilution: a systematic review and meta-analysis. PLoS One. 2019;14(10):e0222105. https://doi.org/10.1371/journal.pone.0222105.
22. Jozwiak M, Mercado P, Teboul JL, et al. What is the lowest change in cardiac output that transthoracic echocardiography can detect? Crit Care. 2019;23(1):116. Published 2019 Apr 11. https://doi.org/10.1186/s13054-019-2413-x.
23. Vincent JL, Cecconi M, De Backer D. The fluid challenge. Crit Care. 2020;24(1):703. https://doi.org/10.1186/s13054-020-03443-y.
24. Michard F. Changes in arterial pressure during mechanical ventilation. Anesthesiology. 2005;103(2):419–28; quiz 449–5. https://doi.org/10.1097/00000542-200508000-00026.
25. Vieillard-Baron A, Naeije R, Haddad F, Bogaard HJ, Bull TM, Fletcher N, Lahm T, Magder S, Orde S, Schmidt G, Pinsky MR. Diagnostic workup, etiologies and management of acute right ventricle failure: a state-of-the-art paper. Intensive Care Med. 2018;44(6):774–90. https://doi.org/10.1007/s00134-018-5172-2.
26. Vignon P, Repessé X, Bégot E, Léger J, Jacob C, Bouferrache K, Slama M, Prat G, Vieillard-Baron A. Comparison of echocardiographic indices used to predict fluid responsiveness in ventilated patients. Am J Respir Crit Care Med. 2017;195(8):1022–32. https://doi.org/10.1164/rccm.201604-0844OC.
27. Upadhyay V, Malviya D, Nath SS, Tripathi M, Jha A. Comparison of superior vena cava and inferior vena cava diameter changes by echocardiography in predicting fluid responsiveness in mechanically ventilated patients. Anesth Essays Res. 2020;14(3):441–7. https://doi.org/10.4103/aer.AER_1_21.
28. Kattan E, Castro R, Miralles-Aguiar F, Hernández G, Rola P. The emerging concept of fluid tolerance: a position paper. J Crit Care. 2022;71:154070. https://doi.org/10.1016/j.jcrc.2022.154070.
29. Beaubien-Souligny W, Rola P, Haycock K, Bouchard J, Lamarche Y, Spiegel R, Denault AY. Quantifying systemic congestion with point-of-care ultrasound: development of the venous excess ultrasound grading system. Ultrasound J. 2020;12(1):16. https://doi.org/10.1186/s13089-020-00163-w.
30. Belletti A, Benedetto U, Biondi-Zoccai G, Leggieri C, Silvani P, Angelini GD, Zangrillo A, Landoni G. The effect of vasoactive drugs on mortality in patients with severe sepsis and septic shock. A network meta-analysis of randomized trials. J Crit Care. 2017;37:91–8. https://doi.org/10.1016/j.jcrc.2016.08.010.
31. Vetrugno L, Baciarello M, Bignami E, Bonetti A, Saturno F, Orso D, Girometti R, Cereser L, Bove T. The "pandemic" increase in lung ultrasound use in response to Covid-19: can we complement computed tomography findings? A narrative review. Ultrasound J. 2020;12(1):39. https://doi.org/10.1186/s13089-020-00185-4.
32. Lichtenstein DA, Mezière GA. The BLUE-points: three standardized points used in the BLUE-protocol for ultrasound assessment of the lung in acute respiratory failure. Crit Ultrasound J. 2011;3:109–10. https://doi.org/10.1007/s13089-011-0066-3.
33. Volpicelli G, Skurzak S, Boero E, Carpinteri G, Tengattini M, Stefanone V, Luberto L, Anile A, Cerutti E, Radeschi G, Frascisco MF. Lung ultrasound predicts well extravascular lung water but is of limited usefulness in the prediction of wedge pressure. Anesthesiology. 2014;121(2):320–7. https://doi.org/10.1097/ALN.0000000000000300.
34. Lichtenstein D, Mezière G, Seitz J. The dynamic air bronchogram. A lung ultrasound sign of alveolar consolidation ruling out atelectasis. Chest. 2009;135(6):1421–5. https://doi.org/10.1378/chest.08-2281.
35. Bouhemad B, Mongodi S, Via G, Rouquette I. Ultrasound for "lung monitoring" of ventilated patients. Anesthesiology. 2015;122(2):437–47. https://doi.org/10.1097/ALN.0000000000000558.
36. Picano E, Pellikka PA. Ultrasound of extravascular lung water: a new standard for pulmonary congestion. Eur Heart J. 2016;37:2097–104.
37. Pino R, Manzella F, Puccio D, Sciortino G, Polizzi G. Sindrome tako-tsubo con transitoria ostruzione dinamica del tratto di efflusso del ventricolo sinistro, complicata da persistente ipotensione

[Transient left ventricular apical ballooning with dynamic outflow tract obstruction complicated by persistent hypotension]. G Ital Cardiol (Rome). 2016;17(10):827–830. Italian. https://doi.org/10.1714/2464.25802.

38. O'Brien J, Mahony S, Byrne RJ, Byrne RA. Dynamic left ventricular outflow tract gradient resulting from Takotsubo cardiomyopathy ameliorated by intra-aortic balloon pump counterpulsation: a case report. Eur Heart J Case Rep. 2021;5(3):ytab082. Published 2021 Mar 3. https://doi.org/10.1093/ehjcr/ytab082.
39. Konstantinides SV, Meyer G, Becattini C, Bueno H, Geersing GJ, Harjola VP, Huisman MV, Humbert M, Jennings CS, Jiménez D, Kucher N, Lang IM, Lankeit M, Lorusso R, Mazzolai L, Meneveau N, Áinle FN, Prandoni P, Pruszczyk P, Righini M, Torbicki A, Van Belle E, Zamorano JL, The Task Force for the Diagnosis and Management of Acute Pulmonary Embolism of the European Society of Cardiology (ESC). 2019 ESC guidelines for the diagnosis and management of acute pulmonary embolism developed in collaboration with the European Respiratory Society (ERS): the Task Force for the Diagnosis and Management of Acute Pulmonary Embolism of the European Society of Cardiology (ESC). Eur Respir J. 2019;54(3):1901647. https://doi.org/10.1183/13993003.01647-2019.
40. Cavayas YA, Girard M, Desjardins G, Denault AY. Transesophageal lung ultrasonography: a novel technique for investigating hypoxemia. Can J Anaesth. 2016;63(11):1266–76. English. https://doi.org/10.1007/s12630-016-0702-2.

Role of Lung Ultrasound and Echocardiography in Acute Respiratory Failure, Acute Respiratory Distress Syndrome, and Weaning in Mechanically Ventilated Patients

Luigi Pisani, Marry R. Smit, and Pieter R. Tuinman

Contents

24.1 Lung Ultrasound and Critical Care Echocardiography in Acute Respiratory Failure (ARF) – 389

24.1.1 Integrating Lung Ultrasound and Critical Care Echocardiography in Acute Respiratory Failure – 389

24.2 LUS and CCE in the Differential Diagnosis and Monitoring of Treatment of Acute Respiratory Distress Syndrome (ARDS) – 393

24.2.1 Basic LUS Findings – 393

24.2.2 Lung Ultrasound Findings in ARDS and Importance of Dishomogeneity – 394

24.2.3 Excluding Left Ventricular Failure in ARDS – 396

24.2.4 LUS and CCE in the Monitoring and Treatment of ARDS – 397

24.2.5 Left Ventricular Systolic Failure and Fluid Overload – 400

© The Author(s), under exclusive license to Springer Nature Switzerland AG 2023
C. Robba et al. (eds.), *Basic Ultrasound Skills "Head to Toe" for General Intensivists*, Lessons from the ICU,
https://doi.org/10.1007/978-3-031-32462-8_24

24.3 CCUS in Weaning from Mechanical Ventilation – 400
24.3.1 Physiological Changes of Weaning – 401
24.3.2 Role of CCUS in Weaning from Mechanical Ventilation – 401
24.3.3 Pitfalls – 404

References – 405

Learning Objectives

- Appraise indications, utility and limitations of lung, cardiac and diaphragm ultrasound in the differential diagnosis of acute respiratory failure.
- Learn the specific lung ultrasound patterns of acute respiratory distress syndrome (ARDS) and use of echocardiography to rule out significant cardiac dysfunction.
- Identify the synergy between lung ultrasound, echocardiography, and diaphragm ultrasound in assessing the patient ready for weaning and potential causes of weaning failure.

24.1 Lung Ultrasound and Critical Care Echocardiography in Acute Respiratory Failure (ARF)

Clinical Case

A 69-year-old male presents to the emergency department (ED) with fever and dyspnea for 3 days. His past medical history shows diabetes, hypertension, and mild heart failure (NYHA 2) due to moderate mitral valve insufficiency.

How can critical care ultrasound contribute to the differential diagnosis?

24.1.1 Integrating Lung Ultrasound and Critical Care Echocardiography in Acute Respiratory Failure

Critical care ultrasound (CCUS) has become a key component in the evaluation and clinical management of patients with acute respiratory failure (ARF). An important challenge is the correct and systematic integration of lung ultrasound (LUS) and critical care echocardiography (CCE) in narrowing down the differential diagnosis. It must be remembered that LUS is a technique with high sensitivity for acute lung pathology, but sometimes lower specificity. CCE should always be added to further fine tune diagnosis (i.e., increasing specificity of LUS findings) and evaluate the presence of a cardiac component to the ARF. Independently from the type of technique, a major difference between ultrasound and static imaging techniques such as X-ray and computed tomography, is that ultrasound provides both morphological and functional information in real time [1].

The mechanically ventilated patient brings additional challenges, as the positive pressure delivered by the ventilator may influence LUS patterns, hinder echocardiographic windows, and modify diaphragmatic movements. A recent expert recommendation issued by the European Society of Intensive Care Medicine (ESICM) identified basic head-to-toe skills for the intensivist, issuing among others 20 recommendations for LUS and 20 for CCE [2].

The proposed LUS diagnostic approaches in patients with ARF are usually based on:

1. The detection of specific LUS *findings* and patterns
2. The understanding of *distribution* of these findings across the two lungs, in order to narrow down the differential diagnosis

While the BLUE protocol was historically the first LUS-based diagnostic approach proposed, several others have followed thereafter [3–5]. Most of these approaches rely on an increasing body of diagnostic accuracy evidence on individual pulmonary diagnosis, rather than a comprehensive validation of the entire approach.

Every single LUS-based diagnostic approach can be integrated with CCE to correctly understand heart–lung interactions, refine the diagnosis, and monitor response to treatment. For example, we can integrate CCE in a recently proposed diagnostic algorithm for seven frequent pulmonary conditions [5], as shown in Fig. 24.1. When an integrated LUS and CCE approach was used alongside standard diagnostic tests in the ED, it was superior to standard diagnostic tests alone in establishing a correct diagnosis within 4 h, although the trial was not powered to test for mortality or other patient-centered outcomes [6].

Several studies have proposed protocols integrating in one way or another LUS and CCE, extending the exam also to venous or abdominal ultrasound. Some of the proposed approaches are summarized in Table 24.1. While detailed knowledge of these approaches is not mandatory and validation data is still scarce, they have been instrumental in fostering a culture of integration between ultrasound modalities, avoiding a dangerous silo mentality in critical care ultrasonography.

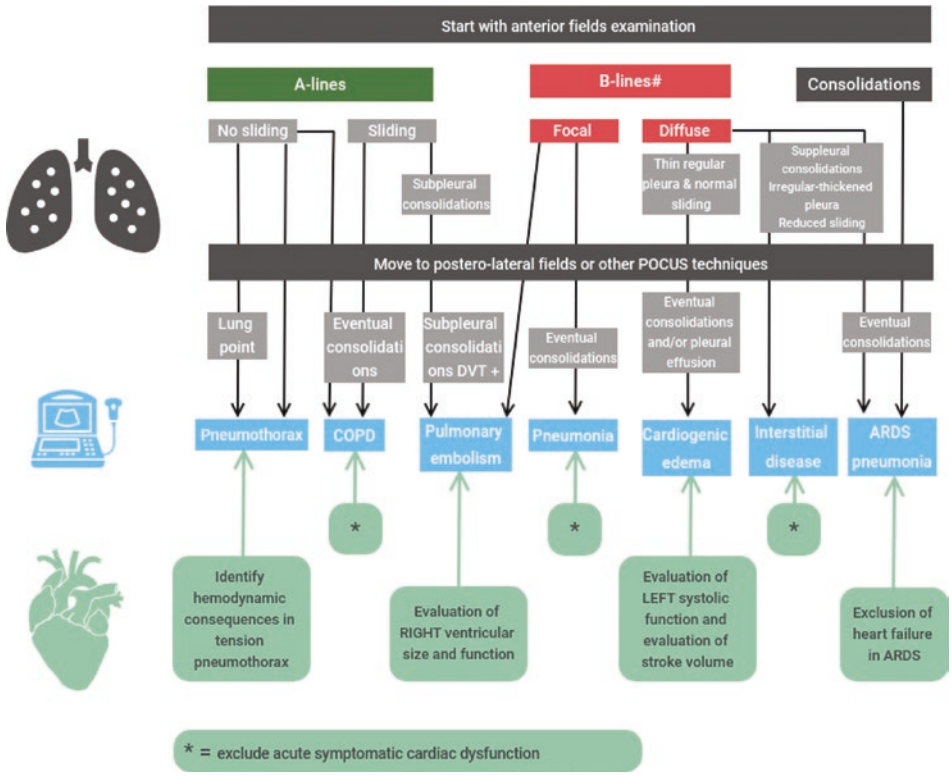

Fig. 24.1 Systematic approach to differential diagnosis of acute respiratory failure using lung ultrasound and critical care echocardiography. Lung ultrasound part of flowchart extracted from Ref. [5]. #At least three or more B-lines. *COPD* chronic obstructive pulmonary disease, *ARDS* acute respiratory distress syndrome

Table 24.1 Proposed approaches integrating LUS and CCE in the diagnostic workflow of the patient with ARF (modified from Ref. [7])

	Description	Clinical utility	Limitations
Cardiac and lung ultrasound			
CAUSE 2008 [8]	LUS + CCE 4 chamber view Diagnosis of (1) pericardial tamponade; (2) tension pneumothorax; (3) pulmonary embolism; and (4) hypovolemia	Aims to detect the four leading causes of non-arrhythmogenic cardiac arrest without interfering with resuscitation.	Poor to moderate sensitivity as routine screening in all patients suspected of pulmonary emboli, but good to excellent specificity.
FALLS 2013 [9]	Combines CCE with LUS (BLUE-protocol) to assess four causes of circulatory failure	Sequentially rule out obstructive, cardiogenic, and hypovolemic shock for expediting the diagnosis of distributive/septic shock.	(1) Presence of diffuse B-lines on initial assessment exclude patients from this protocol and (2) cardiogenic shock due to RV failure (with low wedge pressure) not easily diagnosed as it is usually associated with A-profile. Needs ECG to rule out right-sided myocardial infarction
ORACLE (2020) [10]	O: Left ventricular functiOn; R: Right ventricular disease; A: vAlve disease, C: periCardium; L: Lung ultrasound; E: hEmodynamic parameters	Cardiac and pulmonary evaluations in COVID-19 intensive care unit (ICU) patients.	Intermediate to advanced echo skills needed and requires at least 20 min in trained hands.
PIEPIER (2018) [11]	12 point LUS + CCE: IVC, RV, LV systolic and diastolic function, and afterload assessment	A stepwise approach to diagnosing causes of cardiorespiratory failure, including consideration of etiology, interventions and reassessments.	Requires experience for image interpretation, diagnosis and intermediate level CCE
Cardiac, lung and venous ultrasound			
ASE POCUS protocol for COVID-19 pandemic (2020) [12]	(1) CCE (basic views); (2) LUS; and (3) inferior vena cava and leg veins (optional)	Initial cardiopulmonary assessment of patients with COVID-19	In the case of difficult image acquisition, and it may be more efficient for a skilled sonographer to rapidly scan the patient, rather than have a POCUS operator struggle with prolonged attempts

(continued)

Table 24.1 (continued)

	Description	Clinical utility	Limitations
Cardiac, lung and abdominal ultrasound			
SHoC-ED (2018) [13]	Combines ACES and RUSH	Cardiac: Assess LV/RV function, size and presence of pericardial effusion. Lung: Base of lung and lung sliding. Abdominal-free fluid, AAA, IVC size and collapsibility.	An RCT in ED involving patients with undifferentiated hypotension did not detect significant difference in 30 days or hospital survival, media fluid administered, inotrope administration
Cardiac, lung, venous and abdominal ultrasound			
SESAME (2015) [14]	Five steps: (1) LUS (BLUE followed by FALLS protocol); (2) lower femoral vein vascular ultrasound 'V-point': A distal, lower superficial femoral vein; (3) abdominal ultrasound; (4) pericardium; and (5) CCE	Assess for tension pneumothorax, hypovolemia, pulmonary embolism, pericardial tamponade, free abdominal fluid as a cause of severe shock or cardiac arrest.	Uses a single microconvex probe, which may not be always available; evaluates for VTE only at 1 point on lower limb veins.

CAUSE cardiac arrest ultrasound exam, *LUS* lung ultrasound, *CCE* critical care echocardiography, *FALLS* fluid administration limited by lung sonography, *ASE* American Society of echocardiography, *BLUE* bedside lung ultrasound evaluation, *VTE* venous thromboembolism, *ACES* abdominal and cardiothoracic evaluation with sonography in shock, *RUSH* rapid ultrasound in Shock and Hypotension, *LV* left ventricle, *RV* right ventricle, *AAA* abdominal aortic aneurism

Diaphragm ultrasound is another valuable tool in further narrowing down the diagnosis in patients with unexplained dyspnea and acute respiratory failure. Diaphragm ultrasound is part of a wider set of techniques (respiratory muscles ultrasound) aimed at integrating ultrasound of different organs that comprise the respiratory system. For instance, diaphragm weakness is diagnosed by a diaphragmatic excursion (DE) of less than 10–20 mm during tidal breathing or a thickening fraction (TFdi) (max) of less than 20% [1, 15]. In patients with unilateral diaphragm paralysis, thickness and TFdi of the paralyzed diaphragm will be significantly less compared to the other hemidiaphragm. The use of diaphragm ultrasound in weaning will be explained in a dedicated section below.

Case Study

Ultrasound findings: LUS showed a unilateral consolidation on the right side with dynamic air bronchograms and positive Doppler flow, compatible with pneumonia. However, there were also diffuse bilateral separated B-lines in the lateral lung zones with a thin regular pleura. CCE showed decreased left ventricular systolic function. Diaphragmatic ultrasound showed a DE of 22 mm and a thickening fraction (TFdi) of 30%.

Interpretation: This patient in the ED is suffering from acute basal pneumonia, complicated by mild left ventricular failure and initial interstitial edema, without signs of diaphragmatic dysfunction.

24.2 LUS and CCE in the Differential Diagnosis and Monitoring of Treatment of Acute Respiratory Distress Syndrome (ARDS)

24.2.1 Basic LUS Findings

The clinical application of LUS relies on a combination of artifacts and anatomical patterns that can be observed below the pleura. Ultrasound waves used in diagnostic imaging cannot effectively travel through the lung, as high difference in impedance between the subcutaneous layer and the lung results in a complete reflection of ultrasound waves when lung tissue is normally aerated or in case of a pneumothorax. For this reason, LUS cannot detect small lung pathologies like pulmonary embolisms and malignancies that do not reach the pleura. This exceptionally strong reflection of ultrasound waves causes reverberation of the ultrasound signal between the probe and the pleura, generating horizontal artifacts that look like repetitions of the pleura. These artifacts are called 'A-lines'. 'A-lines' disappear when aeration diminishes because of an increase of mass or fluid or a decrease of air. Lung tissue with coexistence of air and fluid or mass generates vertical artifacts that reach the end of the screen and are called 'B-lines'. B-lines most likely arise from ultrasound waves that are reverberating within thickened interlobular septa and express a higher density of the lung parenchyma. As density is calculated as *density* = *mass*/*volume*, anything that increases parenchymal mass (e.g., cells, blood, fibrosis, lung water), or decreases lung volume (e.g., atelectasis) will generate B-lines. Observation of one or two B-lines in an intercostal space is considered physiological, but more than two is pathological. The extent and confluency of B-lines is closely related to the severity of aeration loss as measured with thermodilution or computed tomography (CT) [16–18]. It is important to consider that, when we visualize A- and B-lines, only the subpleural layer is being assessed with ultrasound [19].

Ultrasound waves travel well through lung tissue that is not aerated, for example, in the case of consolidation/atelectasis. Non-aerated lung tissue is visualized as a hypoechogenic anatomical structure that can be measured in size and is always pathological.

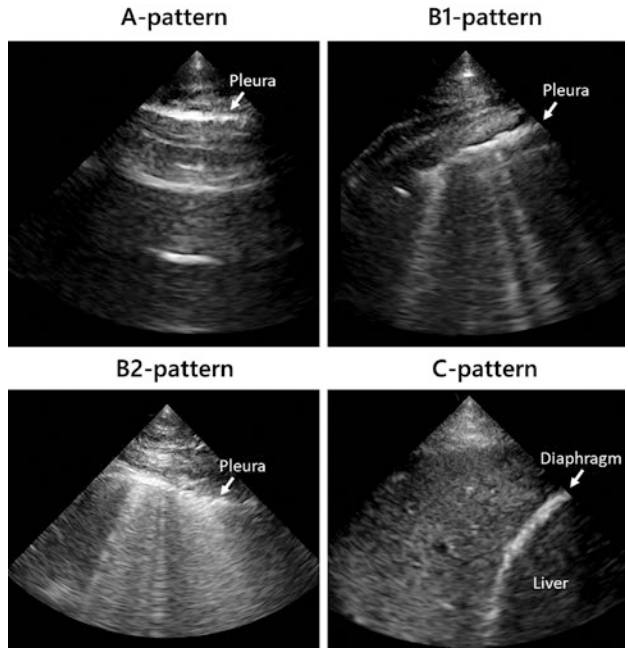

Fig. 24.2 Examples of LUS patterns. White arrows indicate the pleura in the ultrasound images with an artifactual A- or B-pattern. A healthy pleura will appear as thin and smooth on ultrasound (A-pattern). However, disrupted pleurae with subpleural consolidations are common in ultrasound images with a B-pattern (B1- and B2-pattern). A C-pattern is an anatomical image of non-aerated lung tissue

A variety of the above-named LUS findings can be found in critically ill patients as they commonly have altered lung aeration. To structure LUS findings, images are commonly classified in the following patterns (Fig. 24.2):

- A-pattern: If A-lines and a maximum of two B-lines are present in the image.
- B1-pattern: In case more than two B-lines are present covering less than 50% of the pleura.
- B2-pattern: When more than 50% of the pleura is covered by B-lines.
- C-pattern: An anatomical image of non-aerated lung tissue.

24.2.2 Lung Ultrasound Findings in ARDS and Importance of Dishomogeneity

LUS patterns are usually not specific for a certain disease, although they are for certain physiological entities (e.g., C-patterns are nonspecific for pneumonia, but they are 100% specific for loss of aeration; A-lines are 100% specific for presence of air). It is by combining the type and *distribution* of LUS patterns that we increase specificity and reach an accurate diagnosis. The BLUE protocol was proposed as a hierarchical flowchart that integrates LUS findings and scans for deep venous thrombosis into diagnosis of the origin of ARF. This protocol was initially

developed for patients presenting at the ED but can be useful in mechanically ventilated patients as well [3]. However, important differences characterize intensive care unit (ICU) and ED patients. ICU patients often have more than one respiratory diagnosis, and there is overlap in LUS findings between diagnoses, most importantly atelectasis and pneumonia, or cardiogenic pulmonary edema and ARDS [20].

As LUS findings only give an indication of the loss of lung aeration, it is important to assess the distribution of these findings across the thorax. For instance, while a bilateral and diffuse B-pattern is indicative of pulmonary edema, focal distribution of B-pattern is more common for either pneumonia or pulmonary embolism in case deep venous thrombosis is found during further examination.

Clinicians often need to differentiate between pulmonary edema of cardiogenic origin (e.g., hydrostatic edema) and ARDS (e.g., permeability edema) [21]. The appearance of the pleura can be a valuable tool to identify the cause of the pulmonary edema as an abnormal, thickened, fragmented, and/or irregular pleura is commonly present in ARDS while the pleura is thin, smooth, and homogenous in cardiogenic pulmonary edema. A multicenter study showed high specificity of pleural abnormalities for ARDS, but sensitivity is limited. Spared regions are also considered specific for ARDS and are defined as an intercostal space with an A-pattern that is surrounded by B-patterns [22]. However, the value of spared regions is largely based on expert opinion and needs to be prospectively validated. An overview of differences in ultrasound characteristics between cardiogenic edema and ARDS is presented in ◘ Table 24.2. The importance of heterogeneous distribution of findings in ARDS should be retained.

◘ **Table 24.2** Common lung ultrasound findings in cardiogenic pulmonary edema versus acute respiratory distress syndrome (ARDS) [22, 23]

Lung ultrasound characteristic	Cardiogenic pulmonary edema	ARDS
Pleural line appearance	Normal (thin, smooth, and homogeneous)	Abnormal (small subpleural consolidations, thickened, fragmented, irregular)
B-pattern	Present	Present
Distribution of B-pattern	Homogeneous with regularly spaced B-lines	*Heterogeneous* distribution with irregularly spaced B-lines and presence of spared regions (A-pattern surrounded by B-patterns)
Consolidations	Can be found in dependent areas, commonly accompanied with pleural effusion	Commonly present
Lung sliding	Normal	Often reduced
Lung pulse	Absent	Commonly present

LUS has also been used for diagnosis of acute respiratory distress syndrome (ARDS) in low-resource settings within the Kigali modification of the Berlin definition of ARDS. The Kigali LUS criteria were pragmatically defined as at least one region with a B-pattern or consolidation on each hemithorax [24–26].

24.2.3 Excluding Left Ventricular Failure in ARDS

CCE assessment of the left ventricle (LV) can provide crucial information on the origin of acute respiratory failure and in particular pulmonary edema. Failure of the left ventricle causes an increase in hydrostatic pressure in the pulmonary capillaries, with cardiogenic pulmonary edema as result. To diagnose the permeability edema that is the hallmark of ARDS, it is important to exclude severe left ventricular dysfunction that may trigger a cardiogenic pulmonary edema. It is important, however, to underline that ARDS and cardiac dysfunction may coexist generating complex clinical and ultrasound scenarios.

Assessment of LV function with CCE can be performed in several ways depending on the expertise of the sonographer. Basic CCE of the LV consists of a five views 2D transthoracic examination aimed at a qualitative assessment of LV cavity size, LV systolic function, and classification of LV wall movement abnormalities [27]. As with LUS, basic CCE aids the bedside physician to answer simple binary questions, such as whether the left and right ventricles are significantly impaired or if a large pericardial effusion is present [27]. More advanced competencies of LV assessment are determination of the LV ejection fraction, LV fractional area change, stroke volume, identification of regional wall abnormalities, and accurate qualitative assessment of the global systolic function of the LV [28]. Diastolic dysfunction can be assessed by more advanced Doppler measures as the ratio between the mitral E and A wave (E/A ratio), the deceleration time of the mitral E wave (DTE), systolic fraction of the flow in the pulmonary vein, and the ratio between the peak E wave velocity and the peak e′ wave velocity (E/e′ ratio—ratio between early mitral inflow velocity and mitral annular early diastolic velocity—assessed by tissue Doppler imaging).

Case

The patient was subsequently admitted from the ED to the ICU, and antibiotics for community acquired pneumonia were started, together with diuretic therapy. After 2 days, dyspnea and hypoxemia worsened. Continuous positive airway pressure (CPAP) was started with 5 cmH_2O positive end-expiratory pressure (PEEP) and 50% FiO_2 (PaO_2/FiO_2 = 180).

A new ultrasound examination was performed:

Ultrasound findings: LUS showed an increase in bilateral B-lines, with evidence of spared areas, abnormal pleural line, and dishomogeneous patchy bilateral consolidations. CCE showed a slight improvement compared to the admission day, with persistent mild LV dysfunction.

Interpretation: This picture cannot solely be explained by the mild LV failure, and the bilateral dishomogeneous findings are in favor of ARDS, triggered by the initial pneumonia.

24.2.4 LUS and CCE in the Monitoring and Treatment of ARDS

24.2.4.1 LUS Score for Aeration and Recruitment Assessment

Lung aeration can be semiquantified into a score by interpretation of the artifactual and anatomical patterns that can be observed under the probe. LUS scores based on the presence of A-lines, B-lines, or consolidated patterns have shown to be well correlated with both thermodilution methods and quantitative CT. Although the exact scoring system is not standardized yet, there are several studies that use LUS assessment of lung aeration in the management of mechanically ventilated patients [17].

LUS assessment of lung aeration is commonly performed in 12 regions and may be used for monitoring the effect of recruitment maneuvers (◘ Fig. 24.3). Of note, the LUS aeration score can also be used in monitoring aeration in patients with COVID-19, also in resource-poor settings [29].

Changes in the LUS aeration score are associated with PEEP-induced lung recruitment when measured with the pressure-volume curve method [30]. Prediction of response to lung recruitment or prone positioning can be done based on imaging assessment of lung morphology in ARDS patients. Patients with 'focal' lung morphology may respond better to prone positioning, whereas patients with 'non-focal or diffuse' lung morphology may respond better to recruitment maneuvers. The LIVE study showed potential benefit of morphology-guided personalized ventilation, but only in patients in whom morphology was correctly classified. Many patients were misclassified due to the high use of chest X-ray with poor quality [31]. CT is the gold standard for classification of morphology but is limited by need for transport. After the LIVE study, LUS methods that could accurately classify lung morphology (with the major benefit that they can be performed bedside) were developed. When

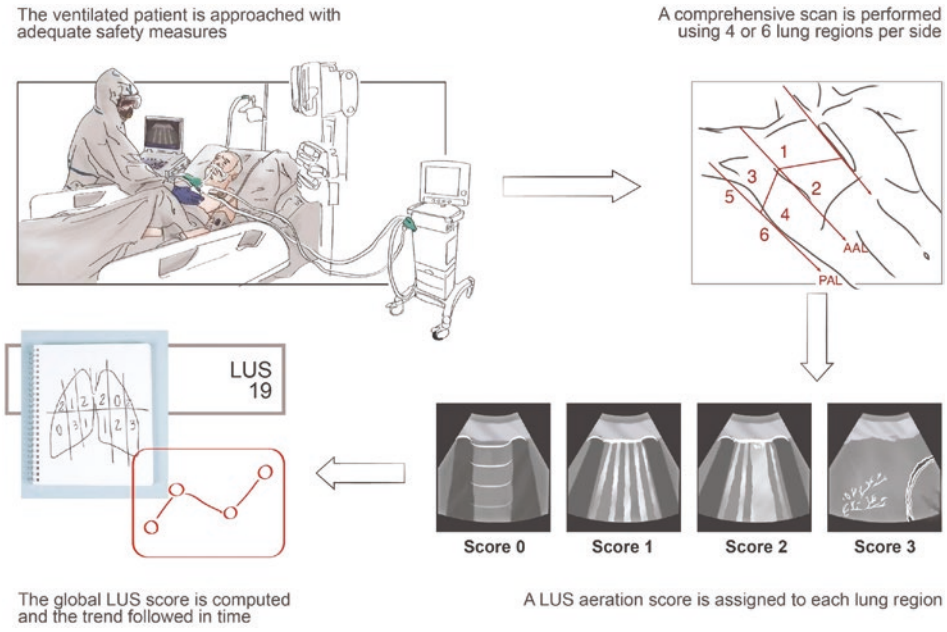

◘ **Fig. 24.3** Lung ultrasound score in monitoring of patients with COVID-19

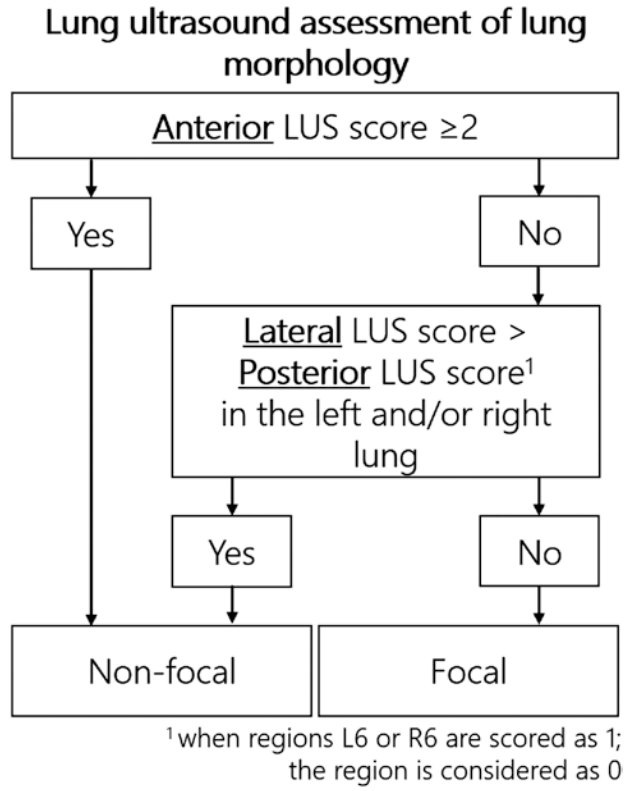
Lung ultrasound assessment of lung morphology
Anterior LUS score ≥2
Yes
No
Lateral LUS score > Posterior LUS score[1] in the left and/or right lung
Yes
No
Non-focal
Focal
[1] when regions L6 or R6 are scored as 1; the region is considered as 0

Fig. 24.4 Lung ultrasound assessment of lung morphology. (Adapted from Ref. [33])

an ARDS patient has normal or nearly normal lung aeration in the easily accessible anterior lung zones, the patient is likely to have 'focal' lung morphology. 'Non-focal' lung morphology can be described by LUS as loss of aeration with B-lines and consolidations present in anterior and lateral fields. Protocols for LUS assessment of lung morphology were proposed in two studies (Fig. 24.4) [32]. Whether LUS-guided personalized ventilation improves outcome in ARDS patients needs to be tested in future trials before we can recommend its use in clinical practice.

24.2.4.2 Detection of Pulmonary Complications in Ventilated Patients

Complications of mechanical ventilation can be monitored with LUS in several ways. Pneumothorax is commonly present in patients suffering from barotrauma as a result of high pressures delivered by the ventilator. Pneumothorax can be rapidly detected using LUS, and the technique has been extensively described in an earlier chapter of this book.

Patients under prolonged mechanical ventilation are also at risk of developing ventilator-associated pneumonia (VAP). Pulmonary consolidation on LUS is specific for pneumonia in the ED but not in the ICU where consolidations can have several origins, and it is complex to distinguish from atelectasis. The LUS clinical pulmonary infection score might be useful in ventilated and non-ventilated ICU patients to distinguish atelectasis from pneumonia. An extended LUS examination,

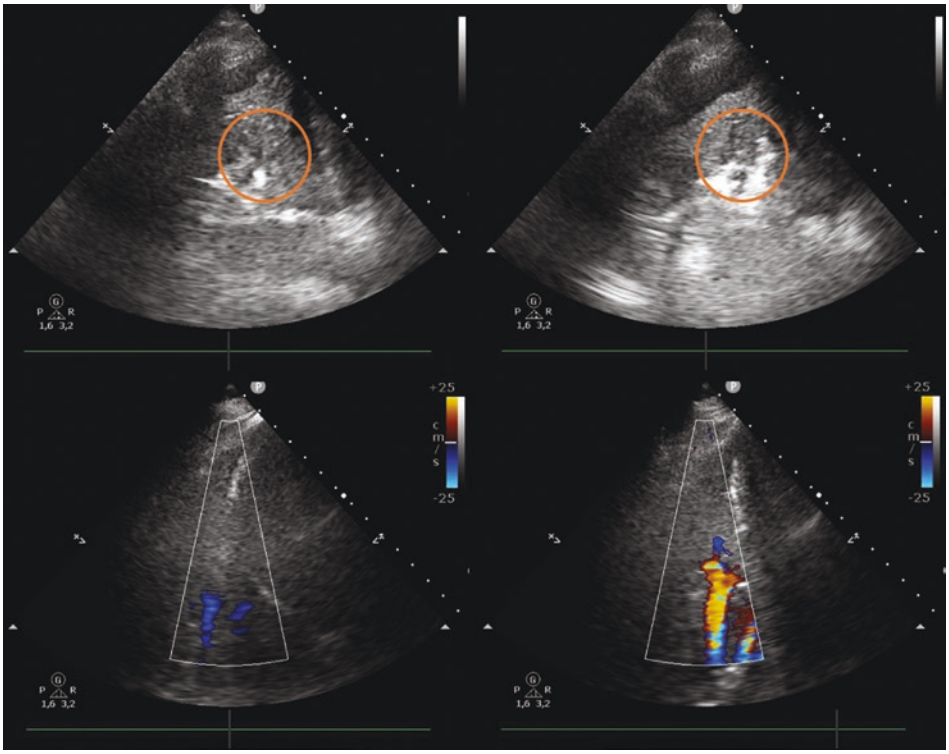

Fig. 24.5 Example of a dynamic air bronchogram (upper two images) and positive Doppler flow (lower two images)

specifically designed to differentiate pneumonia from atelectasis using signs of small subpleural consolidations, positive Doppler flow, and dynamic air bronchograms, outperformed other scores including the aforementioned score [34]. Examples of a dynamic air bronchogram and positive Doppler flow are presented in Fig. 24.5. After diagnosis of pneumonia, LUS can be used to monitor the response to antibiotic therapy. For instance, changes in LUS scores during antibiotic therapy were shown to be strongly related to increase in re-aerated lung volume as measured with CT [35].

24.2.4.3 Detecting Right Ventricular Failure

High PEEP might be indicated in patients with ARDS to ensure that alveoli remain sufficiently opened. The subsequent increase of intrathoracic pressure, however, might have negative side effects on the right ventricle (RV) as preload in the RV is decreased while afterload is increased. Acute cor pulmonale is frequent in patients with ARDS with an incidence of 25% and is associated with negative effects on patient outcome (Fig. 24.6) [36, 37]. CCE is an excellent tool to monitor the effect of positive pressure ventilation on RV size and function, especially in patients with RV dysfunction. CCE assessment of the RV in the ICU can be eyeballed, or the RV size can be assessed, and systolic function evaluated by tricuspid annular plane systolic excursion (TAPSE) measured in M-mode. An RV/LV diameter ratio of <0.6

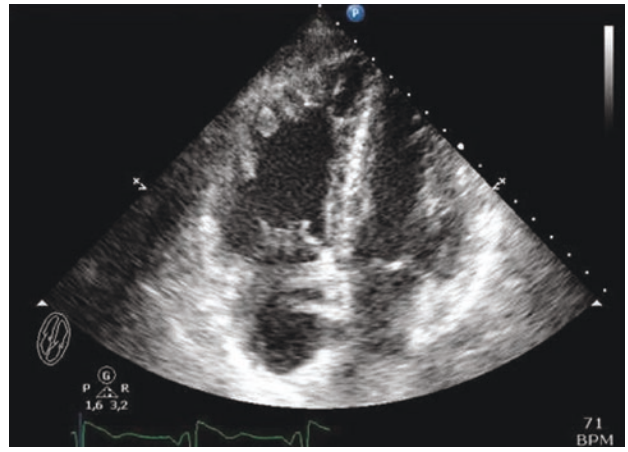

Fig. 24.6 Acute cor pulmonale during acute respiratory distress syndrome (ARDS). The right ventricle diameter not only increases but exceeds that of the left ventricle (RV/LV >1)

and TAPSE of >17 mm are indicative of normal RV size and systolic function, respectively [28, 38]. Daily CCE monitoring of ventilated patients is indicated to closely observe the effect of mechanical ventilation on the RV and adjust plateau pressures if needed [39].

A negative hemodynamic effect of high intrathoracic pressures induced by high PEEP values or excessive tidal volume, may be observed on the RV (which is known to badly tolerate increased pressures). On the other hand, positive pressure ventilation might induce a positive effect on LV function, as it can decrease LV afterload. Cardiac output is, however, also dependent on other factors such as venous return and pulmonary vascular resistance that are often negatively impacted by positive pressure ventilation [40].

24.2.5 Left Ventricular Systolic Failure and Fluid Overload

Please see relevant section in Part I of the book.

24.3 CCUS in Weaning from Mechanical Ventilation

Case

Due to the ARDS and refractory hypoxemia, the patient was intubated. After 8 days of mechanical ventilation (MV) gas exchange improved alongside, and subsequently, FiO_2 and PEEP could be decreased.

Daily spontaneous breathing trial (SBT) is planned by the treating team.

Is the patient ready to be liberated from the ventilator?

A new ultrasound is performed.

Ultrasound findings: The pre-SBT LUS aeration score is 12. LV ejection fraction is eyeballed and estimated to be around 50%. Diaphragmatic thickening fraction during the spontaneous breathing trial is 40%.

Interpretation: The clinical trajectory informs us that the patient is ready to undergo SBTs and eventually proceed to extubation. Although the LUS score is borderline, the LV ejection fraction and diaphragm thickening values are in favor of a successful extubation; there is no impending cardiac and diaphragmatic dysfunction. Ultrasound findings always need to be used in concert with other clinical findings (e.g., cough strength). The decision to extubate a patient should never be made solely on ultrasound findings.

24.3.1 Physiological Changes of Weaning

Weaning from mechanical ventilation is a challenging step during recovery from critical illness. Difficulty in weaning from mechanical ventilation is encountered in approximately one in five ventilated ICU patients. Interestingly, the liberation phase from the ventilator may account for almost 40% of the time spent in the ICU by the patient. The challenge lies in the knowledge that while weaning failure or early reintubation are associated with worse outcomes, also unnecessary prolonged ventilation can potentially lead to severe complications.

Weaning basically represents a stress test for the cardiopulmonary system of the ICU patient. The process of weaning increases a patient's cardiac workload while removing the respiratory assistance the patient has received for hours, days, or weeks. Guidelines for weaning recommend the implementation of a spontaneous breathing trial (SBT) as a tool to predict weaning outcome [41]. However, up to 26% of patients who are extubated following a successful SBT need to be reintubated within 48 h [42].

The principal causes of weaning failure may grossly be divided in respiratory or cardiac origin, although there is increasing evidence on the role of dysfunction of the respiratory muscles, especially diaphragmatic dysfunction.

24.3.2 Role of CCUS in Weaning from Mechanical Ventilation

The cause of weaning failure is often multifactorial across the cardiorespiratory axis. CCUS will help identify the interplay of factors that lead to difficulty in liberating the patient from the ventilator [43, 44]. CCUS can be used to assess lung aeration, cardiac, and diaphragmatic function *before*, *during*, and *after* the patient is disconnected from mechanical ventilation.

Three questions can be answered with the aid of CCUS [45]:

- Is my patient ready to be extubated? (readiness)
- Is there a high risk of failing extubation? (prediction)
- If yes, what is the likely cause of potential failure? (nature)

24.3.2.1 The Lungs

LUS assesses global and regional lung aeration and can detect the decrease in the aeration of the lung parenchyma due to cardiac, respiratory, or diaphragmatic origin. By ultimately providing information on parenchymal density, both before and after a SBT, LUS may inform both on readiness for weaning and prediction of weaning failure.

For instance, a higher baseline LUS score was found more likely to lead to post-extubation respiratory distress [46, 47]. In addition, a pre-and post SBT lung ultrasound can be performed, with patients who fail, demonstrating higher changes in LUS score after the SBT (see ◘ Table 24.4 for reference values).

Weaning induced pulmonary edema (WIPO) was identified in up to 60% of weaning failures [48]. Bilateral B-lines or, more specifically, three or more B-lines in two or more zones on each hemithorax are considered diagnostic for pulmonary edema on LUS [47, 49].

◘ **Table 24.4** ABCDE method to approach the weaning patient (table modified from Ref. [15], additional cutoff values integrated from Refs. [54–57])

	What to measure	Helpful cutoffs
A	**Aeration score and pleural effusion**	Extubation failure associated with LUS aeration score >17 and increase in B-lines during SBT ≥6. Extubation success associated with LUS aeration score <13. *Estimate drainage liquid:* 20 mL X mm
B	**Below the diaphragm** Screen for ascites or abscesses. High intra-abdominal pressure may alter respiratory mechanics.	
C	**Cardiac** Assess LV systolic and diastolic cardiac function, preload dependency and obstructive cardiomyopathy.	*Before SBT*: SBT failure more likely if Systolic dysfunction (LVEF <40%) Moderate to severe diastolic impairment: E′ <8 cm/s If EF reduced → E/A >2 If EF normal → E/e′ >12 *After SBT*: SBT induced cardiogenic pulmonary edema identified if increased E/A or E/e′
D	**Diaphragm** Measure thickness, TFdi and excursions during tidal breathing and maximal effort; assess symmetry.	*Extubation success:* TFdi >30–36%; >10 mm excursions (bilateral DD), >25 mm (unilateral DD, unaffected side during maximal effort)
E	**Extra diaphragmatic respiratory muscles** Evaluate accessory respiratory muscles during SBT: active use indicates high work of breathing/ low diaphragm capacity	*Intercostal muscles*: Increased parasternal muscle thickening fraction (>10%). *Abdominal muscles*: Reduced abdominal muscle (transversus abdominis, internal oblique, and rectus abdominis) thickening during cough (>10%) associated with extubation failure among patients who pass SBTs.

LUS lung ultrasound, *SBT* spontaneous breathing trial, *TFdi* diaphragm thickening fraction, *LVEF* left ventricle ejection fraction, *DD* diaphragm dysfunction, *EF* ejection fraction, *TFdi* diaphragmatic thickening fraction, *E* Doppler mitral early diastolic wave, *A* Doppler mitral late diastolic wave, *E/e′ ratio* ratio between early mitral inflow velocity and mitral annular early diastolic velocity

24.3.2.2 The Heart

Cardiac dysfunction represents the most common cause of weaning failure [50]. Cardiac-related weaning failure may be due to systolic LV dysfunction or isolated diastolic dysfunction, or even by a mix of these two events.

It is debated whether the early changes in interstitial edema that constitute the red flag for failed weaning, should be picked up by LUS alone or whether these are better predicted by the inability of the heart to increase VTI in response to a passive leg raise (PLR). Interestingly, static LV filling pressure was not found to be a good predictor of weaning failure. Using a dynamic parameter, such as VTI change to PLR, may be a better reflection of the stress imposed on the heart by increased work of spontaneous breathing than any other static parameter [47].

Data from CCE in addition to LUS can be used to improve diagnostic accuracy, guide and monitor the response to interventions, and communicate important prognostic information in patients with WIPO and acute heart failure [51]. Not all echocardiographic parameters for systolic and diastolic dysfunction were shown to be meaningful in picturing the weaning phase. Interestingly, the metrics significantly associated with weaning failure are mostly picturing diastolic dysfunction (higher E/e′ ratio, lower e′ wave, higher E wave—where the E wave is the Doppler mitral early diastolic wave, while the e′ represents the tissue Doppler based early diastolic wave at the lateral annulus) [52]. Of note, a typical marker of systolic dysfunction, such as LV ejection fraction, was *not* found to have a predictive value, similarly to a widely used marker of diastolic dysfunction such as ration of the mitral inflow velocity or E/A ratio (where the A wave is the maximal flow velocity during late diastole).

24.3.2.3 The Diaphragm

Being the main driving force of respiration, the diaphragm plays a crucial role in transitioning from mechanical ventilation to spontaneous breathing, and thus, its study should retain predictive potential. Yet, the actual predictive value of diaphragm ultrasound is still uncertain with studies in favor and against its clinical applicability in the assessment of the risk for weaning failure. Overall, the available literature seems to suggest a clear role of diaphragm ultrasound for diagnosing diaphragm weakness in difficult to wean patients but limited utility in predicting extubation outcome.

The measures of diaphragmatic thickening fraction (TFdi) and diaphragmatic excursion (DE) can be used during SBT in spontaneous breathing or during pressure support ventilation [53]. It is important to remember, however, that DE (and to a lesser extent TFdi) are influenced by the amount of mechanical ventilatory support.

24.3.2.4 Integrated Approach

LUS, cardiac, and respiratory muscle ultrasounds should be used holistically in determining the cause and evolution of weaning failure. A recent approach suggested the 'ABCDE' mnemonic to separate the necessary steps when approaching the patient to wean (◘ Table 24.4) [15]. This approach also explores extra-diaphragmatic muscle function assessment, which, being the latest addition to the ultrasound evaluation of the weaning patient, only has limited supportive body of literature [54, 55]. While numerical cutoffs that allow to discriminate the patient failing weaning are still under definition and refinement, it is important to retain some objective numerical values that will also allow adequate follow-up of the patient in time (◘ Table 24.4).

24.3.3 Pitfalls

There are several pitfalls within LUS in mechanically ventilated patients that are inherent to the technique and patient type. At first, ultrasound waves need to be able to travel from the probe to the pleura, which can be challenging in patients with surgical dressings, wounds, or drains. Moreover, lung aeration cannot be assessed in case of subcutaneous emphysema or pneumothorax, although for the latter you can assume a reduced aeration in present. For the same reason, lung pathologies can only be observed when they reach the pleura, which is usually true for pneumonia, edema, or atelectasis but not for early stages of pulmonary embolisms.

Acquisition of ultrasound images in a mechanically ventilated patient can be challenging because these patients are often sedated and difficult to mobilize. Posterior lung zones could be assessed by laterally tilting the patient, but in practice, the most posterior lung zones are commonly scanned just beneath the posterior axillary line as these can be reached in supine patients. When assessing lung aeration with any imaging technique, it is important to remember that PEEP does influence lung aeration and thus the patterns observed with LUS. Similar difficulties are encountered in the cardiac scanning of the critically ill supine patient, where (1) the PEEP induced increased aeration of anterior regions and (2) the impossibility of turning the patient—may hinder acquisition of high-quality images.

As with LUS and CCE, accuracy and reproducibility of diaphragm ultrasound are dependent on the training and skills of the operator. It is advised to mark the skin when follow up measurements are done. In addition, DE should only be measured in patients without pressure support as during assisted ventilation active displacement cannot be distinguished from passive displacement due to driving pressures.

Finally, a general word of caution. In clinical practice, the sonographer is responsible for the acquisition of the ultrasound exam, the interpretation of the findings, and the integration of those findings with the overall clinical picture. Clinicians should, therefore, be well aware of their own ultrasound competence and also of the features of the ultrasound equipment that they use. In addition, physicians should be aware of potential availability bias; in fact the prompt availability of ultrasound apparatuses should not lead to an over enthusiastic (ab-)use. Although the technique is noninvasive, a wrong diagnosis may lead to an increase in invasive procedures and harm.

Take-Home Messages

- Lung ultrasound is a technique with high diagnostic accuracy driven by high sensitivity. Accuracy is increased by understanding lung ultrasound findings, defining their distribution and by integrating lung and cardiac ultrasound findings with the clinical picture.
- In the mechanically ventilated patient, lung ultrasound and critical care echocardiography will help you define the cause of respiratory failure, monitor response to treatment, and identify potential complications.
- Integrating lung, cardiac, and diaphragm ultrasound in the weaning patient helps answer three questions: readiness to start weaning, prediction of weaning outcome, and nature of weaning failure.

References

1. Llamas-Álvarez AM, Tenza-Lozano EM, Latour-Pérez J. Diaphragm and lung ultrasound to predict weaning outcome: systematic review and meta-analysis. Chest. 2017;152(6):1140–50.
2. Robba C, Wong A, Poole D, Al Tayar A, Arntfield RT, Chew MS, et al. Basic ultrasound head-to-toe skills for intensivists in the general and neuro intensive care unit population: consensus and expert recommendations of the European Society of Intensive Care Medicine. Intensive Care Med. 2021;47(12):1347–67.
3. Lichtenstein DA, Mezière GA. Relevance of lung ultrasound in the diagnosis of acute respiratory failure: the BLUE protocol. Chest. 2008;134(1):117–25.
4. Kruisselbrink R, Chan V, Cibinel GA, Abrahamson S, Goffi A. I-AIM (Indication, Acquisition, Interpretation, Medical Decision-making) framework for point of care lung ultrasound. Anesthesiology. 2017;127(3):568–82.
5. Mojoli F, Bouhemad B, Mongodi S, Lichtenstein D. Lung ultrasound for critically ill patients. Am J Respir Crit Care Med. 2019;199(6):701–14.
6. Laursen CB, Sloth E, Lassen AT, dePont CR, Lambrechtsen J, Madsen PH, et al. Point-of-care ultrasonography in patients admitted with respiratory symptoms: a single-blind, randomised controlled trial. Lancet Respir Med. 2014;2(8):638–46.
7. Lau YH, See KC. Point-of-care ultrasound for critically-ill patients: a mini-review of key diagnostic features and protocols. World J Crit Care Med. 2022;11(2):70–84.
8. Hernandez C, Shuler K, Hannan H, Sonyika C, Likourezos A, Marshall J. C.A.U.S.E.: cardiac arrest ultra-sound exam—a better approach to managing patients in primary non-arrhythmogenic cardiac arrest. Resuscitation. 2008;76(2):198–206.
9. Lichtenstein DA. BLUE-protocol and FALLS-protocol: two applications of lung ultrasound in the critically ill. Chest. 2015;147(6):1659–70.
10. García-Cruz E, Manzur-Sandoval D, Rascón-Sabido R, Gopar-Nieto R, Barajas-Campos RL, Jordán-Ríos A, et al. Critical care ultrasonography during COVID-19 pandemic: the ORACLE protocol. Echocardiogr Mt Kisco N. 2020;37(9):1353–61.
11. Yin W, Li Y, Wang S, Zeng X, Qin Y, Wang X, et al. The PIEPEAR workflow: a critical care ultrasound based 7-step approach as a standard procedure to manage patients with acute cardiorespiratory compromise, with two example cases presented. BioMed Res Int. 2018;2018:4687346 [cited 2022 Jul 17]. Available from: https://pubmed.ncbi.nlm.nih.gov/29992144/.
12. Johri AM, Galen B, Kirkpatrick JN, Lanspa M, Mulvagh S, Thamman R. ASE statement on point-of-care ultrasound during the 2019 novel coronavirus pandemic. J Am Soc Echocardiogr. 2020;33(6):670–3.
13. Atkinson PR, Milne J, Diegelmann L, Lamprecht H, Stander M, Lussier D, et al. Does point-of-care ultrasonography improve clinical outcomes in emergency department patients with undifferentiated hypotension? An international randomized controlled trial from the SHoC-ED Investigators. Ann Emerg Med. 2018;72(4):478–89.
14. Lichtenstein DA. How can the use of lung ultrasound in cardiac arrest make ultrasound a holistic discipline. The example of the SESAME-protocol. Med Ultrason. 2014;16(3):252–5.
15. Tuinman PR, Jonkman AH, Dres M, Shi ZH, Goligher EC, Goffi A, et al. Respiratory muscle ultrasonography: methodology, basic and advanced principles and clinical applications in ICU and ED patients-a narrative review. Intensive Care Med. 2020;46(4):594–605.
16. Agricola E, Bove T, Oppizzi M, Marino G, Zangrillo A, Margonato A, et al. "Ultrasound comet-tail images": a marker of pulmonary edema: a comparative study with wedge pressure and extravascular lung water. Chest. 2005;127(5):1690–5.
17. Chiumello D, Mongodi S, Algieri I, Vergani GL, Orlando A, Via G, et al. Assessment of lung aeration and recruitment by CT scan and ultrasound in acute respiratory distress syndrome patients. Crit Care Med. 2018;46(11):1761–8.
18. Bataille B, Rao G, Cocquet P, Mora M, Masson B, Ginot J, et al. Accuracy of ultrasound B-lines score and E/Ea ratio to estimate extravascular lung water and its variations in patients with acute respiratory distress syndrome. J Clin Monit Comput. 2015;29(1):169–76.
19. Smit MR, Pisani L, de Bock EJE, van der Heijden F, Paulus F, Beenen LFM, et al. Ultrasound versus computed tomography assessment of focal lung aeration in invasively ventilated ICU patients. Ultrasound Med Biol. 2021;47(9):2589–97.

20. Smit JM, Haaksma ME, Winkler MH, Heldeweg MLA, Arts L, Lust EJ, et al. Lung ultrasound in a tertiary intensive care unit population: a diagnostic accuracy study. Crit Care Lond Engl. 2021;25(1):339.
21. Heldeweg MLA, Smit MR, Kramer-Elliott SR, Haaksma ME, Smit JM, Hagens LA, et al. Lung ultrasound signs to diagnose and discriminate interstitial syndromes in ICU patients: a diagnostic accuracy study in two cohorts. Crit Care Med. 2022;50:1607.
22. Copetti R, Soldati G, Copetti P. Chest sonography: a useful tool to differentiate acute cardiogenic pulmonary edema from acute respiratory distress syndrome. Cardiovasc Ultrasound. 2008;6:16.
23. Mayo PH, Copetti R, Feller-Kopman D, Mathis G, Maury E, Mongodi S, et al. Thoracic ultrasonography: a narrative review. Intensive Care Med. 2019;45(9):1200–11.
24. Riviello ED, Kiviri W, Twagirumugabe T, Mueller A, Banner-Goodspeed VM, Officer L, et al. Hospital incidence and outcomes of the acute respiratory distress syndrome using the Kigali modification of the Berlin definition. Am J Respir Crit Care Med. 2016;193(1):52–9.
25. Pisani L, De Nicolo A, Schiavone M, Adeniji AO, De Palma A, di Gennaro F, et al. Lung ultrasound for detection of pulmonary complications in critically ill obstetric patients in a resource-limited setting. Am J Trop Med Hyg. 2020;104:478.
26. Vercesi V, Pisani L, van Tongeren PSI, Lagrand WK, Leopold SJ, Huson MMA, et al. External confirmation and exploration of the Kigali modification for diagnosing moderate or severe ARDS. Intensive Care Med. 2018;44(4):523–4.
27. Vieillard-Baron A, Millington SJ, Sanfilippo F, Chew M, Diaz-Gomez J, McLean A, et al. A decade of progress in critical care echocardiography: a narrative review. Intensive Care Med. 2019;45(6):770–88.
28. Mayo PH, Beaulieu Y, Doelken P, Feller-Kopman D, Harrod C, Kaplan A, et al. American College of Chest Physicians/La Société de Réanimation de Langue Française statement on competence in critical care ultrasonography. Chest. 2009;135(4):1050 [cited 2022 Jul 17]. Available from: https://pubmed.ncbi.nlm.nih.gov/19188546/.
29. Schultz MJ, Gebremariam TH, Park C, Pisani L, Sivakorn C, Taran S, et al. Pragmatic recommendations for the use of diagnostic testing and prognostic models in hospitalized patients with severe COVID-19 in low- and middle-income countries. Am J Trop Med Hyg. 2021;104:34–47.
30. Bouhemad B, Brisson H, Le-Guen M, Arbelot C, Lu Q, Rouby JJ. Bedside ultrasound assessment of positive end-expiratory pressure-induced lung recruitment. Am J Respir Crit Care Med. 2011;183(3):341–7.
31. Constantin JM, Jabaudon M, Lefrant JY, Jaber S, Quenot JP, Langeron O, et al. Personalised mechanical ventilation tailored to lung morphology versus low positive end-expiratory pressure for patients with acute respiratory distress syndrome in France (the LIVE study): a multicentre, single-blind, randomised controlled trial. Lancet Respir Med. 2019;7(10):870–80.
32. Costamagna A, Pivetta E, Goffi A, Steinberg I, Arina P, Mazzeo AT, et al. Clinical performance of lung ultrasound in predicting ARDS morphology. Ann Intensive Care. 2021;11(1):51 [cited 2022 Jul 15]. Available from: https://pubmed.ncbi.nlm.nih.gov/33779834/.
33. Pierrakos C, Smit MR, Pisani L, Paulus F, Schultz MJ, Constantin JM, et al. Lung ultrasound assessment of focal and non-focal lung morphology in patients with acute respiratory distress syndrome. Front Physiol. 2021;12:730857.
34. Haaksma ME, Smit JM, Heldeweg MLA, Nooitgedacht JS, de Grooth HJ, Jonkman AH, et al. Extended lung ultrasound to differentiate between pneumonia and atelectasis in critically ill patients: a diagnostic accuracy study. Crit Care Med. 2022;50(5):750–9.
35. Bouhemad B, Liu ZH, Arbelot C, Zhang M, Ferarri F, Le-Guen M, et al. Ultrasound assessment of antibiotic-induced pulmonary reaeration in ventilator-associated pneumonia. Crit Care Med. 2010;38(1):84–92.
36. Boissier F, Katsahian S, Razazi K, Thille AW, Roche-Campo F, Leon R, et al. Prevalence and prognosis of cor pulmonale during protective ventilation for acute respiratory distress syndrome. Intensive Care Med. 2013;39(10):1725–33.
37. Vieillard-Baron A, Schmitt JM, Augarde R, Fellahi JL, Prin S, Page B, et al. Acute cor pulmonale in acute respiratory distress syndrome submitted to protective ventilation: incidence, clinical implications, and prognosis. Crit Care Med. 2001;29(8):1551–5.
38. Vieillard-Baron A. Assessment of right ventricular function. Curr Opin Crit Care. 2009;15(3):254–60.

39. Jardin F, Vieillard-Baron A. Is there a safe plateau pressure in ARDS? The right heart only knows. Intensive Care Med. 2007;33(3):444–7.
40. Mahmood SS, Pinsky MR. Heart-lung interactions during mechanical ventilation: the basics. Ann Transl Med. 2018;6(18):349.
41. Girard TD, Alhazzani W, Kress JP, Ouellette DR, Schmidt GA, Truwit JD, et al. An official American Thoracic Society/American College of Chest Physicians Clinical Practice Guideline: liberation from mechanical ventilation in critically ill adults. rehabilitation protocols, ventilator liberation protocols, and cuff leak tests. Am J Respir Crit Care Med. 2017;195(1):120–33.
42. Frutos-Vivar F, Ferguson ND, Esteban A, Epstein SK, Arabi Y, Apezteguía C, et al. Risk factors for extubation failure in patients following a successful spontaneous breathing trial. Chest. 2006;130(6):1664–71.
43. Haaksma ME, Tuinman PR, Heunks L. Weaning the patient: between protocols and physiology. Curr Opin Crit Care. 2021;27(1):29–36.
44. Doorduin J, van der Hoeven JG, Heunks LMA. The differential diagnosis for failure to wean from mechanical ventilation. Curr Opin Anaesthesiol. 2016;29(2):150–7.
45. Hussain A, Via G, Melniker L, Goffi A, Tavazzi G, Neri L, et al. Multi-organ point-of-care ultrasound for COVID-19 (PoCUS4COVID): international expert consensus. Crit Care Lond Engl. 2020;24(1):702.
46. Soummer A, Perbet S, Brisson H, Arbelot C, Constantin JM, Lu Q, et al. Ultrasound assessment of lung aeration loss during a successful weaning trial predicts postextubation distress. Crit Care Med. 2012;40(7):2064–72.
47. Kundu R, Baidya D, Anand R, Maitra S, Soni K, Subramanium R. Integrated ultrasound protocol in predicting weaning success and extubation failure: a prospective observational study. Anaesthesiol Intensive Ther. 2022;54:46841.
48. Liu J, Shen F, Teboul JL, Anguel N, Beurton A, Bezaz N, et al. Cardiac dysfunction induced by weaning from mechanical ventilation: incidence, risk factors, and effects of fluid removal. Crit Care Lond Engl. 2016;20(1):369.
49. Volpicelli G, Elbarbary M, Blaivas M, Lichtenstein DA, Mathis G, Kirkpatrick AW, et al. International evidence-based recommendations for point-of-care lung ultrasound. Intensive Care Med. 2012;38(4):577–91.
50. Teboul JL, Monnet X, Richard C. Weaning failure of cardiac origin: recent advances. Crit Care Lond Engl. 2010;14(2):211.
51. Price S, Platz E, Cullen L, Tavazzi G, Christ M, Cowie MR, et al. Expert consensus document: Echocardiography and lung ultrasonography for the assessment and management of acute heart failure. Nat Rev Cardiol. 2017;14(7):427–40.
52. Sanfilippo F, Di Falco D, Noto A, Santonocito C, Morelli A, Bignami E, et al. Association of weaning failure from mechanical ventilation with transthoracic echocardiography parameters: a systematic review and meta-analysis. Br J Anaesth. 2021;126(1):319–30.
53. DiNino E, Gartman EJ, Sethi JM, McCool FD. Diaphragm ultrasound as a predictor of successful extubation from mechanical ventilation. Thorax. 2014;69(5):423–7.
54. Dres M, Dubé BP, Goligher E, Vorona S, Demiri S, Morawiec E, et al. Usefulness of parasternal intercostal muscle ultrasound during weaning from mechanical ventilation. Anesthesiology. 2020;132(5):1114–25.
55. Schreiber AF, Bertoni M, Coiffard B, Fard S, Wong J, Reid WD, et al. Abdominal muscle use during spontaneous breathing and cough in patients who are mechanically ventilated: a bi-center ultrasound study. Chest. 2021;160(4):1316–25.
56. Mayo P, Volpicelli G, Lerolle N, Schreiber A, Doelken P, Vieillard-Baron A. Ultrasonography evaluation during the weaning process: the heart, the diaphragm, the pleura and the lung. Intensive Care Med. 2016;42(7):1107–17.
57. Balik M, Plasil P, Waldauf P, Pazout J, Fric M, Otahal M, et al. Ultrasound estimation of volume of pleural fluid in mechanically ventilated patients. Intensive Care Med. 2006;32(2):318.

Use of Ultrasound for the Assessment of Fluid Responsiveness in Critically Ill Patients

Filippo Sanfilippo, Stephen Huang, and Alberto Noto

Contents

25.1 Introduction – 411

25.2 Physiology Behind Fluid Responsiveness – 412
25.2.1 The "Frank–Starling" Mechanism and the Venous Return Curve – 412
25.2.2 Fluid Responsiveness and Fluid Tolerance Concepts – 414
25.2.3 Factors Influencing Fluid Responsiveness – 415

25.3 Use of Ultrasound for the Assessment of FR in ICU – 416

25.4 Ultrasound Assessment at the Heart Level – 417
25.4.1 Assessment of Flow: Stroke Volume and Cardiac Output – 417
25.4.2 VTI and Fluid Responsiveness – 419

25.5 Ultrasound Assessment on the Venous Side – 420
25.5.1 Respiratory Variations of the Inferior Vena Cava – 421
25.5.2 Respiratory Variations of the Superior Vena Cava – 423
25.5.3 Respiratory Variations of the Internal Jugular, Subclavian and/or Femoral Vein – 423
25.5.4 Study of the Hepatic Venous Flow – 424

© The Author(s), under exclusive license to Springer Nature Switzerland AG 2023
C. Robba et al. (eds.), *Basic Ultrasound Skills "Head to Toe" for General Intensivists*, Lessons from the ICU,
https://doi.org/10.1007/978-3-031-32462-8_25

25.6 US Assessment on the Arterial Side – 425
25.6.1 Measurement of Carotid Blood Flow and Carotid Corrected Flow Time – 425
25.6.2 Measurement of Flow in the Aorta (Ascending or Descending) – 426
25.6.3 Other Measurements at Level of Brachial, Femoral, or Splenic Artery – 426

25.7 US for the Assessment of Fluid Tolerance – 427
25.7.1 VExUS and Systemic Congestion – 427
25.7.2 Lung Ultrasound and Pulmonary Congestion – 428

25.8 Conclusions – 428

References – 429

Learning Objectives

- Define the concepts and physiology aspects of fluid responsiveness
- Understand the concepts behind fluid tolerance
- Outline the role of ultrasound in the noninvasive assessment of fluid responsiveness
- Explore the ultrasound techniques to assess fluid responsiveness in different sites:
  - Heart
  - Arteries
  - Veins
- Explore the ultrasound approaches to assess fluid tolerance at bedspace

25.1 Introduction

The concept of fluid responsiveness (FR) is used clinically to indicate a significant increase in cardiac output (CO, or cardiac index) in response to an intravascular volume expansion or other maneuvers that increase preload [1]. Therefore, assessment of FR is of paramount importance in the daily practice of intensive care unit (ICU) physicians dealing with critically ill patients. However, performing a proper assessment of FR is a challenging aspect in the management of ICU patients [2]. Importantly, both hypo- and hypervolemia are associated with poorer outcomes in the critically ill patients [3]. Moreover, the concept of fluid tolerance and of aggressive fluid removal are gaining large attention in the recent literature, and new studies are ongoing to investigate the importance of such aspects [4–6].

The effect of hypovolemia may be quite obvious, where a significant reduction in preload leading to reduced CO could result in hypoperfusion and finally end-organ damage [7]. For such reasons, it is important to correctly identify fluid responders, where the administration of intravenous fluid bolus may increase the venous return to the right ventricle (RV) and in turn generate greater stroke volume (SV or its indexed value, SVI) from the left ventricle (LV) resulting in greater CO and improved systemic perfusion. The CO (or cardiac index) is a measure of flow (L/min) generated by the cardiac pump; in healthy subjects the SVI is about 35–65 mL/m^2/beat and, considering a heart rate (HR) around 75 beats/min, the resulting cardiac index would be around 3.5–4.0 L/min/m^2. Therefore, FR is a physiologic condition where further increase in LV preload leads to an increase in CO. In simple words, FR is a condition where an exogenous fluid administration generates a good biventricular response ultimately resulting in a significant increase in CO. A significant increase in CO is usually defined as a relative change above 15% of its baseline value, although some studies have used lower cut-offs (i.e., 10% change) [8]. Of note, the variations in mean arterial pressure are not sensitive enough to detect changes in organ perfusion and oxygen delivery; consequently, CO should always be the clinical reference target in sick patients. Conversely, "fluid unresponsiveness" is a situation where further volume administration does not produce a significant increase in CO. In this case, the plateau of the Frank–Starling curve (see next paragraph) has been reached, and fluid administration is unlikely to be helpful and may possibly be harmful. Hypervolemia and positive fluid balance may increase the risks of systemic congestion and interstitial edema with decreased organ perfusion and/or function; moreover, pulmonary

congestion may impair oxygenation and gas exchanges, thereby reducing arterial oxygen concentration, hence, affecting oxygen delivery to organs and peripheral tissues. It is, therefore, not surprising that hypervolemia and positive fluid balance have been strongly linked with worse patients' outcomes [9].

As stated above, prediction of FR is a crucial step in the clinical evaluation during the perioperative period and in critically ill patients because it helps clinicians in optimizing fluid status, hence, organ perfusion on one hand and avoiding the deleterious effects of unnecessary fluid infusion on the other. In this regard, point-of-care ultrasound (POCUS) plays an important role in assisting ICU clinicians in managing patients' fluid status, possibly improving patient outcome. Ideally, the perfect test to discriminate FR should be accurate and precise, noninvasive, reproducible, and easy to perform with minimal training. As POCUS offers most of these advantages, in this chapter the authors first introduce the concept of FR (and of fluid tolerance) and then discuss the multiple use of POCUS for the evaluation of FR, finally discussing also other potentials of POCUS in the context of fluid management for critically ill patients.

25.2 Physiology Behind Fluid Responsiveness

25.2.1 The "Frank–Starling" Mechanism and the Venous Return Curve

In order to understand the concepts and theoretical aspects of FR, it is crucial to briefly revisit the two concepts on the relationship between CO and venous return: the "Frank–Starling" curve and the venous return curve.

The "Frank–Starling" law describes the intrinsic cardiac autoregulatory mechanism ensuring that SV changes proportionally to the change in the LV end-diastolic volume, that is, the volume that the LV receives (see ◘ Fig. 25.1a). In other words, the Frank–Starling curves describes the relationship between SV and preload (see below). This mechanism operates continuously on a beat-to-beat basis to ensure the left- and right-side output are matched, despite the cyclical variations in the venous return (preload) as a result of respiratory activity that periodically changes the intrathoracic pressure.

The CO curve, or cardiac function curve, is an extension of the "Frank–Starling" curve by assuming the heart rate remains constant. This curve describes the relationship between the CO in the *y-axis* and the right atrial pressure (RAP, the preload) in the *x-axis*, although RV end-diastolic volume is often used as a surrogate of RAP in echocardiography. The RAP is an important determinant of the venous return since the lower the RAP the greater the venous return. The CO curve contains two parts: the ascending (steep) part and the flat part (plateau). When the ventricular contractility is operating in the ascending (responsive) part of the curve, increase in preload (RV end-diastolic volume) generates larger CO. However, when the ventricular function is operating maximally (the flat portion of the curve), any further increase in preload is not accompanied by larger CO. It is noteworthy that the slope

of the ascending part is less steep in patients with heart dysfunction, and the responsive range to fluid administration is rather smaller in these patients (see Fig. 25.1b).

When discussing the venous return curve, it is important to introduce the concepts of mean systemic filling pressure (*Pmsf*), which is the theoretical mean pressure in the systemic circulation in the absence of blood flow, that is, when the heart stops beating. *Pmsf* is determined by venous vascular resistance and total intravascular volume. The *Pmsf* represents the pressure in the peripheral circulation, which is greater than the RAP and creates the gradient for generating the venous return to the RV. Indeed, the difference between *Pmsf* and RAP represents the driving pressure for venous return, rather than the arterial pressure generated by the heart. Therefore, as already mentioned, the lower the RAP the greater is the venous return, whereas when the RAP equals the *Pmsf* there will be no venous return at all. Finally, it must be immediately clear that there is a limit in the increase in venous return that can be achieved. This limit is usually reached when the RAP is around 0 mmHg (plateau of venous return): under this condition, there is no "suction" effect, and the major (central) veins begin to collapse.

Combining the cardiac function and the venous return curves together allows one to obtain the steady state CO by inspecting the intersection point of the CO and venous return curves. Under conditions of stable cardiac performance (same morphology and steepness of the cardiac function curve), any changes in venous return will produce changes in CO according to intersection point. Figure 25.1 shows what happens when the venous return curve intersects the cardiac function curve at its ascending or flat part. A reduction of venous return (as result of bleeding, stimu-

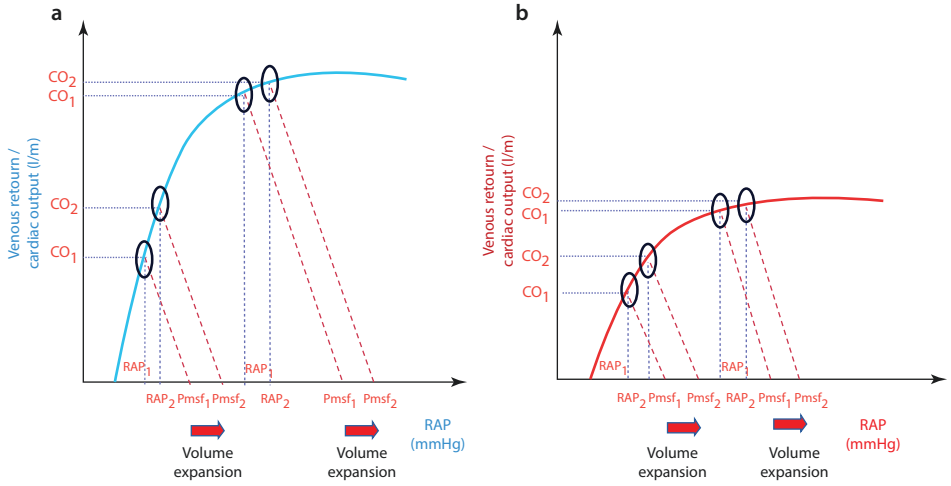

Fig. 25.1 Cardiac function (output) and venous return curves in two patients with different baseline cardiac performance. In the figure on the left **a**, the curve of cardiac function is shown in a healthy patient with normal cardiac function (light blue color). The ascending part of the curve is bigger as compared to the second case. On the right side **b**, a second curve (red color) is shown, and it is typical of a patient with significant cardiac dysfunction (i.e., heart failure) with very limited tolerance to an artificial increase in preload (ascending part of the curve is rather limited). *CO* cardiac output, *Pmsf* mean systemic filling pressure, *RAP* right atrial pressure

lation of diuresis, etc.), or conversely an increase in preload (i.e., due to vasoconstriction, exogenous administration of fluid, etc.), will produce significant variations of CO by shifting the venous return curve. Under this condition, the patient is described as fluid responder. On the contrary, changes in venous return when the patient heart function is already operating on the flat part of the CO curve will not produce significant changes, and the patient will be classified as fluid nonresponder.

25.2.2 Fluid Responsiveness and Fluid Tolerance Concepts

Responsiveness to the administration of fluid is a physiological phenomenon due to normal preload reserve. Therefore, healthy individuals are usually FR. Hence, FR does not mean that fluid must or can always be administered, and decision on fluid administration should rely on the following three characteristics [7]:

1. Identification of hemodynamic instability and/or peripheral hypoperfusion that may benefit from increase in CO
2. Presence of indexes suggesting a condition of FR (or better defined as "biventricular responsiveness")
3. Limited risks of fluid overload in case of fluid administration

Once identified a clinical condition that may be potentially improved with fluid administration, ICU clinicians should evaluate if the patient is a fluid responder, hence if the CO is likely to increase after volume administration. This evaluation is performed with dynamic parameters/maneuvers whose aim is to describe (or anticipate) the clinical response to exogenous fluid administration. This identification is of utmost clinical importance as an excess of fluid administration is associated with worse patient's outcome. Indeed, unnecessary fluid expansion would cause worse oxygen delivery via hemodilution and reduction in hemoglobin, increase in peripheral edema and reduction in perfusion pressure, pulmonary congestion, and worse gas exchanges. Presence of FR should not become a triggering signal for fluid loading without a precise clinical endpoint, and considering the condition of FR as a mandatory trigger for further fluid administration currently represents an inadequate use of this therapeutic approach, which may result in harm. Therefore, when evaluating FR in the ICU patients, clinicians should balance other two concepts for a modern approach to fluid management: fluid overload and fluid tolerance [4]. In particular, fluid overload is usually calculated with adjustment for patient's body weight, and it has been defined as an increase over 10% of body weight due to fluid accumulation; it can be quantified by dividing the cumulative fluid balance by the patient's baseline body weight and multiplying by 100 [4]. Fluid tolerance, on the other hand, is a more theoretical concept and can be defined as the *capacity to accept additional fluids without risk of organ dysfunction due accumulation of tissue edema*. Therefore, it seems apparent that fluid tolerance fills the gap between conditions of fluid responsiveness and fluid overload, stressing the clinical importance of an adequate and timely fluid removal once the patient's conditions have been stabilized [10]. In the context of exploring the patient's tolerance to further fluid administration, the use of POCUS has been explored and may be valuable. In particular, two tools have been recently introduced in clinical practice. The first is represented by the use of lung ultrasound with focus on the search for B-lines pattern, which suggests accumu-

lation of fluids in the lung at interstitial level. The presence of diffuse B-lines pattern suggests cautiousness in the administration of fluids that may worsen gas exchanges and produce further increase in left ventricular filling pressure [11, 12]. The second tool is called VExUS (Venous Excess Ultrasonography Score) and has been introduced with the idea to evaluate systemic congestion. VExUS evaluation integrates a series of ultrasound data, starting from the size of the inferior vena cava (IVC) and proceeding to the interrogation of flows at the levels of hepatic, portal, and intrarenal venous using Doppler [13]. VExUS has been introduced more recently, and its value from clinical perspective is under intense scientific evaluation.

From clinical perspectives, several parameters can be used for the identification of FR, each one with advantages and disadvantages. In terms of cutoffs used to define FR, the most widely accepted change in CO to define FR is ≥15%, although ≥10% has been used too [8]. These cutoffs should not be confused with the values used for the prediction of FR using information gathered from invasive arterial line monitoring (i.e., pulse pressure and stroke volume variation) or from POCUS examination. In terms of assessment of FR, the main advantage of the invasive arterial line system is represented by the continuous monitoring with the ease to track changes over time of the data from the arterial blood pressure signal. Although an arterial line catheter is invasive by nature, this is positioned in the vast majority of critically ill patients not only for the purpose of continuous hemodynamic monitoring, but also to perform blood samples and acquire data from arterial blood gas analyses. While POCUS has the disadvantage of not being continuous, it offers the opportunity to noninvasively evaluate FR and explore fluid tolerance looking for signs of pulmonary and/or systemic venous congestion.

25.2.3 Factors Influencing Fluid Responsiveness

Despite this relatively straightforward physiological background, the practical assessment of FR remains a challenging task for several reasons. The prediction of cardiovascular response based on the interaction of venous return and cardiac function curves works very well when only one variable is altered at a time; however, from clinical perspectives, all of these variables have some degree of continuous interaction, which makes its application in real life more challenging. The factors primarily influencing FR can be divided in those related to (a) the heart function and (b) to the venous return, and can be analyzed separately.

(a) From cardiac perspectives, the FR relies on the performance of both RV and LV, and therefore, it has been suggested that from theoretical perspectives the name of "biventricular responsiveness" would be more appropriate. Indeed, it is important to consider the issue of ventricular interdependence where the dysfunction of one ventricle have pronounced effect on the performance of the other one, as it may happen in case of RV failure and septal displacement toward the left, which consequently impaired LV filling. Even if in absence of significant clinical events (myocardial ischemia, pulmonary embolism, etc.), the cardiac performance remains relatively steady in the short term, and the CO curve does not present rapid variations or shifts; as already mentioned, not all patients have the same shape of CO curve. Indeed, several critically ill patients present a reduction in heart performance, which are described by a flatter CO curve. In other

words, the steep part of the curve is usually more predominant in healthy individuals with good cardiac performance, while this ascending part becomes much smaller in patients with reduced contractility such as those with heart failure and cardiac disease (Fig. 25.1b). In the latter patients, the small ascending part offers little leverage in terms of fluid tolerance, that is, very little tolerance for fluid administration, and there is greater risk of serious adverse effects from hypervolemia and fluid overload.

(b) From the perspectives of the venous return, the variations in preload typically exhibited by critically ill patients can be considerable, and such variations may occur rapidly. For example, sedative drugs have large influence on the vascular tone, and their dose is frequently modified in daily critical care practice; in turn, fluctuations in sedation level and sympathetic stimulation produce rapid changes in in vasomotor tone [14]. Moreover, not only is the intravascular volume influenced by fluid administration, but also by absorption of enteral nutrition, fluctuations in diuresis, and capillary leakage, the latter being grossly conditioned by inflammatory and infective phenomena [15, 16].

Therefore, considering that the aforementioned factors cause high variability and are capable of inducing rapid fluctuations in preload conditions over the entire course of critical illness, it is of utmost importance to repeatedly assess FR as part of usual daily ICU practice. Of course, such assessments should rely on a preliminary understanding of patient's cardiac performance, possibly by performing an echocardiogram whenever feasible and preferably within the first hours after ICU admission. Indeed, a consensus of experts recommends echocardiography as the first line approach for the clinical characterization of a patient in shock. Moreover, it seems reasonable to repeat assessments of cardiac function over the course of ICU stay to exclude significant changes and events that may negatively influence the CO curve position. Further, clinicians must recognize that the introduction of treatment with inotropes or the resolution of the primary insult may produce significant shifts of the cardiac function curve.

25.3 Use of Ultrasound for the Assessment of FR in ICU

There are several methods for repeated FR assessment, each of these presenting strengths and pitfalls. As the assessments are to be performed multiple times in the daily ICU practice, preferences have been given to noninvasive methods such as echocardiography and/or with other POCUS methods. Nonetheless, it must be clarified that, although most of the other non-POCUS methods for the prediction of FR (i.e., pulse pressure variation) require the presence of an indwelling (invasive) arterial line catheter, this catheter is usually already in place in most patients. Therefore, such non-POCUS methods of assessment of FR cannot be truly regarded as "invasive" per se, since the patient is not exposed to further procedures in order to gather the information.

For simplicity, the assessment of FR with POCUS techniques may be divided in three main parts, according to the cardiovascular focus of interrogation:

- the cardiac function (i.e., variation in flow generated by the LV)
- the venous side (i.e., size and variation of main veins)
- the arterial side (i.e., changes in flow time or blood flow in arteries)

Such methods can easily be integrated with each other (or with other "invasive" methods) for a more comprehensive assessment, especially when the findings of one assessment are inconclusive for whatever reason. Of course, one focus of POCUS interrogation does not exclude the use of the other two; moreover, in some cases, it is also recommended to integrate them. For instance, in the case of interrogating the variation of the inferior vena cava (IVC) diameter for FR, the exclusion of conditions confounding its predictive value (i.e., presence of RV dysfunction/failure, significant tricuspid regurgitation, or tamponade) is required.

Before discussing the abovementioned cardiovascular focuses of interrogation with POCUS to gather information on FR, it is useful to consider that POCUS information can be differentiated in measurements of

- Sizes and variations of a heart chamber or a vein, or
- Flow calculated using the Doppler effect with velocity time integral (VTI) assessment

25.4 Ultrasound Assessment at the Heart Level

25.4.1 Assessment of Flow: Stroke Volume and Cardiac Output

The assessment of CO variations as consequence of fluid administration or of preload modifying maneuvers (passive leg raising—PLR—or ventilatory variation as the tidal volume challenge) can be performed noninvasively with echocardiography. In particular, echocardiography allows one to measure variation of the SV or CO by using Doppler principles. When ultrasound beam hits moving red blood cells, the received frequency changes (Doppler shift frequency), and the Doppler equation defines the relation between the angle of incidence of the ultrasound beam, the blood velocity/direction, and the Doppler shift frequency. As previously described, blood velocity is reported in centimeters per second (cm/s) as VTI, which reports the distance that blood travels over a single beat. By means of echocardiography, one can measure the VTI in the left ventricular outflow tract (LVOT), gathering clinically important information, considering that the VTI is proportional to the SV. If required, one can also estimate the SV by measuring the diameter, hence cross-sectional area, of the LVOT. In such case, the area of the LVOT is multiplied by the VTI obtained in the same anatomical region.

However, there are a number of caveats that concern the validity of the results: there should be no significant valve regurgitation, intracardiac shunts, or severe valvular stenosis (pre-stenotic accelerated flow signals must be avoided for a correct calculation). As mentioned, left-sided SV calculation is performed computing forward flow across the LVOT. Similarly, the RV outflow tract (RVOT) can be used to assess right-sided SV changes, while methods relying on trans-mitral and trans-tricuspid flows have not been clinically implemented due to the complex dynamic geometry of these orifices making calculations less practical and unreliable.

The most common echocardiography approach used by ICU clinicians is certainly the transthoracic route (TTE), and in these circumstances, the LVOT size is measured in parasternal long axis view, whereas in case of transesophageal approach

(TEE), the LVOT measurement is performed in mid-esophageal long axis view. In both cases, it is recommended to zoom in the LVOT and aortic valve region in order to maximize precision in LVOT sizing. The LVOT diameter is measured in mid-systole (aortic valve opened) and about 3–10 mm from the aortic valve (AV) plane. A normal LVOT size is between 19 and 26 mm according to patient's body size, but it can be influenced by LV hypertrophy. As shown in ◘ Fig. 25.2a, b, once the LVOT

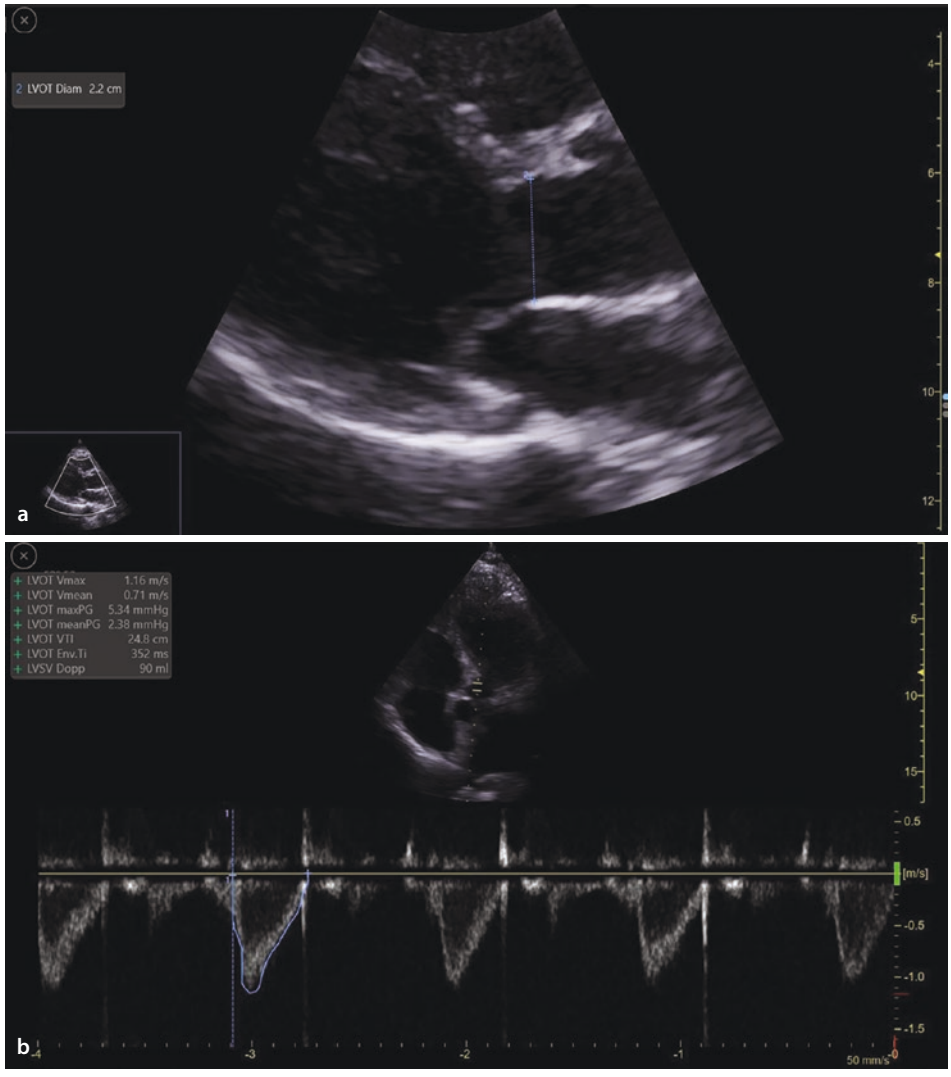

◘ **Fig. 25.2** Two images obtained to calculate the stroke volume (SV) with transthoracic echocardiography. (**a**) Shows a parasternal long axis view with a zoom image focusing on the left ventricular outflow tract (LVOT) with a diameter measured 2.2 cm with the cardiac cycle in meso-systole with aortic valve leaflets well opened. The image on the left (**b**) shows a pulse wave Doppler image obtained at the LVOT from an apical five chambers. The Doppler signal is traced, and, among others, a velocity time integral (VTI) value of 24.8 cm is obtained. Considering the formula ($\pi r^2 \times$ VTI), an LVOT area of 3.45 cm^2 is obtained, and the resulting SV is 85.7 mL

size is measured (Fig. 25.2a), its value is integrated with the LVOT VTI measured in the LVOT region from an apical five chambers view so that the SV is obtained using the formula ($\pi r^2 \times$ VTI). As the value of the radius of the LVOT is squared, extra care is needed in measuring LVOT diameter; indeed, any error in its measurement is squared by the area calculation with significant variation of the SV. Once the SV has been obtained, this value is multiplied by the HR to obtain the CO.

Clinical monitoring of SV and CO is possible with both echocardiography and advanced hemodynamic monitoring devices. While echocardiography has the advantages of being noninvasive and repeatable, it does not provide continuous information as advanced hemodynamic monitoring devices, and this is one of the reasons why the two methods should not be regarded as foes but can be both implemented according to skills, availability, and clinical indications. Another important issue that should be kept in mind is that CO measurement with echocardiography has some degree of inter- and intra-observer variability.

25.4.2 VTI and Fluid Responsiveness

From practical perspectives, the evaluation of changes in VTI is very useful for the estimation of FR. In particular, considering that the LVOT size (anatomy) remains constant, and assuming also that the intrinsic cardiac contractility (function) does not vary if clinical conditions are steady and there is no change in drug infusion, the variation in VTI is a good surrogate for the estimation of FR.

In terms of assessment of FR, the change in VTI can be used as predictor of preload responsiveness in different ways. First of all, based on the heart–lung interaction and the cyclic variation of intrathoracic pressure, the VTI variation on a beat-to-beat base can be used as a surrogate of FR in patients presenting sinus rhythm. The greater the difference between maximal and minimal VTI, the more likely the patient would be fluid responder or, in physiologic terms, the more likely the patient will be on the ascending portion of his/her cardiac function curve. A second use that can be done with the VTI is the measurement of its change before and after performing a preload modifying maneuver such as PLR (where a pool of blood is recruited by lifting the lower extremities) or, less commonly, inducing changes in venous return applying ventilatory maneuvers (such as the tidal volume challenge or the end-expiratory occlusion test). Finally, the VTI change can be used also during a mini-fluid challenge (smaller amount of fluid administered to decrease the risk of fluid overload); however, when performing a mini-fluid challenge, the expected change of the VTI that predicts FR is lower than the one observed in case of larger volume of fluid administered. The assessment of VTI can be performed not only at the LVOT (or RVOT) level, but this measurement can be taken also for the flow through the aortic valve, keeping in mind that the higher velocities recorded at this level warrant the use of continuous wave Doppler instead of pulsed-wave. The aortic VTI (flow) variations due to respiratory cycle can be calculated by tracing the continuous wave Doppler signals when the maximum aortic flow velocity is maximum and minimum. The difference between maximal and minimal aortic VTI (delta) is divided by the mean value, and an index over 12% is usually accepted as a cutoff for FR [17]. Alternatively, also the difference in peak velocities of aortic blood flow can used for

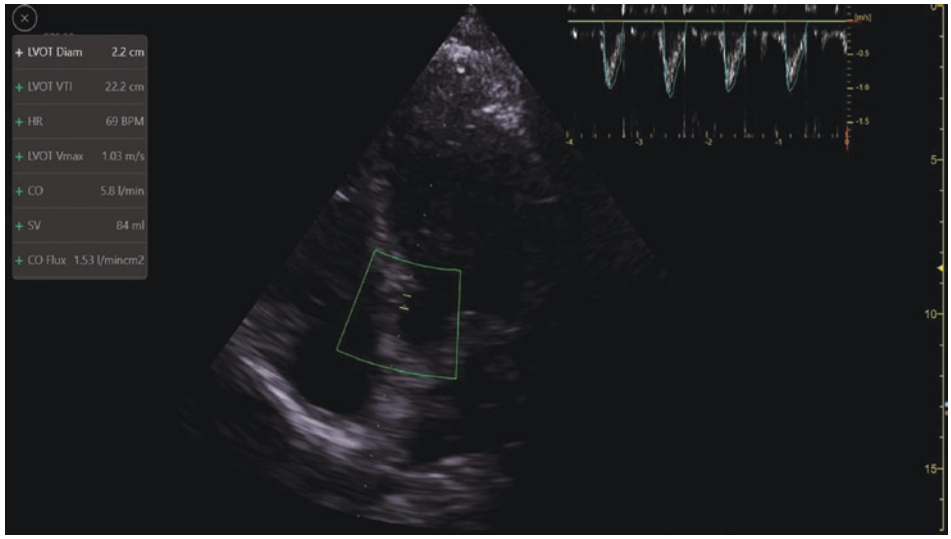

Fig. 25.3 In the same patient shown in Fig. 25.2, an automated calculation of the velocity time integral (VTI) is obtained from the apical five-chamber view with transthoracic echocardiography. The automated calculation at the left ventricular outflow tract (LVOT) is performed by the software with a trace of the Doppler signal in four consecutive beats. The resulting VTI is 22.2 cm, and the stroke volume is 84 mL

the identification of FR, keeping in mind that alignment of the continuous wave Doppler signal and blood flow is essential.

Nowadays, the ICU physicians must be aware of the development of Artificial Intelligence (AI) tools to facilitate, automate, and decrease the intra-operator variability also in the field of POCUS. Among these AI-enabled tools, one is the automatic assessment of the VTI ("auto-VTI"—Fig. 25.3) which, after the operator has achieved a good apical five-chamber view, in just a few seconds automatically detects the correct positioning of the LVOT and starts recording the Doppler signal with automated quantification of the VTI (averaged over a certain number of beats, usually five). Recently, Gonzalez et al. showed that automatic assessment of VTI was possible in most cases (92%), and if compared with manual calculation, it was accurate and precise both in expert and in trainee hands [18]. Theoretically, not only flows but also sizes could be used at heart level for the POCUS assessment of FR. For instance, noninvasive assessment of CO could be gathered indirectly estimating LV volumes at end-systole and end-diastole; however, such method is less reliable to detect changes in CO after preload modifying maneuvers.

25.5 Ultrasound Assessment on the Venous Side

The assessment of FR with POCUS at venous side has gained interest due to its ease of learning and quick mastering of the procedures for such evaluation. As for the evaluation of FR according to the VTI (flow) variation due to oscillations in the degree of LV (or RV) filling and consequently in SV generated by the cardiac pump, the judgment of FR with assessment of the venous side relies on variation in the

interrogated veins according to the breathing cycle. Such variations are mostly assessed in terms of size changes, although the flow of the hepatic veins has gained interest in recent years.

25.5.1 Respiratory Variations of the Inferior Vena Cava

As the TTE is the most common echocardiographic approach used in the general ICU population, the variation of diameters of the IVC (min and max) with respiration has received the greatest interest [19] among the venous targets of evaluation. Clearly, the ease of visualization of the IVC generated enthusiasm in the research and subsequently in the clinical use of this parameter. From practical perspectives, the IVC can be imaged in short (axial) or long (sagittal) axis, each with its own advantages. The assessment can be done in 2-D or in M-mode view (◘ Fig. 25.4a), and it is recommended to evaluate the changes in the vessel diameter usually within 4 cm from the right atrium, distal to the hepatic vein junction with the IVC. Although the visual inspection can suggest FR in extreme cases, it is recommended to precisely measure the vessel size variation using the caliper function and to apply validated formulae for the estimation of FR. Of note, the cutoffs are different for patients receiving or not receiving respiratory support. In particular, the first two studies evaluating FR according to variation of the IVC diameter were conducted in mechanically ventilated patients [20, 21]. While the numerator is represented by the delta of the diameters (IVC*max* − IVC*min*) in both studies, the denominators were different (IVC*min* or IVC*mean* diameter). Consequently, the cutoffs for prediction of FR were ≥18% [21] and ≥12% [20]. Currently, the formula used in the study by Barbier et al. (IVC*max* − IVC*min*)/IVC*min* is the more commonly adopted [21]. A different formula was reported in spontaneously breathing patients, (IVC*max* − IVC*min*)/IVC*max*, in other studies [22–24]. These studies found that the best cutoff for FR is comprised between ≥42% and ≥48%. In terms of terminology, the formulae for the assessment of FR and their cutoffs (or indexes) refer to the changes in the IVC diameter during inspiration; therefore, in mechanically ventilated patients with controlled breathing, the formula defines the distensibility index (IVC-DI), whereas in spontaneously breathing patients, the index is called collapsibility index (IVC-CI).

However, the enthusiasm on the use of IVC parameters of FR has decreased over the years due to the limitations that influences the IVC assessment for FR [25]. Moreover, while the initial studies conducted in mechanically ventilated patients reported promising sensitivity and specificity of the IVC for estimating FR (both around 90%), subsequent larger studies showed lower area under the curve (AUC) values [26]. Indeed, pooled results from meta-analyses suggest an AUC for IVC above 0.80, with slightly higher values in mechanically ventilated patients as compared to those spontaneously breathing. Of note, for the population of critically ill patients with mechanical ventilation, the AUC is higher when the IVC-DI is used to predict FR in patients ventilated with both a tidal volume >8 mL/kg of and a positive end-expiratory pressure of 5 cmH_2O or less (AUC 0.88 vs 0.70 in those not matching both these requirements [27]).

Although used more rarely, the IVC variation can be estimated also using the short axis visualization of the vessel and measuring the IVC area at end-inspiration and end-expiration. Whatever is the choice to assess the IVC diameter variation over

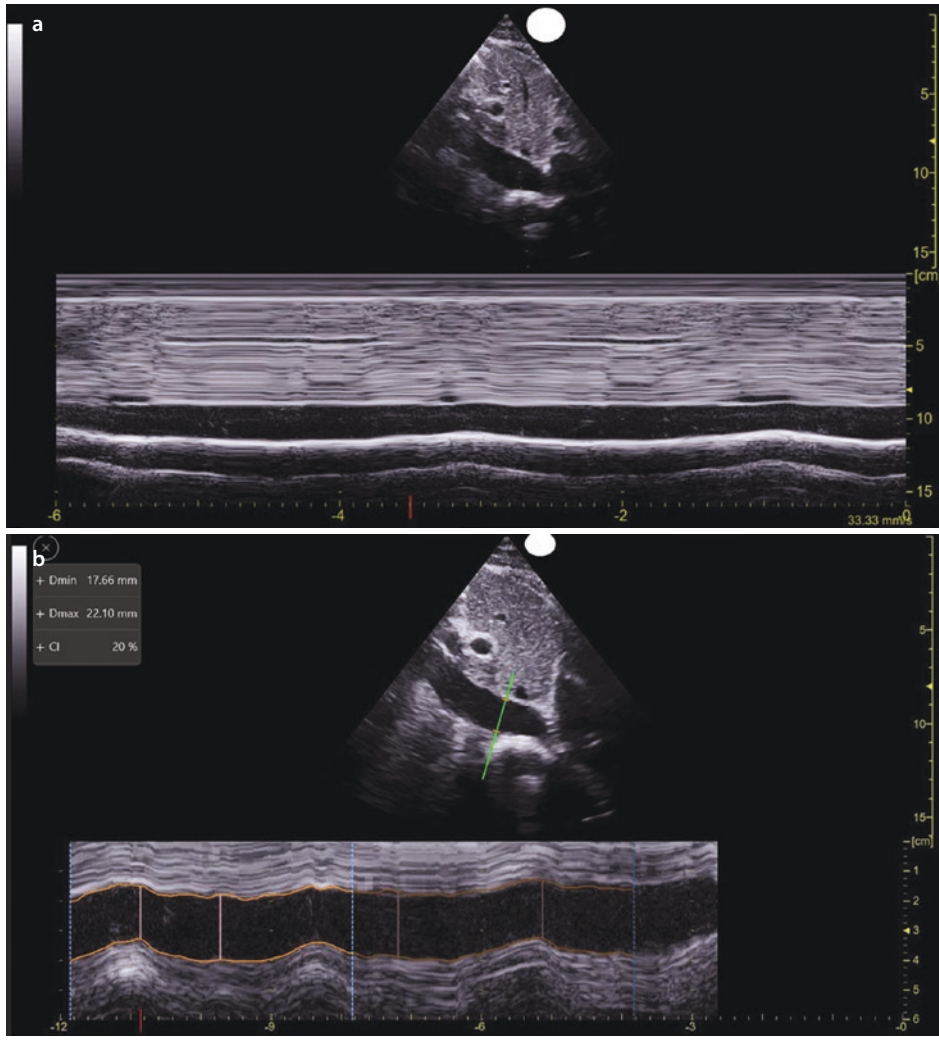

Fig. 25.4 Evaluation of inferior vena cava (IVC) diameter change over time obtained with transthoracic echocardiography in a spontaneously breathing patient. In (**a**), a typical imaging in M-Mode function is recorded for subsequent calculation. In (**b**), the calculation is obtained with automated border tracing function resulting in a real-time calculation (IVC*max* diameter 22.1 mm; IVC*min* diameter 17.66 mm) with a collapsibility index (CI) estimated at 20%

the time during the respiratory cycle, it is important to keep the probe steady and focused on the center of the vessel. Moreover, in terms of limitations, it must be considered that several conditions affect the interpretation of the IVC exam for the prediction of FR. Among these, RV dysfunction, significant tricuspid regurgitation, tamponade, acute asthma, and severe chronic obstructive pulmonary disease are common clinical conditions where the assessment of the IVC is significantly influenced, and its value in the estimation of FR is at least partially compromised. Other factors include body position, intra-abdominal hypertension, obesity, and intra-abdominal masses [25].

Finally, as the IVC is not easily visible or assessable from the subxiphoid region in some types of ICU patients (i.e., obese, median laparotomy, presence of mediastinal drains), some research interest has been developed in the imaging of the IVC in coronal axis through the transhepatic window. Most of the studies have found good feasibility of the coronal IVC imaging, but the measurements do not seem interchangeable with those obtained in sagittal subcostal approach. In particular, in most patients the variation of the IVC in coronal axis is inferior than the one estimated in sagittal view of the vessel [28].

As in the case of the AI tools developed for the calculation of VTI in the LVOT region, an AI software for automated border detection of the IVC has been integrated in some POCUS machines (◘ Fig. 25.4b), allowing clinicians to perform multiple measurements in few seconds once they achieved a good vessel visualization. The AI software will report the vessel diameters and report the IVC-CI or IVC-DI according to the type of ventilation.

25.5.2 Respiratory Variations of the Superior Vena Cava

The variation of the superior vena cava (SVC) follows the same approach described for the IVC, but some important differences must be taken into account. First of all, the vessel can be easily imaged in short and long axis with TEE, the latter on the right of the image called "bicaval view." Moreover, the SVC can be visualized in short axis with miniaturized TEE probes (also known as hemodynamic TEE–hTEE). However, SVC visualization with TTE is rarely achieved, and the assessment of the SVC is reserved to mechanically ventilated patients only. Second, the vessel is intrathoracic, and therefore, the diameter changes follow an opposite pattern to the IVC in mechanically ventilated patients. The adopted formula for FR prediction is the same as the one used for the IVC-DI, (IVC*max* − IVC*min*)/IVC*min*; however, the resulting index is called SVC-CI because of the collapse of SVC during inspiration in mechanically ventilated patients. Clinicians should pay attention in avoiding confusion with the IVC-CI applied to spontaneously breathing patients. Third difference, the commonly accepted cutoff for prediction of FR is ≥36%, and it has shown much higher sensitivity and specificity than the IVC-DI and IVC-CI [29]. As an easy rule of thumb, in mechanically ventilated patients, the cutoff for the SVC-CI is double as compared to the one commonly used for the IVC-DI (18%).

25.5.3 Respiratory Variations of the Internal Jugular, Subclavian and/or Femoral Vein

Considering the same principles of those applied to the variability of the IVC or SVC size according to the respiration, some authors have studied such variations in more distal districts, namely the internal jugular, subclavian, and femoral veins (IJV, SCV, and FV, respectively).

The group of Kent et al. conducted two studies using these districts to predict FR in mixed ICU populations where around two thirds of patients were mechanically ventilated. The first one was conducted pairing measurements of SCV and IVC, and

showed that SCV had moderate correlation with IVC with a mean bias of −3.2% [30]. In a second study from the same group of authors [31], both IJV and FV showed weaker correlations with the IVC data. In particular, mean bias of IJV was −3.5% and similar to the one of the SCV, meaning overestimation by IJV; conversely, FV had a mean bias of +3.8% with consequent underestimation as compared to IVC. In all these studies, the peripheral measurements of SV, IJV, and FV had shorter time of image acquisition than the IVC.

25.5.4 Study of the Hepatic Venous Flow

The study of the hepatic venous blood flow has received growing interest for the assessment of venous congestion in the multiparametric assessment conducted according to the VeXUS principles for POCUS [13]. However, the flow in the middle hepatic vein (MHV) has also been investigated for the potential value of predicting FR [32]. The MHV flow is characterized by four waves seen on Pulse Wave Doppler (Fig. 25.5): A, S, V, and D. In short, the A wave is a positive wave due to return of flow toward the liver due to right atrial contraction. Subsequently, during the ventricular systole, the S wave indicates flow toward the right atrium, which has a drop in pressure due to his relaxation after systole. This S wave ends with the return of the tricuspid annulus toward the resting position after its excursion in systole; at this stage, the excursion of the tricuspid annulus may generate a small positive wave (V), but this is not always visualized. Finally, the negative D wave develops as consequence of the right atrium relaxation and drop in atrial pressure, which in turn facilitates venous flow from liver to the IVC and right atrium. Among the parameters of MHV flow studied for the assessment of FR, the variation of the D wave after volume expansion

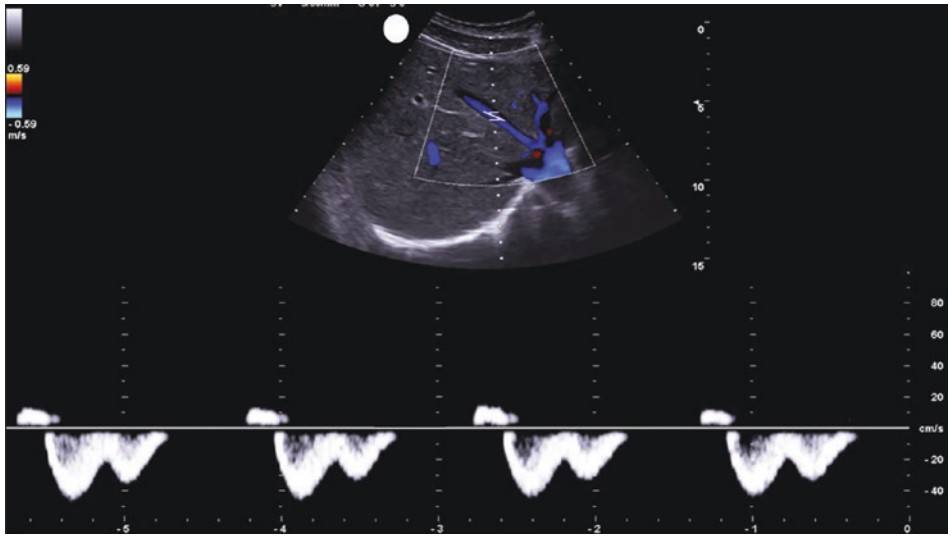

Fig. 25.5 Image of the middle hepatic vein (MHV) flow evaluated with pulse wave Doppler. In the image provided, the A positive wave is followed by two negative (S and then D) waves. A small positive wave (V) is sometimes seen after the S wave but not in the image shown

as compared to its baseline value ($MHV_{expansion} - MHV_{baseline}/MHV_{baseline} \times 100$) has shown excellent sensitivity (100%) and specificity (71%) in detecting patients not responding to volume expansion, with an AUC of 0.92 using a cutoff of >21%. Therefore, the higher the change after volume expansion, the lower the chances of FR.

25.6 US Assessment on the Arterial Side

Clinical discrimination of FR should be ideally performed with a noninvasive, reproducible, and easy to learn approach. In lights of these characteristics, the investigation of accessible arteries has generated significant interest, and it has been explored at the level of carotid, brachial, femoral, and splenic arteries. As discussed in the case of the VTI calculated in the LVOT or RVOT region, also the flow calculated in the arteries is based on the physics of ultrasound and in particular on Doppler shift frequency. Indeed, the Doppler equation allows to calculate the VTI, which defines the distance that blood travels over a single beat. Similar to the calculation performed at heart level, it is possible to obtain information on blood flow in the arteries considering their round shape and integrating the measurements of their diameter (or radius) estimated with caliper function, with the values of VTI. In addition to the use of VTI for the study of FR at the level of the arteries, another ultrasound measure of interest has been the corrected systolic flow time (FTc). The FTc represents duration of the systolic portion of the cardiac cycle, which is then corrected for the HR. Several formulae are available for the calculation of FTc, from the more complex Bazett's formula ($FTc = \frac{FT}{\sqrt{\text{cycle time}}}$) to a simpler one FTc = FTmeasured + [1.29 × (HR − 60)].

25.6.1 Measurement of Carotid Blood Flow and Carotid Corrected Flow Time

The common carotid artery region is easy to study at the bedside, and, considering that it can be visualized with POCUS virtually in all patients, it has been one of the first extra-cardiac sites investigated. The imaging of this region is more easily achieved than the LVOT and may inform on cerebral blood flow. Recently, a systematic review [33] on the role of carotid ultrasound concluded that in most studies (n = 15/17 analyzed) this method was able to predict FR. Also, it must be kept in mind that roughly one quarter of these studies were performed in healthy volunteers, so applying their results to critically ill patients must be done very cautiously. In the included studies reported by the systematic review, the most commonly reported parameter was the FTc (n = 9/17), as absolute value or as change after PLR. The second most reported measure was the change in peak velocity during respiration with a proposed optimal cutoff ranging from 9% to 14% (AUC from 0.81 to 0.91, sensitivities 73–86%, and specificities 78–86%). Of note, the FTc principle was initially studied in the aorta, and it has shown good correlation with preload conditions; unfortunately, the accuracy of FTc measured in the carotid artery has not been very well characterized; to add complexity, the reported cutoffs are quite different and different equations (Bazett and Woodey) have been used to correct for HR.

Overall, the analysis of the available data suggests that carotid ultrasound may represent a promising tool to evaluate the fluid status, especially the change in peak velocity during respiration; the FTc currently does not reach an adequate sensitivity and specificity to be used as standalone tool, and it is more cumbersome to apply in clinical practice [34–36].

25.6.2 Measurement of Flow in the Aorta (Ascending or Descending)

Historically, esophageal Doppler has been introduced with the idea of advanced monitoring of several hemodynamic variables (including CO) at the level of the descending aorta, achieving clinically relevant information by a less invasive mean. The correlation with CO measured by a pulmonary artery catheter using the thermodilution method seemed good [37], and esophageal Doppler was particularly used to measure the changes in flow as response to a particular hemodynamic intervention; therefore, esophageal Doppler was used as a dynamic measure in response to a PLR [38] or changes induced by adjustments of mechanical ventilation [17]. The measurements of blood flow in the aorta accurately reflects the trend ("trend-ability") of any change of SV over time, more than the absolute SV value. Although the esophageal Doppler has several advantages including its continuous monitoring, it is not truly a POCUS method, and it is used predominantly in intubated patients, and its main limitation is the probe positioning and the risk of dislodgement.

Conversely, the ascending aorta and the pulmonary artery can be studied with POCUS. The principles of POCUS for the study of flow in these great vessels rely still on the Doppler equation, and it is common to the use for VTI calculation in LVOT. Of course, it is much easier to study the flow at these levels with TEE rather than with TTE. Therefore, it is not surprising that there are not many studies in critically ill patients assessing blood flow and FR in these vessels.

25.6.3 Other Measurements at Level of Brachial, Femoral, or Splenic Artery

As in the case of variability in VTI measured at the heart level, the same concept has been studies at the level of the brachial artery with measurements of peak velocity; this parameter was studied by Garcia et al. [39] during mechanical ventilation as a tool to predict FR. The brachial artery blood velocity signal was obtained 5–10 cm above the antecubital fossa, then variability was studied as difference between maximum and minimum velocity (ΔVpeak) divided by the mean of them (Vpeak-mean). An increase over 10% after fluid challenge predicted FR with a good accuracy (AUC 0.88). It should be noted that brachial arterial flow seems to be quite sensitive to the mechanical influence of active muscle contraction, thus may be less valuable in awake patients during spontaneous ventilation. Similar to the velocity measured at the heart level, this parameter is largely influenced by the presence of cardiac arrhythmias.

Likewise, the peak velocity flow was studied at the level of the femoral artery in ICU patients [40, 41]. Here, in an initial study an increase of 8% after a PLR predicted FR with excellent accuracy (AUC 0.93). However, Girotto et al. [42] were not able to reproduce these findings (AUC 0.57) and reported a large inter- and intravariability between operators; a possible explanation is that the anatomical landmarks tend to change during PLR.

The splenic Doppler resistive index (SDRI) has been proposed as noninvasive parameter of hypovolemia. This measurement is taken in the main branch of the splenic artery, and it is defined as: (peak systolic velocity − end-diastolic velocity)/peak systolic velocity. Higher values of SDRI were reported in patients with occult bleeding after trauma (0.71 vs. 0.6) [43]. In mechanically ventilated patients receiving a fluid challenge, Brusasco et al. [44] reported that a reduction in SDRI less than 4% excluded the presence of FR (sensitivity 100%, specificity 100%); conversely, an SDRI reduction over 9% was a marker of FR with 100% specificity and 100% positive predictive value.

In conclusion, despite the technical simplicity of these techniques applied to the body arteries, there are several studies indicating low reproducibility and insufficient reliability in the ICU population, as most of the data supporting these techniques are not on critically ill patients. At current stage, data are insufficient for the implementation into the routine practice of FR evaluation by means of POCUS at arterial level.

25.7 US for the Assessment of Fluid Tolerance

25.7.1 VExUS and Systemic Congestion

Venous congestion can be evaluated with the study of the IVC. Its size increases proportionally to the central venous pressure until it reaches its maximum dilation, then the pressure is transmitted in a retrograde fashion through the veins to the abdominal organs. As already briefly mentioned, the VExUS is a protocol that evaluates the presence of congestion in the IVC, moving then to the grading of vein congestion with Doppler ultrasound evaluation at the level of the liver and the kidneys. The VExUS protocol should be performed in four steps. The first step is the evaluation of the IVC diameter, and if the diameter is >2 cm, the VExUS evaluation proceeds and the score ranges between 1 and 3. The second step is the evaluation of the flow pattern in the hepatic veins: normally, the S wave should be much larger than the D wave, but when venous congestion occurs, the magnitude of the S wave decreases until eventually becoming positive (blood flow reversal). The third step is the study of the portal vein; when systemic congestion occurs, the rise in pressure is transmitted from the hepatic to the portal system, and the flow becomes pulsatile (from continuous). The degree of portal vein pulsatility is quantified with the pulsatility index, defined as the difference between maximal and minimal flow divided by the maximal flow. The last step of VExUS is the assessment of the renal vein flow. Normal renal veins have uninterrupted monophasic flow, but as venous congestion increases the systolic component of the flow decreases, until in severe congestion the systolic flow

is absent. The VExUS grading system ranges from 0 to 3; in grade 0, the IVC is non-dilated (<2 cm). The grades from 1 to 3 represent a combination of dilated IVC and normal flow pattern (grade 1), mild congestion pattern (grade 2), or severe congestion (grade 3).

25.7.2 Lung Ultrasound and Pulmonary Congestion

Extravascular lung water is a parameter obtained with transpulmonary thermodilution, and it has been used as a marker of fluid congestion in the lungs. Lung ultrasound represents a bedside tool to detect pulmonary congestion. The lung ultrasound examination is primarily based on the evaluation of artifacts due to air content (A-line pattern), but when this air content decreases and extra-vascular lung water (EVLW) increases; the A-line pattern are progressively substituted with vertical hyperechoic artifacts (B-lines). The B-lines arise from the pleural line and move synchronously with lung sliding. It is paramount to remember that pulmonary congestion depends not only on the fluid status but also on cardiac filling pressure (LV diastolic function) and the pulmonary vasculature permeability (i.e., in cases of pneumonia and lung inflammation). Of note, a B-lines pattern present bilaterally and in two or more lung regions suggests an "interstitial syndrome"; conversely, a monolateral or focal B-lines pattern suggests a pneumonia or lung contusion.

Lung ultrasound examination starts with the identification of six lung regions of interest (for a total 12 regions considering lungs); the regions are delineated by the intersections of parasternal line, anterior axillary line, posterior axillary line, and paravertebral line. Each lung region is evaluated and graded from 0 to 3 points (0 = normal aeration, 1 = interstitial syndrome, 2 = alveolar edema, 3 = consolidation). The total lung ultrasound score is obtained from the sum of the 12 regional scores and may range from 0 to 36. However, more simplified lung ultrasound assessment with evaluation of a reduced number of lung zones has also been clinically adopted. Regarding the concept of FR and fluid tolerance, when a diffuse and bilateral B-profile is found, it is important to consider the occurrence of "fluid intolerance"; conversely, a bilateral A-profile suggests fluid tolerance and limited risk of fluid overload [45]. Among ICU physicians, the use of transthoracic lung ultrasound is becoming a useful and noninvasive tool to evaluate also the lungs fluid "intolerance."

25.8 Conclusions

In conclusions, the evaluation of fluid responsiveness and of fluid tolerance are major daily duties of clinicians assessing critically ill patients. The use of POCUS at different levels (heart, veins, and/or arteries) may offer clinically relevant information for the prediction of fluid responsiveness. Moreover, POCUS can be used to integrate such information with other variables suggesting the patient's tolerance (or not) to further fluid administration.

Take-Home Messages

- Responsiveness to the administration of fluid is a physiological phenomenon due to normal preload reserve.
- Presence of fluid responsiveness does not mean that fluid must be administered.
- Unnecessary fluid expansion may cause worse oxygen delivery due to hemodilution and reduction in hemoglobin, increase in peripheral edema, and reduction in perfusion pressure, pulmonary congestion, and worse gas exchanges.
- Fluid tolerance is the capacity to accommodate administration of additional fluids without increasing the risk of organ dysfunction due to accumulation of tissue edema.
- The fluid responsiveness assessment could be performed with ultrasound techniques directed to several cardiovascular districts: the heart, the veins, or the arteries.
- The volume time integral (VTI) measured in the left ventricular outflow tract (LVOT) is proportional to the stroke volume (SV).
- The change in VTI (LVOT or aorta) can be used as a predictor of preload responsiveness in different ways: cyclic variation of intrathoracic pressure, after fluid administration, and after a passive leg raising.
- The respiratory variations of the inferior or superior vena cava could be used to assess fluid responsiveness. The initial enthusiasm on the use of these measures is limited by many factors (among others the use of protective mechanical ventilation with tidal volume <8 mL/kg).
- It is possible to evaluate fluid responsiveness also investigating changes in arterial blood flow (or flow time) with Doppler ultrasound.
- The venous congestion can be evaluated with the study of the inferior vena cava diameter, the flow pattern in the hepatic and portal veins, and the renal blood flow (VExUS grading system). Also, lung ultrasound is useful to define signs of pulmonary congestion and fluid tolerance.

References

1. Sanfilippo F, Messina A, Cecconi M, Astuto M. Ten answers to key questions for fluid management in intensive care. Med Intensiva (Engl Ed). 2021;45:552–62.
2. Messina A, Collino F, Cecconi M. Fluid administration for acute circulatory dysfunction using basic monitoring. Ann Transl Med. 2020;8:788.
3. Boulain T, Cecconi M. Can one size fit all? The fine line between fluid overload and hypovolemia. Intensive Care Med. 2015;41:544–6.
4. Kattan E, Castro R, Miralles-Aguiar F, Hernández G, Rola P. The emerging concept of fluid tolerance: a position paper. J Crit Care. 2022;71:154070.
5. Díaz-Gómez JL. Fluid tolerance, hemodynamic/organ congestion, or congestion cascade in the critically ill-a must-known evolving concept in 2022. J Crit Care. 2022;71:154071.
6. Malbrain M, Van Regenmortel N, Saugel B, et al. Principles of fluid management and stewardship in septic shock: it is time to consider the four D's and the four phases of fluid therapy. Ann Intensive Care. 2018;8:66.
7. Sanfilippo F, Messina A, Cecconi M, Astuto M. Ten answers to key questions for fluid management in intensive care. Med Intensiva. 2020;45:552.
8. Messina A, Calabrò L, Pugliese L, et al. Fluid challenge in critically ill patients receiving haemodynamic monitoring: a systematic review and comparison of two decades. Crit Care. 2022;26:186.

9. Dhondup T, Tien JC, Marquez A, Kennedy CC, Gajic O, Kashani KB. Association of negative fluid balance during the de-escalation phase of sepsis management with mortality: a cohort study. J Crit Care. 2020;55:16–21.
10. Claure-Del Granado R, Mehta RL. Fluid overload in the ICU: evaluation and management. BMC Nephrol. 2016;17:109.
11. Lichtenstein DA. BLUE-protocol and FALLS-protocol: two applications of lung ultrasound in the critically ill. Chest. 2015;147:1659–70.
12. Lichtenstein DA. Current misconceptions in lung ultrasound: a short guide for experts. Chest. 2019;156:21–5.
13. Bhardwaj V, Vikneswaran G, Rola P, et al. Combination of inferior vena cava diameter, hepatic venous flow, and portal vein pulsatility index: venous excess ultrasound score (VEXUS score) in predicting acute kidney injury in patients with cardiorenal syndrome: a prospective cohort study. Indian J Crit Care Med. 2020;24:783–9.
14. Morelli A, Sanfilippo F, Arnemann P, et al. The effect of propofol and dexmedetomidine sedation on norepinephrine requirements in septic shock patients: a crossover trial. Crit Care Med. 2019;47:e89–95.
15. Rovas A, Seidel LM, Vink H, et al. Association of sublingual microcirculation parameters and endothelial glycocalyx dimensions in resuscitated sepsis. Crit Care. 2019;23:260.
16. Wollborn J, Hassenzahl LO, Reker D, et al. Diagnosing capillary leak in critically ill patients: development of an innovative scoring instrument for non-invasive detection. Ann Intensive Care. 2021;11:175.
17. Feissel M, Michard F, Mangin I, Ruyer O, Faller JP, Teboul JL. Respiratory changes in aortic blood velocity as an indicator of fluid responsiveness in ventilated patients with septic shock. Chest. 2001;119:867–73.
18. Gonzalez FA, Varudo R, Leote J, et al. The automation of sub-aortic velocity time integral measurements by transthoracic echocardiography: clinical evaluation of an artificial intelligence-enabled tool in critically ill patients. Br J Anaesth. 2022;129:e116.
19. Vieillard-Baron A, Millington SJ, Sanfilippo F, et al. A decade of progress in critical care echocardiography: a narrative review. Intensive Care Med. 2019;45:770–88.
20. Feissel M, Michard F, Faller JP, Teboul JL. The respiratory variation in inferior vena cava diameter as a guide to fluid therapy. Intensive Care Med. 2004;30:1834–7.
21. Barbier C, Loubieres Y, Schmit C, et al. Respiratory changes in inferior vena cava diameter are helpful in predicting fluid responsiveness in ventilated septic patients. Intensive Care Med. 2004;30:1740–6.
22. Airapetian N, Maizel J, Alyamani O, et al. Does inferior vena cava respiratory variability predict fluid responsiveness in spontaneously breathing patients? Crit Care. 2015;19:400.
23. Preau S, Bortolotti P, Colling D, et al. Diagnostic accuracy of the inferior vena cava collapsibility to predict fluid responsiveness in spontaneously breathing patients with sepsis and acute circulatory failure. Crit Care Med. 2017;45:e290–7.
24. Muller L, Bobbia X, Toumi M, et al. Respiratory variations of inferior vena cava diameter to predict fluid responsiveness in spontaneously breathing patients with acute circulatory failure: need for a cautious use. Crit Care. 2012;16:R188.
25. Via G, Tavazzi G, Price S. Ten situations where inferior vena cava ultrasound may fail to accurately predict fluid responsiveness: a physiologically based point of view. Intensive Care Med. 2016;42:1164–7.
26. Vignon P, Repesse X, Begot E, et al. Comparison of echocardiographic indices used to predict fluid responsiveness in ventilated patients. Am J Respir Crit Care Med. 2017;195:1022–32.
27. Si X, Xu H, Liu Z, et al. Does respiratory variation in inferior vena cava diameter predict fluid responsiveness in mechanically ventilated patients? A systematic review and meta-analysis. Anesth Analg. 2018;127:1157–64.
28. La Via L, Astuto M, Dezio V, et al. Agreement between subcostal and transhepatic longitudinal imaging of the inferior vena cava for the evaluation of fluid responsiveness: a systematic review. J Crit Care. 2022;71:154108.
29. Vieillard-Baron A, Chergui K, Rabiller A, et al. Superior vena caval collapsibility as a gauge of volume status in ventilated septic patients. Intensive Care Med. 2004;30:1734–9.

30. Kent A, Bahner DP, Boulger CT, et al. Sonographic evaluation of intravascular volume status in the surgical intensive care unit: a prospective comparison of subclavian vein and inferior vena cava collapsibility index. J Surg Res. 2013;184:561–6.
31. Kent A, Patil P, Davila V, et al. Sonographic evaluation of intravascular volume status: can internal jugular or femoral vein collapsibility be used in the absence of IVC visualization? Ann Thoracic Med. 2015;10:44–9.
32. Du W, Wang XT, Long Y, Liu DW. Monitoring changes in hepatic venous velocities flow after a fluid challenge can identify shock patients who lack fluid responsiveness. Chin Med J. 2017;130:1202–10.
33. Beier L, Davis J, Esener D, Grant C, Fields JM. Carotid ultrasound to predict fluid responsiveness: a systematic review. J Ultrasound Med. 2020;39:1965–76.
34. Jung S, Kim J, Na S, Nam WS, Kim DH. Ability of carotid corrected flow time to predict fluid responsiveness in patients mechanically ventilated using low tidal volume after surgery. J Clin Med. 2021;10:2676.
35. Wang H, Chen W, Cheng H, et al. Value of corrected flow time in common carotid artery in predicting volume responsiveness under mechanical ventilation. Shock. 2022;58:28–33.
36. Abbasi A, Azab N, Nayeemuddin M, et al. Change in carotid blood flow and carotid corrected flow time assessed by novice sonologists fails to determine fluid responsiveness in spontaneously breathing intensive care unit patients. Ultrasound Med Biol. 2020;46:2659–66.
37. Baillard C, Cohen Y, Fosse JP, Karoubi P, Hoang P, Cupa M. Haemodynamic measurements (continuous cardiac output and systemic vascular resistance) in critically ill patients: transoesophageal Doppler versus continuous thermodilution. Anaesth Intensive Care. 1999;27:33–7.
38. Monnet X, Rienzo M, Osman D, et al. Passive leg raising predicts fluid responsiveness in the critically ill. Crit Care Med. 2006;34:1402–7.
39. Monge García MI, Gil Cano A, Díaz Monrové JC. Brachial artery peak velocity variation to predict fluid responsiveness in mechanically ventilated patients. Crit Care. 2009;13:R142.
40. Luzi A, Marty P, Mari A, et al. Noninvasive assessment of hemodynamic response to a fluid challenge using femoral Doppler in critically ill ventilated patients. J Crit Care. 2013;28:902–7.
41. Préau S, Saulnier F, Dewavrin F, Durocher A, Chagnon JL. Passive leg raising is predictive of fluid responsiveness in spontaneously breathing patients with severe sepsis or acute pancreatitis. Crit Care Med. 2010;38:819–25.
42. Girotto V, Teboul JL, Beurton A, et al. Carotid and femoral Doppler do not allow the assessment of passive leg raising effects. Ann Intensive Care. 2018;8:67.
43. Corradi F, Brusasco C, Garlaschi A, et al. Splenic Doppler resistive index for early detection of occult hemorrhagic shock after polytrauma in adult patients. Shock. 2012;38:466–73.
44. Brusasco C, Tavazzi G, Robba C, et al. Splenic Doppler resistive index variation mirrors cardiac responsiveness and systemic hemodynamics upon fluid challenge resuscitation in postoperative mechanically ventilated patients. Biomed Res Int. 2018;2018:1978968.
45. Lichtenstein D, Mézière G, Biderman P, Gepner A, Barré O. The comet-tail artifact. An ultrasound sign of alveolar-interstitial syndrome. Am J Respir Crit Care Med. 1997;156:1640–6.

Extended-FAST Protocol in Polytrauma Patients

Francesco Corradi, Federico Dazzi, Erika Taddei, Giada Cucciolini, and Samuele Ferrari

Contents

26.1 Introduction – 434

26.2 e-FAST Applications – 435

26.2.1 Primary Assessment Following an "A, B, C, D, E" ATLS Resuscitation Sequence – 436

26.2.2 Secondary Assessment: Monitoring the Adequacy of Resuscitation – 445

References – 448

© The Author(s), under exclusive license to Springer Nature Switzerland AG 2023
C. Robba et al. (eds.), *Basic Ultrasound Skills "Head to Toe" for General Intensivists*, Lessons from the ICU,
https://doi.org/10.1007/978-3-031-32462-8_26

Learning Objectives

- Airway management
- Characterization of acute respiratory failure
- Detection of free abdominal fluid
- Assessment of the inferior vena cava and volume status
- Focused cardiac examination to identify hemopericardium.
- Assessment of closed head injury
- Assessment of splanchnic perfusion

26.1 Introduction

Traumatic injury currently constitutes 16% of the world's burden of disease and represents the leading cause of death and disability in the developing world [1]. As these deaths are potentially preventable, they demand urgent attention.

Ultrasound (US) represents a powerful, easy-to-use, tool capable of rapidly confirming or refuting life-threatening diagnoses.

Since the 1970s, Focused Abdominal Sonography for Trauma (FAST) has become a basic component in the evaluation of polytrauma patients; it is based on the sequential assessment of pericardial, perihepatic, pelvic, and perisplenic views (Fig. 26.1).

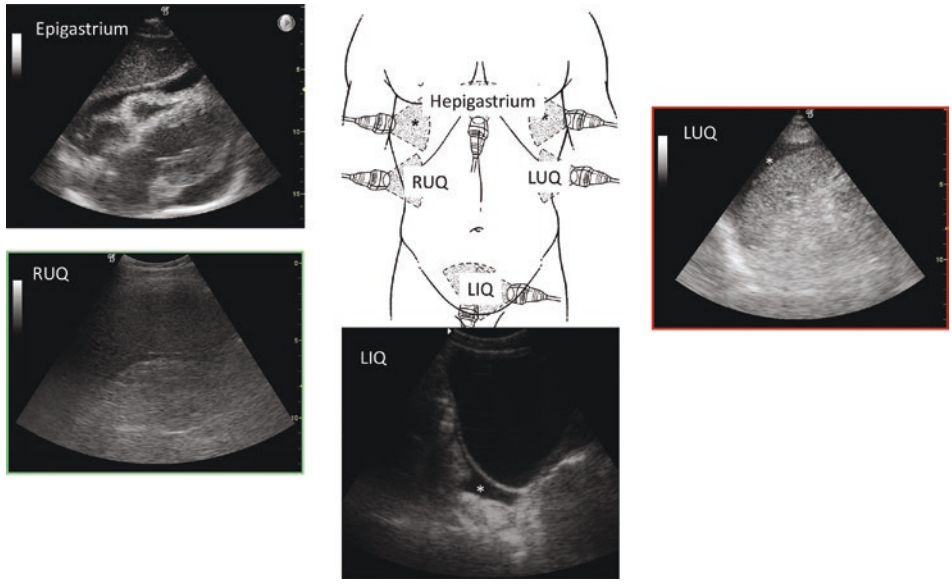

Fig. 26.1 Epigastrium: subxiphoid views of the heart are obtained by placing the transducer on the epigastrium aiming superiorly toward the left shoulder. The liver aids as an acoustic window. A pericardial effusion is seen as an anechoic space surrounding the heart. The right upper quadrant (RUQ) corresponding to the Morrison pouch, the lower inferior quadrant (LIQ) corresponding to the Pouch of Douglas, the left upper quadrant (LUQ) corresponding to the pouch between the spleen and the left kidney. White stars (*) point at peritoneal effusion

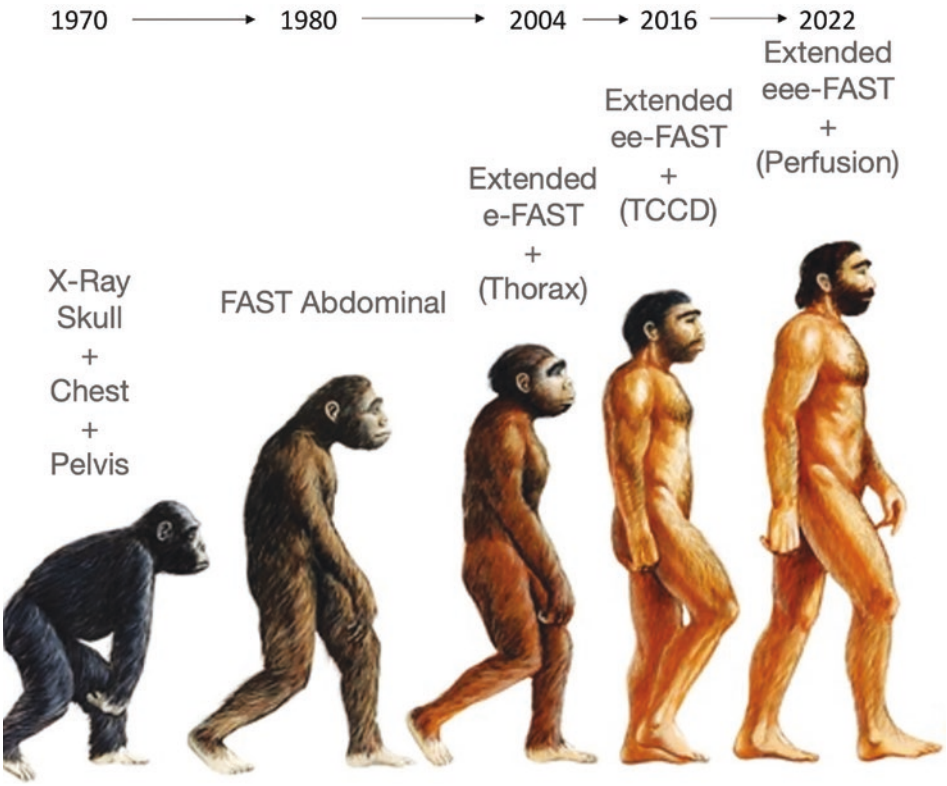

Fig. 26.2 The evolution in FAST: from free fluid to splanchnic perfusion assessment

Due to its ability to be performed quickly and safely during resuscitation, it rapidly replaced the diagnostic peritoneal lavage during the 1980s, and it was later integrated into the Advanced Trauma Life Support (ATLS) protocol developed by the American College of Surgeons [2–4].

The examination was further extended to evaluate several organs in the following years and still remains a point-of-care examination. It provides a complete overview of the patient in real time by evaluating the airways, the thorax bilaterally, the heart via a subcostal window, the abdomen with splanchnic perfusion, and the brain with transcranial Doppler and cerebral US. The actual name was therefore changed to "extended Focused Assessment Sonography for Trauma" (or e-FAST protocol) [5] (Fig. 26.2).

26.2 e-FAST Applications

The environment around polytraumatized patients is often crowded and messy; performing e-FAST can present a challenge to the practitioner. Moreover, the nature of trauma (e.g., the presence of subcutaneous emphysema) and patient status (e.g., agitation or distress) could further hamper proper US assessment. Therefore, the exam-

ination protocol must be as simple as possible and quickly target main goals by following an "A, B, C, D, E" ATLS resuscitation sequence. The examination objectives differ in the pre- and in-hospital setting: in the former, the objective is to choose the proper hospital allocation, avoiding secondary transports; in the latter, the objective is to promptly detect the need for potential urgent/emergency procedures, such as laparotomy or pericardial and/or pleural drainage.

26.2.1 Primary Assessment Following an "A, B, C, D, E" ATLS Resuscitation Sequence

26.2.1.1 Airways

The rate of endotracheal tube (ETT) malposition in the emergency setting is still high [6]. US is a valuable tool capable of confirming proper ETT placement by directly visualizing it inside the trachea. Anterior and lateral walls of the upper airways are visible by US, and the ETT appears as a hyperechoic line distinguishable from surrounding tissues (◘ Fig. 26.3). Additionally, lung US can be used to rule out esophageal and right mainstem intubation through bilateral visualization of pleural sliding, B-lines, or diaphragmatic movements [7, 8].

26.2.1.2 Breathing

Ultrasonography of the Chest

Key findings:
- Pneumothorax
- Lung contusions
- Respiratory failure characterization and reduction/loss of lung aeration
- Free fluid

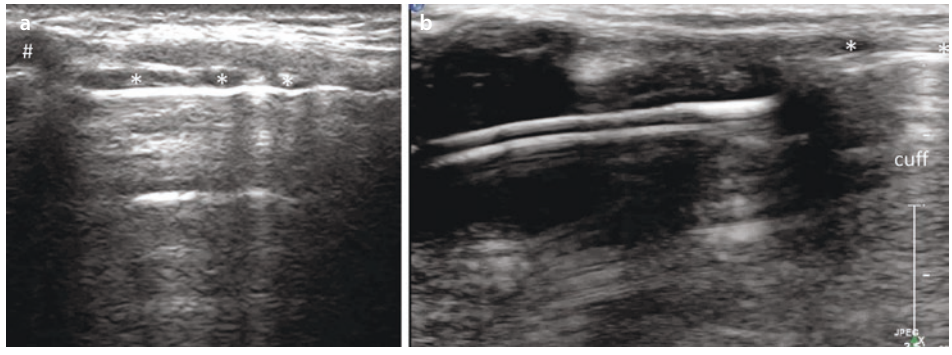

◘ **Fig. 26.3** Panel **a**: the neck in a longitudinal scan. The cricoid cartilage (#) is represented by an acoustic shadow; to follow a hyperechoic layer corresponding to the tracheal wall and the first three tracheal rings (white stars). Panel **b**: the neck after oro-tracheal intubation. The hyperechoic double layer represents the endotracheal tube within the trachea. Immediately after several hyperechoic reflections caused by the air contained in the cuff of the tube. Immediately above two circular hypoechoic structures are the tracheal rings (*). This scan allows to confirm the correct positioning of the oro-tracheal tube

Probes

Any probe can be used, even though a high-frequency (>7 MHz) linear transducer probe is preferred for pneumothorax detection.

Sites of Evaluation

A six-quadrant area of examination for each hemithorax is recommended [9]; the anterior, lateral, and posterior fields are identified by the sternum, anterior and posterior axillary lines. All of these must be scanned to detect either a hemothorax posteriorly or a pneumothorax anteriorly.

The diaphragm represents a basic landmark allowing for correct differentiation of intrathoracic and intra-abdominal structures and findings. The transducer should be placed longitudinally, perpendicularly to the ribs, to identify the pleural line in reference to the overlying ribs and then rotated transversely in the intercostal spaces. Multiple areas of the thorax should be assessed, with comparison to the contralateral side to identify any pneumothorax.

Main Concepts

Since 2004, lung US has been integrated in the standard approach to trauma (e-FAST) [4] as an extension of the FAST examination to the chest. This probably represented the greatest advancement in management of polytrauma patients, as up to 70% of pneumothoraxes are not seen on chest-X-ray even if they are large (6% of cases) [10].

The accuracy and sensitivity of lung US for pneumothorax detection are higher than that of chest X-ray [11] and auscultation [12, 13]. In fact, there is now robust evidence demonstrating that lung US is as accurate as CT scans at detecting pneumothorax, especially if traumatic in nature [14].

The identification of just one of the following signs rules out the presence of pneumothorax: lung sliding, lung pulse, and/or B-lines. On the contrary, the simultaneous absence of B-lines, lung sliding, and lung pulse in the anterior thorax of unstable supine patients indicates the need for immediate chest tube drainage.

In stable patients, this technique can be extended laterally to look for the lung point. Its location on the thorax allows semi-quantification of lung collapse [14] and monitoring of its evolution, especially if the patient is on positive pressure ventilation. However, though highly specific, lung point has a low sensitivity since it cannot be visualized in a totally collapsed lung.

Lung US is also effective in diagnosing lung contusions (◘ Fig. 26.4) [15], with high sensitivity and specificity, by visualizing the presence of either increased parenchymal density (described as B-lines) or subpleural consolidations in the context of blunt chest trauma [16]. This method has an accuracy comparable to that of CT scans, though the diameter of the consolidations and their distance from the pleural line could affect its sensitivity [17].

Pleural effusion appears as an anechoic space between two pleural layers, above the diaphragm (◘ Fig. 26.5). Despite its non-specificity, in the context of blunt chest trauma, the anechoic pattern is suggestive of hemorrhagic effusion, while an heterogeneous pattern of echoes within an effusion is somewhat specific for active bleeding (◘ Fig. 26.6).

In addition, lung US can provide an early ARDS diagnosis by demonstrating B-lines with heterogeneous and gravity-independent distribution, spared areas, pleural line thickening, and subpleural consolidations [18]; it also allows quantification

Fig. 26.4 Coronal scan with a basal right pulmonary contusion. The ultrasonographic pattern shows an increased lung density with multiple B-lines and a subpleural anechoic effusion. The hyperechoic line between the right hemithorax and the liver represents the diaphragm

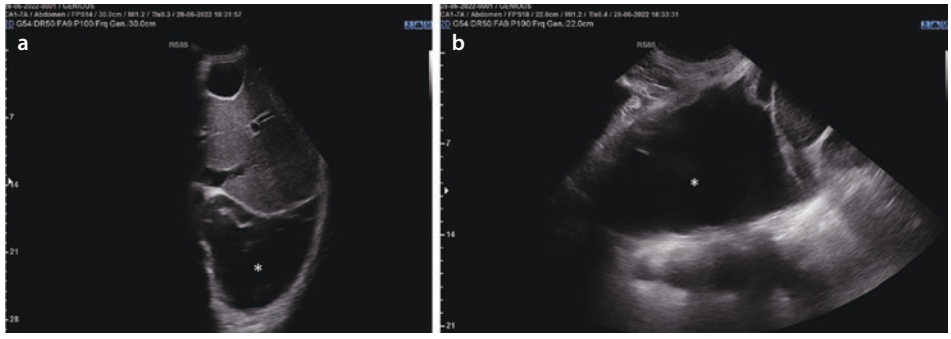

Fig. 26.5 Subcostal scan of the right hemithorax (panel **a**) and coronal scan of the left hemithorax (panel **b**) showing pleural effusions (*)

Fig. 26.6 Echogenic particles of blood (*) precipitate to the dependent areas of the hemithorax within a pleural effusion, suggesting an hemothorax in the context of a blunt chest trauma

of extravascular lung water and lung density [19], proving to be an important tool in the evaluation and ventilatory management of ARDS [20, 21]. In conclusion, lung US outperforms chest X-ray for the diagnosis of pneumothorax, hemothorax, and lung contusions in acute assessment after trauma [22].

26.2.1.3 Circulation

US of the Abdomen

Key findings:
- Peritoneal free fluid/blood
- Characterizations of effusions

Probe Selection

Probe selection, in the context of polytrauma, relies on the target of examination. In most cases, a 3–5 MHz sector probe is generally suitable for examining solid organs and determining the presence of free fluid in the abdomen or thorax and pneumothorax.

Sites of Evaluation

Evaluation consists of the sequential assessment of (1) the right upper quadrant, which includes the hepatorenal space or Morison's pouch, (2) the suprapubic region, including the Douglas's pouch posterior to the bladder, and (3) the left upper quadrant, encompassing the splenorenal recess (Koller's pouch).

Main Concepts

The hepatorenal space is the most common location for free fluid, the presence of which is associated with significant parenchymal injuries [22, 23]. Nevertheless, a multiple-view e-FAST examination is recommended: it requires minimal additional time but it increases the sensitivity for the identification of free fluid [24–27]. US has a good diagnostic accuracy for peritoneal effusion with a specificity and sensitivity between 70% and 90% [28, 29].

Hemoperitoneum usually appears anechoic or hypoechoic compared to adjacent solid organs (◘ Figs. 26.7 and 26.8), though it may become more echogenic with time.

Different protocols and scores have been developed to quantify free abdominal fluid; they primarily depend on the number of abdominal collections or the vertical height of fluid collection. It is assumed that the higher the number of the sites and the amount of fluid, the higher the severity of injury and likelihood of a surgical intervention [27, 30, 31].

However, it is of outmost importance to realize that even when a peritoneal effusion is detected, the localization of bleeding cannot be determined; indeed, in cases of isolated splenic trauma, fluid is more often found in the right upper quadrant than the left [32]. Since in clinical practice, it is possible to determine the presence of peritoneal effusion but not its origin, a common mistake would be to attribute the cause

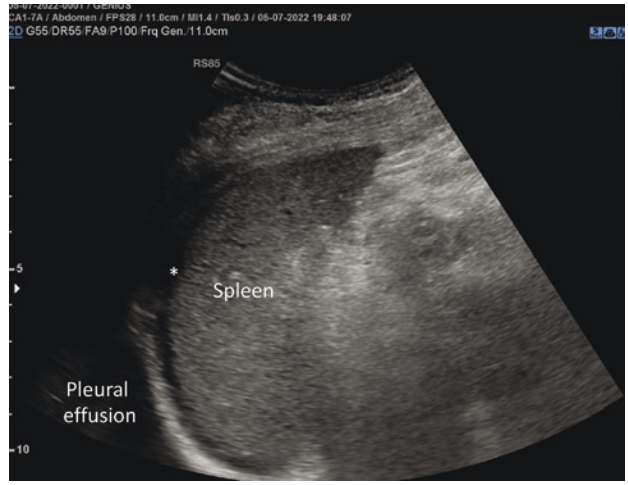

Fig. 26.7 Left coronal scan showing perisplenic fluid. Abdominal free fluid (*) is located between the diaphragm and the spleen

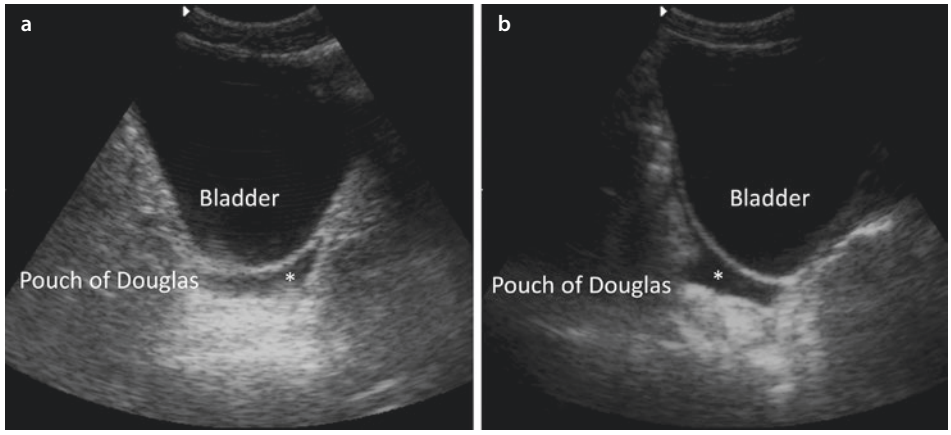

Fig. 26.8 Suprapubic view showing free abdominal fluid in the pouch of Douglas. Abdominal free fluid (*) is located posteriorly to the bladder. Lower Inferior Quadrant transversal scan (**a**); Lower Inferior Quadrant longitudinal scan (**b**)

of hemodynamic instability to a peritoneal effusion when the cause may be a retroperitoneal bleeding. Besides, even when a patient is unstable and has a peritoneal effusion, there is only a 50% chance that the bleeding is ongoing.

Considering hemoperitoneum as a marker of active bleeding may lead to misdiagnosis and delay necessary hemostatic treatment (e.g., in patients with pelvic fractures, hemoperitoneum is not always an indication for emergency laparotomy) [33].

This concern emphasizes the recommendation to perform, whenever possible, a whole-body CT scan in polytrauma patients [34, 35] to differentiate a peritoneal from active retroperitoneal bleeding as it is impossible to do so with US.

Other limitations can also affect the use of US during FAST. In fact, small amounts of free fluid cannot be detected, especially after bladder decompression via Foley catheterization. The mean minimum detectable free-fluid volume can be as large as 600 mL (possibly even more in Morison's pouch) [26, 36].

Several studies have shown underdiagnosis of intra-abdominal injury to be a potential pitfall of FAST [37]. This is in large part due to the fact that US is inferior to abdominal CT in detecting parenchymal lesions [38], and that relevant isolated solid organ injury may indeed coexist without the concomitant presence of detectable intra-abdominal free fluid.

Following patient stabilization, any change in patient condition is an indication for serial FAST exams, to identify potential development of previously undetectable free fluid collections [9]. Serial FAST exams also decrease false-negative rate by 50% and increase sensitivity for free fluid detection from 69% to 85% [39–41].

In polytrauma patients with an initial negative FAST, mechanism of injury, hemodynamic status, and clinical suspicion should always inform decisions for further diagnostic work-up. This may include a CT scan or a splanchnic Doppler-US evaluation, aimed at finding potential occult bleeding or splanchnic hypoperfusion [42–46].

Ultrasonography of the Heart

Key findings:
- Detection of pericardial effusion
- Detection of cardiac tamponade
- Volume status evaluation through inferior vena cava assessment

Probe

A 3–5 MHz sector probe is commonly used.

Sites of Evaluation

Subxiphoid views of the heart are obtained by placing the transducer on the epigastrium pointing superiorly toward the left shoulder. The proximity of the liver aids in propagating the US waves.

Main Concepts/Findings

A pericardial effusion is seen as an anechoic space surrounding the heart (Fig. 26.9). This view has proved to accurately diagnose post-traumatic cardiac injury, with 92–100% sensitivity and 99–100% specificity in the diagnosis of pericardial effusion [47, 48].

The thin-walled right heart chambers are usually the first to be compressed in the setting of cardiac tamponade. Signs of cardiac tamponade include (but are not limited to) swinging motion of the heart in the pericardial sac, diastolic collapse of right atrium and/or ventricle, cardiac chamber compression, and inferior vena cava plethora.

The absence of pericardial effusion rules out tamponade, but not cardiac injury.

Trans-thoracic echocardiography may be difficult to perform in patients with subcutaneous emphysema or pneumothorax. Additionally, concurrent massive hemothorax surrounding the pericardium may lead to either false-positive or false-negative results [22, 49, 50] because fluid in the posterior pericardial space may be difficult to distinguish from fluid in the posteromedial pleural cavity.

Fig. 26.9 Subxiphoid views of the heart are obtained by placing the transducer on the epigastrium aiming superiorly towards the left shoulder. The liver aids as an acoustic window. A pericardial effusion is seen as an anechoic space surrounding the heart

Inferior Vena Cava (IVC)

Key findings:
- Volume depletion

Probe

A 3–5 MHz sector or convex probe is suitable.

Site of Evaluation

The diameter is measured 2 cm below the cavoatrial junction by a subxiphoid approach, with the patient supine and the transducer in sagittal orientation. Inspiratory and expiratory diameters are obtained for comparison (Fig. 26.10).

A general relationship exists between the diameter of the inferior vena cava and central venous pressure; a small diameter (<1.5 cm) with substantial collapse may indicate volume depletion. However, the opposite is not true, as mechanical ventilation with positive end-expiratory pressure, severe chronic obstructive pulmonary disease, right heart failure, and pulmonary hypertension can underestimate the severity of shock [51] (Fig. 26.11).

Previous studies on trauma patients have shown that inferior vena cava diameter and collapsibility index values are good indicators of blood loss [52] and can predict the occurrence of shock [53], its recurrence after initial response [54] and 24-h fluid resuscitation requirements [55].

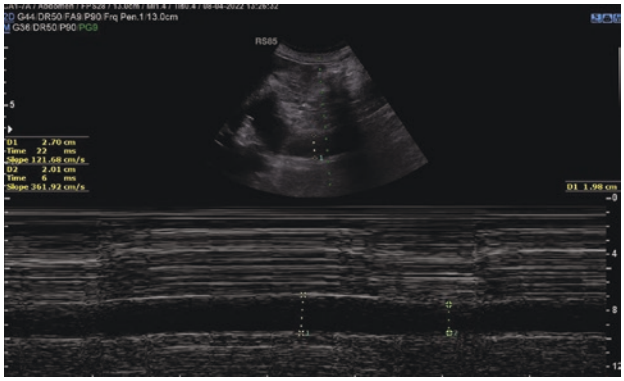

Fig. 26.10 Determination of respiratory-related changes diameters of the inferior vena cava by M-mode

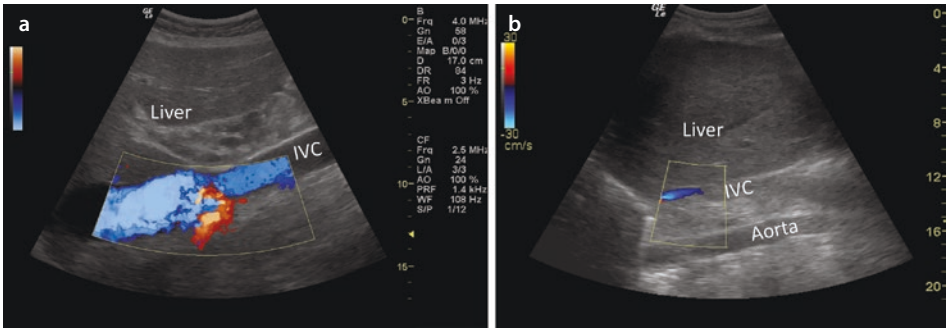

Fig. 26.11 Visualization of the inferior vena cava dilated (panel **a**) or reduced in diameter (panel **b**)

26.2.1.4 Disability

Brain US

Key findings:
- Detection of major intracranial complications such as midline shift (MLS)
- Triage or clinical suspicion of intracranial hypertension
- Prediction of secondary deterioration

Probes

A 3–5 MHz sector probe is used for brain structures or transcranial Doppler examination; a high-frequency (7–15 MHz) linear transducer is used to evaluate optic nerve sheath diameter (ONSD).

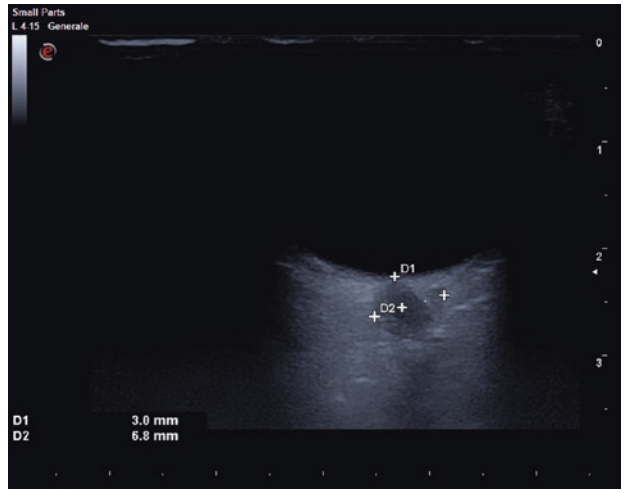

Fig. 26.12 Caliper placement at 3 mm from the vitreoretinal interface (D1) for the measurement of the optic nerve sheath diameter (D2)

26

Sites of Evaluation

The four commonly used acoustic windows in transcranial Doppler examination are the transtemporal, submandibular, transorbital, and suboccipital or transforaminal windows. Transtemporal approach allows for flow velocity measurement in the middle cerebral artery (MCA).

The ONSD is visualized by a linear probe placed on the upper eyelid, slightly on the temporal side. The optic nerve is represented by a hypoechoic linear structure stretching perpendicularly to the probe, posterior to the retina; the ONSD is measured 3 mm behind the retina (Fig. 26.12). ONSD measurements should be attempted in both the coronal and sagittal planes. A value higher than 5–6mm may suggest elevated intracranial pressure.

Main Concepts: Background

In major trauma, evaluation of brain injuries has been traditionally assigned to head CT scans, so that in comatose patients with a positive FAST for intra-abdominal bleeding, any brain-oriented evaluation and strategy were delayed until emergency surgery had been performed.

The introduction of brain US into the FAST routine can potentially provide information concerning the presence of intracranial hypertension and, in some cases, allow visualization of subdural or epidural hematomas and contusions.

Brain midline shift (MLS) is a life-threatening complication of acute brain injury and calls for expedited diagnosis and treatment. Brain US allows visualization of the third ventricle, which in sonographic anatomy can be considered a point of reference for midline structures. US-measured MLS shows a positive correlation with that of CT-measured MLS (gold standard), with a tendency of the former to slightly underestimate measurements [56].

Cerebral US may detect indirect signs of elevated intracranial pressure, as an elevated pulsatility index (PI) at transcranial color couded Doppler (TCCD) (Fig. 26.13) or an increased ONSD.

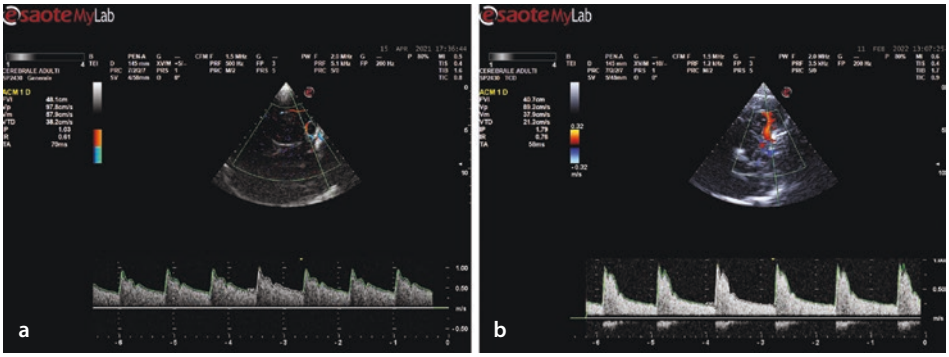

Fig. 26.13 Panel **a**: normal morphology flow velocity waveform from the middle cerebral artery. Panel **b**: flow abnormalities in the middle cerebral artery depicted by increments in peak systolic velocity while diastolic and mean velocities are decreased resulting in increased pulsatility index (PI)

The PI, expressed as (peak systolic—end-diastolic velocities)/mean middle cerebral artery (MCA) flow velocity, shows a close correlation with invasive intracranial pressure measurements [57]. In patients with mid-to-moderate traumatic brain injury, a PI >1.2 and a diastolic flow velocity <25 cm/s could predict a secondary cerebral deterioration within the first post-traumatic week [58].

ONSD increases almost directly with ICP making it a useful tool to evaluate intracranial hypertension in binary mode identifying an ICP >20 mmHg with the best cutoff of 0.58 mm in the emergency setting or when invasive monitoring is not available [59].

26.2.2 Secondary Assessment: Monitoring the Adequacy of Resuscitation

26.2.2.1 Splanchnic Perfusion Assessment

Key findings:
- Occult splanchnic hypoperfusion
- Occult bleeding
- Fluid responsiveness

The evaluation of visceral end-organ perfusion by color Doppler resistive indexes can provide useful insights into early hemodynamic abnormalities related to organ dysfunction before the occurrence of biochemical or macro-hemodynamic derangements [42–45, 60].

Probe

A sector or convex array probe with a color-pulsed wave Doppler is used for splanchnic perfusion assessment; the patient is commonly resting supine.

Sites of Evaluation

The transducer is positioned over the right and left intercostal spaces to evaluate perfusion of the spleen and kidneys. Color Doppler mode allows identification of the main branches of the renal and splenic arteries (Fig. 26.14).

Splenic artery flow should be sampled over a straight tract of the vessel inside the spleen, 1 cm from the hilum. Intrarenal vascular blood flow must be measured by acquiring at least three consecutive Doppler traces of the interlobar arteries for each renal area (upper, middle, and lower), which are then averaged to derive an index for the whole organ. Doppler resistive index is calculated according to the protocol of Planiol and Pourcelot as the ratio (S − D)/S, where S and D are peak systolic and end-diastolic velocities, respectively [42, 43].

The Kidney

The kidneys deserve particular attention in critically ill patients. Renal blood flow (RBF) can be easily monitored using Doppler metrics of the renal artery, the major determinants of which are drugs, vascular compliance, and renal vascular resistance [61]. Renal Doppler resistive index (RDRI) is the most important and commonly used index, reflecting all major determinants of systemic hemodynamics. It is effective in ensuring an adequate splanchnic perfusion and can identify high-risk patients for acute kidney injury (AKI) in intensive care units (ICU) [62].

During initial hypovolemia, renal blood flow can be reduced from normal 1300 to <200 mL/min, acting to protect against severe hypoperfusion of core organs [63]. Studies analyzing RDRI in humans have found that RDRI is related to hypoxemia in patients with acute lung injury [64] and can also detect occult euvolemic anemia in hemodynamically stable patients [42]. Thus, RDRI could be a promising independent predictive index for blood transfusion requirements, hemodynamic instability, and incipient hypovolemic shock in polytrauma patients.

This concept is also supported by a significant correlation between RDRI and arterial standard base excess, a marker of tissue hypoxia consistently found in critically ill (polytrauma) patients [65]. This establishes the clinical usefulness of RDRI as a non-invasive method for studying splanchnic hypoperfusion and possibly help instigate early surgical or radiological interventions. Additionally, RDRI has a pre-

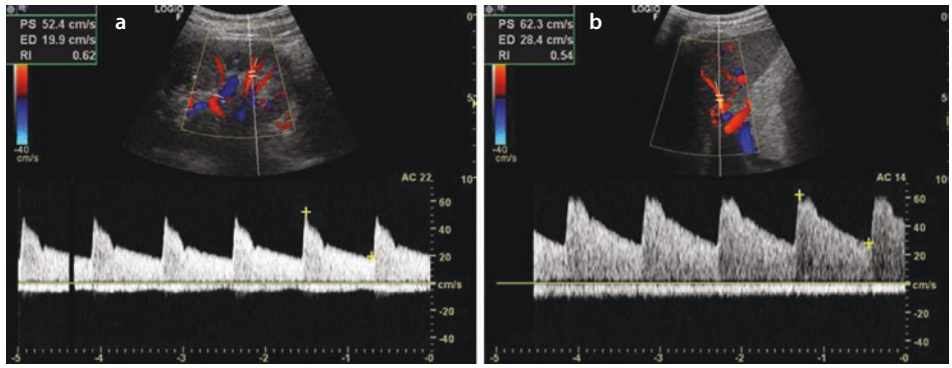

Fig. 26.14 Panel **a**: longitudinal ultrasonographic scan showing renal Doppler resistive index of the interlobar arteries of the kidney. Panel **b**: longitudinal scan of the spleen showing splenic Doppler resistive index of the main branch of the splenic artery

dictive function and it can detect hypoperfusion caused by low central venous oxygen in hemodynamically stable patients [60].

The Spleen

The spleen receives roughly 10% of cardiac output and plays an important role in maintaining vascular volume and pressure. Its regulatory mechanisms are mediated through changes in intra-splenic microvascular tone and neurohormonal modulation of renal and mesenteric vascular beds. Splenic effects on renal perfusion are mediated through reflex activation of splenic and renal sympathetic nerves [66]. The spleen can also regulate venous return by acting as a fluid reservoir; it mobilizes blood in event of hypovolemia and, through sympathetic regulation, it pools blood in the veins. These observations suggest that the spleen provides an insight into splanchnic circulation.

In a study by Corradi et al. [46], significant changes in splenic Doppler resistive index (SDRI) mirrored significant hemodynamic variations induced by a fluid challenge. SDRI was a valuable and reproducible bedside method to assess splanchnic perfusion regardless of fluid responsiveness. The main findings were that an SDRI reduction >9% was a marker of fluid responsiveness, with 100% specificity and 100% positive predictive value and a reduction >4% was associated with improved splanchnic hypoperfusion, increased lactate clearance, and reduced systemic vascular resistance, regardless of fluid responsiveness.

A SDRI reduction <4% excluded fluid responsiveness, with 100% sensitivity and 100% negative predictive value, without improvement in splanchnic perfusion but identifying congestion, fluid overload, and increased splanchnic parenchymal wedge pressures.

A ΔSDRI between 4% and 9% was always associated with improved splanchnic perfusion, reflected by an increase in lactate clearance regardless of cardiac fluid responsiveness. These findings confirm the spleen as a precisely regulated reservoir responding to hemodynamic variations induced by a fluid challenge. The role of SDRI is further validated by work on occult hemorrhagic shock after polytrauma in patients with persistently high SDRI and occult hypoperfusion despite a restored mean arterial pressure, heart rate, and cardiac index thus indicating SDRI as a target for appropriate resuscitation therapy.

Further studies in this emerging field of investigation are warranted as SDRI is potentially able to guide treatments that improve patient outcomes by restoring adequate regional perfusion pressure, avoiding vasoconstriction and splanchnic hypoperfusion.

Take-Home Messages

- E-FAST represents a rapid protocol to detect pericardial, intrathoracic, and intra-bdominal effusions.
- Detection of free fluid should prompt immediate further diagnostic procedures and/or interventions.
- Focused Assessment with Sonography for Trauma examination to identify pathological presence of free fluid/blood (i.e., pericardial sac, pleural space, and peritoneum) in traumatic acute abdomen should be considered as a basic skill.
- Focused Assessment with Sonography for Trauma examination should be considered as an integral component of trauma resuscitation.

References

1. Krug EG, Sharma GK, Lozano R. The global burden of injuries. Am J Public Health. 2000;90:523–6.
2. Carmont MR. The Advanced Trauma Life Support course: a history of its development and review of related literature. Postgrad Med J. 2005;81:87–91.
3. Kool DR, Blickman JG. Advanced Trauma Life Support. ABCDE from a radiological point of view. Emerg Radiol. 2007;14:135–41.
4. Kirkpatrick AW, Sirois M, Laupland KB, et al. Hand-held thoracic sonography for detecting post-traumatic pneumothoraces: the Extended Focused Assessment with Sonography for Trauma (EFAST). J Trauma. 2004;57:288–95.
5. Scalea TM, Rodriguez A, Chiu WC, Brenneman FD, Fallon WF, Kato K, McKenney MG, Nerlich ML, Ochsner MG, Yoshii H. Focused Assessment with Sonography for Trauma (FAST): results from an international consensus conference. J Trauma. 1999;46:466–72.
6. Dronen S, Chadwick O, Nowak R. Endotracheal tip position in the arrested patient. Ann Emerg Med. 1982;11:116–7.
7. Hosseini JS, Talebian MT, Ghafari MH, Eslami V. Secondary confirmation of endotracheal tube position by diaphragm motion in right subcostal ultrasound view. Int J Crit Illn Inj Sci. 2013;3:113–7.
8. Hsieh K-S, Lee C-L, Lin C-C, Huang T-C, Weng K-P, Lu W-H. Secondary confirmation of endotracheal tube position by ultrasound image. Crit Care Med. 2004;32:S374–7.
9. Robba C, Wong A, Poole D, et al. Basic ultrasound head-to-toe skills for intensivists in the general and neuro intensive care unit population: consensus and expert recommendations of the European Society of Intensive Care Medicine. Intensive Care Med. 2021;47:1347–67.
10. Charbit J, Millet I, Maury C, Conte B, Roustan J-P, Taourel P, Capdevila X. Prevalence of large and occult pneumothoraces in patients with severe blunt trauma upon hospital admission: experience of 526 cases in a French level 1 trauma center. Am J Emerg Med. 2015;33:796–801.
11. Volpicelli G. Sonographic diagnosis of pneumothorax. Intensive Care Med. 2011;37:224–32.
12. Hamada SR, Delhaye N, Kerever S, Harrois A, Duranteau J. Integrating eFAST in the initial management of stable trauma patients: the end of plain film radiography. Ann Intensive Care. 2016;6:62.
13. Vezzani A, Manca T, Brusasco C, Santori G, Valentino M, Nicolini F, Molardi A, Gherli T, Corradi F. Diagnostic value of chest ultrasound after cardiac surgery: a comparison with chest X-ray and auscultation. J Cardiothorac Vasc Anesth. 2014;28:1527–32.
14. Volpicelli G, Boero E, Sverzellati N, et al. Semi-quantification of pneumothorax volume by lung ultrasound. Intensive Care Med. 2014;40:1460–7.
15. Soldati G, Testa A, Silva FR, Carbone L, Portale G, Silveri NG. Chest ultrasonography in lung contusion. Chest. 2006;130:533–8.
16. Corradi F, Ball L, Brusasco C, Riccio AM, Baroffio M, Bovio G, Pelosi P, Brusasco V. Assessment of extravascular lung water by quantitative ultrasound and CT in isolated bovine lung. Respir Physiol Neurobiol. 2013;187:244–9.
17. Corradi F, Brusasco C, Garlaschi A, Paparo F, Ball L, Santori G, Pelosi P, Altomonte F, Vezzani A, Brusasco V. Quantitative analysis of lung ultrasonography for the detection of community-acquired pneumonia: a pilot study. Biomed Res Int. 2015;2015:868707.
18. Corradi F, Brusasco C, Pelosi P. Chest ultrasound in acute respiratory distress syndrome. Curr Opin Crit Care. 2014;20:98–103.
19. Pelosi P, Corradi F. Ultrasonography in the intensive care unit: looking at the world through colored glasses. Anesthesiology. 2012;117:696–8.
20. Luecke T, Corradi F, Pelosi P. Lung imaging for titration of mechanical ventilation. Curr Opin Anaesthesiol. 2012;25:131–40.
21. Hyacinthe A-C, Broux C, Francony G, Genty C, Bouzat P, Jacquot C, Albaladejo P, Ferretti GR, Bosson J-L, Payen J-F. Diagnostic accuracy of ultrasonography in the acute assessment of common thoracic lesions after trauma. Chest. 2012;141:1177–83.
22. Rozycki GS, Ballard RB, Feliciano DV, Schmidt JA, Pennington SD. Surgeon-performed ultrasound for the assessment of truncal injuries: lessons learned from 1540 patients. Ann Surg. 1998;228:557–67.

23. Rozycki GS, Feliciano DV, Ochsner MG, et al. The role of ultrasound in patients with possible penetrating cardiac wounds: a prospective multicenter study. J Trauma. 1999;46:543–51; discussion 551–2.
24. Goldberg BB, Goodman GA, Clearfield HR. Evaluation of ascites by ultrasound. Radiology. 1970;96:15–22.
25. Paajanen H, Lahti P, Nordback I. Sensitivity of transabdominal ultrasonography in detection of intraperitoneal fluid in humans. Eur Radiol. 1999;9:1423–5.
26. Abrams BJ, Sukumvanich P, Seibel R, Moscati R, Jehle D. Ultrasound for the detection of intraperitoneal fluid: the role of Trendelenburg positioning. Am J Emerg Med. 1999;17:117–20.
27. Huang MS, Liu M, Wu JK, Shih HC, Ko TJ, Lee CH. Ultrasonography for the evaluation of hemoperitoneum during resuscitation: a simple scoring system. J Trauma. 1994;36:173–7.
28. Ma OJ, Mateer JR, Ogata M, Kefer MP, Wittmann D, Aprahamian C. Prospective analysis of a rapid trauma ultrasound examination performed by emergency physicians. J Trauma. 1995;38:879–85.
29. Ingeman JE, Plewa MC, Okasinski RE, King RW, Knotts FB. Emergency physician use of ultrasonography in blunt abdominal trauma. Acad Emerg Med. 1996;3:931–7.
30. Sirlin CB, Casola G, Brown MA, Patel N, Bendavid EJ, Hoyt DB. Quantification of fluid on screening ultrasonography for blunt abdominal trauma: a simple scoring system to predict severity of injury. J Ultrasound Med. 2001;20:359–64.
31. McKenney KL, McKenney MG, Cohn SM, Compton R, Nunez DB, Dolich M, Namias N. Hemoperitoneum score helps determine need for therapeutic laparotomy. J Trauma. 2001;50:650–4; discussion 654–6.
32. Rozycki GS, Ochsner MG, Feliciano DV, Thomas B, Boulanger BR, Davis FE, Falcone RE, Schmidt JA. Early detection of hemoperitoneum by ultrasound examination of the right upper quadrant: a multicenter study. J Trauma. 1998;45:878–83.
33. Charbit J, Millet I, Lakhal K, Brault-Noble G, Guillon F, Taourel P, Capdevila X. A haemoperitoneum does not indicate active bleeding in the peritoneum in 50% of hypotensive blunt trauma patients: a study of 110 severe trauma patients. Injury. 2014;45:88–94.
34. Yeguiayan J-M, Yap A, Freysz M, Garrigue D, Jacquot C, Martin C, Binquet C, Riou B, Bonithon-Kopp C, FIRST Study Group. Impact of whole-body computed tomography on mortality and surgical management of severe blunt trauma. Crit Care. 2012;16:R101.
35. Bouzat P, Valdenaire G, Gauss T, et al. Early management of severe abdominal trauma. Anaesth Crit Care Pain Med. 2020;39:269–77.
36. Branney SW, Wolfe RE, Moore EE, Albert NP, Heinig M, Mestek M, Eule J. Quantitative sensitivity of ultrasound in detecting free intraperitoneal fluid. J Trauma. 1995;39:375–80.
37. Kornezos I, Chatziioannou A, Kokkonouzis I, Nebotakis P, Moschouris H, Yiarmenitis S, Mourikis D, Matsaidonis D. Findings and limitations of focused ultrasound as a possible screening test in stable adult patients with blunt abdominal trauma: a Greek study. Eur Radiol. 2010;20:234–8.
38. Richards JR, McGahan JP, Jones CD, Zhan S, Gerscovich EO. Ultrasound detection of blunt splenic injury. Injury. 2001;32:95–103.
39. Nunes LW, Simmons S, Hallowell MJ, Kinback R, Trooskin S, Kozar R. Diagnostic performance of trauma US in identifying abdominal or pelvic free fluid and serious abdominal or pelvic injury. Acad Radiol. 2001;8:128–36.
40. Blackbourne LH, Soffer D, McKenney M, et al. Secondary ultrasound examination increases the sensitivity of the FAST exam in blunt trauma. J Trauma. 2004;57:934–8.
41. Rajabzadeh Kanafi A, Giti M, Gharavi MH, Alizadeh A, Pourghorban R, Shekarchi B. Diagnostic accuracy of secondary ultrasound exam in blunt abdominal trauma. Iran J Radiol. 2014;11:e21010.
42. Corradi F, Brusasco C, Vezzani A, Palermo S, Altomonte F, Moscatelli P, Pelosi P. Hemorrhagic shock in polytrauma patients: early detection with renal Doppler resistive index measurements. Radiology. 2011;260:112–8.
43. Corradi F, Brusasco C, Garlaschi A, Santori G, Vezzani A, Moscatelli P, Pelosi P. Splenic Doppler resistive index for early detection of occult hemorrhagic shock after polytrauma in adult patients. Shock. 2012;38:466–73.
44. Corradi F, Brusasco C, Via G, Tavazzi G, Forfori F. Renal Doppler-based assessment of regional organ perfusion in the critically ill patient. Shock. 2021;55:842–3.

45. Corradi F, Via G, Tavazzi G. What's new in ultrasound-based assessment of organ perfusion in the critically ill: expanding the bedside clinical monitoring window for hypoperfusion in shock. Intensive Care Med. 2020;46:775–9.
46. Brusasco C, Tavazzi G, Robba C, Santori G, Vezzani A, Manca T, Corradi F. Splenic Doppler resistive index variation mirrors cardiac responsiveness and systemic hemodynamics upon fluid challenge resuscitation in postoperative mechanically ventilated patients. Biomed Res Int. 2018;2018:1978968.
47. Kelsey JH, Henderson SO, Newton K. Bedside ultrasound in delayed traumatic pericardial effusion. Am J Emerg Med. 1999;17:313–4.
48. Spodick DH. Acute cardiac tamponade. N Engl J Med. 2003;349:684–90.
49. Ball CG, Williams BH, Wyrzykowski AD, Nicholas JM, Rozycki GS, Feliciano DV. A caveat to the performance of pericardial ultrasound in patients with penetrating cardiac wounds. J Trauma. 2009;67:1123–4.
50. Meyer DM, Jessen ME, Grayburn PA. Use of echocardiography to detect occult cardiac injury after penetrating thoracic trauma: a prospective study. J Trauma. 1995;39:902–7; discussion 907–9.
51. Via G, Tavazzi G, Price S. Ten situations where inferior vena cava ultrasound may fail to accurately predict fluid responsiveness: a physiologically based point of view. Intensive Care Med. 2016;42:1164–7.
52. Yanagawa Y, Nishi K, Sakamoto T, Okada Y. Early diagnosis of hypovolemic shock by sonographic measurement of inferior vena cava in trauma patients. J Trauma. 2005;58:825–9.
53. Sefidbakht S, Assadsangabi R, Abbasi HR, Nabavizadeh A. Sonographic measurement of the inferior vena cava as a predictor of shock in trauma patients. Emerg Radiol. 2007;14:181–5.
54. Yanagawa Y, Sakamoto T, Okada Y. Hypovolemic shock evaluated by sonographic measurement of the inferior vena cava during resuscitation in trauma patients. J Trauma. 2007;63:1245–8. discussion 1248
55. Doucet JJ, Ferrada P, Murthi S, et al. Ultrasonographic inferior vena cava diameter response to trauma resuscitation after 1 hour predicts 24-hour fluid requirement. J Trauma Acute Care Surg. 2020;88:70–9.
56. Assessment of brain midline shift using sonography in neurosurgical ICU patients. https://pubmed.ncbi.nlm.nih.gov/25488604/. Accessed 1 Aug 2022.
57. Bellner J, Romner B, Reinstrup P, Kristiansson K-A, Ryding E, Brandt L. Transcranial Doppler sonography pulsatility index (PI) reflects intracranial pressure (ICP). Surg Neurol. 2004;62:45–51; discussion 51.
58. Bouzat P, Almeras L, Manhes P, et al. Transcranial Doppler to predict neurologic outcome after mild to moderate traumatic brain injury. Anesthesiology. 2016;125:346–54.
59. Robba C, Santori G, Czosnyka M, Corradi F, Bragazzi N, Padayachy L, Taccone FS, Citerio G. Optic nerve sheath diameter measured sonographically as non-invasive estimator of intracranial pressure: a systematic review and meta-analysis. Intensive Care Med. 2018;44:1284–94.
60. Corradi F, Brusasco C, Paparo F, et al. Renal Doppler resistive index as a marker of oxygen supply and demand mismatch in postoperative cardiac surgery patients. Biomed Res Int. 2015;2015:763940.
61. Di Nicolò P, Granata A. Renal intraparenchymal resistive index: the ultrasonographic answer to many clinical questions. J Nephrol. 2019;32:527–38.
62. Le Dorze M, Bouglé A, Deruddre S, Duranteau J. Renal Doppler ultrasound: a new tool to assess renal perfusion in critical illness. Shock. 2012;37:360–5.
63. Lucas CE. Renal considerations in the injured patient. Surg Clin North Am. 1982;62:133–48.
64. Darmon M, Schortgen F, Leon R, Moutereau S, Mayaux J, Di Marco F, Devaquet J, Brun-Buisson C, Brochard L. Impact of mild hypoxemia on renal function and renal resistive index during mechanical ventilation. Intensive Care Med. 2009;35:1031–8.
65. Vezzani A, Corradi F, Palermo S, Altomonte F, Moscatelli P, Brusasco C. Renal Doppler resistance index: early marker of splanchnic hypoperfusion and bleeding in major trauma with a borderline hemodynamic status. Intensive Care Med. 2009;35:s257.
66. Hamza SM, Kaufman S. Role of spleen in integrated control of splanchnic vascular tone: physiology and pathophysiology. Can J Physiol Pharmacol. 2009;87:1–7.